

UC Berkeley

UC Berkeley Electronic Theses and Dissertations

Title

Toward the Rational Design of Asymmetric Catalysts using Attractive Non-Covalent Interactions and Design Elements

Permalink

<https://escholarship.org/uc/item/34d2396n>

Author

Neel, Andrew James

Publication Date

2016

Peer reviewed|Thesis/dissertation

Toward the Rational Design of Asymmetric Catalysts using Attractive Non-Covalent
Interactions as Design Elements

by

Andrew James Neel

A dissertation submitted in partial satisfaction of the

requirements for the degree of

Doctor of Philosophy

in

Chemistry

in the

Graduate Division

of the

University of California, Berkeley

Committee in charge:

Professor F. Dean Toste, Chair

Professor Richmond Sarpong

Professor Dmitry Budker

Spring 2016

Abstract

Toward the Rational Design of Asymmetric Catalysts using Attractive Noncovalent Interactions as Design Elements

by

Andrew James Neel

Doctor of Philosophy in Chemistry

University of California, Berkeley

Professor F. Dean Toste, Chair

Throughout my doctoral studies, I have endeavored to address the question of how to rationally design chiral catalysts to control enantioselectivity in a predictable fashion. To approach this problem, I have focused on the strategic implementation of attractive non-covalent interactions between catalysts and their substrates at the enantiodetermining transition state. A significant portion of this work involved the development of an approach to elucidating the structural origins of selectivity in complex data sets, with an eye towards rational catalyst design. The insights gained from these studies constitute the subject matter of this dissertation.

Chapter 1 provides an overview of a subset of attractive non-covalent interactions involving aromatic rings. Examples are highlighted in which these interactions have been characterized in the ground state with the explicit intention of quantifying their strengths and geometric requirements. Using the lessons learned from these reports, case studies are presented in which the interactions under discussion have been leveraged to catalyze chemical reactions *via* the paradigm of transition state stabilization. The insight gleaned from this literature survey is intended to provide a framework for the discussion of the catalyst design concepts outlined in the following chapters.

Chapter 2 describes the development of a novel class of axially chiral triazole containing phosphoric acid catalysts designed to impart enantioselectivity *via* attractive non-covalent interactions with a substrate at the enantiodetermining TS. This strategy stands in contrast to that typically discussed in the literature in which catalyst steric bulk is frequently invoked to rationalize asymmetric induction. Using this newly prepared catalyst library, an enantioselective cross dehydrogenative coupling was developed within the conceptual framework of the Toste group's strategy of chiral anion phase transfer catalysis. Preliminary experiments suggested that the triazole substituents played a role in the determination of asymmetric induction beyond steric bulk, as initially hypothesized.

The third chapter describes our efforts to elucidate the structural origins of enantioselectivity in the oxidative coupling reaction presented in Chapter 2. By obtaining an enantioselectivity data set based on strategically modulated catalysts and substrates, we applied linear regression techniques to correlate our experimental data with molecular descriptors describing the structural variation

throughout the data set. The resulting models, along with the overall enantioselectivity trends, were used to develop intuitively sensible mechanistic hypotheses that were subsequently tested through the application of new catalysts specifically tailored to address them. Based on the hypothesis that the triazole catalysts were engaged in enantiodetermining π - π interactions with the substrates at the TS, we rationally designed catalysts that afforded the products with the highest enantiomeric excesses reported to date.

Chapter 4 builds on the strategy outlined in Chapter 3 in the context of a boronic acid-directed phosphoric acid catalyzed enantioselective fluorination of allylic alcohols. Specifically, the logic developed in this chapter allows for the generalization of our data intensive strategy to scenarios in which the mechanism for selectivity determination changes throughout a data set. Through the careful organization of enantioselectivity data and strategically implemented mechanistic experiments, we identified a region of structural space in which we propose that a lone pair- π interaction governs enantioselectivity. Based on this hypothesis, we rationally designed a catalyst system capable of producing either enantiomer of a chiral fluorinated building block in high enantiomeric excess using the same chiral catalyst.

Table of Contents

List of Figures	v
List of Schemes	ix
List of Tables	x
Acknowledgements.....	xii
Chapter 1. Attractive Non-Covalent Interactions Beyond Hydrogen Bonding in Transition State Stabilization	
Introduction	2
π - π	5
Cation- π	9
Anion- π	14
Lone pair- π	18
Conclusions and Outlook	21
Chapter 2. Enantioselective Cross Dehydrogenative Coupling Enabled by the Design and Application of Chiral Triazole Containing Phosphoric Acids	
Introduction	27
Results and Discussion	30
Reaction development	30
Mechanistic studies	37
Conclusion	40
Experimental Section	40
General information	40
Materials and methods	41

Synthesis and characterization of catalysts	41
Synthesis and characterization of substrates	60
Synthesis and characterization of products	68
HPLC traces	77
Kinetic isotope effect experimental details	93
References and notes	104
Appendix A. NMR spectra for compounds in Chapter 2	108
NMR spectra of catalysts	108
NMR spectra of substrates	154
NMR spectra of products	174

Chapter 3. Development of a Data-Intensive Method for Mechanistic Elucidation using Structurally Diverse Enantioselectivity Datasets

Introduction	197
Background	199
Results and Discussion	206
Experimental design	206
Library design and parameter selection	207
Modeling catalyst heterocyclic rings	210
Modeling of individual substrates and catalysts	212
Trend Analysis	215
Trend Interpretation	216
Comprehensive model and probes of mechanistic hypotheses	218
Conclusion	220

Experimental Section	221
General information	221
Materials and methods	222
Computations	222
Modeling	222
Synthesis and characterization of catalysts	242
Synthesis and characterization of substrates	257
Synthesis and characterization of products	261
HPLC Traces	265
References and Notes	278
Appendix B. NMR spectra for compounds in Chapter 3.....	280
NMR spectra of catalysts	280
NMR spectra of substrates	318
NMR spectra of products	325
Chapter 4. Development of a Strategy for the Identification of Mechanistic Breaks using Judiciously Designed Enantioselectivity Datasets	
Introduction	333
Background	334
Results and Discussion	335
Control experiments	335
Dataset design	338
Data collection	339
Nonlinear effect studies	340
Examination of 4- <i>i</i> -Pr substituted catalyst 4.7e	345

Isotopic substitution experiments	346
Probing direct interaction	348
Trend analysis	350
Conclusion	352
Experimental Section	353
General information	353
Materials and methods	353
Synthesis and characterization of catalysts	353
Synthesis and characterization of boronic acids	356
Synthesis and characterization of 4.1-<i>d</i>₃	358
General procedure for enantioselective fluorination reactions	359
Complete enantioselectivity dataset	360
Data used for nonlinear effect studies	363
Data used for construction of Hammett plots	364
Computations	364
Model Development	364
HPLC traces	371
References and Notes	373
Appendix C. NMR spectra for compounds in Chapter 4	379
NMR spectra of catalysts	379
NMR spectra of boronic acids	382

List of Figures

Figure 1.1. Qualitative description of catalysis	2
Figure 1.2. Qualitative depiction of catalysis <i>via</i> change in mechanism	2
Figure 1.3. Qualitative depiction of catalysis <i>via</i> TS stabilization	3
Figure 1.4. Summary of noncovalent interactions under discussion	4
Figure 1.5. π - π interaction geometries (left) and example ESP maps (right)	5
Figure 1.6. Solution study supporting polar- π model	6
Figure 1.7. Hammett correlations supporting direct interaction model	6
Figure 1.8. Correlations demonstrating geometric consequences of direct interaction model	7
Figure 1.9. Experimental study supporting direct interaction model	8
Figure 1.10. Experimental study quantifying contributions of π - π interactions to catalysis	8
Figure 1.11. Depiction of the aromatic box from HP1 chromodomain	10
Figure 1.12. Contribution of cation- π interactions to trimethyllysine binding by HP1 chromodomain	11
Figure 1.13. Quantification of cation- π interactions in squalene-hopene cyclase	12
Figure 1.14. Quantification of cation- π interactions in aristolochene synthase	13
Figure 1.15. Control of enantioselectivity using synthetic catalysts designed to employ cation- π interactions	13
Figure 1.16. Anion- π geometries (left) and ESP maps for electron-poor arenes (right)	14
Figure 1.17. Computational investigation of compensatory effects in anion- π interactions	15
Figure 1.18. Experimental study of anion- π interactions in solution	16
Figure 1.19. Anion- π catalysis of Kemp elimination	16
Figure 1.20. Enolate stabilization <i>via</i> anion- π interactions	17
Figure 1.21. Control of reaction selectivity using anion- π interactions	18

Figure 1.22. Example lone pair- π interactions in Z-DNA and an RNA pseudoknot	19
Figure 1.23. Quantification of lone pair- π interaction in solution	20
Figure 1.24. Quantification of lone pair-p interactions using molecular torsion balances	21
Figure 2.1. Selected examples of axially chiral phosphoric acids	27
Figure 2.2. Proposed catalytic cycle for CAPT fluorination	30
Figure 2.3. Mechanistic hypothesis for chiral phosphate-catalyzed enantioselective CDC reaction	31
Figure 2.4. Conceptual difference between using repulsive (left) versus attractive (right) interactions to influence enantioselectivity in chiral phosphate catalysis	32
Figure 2.5. Simplified reaction coordinate diagram illustrating the enantiodetermining transition state of an asymmetric reaction and the associated energy differences required for asymmetric induction (top) and examples of noncovalent interactions that might be leveraged for asymmetric catalysis (bottom)	33
Figure 2.6. Illustration of peptidomimetic qualities of 1,2,3-triazole resulting from its large dipole moment	34
Figure 2.7. Preliminary substrate scope of asymmetric CDC reaction	36
Figure 2.8. Summary of enantiomer-dependent kinetic isotope effect experiments	37
Figure 2.9. Mechanistic rational for enantiomer-dependent kinetic isotope effect illustrating that oxidation and cyclization are de-coupled	38
Figure 2.10. Proposed mechanism for chiral anion catalyzed asymmetric CDC reaction	39
Figure 2.11. Experiments probing structural role of 1,2,3-triazole in catalysts 2.11	39
Figure 3.1. Summary of triazolyl PA-catalyst CDC reaction	197
Figure 3.2. Subset of nonintuitive enantioselectivity trends from asymmetric CDC reaction ..	198
Figure 3.3. Example reaction coordinate diagram depicting energy difference between competing diastereomeric TS's required for asymmetric induction	199
Figure 3.4. LFER correlating ee of asymmetric epoxidation to Hammett σ constant	
Figure 3.5. LFER correlating ee of asymmetric NHK allylation with Taft-Charton steric parameter (ν) ...	201

Figure 3.5. LFER correlating ee of asymmetric NHK allylation with Taft-Charton steric parameter (ν)	202
Figure 3.6. Systematically modified ligand library for evaluation in NHK propargylation	203
Figure 3.7. Three-dimensional surface illustrating interplay of steric and electronic effects in NHK propargylation	203
Figure 3.8. Pictorial representation of Sterimol parameters B_1 , B_5 , and L	204
Figure 3.9. Comparison of ability of Taft-Charton (left) and Sterimol (right) parameters to correlate with ee in desymmetrization of <i>bis</i> -phenols	204
Figure 3.10. Improvement of correlation between predicted and measured ee upon switching from steric (left) to vibrational (right) analysis	205
Figure 3.11. <i>Bis</i> -phenol vibrational modes relevant for modeling enantioselectivity in peptide-catalyzed desymmetrization	206
Figure 3.12. Outline of strategy for studying origin of enantioselectivity	207
Figure 3.13. Substrate and catalyst libraries used for modeling	208
Figure 3.14. Substrate molecular descriptors used for modeling.....	209
Figure 3.15. Catalyst molecular descriptors used for modeling	209
Figure 3.16. Example catalyst vibrational frequencies	209
Figure 3.17. Nitrogen deletion experiments	211
Figure 3.18. Mathematical correlation of normalized catalyst and substrate vibrational parameters to enantioselectivity and associated measured vs. predicted $\Delta\Delta G^\ddagger$ plot	211
Figure 3.19. Example mathematical correlation of catalyst vibrational parameters to enantioselectivity for a single substrate with 11 catalysts and associated predicted vs. measured $\Delta\Delta G^\ddagger$ plot	213
Figure 3.20. General form of initial substrate models	213
Figure 3.21. Graphical representation of catalyst structure-selectivity trends as a function of substrate	214
Figure 3.22. Graphical representation of substrate structure-selectivity trends as a function of catalyst	214

Figure 3.23. Mathematical correlation of torsion angle to catalyst vibrational frequencies	215
Figure 3.24. Qualitative depiction of data interpretation	217
Figure 3.25. Predicted vs. measured $\Delta\Delta G^\ddagger$ plot for normalized global model relating enantioselectivity to both catalyst and substrate structural features	218
Figure 3.26. Individual models and plots for substrates 3.1	237
Figure 3.27. Individual models and plots for catalysts 3.4	240
Figure 3.28. Enantioselectivity data for all catalyst-substrate combinations	242
Figure 4.1. Example Hammett plot demonstrating how change in slope suggests change in mechanism	333
Figure 4.2. Conceptual diagram of chiral anion phase-transfer catalysis	334
Figure 4.3. Phosphate-catalyzed aryl BA-directed asymmetric fluorination of allylic alcohols.....	335
Figure 4.4. Preliminary results demonstrating effect of BA structure on enantioselectivity	335
Figure 4.5. Proposed mechanism asymmetric fluorination	336
Figure 4.6. Boron speciation during titration of 4.3 with 4.1	337
Figure 4.7. Effect of BA structure on enantioselectivity using (<i>S</i>)-TRIP	338
Figure 4.8. Visualization of enantioselectivity range accessible through alteration BA structure	338
Figure 4.9. Enantioselectivity data obtained by variation of PA and BA substitution pattern ..	340
Figure 4.10. Graphical representation of BA structure-selectivity trends as a function of catalyst structure	341
Figure 4.11. Relationship between product and catalyst enantiomeric excess for various PA-BA combinations	342
Figure 4.12. Effect of catalyst enantiopurity on rate of product formation	343
Figure 4.13. Effect of Selectfluor counteranion on reaction outcome	343
Figure 4.14. Relationship between product and catalyst enantiomeric excess for 4.7f and 4.6p	344

Figure 4.15. Effect of catalyst <i>para</i> -substituent identity on enantioselectivity	344
Figure 4.16. Relationship between product and catalyst enantiomeric excess for 4.7b and 4.6o	345
Figure 4.17. Correlation between enantiomeric excess of 4.2 ($\Delta\Delta G^\ddagger$) and σ_{para} for various BAs using catalyst 4.7e	345
Figure 4.18. Reaction time course data for formation of 4.2 with varying BA structure	346
Figure 4.19. Comparison of enantiomeric excess of 4.2 and 4.2-<i>d</i>₂ for various BA-PA combinations	347
Figure 4.20. Plausible mechanistic rationale for variable dependence of enantioselectivity on isotopic substitution	347
Figure 4.21. (A) Comparison of enantiomeric excess of 4.2 using hybrid BA 4.6w vs. 4.6o and 4.6m . (B) Effect of variation of alkyl vs. alkoxy substituents for various 3,5-disubstituted hybrid BAs	348
Figure 4.22. Qualitative depiction of the lone pair- π interaction as a stabilizing structural element of Z-DNA (left) and analogy to the present system	349
Figure 4.23. Inversion of enantiomeric excess of 4.2 using catalyst 4.7i	350
Figure 4.24. Graphical representation of catalyst structure-selectivity trends as a function of BA structure	351
Figure 4.25. Mathematical correlations of normalized normalized catalyst and BA molecular descriptors to enantioselectivity ($\Delta\Delta G^\ddagger$) for 2- and 4-substituted aryl BAs (A), all 3,5-disubstituted aryl BAs (B), 3,5-disubstituted aryl BAs with symmetrical substitution or a methoxy substituent (C), and 3-alkoxy-5-methyl substituted aryl BAs (D)	352
Figure 4.26. Complete set of enantioselectivity data for all BA-PA combinations	360
Figure 4.27. Enantioselectivity data used for creation of NLE plots	363
Figure 4.28. Carboxylic acid vibrational modes used for modeling enantioselectivity	365
Figure 4.29. Correlation between carboxylic acid and boronic acid vibrational modes for various aryl substitution patterns	366
Figure 4.30. Examples of parameters used for modeling	366

Figure 4.31. Sample ^1H NMR titration spectrum. Initial concentrations: 0.0438 M boroxine, 0.175 M alcohol in benzene- d_6 . Final concentrations: 0.0114 M boroxine, 0.0499 M *mono*-ester, 0.0381 M *bis*-ester, 0.0512 M alcohol373

List of Schemes

Scheme 2.1. Seminal examples of axially chiral PAs as Brønsted acid catalysts	28
Scheme 2.2. Seminal report of chiral anion catalysis with phosphate anions	28
Scheme 2.3. Seminal examples of asymmetric cationic (top) and anionic (bottom) PTC	29
Scheme 2.4. Oxoammonium mediated oxidation of a secondary amine	30
Scheme 2.5. Synthesis of triazolyl PA catalysts	35
Scheme 2.6. Chiral substrate demonstrating catalyst control over absolute configuration of newly-formed stereocenter	37
Scheme 2.7. Synthesis of <i>pyr</i> - and <i>imid</i> - 2.111	57
Scheme 2.8. Synthesis of substrates 2.6	60
Scheme 2.9. Synthesis of substrate 2.6a-d₁	93
Scheme 2.10. Determination of er of 2.6a-d₁	97
Scheme 2.11. Determination of KIE_{Real}	102
Scheme 3.1. Synthesis of triazolyl phosphoric acids 3.4	242
Scheme 3.2. Synthesis of substrates 3.1	257
Scheme 4.1. Synthesis of catalysts 4.7	354
Scheme 4.2. Synthesis of hybrid aryl BAs	356
Scheme 4.3. Synthesis of deuterated substrate 4.1-d₃	358

List of Tables

Table 2.1. Initial survey of axially chiral PAs in model asymmetric CDC reaction	32
Table 2.2. Summary of effects of catalyst, oxidant, base and solvent on conversion and enantiomeric excess of model asymmetric CDC reaction	35

Table 2.3. Kinetic isotope effect data	101
Table 3.1. Selected values of parameters used for modeling of <i>bis</i> -phenol desymmetrization	206
Table 3.2. Predicted and measured enantioselectivities for adamantyl-substituted catalysts	212
Table 3.3. Summary of simplified substrate models using torsion angle as a parameter	216
Table 3.4. Hypothesis-driven external validation using catalyst 3.4l	219
Table 3.5. Hypothesis-driven external validation using catalyst 3.4m	220
Table 3.6. Hypothesis-driven external validation using catalyst 3.4n	220
Table 3.7. Parameters used for substrates 3.1	224
Table 3.8. Normalized reduced parameter set used for substrates	226
Table 3.9. Parameters used for catalysts 3.4	227
Table 3.10. Normalized reduced parameter set used for aryl triazole catalysts	229
Table 3.11. Measured vs. predicted $\Delta\Delta G^\ddagger$ values (black represents training set, red represents external validations, and blue represents external predictions)	229
Table 3.12. $\Delta\Delta G^\ddagger$ values used as inputs for modeling	233
Table 4.1. Selected control experiments	336
Table 4.2. NMR titration experiments	337
Table 4.3. Complete enantioselectivity data using catalyst 4.7e	364
Table 4.4. Full set of BA molecular descriptors used for modeling	367
Table 4.5. Full set of catalyst molecular descriptors used for modeling	369

Acknowledgements

First and foremost, I would like to acknowledge my parents, Dr. James and Louisa Neel, for their unwavering support of any and all pursuits in which I have ever been engaged. Perhaps even more importantly, I am indebted to you for providing an example of hard work and responsibility that spoke louder than words ever could have.

I would like to express gratitude towards my friends from Wichita- in particular Mitch, Connor, Alan, Ryley, Thomas, Megan, Katie, Tommy and Dustin- for not only their friendship over multiple decades but especially for centering me and providing reminders when they were needed most that life goes on outside of the strange bubble of graduate school at UC Berkeley.

I would like to thank my high school Latin and Chemistry teachers, Virginia Kehoe and Janice Crowley respectively, for challenging me to think critically- a skill without which my scientific pursuits would have undoubtedly failed to launch.

I credit Professor Marcey Waters at UNC for first exposing me to organic chemistry, ultimately leading to my decision to pursue it as a career. I am also grateful to Professor Jeffrey S. Johnson for affording me my first true research experience and for providing an illuminating view into the world of academic research. Additionally, I am indebted to Dr. Andrew Parsons and Dr. Austin Smith for their mentorship and patience during my initial foray into research and for truly setting the bar for what a successful graduate student should look like.

Moving all the way across the country to Berkeley for graduate school in the fall of 2011 was a major life change, but it could not have been any smoother, due in no small part to my roommates Anna Parker and Richard Cooper. I don't think that I can name another person who stayed with the same people for the entirety of his/her graduate career and I attribute this success to our aligned ideals- from cleanliness standards to beer consumption, the pleasure has been all mine. I'd also like to thank Tony, Kelly, Andrew, Karla, Alex, Scott and Cheri for being great friends from the beginning- many of the best times from the Berkeley years have been with you guys.

In contrast to the many horror stories that precede the beginning of any graduate career, my experience in the Toste group has been, if not sophisticated, extremely fun. In addition to being hands down the most intellectually stimulating environment to which I have been exposed, I have made some great friends from all over the globe that have challenged the ways in which I think about everything from science to politics. In particular, I would like to thank former postdocs Dr. Vivek Rauniar, Dr. Robert Phipps and Dr. Matthew Winston for setting examples early in my graduate career of the different forms that excellence can take and have made an effort to assimilate habits from each into my own work. I would also like to thank the graduate students who came before me (Drs. Jane Wang, Chris Boyd, Aaron Lackner, Yiming Wang, Jeff Wu, Mika Shiramizu, Chen Zhao, Hunter Shunatona and Miles Johnson) and after (Mark Levin, Drew Samant, Rebecca Triano, Dave Kaphan, Cindy Hong, Richard Thornbury, Patrick Bohan, Alec Christian, Suhong Kim and John Lee) for giving the group the ever-evolving but always unique character.

Given that the second half of my PhD was spent as part of a collaboration, it would be remiss not to acknowledge Professor Matthew Sigman for being a superb and thorough collaborator and research mentor. Additionally, special thanks to Dr. Anat Milo, who is truly the most outside the box person I've ever worked with- rest assured that my views towards the world will forever be couched in terms of probabilistic thinking for better or worse.

The student-advisor relationship can make or break a PhD experience and I am forever indebted to my advisor, Prof. F. Dean Toste, for making mine so positive. Your commitment to supporting both crazy ideas and a rigorous application of the scientific method to challenging

questions makes for a stimulating and fulfilling environment. You've also just been a cool dude to talk to-sometimes that's just as important.

I would like to give a particularly special thanks to my classmates in the Toste group-Dillon Miles, Dimitri Khrakovsky, Jigar Patel and Willie Wolf. I would venture to guess that it is somewhat unusual to have lab mates that are also such great friends. I could say much more but I've opted for brevity because I truly couldn't say enough. Grad school would've sucked without you guys-thanks.

Finally, Frances. We've come a long way since the days when I was afraid to ask you to go to dinner with me. Now I've asked you to move across the country with me. You've been my best friend for the last four years and I don't know how I would have gotten through the low points without you. You are devastatingly beautiful, intimidatingly intelligent and, most importantly, a complete badass. I love you and I'm excited for what's next.

Chapter 1

Attractive Non-Covalent Interactions Beyond Hydrogen Bonding in Transition State Stabilization

Introduction

In its broadest chemical sense, catalysis can be understood as the lowering of a reaction's free energy of activation (ΔG^\ddagger by the Eyring convention) by a molecular entity (the catalyst) that is not itself consumed. As ΔG^\ddagger merely describes the difference between the lowest and highest energy points along a reaction coordinate, catalysis must be achieved through transition state (TS) stabilization, either alone or a combination with ground state (GS) destabilization (Figure 1.1). A catalyst can not alter the thermodynamics of a system, only the rate at which equilibrium is achieved.

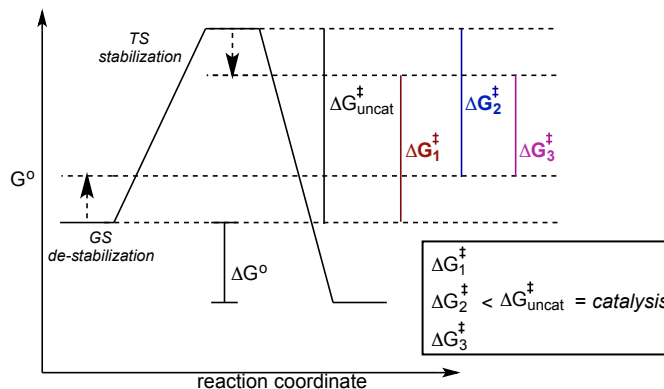


Figure 1.1. Qualitative description of catalysis

As such, catalysis is often understood in terms of a change in the mechanism (*i.e.*, the relative ordering and nature of bond making and breaking events) by which a reactant is converted into a product. Indeed, practitioners of chemical synthesis have traditionally held this viewpoint, developing catalytic reactions whose mechanisms have no natural counterparts, realizing a decrease in ΔG^\ddagger by accessing an orthogonal energetic landscape.

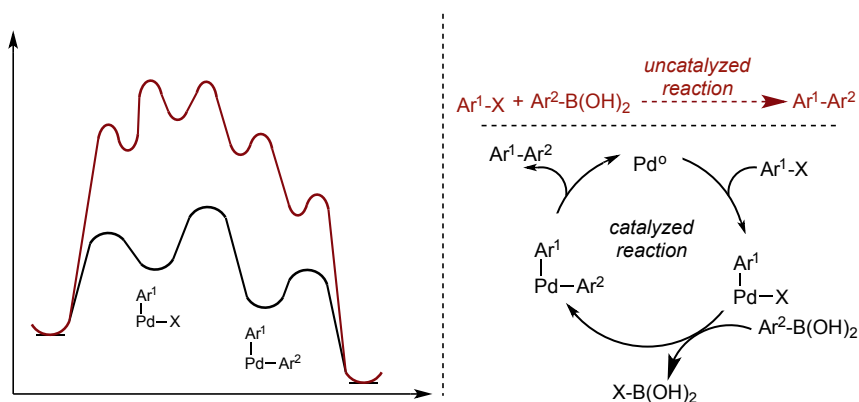


Figure 1.2. Qualitative depiction of catalysis *via* change in mechanism

An illustrative example is the Suzuki-Miyaura reaction between an aryl halide and an aryl boronic acid, whose accepted mechanism involves a palladium catalyst effecting oxidative addition, transmetalation and reductive elimination steps (Figure 1.2). This mechanism stands in

stark contrast to that of the uncatalyzed process in which aryl-aryl bond formation might occur by a mechanism involving extremely high energy intermediates with TS's completely unrelated to those of the palladium-catalyzed process, or indeed *not at all* due to the absence of a viable pathway.

Alternatively, a catalyst need not achieve the required lowering of a reaction's ΔG^\ddagger *via* the wholesale overhaul of the intermediates and transition states involved in the mechanism. Catalysis can occur *via* the stabilization of a TS or TS's along a reaction coordinate that are otherwise quite similar to those of the uncatalyzed background reaction (Figure 1.3). Although subtle, this difference has an important consequence: as transition structures are necessarily composites of the ground state structures immediately preceding and following them, a catalyst that favorably binds a TS will also likely do so for these latter entities. Thus, the key to achieving rate acceleration in this scenario is for the catalyst to bind the TS more tightly than the GS. Covalent catalysis notwithstanding, this is the strategy employed by a large portion of Nature's catalysts, enzymes (Figure 1.3).

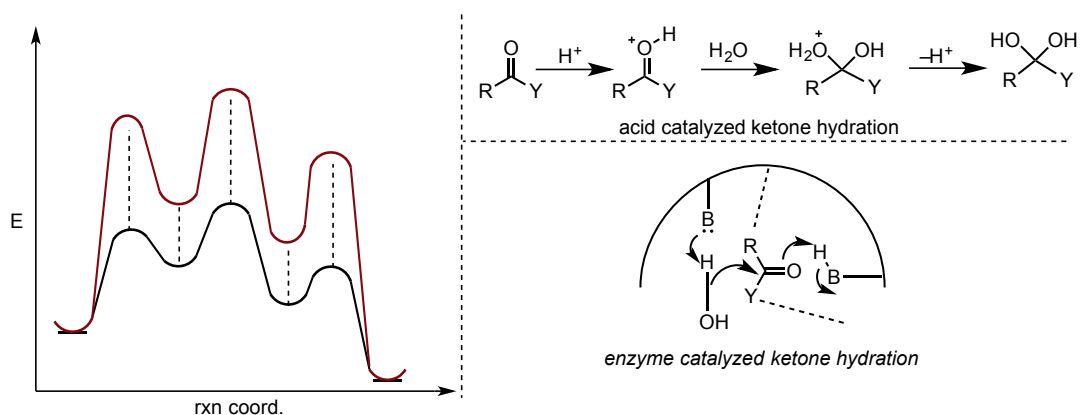


Figure 1.3. Qualitative depiction of catalysis *via* TS stabilization

Products of billions of years of evolutionary pressure, enzyme active sites are flawlessly engineered spaces; cavities comprised of amino acid residues precisely positioned to be complementary to the transition states of the reactions that they catalyze with regard to size, shape, charge, and any number of additional features. Although the diversity of reactivity observed in Nature is vast, the underlying principles of molecular recognition (both for the substrate and TS) are similar and are typically understood as emanating from the concerted action of multiple noncovalent substrate-catalyst interactions (*e.g.* steric repulsion, Van der Waals forces, the hydrophobic effect, or electrostatic interactions), which are individually weak (~ 1 - 3 kcal/mol) but collectively substantial. These interactions result in a decrease in free energy (ΔG) as the enzyme-substrate complex approaches the TS that partially compensates for the energetic uptake required to achieve the structure of the activated complex, leading to catalysis. The array of attractive noncovalent interactions (NCI's) that exists affords seemingly endless approaches to the design of synthetic catalysts that operate by similar principles. However, in order to leverage NCIs to this end, one needs to first consider the principles of molecular association, or *binding*, which have been studied extensively in the ground state.

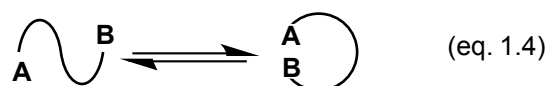
The reversible association of two molecules A and B to form a complex A:B is described by the equilibrium expression in equation 1.1, alongside the associated equilibrium constant (K_{eq})

(equation 1.2) and the corresponding free energy of association (equation 1.3). A similar analysis applies to the different conformational states of a molecule (equation 1.4). By studying molecular systems, either contrived or naturally occurring, in which a particular NCI can be isolated as primarily responsible for molecular association, the contribution of that NCI to complex stability can be quantified.



$$K_{\text{eq}} = \frac{[AB]}{[A][B]} \quad (\text{eq. 1.2})$$

$$\Delta G^\circ = -RT \ln K_{\text{eq}} \quad (\text{eq. 1.3})$$



Through this process, chemists have developed a relatively sophisticated view of the physical principles underlying these interactions to the extent that they can often rationally build them into supramolecular architectures, for example, in the fields of crystal or protein engineering. As transition state theory fundamentally relies on the treatment of the ground and transition states as being in equilibrium, the factors that govern binding in the former (ΔG and K_{eq}) are perfectly analogous to those in the latter (ΔG^\ddagger and k). As such, by understanding the contributions of various aspects of NCIs (distance, orientation, substituent effects, *etc.*) to the strength of ground state binding, the prospect of achieving catalysis through the rational design of molecules that bind the TS in the same way becomes entirely reasonable.

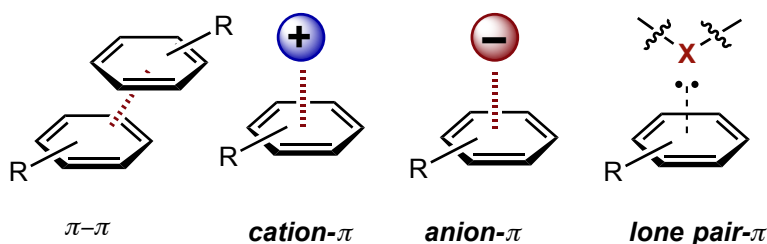


Figure 1.4. Summary of noncovalent interactions under discussion

Here, a brief survey will be provided of a subset of these interactions that is increasingly being acknowledged as a potentially transformative design element for catalysis: π -interactions (sometimes referred to as aromatic interactions) including π - π , cation- π , anion- π , and lone pair- π (Figure 1.4). Drawing from the extensive knowledge that exists in fields as diverse as crystallographic engineering, supramolecular chemistry, structural biology, organic synthesis and computational chemistry, illustrative examples of each interaction in the ground state will be presented, followed by those where the same principles have been applied to the acceleration of a chemical transformation. Emphasis will be placed on examples where the NCI under discussion has been quantified through rigorous means with the explicit intention of delineating the underlying physical organic principles. Finally, an outlook will be provided on the prospects of truly *de novo* catalyst design for any given transformation *via* the paradigm of transition state

recognition using π -interactions as a design element, with an eye towards impacting the field of synthetic organic chemistry.

π - π

The noncovalent attraction between neutral, closed shell aromatic rings is often characterized using the terms π - π or π -stacking.¹⁻⁵ Three geometries are characteristic of π - π interactions: T-shaped, parallel stacked (PS), and parallel displaced (PD, Figure 1.5). For the benzene dimer, the T-shaped and PD geometries have been calculated to be approximately equal in stability (*ca.* -2.5 kcal/mol), with the PS significantly less so (*ca.* -1.6 kcal/mol). Qualitatively, this geometric preference can be understood in terms of molecular quadrupole moments. The six radially oriented C-H bonds of benzene confer a quadrupole moment to the molecule (described by the z^2 component of the quadrupole moment tensor, Q_{zz}) such that regions of negative electrostatic potential are found above and below the ring plane, and positive potential around the ring periphery. Electrostatic potential (ESP) maps provide a useful way of visualizing this charge distribution (Figure 1.5). From this perspective, the T-shaped and PD geometries reflect an interaction between regions of positive and negative potential, whereas the PS geometry is electrostatically repulsive for benzene due to overlapping regions of negative potential. However, based on a number of high level *ab initio* studies, it is now generally accepted that dispersion plays a major role in the attractive nature of π - π interactions but is largely cancelled by exchange repulsion.^{5,6} As such, the electrostatic contribution is significant when comparing the interaction strengths across a series of substituted homologues (*vide infra*).

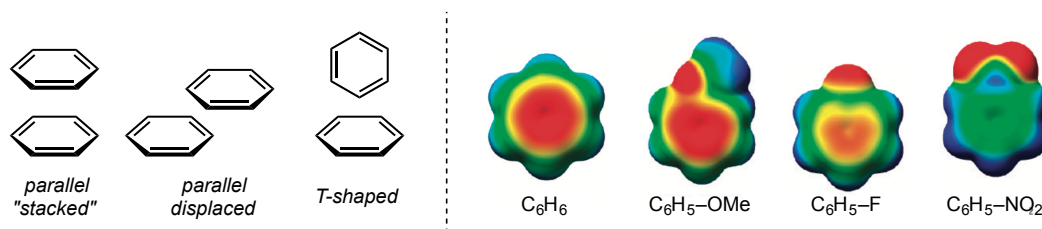


Figure 1.5. π - π interaction geometries (left) and example ESP maps (right)

There have been numerous studies in the past two decades devoted to the understanding of the physical origins of substituent effects in tuning the strength of π - π interactions. Until recently, the prevailing viewpoint, initially put forth by Hunter and Sanders,⁷ was based on a π -polarization argument wherein electron withdrawing substituents were proposed to remove electron density from an arene's π -system *via* π -resonance effects (and vice versa for electron donating substituents).⁸⁻¹⁴ As such, this model predicts that the interaction between two rings in a stacked geometry will be strengthened upon introduction of an electron withdrawing substituent into one of the partners due to a decrease in repulsion between the two π -systems, whereas introduction of an electron donating substituent should weaken the interaction by the opposite mechanism. ESP maps have often been employed to support this viewpoint, based on the assumption that the ESP above and below a ring centroid is reflective of its π -electron density (Figure 1.5).

An early experimental study corroborating the Hunter-Sanders model was reported by Cozzi and Siegel, who prepared a series of 1,8-diaryl naphthalenes in which the aryl groups were necessarily in a face to face stacking geometry in the ground state due to steric constraints (Figure

1.6).¹¹ Assuming that the π - π interaction between the two parallel rings would be completely attenuated at the transition state for rotation about the aryl-naphthyl bond, measurement of the barrier to this rotation would be reflective of the ground state stabilization of the stacked geometry. Electron donating substituents were expected to destabilize the ground state *via* π -electron donation, whereas electron withdrawing substituents were expected to have the opposite effect. In practice, an excellent correlation was found between ΔG^\ddagger for ring rotation and σ_{para} , consistent with the notion that π -resonance effects were the dominant factor underlying the observed substituent effect.

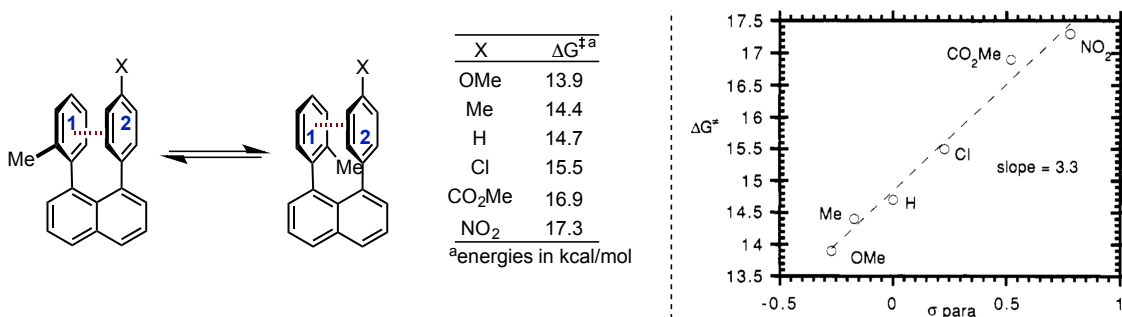


Figure 1.6. Solution study supporting polar- π model

In recent years, however, the π -polarization model has been a source of controversy.^{4,15,16} High level *ab initio* studies have suggested that the introduction of *any* substituent (*i.e.* electron donating or withdrawing) should increase the strength of π - π interactions compared with the benzene dimer.¹⁷ In fact, the notion that the π -systems of the interacting partners are even involved in “ π - π interactions” has been increasingly called into question.^{4,15,16} For example, computations by Grimme have suggested that the interaction energy of cyclohexane “stacking” (3.09 kcal/mol) is actually stronger than that of benzene (PD orientation, 2.62 kcal/mol),¹⁵ and

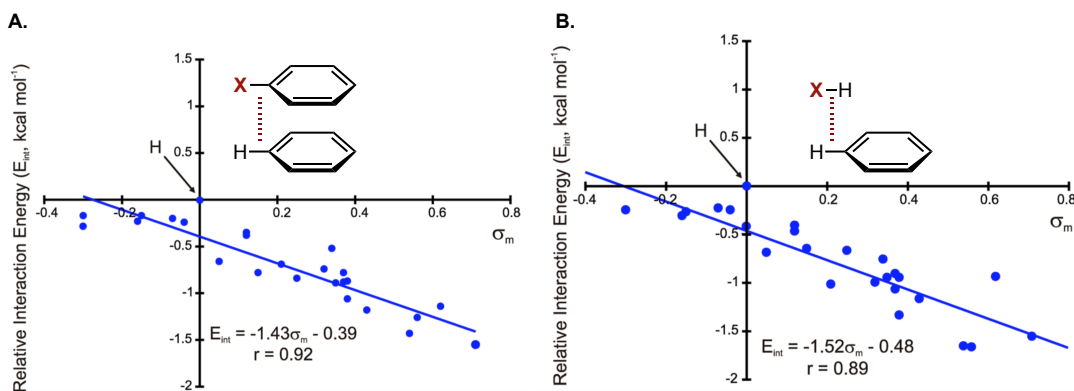


Figure 1.7. Hammett correlations supporting direct interaction model

Wheeler has shown that the interaction between benzene and cyclohexane (−2.91 kcal/mol) is stronger than that of the benzene dimer (PS orientation, −1.63 kcal/mol).¹⁶ It has thus been

proposed that the π - π terminology be reserved for larger aromatic systems in which special π -electron correlation effects do appear to exist. Nonetheless, as it is not our goal to coin new terminology but rather to describe the current state of the art, we have chosen to use the terms “ π - π ” or “ π -stacking” fully aware of their shortcomings.

A more recent model that is consistent with the majority of available data is that popularized by Wheeler and Houk, which posits that it is the direct interactions between the local C-X/H dipoles of substituted aromatic rings that determine the strength of a “ π - π ” interaction.^{3,5,16,18–23} Viewed from this perspective, aromatic rings primarily serve as platforms upon which to place substituents in a spatial arrangement that will either be attractive or repulsive depending on the relative geometries between the interacting dipoles. Figure 1.7 depicts a compelling piece of computational evidence to this end. For a given intermolecular separation, the calculated interaction energy between benzene and a monosubstituted benzene derivative was found to correlate strongly with σ_{meta} and was notably attractive for all substituents evaluated (Figure 1.7, left), including those considered to be inductively electron donating (negative σ_{meta}).^{18,23} Keeping the same intermolecular separation but replacing the substituted benzene ring with a hydrogen atom (Figure 1.7, right) afforded an essentially identical correlation, suggesting that the aromatic ring itself is not actually involved in the interaction! Another prediction of the Wheeler-Houk direct interaction model is that substituent effects should be additive-*i.e.*, the interaction between two substituted benzene derivatives should be equal to the sum of the individual interaction energies of each substituted ring with benzene (Figure 1.8, left).²¹ However, this relationship is expected to break down if the substituents on the two substituted rings interact directly as other intermolecular interactions, such as steric repulsion, become relevant (Figure 1.8, right).

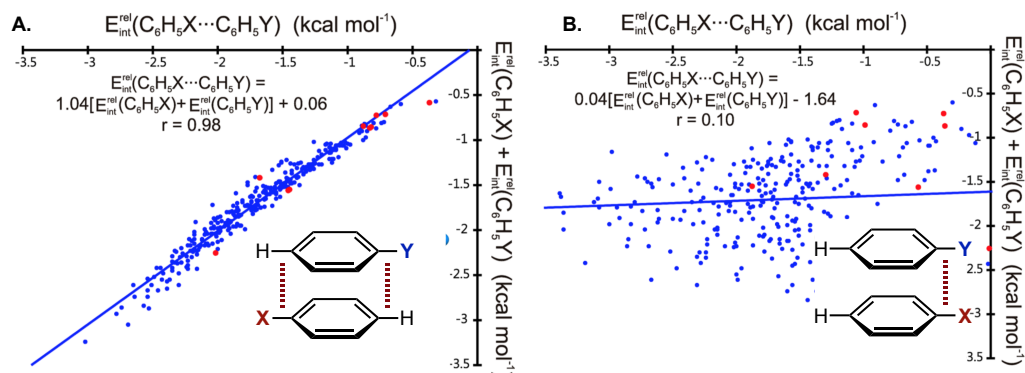


Figure 1.8. Correlations demonstrating geometric consequences of direct interaction model

A recent study by Shimizu and coworkers²⁴ provided direct experimental support for the Wheeler-Houk additivity hypothesis (Figure 1.9). Due to restricted rotation about the imide N-aryl bond, molecular torsion balance **1.1** was found to exhibit discrete unfolded and folded conformations in solution. Furthermore, it was demonstrated that the phenyl ether substituent and phenanthrene shelf were forced into a PD stacking interaction in the folded conformation. Thus, measuring the unfolded to folded ratio as a function of phenyl ether substitution allowed the authors to quantify the strength of the π - π interaction in the ground state. By comparison with a control balance (**1.2**) in which the π - π interaction was precluded, the authors defined a substituent

effect (SE) for several electronically diverse substituents (Figure 1.9, bottom). Notably, the magnitude of the SE's for monosubstituted aryl ethers were dependent on the positions of the substituents on the ring (compare *m*-Cl and *p*-Cl), as would be expected based on the direct

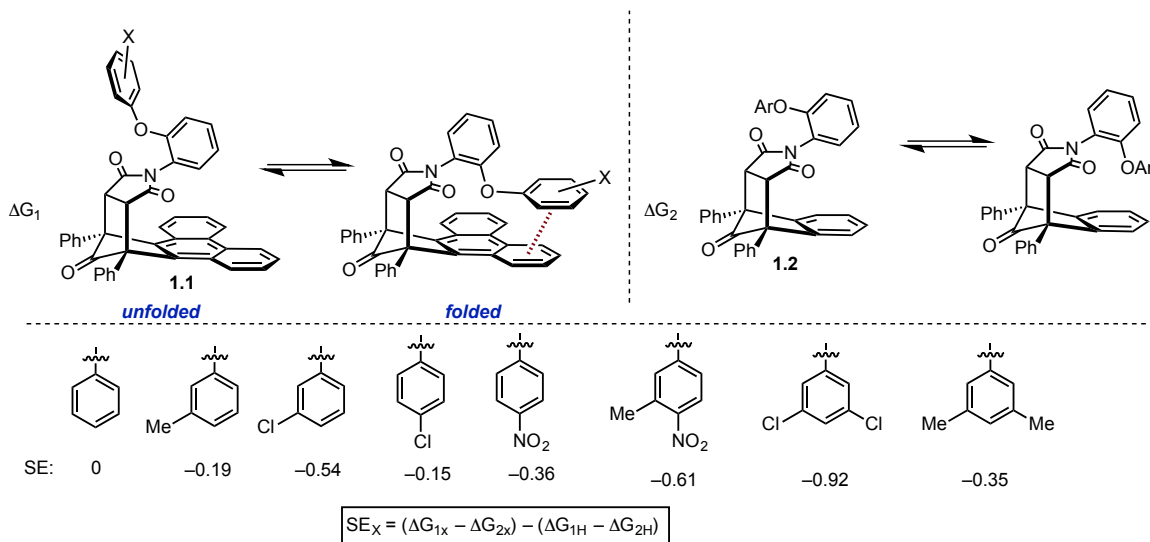


Figure 1.9. Experimental study supporting direct interaction model

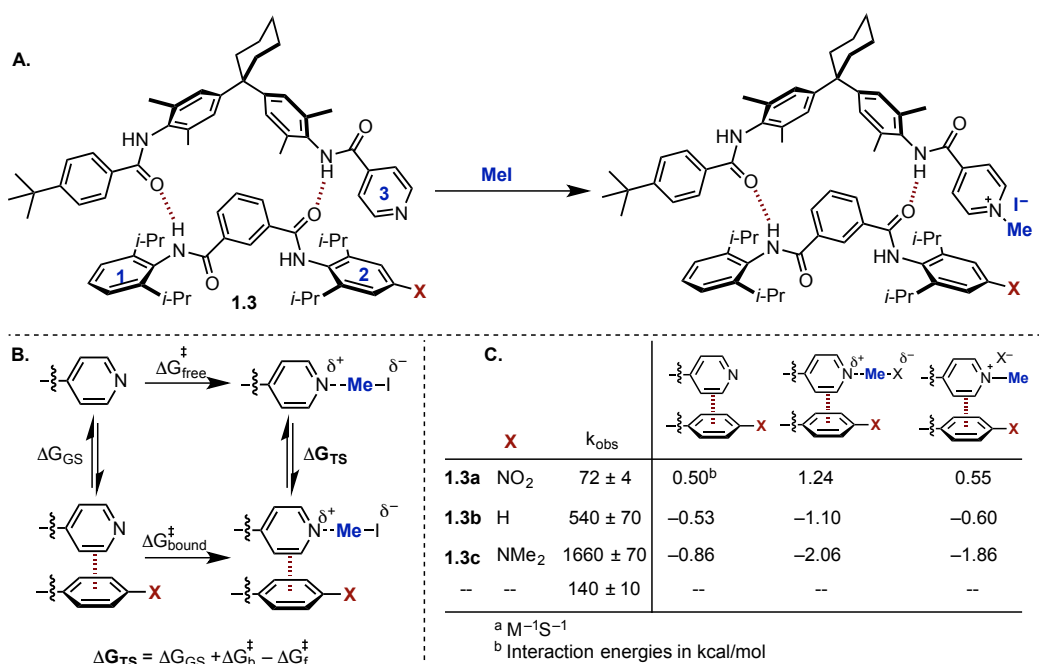


Figure 1.10. Experimental study quantifying contributions of π - π interactions to catalysis

interaction model. Furthermore, using the calculated SE's for the monosubstituted derivatives, the authors were able to predict those for di- and trisubstituted analogues with reasonable accuracy

(Figure 1.9, bottom). As the Hunter-Sanders π -polarization model does not predict that SE's will be additive, these results, along with the observation of a positional dependence of the magnitude of the SE, were taken as evidence to support the Wheeler-Houk direct interaction model.

Considering the manner in which π - π interactions can be employed for the ground state stabilization of, for example, the more crowded folded conformation in torsion balance **1.1**, it stands to reason that they might analogously be leveraged to effect transition state binding for catalysis. An excellent example of this phenomenon was reported by Hunter and coworkers for the alkylation of pyridine in a supramolecular zipper complex (**1.3**, Figure 1.10).⁸ It was hypothesized that a π -interaction between the pyridine ring (ring 3) and ring 2 would be more stabilizing in the polarizable S_N2 transition state than in the ground state reactant or product complexes. Furthermore, it was anticipated that tuning the electronics of ring 2 might allow for the modulation of the putative TS π -interaction, thereby controlling the reaction rate. Measurement of the ground state binding constants (ΔG_{GS}) for a series of zipper complexes **1.3a-c** ($X = \text{NO}_2, \text{H}, \text{NMe}_2$) and the rates of both the uncatalyzed and catalyzed alkylation reactions ($\Delta G_{\text{free}}^\ddagger$ and $\Delta G_{\text{bound}}^\ddagger$) enabled the authors to estimate the binding constant between rings 2 and 3 at the alkylation TS (ΔG_{TS} , Figure 1.10B). Using this information, a double mutant cycle analysis^{9,25} allowed for the determination of the isolated contribution of a π -interaction between rings 2 and 3 to TS stabilization (as well as stabilization of both the reactant and product complexes, Figure 1.10C) in the absence of any confounding factors contributing to complex stability (*e.g.* dispersion, sterics, hydrogen bonding, etc). For complex **1.3a**, rings 2 and 3 were engaged in stronger π - π interactions in the reactant and product complexes than in the TS, implicating negative catalysis. In contrast, complexes **1.3b** and **1.3c** exhibited stronger ring 2-ring 3 π - π interactions in TS relative to GS, definitively demonstrating the contribution of these interactions to the acceleration of pyridine methylation. The nature of the substituent effect is difficult to discern given the aforementioned geometric complexities the direct interaction model. However, the clear electronic trend lends credence to the notion that π - π interactions can be substantially modulated through subtle electronic perturbations of the structures of the interacting partners to impact chemical reactivity.

Cation- π

The cation- π interaction describes the association between a cation and the face of a molecule containing a pi system.²⁶⁻³¹ First reported for the binding of K^+ to benzene in the gas phase, subsequent experimental studies demonstrated association free enthalpies (ΔH) for the alkali metals with benzene of 38.3, 28.0, 19.2 kcal/mol for Li^+ , Na^+ , and K^+ respectively, placing the cation- π interaction among the strongest NCI's known.²⁶ Although it is most often discussed in a context where an aromatic ring acts as the π -component, other π -electron containing molecules, such as ethylene, can serve in this capacity. In the case of benzene, the six radially oriented C-H dipoles confer a quadrupole moment of -8.7 B ($\text{B} = \text{Buckingham}, 1 \text{ B} = 1 \text{ Debye-Angstrom}$) to the molecule, with negative regions above and below the ring plane (*vide supra*). Electron donating and withdrawing substituents lead to increasingly negative and positive Q_{zz} values respectively. Thus, to a first approximation, the cation- π interaction can be understood as one between an ion and an electric quadrupole (although it cannot be modeled quantitatively this way) and is thus primarily electrostatic in nature. In certain instances however, particularly those involving large, polarizable π -systems, the role of induction has been suggested to be significant.^{28,32,33} For benzene derivatives, electrostatic potential (ESP) maps generally serve as good qualitative predictors of the strength of the cation- π interaction as a function of ring

substitution,^{34,35} with increasingly electron donating substituents affording progressively negative ESP's above and below the ring plane and thus predicting a stronger interaction with a cation. Wheeler and Houk have cautioned against misinterpretation of this correlation however, suggesting that it is the orientations of the local dipoles of the C-H/X bonds around the ring periphery, not the donation or withdrawal of π -electron density from the ring center by the substituent, that are responsible for the negative ESPs in the case of electron rich aromatics.³⁶ Thus, for aromatic systems, ring substitution and adjustment of the spatial extent of a π -system can both serve as handles for the predictable modulation of the strength of cation- π interactions (*vide infra*).

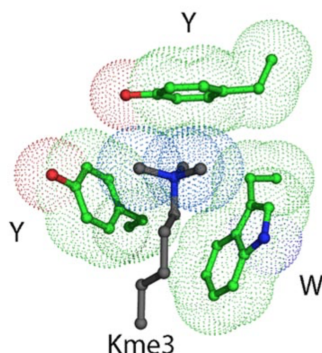


Figure 1.11. Depiction of the aromatic box from HP1 chromodomain

Nature provides several excellent platforms for studying cation- π interactions in both the ground and transition states. A recurring motif in proteins for the recognition of cationic moieties is the so-called aromatic box^{30,37}-a term that characterizes binding pockets comprised of various combinations of three to four tryptophan (Trp), tyrosine (Tyr) or phenylalanine (Phe) residues precisely arranged to stabilize positive charge *via* cation- π interactions (Figure 1.11). A prototypical example that has been studied by the groups of Lester and Dougherty is that of the nicotinic acetylcholine receptor (nAChR), a ligand gated ion channel that is modulated *via* the binding of the ammonium group of acetylcholine. In a classic physical organic study,³⁸ these groups demonstrated that the EC_{50} of nAChR resulting from ACh could be modulated over 2 orders of magnitude (1.2-114 μ M, > 2.0 kcal/mol) simply through the mutation of a single aromatic box constituent (α Trp 149) to substituted analogues with attenuated cation binding affinity (*e.g.* F-Trp, CN-Trp). An excellent linear correlation was found between mutant EC_{50} values and the computationally-determined cation- π binding energies between the mutated residues and a sodium cation. A subsequent study by the same groups³⁹ implicated a cation- π interaction in distinguishing nicotine binding affinity of neuronal versus muscular ACh receptors, partially explaining the physical origin of nicotine addiction.

Also featured among the many classes of proteins known to possess the aromatic box motif are those that recognize methylated lysine, which represents a post translational modification (PTM) implicated in gene regulation. In 2007, Waters and coworkers reported a study seeking to elucidate the physical origins of the recognition of a cationic methylated lysine (Lys or K) residue on the tail of histone 3 (H3) by the aromatic box of HP1 chromodomain.⁴⁰⁻⁴² Although the interaction between H3 and HP1 was known to increase with increasing methylation (*i.e.* $KMe_3 > KMe_2 > KMe$), it was unclear if this primarily was due to a cation- π interaction or a

hydrophobic effect, as the latter may be expected considering the increase in lipophilicity with each methylation. To answer this question, a model system was analyzed in which the positively charged trimethyllysine (KMe₃) and a neutral isostere (*t*-BuNle) were incorporated into a β -hairpin oligopeptide (**1.4**, Figure 1.12A) designed to facilitate inter-residue contact between position **X** and the good cation- π donor tryptophan (Trp).

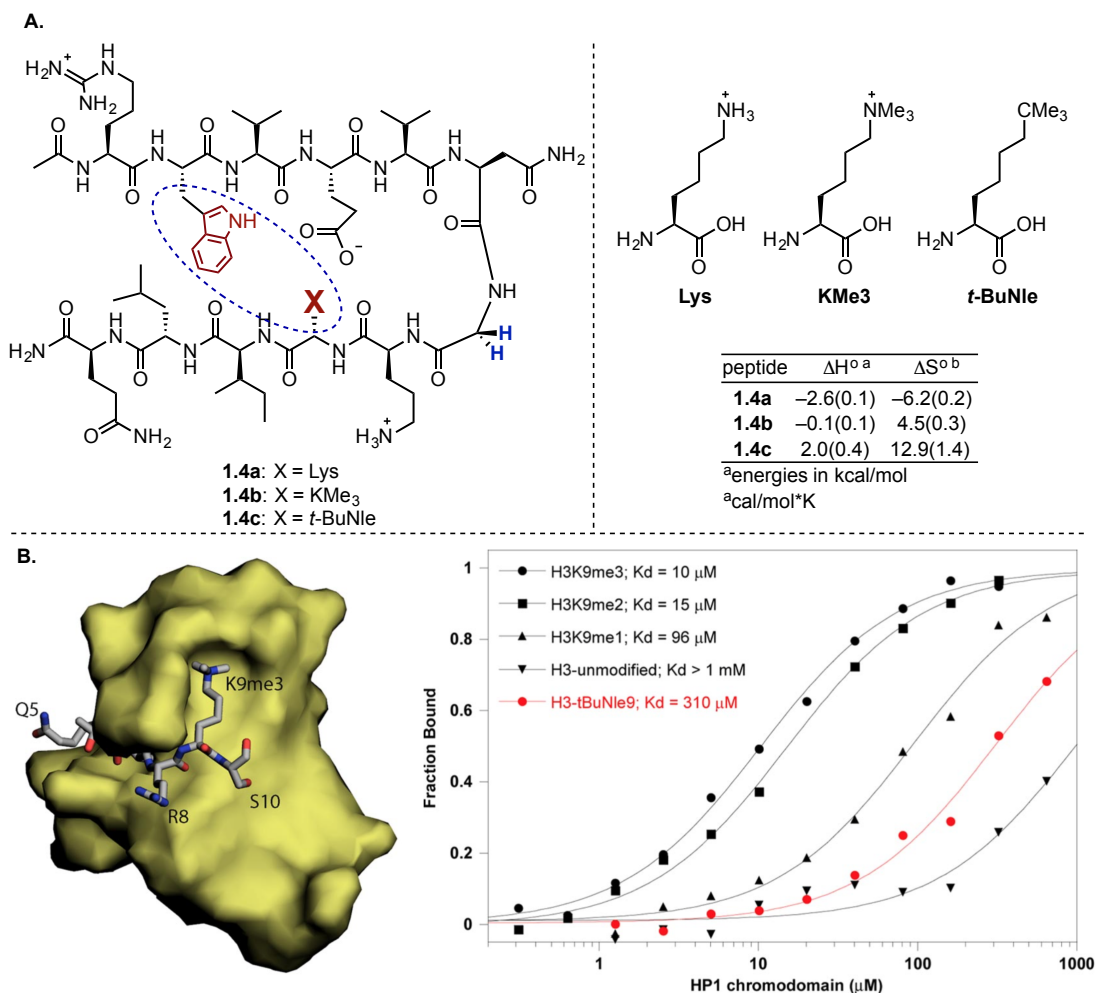


Figure 1.12. Contribution of cation- π interactions to trimethyllysine binding by HP1 chromodomain

Chemical double mutant cycles²⁵ revealed interaction energies of -1.0 and -0.6 kcal/mol for KMe₃-Trp (**1.4b**) and *t*-BuNle-Trp (**1.4c**) respectively.⁴² Furthermore, a modified Van't Hoff analysis demonstrated a favorable entropy ($\Delta\Delta S^\circ = 8.4$ cal/molK relative to KMe₃) but unfavorable enthalpy ($\Delta\Delta H^\circ = +2.1$ kcal/mol relative to KMe₃) for the *t*-BuNle-Trp interaction (Figure 1.12A). Collectively, these results suggested that although there is likely a hydrophobic component to the KMe₃-Trp interaction, a cation- π component is required to explain the specificity over *t*-BuNle. These findings were corroborated by subsequent experiments in which the binding of wild type H3 protein and four mutants (H3K9Me₃, H3K9Me₂, H3K9Me₁ and H3K9*t*BuNle) to the HP1 chromodomain (Figure 1.12B) was examined. Diminished binding was observed with each

successive methyl removal, with uncharged mutant H3K9tBuNle displaying 31-fold weaker binding relative to H3K9Me₃. Given the similar sizes and shapes of these mutants, this result was taken as strong evidence of a cation- π interaction between the cationic H3 mutants and the aromatic residues in HP1 chromodomain.⁴²

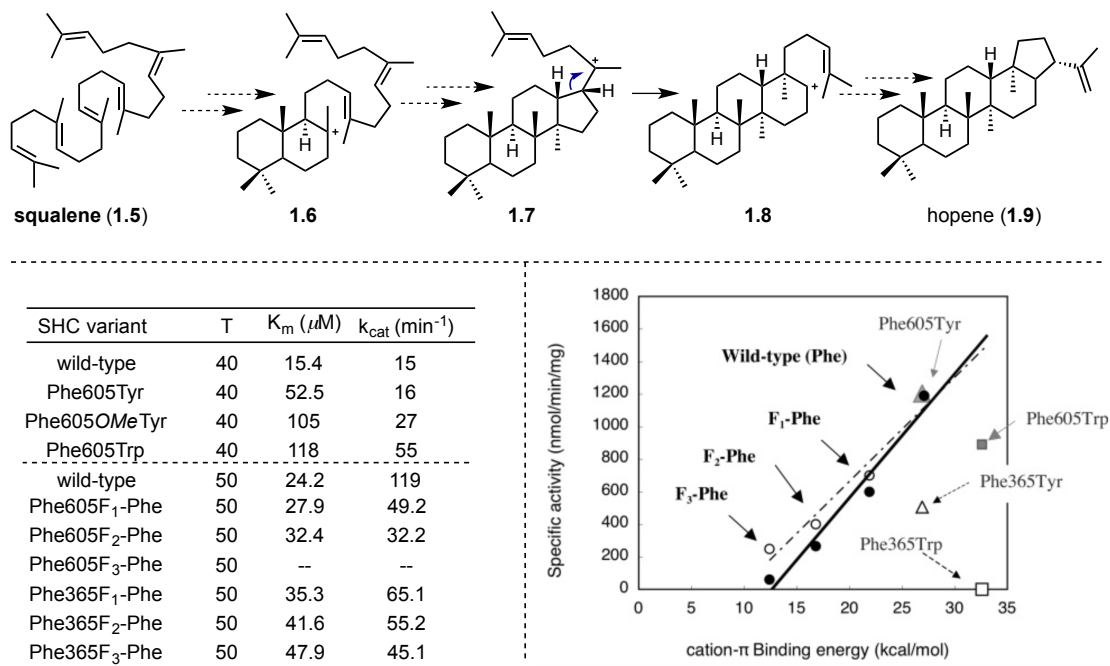


Figure 1.13. Quantification of cation- π interactions in squalene-hopene cyclase.

In the same way that the ground state recognition of methyllysine is dictated by cation- π interactions, transition state stabilization can also be effected. A field where this paradigm is frequently invoked is that of terpene biosynthesis.⁴³ In the first definitive example, Hoshino and coworkers executed a beautiful study⁴⁴ on the enzyme squalene-hopene cyclase (SHC)^{45,46} from *Alicyclobacillus acidocaldarius*, which catalyzes the formation of hopene (**1.9**) via a complex cationic polycyclization cascade from the acyclic precursor squalene (**1.5**, Figure 1.13). Site directed mutagenesis studies were conducted on Phe 356 and Phe 605, which are components of different aromatic box regions in SHC implicated in stabilizing cationic intermediates **1.6** and **1.7** respectively. At low temperatures (< 40 °C), Phe 605 mutants with electron rich aromatic residues expected to enhance cation- π binding (Phe605Tyr, Phe605OMe-Tyr, Phe605Trp) displayed higher specific activities than the wild-type enzyme. Estimation of Michaelis-Menten parameters revealed that, although the mutants displayed looser binding relative to the wild type, catalytic activity increased in the expected order based on the ability of the mutated residue to favorably interact with positive charge (Figure 1.13). A complementary set of experiments conducted using fluorinated Phe mutants (F₁-Phe, F₂-Phe, F₃-Phe) at positions 365 and 605 demonstrated progressively diminished catalytic activity with each successive fluorination (K_m was affected to a lesser extent, presumably due to the minimal steric perturbation resulting from fluorine substitution). A linear correlation was observed between the specific activity of the SHC mutants and the previously-computed cation- π binding energies³⁸ of the F_nPhe residues (Figure 1.13). These results convincingly support in a quantitative manner the hypothesis that cation- π

interactions at both positions are essential to hopene biosynthesis, presumably *via* both ground and transition state stabilization.

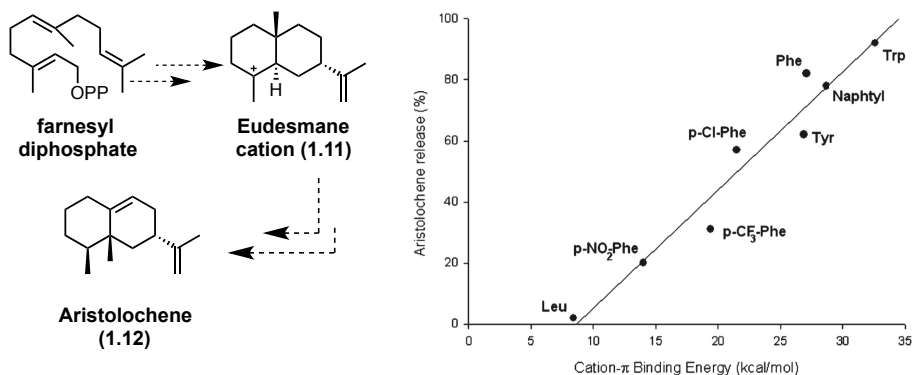


Figure 1.14. Quantification of cation- π interactions in aristolochene synthase

More recently, Allemann and coworkers⁴⁷ conducted a site directed mutagenesis study to explore the importance of a cation- π interaction in stabilizing eudesmane cation **1.11** (and presumably the prior and subsequent transition states) during the biosynthesis of aristolochene (**1.12**) by aristolochene synthase from *Penicillium roqueforti* (Figure 1.14). A series of natural (Leu, Tyr, Phe) and unnatural (*e.g.* *p*-NO₂Phe, *p*-CF₃-Phe, *p*-Cl-Phe) amino acids were incorporated in place of Tyr 334 and a robust correlation was observed between % aristolochene release and calculated cation- π binding energy of each aromatic residue, further supporting the role of this interaction in terpene biosynthesis.

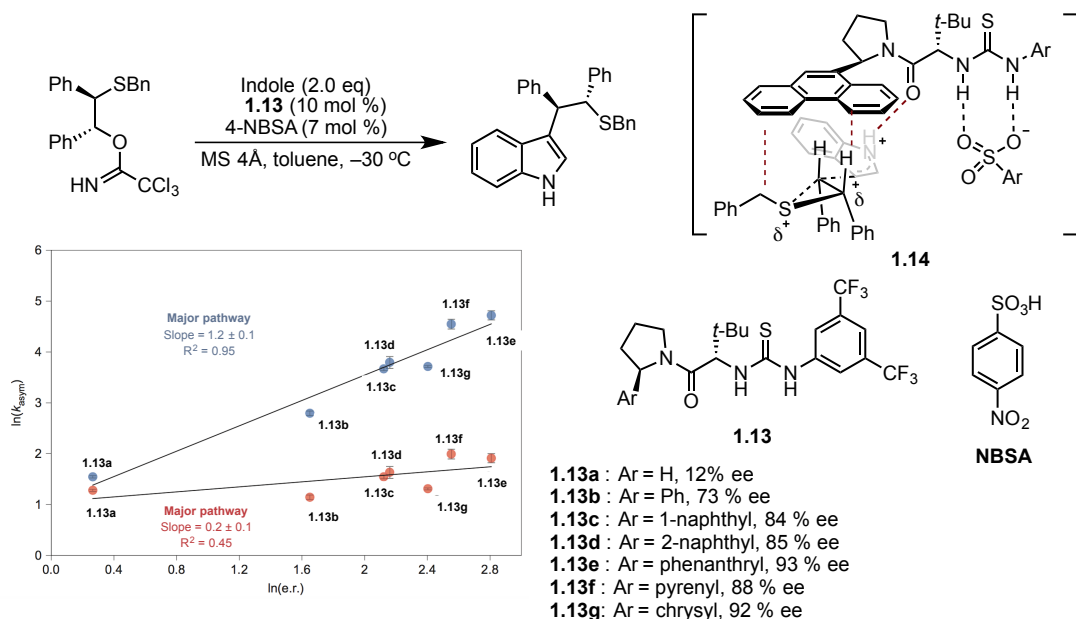


Figure 1.15. Control of enantioselectivity using synthetic catalysts designed to employ cation- π interactions

Considering the lessons learned from examples such as those presented above, it should in principle be possible to design synthetic catalysts that accelerate novel reactions *via* stabilizing cation- π interactions at the TS. To this end, Jacobsen and coworkers have hypothesized that enantioselectivity, a necessarily kinetic phenomenon, can be dictated in part or in full by aromatic substituents deliberately incorporated into synthetic catalyst scaffolds for this purpose.⁴⁸⁻⁵¹ Figure 1.15 depicts an excellent example in the chiral thiourea catalyzed enantioselective nucleophilic ring opening of episulfonium ions with indole.⁵¹ Mechanistically, the authors proposed that an episulfonium ion was generated upon trichloroacetimidate protonation by 4-nitrobenzenesulfonic acid (NBSA). A bifunctional thiourea catalyst (**1.13**) could then bind the conjugate base of NBSA and the episulfonium ion in a spatially resolved ion pair through a combination of hydrogen bonding and cation- π interactions respectively (**1.14**). The presence of the latter interaction was hypothesized based on the observation that reaction enantioselectivity generally correlated with the size of the π -system of the catalyst aryl substituent (Figure 1.15), an assertion that was supported through NMR studies and a series of correlations between reaction kinetic parameters (rate, enantiomeric ratio) and arene molecular descriptors expected to impact cation-binding affinity (quadrupole moment and polarizability). To unambiguously distinguish whether enantioselection was occurring due to a TS-stabilizing cation- π interaction in the major pathway or a destabilizing steric interaction in the minor pathway, the authors took advantage of the observation that indole addition to the episulfonium-thiourea complex (**1.14**) was both rate and enantio-determining. Using a combination of rate constants from both the catalyzed and uncatalyzed reactions along with enantioselectivity data, the rate constants for the pathways leading to the major and minor enantiomers could be distinguished and were each shown to independently correlate with reaction enantioselectivity (Figure 1.15). This experiment rigorously demonstrates that the cation- π interaction can be leveraged to achieve TS stabilization in a completely designed system that operates by the same principles observed in fundamental, ground state studies (*vide supra*).

Anion- π

Superficially, anion- π interactions emerge as the natural complement to their cationic counterparts, typically describing the attractive association between a negatively charged atom or molecule and the π -face of an electron *deficient* (hetero)arene.⁵²⁻⁵⁸ However, this interaction is

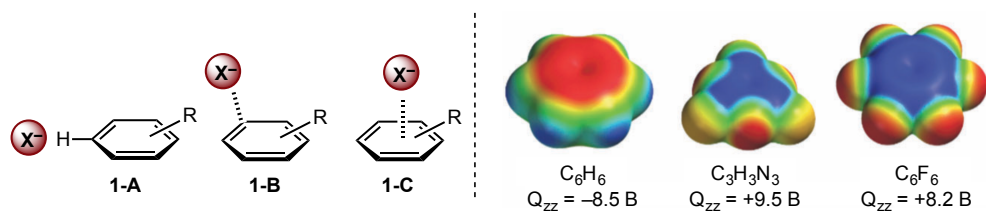


Figure 1.16. Anion- π geometries (left) and ESP maps for electron-poor arenes (right)

somewhat counterintuitive considering the expected electron repulsion between an anion and the π -electron cloud of an arene. Since its original proposal in a series of *ab initio* studies in 2002,⁵⁹⁻⁶¹ the anion- π interaction has been extensively studied theoretically and experimentally in the solution, solid and gas phases. Compared with cation- π , anion- π interactions have more shallow potential energy surfaces resulting in laxer geometric requirements.^{54,57,62} As such, in the solid

state, as opposed to residing directly above the ring centroid (**1-C**), anions are more frequently observed either in the same plane as the aromatic ring interacting with polarized C-H bonds (**1-A**), or interacting with a ring π^* orbital as in a Meisenheimer complex (**1-B**, Figure 1.16).^{54,63}

The stabilizing nature of anion- π interactions is typically attributed to a combination of electrostatic and ion-induced polarization effects, which can be described by the Q_{zz} component of the arene's quadrupole moment and its polarizability respectively. Notably, these features can display a compensatory effect. As illustrated in Figure 1.17, Frontera and coworkers⁶⁴ demonstrated computationally that the interaction energy of a chloride anion with a series of (thio)isocyanuric acid derivatives is essentially constant despite a decrease in the Q_{zz} because of a systematic increase in polarizability (α) with each replacement of oxygen with sulfur. Additionally, the nature of the anion has a substantial impact on the interaction, with smaller anions inducing greater polarization in the π -system and strengthening the association and planar, polyatomic ions such as NO_3^- benefitting from a π - π contribution to the overall interaction.

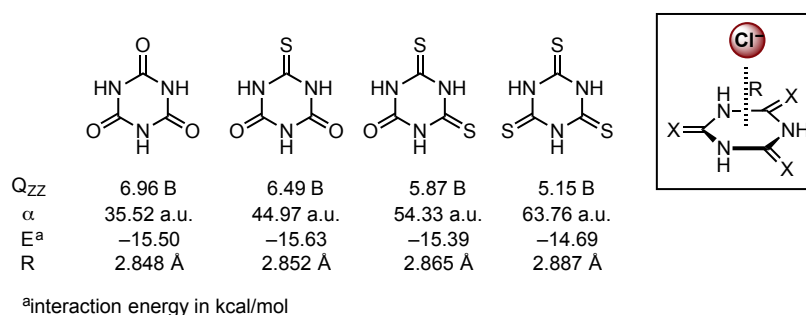


Figure 1.17. Computational investigation of compensatory effects in anion- π interactions

For substituted benzene derivatives, substituent effects generally follow the expected trends based on electrostatics, with increasingly electron-withdrawing substituents contributing to an increasingly positive electrostatic potential above and below the π -face, strengthening the interaction (Figure 1.16, right). Like other NCI's involving aromatic rings, this has traditionally been attributed to π -polarization effects, but has more recently been explained on the basis of the Wheeler-Houk direct interaction model in which an anion experiences direct, stabilizing interactions with the local dipoles of the C-X bonds located around the periphery of the arene.^{5,16,65,66} Electron deficient nitrogenous heterocycles have featured particularly prominently in both theoretical and experimental explorations of anion- π interactions given their intrinsically positive Q_{zz} and molecular ESP values.^{59-61,67} It was recently suggested that these latter features are consequences of the influx of positive nuclear charge towards the ring center upon nitrogen incorporation rather than π -polarization effects.⁶⁶ Regardless of their physical origin, both quadrupole moments and molecular ESP maps provide reasonable qualitative guides in tuning the strength of anion- π interactions.

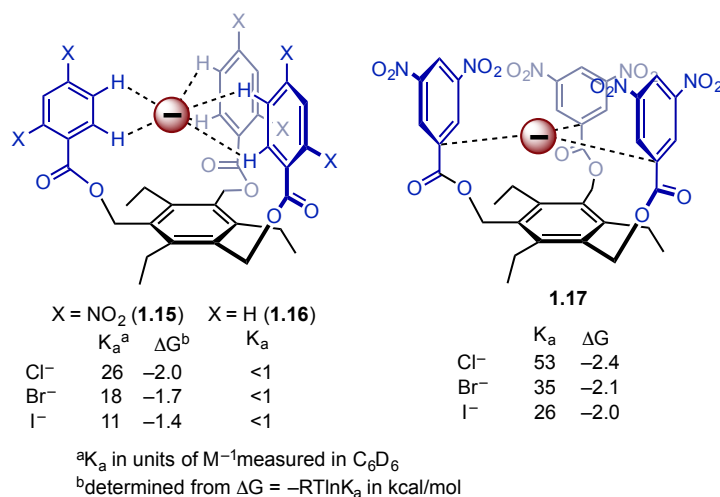


Figure 1.18. Experimental study of anion- π interactions in solution

In an early example of quantifying the ground state association between anions and electron poor arenes in solution, Johnson and coworkers measured the association constants (K_a) between the *n*-heptylammonium salts of Cl⁻, Br⁻, and I⁻ and a series of neutral tripodal receptors (**1.15-1.17**, Figure 1.18).⁶⁸ The authors anticipated that 2,4-dinitro substituted host **1.15** would interact with the halide series *via* C-H hydrogen bonding. However, due to steric constraints, this binding mode was expected to be precluded for 3,5-dinitro analogue **1.17**, necessitating involvement of the arene faces in anion recognition. Significant association with all three halides was apparent by NMR titration in C₆D₆ ($K_a = 11-53 \text{ M}^{-1}$, $\Delta G = -1.4 - -2.4 \text{ kcal/mol}$), with the 3,5-disubstituted receptor exhibiting superior binding in all cases in the expected order based on size (i.e. Cl⁻ > Br⁻ > I⁻). Electron rich control receptor **1.16** did not exhibit measurable binding. On the basis of both these NMR studies and DFT calculations, it was proposed that receptor **1.17** bound the halides *via* a σ -complex rather than a true anion- π complex, demonstrating the ambiguity often associated with the geometric nature of anion- π interactions.

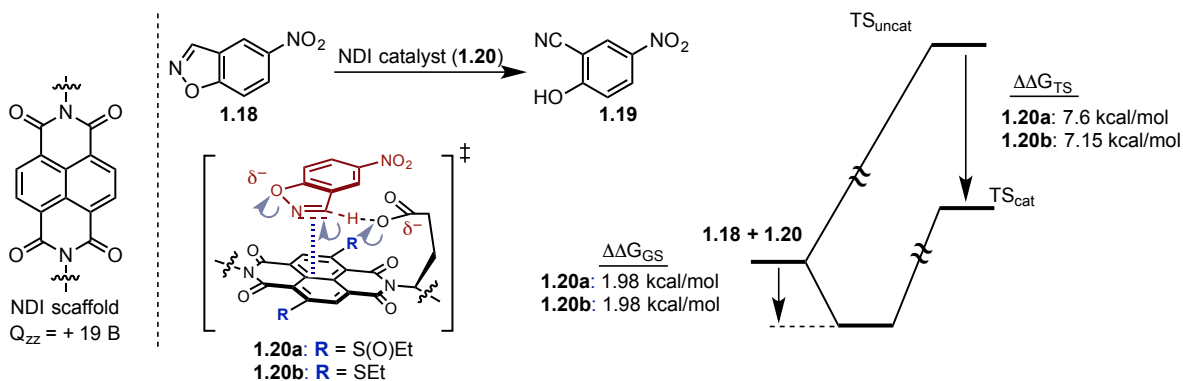


Figure 1.19. Anion- π catalysis of Kemp elimination

The ability of anion- π interactions to stabilize both ground and transition states has been investigated intensively by Matile and coworkers.⁶⁹⁻⁷⁹ To explore the prospect of anion- π catalysis

conceptually, the Kemp elimination (**1.18** to **1.19**, Figure 1.19) was chosen as a model reaction given that the transition state for C-N bond breakage was expected to exhibit significantly anionic character relative to the ground state.^{73,74} Catalysts were designed to place a carboxylate base near the the surface of a naphthalenediimide scaffold (**1.20**), which was expected to engage the anionic C-N bond breaking TS in stabilizing anion- π interactions given the parent NDI's significantly positive ($Q_{zz} = +19$ B) quadrupole moment (Figure 1.19). Furthermore, the authors proposed that introduction of sulfur substituents into the NDI scaffold would allow for fine-tuning of the catalyst's anion stabilizing ability through standard redox manipulations (*i.e.* SEt \rightarrow S(O)Et \rightarrow SO₂Et). In practice, Michaelis-Menten analysis enabled the authors to estimate GS and TS stabilization energies of 1.98 and 7.15 kcal/mol respectively for catalyst **1.20a** relative to the uncatalyzed background reaction. Upon moving to the more electron poor variant (**1.20b**), increased TS stabilization was observed ($\Delta\Delta G_{TS} = 7.6$ kcal/mol) with no measurable effect on ground state stabilization relative to **1.20a** (Figure 1.19). These results provide compelling evidence that anion- π interactions can indeed be leveraged for the acceleration of chemical reactions in a manner analogous to cation- π interactions (*vide supra*).

The Matile group has further extended the concept of anion- π catalysis to the realm of enolate chemistry⁷⁵⁻⁸⁰ through both ground and transition state studies. Using a model system in which a malonate moiety was situated on a π -acidic NDI surface (**1.21**, Figure 1.20), it was shown that tuning of the NDI's electronic character enabled the malonate's pK_a to be adjusted over six orders of magnitude ($\Delta\Delta G_{GS} = -3.25 - +0.287$) compared with diethyl malonate (**1.22**) as a control ($pK_a = 16.4$).⁷⁵ An excellent correlation was observed between the LUMO energies of the substituted NDI's and the observed pK_a 's. These results were attributed to the ability of the NDI surfaces to engage the enolate conjugate bases in attractive anion- π interactions in a manner that could be precisely controlled.

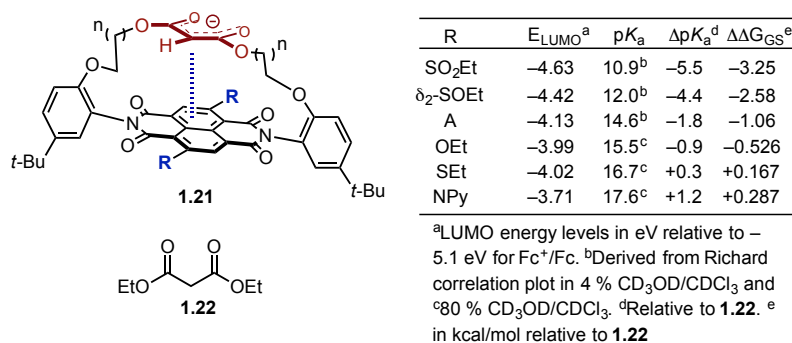


Figure 1.20. Enolate stabilization *via* anion- π interactions.

The ability of NDI surfaces to stabilize enolates in the ground state was able to be exploited for transition state stabilization to control catalytic selectivity (Figure 1.21).^{77,80} The addition of malonic acid half thioester **1.23** to β -nitrostyrene was observed to proceed in low yields when catalyzed by triethylamine due to competitive decarboxylation (addition/decarboxylation = 0.6). It was anticipated that, in the presence of an appropriate NDI catalyst, the planar enolate tautomer leading to the desired addition (a) would be stabilized to a greater degree than the nonplanar tautomer leading to decarboxylation (d) and, correspondingly, that the TS for each would be affected to differing degrees, impacting selectivity (a/d). This hypothesis was verified in practice,

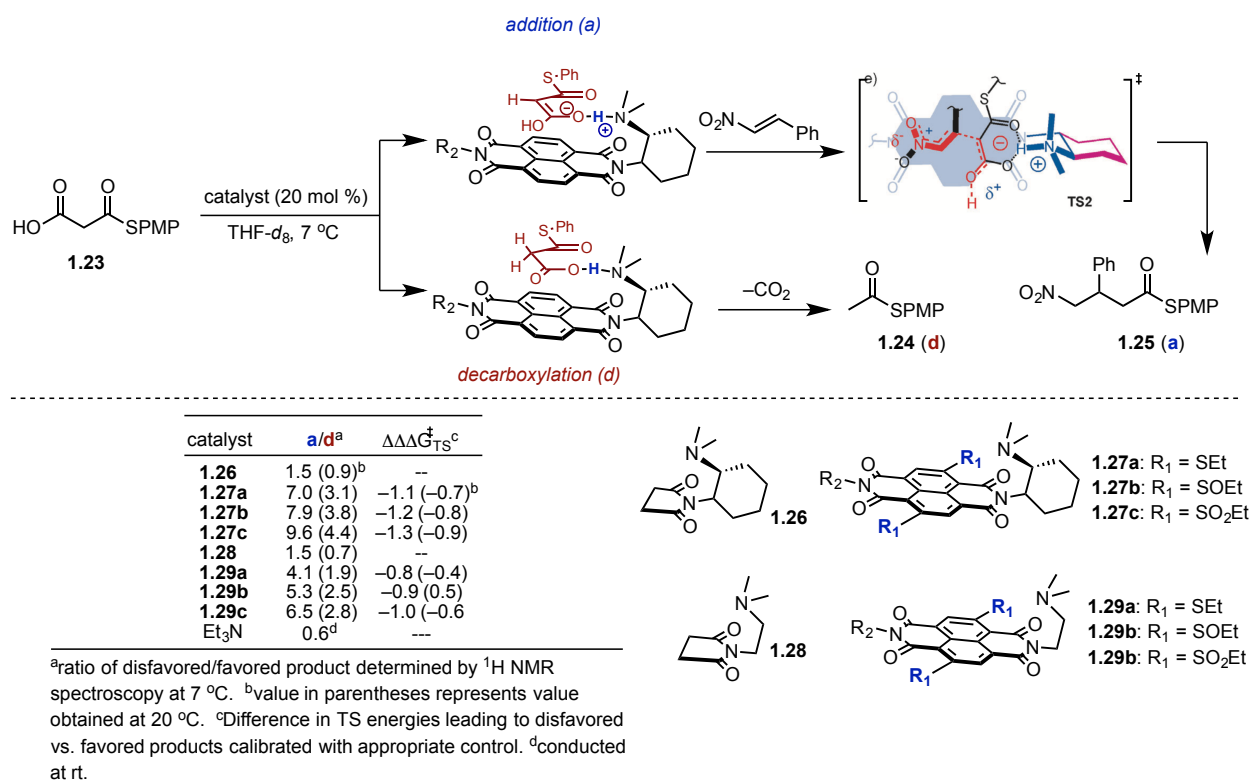


Figure 1.21. Control of reaction selectivity using anion- π interactions

as illustrated for catalysts **1.27** and **1.29** (Figure 1.21).⁸⁰ Increasing the π -acidity of the NDI surface through oxidation of the sulfur substituents was observed to progressively improve selectivity in favor of the addition product **1.25** up to a ratio of 9.6. Furthermore, it was noted that rigidification of the “Leonard turn” connecting the amine functionality to the NDI surface (**1.27**) led to improved selectivity (compare with **1.29**), presumably by enabling closer contact between the surface and the TS leading to the major product.⁸⁰ Comparison with control catalysts **1.26** and **1.28** lent further support to the notion that anion- π interactions were responsible for the inversion in product selectivity and initial rate experiments led the authors to conclude that the selectivity inversion was due to simultaneous deceleration of decarboxylation and acceleration of addition.⁷⁷ Collectively, these examples serve as excellent examples of the ways in which the principles underlying ground state association can be brought to bear on the challenge of rational catalyst design.

Lone Pair- π

The lone pair- π (lp- π , also referred to as n to π^*) interaction⁸¹ describes the stabilizing association between a lone pair of electrons and the face of a π system and is somewhat counterintuitive considering the presumptive electron-electron repulsion between these components. Like the anion- π interaction, it is typically expected to be more significant for electron-deficient π -systems and can qualitatively be understood as the interaction between regions of negative (the lone pair) and positive (the Q_{zz} component of the traceless quadrupole moment tensor above and below the face of the π -system) electrostatic potential.^{82,83} However, several

studies, both theoretical^{84–86} and experimental, have noted the shortcomings of this picture and acknowledge the likely significance of electron correlation, or dispersion effects, with weak attractive interactions having been observed for electron rich aromatic systems with negative quadrupole moments.⁸⁷ Although it is expected to be individually quite weak, the significance of the lp- π interaction has been noted in cooperation with other NCI's such as H-bonding (*vide infra*).^{88,89}

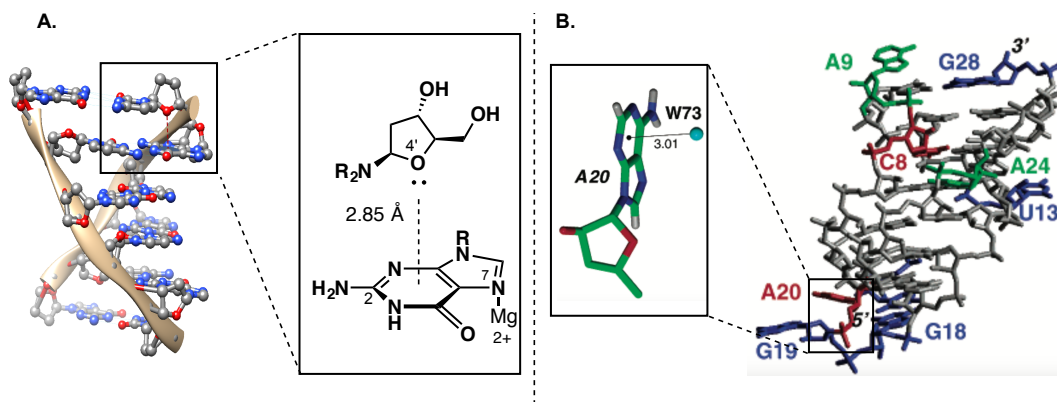


Figure 1.22. Example lone pair- π interactions in Z-DNA (left) and an RNA pseudoknot (right)

The first lp- π interaction to be acknowledged explicitly as such has its origin in the field of structural biology as a stabilizing structural element for Z-DNA.^{90,91} As shown in Figure 1.22 (left), the O4' oxygen atom of cytosine was crystallographically observed to lie within 2.9 Å of guanine C2 for each d(CpG) step,⁹⁰ and a subsequent *ab initio* study⁹¹ estimated the stabilization gained from this interaction to be on the order of 2 kcal/mol when guanine is coordinated by Mg at N7 (Figure 1.22). The interaction between water lone pairs and biomolecular arenes is also proposed to be of import,⁹² as demonstrated in the crystal structure of the ribosomal frameshifting RNA pseudoknot from beet western yellow virus in Figure 1.22 (right).⁹³ The significance of the lone pair- π interaction in crystal engineering has been noted by Reedijk and coworkers, who performed a thorough analysis of the crystallographic database (CSD) for F, Cl, Br, O, S, Se or N atoms that lie within 4Å of any atom or centroid of a six-membered (hetero)aromatic ring, revealed 25,297 such contacts.⁹⁴ Notably, the same search criteria resulted in significantly fewer hits for cation- π and anion- π interactions (1076 and 5254 respectively), suggesting that lone pair- π interaction may actually occur much more frequently than acknowledged.

Several key experimental studies have contributed to the understanding of the strength and nature of lp- π interactions. Based on the observance of a close contact (3.08 Å) between the alcohol oxygen and C₆F₅ ring centroid in the crystal structure of amino alcohol **1.30** (Figure 1.23),⁹⁵ Korenaga and coworkers conducted a study on a simplified model system to support or refute the existence of a *bona fide* lp- π interaction.⁹⁶ By studying the association between a series of N,N-dimethylamino arylethylamines and methanol in CDCl₃ by ¹H NMR spectroscopy, the authors expected to observe a linear relationship between amine basicity and enthalpy of association (ΔH_{obs}) if H-bonding were solely driving the interaction. As shown in Figure 1.23, a good correlation was found between ΔH_{obs} and Taft's σ^* parameter for a range of electronically diverse arylethylamines (**1.31a-e**, -6.09 to -5.72 kcal/mol), with the exception of

pentafluorophenyl derivative **1.32** (−6.15 kcal/mol). This latter outlier was rationalized on the basis of an intramolecular lp- π interaction supplementing the otherwise weaker H-bond in this

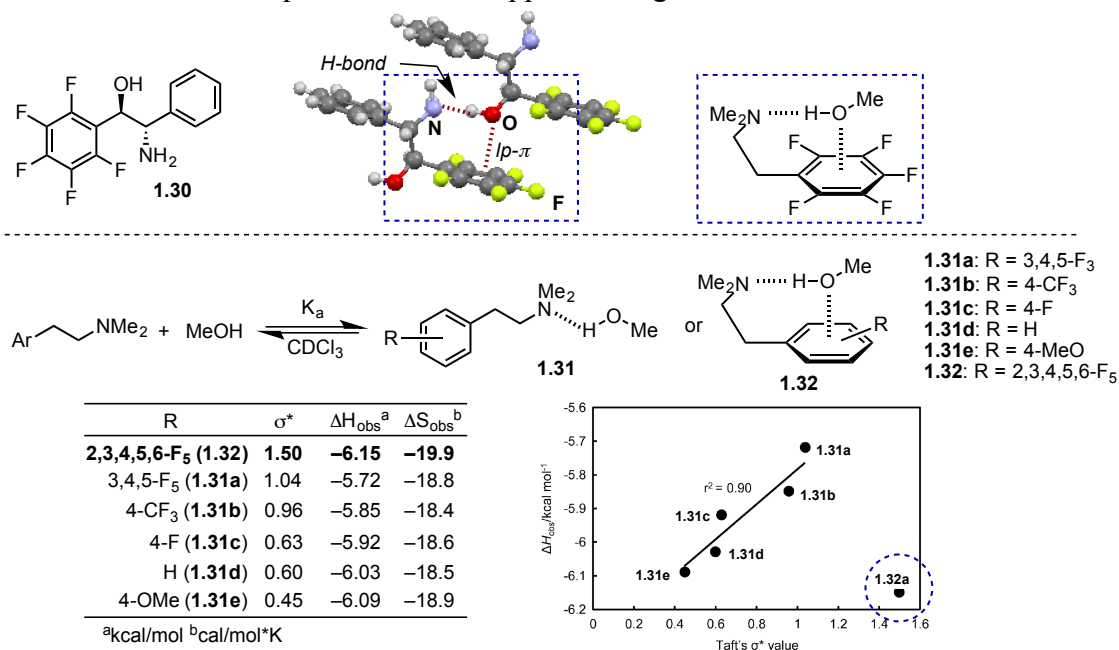


Figure 1.23. Quantification of lone pair- π interaction in solution

complex (**1.32**), whose electron-deficient aryl substituent would be expected to interact favorably with a lone pair. This proposal was corroborated by a significantly negative entropy of association (ΔS_{obs} , −19.9 cal/molK) as might be expected for the proposed conformationally restricted complex **1.32**, and by a computational analysis that showed good qualitative agreement between the predicted and measured ΔH_{obs} for the full dataset.

Molecular torsion balances are rigid molecules designed to exhibit discrete conformational preferences based on the presence or absence of interactions between carefully positioned groups and have proven useful for probing the strengths of NCIs in the 0.5-2 kcal/mol range in solution. Gung and Amicangelo have investigated lp- π interactions using a molecular torsion balance based on a triptycene scaffold (**1.33**, Figure 1.24 top).^{87,97} The relative populations of the *syn* and *anti* conformers, which were readily determined by ¹H NMR spectroscopy, were expected to be dictated by the lp- π interaction strength between the C9 benzyl and the C1 methoxymethyl (MOM) substituents. As shown in Figure 1.24, the expected trend was observed based on electrostatic reasoning ($\Delta G = 1.2$ kcal/mol for C₆F₅ to −0.19 for 4-NMe₂). However, the fact that the interaction was attractive even for electron neutral to rich derivatives (H, Me, NMe₂) could not be explained with electrostatic reasoning alone, leading the authors to invoke dispersion as the dominant force in these latter cases, concluding that aromatic rings cannot be treated as simple quadrupolar groups at the short distances required for many NCIs.⁸⁷

In addition to ring substitution, the incorporation of heteroatoms into a ring system serves as a means to tune the systems electronic features and thus modulated the strengths of various NCIs. In a recent report, Aliev and Motherwell studied the lp- π interaction between an alcohol oxygen and two different azines in a top-pan molecular balance based on the dibenzobicyclo[3.2.2]nonane framework (**1.34-1.40**, Figure 1.24 bottom).⁹⁸ The percentage of the

conformer in which the oxygen resided over the aromatic ring increased significantly upon moving from the benzene (**1.34**) to the pyrazine (**1.35**) and quinoxaline (**1.36**) variants, as would be qualitatively expected based on their corresponding quadrupole moments ($Q_{zz} = -8.9$ and -2.9 B for benzene and pyrazine respectively). The same trend was observed for dimethoxy (**1.37** and **1.38**) and difluorinated (**1.39** and **1.40**) derivatives, suggesting the possibility that heteroatom substitution might serve as a means to tune the strength of lp- π interactions in a rationally designed system.

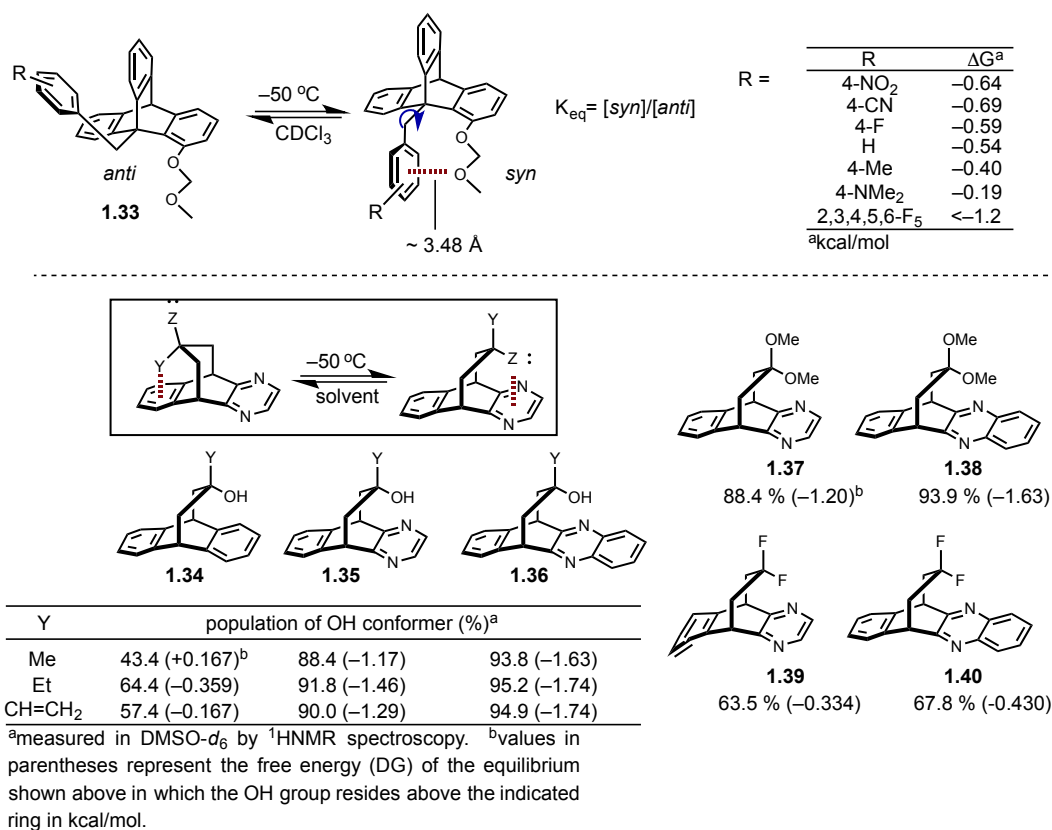


Figure 1.24. Quantification of lone pair- π interactions using molecular torsion balances

To our knowledge, no explicit examples exist of rational catalyst design using lessons from ground state studies such as those highlighted. However, in direct analogy to π - π , cation- π and anion- π , we fully anticipate examples to be forthcoming. Although not rigorously verified as such, progress to this end will be described in Chapter 4 of this dissertation in which we invoked a TS lp- π interaction between a chiral catalyst and an achiral additive to rationalize a major inversion in the sense of enantioinduction in an asymmetric fluorination of allylic alcohols (77 % *R* to 92 % ee *S*) based on a series of structure-selectivity studies.

Conclusions and Outlook

The preceding paragraphs have laid the conceptual foundation upon which the catalyst design elements described in this dissertation are based. Specifically, the following chapters will describe progress towards to goal of rationally modulating attractive noncovalent interactions involving aromatic rings to control enantioselectivity in organocatalytic reactions. As described

above, the weakly attractive nature of such interactions, their complex geometric requirements, and the lack of detailed knowledge of transition state structure at the outset of a synthetic methodology project render the truly *de novo* design of effective catalysts challenging. However, considering the sizable body of knowledge regarding both ground and transition state stabilization conferred by noncovalent interactions, the prospects for their deliberate modulation once identified seem bright. It will be argued that the proper organization of data allows for the recognition of situations in which noncovalent interactions may be playing a role in catalysis, enabling the generation of testable hypotheses that enable detailed mechanistic and structural insight. It is our hope that the conclusions of these studies will challenge the conventional thinking that synthetic chiral catalysts need exert their influence on transition states solely *via* steric repulsion, moving a step closer to ultimate goal of truly rational catalyst design.

References

- (1) Sinnokrot, M. O.; Sherrill, C. D. *J. Phys. Chem. A* **2006**, *110* (37), 10656.
- (2) Lee, E. C.; Kim, D.; Jurečka, P.; Tarakeshwar, P.; Hobza, P.; Kim, K. S. *J. Phys. Chem. A* **2007**, *111* (18), 3446.
- (3) Raju, R. K.; Bloom, J. W. G.; An, Y.; Wheeler, S. E. *ChemPhysChem* **2011**, *12* (17), 3116.
- (4) Martinez, C. R.; Iverson, B. L. *Chem. Sci.* **2012**, *3* (7), 2191.
- (5) Wheeler, S. E.; Bloom, J. W. G. *J. Phys. Chem. A* **2014**, *118* (32), 6133.
- (6) Tsuzuki, S.; Honda, K.; Uchimaru, T.; Mikami, M.; Tanabe, K. *J. Am. Chem. Soc.* **2002**, *124* (1), 104.
- (7) Hunter, C. A.; Sanders, J. K. M. *J. Am. Chem. Soc.* **1990**, *112* (14), 5525.
- (8) Hunter, C. A.; Low, C. M. R.; Vinter, J. G.; Zonta, C. *J. Am. Chem. Soc.* **2003**, *125* (33), 9936.
- (9) Cockroft, S. L.; Hunter, C. A.; Lawson, K. R.; Perkins, J.; Urch, C. J. *J. Am. Chem. Soc.* **2005**, *127* (24), 8594.
- (10) Cockroft, S. L.; Hunter, C. A. *Chem. Commun.* **2006**, No. 36, 3806.
- (11) Cozzi, F.; Cinquini, M.; Annunziata, R.; Dwyer, T.; Siegel, J. S. *J. Am. Chem. Soc.* **1992**, *114* (14), 5729.
- (12) Cozzi, F.; Cinquini, M.; Annunziata, R.; Siegel, J. S. *J. Am. Chem. Soc.* **1993**, *115* (12), 5330.
- (13) Cozzi, F.; Ponzini, F.; Annunziata, R.; Cinquini, M.; Siegel, J. S. *Angew. Chem. Int. Ed. Engl.* **1995**, *34* (9), 1019.
- (14) Cozzi, F.; Annunziata, R.; Benaglia, M.; Cinquini, M.; Raimondi, L.; Baldrige, K. K.; Siegel, J. S. *Org. Biomol. Chem.* **2003**, *1* (1), 157.
- (15) Grimme, S. *Angew. Chem. Int. Ed.* **2008**, *47* (18), 3430.
- (16) Bloom, J. W. G.; Wheeler, S. E. *Angew. Chem. Int. Ed.* **2011**, *50* (34), 7847.
- (17) Sinnokrot, M. O.; Sherrill, C. D. *J. Am. Chem. Soc.* **2004**, *126* (24), 7690.
- (18) Wheeler, S. E.; Houk, K. N. *J. Am. Chem. Soc.* **2008**, *130* (33), 10854.
- (19) Wheeler, S. E.; Houk, K. N. *Mol. Phys.* **2009**, *107* (8-12), 749.
- (20) Wheeler, S. E.; Houk, K. N. *J. Chem. Theory Comput.* **2009**, *5* (9), 2301.
- (21) Wheeler, S. E. *J. Am. Chem. Soc.* **2011**, *133* (26), 10262.
- (22) Raju, R. K.; Bloom, J. W. G.; Wheeler, S. E. *J. Chem. Theory Comput.* **2013**, *9* (8), 3479.
- (23) Wheeler, S. E. *Acc. Chem. Res.* **2013**, *46* (4), 1029.
- (24) Hwang, J.; Li, P.; Carroll, W. R.; Smith, M. D.; Pellechia, P. J.; Shimizu, K. D. *J. Am. Chem. Soc.* **2014**.

- (25) Cockroft, S. L.; Hunter, C. A. *Chem. Soc. Rev.* **2007**, 36 (2), 172.
- (26) Ma, J. C.; Dougherty, D. A. *Chem. Rev.* **1997**, 97 (5), 1303.
- (27) Meyer, E. A.; Castellano, R. K.; Diederich, F. *Angew. Chem. Int. Ed.* **2003**, 42 (11), 1210.
- (28) An, Y.; Wheeler, S. E. In *Encyclopedia of Inorganic and Bioinorganic Chemistry*; John Wiley & Sons, Ltd, 2011.
- (29) Salonen, L. M.; Ellermann, M.; Diederich, F. *Angew. Chem. Int. Ed.* **2011**, 50 (21), 4808.
- (30) Dougherty, D. A. *Acc. Chem. Res.* **2013**, 46 (4), 885.
- (31) Mahadevi, A. S.; Sastry, G. N. *Chem. Rev.* **2013**, 113 (3), 2100.
- (32) Cubero, E.; Luque, F. J.; Orozco, M. *Proc. Natl. Acad. Sci.* **1998**, 95 (11), 5976.
- (33) Tsuzuki, S.; Mikami, M.; Yamada, S. *J. Am. Chem. Soc.* **2007**, 129 (27), 8656.
- (34) Mecozzi, S.; West, A. P.; Dougherty, D. A. *Proc. Natl. Acad. Sci.* **1996**, 93 (20), 10566.
- (35) Mecozzi, S.; West, A. P.; Dougherty, D. A. *J. Am. Chem. Soc.* **1996**, 118 (9), 2307.
- (36) Wheeler, S. E.; Houk, K. N. *J. Am. Chem. Soc.* **2009**, 131 (9), 3126.
- (37) Daze, K. D.; Hof, F. *Acc. Chem. Res.* **2013**, 46 (4), 937.
- (38) Zhong, W.; Gallivan, J. P.; Zhang, Y.; Li, L.; Lester, H. A.; Dougherty, D. A. *Proc. Natl. Acad. Sci.* **1998**, 95 (21), 12088.
- (39) Xiu, X.; Puskar, N. L.; Shanata, J. A. P.; Lester, H. A.; Dougherty, D. A. *Nature* **2009**, 458 (7237), 534.
- (40) Jacobs, S. A.; Khorasanizadeh, S. *Science* **2002**, 295 (5562), 2080.
- (41) Nielsen, P. R.; Nietlispach, D.; Mott, H. R.; Callaghan, J.; Bannister, A.; Kouzarides, T.; Murzin, A. G.; Murzina, N. V.; Laue, E. D. *Nature* **2002**, 416 (6876), 103.
- (42) Hughes, R. M.; Wiggins, K. R.; Khorasanizadeh, S.; Waters, M. L. *Proc. Natl. Acad. Sci.* **2007**, 104 (27), 11184.
- (43) Christianson, D. W. *Chem. Rev.* **2006**, 106 (8), 3412.
- (44) Morikubo, N.; Fukuda, Y.; Ohtake, K.; Shinya, N.; Kiga, D.; Sakamoto, K.; Asanuma, M.; Hirota, H.; Yokoyama, S.; Hoshino, T. *J. Am. Chem. Soc.* **2006**, 128 (40), 13184.
- (45) Wendt, K. U. *Science* **1997**, 277 (5333), 1811.
- (46) Wendt, K. U.; Lenhart, A.; Schulz, G. E. *J. Mol. Biol.* **1999**, 286 (1), 175.
- (47) Faraldos, J. A.; Antonczak, A. K.; González, V.; Fullerton, R.; Tippmann, E. M.; Allemann, R. K. *J. Am. Chem. Soc.* **2011**, 133 (35), 13906.
- (48) Knowles, R. R.; Jacobsen, E. N. *Proc. Natl. Acad. Sci.* **2010**, 107 (48), 20678.
- (49) Knowles, R. R.; Lin, S.; Jacobsen, E. N. *J. Am. Chem. Soc.* **2010**, 132 (14), 5030.
- (50) Uyeda, C.; Jacobsen, E. N. *J. Am. Chem. Soc.* **2011**, 133 (13), 5062.
- (51) Lin, S.; Jacobsen, E. N. *Nat. Chem.* **2012**, 4 (10), 817.
- (52) Ahuja, R.; Samuelson, A. G. *CrystEngComm* **2003**, 5 (69), 395.
- (53) Gamez, P.; Mooibroek, T. J.; Teat, S. J.; Reedijk, J. *Acc. Chem. Res.* **2007**, 40 (6), 435.
- (54) Frontera, A.; Gamez, P.; Mascal, M.; Mooibroek, T. J.; Reedijk, J. *Angew. Chem. Int. Ed.* **2011**, 50 (41), 9564.
- (55) Bauzá, A.; Mooibroek, T. J.; Frontera, A. *CrystEngComm* **2015**, 18 (1), 10.
- (56) Giese, M.; Albrecht, M.; Rissanen, K. *Chem. Rev.* **2015**, 115 (16), 8867.
- (57) Giese, M.; Albrecht, M.; Rissanen, K. *Chem. Commun.* **2016**, 52 (9), 1778.
- (58) Lucas, X.; Bauzá, A.; Frontera, A.; Quiñonero, D. *Chem. Sci.* **2016**, 7 (2), 1038.
- (59) Alkorta, I.; Rozas, I.; Elguero, J. *J. Am. Chem. Soc.* **2002**, 124 (29), 8593.
- (60) Mascal, M.; Armstrong, A.; Bartberger, M. D. *J. Am. Chem. Soc.* **2002**, 124 (22), 6274.
- (61) Quiñonero, D.; Garau, C.; Frontera, A.; Ballester, P.; Costa, A.; Deyà, P. M. *Chem. Phys. Lett.* **2002**, 359 (5–6), 486.

- (62) Estarellas, C.; Bauzá, A.; Frontera, A.; Quiñonero, D.; Deyà, P. M. *Phys. Chem. Chem. Phys.* **2011**, *13* (13), 5696.
- (63) Hay, B. P.; Custelcean, R. *Cryst. Growth Des.* **2009**, *9* (6), 2539.
- (64) Frontera, A.; Saczewski, F.; Gdaniec, M.; Dziemidowicz-Borys, E.; Kurland, A.; Deyà, P. M.; Quiñonero, D.; Garau, C. *Chem. – Eur. J.* **2005**, *11* (22), 6560.
- (65) Lu, T.; Wheeler, S. E. *Org. Lett.* **2014**, *16* (12), 3268.
- (66) Wheeler, S. E.; Bloom, J. W. G. *Chem. Commun.* **2014**, *50* (76), 11118.
- (67) Estarellas, C.; Frontera, A.; Quiñonero, D.; Deyà, P. M. *Angew. Chem. Int. Ed.* **2011**, *50* (2), 415.
- (68) Berryman, O. B.; Sather, A. C.; Hay, B. P.; Meisner, J. S.; Johnson, D. W. *J. Am. Chem. Soc.* **2008**, *130* (33), 10895.
- (69) Dawson, R. E.; Hennig, A.; Weimann, D. P.; Emery, D.; Ravikumar, V.; Montenegro, J.; Takeuchi, T.; Gabutti, S.; Mayor, M.; Mareda, J.; Schalley, C. A.; Matile, S. *Nat. Chem.* **2010**, *2* (7), 533.
- (70) Matile, S.; Jentzsch, A. V.; Montenegro, J.; Fin, A. *Chem. Soc. Rev.* **2011**, *40* (5), 2453.
- (71) Adriaenssens, L.; Estarellas, C.; Vargas Jentzsch, A.; Martinez Belmonte, M.; Matile, S.; Ballester, P. *J. Am. Chem. Soc.* **2013**, *135* (22), 8324.
- (72) Vargas Jentzsch, A.; Hennig, A.; Mareda, J.; Matile, S. *Acc. Chem. Res.* **2013**, *46* (12), 2791.
- (73) Zhao, Y.; Domoto, Y.; Orentas, E.; Beuchat, C.; Emery, D.; Mareda, J.; Sakai, N.; Matile, S. *Angew. Chem. Int. Ed.* **2013**, *52* (38), 9940.
- (74) Zhao, Y.; Beuchat, C.; Domoto, Y.; Gajewy, J.; Wilson, A.; Mareda, J.; Sakai, N.; Matile, S. *J. Am. Chem. Soc.* **2014**, *136* (5), 2101.
- (75) Zhao, Y.; Sakai, N.; Matile, S. *Nat. Commun.* **2014**, *5*, 3911.
- (76) Miros, F. N.; Huang, G.; Zhao, Y.; Sakai, N.; Matile, S. *Supramol. Chem.* **2015**, *27* (5-6), 303.
- (77) Zhao, Y.; Benz, S.; Sakai, N.; Matile, S. *Chem. Sci.* **2015**, *6* (11), 6219.
- (78) Zhao, Y.; Cotelle, Y.; Avestro, A.-J.; Sakai, N.; Matile, S. *J. Am. Chem. Soc.* **2015**, *137* (36), 11582.
- (79) Miros, F. N.; Zhao, Y.; Sargsyan, G.; Besnard, C.; Beuchat, C.; Mareda, J.; Sakai, N.; Matile, S. *Chem. – Eur. J.* **2016**, *22* (8), 2648.
- (80) Cotelle, Y.; Benz, S.; Avestro, A.-J.; Ward, T. R.; Sakai, N.; Matile, S. *Angew. Chem. Int. Ed.* **2016**, n/a.
- (81) Singh, S. K.; Das, A. *Phys. Chem. Chem. Phys.* **2015**, *17* (15), 9596.
- (82) Alkorta, I.; Rozas, I.; Elguero, J. *J. Org. Chem.* **1997**, *62* (14), 4687.
- (83) Gallivan, J. P.; Dougherty, D. A. *Org. Lett.* **1999**, *1* (1), 103.
- (84) Amicangelo, J. C.; Gung, B. W.; Irwin, D. G.; Romano, N. C. *Phys. Chem. Chem. Phys.* **2008**, *10* (19), 2695.
- (85) Ran, J.; Hobza, P. *J. Chem. Theory Comput.* **2009**, *5* (4), 1180.
- (86) Badri, Z.; Foroutan-Nejad, C.; Kozelka, J.; Marek, R. *Phys. Chem. Chem. Phys.* **2015**, *17* (39), 26183.
- (87) Gung, B. W.; Zou, Y.; Xu, Z.; Amicangelo, J. C.; Irwin, D. G.; Ma, S.; Zhou, H.-C. *J. Org. Chem.* **2008**, *73* (2), 689.
- (88) Singh, S. K.; Kumar, S.; Das, A. *Phys. Chem. Chem. Phys.* **2014**, *16* (19), 8819.
- (89) Ao, M.-Z.; Tao, Z.; Liu, H.-X.; Wu, D.-Y.; Wang, X. *Comput. Theor. Chem.* **2015**, *1064*, 25.
- (90) Egli, M.; Gessner, R. V. *Proc. Natl. Acad. Sci.* **1995**, *92* (1), 180.

- (91) Egli, M.; Sarkhel, S. *Acc. Chem. Res.* **2007**, *40* (3), 197.
- (92) Jain, A.; Ramanathan, V.; Sankararamkrishnan, R. *Protein Sci.* **2009**, *18* (3), 595.
- (93) Sarkhel, S.; Rich, A.; Egli, M. *J. Am. Chem. Soc.* **2003**, *125* (30), 8998.
- (94) Mooibroek, T. J.; Gamez, P.; Reedijk, J. *CrystEngComm* **2008**, *10* (11), 1501.
- (95) Korenaga, T.; Tanaka, H.; Ema, T.; Sakai, T. *J. Fluor. Chem.* **2003**, *122* (2), 201.
- (96) Korenaga, T.; Shoji, T.; Sakai, T. *Chem. Commun.* **2009**, No. 31, 4678.
- (97) Gung, B. W.; Xue, X.; Reich, H. J. *J. Org. Chem.* **2005**, *70* (18), 7232.
- (98) Pavlakos, I.; Arif, T.; Aliev, A. E.; Motherwell, W. B.; Tizzard, G. J.; Coles, S. J. *Angew. Chem. Int. Ed.* **2015**, *54* (28), 8169.

Chapter 2

Enantioselective Cross Dehydrogenative Coupling Enabled by the Design and Application of Chiral Triazole Containing Phosphoric Acids

Portions of this chapter were adapted with permission from (Neel, A. J.; Hehn, J. P.; Tripet, P. F.; Toste, F. D. *J. Am. Chem. Soc.* **2013**, *135*, 14044. “Asymmetric Cross-Dehydrogenative Coupling Enabled by the Design and Application of Chiral Triazole-Containing Phosphoric Acids”). Copyright (2013) American Chemical Society and (Milo, A.*; Neel, A. J.*, Toste, F. D; Sigman, M. S. *Science* **2015**, *347*, 737. “A Data-Intensive Approach to Mechanistic Elucidation Applied to Chiral Anion Catalysis). Copyright (2015) The American Association for the Advancement of Science.

Chapter 2. Enantioselective Cross Dehydrogenative Coupling Enabled by the Design and Application of Chiral Triazole Containing Phosphoric Acids

Introduction

In contrast to the myriad branches of science whose focus is the observation and subsequent rationalization of naturally occurring phenomena, synthetic chemistry, and in particular organic synthesis, provides a unique opportunity for *ab initio* invention limited only by the creativity of the practitioner. Indeed, some of the most impressive advances in the field include the development of novel reactivity paradigms entirely lacking natural counterparts. As a result of the freedom afforded by the practice of synthetic organic chemistry, different approaches to the development of new reactions have emerged that continue to result in innovative solutions to outstanding synthetic challenges. Broadly, strategies for reaction development can be classified into three major categories on the basis of the motivation underlying the work: motif-based, bond-based, and reactivity-based.¹ The motif-based approach to reaction development is perhaps the most familiar, entailing the development of methodology targeting the synthesis of a particular functional group or functional group array that is present in, for example, a naturally occurring secondary metabolite or pharmaceutical compound of interest. The bond-based approach seeks to identify catalysts or reaction conditions that enable the formation of a specific type of bond that may allow for new, simplifying disconnections in retrosynthetic planning. In contrast to these strategies, which are rooted in the synthesis of specific molecular entities, the reactivity-based approach to reaction development focuses on identifying reactivity patterns that allow for the development of hypotheses such that successful reaction development serves as a validation of the proposed reactivity. Thus, this latter approach enables the synthesis of many different structural motifs from a single reactivity manifold.

It is within this conceptual framework that the Toste group has made advances in the field of chiral anion catalysis (CAC).²⁻⁴ Unlike more conventional methods for catalytically introducing stereocenters into organic molecules, such as chiral Lewis or Brønsted acid catalysis or the implementation of transition metals supported by chiral ligands, CAC is predicated on the formation of a tight ion pair between a chiral anion and a cationic reaction component. The power of this strategy lies in its generalizability to any situation in which a cationic reagent or reaction intermediate is involved at any point prior to or during the enantiodetermining event along a reaction coordinate. Although controversy can exist as to whether the association between the catalyst and substrate is purely electrostatic in nature,⁵ this concept has provided chemists with an intriguing approach to reaction design. Indeed, in the past decade CAC has evolved into a sub-field in its own right with numerous catalyst structures and reaction classes having been reported.^{2-4,6-16}

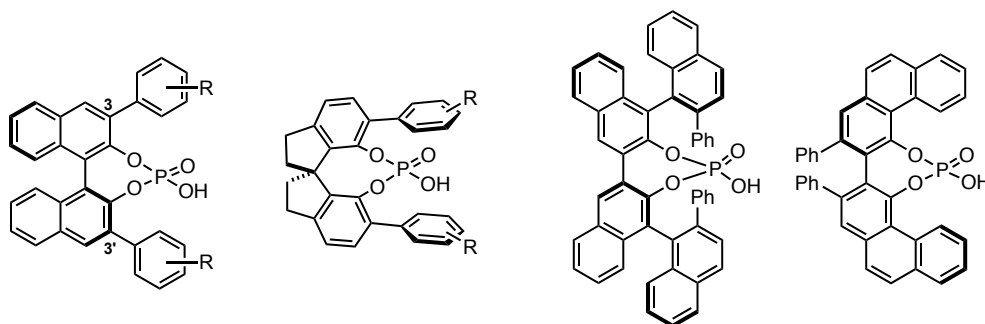
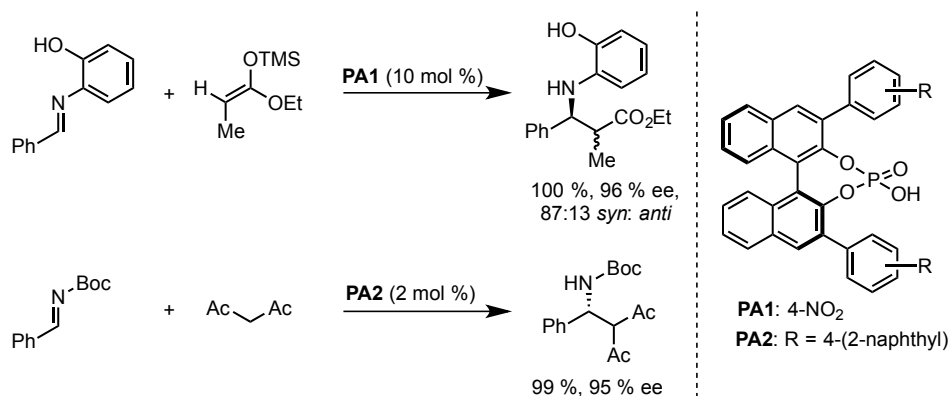


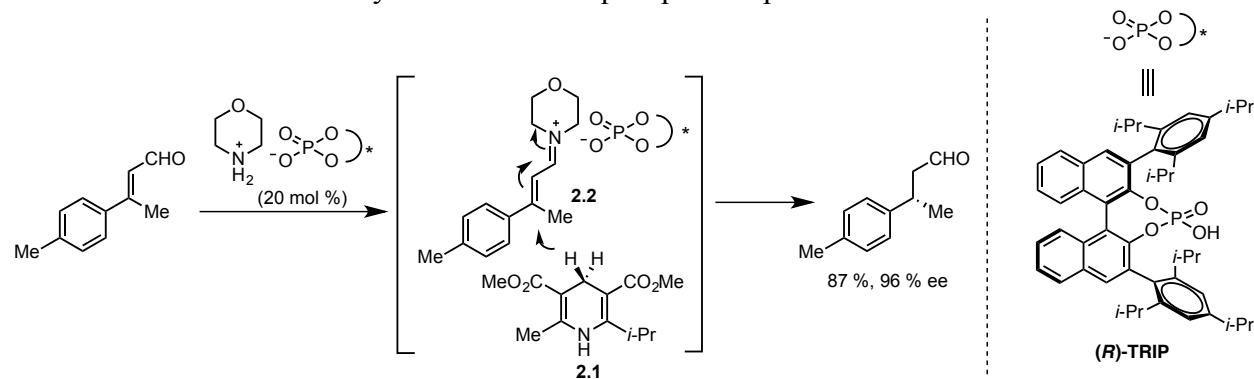
Figure 2.1. Selected examples of axially chiral phosphoric acids

Among the chiral anionic catalysts employed, the conjugate bases of axially chiral phosphoric acids (PAs) have featured particularly prominently.¹⁷⁻²⁰ The most common catalyst structures are those based on the 1,1'-bi-2-naphthol (BINOL) structure (Figure 2.1, left) due to BINOL's relatively low cost and the modularity that this structure affords with respect to the groups that may be installed at the 3 and 3' positions. This latter feature allows one to tune the steric and electronic properties of the catalyst. Originally reported independently by Akiyama²¹ and Terada²² in 2004 for enantioselective Mannich-type reactions (Scheme 2.1), PAs of this general structure have seen extensive use as chiral Brønsted acids.²⁰

Scheme 2.1. Seminal examples of axially chiral PAs as Brønsted acid catalysts (refs. 21-22)



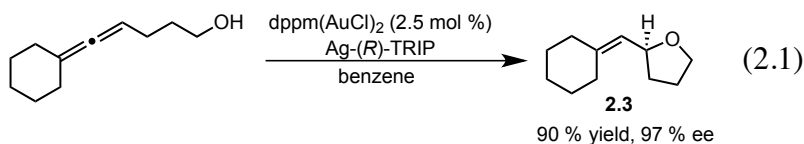
In 2006 Mayer and List reported the first use of the conjugate base of an axially chiral PA as a chiral anion in catalysis.²³ As shown in Scheme 2.2, the formation of an ion pair between an achiral iminium and a chiral phosphate (**2.2**) enabled a highly enantioselective conjugate reduction using Hantzsch ester **2.1**. In this instance, the association between the phosphate and iminium (**2.2**) is necessarily ionic in nature, as other interactions such as hydrogen bonding are precluded. Also of note was the introduction of the chiral phosphate catalyst (*R*)-TRIP bearing (2,4,6-*i*-Pr)₃Ph-substituents at the 3 and 3' positions of the binaphthyl backbone, as this catalyst has likely seen the most extensive use of any other chiral PA/phosphate reported to date.²⁴



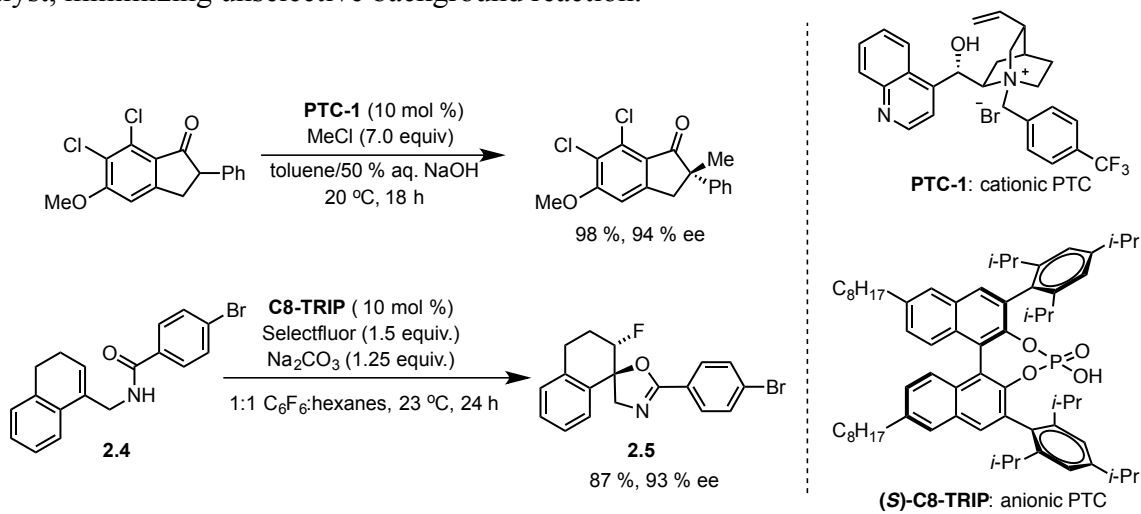
Scheme 2.2. Seminal report of chiral anion catalysis with phosphate anions (ref. 23)

Toste and coworkers reported independently in 2007 that transition metal-catalyzed reactions could also be rendered highly enantioselective through the action of a chiral anion (eq.

2.1).²⁵ This achievement was particularly noteworthy, as it addressed the issue of designing chiral ligands for Au(I), which is challenging due to its preference for a linear coordination geometry. By combining an achiral cationic Au(I) species with an appropriately designed chiral phosphate anion ((*R*)-TRIP), cyclization product **2.3** was obtained in excellent yield and enantiomeric excess.



In 2011, the Toste group further extended the idea of CAC into the realm of enantioselective phase transfer catalysis (PTC, Scheme 2.3 bottom),^{26,27} which had only previously been demonstrated for the charge inverted strategy of using cationic species as the catalytic sources of chirality (Scheme 2.3 top).²⁸ Specifically, it was envisioned that an insoluble, cationic reagent could be rendered soluble as the result of ion pairing with a lipophilic chiral anion, ensuring that any of the reagent available for subsequent reaction would be in the chiral environment of the catalyst, minimizing unselective background reaction.²⁹



Scheme 2.3. Seminal examples of asymmetric cationic (top, ref. 28) and anionic (bottom, ref. 29) PTC

As a proof of concept, enantioselective fluorination was targeted, given the ability of fluorine to impart desirable properties to pharmaceutical compounds and the dearth of methods available for its enantioselective introduction.^{30–38} Using the doubly cationic, commercially available reagent Selectfluor^{39–42} in combination with the chiral phosphoric acid (*S*)-C8-TRIP (Scheme 2.3), a number of fluorinated spiro-fused dihydrooxazoles (**2.5**) were prepared in highly enantioenriched form from the corresponding dihydropyran-derived substrates **2.4** (Scheme 2.3). Mechanistically, it was proposed²⁹ (Figure 2.2) that the soluble chiral phosphate (**2-A**) underwent anion metathesis with Selectfluor, resulting in a chiral ion pair (**2-B**). The presence of multiple phosphate anions was supported by the observation of a nonlinear relationship between catalyst and product enantiomeric excess (ee) using catalyst mixtures of varying enantiopurity. Subsequent fluorocyclization afforded the dihydrooxazole product and phosphoric acid (**2-C**), which could be deprotonated by an equivalent of inorganic base to regenerate the phosphate anion.

Conceptualization of chiral anion phase-transfer (CAPT) catalysis in this way has allowed for several additional substrate classes to be halogenated with excellent enantioselectivity.^{43–56}

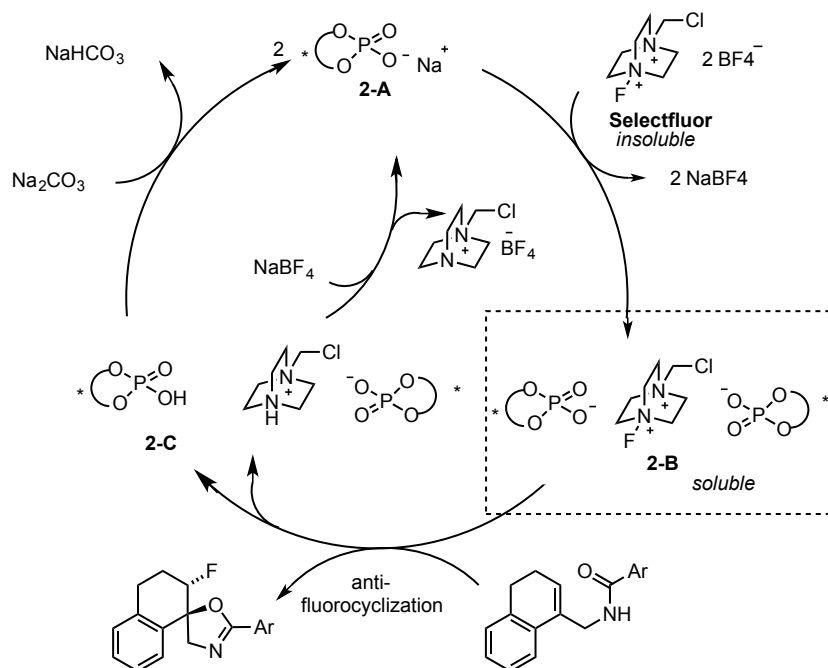
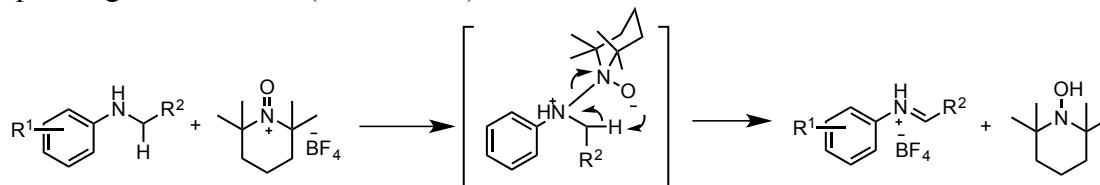


Figure 2.2. Proposed catalytic cycle for CAPT fluorination (ref. 29)

Bearing in mind our reactivity-based approach to reaction development, we were intrigued by the possibility of using CAPT to enable the formation of an ion pair between a chiral phosphate and a reactive intermediate (in contrast to a cationic metal complex or cationic reagent). Specifically, we sought to identify an insoluble, positively charged reagent that, upon solubilization by a chiral phosphate, could react with a substrate to afford a cationic intermediate. Introduction of the reagent into solution in this way would ensure that the phosphate would be in position to form a tight ion pair with the cationic reaction intermediate by virtue of proximity. With these criteria in mind, we chose to explore the use of oxoammonium salts,⁵⁷ which are cationic and have been shown to serve as competent oxidants towards amine substrates to give the corresponding iminium ions (Scheme 2.4).^{58–61}



Scheme 2.4. Oxoammonium mediated oxidation of a secondary amine

Results and Discussion

Reaction Development

We selected the model reaction shown in Table 2.1 to test our hypothesis that CAPT could be used as a mechanism to enforce ion pairing between a chiral phosphate and a prochiral reactive

intermediate. Additionally, this would represent a novel approach to enantioselective cross-dehydrogenative coupling (CDC), a term coined by Li⁶² to describe the functionalization of C-H bonds alpha to heteroatoms in the presence of a hydrogen acceptor.⁶²⁻⁶⁵ Mechanistically, we envisioned that a chiral phosphate (**2-D**, Figure 2.3) could undergo anion-exchange with an appropriately-chosen cationic oxidant ensuring that the phosphate would be in close proximity to form a tight ion-pair (**2-E**) with the substrate upon oxidation. Preferential attack on one of the prochiral faces of the resulting ionic complex would provide an enantioenriched product (**2-F**) and release the chiral phosphate.

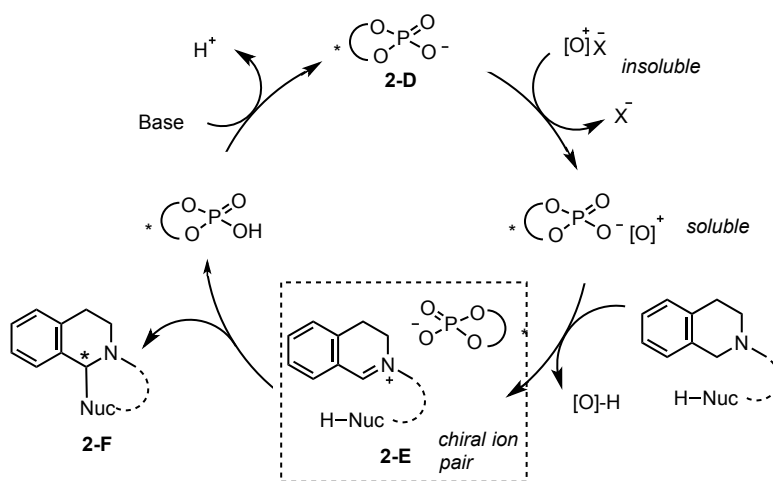


Figure 2.3. Mechanistic hypothesis for chiral phosphate-catalyzed enantioselective CDC reaction

We began our studies by evaluating a number of conventional axially chiral PAs in combination with amide-tethered tetrahydroisoquinoline substrate **2.6** and oxoammonium salt **2.8** (Table 2.1). Promising conversion to the desired product (**2.7**) was observed in each case along with detectable levels of enantioselectivity; however, none of the catalysts initially tested afforded **2.7** with enantiomeric excess greater than 31% ee. We reasoned that although the putative substrate-phosphate complex (**2-E**) may be forming, the chiral environment created by these catalysts was inadequate to differentiate the prochiral faces of the substrate, leading us to consider alternative substrate-catalyst interactions beyond sterics that might influence enantioselectivity.

In chiral PA/phosphate catalysis, asymmetric induction has generally been achieved by the strategic installation of bulky groups that serve to project the catalyst's axial chirality, coercing the prochiral substrate into a position within the chiral pocket that minimizes unfavorable steric interactions with the catalyst (Figure 2.4, left).⁶⁶ Thus, achieving high levels of enantioselectivity often hinges on the identification and synthesis of catalysts bearing increasingly large substituents. Although remarkable success has been realized using this strategy,⁶⁷⁻⁷¹ the enzyme-inspired principle of preferentially stabilizing one diastereomeric transition state *via* attractive, non-covalent interactions⁷²⁻⁷⁶ had not been explicitly explored in the realm of PA catalysis, despite having seen great success with other classes of organic catalysts.

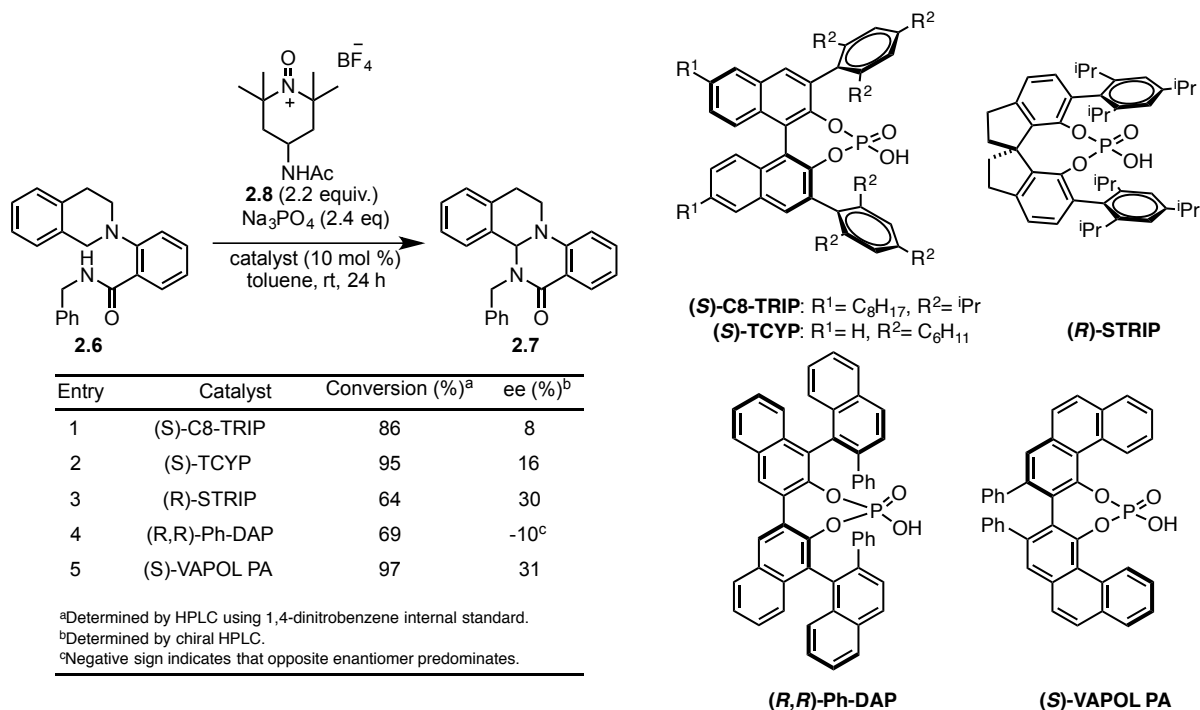


Table 2.1. Initial survey of axially chiral PAs in model asymmetric CDC reaction

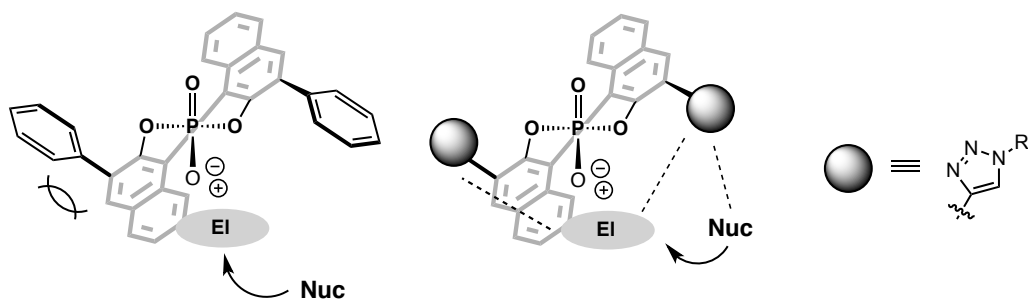


Figure 2.4. Conceptual difference between using repulsive (left) and attractive (right) interactions to influence enantioselectivity in chiral phosphate catalysis

According to the Curtin Hammett principle,^{77,78} the observed enantiomeric ratio of the product of an enantioselective reaction is directly related to the free energy difference between the competing diastereomeric transition states leading to each enantiomer ($\Delta\Delta G^\ddagger = -RT\ln([\text{enantiomer}_{\text{major}}]/[\text{enantiomer}_{\text{minor}}])$).⁷⁹ As such, the transition state energy difference required for a highly enantioselective reaction is actually quite small (Figure 2.5, top). As recently discussed by Knowles and Jacobsen,⁷⁴ these energies are on the same order as those typically attributed to a number of weak, attractive, noncovalent interactions, such as hydrogen bonding, aromatic interactions or dispersion forces (Figure 2.5, bottom). We reasoned that judiciously-chosen atoms or groups incorporated at the 3 and 3' positions of the binaphthyl backbone would be appropriately positioned to form attractive interactions with a substrate at a site remote from the phosphate moiety, providing an alternative type of organizational element (Figure 2.4, right).

With respect to both modularity and function, the 1,2,3-triazole seemed well suited to this purpose.^{80,81}

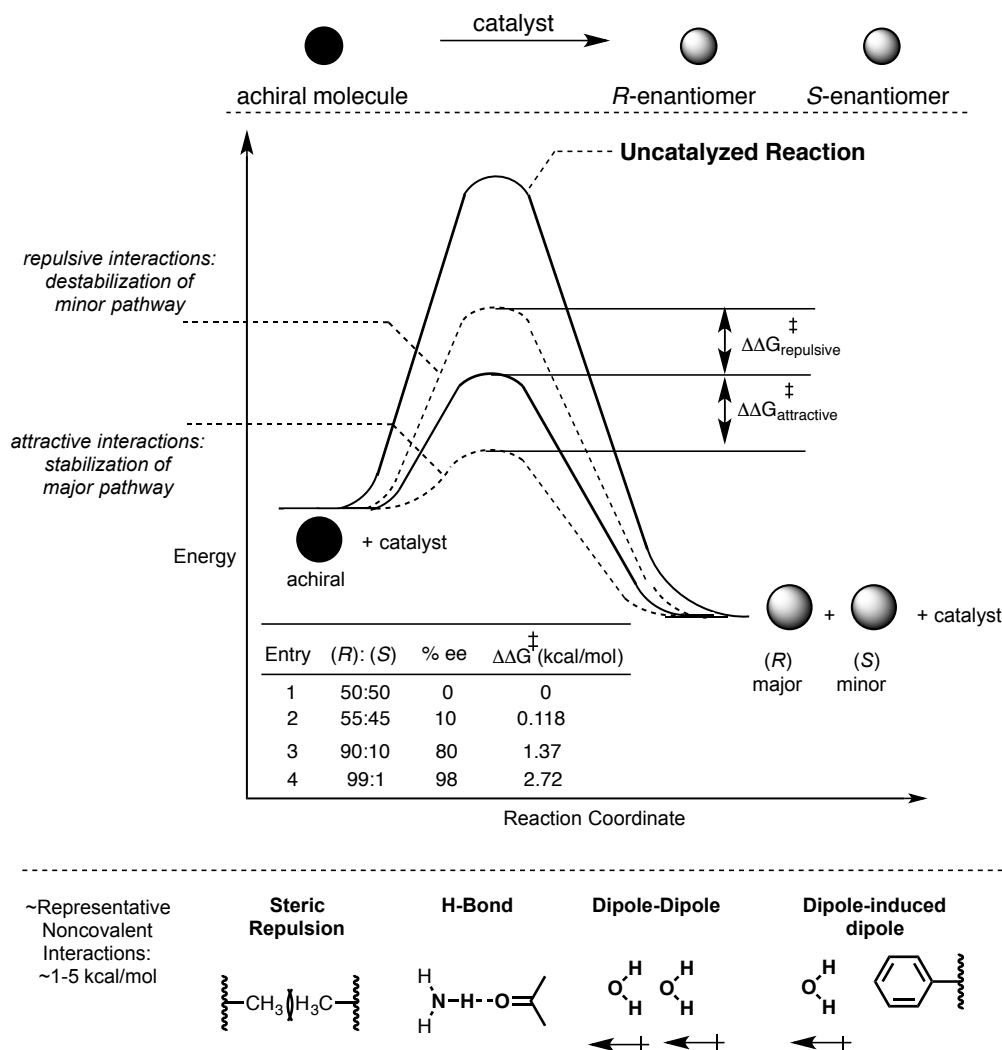


Figure 2.5. Simplified reaction coordinate diagram illustrating the enantiodetermining transition state of an asymmetric reaction and the associated energy differences required for asymmetric induction (top) and examples of noncovalent interactions that might be leveraged for asymmetric catalysis (bottom).

The advent of click chemistry,⁸² in particular the copper-catalyzed azide-alkyne cycloaddition (CuAAC),⁸³⁻⁸⁵ has provided a tool for rapid generation of 1,2,3-triazole-containing compounds that have found widespread application. From the standpoint of modular catalyst design, the click chemistry approach is ideal in that the broad alkyne/azide scope allows for the facile preparation of numerous sterically and electronically diverse derivatives from a common intermediate. In addition to synthetic accessibility, the 1,2,3-triazole displays interesting hydrogen-bonding properties as exemplified by its ability to serve as an effective anion binder⁸⁶⁻⁹⁰ and peptide bond surrogate (Figure 2.6).⁹¹⁻⁹⁴ With respect to this latter feature, we hypothesized that in addition to the ionic phosphate-substrate association, the amide bond-containing substrate 2.6

might undergo attractive hydrogen-bonding interaction with the triazole, resulting in additional rigidity within the chiral pocket created by the catalyst and stabilization of the diastereomeric transition state.

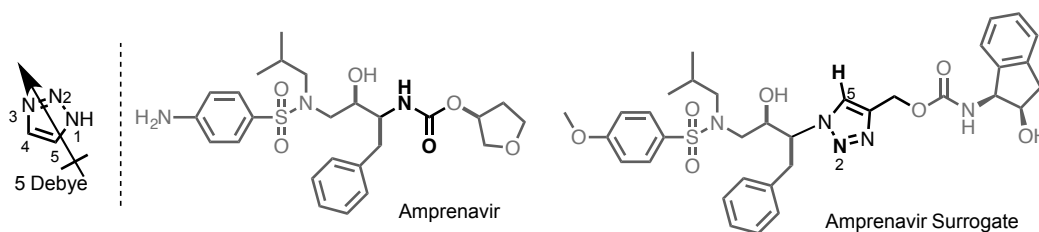
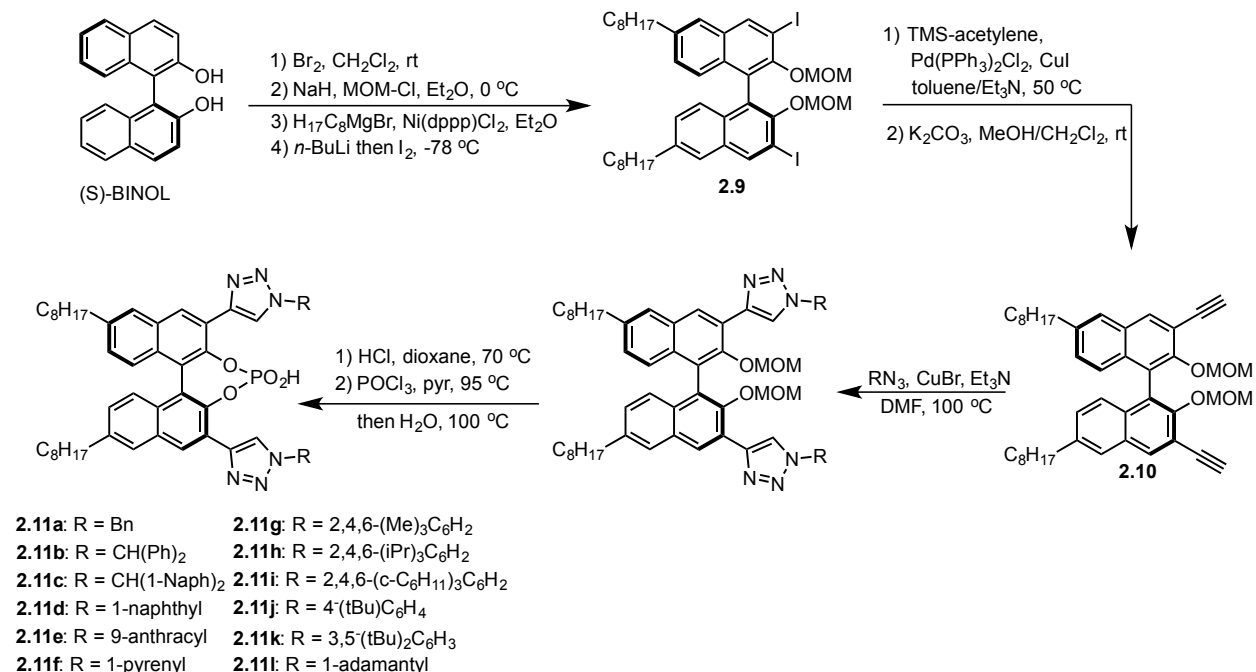


Figure 2.6. Illustration of peptidomimetic qualities of 1,2,3-triazole resulting from its large dipole moment (ref. 91)

To this end, we set out to develop a modular synthesis of 3,3'-triazolyl BINOL-derived phosphoric acids that would allow for the late stage introduction of diversity, enabling the rapid preparation of a library of catalysts from a common intermediate. This synthesis is outlined in Scheme 2.5. Beginning from (*S*)-BINOL, selective bromination of the 6 and 6' positions, protection of the phenol oxygen atoms by chloromethyl methyl ether (MOM-Cl), Kumada coupling with octylmagnesium bromide and directed *ortho*-lithiation/iodination gave *bis*-iodide **2.9**. The installation of the alkyl groups on the catalyst backbone was deemed necessary to ensure solubility of the final triazolyl catalysts in the nonpolar organic solvents required for our phase-transfer strategy. Intermediate **2.9** was transformed into the key *bis*-alkyne **2.10** after Sonogashira coupling with trimethylsilylacetylene and alkyne deprotection with potassium carbonate in methanol. From *bis*-alkyne **2.10**, the final catalysts **2.11** were prepared *via* a three step, two-pot sequence involving CuAAC with an azide, phenol deprotection and phosphorylation/hydrolysis. Using this procedure, twelve catalysts (**2.11a-l**) were prepared from common intermediate **2.10**, offering an advantage over the syntheses of the more conventional chiral PA catalysts that are often tailored to the specific derivative of interest.

When these novel catalysts were tested in our model reaction, an improvement in the observed enantiomeric excess of **2.7** over that using aryl-substituted catalysts was observed in every case, while maintaining excellent levels of conversion (Table 2.2, compare entries 1-5 to entries 6-17). Notably, the major enantiomer of **2.7** produced using the triazolyl PA catalysts was opposite to that produced using the aryl-substituted PA catalysts in all cases (*vide infra*). Furthermore, we were surprised to discover that the reaction reached comparable conversion even in the absence of the PA (Table 2.2, entry 38), suggesting a remarkable acceleration of the enantiodetermining step in the presence of the catalyst. A series of standard optimization experiments revealed that N-acyl oxoammonium salt **2.8**, tribasic sodium phosphate and *p*-xylene provided an ideal balance of yield and enantioselectivity.



Scheme 2.5. Synthesis of triazolyl PA catalysts

Entry	Catalyst	Oxidant	Base	Solvent	Conversion ^a	ee (%) ^b	Entry	Catalyst	Oxidant	Base	Solvent	Conversion ^a	ee (%) ^b
1	(S)-C8-TRIP	2.8	Na ₃ PO ₄	toluene	86	8	23	2.111	2.8	Na ₃ PO ₄	hexanes	91	-27
2	(S)-TCYP	2.8	Na ₃ PO ₄	toluene	95	16	24	2.111	2.8	Na ₃ PO ₄	Et ₂ O	86	-78
3	(R)-STRIP	2.8	Na ₃ PO ₄	toluene	64	30	20	2.111	2.8	Na ₃ PO ₄	THF	95	-55
4	(R,R)-Ph-DAP	2.8	Na ₃ PO ₄	toluene	69	-10 ^c	25	2.111	2.8	Na ₃ PO ₄	MeCN	69	4
5	(S)-VAPOL PA	2.8	Na ₃ PO ₄	toluene	97	31	26	2.111	2.8	Na ₃ PO ₄	CH ₂ Cl ₂	43	-18
6	2.11a	2.8	Na ₃ PO ₄	toluene	97	-70	27	2.111	2.8	Na ₃ PO ₄	benzene	96	-73
7	2.11b	2.8	Na ₃ PO ₄	toluene	99	-69	28	2.111	2.8	Na ₃ PO ₄	<i>o</i> -xylene	95	-82
8	2.11c	2.8	Na ₃ PO ₄	toluene	75	-52	29	2.111	2.8	Na ₃ PO ₄	<i>m</i> -xylene	95	-81
9	2.11d	2.8	Na ₃ PO ₄	toluene	97	-63	30	2.111	2.8	Na ₃ PO ₄	<i>p</i> -xylene	94	-82
10	2.11e	2.8	Na ₃ PO ₄	toluene	92	-41	31	2.111	2.8	Na ₃ PO ₄	mesitylene	92	-84
11	2.11f	2.8	Na ₃ PO ₄	toluene	77	56	32	2.111	2.8	Na ₃ PO ₄	fluorobenzene	92	-61
12	2.11g	2.8	Na ₃ PO ₄	toluene	92	-78	33	2.111	2.8	Na ₂ HPO ₄	<i>p</i> -xylene	65	-88
13	2.11h	2.8	Na ₃ PO ₄	toluene	92	-80	34	2.111	2.8	Na ₂ CO ₃	<i>p</i> -xylene	38	-88
14	2.11i	2.8	Na ₃ PO ₄	toluene	91	-77	35	2.111	2.8	NaHCO ₃	<i>p</i> -xylene	24	-88
15	2.11j	2.8	Na ₃ PO ₄	toluene	91	-37	36	2.111	2.8	K ₂ CO ₃	<i>p</i> -xylene	21	-88
16	2.11k	2.8	Na ₃ PO ₄	toluene	92	-50	37	2.111	2.8	LiCO ₃	<i>p</i> -xylene	38	-82
17	2.11l	2.8	Na ₃ PO ₄	toluene	75	-81	38	none	2.8	Na ₃ PO ₄	toluene	92	nd
18	2.11h	2.12	Na ₃ PO ₄	toluene	95	-79							
19	2.11h	2.13	Na ₃ PO ₄	toluene	88	-78							
20	2.11h	2.14	Na ₃ PO ₄	toluene	32	-56							
21	2.11h	2.15	Na ₃ PO ₄	toluene	0	nd							
22	2.11h	2.16	Na ₃ PO ₄	toluene	4	nd							

^a Determined by HPLC using 1,4-dinitrobenzene internal standard. ^b Determined by chiral HPLC. ^c Negative sign indicates that opposite enantiomer predominates.

Table 2.2. Summary of effects of catalyst, oxidant, base and solvent on conversion and enantiomeric excess of model asymmetric CDC reaction

Using this set of conditions, the scope of this C-N bond forming reaction was explored. Benzylic groups bearing both electron-rich and electron-poor substituents at the *para* position were

tolerated on the nucleophilic nitrogen atom (Figure 2.7, **2.7b-d**), resulting in both good yields and enantioselectivities. Furthermore, *ortho*-methoxy-substituted benzylic substrate **2.7e** afforded the product in excellent ee. We next turned our attention to substrates bearing *N*-aryl groups. Although only modest selectivities were observed using *N*-phenyl substrate **2.7f** and its 3-methyl substituted analogue **2.7g**, switching to 2-substitution (**2.7h**) resulted in a dramatic increase in enantioselectivity, although reactivity was sluggish. A range of *ortho* functional groups were tolerated, including naphthyl (**2.7i**) chloro (**2.7j**), and, perhaps surprisingly, hydroxyl (**2.7k**). Moreover, substrates with bulky alkyl substituents underwent the transformation with good enantioselectivity (**2.7l-m**). The tetrahydroisoquinoline *N*-aryl ring could also be substituted with both electron-donating and withdrawing groups, while still maintaining excellent levels of enantioselectivity (**2.7n-p**). It is worth mentioning that no general catalyst emerged during these preliminary scope studies. For each substrate, several catalysts **2.11** were tested and it was observed that different catalysts provided superior results depending on the substrate employed (Figure 2.7). These observations suggested an intriguing structural interplay between catalyst and substrate structure whose origin was difficult to discern at this juncture (*vide infra*).

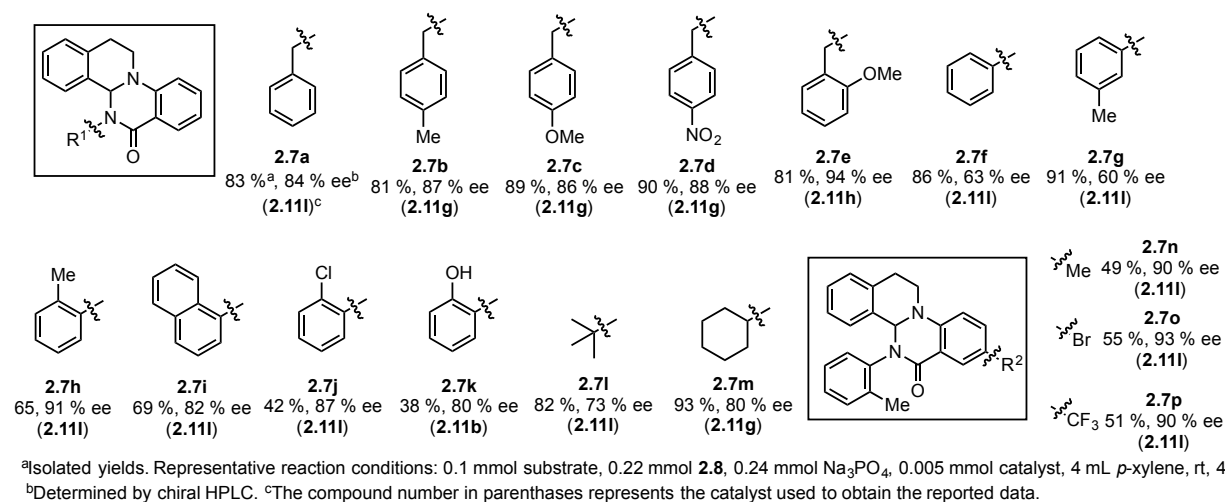
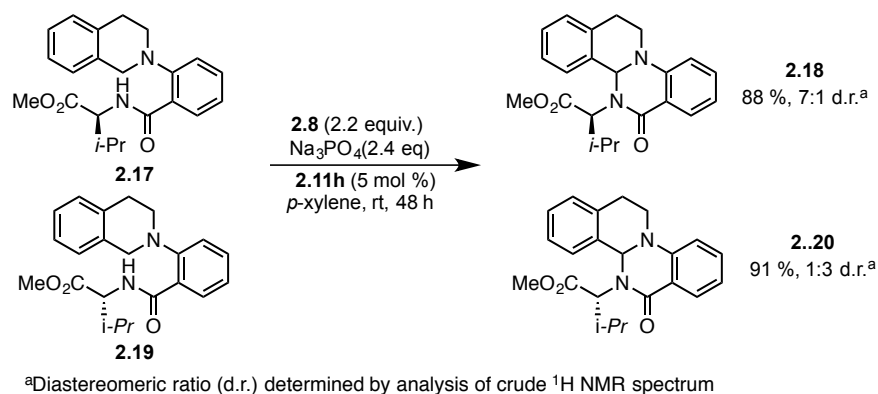


Figure 2.7. Preliminary substrate scope of asymmetric CDC reaction

To explore the extent to which triazolyl catalysts **2.11** could control the absolute configuration of the newly-formed stereocenter, both antipodes of the amino acid valine were incorporated into the substrate scaffold as their corresponding methyl esters and subjected to the standard reaction conditions (Scheme 2.6). In the absence of catalyst, a 1:1 mixture of diastereomers was produced. However, when **2.11h** was employed, *L*-valine-derived substrate **2.17** produced the product (**2.18**) as a 7:1 mixture of diastereomers, while *D*-valine-derived substrate **2.19** afforded a 1:3 mixture in favor of the opposite diastereomer (**2.20**), demonstrating the catalyst's ability to control the absolute configuration of the newly-formed stereocenter in the presence of an existing one.



Scheme 2.6. Chiral substrate demonstrating catalyst control over absolute configuration of newly-formed stereocenter

Mechanistic Studies

We next endeavored to gather evidence to support or refute our original hypothesis that ion pairing between the phosphate and oxoammonium salt was a necessary prerequisite for ion pairing with the oxidized tetrahydroisoquinolinium intermediate. With respect to the general mechanism in Figure 2.3, we sought to distinguish two scenarios: i) enantioselectivity is determined during oxidation of substrate (**2-H**, Figure 2.8) or ii) enantioselectivity is determined during the cyclization of an oxidized intermediate (**2-G**, Figure 2.8). In the former scenario, it was conceivable that although the stereogenic center is formally set in the cyclization from the oxidized intermediate (**2-G**), the interactions between the substrate and catalyst during the oxidation event may pre-organize the system for effective enantioselection.

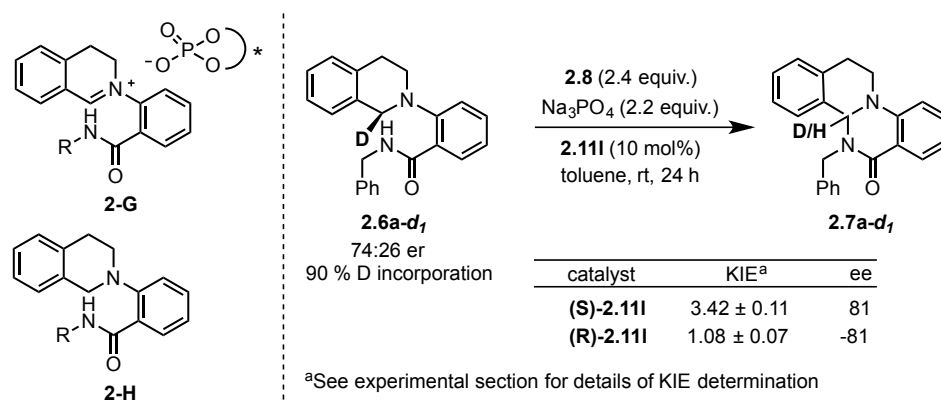


Figure 2.8. Summary of enantiomer-dependent kinetic isotope effect experiments

To distinguish between these possibilities, a set of intramolecular kinetic isotope effect (KIE) experiments was performed using **2.6a-d₁** (90 % D incorporation, 74:26 er, see the Experimental Section for details). We anticipated that, if the chiral phosphate were involved in substrate oxidation, different product H/D ratios would be observed for the formation of **2.7a-d₁** when using enantiomeric catalysts. In practice, (*R*)- and (*S*)-**2.11I** promoted the reaction with KIEs of 3.42 and 1.08 respectively, suggesting the involvement of the catalyst in the oxidation (Figure 2.8), as originally hypothesized. If enantioselectivity were also established in this step, different

product ee values would be expected using the enantiomeric catalysts. However, the observation that the final products exhibited equal but opposite levels of enantioselectivity is consistent with enantioselection occurring during the bond-forming event from an oxidized intermediate such as **2-G**. This result indicated that the two key steps of this reaction (oxidation and cyclization) proceed under independent Curtin-Hammett control, with similar interactions likely governing selectivity in both cases (Figure 2.9).

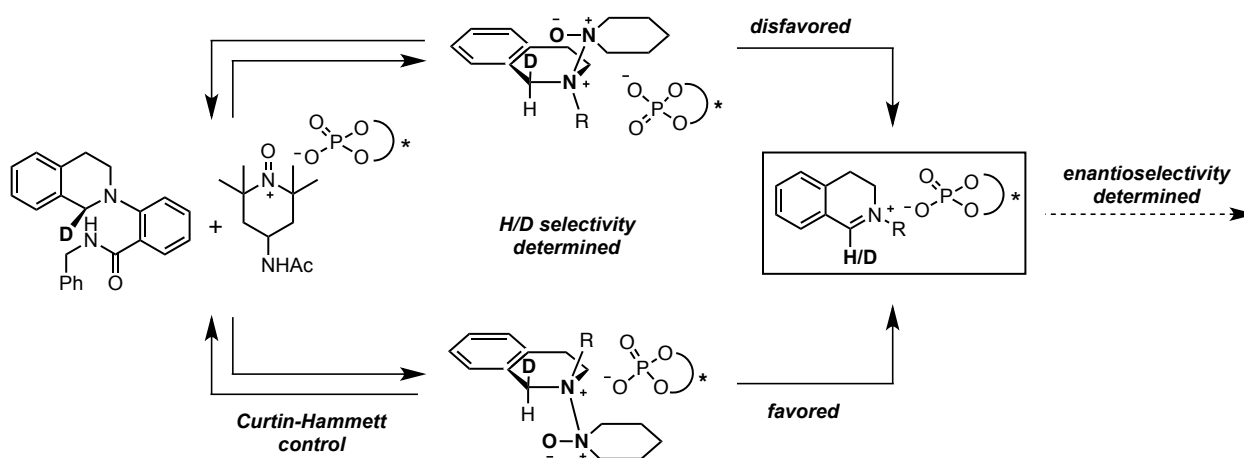


Figure 2.9. Mechanistic rationale for enantiomer-dependent kinetic isotope effect illustrating that oxidation and cyclization are de-coupled

Collectively, the available data are consistent with the mechanism depicted in Figure 2.10. Based on the observation that the qualitative rate of product formation is the same in the presence and absence of the phosphate catalyst (Table 2.2, entry 38), we propose that dissolution of oxoammonium salt **2.8**, unassisted by the phosphate, is rate-limiting. Indeed, the racemic product samples required for high performance liquid chromatography (HPLC) analysis were prepared in every case (i.e. *rac*-**2.7a-p**) simply by running the reaction using the conditions from Figure 2.7 but omitting the catalyst (**2.11**). Given the minimal solubility of **2.8** in *p*-xylene, the 5 mol % of phosphate catalyst in solution will always be present in excess, ensuring that any **2.8** in solution will be part of a chiral ion pair (**2-I**). Thus, although it does not appear that catalysts **2.11** are functioning explicitly as phase transfer catalysts in this system, precise control of the relative solubility of the reacting components is essential for limiting the unselective background reaction by ensuring the phosphate's presence each time a substrate molecule is oxidized. The observation of an enantiomer-dependent kinetic isotope effect supports the claim that the oxoammonium and phosphate are associated during substrate oxidation, resulting chiral isoquinolinium salt **2-J**. That equal and opposite levels of asymmetric induction of **2.7a-d₁** were observed using enantiomeric catalysts (*S*) and (*R*)-**2.11** regardless of the corresponding oxidation KIE suggests that the oxidation and cyclization events are de-coupled that enantioselectivity results from a chiral ion pair between a chiral phosphate and a cationic reaction intermediate, as initially hypothesized.

Although compelling evidence had been obtained that enantioselectivity was determined from a chiral ion pair such as **2-J**, questions still remained regarding the origin of the drastic improvement in ee using triazolyl catalysts **2.11** relative to the more conventional aryl-substituted derivatives. Considering our original hypothesis that **2.11** might improve enantioselectivity by undergoing attractive noncovalent interactions with the substrate, we wanted to design an

experiment that would distinguish this scenario from one in which the selectivity change was purely steric in origin. Thus, pyrazolyl (*pyr-2.111*) and imidazolyl (*imid-2.111*) PAs were prepared (Figure 2.11), which were expected to impose steric environments similar to that of **2.111**, but with

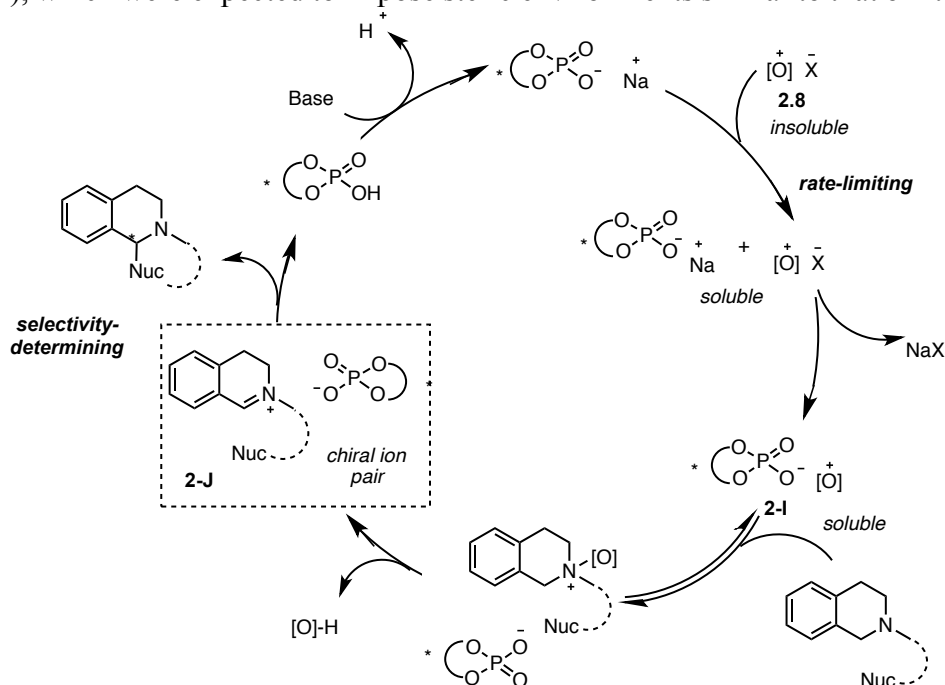


Figure 2.10. Proposed mechanism for chiral anion catalyzed asymmetric CDC reaction

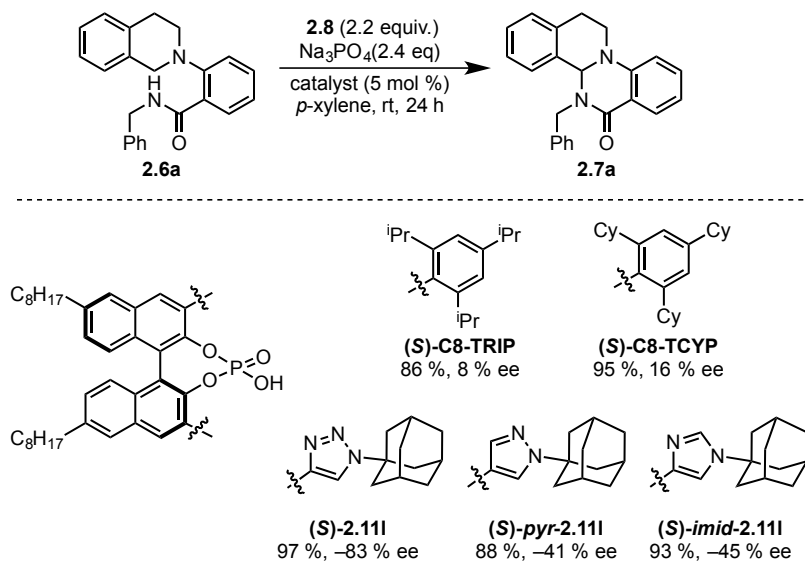


Figure 2.11. Experiments probing structural role of 1,2,3-triazole in catalysts **2.11**

inherently different electronic properties. When these isosteric analogues were tested in the CDC reaction with substrate **2.6a**, similar levels of conversion were observed, but with significantly

reduced enantioselectivities compared with **2.111**, albeit with the same sense of enantioinduction. The observation that **2.11a-I** (Table 2.2, entries 6-17), *pyr-2.111*, and *imid-2.111* all provided the product enantiomer opposite that given by conventional PAs⁹⁵⁻⁹⁸ may be rationalized by either 1) attractive interactions between the heterocyclic substituents and substrate that override the selectivity based purely on sterics or 2) a fundamentally different steric environment created by these catalysts.⁹⁹ However, the diminished enantioselectivities afforded by *pyr-2.111* and *imid-2.111* vs. **2.111** suggests that electronic rather than steric properties of the triazolyl substituents in catalysts **2.11** are primarily responsible for the high enantioselectivities reported herein. We were now in a position to begin investigating the origins of enantioselectivity. This work will be described in Chapter 3.

Conclusion

In conclusion, we have extended the reactivity-based strategy of chiral anion phase-transfer catalysis to a reaction class beyond halogenation to develop a novel oxidative cyclization reaction using oxoammonium salts. Conceptually, this work demonstrates that ion pairing with a sparingly soluble reagent can be an effective mechanism for the delivery of a chiral anion to a cationic reactive intermediate. Central to the success of this approach was the use click chemistry to develop a new class of axially chiral PAs based on BINOL bearing 1,2,3-triazoles at the 3 and 3' positions. Using these molecules as catalysts, we were able to achieve enantioselectivities in a novel C-N bond forming reaction that were unattainable using conventional PAs. Our results suggest that, in addition to being an easily-modified catalyst substituent, the triazole may serve an organizational function other than simply creating a sterically hindered environment around the catalyst active site. These findings will hopefully lead to the increased consideration of strategic use of interactions beyond steric repulsion as elements of catalyst design.

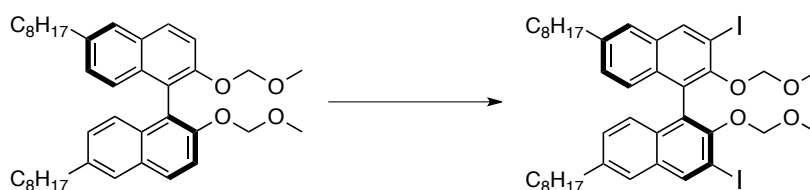
Experimental Section

General Information

Unless otherwise noted, all reagents were purchased from commercial suppliers and used without further purification. Enantioselective cross-dehydrogenative coupling (CDC) reactions were run in 2 dram (15 X 60 mm) vials equipped with a screw cap and stirred using a magnetic Teflon stir bar (1/2" X 5/16"), placed on the surface of a magnetic stir plate. Due to the heterogeneous nature of these reactions, it was important that fast and efficient stirring be maintained over the course of the reaction in order to obtain optimal results. Tetrahydrofuran, dichloromethane, diethyl ether, toluene, triethylamine and N,N-dimethylformamide were purified by passage through an activated alumina column under argon. Thin-layer chromatography (TLC) analysis of reaction mixtures was performed using Merck silica gel 60 F254 TLC plates, and visualized under UV or by staining with ceric ammonium molybdate or KMNO₄. Column chromatography was performed on Merck Silica Gel 60 Å, 230 X 400 mesh. Nuclear magnetic resonance (NMR) spectra were recorded using Bruker AV-600, AV-500, DRX-500, AVQ-400, AVB-400 and AV-300 spectrometers. ¹H and ¹³C chemical shifts are reported in ppm downfield of tetramethylsilane and referenced to residual solvent peak (CHCl₃; δH = 7.26 ppm and δC = 77.0 ppm, DMSO; δH = 2.50 and δC = 39.5 ppm). Multiplicities are reported using the following abbreviations: s = singlet, d = doublet, t = triplet, q = quartet, app t = apparent triplet, m = multiplet, br = broad resonance. Solvent abbreviations are reported as follows: EtOAc = ethyl acetate, hex = hexanes, DCM = dichloromethane, Et₂O = diethyl ether, MeOH = methanol, THF = tetrahydrofuran, DMF = N,N-dimethylformamide, Et₃N

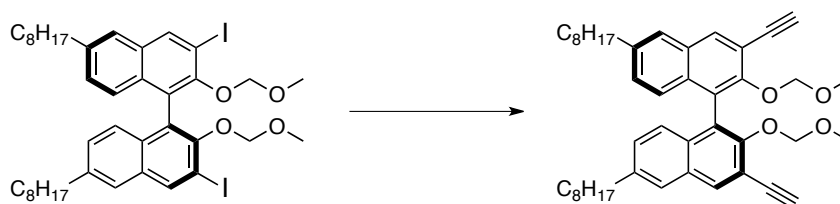
= triethylamine. Mass spectral data were obtained from the Micro-Mass/Analytical Facility operated by the College of Chemistry, University of California, Berkeley. Enantiomeric excesses were measured on a Shimadzu VP Series Chiral HPLC using Chiralpak IA, IB, or IC columns. The syntheses of TRIP¹⁰⁰, C8-TRIP²⁹, TCYP⁴⁴, STRIP¹⁰¹, and VAPOL PA¹⁰² have been previously reported. Caution: Although we have not experienced any problems during the preparation and handling of the azides reported herein, appropriate safety precautions should be taken due to the explosive nature of organic azides, including the use of a blast shield during any manipulations involving azides. Azides 2.22¹⁰³ and 2.32¹⁰⁴ have been previously reported. Azide S3c was prepared by the method of Zhang,¹⁰³ S3d, S3e and S3f by the method of Guo,¹⁰⁵ and S3g, S3h, S3i, S3j and S3k by the method of Tor.¹⁰⁶ All azides were used directly without further purification. Racemic CDC products were synthesized by carrying out the reactions in toluene in the absence of catalyst.

(S)-3,3'-diiodo-2,2'-bis(methoxymethyl)-6,6'-dioctyl-1,1'-binaphthalene (2.9)



A magnetically stirred solution of (*S*)-2,2'-bis(methoxymethyl)-6,6'-dioctyl-1,1'-binaphthalene¹⁰⁷ (31.35 g, 52.35 mmol) in THF (500 mL) was cooled to -78 °C and *n*-butyllithium (2.5 M solution in hexanes, 73 mL, 183.2 mmol) was added dropwise over the course of 15 min. After 30 min, the solution was warmed to 0 °C and stirred at this temperature for 2 h. The dark brown reaction mixture was then cooled to -78 °C and iodine (49.82 g, 196.31 mmol) was added as a single portion. The solution was warmed to room temperature and stirred for an additional 2 h at which point saturated aqueous Na₂S₂O₃ (200 mL) was carefully added and the resulting mixture was allowed to stir at room temperature for 30 min. The mixture was extracted with EtOAc (2 X 200 mL) and the organic extracts were washed with H₂O (200 mL) and brine (100 mL), dried (Na₂SO₄) and concentrated *in vacuo*. Purification of the crude residue by column chromatography on silica gel using Hex/Et₂O as eluent (20:1) afforded the title compound (33.22 g, 39.05 mmol, 75 % yield) as a yellow oil. ¹H NMR (500 MHz, CDCl₃) δ 8.47 (s, 1H), 7.54 (s, 2H), 7.17 (d, *J* = 9.0 Hz, 2H), 7.11 (d, *J* = 9.0 Hz, 2H), 4.81 (d, *J* = 5.7 Hz, 2H), 4.70 (d, *J* = 5.6 Hz, 2H), 2.73 (t, *J* = 7.7 Hz, 4H), 2.62 (s, 6H), 1.74 - 1.63 (m, 4H), 1.39 - 1.22 (m, 20H), 0.89 (t, *J* = 6.7 Hz, 6H). ¹³C NMR (126 MHz, CDCl₃) δ 151.33, 140.58, 139.40, 132.47, 132.23, 128.76, 126.41, 126.23, 125.00, 99.35, 92.31, 56.53, 35.84, 31.89, 31.10, 29.48, 29.37, 29.27, 22.69, 14.15. HRMS (EI) found [M+Na]⁺ 873.1852, C₄₀H₅₂O₄I₂Na requires 873.1847.

(S)-3,3'-diethynyl-2,2'-bis(methoxymethyl)-6,6'-dioctyl-1,1'-binaphthalene (2.10)



To a magnetically stirred solution of (*S*)-3,3'-diiodo-2,2'-bis(methoxymethyl)-6,6'-dioctyl-1,1'-binaphthalene (**2.9**, 18.22 g, 21.42 mmol) in toluene (110 mL) and Et₃N (110 mL) were added bis(triphenylphosphine)palladium (II) dichloride (0.601 g, 0.857 mmol) and copper (I) bromide (1.63 g, 8.57 mmol). After degassing this solution under vacuum (3 x 30 s), trimethylsilylacetylene (9.76 mL, 68.54 mmol) was added. The reaction mixture was stirred at 50 °C for 12 h at which point TLC indicated complete consumption of the starting material. After cooling to room temperature, the reaction mixture was diluted with Et₂O (150 mL), filtered through Celite and concentrated *in vacuo*. The crude residue was taken up in MeOH (455 mL) and DCM (45 mL). To this vigorously-stirred solution was added K₂CO₃ (29.6 g, 214.2 mmol). The reaction mixture was stirred at room temperature for 1 h at which point TLC indicated consumption of the starting material. The reaction mixture was filtered through Celite and the filtrate partitioned between H₂O (200 mL) and DCM (200 mL). The organic phase was separated and the aqueous phase was extracted with DCM (3 x 50 mL). The combined organic extracts were washed with saturated aqueous NH₄Cl, dried (Na₂SO₄), and concentrated *in vacuo*. The residue was purified by column chromatography on silica gel using Hex/Et₂O as eluent (20:1) to give the title compound (10.15 g, 15.64 mmol, 73 % yield over 2 steps) as a viscous, brown oil. ¹H NMR (500 MHz, CDCl₃) δ 8.14 (s, 2H), 7.61 (s, 2H), 7.19 (d, *J* = 9.0 Hz, 2H), 7.16 (d, *J* = 9.0 Hz, 2H), 5.09 (d, *J* = 6.0 Hz, 2H), 4.90 (d, *J* = 6.0 Hz, 2H), 3.34 (s, 2H), 2.74 (t, *J* = 7.8 Hz, 4H), 2.57 (s, 6H), 1.72 - 1.63 (m, 4H), 1.45 - 1.21 (m, 20H), 0.90 (t, *J* = 6.8 Hz, 6H). ¹³C NMR (126 MHz, CDCl₃) δ 152.66, 140.24, 134.64, 132.41, 130.32, 129.15, 126.40, 125.87, 125.74, 116.04, 98.84, 81.30, 80.82, 56.06, 35.83, 31.89, 31.14, 29.48, 29.36, 29.28, 22.69, 14.13. HRMS (EI) found [M]⁺ 646.4031, C₄₄H₅₄O₄ requires 646.4022.

General Procedure A: Synthesis of triazolyl diols *diol-2.11a-c* and *diol-2.11g-l*:

To a magnetically stirred solution of *bis*-alkyne **2.10** (1.0 equiv) in DMF (0.05 M) were added copper (I) bromide (0.25 equiv.), Et₃N (2.0 equiv.), H₂O (4.0 equiv), and azide (2.2 equiv.). The reaction mixture was degassed under vacuum (3 X 30 s), and then heated for 12 h at 100 °C under an atmosphere of N₂. Upon complete consumption of the starting material, as judged by TLC, the reaction mixture was allowed to cool to room temperature and diluted with saturated aqueous NH₄Cl. The aqueous layer was extracted with ethyl acetate (x3) and the combined organic extracts were washed with H₂O (x4), dried (Na₂SO₄) and concentrated *in vacuo*. The crude residue was dissolved in 1,4-dioxane (0.05 M), concentrated HCl (2 mL) was added, and the mixture was heated at 70 °C. Upon complete consumption of the starting material as judged by TLC, the reaction mixture was allowed to cool to room temperature and then concentrated *in vacuo*. The residue was partitioned between DCM and saturated aqueous NaHCO₃. The aqueous layer was extracted with DCM (x3) and the combined organics were dried (Na₂SO₄) and concentrated *in vacuo*. The crude residue was purified by column chromatography (EtOAc/Hex).

General Procedure B: Synthesis of triazolyl diols *diol-2.11d-f*:

i. Preparation of azides: To a magnetically stirred solution of sodium azide (3.2 equiv.) and copper sulfate pentahydrate (0.3 equiv.) in MeOH (0.4 M) was added the appropriate boronic acid (3 equiv.). The brown suspension was stirred at room temperature for 3 h under air and then diluted with EtOAc and saturated aqueous sodium bicarbonate. The organic layer was separated and the aqueous layer was extracted with EtOAc (3x). The combined organic layers were concentrated *in vacuo* to furnish a crude oil, which was directly taken forward in the next step without further purification.

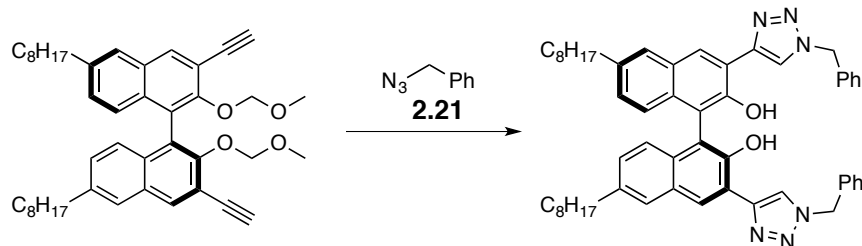
ii. Copper Catalyzed Alkyne-Azide Cycloaddition (CuAAC): The crude azide was dissolved in DCM and transferred to a magnetically stirred solution of *bis*-alkyne **2.10** (1.0 equiv) in DCM/H₂O (1:1, v/v, 0.05 M). Then CuSO₄·5H₂O (0.3 equiv.) and sodium ascorbate (1 equiv.) were successively added and the mixture was stirred at room temperature under an atmosphere of N₂. Every 24 h, sodium ascorbate (0.5 equiv.) was added until complete disappearance of *bis*-alkyne and mono-triazole product as judged by TLC (EtOAc/Hex). The reaction mixture was diluted with DCM, washed with saturated aqueous sodium bicarbonate and extracted with EtOAc (x3). The combined organic extracts were washed with brine, dried (Na₂SO₄) and concentrated *in vacuo*. The crude residue was purified by flash column chromatography using EtOAc/Hex as eluent.

iii. MOM Deprotection: To a magnetically stirred solution of MOM-protected intermediate in 1,4-dioxane (0.025 M) was added concentrated HCl (2 mL) and the mixture was stirred at room temperature overnight. Upon complete consumption of the starting material, as judged by TLC, the reaction mixture was concentrated *in vacuo*. The residue was partitioned between DCM and saturated aqueous NaHCO₃. The aqueous layer was extracted with DCM (x3) and the combined organic layers were dried (Na₂SO₄) and concentrated *in vacuo*. The crude residue was purified by column chromatography using EtOAc/Hex as eluent or by recrystallization from CHCl₃/Hex.

General Procedure C: Synthesis of phosphoric acids:

To a magnetically stirred solution of triazolyl diol *diol-2.11* in pyridine (0.05 M) was added phosphorus (V) oxychloride (2.0 equiv.) and the reaction mixture was heated at 95 °C under an atmosphere of N₂. Upon complete consumption of the starting material, as judged by TLC, the reaction mixture was allowed to cool to room temperature. H₂O (5 mL) was added and the mixture was stirred at 100 °C. Upon complete consumption of the intermediate, as judged by TLC, the reaction mixture was diluted with DCM (20 mL) and washed with 3N HCl (3 x 20 mL). The combined organic extracts were dried (Na₂SO₄) and concentrated *in vacuo*. The crude residue was purified by column chromatography (DCM/MeOH or EtOAc/Hex/TFA).

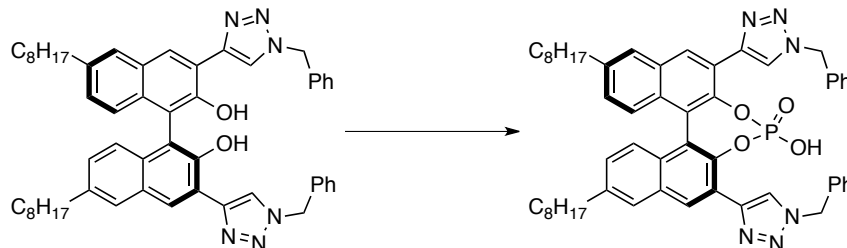
(*S*)-3,3'-bis(1-benzyl-1*H*-1,2,3-triazol-4-yl)-6,6'-dioctyl-[1,1'-binaphthalene]-2,2'-diol (*diol-2.11a*)



Subjection of *bis*-alkyne **2.10** (0.636 g, 0.980 mmol) and azide **2.21** (0.287 g, 2.16 mmol) to General Procedure A gave the title compound (0.597 g, 0.724 mmol, 74 % yield) as a yellow solid after purification by column chromatography on silica gel using Hex:EtOAc as eluent (3:2). ¹H NMR (500 MHz, CDCl₃) δ 9.98 (s, 2H), 8.16 (s, 2H), 8.00 (s, 2H), 7.58 (s, 2H), 7.44 - 7.35 (m, 6H), 7.35 - 7.25 (m, 4H), 7.17 (d, *J* = 8.5 Hz, 2H), 7.10 (d, *J* = 8.5 Hz, 2H), 5.54 (s, 4H), 2.69 (t, *J* = 7.7 Hz, 4H), 1.75 - 1.61 (m, 4H), 1.43 - 1.15 (m, 20H), 0.91 (t, *J* = 6.7 Hz, 6H). ¹³C NMR (126 MHz, CDCl₃) δ 150.27, 147.20, 138.09, 134.39, 132.31, 129.18, 128.86, 128.71, 128.53,

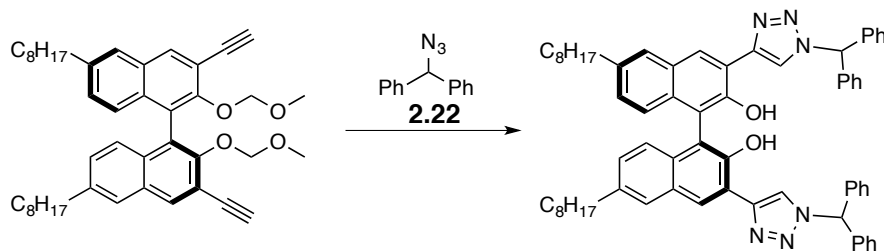
128.14, 126.55, 125.81, 124.72, 120.84, 116.93, 116.56, 54.44, 35.85, 31.94, 31.31, 29.56, 29.46, 29.32, 22.71, 14.16. **HRMS** (ESI) found $[M+H]^+$ 825.4856, $C_{54}H_{61}N_6O_2$ requires 825.4851.

(4*R*,11*bS*)-2,6-bis(1-benzyl-1*H*-1,2,3-triazol-4-yl)-4-hydroxy-9,14-dioctyldinaphtho[2,1-*d*:1',2'-*f*][1,3,2]dioxaphosphepine 4-oxide (2.11a)



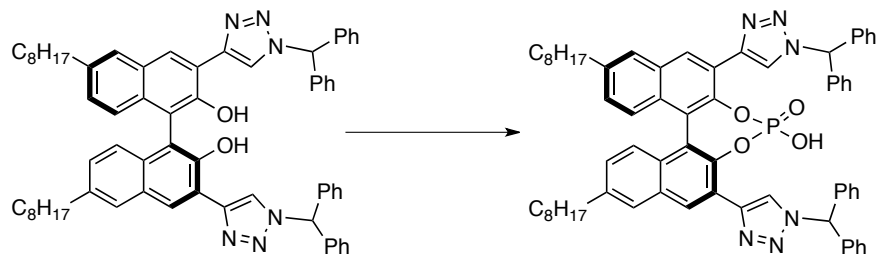
Subjection of diol **diol-2.11a** (0.500 g, 0.606 mmol) to General Procedure C gave the title compound (0.498 g, 0.561 mmol, 93 % yield) as a yellow solid after purification by column chromatography on silica gel using DCM/MeOH as eluent (20:1 to 10:1). **1H NMR** (500 MHz, $CDCl_3$: DMSO, 1:1) δ 8.82 (s, 2H), 8.72 (s, 2H), 7.94 (s, 2H), 7.30 - 7.23 (m, 8H), 7.18 (d, $J = 8.7$ Hz, 4H), 7.05 (d, $J = 8.6$ Hz, 2H), 5.70 (d, $J = 15.5$ Hz, 2H), 5.65 (d, $J = 16.0$ Hz, 2H), 2.71 (t, $J = 7.6$ Hz, 4H), 1.80 - 1.56 (m, 4H), 1.40 - 1.14 (m, 20H), 0.82 (t, $J = 6.7$ Hz, 6H). **^{13}C NMR** (126 MHz, $CDCl_3$: DMSO, 1:1) δ 144.20 (d, $J = 8.9$ Hz), 142.18, 140.34, 136.16, 131.31, 130.25, 128.86, 128.50, 128.14, 127.90, 127.54, 127.17, 126.52, 124.96, 123.24, 122.73, 53.23, 35.63, 31.80, 31.11, 29.39, 29.29, 29.18, 22.61, 14.34. **^{31}P NMR** (243 MHz, $CDCl_3$: DMSO, 1:1) δ 0.95. **HRMS** (ESI) found $[M-H]^-$ 885.4252, $C_{54}H_{58}N_6O_4P_1$ requires 885.4263.

(*S*)-3,3'-bis(1-benzhydryl-1*H*-1,2,3-triazol-4-yl)-6,6'-dioctyl-[1,1'-binaphthalene]-2,2'-diol (diol-2.11b)



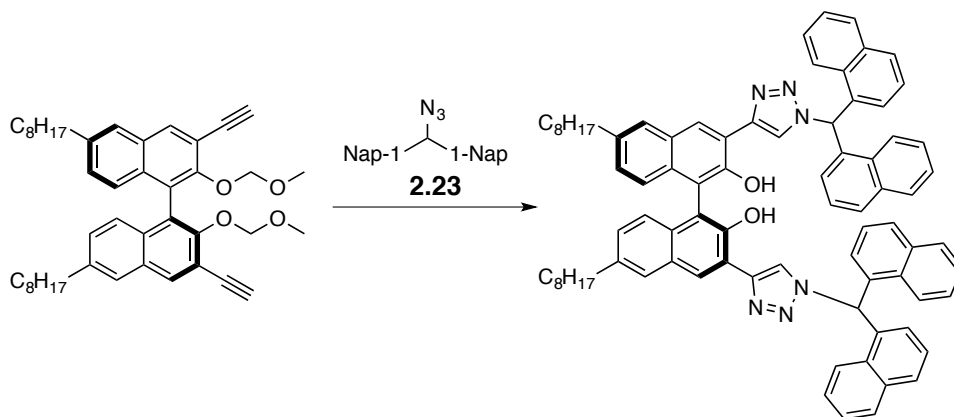
Subjection of *bis*-alkyne **2.10** (0.500 g, 0.771 mmol) and azide **2.22** (0.354 g, 1.69 mmol) to General Procedure A gave the title compound (0.390 g, 0.399 mmol, 52 % yield) as a yellow solid after purification by column chromatography on silica gel using Hex/EtOAc as eluent (9:1). **1H NMR** (500 MHz, $CDCl_3$) δ 9.76 (s, 2H), 8.29 (s, 2H), 8.02 (s, 2H), 7.65 (s, 2H), 7.53 - 7.33 (m, 12H), 7.30 - 7.16 (m, 12H), 7.13 (d, $J = 8.5$ Hz, 2H), 2.73 (t, $J = 7.2$ Hz, 4H), 1.79 - 1.57 (m, 4H), 1.50 - 1.19 (m, 20H), 0.93 (t, $J = 6.3$ Hz, 6H). **^{13}C NMR** (126 MHz, $CDCl_3$) δ 150.26, 146.62, 138.13, 137.81, 132.38, 129.12, 129.10, 128.84, 128.80, 128.61, 128.23, 128.14, 126.57, 125.93, 124.75, 121.07, 117.10, 116.44, 68.54, 35.87, 31.97, 31.29, 29.59, 29.43, 29.34, 22.75, 14.21. **HRMS** (ESI) found $[M+H]^+$ 977.5475, $C_{66}H_{69}N_6O_2$ requires 977.5477.

(4*R*,11*bS*)-2,6-bis(1-benzhydryl-1*H*-1,2,3-triazol-4-yl)-4-hydroxy-9,14-dioctyldinaphtho[2,1-*d*:1',2'-*f*][1,3,2]dioxaphosphepine 4-oxide (2.11*b*)



Subjection of diol **diol-2.11*b*** (0.380 g, 0.388 mmol) to General Procedure C gave the title compound (0.351 g, 0.338 mmol, 87 % yield) as a yellow solid after purification by column chromatography on silica gel using DCM/MeOH as eluent (20:1 to 10:1). $^1\text{H NMR}$ (500 MHz, DMSO, 1:1) δ 8.78 (s, 2H), 8.68 (s, 2H), 7.94 (s, 2H), 7.46 (s, 2H), 7.42 - 7.11 (m, 20H), 7.06 (d, $J = 8.8$ Hz, 2H), 2.85 - 2.62 (m, 4H), 1.76 - 1.55 (m, 4H), 1.39 - 1.09 (m, 20H), 0.83 (t, $J = 6.7$ Hz, 6H). $^{13}\text{C NMR}$ (151 MHz, DMSO) δ 144.79(d, $J = 10.0$ Hz), 140.12, 139.30, 139.15, 131.12, 130.25, 129.07, 128.63, 128.54, 128.44, 128.24, 127.55, 127.46, 127.40, 126.34, 125.28, 123.49, 123.48, 122.77, 122.75, 66.92, 35.35, 31.67, 30.93, 29.24, 29.13, 29.06, 22.49, 14.35. $^{31}\text{P NMR}$ (202 MHz, DMSO) δ 2.37. **HRMS** (ESI) found $[\text{M}+\text{H}]^+$ 1039.5036, $\text{C}_{66}\text{H}_{68}\text{N}_6\text{O}_4\text{P}_1$ requires 1039.5034.

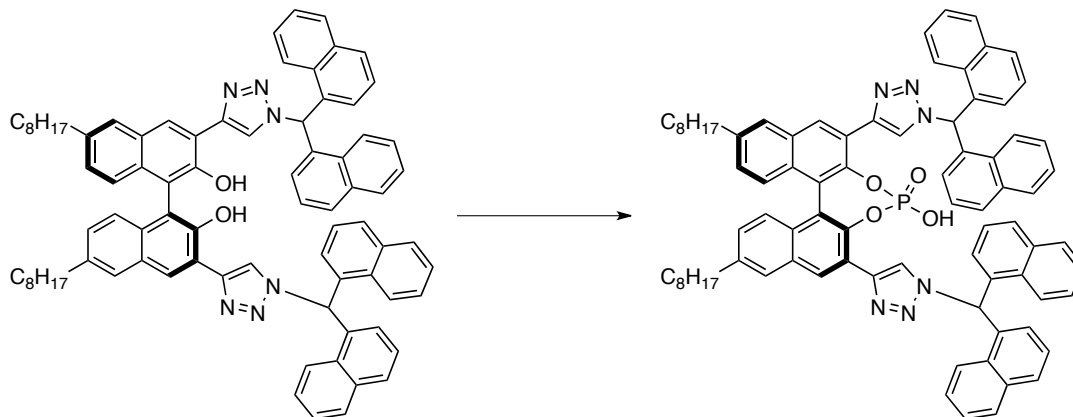
(*S*)-3,3'-bis(1-(di(naphthalen-1-yl)methyl)-1*H*-1,2,3-triazol-4-yl)-6,6'-dioctyl-[1,1'-binaphthalene]-2,2'-diol (diol-2.11*c*)



Subjection of *bis*-alkyne **2.10** (0.500 g, 0.771 mmol) and azide **2.23** (0.524 g, 1.69 mmol) to General Procedure A gave the title compound (0.706 g, 0.600 mmol, 78 % yield) as a brown solid after purification by column chromatography on silica gel using Hex/EtOAc as eluent (4:1). $^1\text{H NMR}$ (500 MHz, CDCl_3) δ 9.84 (s, 2H), 8.71 (s, 2H), 8.21 (s, 2H), 8.04 - 7.85 (m, 14H), 7.62 - 7.54 (m, 6H), 7.54 - 7.47 (m, 4H), 7.44 (app t, $J = 7.2$ Hz, 4H), 7.16 (d, $J = 8.4$ Hz, 2H), 7.10 (d, $J = 8.5$ Hz, 2H), 7.03 (dd, $J = 16.2, 7.0$ Hz, 4H), 2.70 (t, $J = 7.2$ Hz, 4H), 1.76 - 1.61 (m, 4H), 1.45 - 1.24 (m, 20H), 0.94 (t, $J = 6.7$ Hz, 6H). $^{13}\text{C NMR}$ (126 MHz, CDCl_3) δ 150.21, 146.61, 138.08, 134.06, 134.04, 133.31, 133.28, 132.39, 130.72, 130.67, 129.99, 129.95, 129.19, 129.17, 128.80, 128.54, 127.55, 127.52, 126.49, 126.46, 126.44, 126.39, 126.23, 125.90, 125.44, 124.71, 122.82,

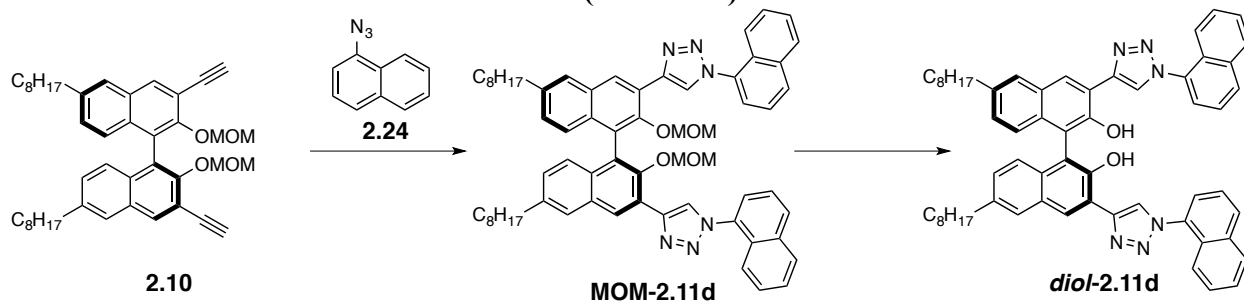
121.89, 116.95, 116.51, 62.75, 35.84, 31.97, 31.24, 29.58, 29.38, 29.33, 22.75, 14.21. **HRMS** (ESI) found $[M+H]^+$ 1176.6118, $C_{82}H_{77}N_6O_4$ requires 1177.6103.

(4*R*,11*S*)-2,6-bis(1-(di(naphthalen-1-yl)methyl)-1*H*-1,2,3-triazol-4-yl)-4-hydroxy-9,14-dioctyldinaphtho[2,1-*d*:1',2'-*f*][1,3,2]dioxaphosphepine 4-oxide (2.11c)



Subjection of diol **diol-2.11c** (0.280 g, 0.236 mmol) to General Procedure C gave the title compound (0.132 g, 0.106 mmol, 45 % yield) as a beige solid after purification by column chromatography on silica gel using DCM/MeOH as eluent (20:1). **¹H NMR** (500 MHz, $CDCl_3$: DMSO, 1:1) δ 8.76 (s, 2H), 8.49 (s, 2H), 8.02 (d, $J = 6.3$ Hz, 2H), 7.99 - 7.81 (m, 10H), 7.76 (s, 2H), 7.56 - 7.44 (m, 6H), 7.40 (app t, $J = 6.9$ Hz, 4H), 7.35 (app t, $J = 7.2$ Hz, 2H), 7.08 (app s, 4H), 7.06 - 6.92 (m, 4H), 2.69 (t, $J = 7.7$ Hz, 4H), 1.72 - 1.55 (m, 4H), 1.37 - 1.15 (m, 20H), 0.84 (t, $J = 6.5$ Hz, 6H). **¹³C NMR** (126 MHz, $CDCl_3$: DMSO, 1:1) δ 143.73 (d, $J = 9.9$ Hz), 142.08, 140.60, 134.31, 133.94, 133.87, 131.39, 130.76, 130.57, 130.24, 129.69, 129.37, 129.17, 129.14, 129.00, 128.64, 127.99, 127.49, 127.24, 127.11, 126.82, 126.54, 126.45, 126.33, 126.18, 125.69, 125.68, 125.34, 123.30, 123.04, 122.88, 122.59, 61.75, 35.65, 31.80, 31.06, 29.38, 29.28, 29.20, 22.62, 14.31. **³¹P NMR** (202 MHz, $CDCl_3$: DMSO, 1:1) δ 1.35. **HRMS** (ESI) found $[M-H]^-$ 1237.5513, $C_{82}H_{74}N_6O_4P_1$ requires 1237.5515.

(*S*)-3,3'-bis(1-(naphthalen-1-yl)-1*H*-1,2,3-triazol-4-yl)-6,6'-dioctyl-[1,1'-binaphthalene]-2,2'-diol (diol-2.11d)

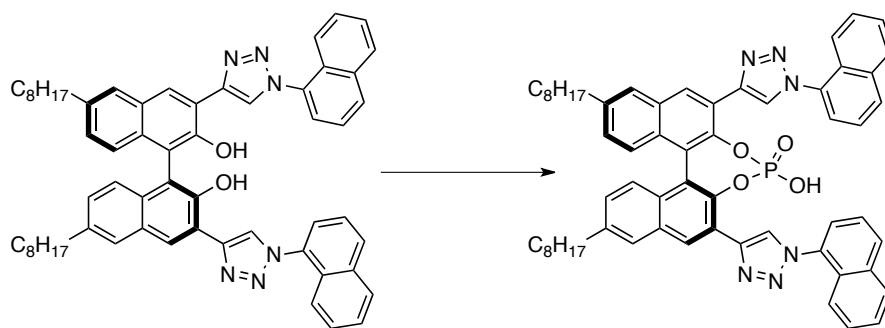


Subjection of *bis*-alkyne **2.10** (0.500 g, 0.773 mmol) to General Procedure Bi-Bii, gave intermediate **MOM-2.11d** (0.585 g, 0.594 mmol, 77 % yield) as an orange solid after purification by column chromatography on silica gel using Hex/ Et_2O as eluent (5:2). **¹H NMR** (400 MHz, $CDCl_3$) δ 9.04 (s, 2H), 8.71 (s, 2H), 8.02 (d, $J = 7.6$ Hz, 2H), 7.96 (d, $J = 7.6$ Hz, 2H), 7.83 (s, 2H), 7.79 (d, $J = 7.6$ Hz, 2H), 7.65 (d, $J = 7.2$ Hz, 2H), 7.60 - 7.52 (m, 6H), 7.26 (d, $J = 7.6$ Hz, 2H),

7.21 (d, $J = 7.6$ Hz, 2H), 4.67 (d, $J = 4.8$ Hz, 2H), 4.45 (d, $J = 4.8$ Hz, 2H), 2.78 (t, $J = 7.8$ Hz, 4H), 2.69 (s, 6H), 1.76-1.69 (m, 4H), 1.43-1.21 (m, 20H), 0.88 (t, $J = 6.7$ Hz, 6H).

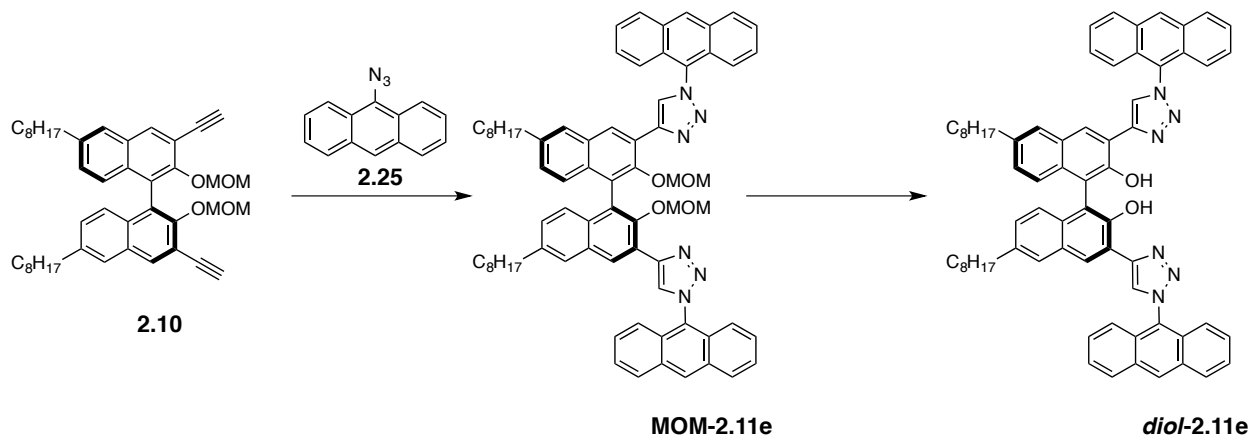
Subjection of **MOM-2.11d** (0.530 g, 0.538 mmol) to General Procedure Biii gave the title compound (0.480 g, 0.535 mmol, 99 % yield) as a brown solid after purification by column chromatography on silica gel using EtOAc/Hex as eluent (0 to 40 %). $^1\text{H NMR}$ (500 MHz, CDCl_3) δ 9.45 (s, 2H), 8.49 (d, $J = 11.8$ Hz, 4H), 8.05 (d, $J = 8.2$ Hz, 2H), 7.98 (d, $J = 7.5$ Hz, 2H), 7.74 (d, $J = 8.1$ Hz, 2H), 7.70 (s, 2H), 7.65 (d, $J = 7.0$ Hz, 2H), 7.63 - 7.53 (m, 6H), 7.26 (d, $J = 8.5$ Hz, 2H), 7.17 (d, $J = 8.8$ Hz, 2H), 2.75 (t, $J = 7.7$ Hz, 4H), 1.79 - 1.64 (m, 4H), 1.54 - 1.14 (m, 20H), 0.92 (t, $J = 6.7$ Hz, 6H). $^{13}\text{C NMR}$ (126 MHz, CDCl_3) δ 150.20, 146.34, 138.38, 134.17, 133.48, 132.40, 130.66, 128.96, 128.81, 128.46, 128.34, 128.09, 127.19, 126.78, 126.45, 125.04, 124.75, 123.92, 123.71, 122.29, 117.13, 116.10, 35.91, 31.96, 31.36, 29.59, 29.50, 29.35, 22.73, 14.18. **HRMS** (ESI) found $[\text{M}+\text{H}]^+$ 897.4861, $\text{C}_{60}\text{H}_{61}\text{N}_6\text{O}_2$ requires 897.4851.

(4*R*,11*bS*)-4-hydroxy-2,6-bis(1-(naphthalen-1-yl)-1*H*-1,2,3-triazol-4-yl)-9,14-dioctyldinaphtho[2,1-*d*:1',2'-*f*][1,3,2]dioxaphosphine 4-oxide (2.11d)



Subjection of diol **diol-2.11d** (0.090 g, 0.100 mmol) to General Procedure C gave the title compound (0.041 g, 0.043 mmol, 43 % yield) as a yellow solid after purification by column chromatography on silica gel using DCM/MeOH as eluent (20:1). $^1\text{H NMR}$ (500 MHz, DMSO) δ 9.15 (s, 2H), 8.82 (s, 2H), 8.22 (d, $J = 8.2$ Hz, 2H), 8.14 (d, $J = 8.1$ Hz, 2H), 7.98 (s, 2H), 7.81 (d, $J = 7.1$ Hz, 2H), 7.73 (app t, $J = 7.7$ Hz, 2H), 7.70 - 7.63 (m, 4H), 7.63 - 7.43 (m, 2H), 7.22 (d, $J = 8.9$ Hz, 2H), 7.12 (d, $J = 8.7$ Hz, 2H), 2.76 (t, $J = 7.6$ Hz, 4H), 1.81 - 1.59 (m, 4H), 1.44 - 1.15 (m, 20H), 0.86 (t, $J = 6.6$ Hz, 6H). $^{13}\text{C NMR}$ (126 MHz, DMSO) δ 164.54, 145.99, 145.96, 139.85, 134.08, 133.78, 130.91, 130.71, 130.41, 128.55, 128.27, 128.16, 128.10, 127.59, 127.30, 127.02, 126.63, 125.43, 123.74, 123.64, 123.18, 122.67, 35.70, 31.84, 31.21, 29.44, 29.38, 29.26, 22.66, 14.37. $^{31}\text{P NMR}$ (162 MHz, DMSO) δ 4.52. **HRMS** (ESI) found $[\text{M}-\text{H}]^-$ 957.4247, $\text{C}_{60}\text{H}_{58}\text{N}_6\text{O}_4\text{P}_1$ requires 957.4263.

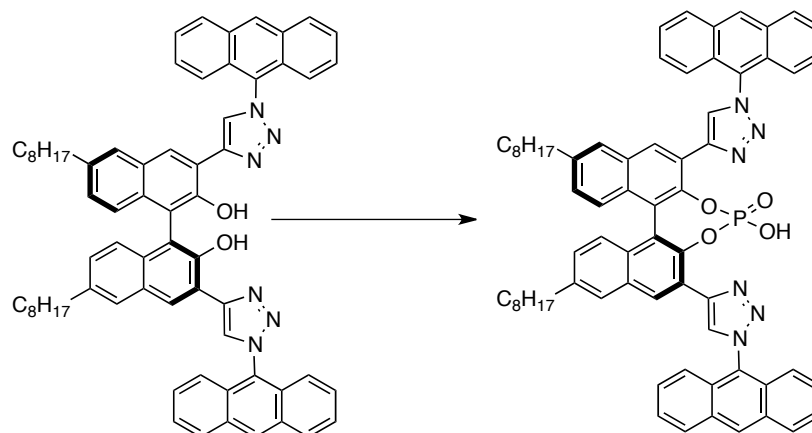
(S)-3,3'-bis(1-(anthracen-9-yl)-1*H*-1,2,3-triazol-4-yl)-6,6'-dioctyl-[1,1'-binaphthalene]-2,2'-diol (*diol-2.11e*)



Subjection of *bis*-alkyne **2.10** (0.500 g, 0.773 mmol) to General Procedure Bi-Bii, gave intermediate **MOM-2.11e** (0.639 g, 0.589 mmol, 76 % yield) as a yellow solid after purification by flash column chromatography on silica gel using EtOAc/Hex as eluent (0 to 25 %). $^1\text{H NMR}$ (400 MHz, CDCl_3) δ 9.11 (s, 2H), 8.72 (s, 2H), 8.66 (s, 2H), 8.15 - 7.99 (m, 4H), 7.85 (s, 2H), 7.57 - 7.38 (m, 12H), 7.30 (d, $J = 8.8$ Hz, 2H), 7.22 (d, $J = 8.8$ Hz, 2H), 4.67 (d, $J = 5.1$ Hz, 2H), 4.50 (d, $J = 5.1$ Hz, 2H), 2.79 (t, $J = 7.7$ Hz, 4H), 2.67 (s, 6H), 1.81 - 1.67 (m, 4H), 1.49 - 1.20 (m, 20H), 0.88 (t, $J = 6.8$ Hz, 6H).

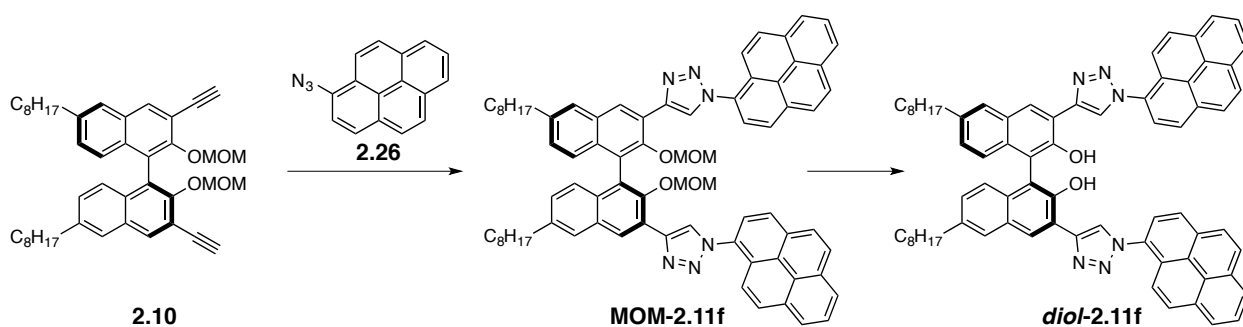
Subjection of **S1e-i** (0.300 g, 0.276 mmol) to General Procedure Biii gave the title compound (0.273 g, 0.274 mmol, 99 %) as an orange solid after recrystallization from CHCl_3/Hex . $^1\text{H NMR}$ (300 MHz, CDCl_3) δ 9.47 (s, 2H), 8.73 (s, 2H), 8.58 (s, 2H), 8.56 (s, 2H), 8.20 - 8.08 (m, 4H), 7.71 (d, $J = 1.4$ Hz, 2H), 7.65 - 7.51 (m, 8H), 7.45 (dd, $J = 10.3, 7.2$ Hz, 4H), 7.29 (d, $J = 8.4$ Hz, 2H), 7.19 (d, $J = 8.4$ Hz, 2H), 2.74 (t, $J = 7.7$ Hz, 4H), 1.82 - 1.61 (m, 4H), 1.46 - 1.18 (m, 20H), 0.86 (t, $J = 6.0$ Hz, 6H). $^{13}\text{C NMR}$ (151 MHz, CDCl_3) δ 150.26, 146.55, 138.40, 132.48, 131.11, 130.04, 129.01, 128.83, 128.40, 128.28, 128.21, 127.96, 126.72, 126.48, 126.02, 125.61, 124.78, 121.97, 117.11, 116.21, 35.86, 31.89, 31.28, 29.52, 29.41, 29.27, 22.66, 14.10. **HRMS** (ESI) found $[\text{M}-\text{H}]^-$ 997.5184, $\text{C}_{68}\text{H}_{65}\text{N}_6\text{O}_2$ requires 997.5164.

(4*R*,11*bS*)-2,6-bis(1-(anthracen-9-yl)-1*H*-1,2,3-triazol-4-yl)-4-hydroxy-9,14-dioctyldinaphtho[2,1-*d*:1',2'-*f*][1,3,2]dioxaphosphepine 4-oxide (2.11e)



Subjection of diol **diol-2.11e** (0.150 g, 0.150 mmol) to General Procedure C gave the title compound (0.136 g, 0.128 mmol, 85 % yield) as a yellow solid after purification by column chromatography on silica gel using DCM/MeOH as eluent (30:1 to 20:1). $^1\text{H NMR}$ (600 MHz, DMSO) δ 9.04 (s, 2H), 8.98 (d, J = 10.1 Hz, 4H), 8.26 (d, J = 8.3 Hz, 4H), 8.03 (s, 2H), 7.67 - 7.51 (m, 8H), 7.38 (d, J = 8.8 Hz, 2H), 7.34 (d, J = 8.6 Hz, 2H), 7.26 (d, J = 8.7 Hz, 2H), 7.20 (d, J = 8.6 Hz, 2H), 2.75 (t, J = 7.5 Hz, 4H), 1.77 - 1.58 (m, 4H), 1.42 - 1.10 (m, 20H), 0.83 (t, J = 6.6 Hz, 6H). $^{13}\text{C NMR}$ (151 MHz, DMSO) δ 144.78 (d, J = 9.5 Hz), 142.44, 139.86, 130.86, 130.69, 130.13, 129.98, 128.71, 128.55, 128.46, 128.40, 127.81, 127.78, 127.59, 127.11, 126.16, 126.06, 122.95, 122.57, 121.61, 54.90, 35.00, 31.28, 30.57, 28.87, 28.76, 28.69, 22.10, 13.93. $^{31}\text{P NMR}$ (162 MHz, DMSO) δ 2.93. **HRMS** (ESI) found $[\text{M}-\text{H}]^-$ 1057.4543, $\text{C}_{68}\text{H}_{62}\text{N}_6\text{O}_2\text{P}$ requires 1057.4552.

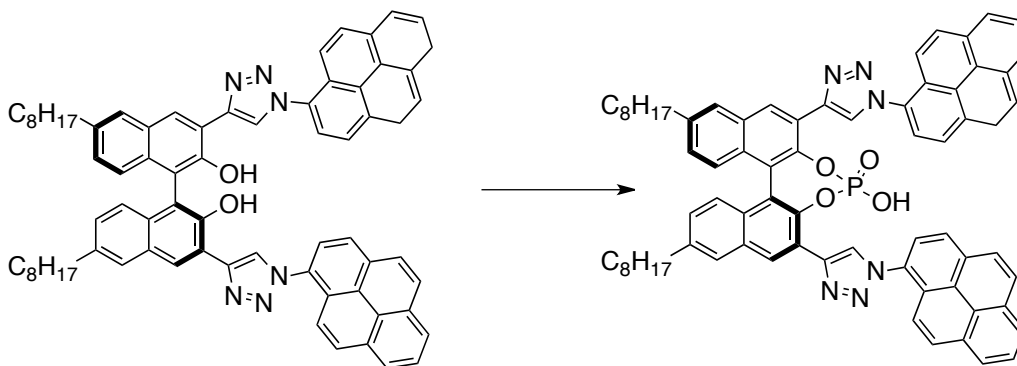
(*S*)-6,6'-dioctyl-3,3'-bis(1-(pyren-2-yl)-1*H*-1,2,3-triazol-4-yl)-[1,1'-binaphthalene]-2,2'-diol (diol-2.11f**)**



Subjection of *bis*-alkyne **2.10** (0.200 g, 0.309 mmol) to General Procedure Bi-Bii, gave intermediate **MOM-2.11f** (0.235 g, 0.207 mmol, 67 % yield) as a dark green solid after purification by column chromatography on silica gel using $\text{Et}_2\text{O}/\text{Hex}$ as eluent (0 to 50 %). $^1\text{H NMR}$ (400 MHz, CDCl_3) δ 9.09 (s, 2H), 8.87 (s, 2H), 8.34 - 8.25 (m, 4H), 8.25 - 8.19 (m, 2H), 8.18 (s, 2H), 8.16 - 8.10 (m, 6H), 8.10 - 7.99 (m, 4H), 7.86 (s, 2H), 7.30 (d, J = 8.8 Hz, 2H), 7.23 (d, J = 8.8 Hz, 2H), 4.73 (d, J = 5.0 Hz, 2H), 4.51 (d, J = 5.0 Hz, 2H), 2.80 (t, J = 7.6 Hz, 4H), 2.74 (s, 6H), 1.85 - 1.67 (m, 4H), 1.48 - 1.19 (m, 20H), 0.89 (t, J = 6.5 Hz, 6H).

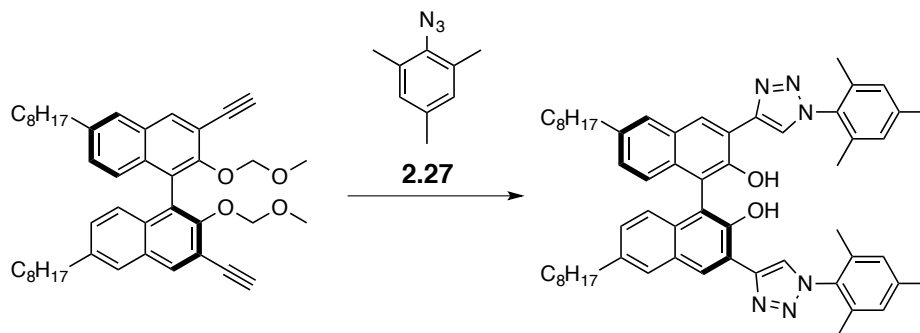
Subjection of **diol-2.11f** (0.200 g, 0.176 mmol) to General Procedure Biii gave the title compound (0.183 g, 0.175 mmol, 99 % yield) as a green solid after purification by column chromatography on silica gel using EtOAc/Hex as eluent (0 to 40 %). $^1\text{H NMR}$ (300 MHz, CDCl_3) δ 9.36 (s, 2H), 8.65 (s, 2H), 8.56 (s, 2H), 8.38 - 8.05 (m, 16H), 7.96 (d, $J = 9.2$ Hz, 2H), 7.72 (s, 2H), 7.27 (d, $J = 8.7$ Hz, 2H), 7.18 (d, $J = 8.7$ Hz, 2H), 2.73 (t, $J = 7.7$ Hz, 4H), 1.79 - 1.62 (m, 4H), 1.44 - 1.14 (m, 20H), 0.86 (t, $J = 6.4$ Hz, 6H). $^{13}\text{C NMR}$ (126 MHz, CDCl_3) δ 150.40, 146.50, 138.33, 132.54, 132.14, 130.90, 130.43, 129.92, 129.70, 128.95, 128.89, 126.86, 126.82, 126.66, 126.55, 126.37, 126.04, 125.83, 124.87, 124.76, 124.66, 124.31, 123.87, 123.17, 120.86, 117.23, 116.39, 35.95, 32.01, 31.41, 29.65, 29.60, 29.41, 22.78, 14.25. **HRMS** (ESI) found $[\text{M}+\text{H}]^+$ 1045.5168, $\text{C}_{72}\text{H}_{65}\text{N}_6\text{O}_2$ requires 1045.5164.

(4*R*,11*cS*)-2-(1-(4,6-dihydropyren-1-yl)-1*H*-1,2,3-triazol-4-yl)-4-hydroxy-9,14-dioctyl-6-(1-(pyren-1-yl)-1*H*-1,2,3-triazol-4-yl)dinaphtho[2,1-*d*:1',2'-*f*][1,3,2]dioxaphosphepine 4-oxide (2.11f)



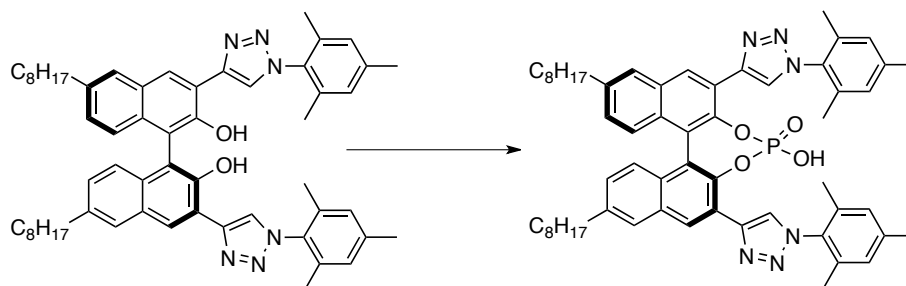
Subjection of diol **diol-2.11f** (0.150 g, 0.143 mmol) to General Procedure C gave the title compound (0.105 g, 0.095 mmol, 66 % yield) as a green solid after purification by column chromatography on silica gel using MeOH/DCM as eluent (0 to 5 %). $^1\text{H NMR}$ (400 MHz, DMSO) δ 9.28 (s, 2H), 8.90 (s, 2H), 8.50 (d, $J = 7.6$ Hz, 2H), 8.44 (d, $J = 7.4$ Hz, 2H), 8.41 - 8.22 (m, 10H), 8.16 (t, $J = 7.6$ Hz, 2H), 8.02 (s, 2H), 7.96 (d, $J = 9.3$ Hz, 2H), 7.26 (d, $J = 8.7$ Hz, 2H), 7.17 (d, $J = 8.7$ Hz, 2H), 2.78 (t, $J = 7.5$ Hz, 4H), 1.85 - 1.60 (m, 4H), 1.47 - 1.14 (m, 20H), 0.86 (t, $J = 5.8$ Hz, 6H). $^{13}\text{C NMR}$ (151 MHz, DMSO) δ 145.43 (d, $J = 7.9$ Hz), 142.64, 139.45, 131.58, 130.59, 130.19, 130.02, 129.99, 129.70, 128.73, 128.15, 127.41, 126.99, 126.48, 126.07, 126.03, 125.14, 125.07, 124.00, 123.51, 123.19, 122.68, 120.76, 34.97, 31.25, 30.55, 28.84, 28.76, 28.66, 22.07, 13.93. $^{31}\text{P NMR}$ (162 MHz, DMSO) δ 4.13. **HRMS** (ESI) found $[\text{M}-\text{H}]^-$ 1105.4553, $\text{C}_{72}\text{H}_{62}\text{N}_6\text{O}_4\text{P}$ requires 1105.4576.

(S)-3,3'-Bis(1-mesityl-1*H*-1,2,3-triazol-4-yl)-6,6'-dioctyl-[1,1'-binaphthalene]-2,2'-diol (diol-2.11g)



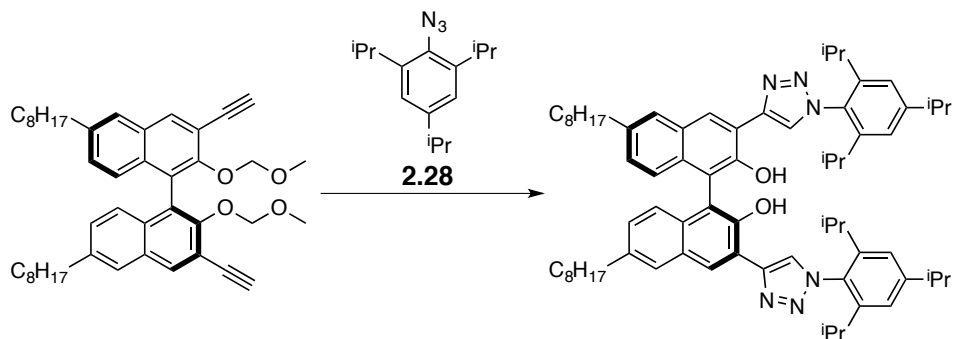
Subjection of *bis*-alkyne **2.10** (0.783 g, 1.20 mmol) and azide **2.27** (0.426 g, 2.64 mmol) to General Procedure A gave the title compound (0.157 g, 0.178 mmol, 15 % yield) as a yellow solid after purification by column chromatography on silica gel using Hex/EtOAc as eluent (4:1). ¹H NMR (500 MHz, CDCl₃) δ 9.69 (s, 2H), 8.43 (s, 2H), 8.21 (s, 2H), 7.70 (s, 2H), 7.22 (d, *J* = 8.5 Hz, 2H), 7.16 (d, *J* = 8.5 Hz, 2H), 7.06 (s, 4H), 2.81 - 2.67 (m, 4H), 2.41 (s, 6H), 2.07 (s, 12H), 1.79 - 1.64 (m, 4H), 1.42 - 1.21 (m, 20H), 0.89 (t, *J* = 6.6 Hz, 6H). ¹³C NMR (126 MHz, CDCl₃) δ 150.23, 146.58, 140.33, 138.27, 135.11, 133.28, 132.38, 129.20, 128.87, 128.68, 126.58, 126.04, 124.75, 122.85, 117.11, 116.34, 35.87, 31.92, 31.31, 29.55, 29.41, 29.31, 22.70, 21.21, 17.39, 14.14. HRMS (ESI) found [M+H]⁺ 881.5472, C₅₈H₆₉O₂N₆ requires 881.5477.

(4*R*,11*bS*)-4-Hydroxy-2,6-bis(1-mesityl-1*H*-1,2,3-triazol-4-yl)-9,14-dioctyldinaphtho[2,1-*d*:1',2'-*f*][1,3,2]dioxaphosphepine 4-oxide (2.11g)



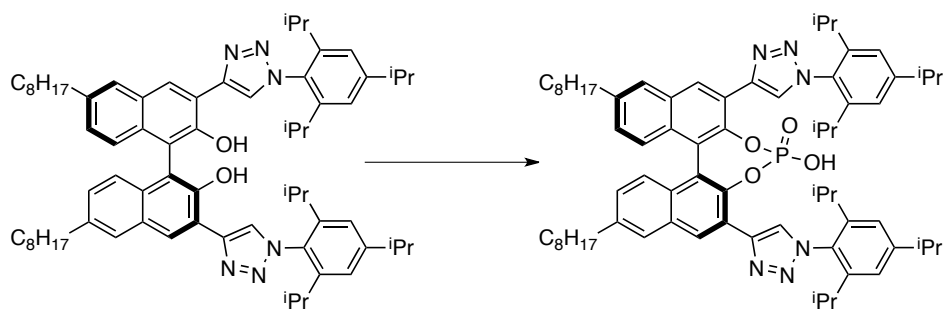
Subjection of diol **diol-2.11g** (0.143 g, 0.162 mmol) to General Procedure C gave the title compound (0.113 g, 0.119 mmol, 74 % yield) as a yellow solid after purification by column chromatography on silica gel using DCM/MeOH as eluent (20:1 to 10:1). ¹H NMR (400 MHz, CDCl₃: DMSO, 1:1) δ 8.75 (s, 2H), 8.69 (s, 2H), 7.92 (s, 2H), 7.17 (d, *J* = 8.7 Hz, 2H), 7.10 (s, 4H), 7.06 (d, *J* = 8.5 Hz, 2H), 2.88 - 2.58 (m, 4H), 2.31 (s, 6H), 1.94 (s, 12H), 1.75 - 1.49 (m, 4H), 1.42 - 1.05 (m, 20H), 0.81 (t, *J* = 6.4 Hz, 6H). ¹³C NMR (126 MHz, CDCl₃: DMSO, 1:1) δ 145.57 (d, *J* = 8.9 Hz), 139.81, 139.74, 134.99, 133.78, 131.85, 131.02, 130.52, 129.18, 128.18, 127.36, 127.08, 126.59, 123.66, 123.04. ³¹P NMR (162 MHz, CDCl₃: DMSO, 1:1) δ 3.26. HRMS (ESI) found [M-H]⁻ 941.4854, C₅₈H₆₆O₄N₆P₁ requires 941.4889.

(S)-6,6'-Dioctyl-3,3'-bis(1-(2,4,6-triisopropylphenyl)-1H-1,2,3-triazol-4-yl)-[1,1'-binaphthalene]-2,2'-diol (diol-2.11h)



Subjection of *bis*-alkyne **2.10** (0.320 g, 0.494 mmol) and azide **2.28** (0.267 g, 1.09 mmol) to General Procedure A gave the title compound (0.328 g, 0.313 mmol, 63 % yield) as a yellow solid after purification by column chromatography on silica gel using Hex/EtOAc as eluent (4:1). ¹H NMR (500 MHz, CDCl₃) δ 9.84 (s, 2H), 8.42 (s, 2H), 8.23 (s, 2H), 7.71 (s, 2H), 7.23 (d, *J* = 8.5 Hz, 2H), 7.19 (s, 4H), 7.16 (d, *J* = 8.5 Hz, 2H), 3.03 (sept, *J* = 7.0 Hz, 2H), 2.79 - 2.71 (m, 4H), 2.48 - 2.26 (m, 4H), 1.77 - 1.65 (m, 4H), 1.35 (d, *J* = 6.8 Hz, 24H), 1.31 (d, *J* = 6.8 Hz, 12H), 1.24 - 1.18 (m, 20H), 0.90 (t, *J* = 6.7 Hz, 6H). ¹³C NMR (126 MHz, CDCl₃) δ 151.81, 150.35, 146.48, 145.86, 145.77, 138.26, 132.49, 130.78, 128.88, 128.68, 126.59, 126.01, 124.81, 123.89, 121.90, 121.87, 117.10, 116.57, 35.91, 34.56, 31.95, 31.36, 29.58, 29.43, 29.33, 28.58, 28.55, 24.36, 24.31, 24.16, 24.05, 22.73, 14.18. HRMS (ESI) found [M+H]⁺ 1049.7347, C₇₀H₉₃O₂N₆ requires 1049.7355.

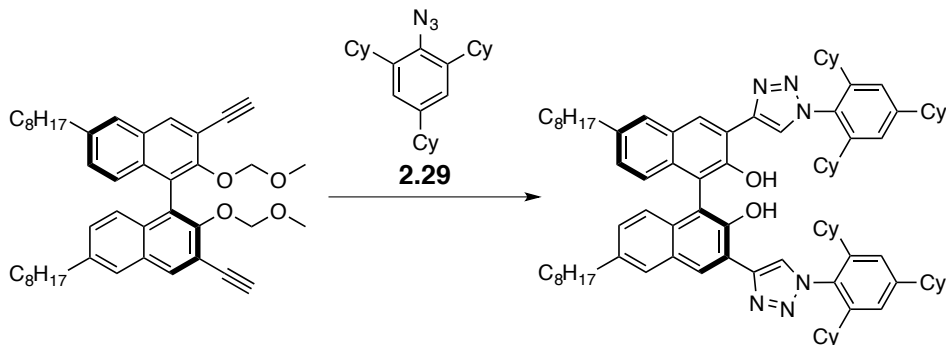
(4R,11bS)-4-Hydroxy-9,14-dioctyl-2,6-bis(1-(2,4,6-triisopropylphenyl)-1H-1,2,3-triazol-4-yl)dinaphtho[2,1-d':1',2'-f][1,3,2]dioxaphosphepine 4-oxide (2.11h)



Subjection of diol **diol-2.11h** (0.230 g, 0.219 mmol) to General Procedure C gave the title compound (0.240 g, 0.216 mmol, 99 % yield) as an orange solid after purification by column chromatography on silica gel using Hex/EtOAc (1:1) with 1 % TFA as eluent. ¹H NMR (400 MHz, DMSO) δ 8.79 (s, 2H), 8.73 (s, 2H), 7.92 (s, 2H), 7.22 (s, 4H), 7.17 (d, *J* = 8.7 Hz, 2H), 7.05 (d, *J* = 8.7 Hz, 2H), 2.95 (sept, *J* = 6.8 Hz, 2H), 2.81 - 2.66 (m, 4H), 2.35 - 2.20 (m, 2H), 2.20 - 2.07 (m, 2H), 1.81 - 1.50 (m, 4H), 1.46 - 1.16 (m, 26H), 1.16 - 0.91 (m, 20H), 0.81 (t, *J* = 6.5 Hz, 6H). ¹³C NMR (151 MHz, DMSO) δ 151.71 (d, *J* = 3.6 Hz), 145.69, 145.59, 139.89, 131.24, 131.01, 130.44, 128.51, 128.34, 127.63, 127.39, 126.42, 123.58, 122.94, 122.07, 122.05, 35.38, 34.22, 31.68, 30.97, 29.26, 29.14, 29.09, 28.53, 28.45, 24.30, 24.26, 24.23, 24.14, 22.50, 14.35.

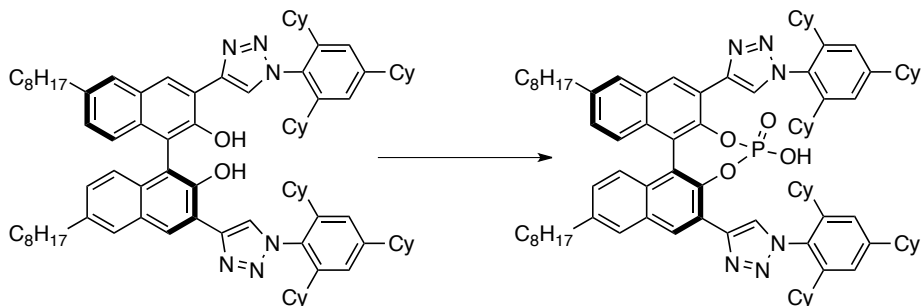
^{31}P NMR (162 MHz, DMSO) δ 4.20. HRMS (ESI) found $[\text{M}+\text{H}]^+$ 1111.6904, $\text{C}_{70}\text{H}_{92}\text{O}_4\text{N}_6\text{P}_1$ requires 1111.6912.

(S)-6,6'-Dioctyl-3,3'-bis(1-(2,4,6-tricyclohexylphenyl)-1H-1,2,3-triazol-4-yl)-[1,1'-binaphthalene]-2,2'-diol (diol-2.11i)



Subjection of *bis*-alkyne **2.10** (0.380 g, 0.586 mmol) and azide **2.29** (0.472 g, 1.29 mmol) to General Procedure A gave the title compound (0.300 g, 0.232 mmol, 40 % yield) as a yellow solid after purification by column chromatography on silica gel using Hex/Et₂O as eluent (20:1). ^1H NMR (300 MHz, CDCl₃) δ 10.25 (s, 2H), 8.34 (s, 2H), 8.16 (s, 2H), 7.69 (s, 2H), 7.24 (d, J = 8 Hz 2H), 7.17-7.13 (m, 6H), 2.72 (app t, J = 8 Hz, 4H), 2.63-2.34 (m, 6H), 1.47-1.19 (m, 86H), 0.87 (t, J = 8 Hz, 6H). ^{13}C NMR (126 MHz, CDCl₃) δ 150.58, 150.54, 146.61, 144.87, 144.75, 138.18, 132.52, 130.85, 128.82, 128.56, 126.50, 125.80, 124.85, 123.44, 123.03, 122.99, 117.06, 116.90, 44.95, 39.17, 35.90, 34.87, 34.70, 34.66, 34.46, 33.15, 31.93, 31.35, 29.55, 29.39, 29.30, 27.27, 27.12, 26.88, 26.67, 26.59, 26.54, 26.50, 26.46, 26.29, 26.13, 25.95, 22.70, 14.14. HRMS (ESI) found $[\text{M}+\text{H}]^+$ 1289.9248, $\text{C}_{88}\text{H}_{117}\text{O}_2\text{N}_6$ requires 1289.9233.

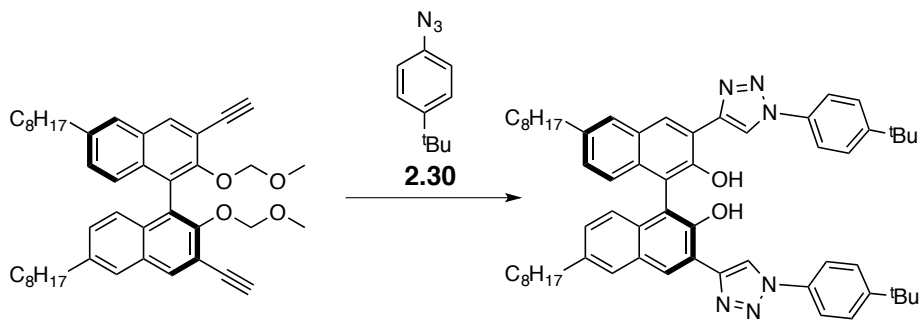
(4R,11bS)-4-Hydroxy-9,14-dioctyl-2,6-bis(1-(2,4,6-tricyclohexylphenyl)-1H-1,2,3-triazol-4-yl)dinaphtho[2,1-d:1',2'-f][1,3,2]dioxaphosphine 4-oxide (2.11i)



Subjection of diol **diol-2.11i** (0.271 g, 0.210 mmol) to General Procedure C gave the title compound (0.250 g, 0.185 mmol, 88 % yield) as a beige solid after purification by column chromatography on silica gel using Hex/EtOAc (1:1) with 0.5 % TFA as eluent. ^1H NMR (400 MHz, CDCl₃: DMSO, 1:1) δ 8.76 (s, 2H), 8.74 (s, 2H), 7.96 (s, 2H), 7.19 - 7.13 (m, 4H), 7.09 (d, J = 8.4 Hz, 2H), 7.03 (s, 2H) 2.92 - 2.66 (m, 4H), 2.65 - 2.50 (m, 6H), 2.05 - 0.89 (m, 84H), 0.81 (t, J = 6.4 Hz, 6H). ^{13}C NMR (126 MHz, CDCl₃: DMSO, 1:1) δ 148.22, 142.82, 142.62, 137.95, 129.57, 129.15, 128.55, 126.31, 126.01, 125.10, 124.73, 121.69, 121.35, 120.99, 120.92, 120.83, 42.76, 42.31, 37.15, 36.90, 35.73, 33.65, 32.74, 32.41, 32.38, 32.32, 31.99, 31.98, 31.92, 29.81,

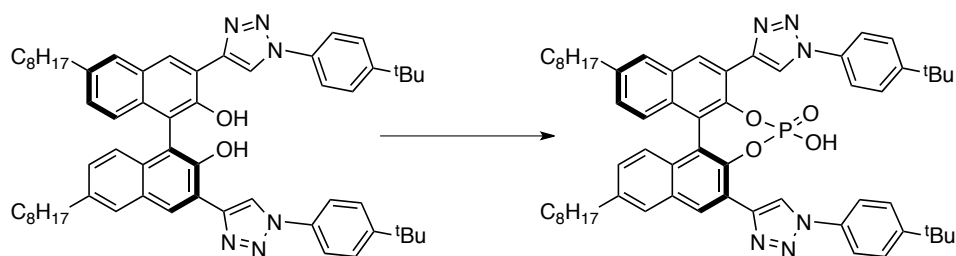
29.13, 27.40, 27.26, 27.21, 24.83, 24.78, 24.74, 24.64, 24.44, 24.03, 24.00, 23.95, 23.83, 20.62, 12.35. ^{31}P NMR (162 MHz, CDCl_3 : DMSO, 1:1) δ 9.16. HRMS (ESI) found $[\text{M}-\text{H}]^-$ 1349.8649, $\text{C}_{88}\text{H}_{114}\text{O}_2\text{N}_6\text{P}_1$ requires 1349.8645.

(S)-3,3'-bis(1-(4-(*tert*-butyl)phenyl)-1*H*-1,2,3-triazol-4-yl)-6,6'-dioctyl-[1,1'-binaphthalene]-2,2'-diol (diol-2.11j)



Subjection of *bis*-alkyne **2.10** (0.351 g, 0.541 mmol) and azide **2.30** (0.209 g, 1.19 mmol) to General Procedure A gave the title compound (0.210 g, 0.231 mmol, 43 % yield) as a yellow solid after purification by column chromatography on silica gel using Hex/EtOAc as eluent (10:1). ^1H NMR (500 MHz, CDCl_3) δ 9.30 (s, 2H), 8.55 (s, 2H), 8.46 (s, 2H), 7.76 (d, $J = 8.3$ Hz, 4H), 7.69 (s, 2H), 7.58 (d, $J = 8.4$ Hz, 4H), 7.18 (d, $J = 9.1$ Hz, 2H), 7.13 (d, $J = 9.1$ Hz, 2H), 2.72 (t, $J = 6.0$ Hz, 4H), 1.76 - 1.62 (m, 4H), 1.40 (s, 18H), 1.37 - 1.20 (m, 20H), 0.89 (t, $J = 6.5$ Hz, 6H). ^{13}C NMR (126 MHz, CDCl_3) δ 164.55, 152.47, 150.10, 138.36, 134.46, 132.28, 128.93, 128.75, 126.74, 126.69, 126.29, 124.69, 120.40, 119.19, 117.15, 115.93, 35.87, 34.86, 31.93, 31.31, 31.29, 29.55, 29.45, 29.31, 22.70, 14.15. HRMS (ESI) found $[\text{M}+\text{H}]^+$ 909.5801, $\text{C}_{60}\text{H}_{73}\text{N}_6\text{O}_2$ requires 909.5790.

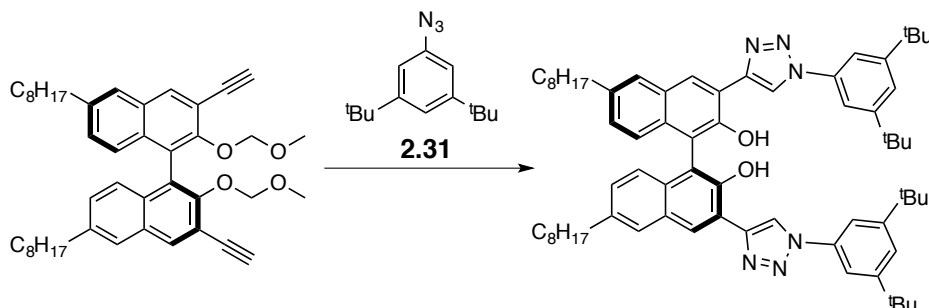
(4*R*,11*bS*)-2,6-bis(1-(4-(*tert*-butyl)phenyl)-1*H*-1,2,3-triazol-4-yl)-4-hydroxy-9,14-dioctyldinaphtho[2,1-*d*:1',2'-*f*][1,3,2]dioxaphosphepine 4-oxide (2.11j)



Subjection of diol **diol-2.11j** (0.181 g, 0.200 mmol) to General Procedure C gave the title compound (0.151 g, 0.155 mmol, 78 % yield) as a brown solid after purification by column chromatography on silica gel using Hex/EtOAc (1:1) with 1 % TFA as eluent. ^1H NMR (500 MHz, CDCl_3 : DMSO, 1:1) δ 8.98 (s, 2H), 8.73 (s, 2H), 7.79 (s, 2H), 7.69 (d, $J = 8.4$ Hz, 4H), 7.40 (d, $J = 8.1$ Hz, 4H), 7.11 (s, 4H), 2.72 (t, $J = 7.6$ Hz, 4H), 1.77 - 1.55 (m, 4H), 1.45 - 1.08 (m, 38H), 0.85 (t, $J = 6.3$ Hz, 6H). ^{13}C NMR (126 MHz, CDCl_3 : DMSO, 1:1) δ 164.54, 151.64, 144.42 (d, $J = 7.6$ Hz), 143.06, 140.32, 134.55, 131.23, 130.41, 128.54, 128.19, 127.15, 126.67, 122.97, 122.76, 122.25, 120.11, 35.68, 34.72, 31.83, 31.32, 31.10, 29.43, 29.38, 29.24, 22.64,

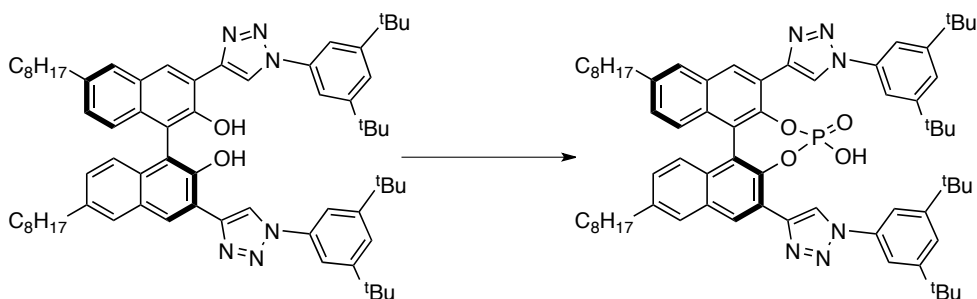
14.33. ^{31}P NMR (202 MHz, CDCl_3 : DMSO, 1:1) δ 3.50. HRMS (ESI) found $[\text{M}+\text{H}]^+$ 971.5355, $\text{C}_{60}\text{H}_{72}\text{N}_6\text{O}_4\text{P}_1$ requires 971.5347.

(S)-3,3'-bis(1-(3,5-di-*tert*-butylphenyl)-1*H*-1,2,3-triazol-4-yl)-6,6'-dioctyl-[1,1'-binaphthalene]-2,2'-diol (*diol*-2.11k)



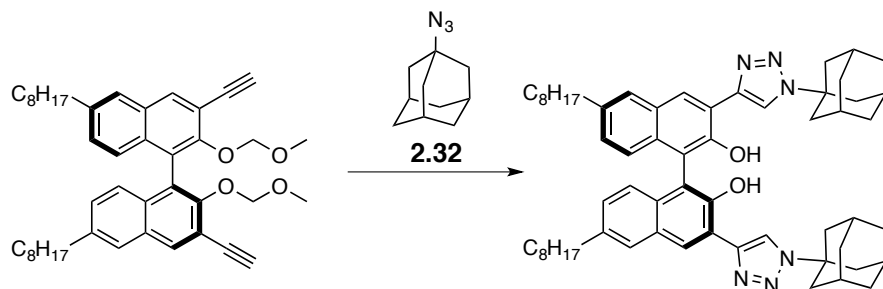
Subjection of *bis*-alkyne **2.10** (0.500 g, 0.771 mmol) and azide **2.31** (0.391 g, 1.69 mmol) to General Procedure A gave the title compound (0.409 g, 0.400 mmol, 52 % yield) as a yellow solid after purification by column chromatography on silica gel using Hex/EtOAc as eluent (20:1). ^1H NMR (300 MHz, CDCl_3) δ 9.60 (s, 2H), 8.56 (s, 2H), 8.43 (s, 2H), 7.67 (s, 2H), 7.63 (s, 4H), 7.56 (s, 2H), 7.21 (d, $J = 8.5$ Hz, 2H), 7.11 (d, $J = 8.5$ Hz, 2H), 2.71 (app t, $J = 7.4$ Hz, 4H), 1.79 - 1.58 (m, 4H), 1.48 - 1.17 (m, 56H), 0.87 (t, $J = 6.7$ Hz, 6H). ^{13}C NMR (75 MHz, CDCl_3) δ 153.22, 150.49, 147.26, 138.49, 136.89, 132.60, 129.09, 129.02, 126.95, 126.42, 124.93, 123.57, 119.75, 117.35, 116.47, 115.87, 36.13, 35.49, 32.20, 31.64, 31.56, 29.82, 29.71, 29.58, 22.96, 14.42. HRMS (ESI) found $[\text{M}+\text{H}]^+$ 1021.7058, $\text{C}_{68}\text{H}_{89}\text{N}_6\text{O}_2$ requires 1021.7042.

(4*R*,11*bS*)-2,6-bis(1-(3,5-di-*tert*-butylphenyl)-1*H*-1,2,3-triazol-4-yl)-4-hydroxy-9,14-dioctyldinaphtho[2,1-*d*:1',2'-*f*][1,3,2]dioxaphosphepine 4-oxide (2.11k**)**



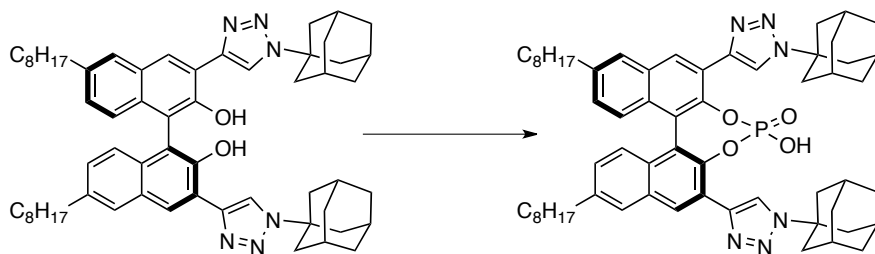
Subjection of diol **diol-2.11k** (0.352 g, 0.345 mmol) to General Procedure C gave the title compound (0.341 g, 0.315 mmol, 91 % yield) as a brown solid after purification by column chromatography on silica gel using Hex/EtOAc (1:1) with 1 % TFA as eluent. ^1H NMR (500 MHz, CDCl_3 : DMSO, 1:1) δ 9.01 (s, 2H), 8.80 (s, 2H), 7.85 (s, 2H), 7.64 (s, 4H), 7.50 (s, 2H), 7.21 (d, $J = 8.5$ Hz, 2H), 7.17 (t, $J = 8.5$ Hz, 2H), 2.74 (t, $J = 7.2$ Hz, 4H), 1.80 - 1.62 (m, 4H), 1.45 - 1.08 (m, 56H), 0.84 (t, $J = 6.1$ Hz, 6H). ^{13}C NMR (126 MHz, CDCl_3 : DMSO, 1:1) δ 152.83, 144.05 (d, $J = 8.9$ Hz), 143.04, 140.63, 136.85, 131.44, 130.42, 128.75, 128.35, 127.22, 126.61, 122.95, 122.84, 122.73, 115.40, 35.70, 35.24, 31.82, 31.47, 31.11, 29.41, 29.33, 29.22, 22.63, 14.31. ^{31}P NMR (202 MHz, CDCl_3 : DMSO, 1:1) δ 2.35. HRMS (ESI) found $[\text{M}+\text{H}]^+$ 1083.6586, $\text{C}_{68}\text{H}_{88}\text{N}_6\text{O}_4\text{P}_1$ requires 1083.6599.

(S)-3,3'-bis(adamantan-1-yl-1*H*-1,2,3-triazol-4-yl)-6,6'-dioctyl-[1,1'-binaphthalene]-2,2'-diol (diol-2.111)



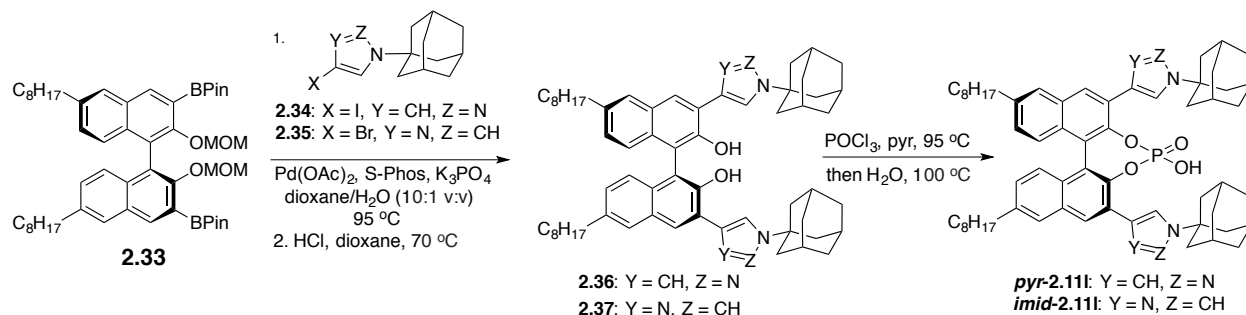
Subjection of *bis*-alkyne **2.10** (1.00 g, 1.54 mmol) and azide **2.32** (0.601 g, 3.39 mmol) to General Procedure A gave the title compound (0.900 g, 0.981 mmol, 64 % yield) as a brown solid after purification by column chromatography on silica gel using Hex/EtOAc as eluent (10:1). $^1\text{H NMR}$ (300 MHz, CDCl_3) δ 10.16 (s, 2H), 8.21 (s, 2H), 8.17 (s, 2H), 7.59 (s, 2H), 7.12 (d, $J = 8.7$ Hz, 2H), 7.05 (d, $J = 8.7$ Hz, 2H), 2.82 - 2.58 (m, 4H), 2.43 - 2.24 (m, 18H), 1.82 (s, 12H), 1.49 - 1.04 (m, 20H), 0.85 (t, $J = 6.3$ Hz, 6H). $^{13}\text{C NMR}$ (126 MHz, CDCl_3) δ 150.59, 146.30, 137.65, 132.33, 128.52, 128.29, 126.43, 125.27, 124.79, 117.32, 117.15, 117.05, 60.23, 59.06, 42.92, 41.56, 35.93, 35.86, 35.81, 31.97, 31.38, 29.84, 29.76, 29.62, 29.55, 29.50, 29.36, 22.74, 14.19. **HRMS** (ESI) found $[\text{M}+\text{H}]^+$ 913.6100, $\text{C}_{60}\text{H}_{77}\text{O}_2\text{N}_6$ requires 913.6103.

(4*R*,11*bS*)-4-hydroxy-2,6-bis(adamantan-1-yl-1*H*-1,2,3-triazol-4-yl)-9,14-dioctyldinaphtho[2,1-*d*:1',2'-*f*][1,3,2]dioxaphosphepine 4-oxide (2.111)



Subjection of diol **diol-2.111** (0.850 g, 0.927 mmol) to General Procedure C gave the title compound (0.882 g, 0.905 mmol, 98 % yield) as a brown solid after purification by column chromatography on silica gel using DCM/MeOH as eluent. (20:1). $^1\text{H NMR}$ (500 MHz, CDCl_3 : DMSO, 1:1) δ 8.70 (s, 2H), 8.56 (s, 2H), 7.80 (s, 2H), 7.11 (d, $J = 8.5$ Hz, 2H), 7.09 (d, $J = 8.5$ Hz, 2H), 2.81 - 2.62 (m, 4H), 2.34 - 2.13 (m, 18H), 1.77 (s, 12H), 1.70 - 1.52 (m, 4H), 1.44 - 1.11 (m, 20H), 0.83 (t, $J = 6.7$ Hz, 6H). $^{13}\text{C NMR}$ (126 MHz, CDCl_3 : DMSO, 1:1) δ 144.00 (d, $J = 9.6$ Hz), 141.28, 140.44, 131.35, 130.19, 128.54, 128.07, 127.15, 126.57, 123.23, 122.58, 120.91, 59.75, 42.87, 35.84, 35.62, 31.79, 31.09, 29.39, 29.37, 29.31, 29.19, 22.61, 14.33. $^{31}\text{P NMR}$ (202 MHz, CDCl_3 : DMSO, 1:1) δ 2.91. **HRMS** (ESI) found $[\text{M}+\text{H}]^+$ 975.5638, $\text{C}_{60}\text{H}_{76}\text{O}_2\text{N}_6\text{P}_1$ requires 975.5660.

Compounds *pyr*-**2.111** and *imid*-**2.111** were prepared according to the reaction sequence depicted in Scheme 2.7.



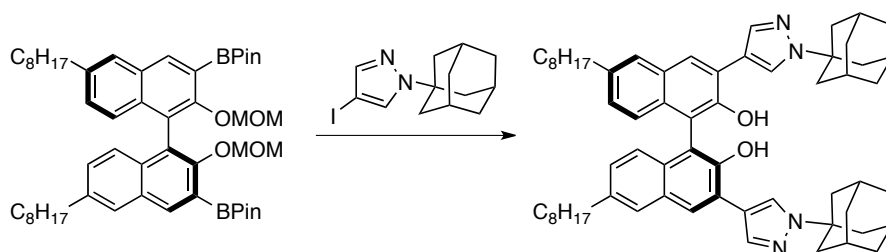
Scheme 2.7. Synthesis of *pyr*- and *imid*-2.111

1-((3*s*,5*s*,7*s*)-adamantan-1-yl)-4-iodo-1*H*-pyrazole (2.34)¹⁰⁸



To a magnetically stirred solution of iodic acid (0.176 g, 1.0 mmol) and iodine (0.302 g, 1.19 mmol) in carbon tetrachloride (0.5 mL), water (1 mL) and acetic acid (1 mL) was added 1-((3*s*,5*s*,7*s*)-adamantan-1-yl)-1*H*-pyrazole (0.750 g, 3.71 mmol).¹⁰⁹ The reaction mixture was heated at 50 °C for 12 h at which point TLC indicated complete consumption of the starting material. After being allowed to cool to room temperature, the reaction mixture was diluted with saturated aqueous Na₂SO₃ (3 mL) and then basified by 1 N NaOH. The resulting suspension was extracted with EtOAc (3 X 20 mL), dried and concentrated *in vacuo* to afford the title compound (0.925 g, 2.83 mmol, 76 % yield) as a white semi-solid. ¹H NMR (500 MHz, CDCl₃) δ 7.55 (s, 1H), 7.54 (s, 1H), 2.24 (s, 3H), 2.15 - 2.09 (m, 6H), 1.79 - 1.73 (m, 6H). ¹³C NMR (126 MHz, CDCl₃) δ 143.40, 129.61, 59.36, 54.96, 42.72, 36.05, 29.53. HRMS (ESI) found [M+H]⁺ 329.0512, C₁₃H₁₈N₂I requires 329.0509.

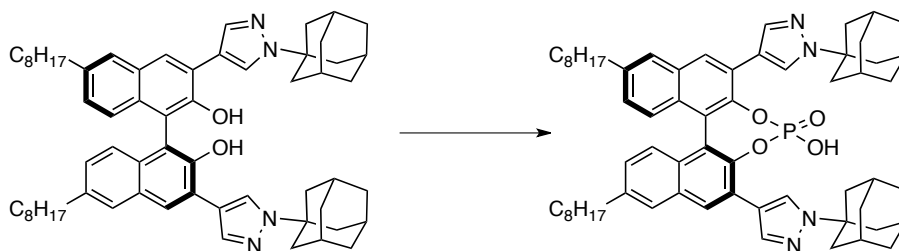
(*S*)-3,3'-bis(adamantan-1-yl)-1*H*-pyrazol-4-yl)-6,6'-dioctyl-[1,1'-binaphthalene]-2,2'-diol (2.36)



To a magnetically stirred solution of *bis*-boronate ester **2.33** (0.868 g, 1.02 mmol) and pyrazole **2.34** (0.900 g, 2.75 mmol) in 1,4-dioxane/H₂O (6.2/0.6 mL) were added Pd(OAc)₂ (0.011 g, 0.051 mmol), S-Phos (0.042 g, 0.102 mmol), and K₃PO₄ (0.650 g, 3.06 mmol). The reaction mixture was degassed under vacuum (3 X 30 s) and stirred at 95 °C for 15 h. The reaction mixture was allowed to cool to room temperature and then filtered through celite, dried (Na₂SO₄) and concentrated *in vacuo*. The crude residue was dissolved in 1,4-dioxane (20 mL) and concentrated HCl (2 mL) was added. The reaction mixture was stirred at 70 °C for 2 h, and then allowed to cool to room temperature and concentrated *in vacuo*. The residue was dissolved in DCM and washed

with saturated aqueous Na₂CO₃ (20 mL), H₂O (20 mL) and brine (20 mL). The organic extracts were dried (Na₂SO₄) and concentrated *in vacuo*. The crude residue was purified by column chromatography on silica gel using Hex/EtOAc as eluent (20:1 to 10:1) to afford the title compound (0.275 g, 0.302 mmol, 30 % yield) as a yellow solid. ¹H NMR (500 MHz, CDCl₃) δ 8.18 (s, 2H), 8.15 (s, 2H), 8.08 (s, 2H), 7.69 (s, 2H), 7.17 - 6.99 (m, 4H), 5.73 (s, 2H), 2.77 - 2.68 (m, 4H), 2.31 - 2.13 (m, 18H), 1.84 - 1.67 (m, 16H), 1.44 - 1.24 (m, 20H), 0.90 (t, *J* = 6.5 Hz, 6H). ¹³C NMR (126 MHz, CDCl₃) δ 149.52, 138.87, 137.47, 130.24, 129.76, 128.32, 126.71, 126.45, 125.26, 124.07, 122.07, 116.97, 111.95, 58.63, 42.83, 36.16, 35.92, 31.94, 31.42, 29.57, 29.54, 29.45, 29.32, 22.72, 14.17. HRMS (ESI) found [M-H]⁻ 909.6046, C₆₂H₇₇N₄O₂ requires 909.6052.

(4*R*,11*bS*)-4-hydroxy-2,6-bis(adamantan-1-yl-1*H*-pyrazol-4-yl)-9,14-dioctyldinaphtho[2,1-*d*:1',2'-*f*][1,3,2]dioxaphosphepine 4-oxide (pyr-2.111)



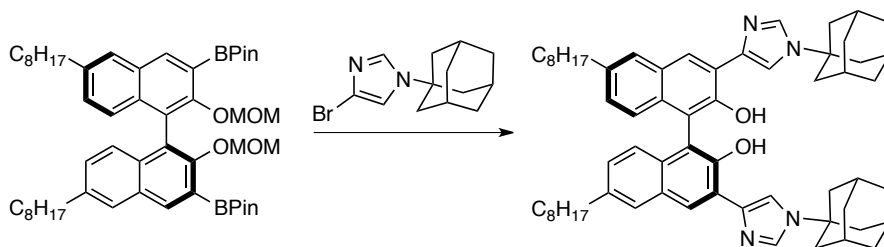
Subjection of diol **2.36** (0.080 g, 0.088 mmol) to General Procedure C gave the title compound (0.078 g, 0.080 mmol, 91 % yield) as a dark-yellow solid. ¹H NMR (400 MHz, DMSO) δ 8.32 (s, 2H), 8.14 (s, 2H), 8.04 (s, 2H), 7.66 (s, 2H), 7.01 (s, 4H), 2.65 (t, *J* = 7.6 Hz, 4H), 2.28 - 2.07 (m, 18H), 1.80 - 1.67 (m, 12H), 1.67 - 1.49 (m, 4H), 1.35 - 1.14 (m, 20H), 0.80 (t, *J* = 6.5 Hz, 6H). ¹³C NMR (126 MHz, DMSO) δ 164.54, 144.21 (d, *J* = 9.6 Hz), 140.11, 137.88, 131.65, 129.37, 127.68, 127.22, 126.56, 126.45, 125.59, 125.42, 122.68, 116.64, 58.62, 42.82, 36.12, 35.66, 31.81, 31.07, 29.47, 29.44, 29.40, 29.28, 29.20, 22.62, 14.34. ³¹P NMR (162 MHz, DMSO) δ 1.91. HRMS (ESI) found [M-H]⁻ 971.5584, C₆₂H₇₆N₄O₄P₁ requires 971.5610.

1-((3*s*,5*s*,7*s*)-adamantan-1-yl)-4-bromo-1*H*-imidazole (2.35)



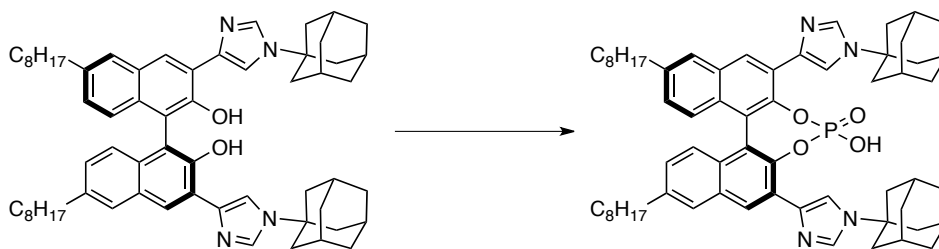
To a magnetically stirred solution of 1-((1*r*,3*R*,5*S*)-adamantan-1-yl)-1*H*-imidazole¹¹⁰ (0.782 g, 3.87 mmol) in DMF (40 mL) was added N-bromosuccinimide (0.757 g, 4.25 mmol) and the reaction mixture was stirred at room temperature for 24 h. The crude reaction mixture was poured into H₂O (50 mL) and extracted with EtOAc (50 mL). The organic extracts were washed with H₂O (4 X 50 mL), dried (Na₂SO₄) and concentrated *in vacuo*. Purification of the crude residue by column chromatography on silica gel using Hex/EtOAc as eluent (3:1) afforded the title compound (0.400 g, 1.42 mmol, 37 % yield) as a white solid. ¹H NMR (600 MHz, CDCl₃) δ 7.45 (s, 1H), 6.99 (s, 1H), 2.19 (s, 3H), 2.01 (s, 6H), 1.72 (dd, *J* = 34.6, 12.9 Hz, 6H). ¹³C NMR (151 MHz, CDCl₃) δ 133.16, 114.93, 114.72, 56.06, 43.49, 35.76, 29.34. HRMS (ESI) found [M+H]⁺ 281.0649, C₁₃H₁₈N₂Br requires 281.0648.

(S)-3,3'-bis(adamantan-1-yl-1*H*-imidazol-4-yl)-6,6'-dioctyl-[1,1'-binaphthalene]-2,2'-diol
(**2.37**)



To a magnetically stirred solution of *bis*-boronate ester **2.33** (0.408 g, 0.479 mmol) and imidazole **2.35** (0.363 g, 1.29 mmol) in 1,4-dioxane/H₂O (6.2/0.6 mL) were added Pd(OAc)₂ (0.011 g, 0.051 mmol), S-Phos (0.042 g, 0.102 mmol), and K₃PO₄ (0.650 g, 3.06 mmol). The reaction mixture was degassed under vacuum (3 x 30 s) and stirred at 95 °C for 15 h. The reaction mixture was allowed to cool to room temperature and then filtered through Celite, dried (Na₂SO₄) and concentrated *in vacuo*. The crude residue was dissolved in 1,4-dioxane (20 mL) and concentrated HCl (2 mL) was added. The reaction mixture was stirred at 70 °C for 2 h, and the allowed to cool to room temperature and concentrated *in vacuo*. The residue was dissolved in DCM and washed with saturated aqueous Na₂CO₃ (20 mL), H₂O (20 mL) and brine (20 mL). The organic extracts were dried (Na₂SO₄) and concentrated *in vacuo*. The crude residue was purified by column chromatography on silica gel using Hex/EtOAc as eluent (20:1 to 10:1) to afford the title compound (0.275 g, 0.302 mmol, 30 % yield) as a yellow solid. ¹H NMR (500 MHz, CDCl₃) δ 8.11 (s, 2H), 7.67 (s, 2H), 7.66 (s, 2H), 7.59 (s, 2H), 7.20 (d, *J* = 8.6 Hz, 2H), 7.03 (d, *J* = 8.6 Hz, 2H), 2.71 (t, *J* = 7.7 Hz, 4H), 2.29 (s, 6H), 2.18 (s, 12H), 1.90 - 1.76 (m, 12H), 1.73 - 1.62 (m, 4H), 1.49 - 1.23 (m, 20H), 0.91 (t, *J* = 6.3 Hz, 6H). ¹³C NMR (126 MHz, CDCl₃) δ 151.70, 141.09, 136.92, 132.10, 131.41, 128.35, 127.39, 126.03, 124.98, 122.95, 119.71, 117.33, 111.65, 55.83, 43.80, 35.95, 35.84, 31.96, 31.37, 29.60, 29.51, 29.47, 29.33, 22.72, 14.15. HRMS (ESI) found [M+H]⁺ 911.6201, C₆₂H₇₉N₄O₂ requires 911.6198.

(4*R*,11*bS*)-4-hydroxy-2,6-bis(adamantan-1-yl-1*H*-imidazol-4-yl)-9,14-dioctyldinaphtho[2,1-*d*:1',2'-*f*][1,3,2]dioxaphosphine 4-oxide (imid-2.111)

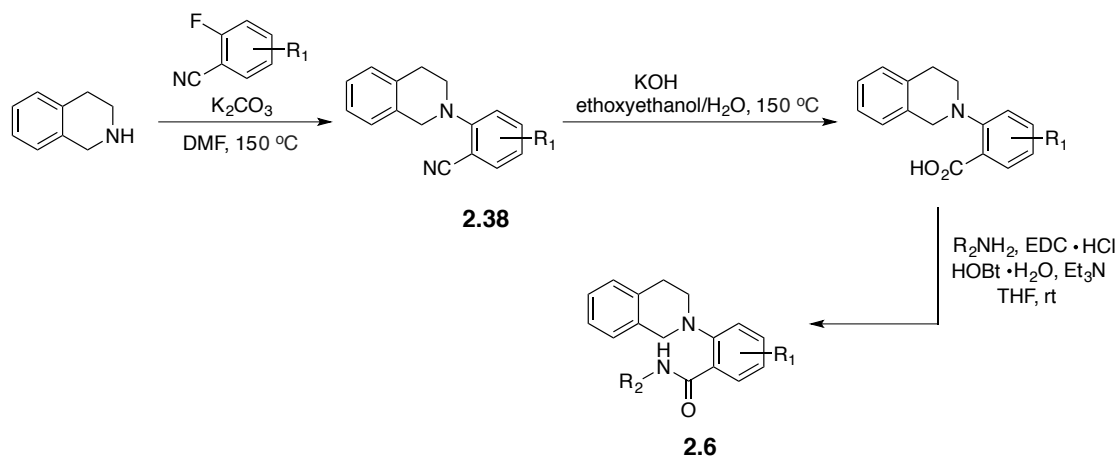


Subjection of diol **2.37** (0.051 g, 0.056 mmol) to General Procedure C gave the title compound (0.013 g, 0.013 mmol, 23 % yield) as a dark-yellow solid. ¹H NMR (500 MHz, CDCl₃: DMSO, 1:1) δ 8.37 (s, 2H), 8.09 (s, 2H), 7.93 (s, 2H), 7.60 (s, 2H), 7.03 (d, *J* = 8.8 Hz, 2H), 6.88 (d, *J* = 8.6 Hz, 2H), 2.64 (t, *J* = 7.8 Hz, 4H), 2.26 (s, 6H), 2.18 (s, 12H), 1.82 - 1.68 (m, 12H), 1.67 - 1.53 (m, 4H), 1.36 - 1.12 (m, 20H), 0.81 (t, *J* = 6.6 Hz, 6H). ¹³C NMR (126 MHz, CDCl₃: DMSO, 1:1) δ 151.79, 140.30, 136.78, 132.44, 131.85, 128.21, 127.20, 124.86, 122.82, 119.77, 117.36, 113.17, 99.99, 56.18, 43.41, 35.86, 35.68, 31.81, 31.37, 29.48, 29.42, 29.29, 29.19, 22.59, 14.33. ³¹P NMR

(202 MHz, CDCl₃: DMSO, 1:1) δ 9.12. HRMS (ESI) found $[M+H]^+$ 973.5771, C₆₂H₇₈N₄O₄P requires 973.5755.

Synthesis of Substrates

Compounds **2.6a-p**, **2.17**, and **2.18** were prepared according to the reaction sequence depicted in Scheme 2.8. Compounds **2.6a-m**, **2.17**, and **2.18** were prepared from known compound 2-(3,4-dihydroisoquinolin-2(1*H*)-yl)benzoic acid.¹¹¹



Scheme 2.8. Synthesis of substrates **2.6**

General Procedure D: Synthesis of Compounds **2.6a-m**, **2.17**, and **2.18**

To a magnetically stirred solution of 2-(3,4-dihydroisoquinolin-2(1*H*)-yl)benzoic acid (1.0 equiv.) in THF (0.1 M) were added *N*-(3-dimethylaminopropyl)-*N'*-ethylcarbodiimide hydrochloride (1.2 equiv.), 1-hydroxybenzotriazole hydrate (1.2 equiv.), triethylamine (1.3 equiv.), and the appropriate primary amine (1.2 equiv.) in succession and the reaction mixture was stirred at room temperature. Upon complete consumption of the starting material, as judged by TLC, the reaction mixture was filtered through silica gel using EtOAc/Hex (1:1) as eluent. The resulting filtrate was concentrated *in vacuo*. The crude residue was purified by column chromatography or recrystallization.

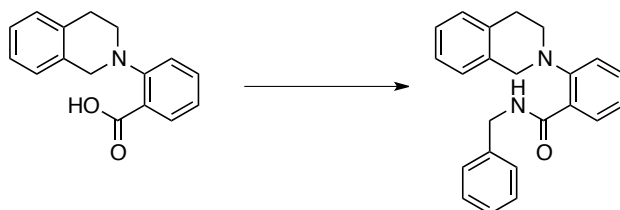
General Procedure E: Synthesis of *N*-arylated tetrahydroisoquinolines **2.38**

To a magnetically stirred solution of 1,2,3,4-tetrahydroisoquinoline (2.0 equiv.) in DMF (2.0 M) was added K₂CO₃ (2.0 equiv.) followed by the appropriate 2-fluorobenzotrile (1.0 equiv.). The reaction mixture was heated at 150 °C until TLC indicated complete consumption of the starting material. After being allowed to cool to room temperature, the reaction mixture was diluted with EtOAc, extracted with saturated aqueous NH₄Cl, washed with H₂O (x 4), dried (Na₂SO₄) and concentrated *in vacuo*. The crude residue was purified by column chromatography on silica gel using EtOAc/Hex as eluent.

General Procedure F: Synthesis of Compounds 2.6n-p

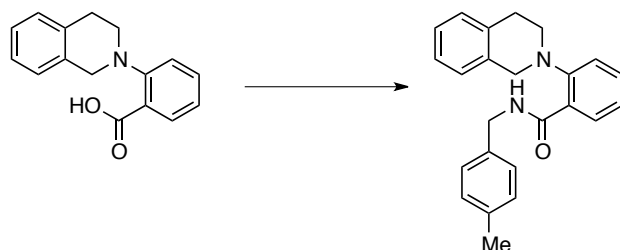
To a magnetically stirred solution of N-arylated 1,2,3,4-tetrahydroisoquinoline derivative **2.38** (1.0 equiv.) in ethoxyethanol/H₂O (8:1 v:v, 1.0 M) was added freshly-ground KOH (6.0 equiv.). The reaction mixture was heated at 150 °C for 2h, at which point a precipitate was observed. The reaction mixture was allowed to cool to room temperature and the solid was filtered and dissolved in H₂O. This solution was acidified to pH = 7 using 3N HCl and extracted with DCM (x 2), dried (Na₂SO₄), and concentrated *in vacuo* to afford the crude carboxylic acid. Assuming quantitative yield, the crude product was dissolved in THF (0.1 M). To this magnetically stirred solution were added N-(3-dimethylaminopropyl)-N'-ethylcarbodiimide hydrochloride (1.2 equiv.), 1-hydroxybenzotriazole hydrate (1.2 equiv.), triethylamine (1.3 equiv.), and the appropriate primary amine (1.2 equiv.) in succession and the reaction mixture was stirred at room temperature. Upon complete consumption of the starting material, as judged by TLC, the reaction mixture was filtered through silica gel using EtOAc/Hex (1:1) as eluent. The resulting filtrate was concentrated *in vacuo*. The crude residue was purified by column chromatography or recrystallization.

N-benzyl-2-(3,4-dihydroisoquinolin-2(1H)-yl)benzamide (2.6a)



Subjection of 2-(3,4-dihydroisoquinolin-2(1H)-yl)benzoic acid (1.00 g, 3.94 mmol) to General Procedure D gave the title compound (1.02 g, 2.98 mmol, 76 % yield) as a white solid after purification by column chromatography on silica gel using Hex/EtOAc as eluent (9:1). ¹H NMR (600 MHz, CDCl₃) δ 10.21 (s, 1H), 8.28 (d, *J* = 7.3 Hz, 1H), 7.47 (t, *J* = 7.6 Hz, 1H), 7.32 - 7.24 (m, 2H), 7.23 - 7.11 (m, 3H), 7.11 - 7.04 (m, 3H), 7.03 - 6.96 (m, 3H), 4.48 (d, *J* = 5.1 Hz, 2H), 4.08 (s, 2H), 3.26 (t, *J* = 5.8 Hz, 2H), 2.76 (t, *J* = 5.8 Hz, 2H). ¹³C NMR (126 MHz, CDCl₃) δ 166.03, 151.23, 137.99, 133.78, 133.40, 132.17, 131.64, 129.02, 128.49, 127.96, 127.88, 127.14, 126.70, 126.31, 126.10, 125.18, 121.00, 56.77, 50.40, 44.06, 29.24. HRMS (ESI) found [M+H]⁺ 343.1800, C₂₃H₂₃N₂O requires 343.1805.

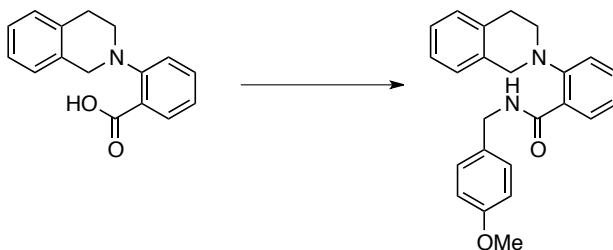
2-(3,4-dihydroisoquinolin-2(1H)-yl)-N-(4-methylbenzyl)benzamide (2.6b)



Subjection of 2-(3,4-dihydroisoquinolin-2(1H)-yl)benzoic acid (1.00 g, 3.94 mmol) to General Procedure D gave the title compound (0.587 g, 1.65 mmol, 42 % yield) as a white solid after recrystallization from hot EtOAc. ¹H NMR (500 MHz, CDCl₃) δ 10.18 (s, 1H), 8.29 (d, *J* = 9.3

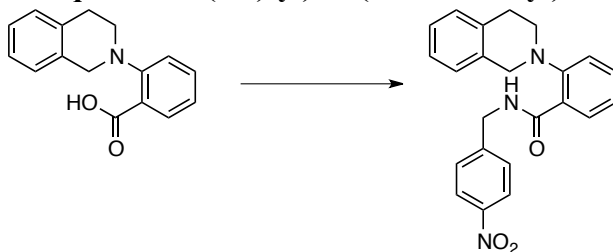
Hz, 1H), 7.48 (app t, $J = 7.6$ Hz, 1H), 7.33 - 7.15 (m, 4H), 7.06 (d, $J = 7.5$ Hz, 1H), 7.00 (d, $J = 7.2$ Hz, 1H), 6.91 (d, $J = 13.0$ Hz, 2H), 6.88 (d, $J = 13.0$ Hz, 2H), 4.45 (d, $J = 5.0$ Hz, 2H), 4.08 (s, 2H), 3.27 (t, $J = 5.9$ Hz, 2H), 2.78 (t, $J = 5.9$ Hz, 2H), 2.28 (s, 3H). ^{13}C NMR (126 MHz, CDCl_3) δ 165.91, 151.23, 136.65, 134.88, 133.76, 133.42, 132.12, 131.61, 129.15, 128.91, 128.01, 127.85, 126.55, 126.29, 126.01, 125.16, 121.01, 56.70, 50.37, 43.83, 29.26, 21.13. HRMS (ESI) found $[\text{M}+\text{H}]^+$ 357.1958, $\text{C}_{24}\text{H}_{25}\text{N}_2\text{O}$ requires 357.1961.

2-(3,4-dihydroisoquinolin-2(1H)-yl)-N-(4-methoxybenzyl)benzamide (2.6c)



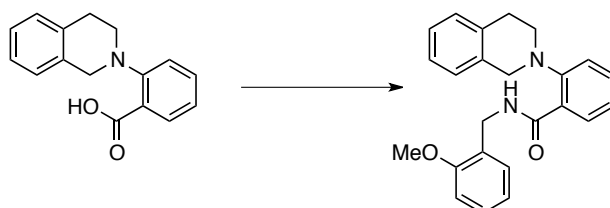
Subjection of 2-(3,4-dihydroisoquinolin-2(1H)-yl)benzoic acid (1.00 g, 3.94 mmol) to General Procedure D gave the title compound (0.680 g, 1.82 mmol, 46 % yield) as a white solid after recrystallization from hot EtOAc. ^1H NMR (500 MHz, CDCl_3) δ 10.17 (s, 1H), 8.29 (d, $J = 9.1$ Hz, 1H), 7.48 (app t, $J = 7.6$ Hz, 1H), 7.34 - 7.15 (m, 4H), 7.08 (d, $J = 7.2$ Hz, 1H), 7.00 (d, $J = 7.3$ Hz, 1H), 6.93 (d, $J = 8.5$ Hz, 2H), 6.60 (d, $J = 8.5$ Hz, 2H), 4.43 (d, $J = 5.0$ Hz, 2H), 4.07 (s, 2H), 3.80 (s, 3H), 3.27 (t, $J = 5.8$ Hz, 2H), 2.78 (t, $J = 5.7$ Hz, 2H). ^{13}C NMR (126 MHz, CDCl_3) δ 165.85, 158.60, 151.22, 133.79, 133.44, 132.12, 131.58, 130.06, 129.17, 128.95, 128.00, 126.62, 126.30, 126.03, 125.17, 120.99, 113.81, 56.80, 55.18, 50.27, 43.50, 29.31. HRMS (ESI) found $[\text{M}+\text{H}]^+$ 373.1906, $\text{C}_{24}\text{H}_{25}\text{N}_2\text{O}_2$ requires 373.1911.

2-(3,4-dihydroisoquinolin-2(1H)-yl)-N-(4-nitrobenzyl)benzamide (2.6d)



Subjection of 2-(3,4-dihydroisoquinolin-2(1H)-yl)benzoic acid (1.00 g, 3.94 mmol) to General Procedure D gave the title compound (0.473 g, 1.22 mmol, 31 % yield) as a white solid after recrystallization from hot EtOAc. ^1H NMR (500 MHz, CDCl_3) δ 10.58 (s, 1H), 8.30 (d, $J = 7.8$ Hz, 1H), 7.91 (d, $J = 8.6$ Hz, 2H), 7.53 (app t, $J = 7.6$ Hz, 1H), 7.36 - 7.29 (m, 2H), 7.23 - 7.12 (m, 4H), 7.05 (d, $J = 7.5$ Hz, 1H), 6.92 (d, $J = 7.5$ Hz, 1H), 4.57 (d, $J = 5.4$ Hz, 2H), 4.02 (s, 2H), 3.32 (t, $J = 5.9$ Hz, 2H), 2.86 (t, $J = 5.9$ Hz, 2H). ^{13}C NMR (126 MHz, CDCl_3) δ 166.16, 151.28, 147.00, 145.50, 133.48, 133.01, 132.60, 131.62, 128.92, 128.57, 127.51, 126.90, 126.28, 126.18, 125.57, 123.71, 121.35, 57.27, 50.11, 43.27, 29.58. HRMS (ESI) found $[\text{M}+\text{H}]^+$ 388.1651, $\text{C}_{23}\text{H}_{22}\text{N}_3\text{O}_3$ requires 388.1656.

2-(3,4-dihydroisoquinolin-2(1*H*)-yl)-*N*-(2-methoxybenzyl)benzamide (2.6e)



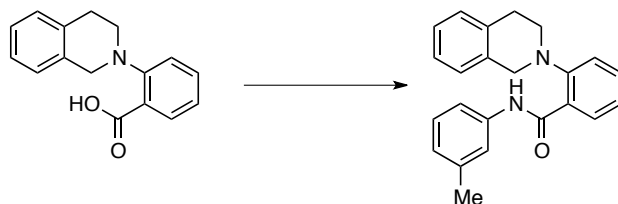
Subjection of 2-(3,4-dihydroisoquinolin-2(1*H*)-yl)benzoic acid (1.00 g, 3.94 mmol) to General Procedure D gave the title compound (0.251 g, 0.673 mmol, 17 % yield) as a white solid after recrystallization from hot EtOAc. $^1\text{H NMR}$ (500 MHz, CDCl_3) δ 9.98 (s, 1H), 8.26 (d, $J = 8.1$ Hz, 1H), 7.45 (app t, $J = 7.7$ Hz, 1H), 7.31 - 7.24 (m, 2H), 7.24 - 7.12 (m, 4H), 7.08 (d, $J = 7.4$ Hz, 1H), 7.01 (d, $J = 7.7$ Hz, 1H), 6.79 (app t, $J = 7.4$ Hz, 1H), 6.61 (d, $J = 8.1$ Hz, 1H), 4.58 (d, $J = 5.5$ Hz, 2H), 4.13 (s, 2H), 3.42 (s, 3H), 3.23 (t, $J = 5.8$ Hz, 2H), 2.76 (t, $J = 5.9$ Hz, 2H). $^{13}\text{C NMR}$ (126 MHz, CDCl_3) δ 166.04, 157.41, 151.10, 134.05, 133.62, 131.86, 131.75, 129.87, 129.02, 128.63, 128.30, 126.44, 126.31, 126.23, 126.00, 124.80, 120.54, 120.44, 110.13, 55.24, 54.77, 51.59, 39.07, 28.97. **HRMS** (ESI) found $[\text{M}+\text{H}]^+$ 373.1906, $\text{C}_{24}\text{H}_{25}\text{N}_2\text{O}_2$ requires 373.1911.

2-(3,4-dihydroisoquinolin-2(1*H*)-yl)-*N*-phenylbenzamide (2.6f)



Subjection of 2-(3,4-dihydroisoquinolin-2(1*H*)-yl)benzoic acid (0.506 g, 2.0 mmol) to General Procedure D gave the title compound (0.500 g, 0.673 mmol, 76 % yield) as a white solid after purification by column chromatography on silica gel using Hex/EtOAc as eluent (10:1). $^1\text{H NMR}$ (500 MHz, CDCl_3) δ 12.51 (s, 1H), 8.41 (d, $J = 7.5$ Hz, 1H), 7.56 (app t, $J = 8.4$ Hz, 1H), 7.43 - 7.35 (m, 2H), 7.35 - 7.25 (m, 4H), 7.25 - 7.14 (m, 3H), 7.09 (d, $J = 7.6$ Hz, 1H), 7.02 (t, $J = 7.4$ Hz, 1H), 4.23 (s, 2H), 3.46 (t, $J = 6.0$ Hz, 2H), 3.20 (t, $J = 6.0$ Hz, 2H). $^{13}\text{C NMR}$ (126 MHz, CDCl_3) δ 163.84, 150.90, 138.72, 133.77, 133.13, 132.61, 131.93, 129.05, 128.91, 128.12, 127.15, 126.78, 126.32, 125.71, 123.59, 121.43, 119.60, 56.75, 51.14, 29.41. **HRMS** (ESI) found $[\text{M}+\text{H}]^+$ 329.1647, $\text{C}_{22}\text{H}_{21}\text{N}_2\text{O}_1$ requires 329.1648.

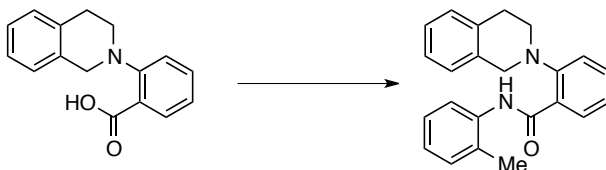
2-(3,4-dihydroisoquinolin-2(1*H*)-yl)-*N*-(*m*-tolyl)benzamide (2.6g)



Subjection of 2-(3,4-dihydroisoquinolin-2(1*H*)-yl)benzoic acid (1.00 g, 3.94 mmol) to General Procedure D gave the title compound (0.785 g, 2.29 mmol, 58 % yield) as a white solid after recrystallization from hot EtOAc. $^1\text{H NMR}$ (500 MHz, CDCl_3) δ 12.52 (s, 1H), 8.41 (d, $J = 6.6$ Hz, 1H), 7.56 (app t, $J = 7.6$ Hz, 1H), 7.42 - 7.35 (m, 2H), 7.35 - 7.27 (m, 2H), 7.27 - 7.16 (m,

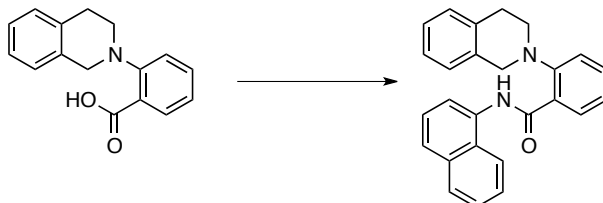
2H), 7.12 - 7.03 (m, 2H), 6.93 (s, 1H), 6.83 (d, $J = 7.4$ Hz, 1H), 4.22 (s, 2H), 3.47 (t, $J = 5.9$ Hz, 2H), 3.21 (t, $J = 6.0$ Hz, 2H), 2.18 (s, 3H). $^{13}\text{C NMR}$ (126 MHz, CDCl_3) δ 163.71, 150.88, 138.64, 138.61, 133.86, 133.25, 132.57, 131.90, 129.01, 128.74, 128.18, 127.20, 126.89, 126.26, 125.74, 124.39, 121.48, 120.25, 116.77, 56.95, 50.98, 29.44, 21.44. **HRMS** (ESI) found $[\text{M}+\text{H}]^+$ 343.1803, $\text{C}_{23}\text{H}_{23}\text{N}_2\text{O}_1$ requires 343.1805.

2-(3,4-dihydroisoquinolin-2(1H)-yl)-*N*-(*o*-tolyl)benzamide (2.6h)



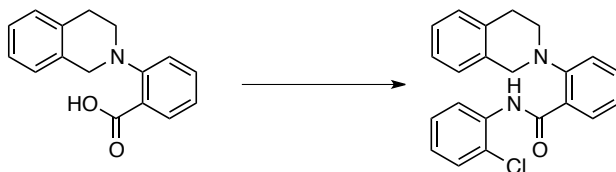
Subjection of 2-(3,4-dihydroisoquinolin-2(1H)-yl)benzoic acid (1.00 g, 3.94 mmol) to General Procedure D gave the title compound (0.695 g, 2.03 mmol, 52 % yield) as a white solid after purification by column chromatography on silica gel using Hex/EtOAc as eluent (4:1). $^1\text{H NMR}$ (500 MHz, CDCl_3) δ 11.57 (s, 1H), 8.37 (d, $J = 7.7$ Hz, 1H), 8.13 (d, $J = 8.1$ Hz, 1H), 7.53 (app t, $J = 7.6$ Hz, 1H), 7.40 - 7.32 (m, 2H), 7.26 - 7.20 (m, 3H), 7.17 (d, $J = 7.6$ Hz, 1H), 7.15 - 7.07 (m, 2H), 7.04 (app t, $J = 7.3$ Hz, 1H), 4.36 (s, 2H), 3.45 (t, $J = 5.9$ Hz, 2H), 3.02 (t, $J = 5.9$ Hz, 2H), 1.98 (s, 3H). $^{13}\text{C NMR}$ (126 MHz, CDCl_3) δ 164.56, 150.73, 136.58, 133.73, 133.39, 132.45, 132.16, 130.33, 128.97, 128.63, 128.51, 126.95, 126.57, 126.41, 126.36, 125.36, 124.39, 122.77, 121.04, 55.60, 52.11, 28.58, 17.60. **HRMS** (ESI) found $[\text{M}+\text{H}]^+$ 343.1802, $\text{C}_{23}\text{H}_{23}\text{N}_2\text{O}$ requires 343.1805.

2-(3,4-dihydroisoquinolin-2(1H)-yl)-*N*-(naphthalen-1-yl)benzamide (2.6i)



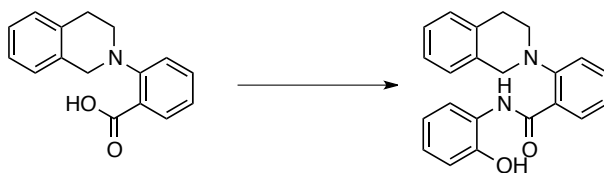
Subjection of 2-(3,4-dihydroisoquinolin-2(1H)-yl)benzoic acid (0.500 g, 1.97 mmol) to General Procedure D gave the title compound (0.304 g, 0.803 mmol, 41 % yield) as a white solid after recrystallization from hot EtOAc. $^1\text{H NMR}$ (300 MHz, CDCl_3) δ 12.61 (s, 1H), 8.45 (d, $J = 7.8$ Hz, 2H), 7.75 (d, $J = 8.1$ Hz, 1H), 7.63 - 7.52 (m, 3H), 7.47 (app t, $J = 7.9$ Hz, 2H), 7.39 (app t, $J = 7.5$ Hz, 1H), 7.33 - 7.14 (m, 4H), 7.06 (d, $J = 6.7$ Hz, 1H), 6.63 (app t, $J = 7.7$ Hz, 1H), 4.45 (s, 2H), 3.43 (t, $J = 5.9$ Hz, 2H), 2.98 (t, $J = 6.0$ Hz, 2H). $^{13}\text{C NMR}$ (126 MHz, CDCl_3) δ 164.62, 151.12, 133.90, 133.71, 133.70, 133.51, 132.65, 132.29, 129.20, 128.74, 128.48, 126.98, 126.51, 126.41, 126.00, 125.86, 125.58, 125.26, 124.26, 121.54, 120.97, 118.62, 55.86, 52.52, 29.18. **HRMS** (ESI) found $[\text{M}+\text{H}]^+$ 379.1801, $\text{C}_{26}\text{H}_{23}\text{N}_2\text{O}$ requires 379.1805.

***N*-(2-chlorophenyl)-2-(3,4-dihydroisoquinolin-2(1*H*)-yl)benzamide (2.6j)**



Subjection of 2-(3,4-dihydroisoquinolin-2(1*H*)-yl)benzoic acid (0.500 g, 1.97 mmol) to General Procedure D gave the title compound (0.204 g, 0.562 mmol, 29 % yield) as a white solid after recrystallization from hot EtOAc. $^1\text{H NMR}$ (300 MHz, CDCl_3) δ 12.21 (s, 1H), 8.63 (d, $J = 8.2$ Hz, 1H), 8.28 (d, $J = 7.8$ Hz, 1H), 7.46 (app t, $J = 7.5$ Hz, 1H), 7.34 - 7.22 (m, 4H), 7.22 - 7.04 (m, 4H), 6.98 (app t, $J = 6.9$ Hz, 1H), 4.38 (s, 2H), 3.42 (t, $J = 5.9$ Hz, 2H), 2.94 (t, $J = 5.9$ Hz, 2H). $^{13}\text{C NMR}$ (126 MHz, CDCl_3) δ 164.82, 150.88, 135.83, 134.00, 133.98, 132.64, 132.15, 129.12, 128.88, 128.14, 127.47, 126.62, 126.26, 126.12, 125.13, 124.23, 123.15, 122.50, 121.49, 54.93, 52.12, 27.76. **HRMS** (ESI) found $[\text{M}+\text{H}]^+$ 363.1258, $\text{C}_{22}\text{H}_{20}\text{N}_2\text{OCl}$ requires 363.1259.

2-(3,4-dihydroisoquinolin-2(1*H*)-yl)-*N*-(2-hydroxyphenyl)benzamide (2.6k)



Subjection of 2-(3,4-dihydroisoquinolin-2(1*H*)-yl)benzoic acid (0.415 g, 1.65 mmol) to General Procedure D gave the title compound (0.335 g, 0.973 mmol, 59 % yield) as a white solid after recrystallization from hot EtOAc. $^1\text{H NMR}$ (500 MHz, CDCl_3) δ 13.23 (s, 1H), 9.98 (s, 1H), 8.41 (d, $J = 7.8$ Hz, 1H), 7.61 (t, $J = 7.6$ Hz, 1H), 7.50 - 7.36 (m, 2H), 7.35 - 7.20 (m, 3H), 7.12 (d, $J = 7.5$ Hz, 1H), 7.08 - 6.92 (m, 2H), 6.52 (app t, $J = 8.0$ Hz, 1H), 6.10 (d, $J = 7.8$ Hz, 1H), 4.24 (s, 2H), 3.49 (t, $J = 5.9$ Hz, 2H), 3.18 (t, $J = 5.9$ Hz, 2H). $^{13}\text{C NMR}$ (126 MHz, CDCl_3) δ 164.87, 151.44, 149.33, 133.47, 133.36, 133.05, 132.04, 129.16, 127.30, 126.84, 126.72, 126.43, 126.23, 126.15, 126.00, 122.08, 121.99, 120.04, 119.97, 57.26, 50.56, 29.32. **HRMS** (ESI) found $[\text{M}+\text{H}]^+$ 345.1592, $\text{C}_{22}\text{H}_{21}\text{N}_2\text{O}_2$ requires 345.1598.

***N*-(*tert*-butyl)-2-(3,4-dihydroisoquinolin-2(1*H*)-yl)benzamide (2.6l)**



Subjection of 2-(3,4-dihydroisoquinolin-2(1*H*)-yl)benzoic acid (0.500 g, 1.97 mmol) to General Procedure D gave the title compound (0.391 g, 1.27 mmol, 64 % yield) as a white solid after purification by column chromatography on silica gel using Hex/EtOAc as eluent (9:1 to 4:1). $^1\text{H NMR}$ (500 MHz, CDCl_3) δ 9.82 (s, 1H), 8.21 (d, $J = 9.3$ Hz, 1H), 7.46 (app t, $J = 8.4$ Hz, 1H), 7.30 - 7.17 (m, 5H), 7.07 (d, $J = 7.2$ Hz, 1H), 4.09 (s, 2H), 3.43 (t, $J = 5.9$ Hz, 2H), 3.12 (t, $J = 6.0$ Hz, 2H), 1.17 (s, 9H). $^{13}\text{C NMR}$ (126 MHz, CDCl_3) δ 165.01, 150.79, 134.03, 133.51, 131.77,

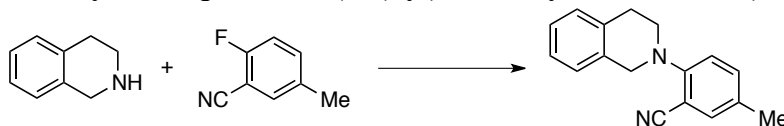
131.31, 129.08, 128.89, 126.92, 126.35, 126.11, 124.95, 120.43, 57.98, 50.57, 49.28, 29.69, 28.33. **HRMS** (ESI) found $[M+H]^+$ 309.1959, $C_{20}H_{25}N_2O$ requires 309.1961.

***N*-cyclohexyl-2-(3,4-dihydroisoquinolin-2(1*H*)-yl)benzamide (2.6m)**



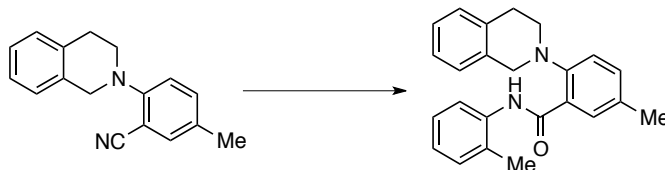
Subjection of 2-(3,4-dihydroisoquinolin-2(1*H*)-yl)benzoic acid (0.500 g, 1.97 mmol) to General Procedure D gave the title compound (0.425 g, 1.23 mmol, 63 % yield) as a white solid after purification by column chromatography on silica gel using Hex/EtOAc as eluent (9:1). **¹H NMR** (500 MHz, $CDCl_3$) δ 9.83 (d, $J = 8.0$ Hz, 1H), 8.25 (d, $J = 6.2$ Hz, 1H), 7.46 (app t, 1H), 7.32 - 7.14 (m, 5H), 7.04 (d, $J = 7.4$ Hz, 1H), 4.10 (s, 2H), 3.93 - 3.77 (m, 1H), 3.40 (t, $J = 5.9$ Hz, 2H), 3.10 (t, $J = 5.9$ Hz, 2H), 1.88 - 1.66 (m, 2H), 1.57 - 1.38 (m, 3H), 1.33 - 1.12 (m, 2H), 1.02 - 0.87 (m, 1H), 0.82 (app q, $J = 12.7$ Hz, 2H). **¹³C NMR** (126 MHz, $CDCl_3$) δ 165.05, 151.04, 134.06, 133.45, 131.92, 131.60, 128.91, 128.31, 126.82, 126.44, 126.04, 125.01, 120.83, 57.57, 49.68, 47.94, 32.56, 29.57, 25.58, 24.61. **HRMS** (ESI) found $[MH]^+$ 335.2119, $C_{22}H_{27}N_2O$ requires 335.2118.

2-(3,4-dihydroisoquinolin-2(1*H*)-yl)-5-methylbenzonitrile (2.38n)



Subjection of 1,2,3,4-tetrahydroisoquinoline (6.70 g, 50.3 mmol) and 2-fluoro-5-methylbenzonitrile (3.4 g, 25.2 mmol) to General Procedure E gave the title compound (3.28 g, 13.2 mmol, 52 % yield) as a colorless oil after purification by column chromatography on silica gel using Hex/EtOAc as eluent (9:1). **¹H NMR** (500 MHz, $CDCl_3$) δ 7.41 (s, 1H), 7.31 (d, $J = 8.4$ Hz, 1H), 7.24 - 7.17 (m, 3H), 7.17 - 7.12 (m, 1H), 7.01 (d, $J = 8.4$ Hz, 1H), 4.37 (s, 2H), 3.62 (t, $J = 5.8$ Hz, 2H), 3.10 (t, $J = 5.8$ Hz, 2H), 2.33 (s, 3H). **¹³C NMR** (126 MHz, $CDCl_3$) δ 153.12, 134.53, 134.51, 133.93, 133.39, 131.00, 129.01, 126.53, 126.39, 126.01, 118.83, 118.39, 104.88, 52.55, 51.20, 29.34, 20.24. **HRMS** (ESI) found $[M-H]^-$ 247.1229, $C_{17}H_{15}N_2$ requires 247.1230.

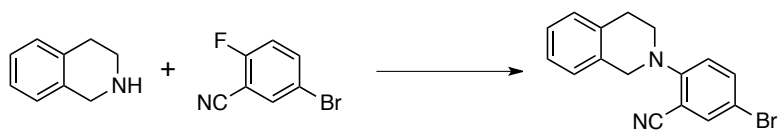
2-(3,4-dihydroisoquinolin-2(1*H*)-yl)-5-methyl-*N*-(*o*-tolyl)benzamide (2.6n)



Subjection of nitrile **2.38n** (0.954 g, 3.84 mmol) to General Procedure F gave the title compound (0.306 g, 0.858 mmol, 22 % yield) as a white solid after purification by column chromatography on silica gel using Hex/EtOAc as eluent (9:1). **¹H NMR** (500 MHz, $CDCl_3$) δ 11.72 (s, 1H), 8.19 (s, 1H), 8.10 (d, $J = 8.1$ Hz, 1H), 7.33 (d, $J = 8.1$ Hz, 1H), 7.28 - 7.25 (m, 1H), 7.24 - 7.18 (m, 3H), 7.16 (d, $J = 6.4$ Hz, 1H), 7.10 (app t, $J = 7.9$ Hz, 2H), 7.03 (app t, $J = 7.3$ Hz, 1H), 4.31 (s, 2H),

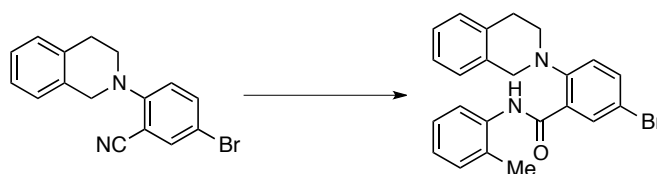
3.40 (t, $J = 5.9$ Hz, 2H), 3.01 (t, $J = 5.9$ Hz, 2H), 2.43 (s, 3H), 1.96 (s, 3H). ^{13}C NMR (126 MHz, CDCl_3) δ 164.60, 148.38, 136.67, 135.16, 133.90, 133.42, 132.99, 132.49, 130.30, 128.94, 128.71, 128.14, 126.86, 126.51, 126.40, 126.30, 124.31, 122.85, 121.12, 55.79, 52.07, 28.70, 20.84, 17.61. HRMS (ESI) found $[\text{M}+\text{H}]^+$ 357.1958, $\text{C}_{24}\text{H}_{25}\text{N}_2\text{O}$ requires 357.1961.

5-bromo-2-(3,4-dihydroisoquinolin-2(1H)-yl)benzonitrile (2.38o)



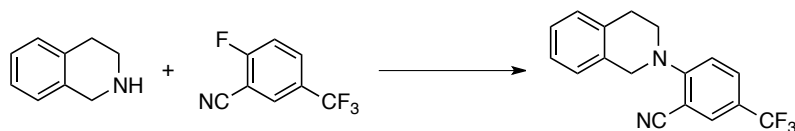
Subjection of 1,2,3,4-tetrahydroisoquinoline (1.82 g, 13.7 mmol) and 5-bromo-2-fluorobenzonitrile (1.3 g, 6.50 mmol) to General Procedure E gave the title compound (1.44 g, 4.61 mmol, 71 % yield) as a yellow oil after purification by column chromatography on silica gel using Hex/EtOAc as eluent (20:1). ^1H NMR (500 MHz, CDCl_3) δ 7.68 (s, 1H), 7.56 (d, $J = 11.1$ Hz, 1H), 7.27 - 7.18 (m, 3H), 7.17 - 7.11 (m, 1H), 6.96 (d, $J = 8.9$ Hz, 1H), 4.42 (s, 2H), 3.69 (t, $J = 5.8$ Hz, 2H), 3.10 (t, $J = 5.8$ Hz, 2H). ^{13}C NMR (126 MHz, CDCl_3) δ 154.00, 136.65, 136.61, 134.37, 133.27, 129.01, 126.78, 126.35, 126.22, 119.67, 117.51, 112.21, 105.52, 52.14, 50.66, 29.17. HRMS (ESI) found $[\text{M}-\text{H}]^-$ 311.0177, $\text{C}_{16}\text{H}_{12}\text{N}_2\text{Br}$ requires 311.0178.

5-bromo-2-(3,4-dihydroisoquinolin-2(1H)-yl)-N-(o-tolyl)benzamide (2.6o)



Subjection of nitrile **2.38o** (0.406 g, 1.3 mmol) to General Procedure F gave the title compound (0.444 g, 1.05 mmol, 81 % yield) as a white solid after purification by column chromatography on silica gel using Hex/EtOAc as eluent (9:1). ^1H NMR (500 MHz, CDCl_3) δ 11.40 (s, 1H), 8.47 (s, 1H), 8.07 (d, $J = 8.1$ Hz, 1H), 7.61 (d, $J = 8.5$ Hz, 1H), 7.27 - 7.20 (m, 4H), 7.16 (d, $J = 7.2$ Hz, 1H), 7.14 - 7.08 (m, 2H), 7.05 (d, $J = 7.3$ Hz, 1H), 4.32 (s, 2H), 3.42 (t, $J = 5.9$ Hz, 2H), 3.00 (t, $J = 5.9$ Hz, 2H), 1.97 (s, 3H). ^{13}C NMR (126 MHz, CDCl_3) δ 163.04, 149.70, 136.26, 135.14, 134.92, 133.35, 133.22, 130.40, 129.00, 128.61, 127.07, 126.64, 126.47, 126.38, 124.65, 122.94, 122.70, 118.76, 55.55, 52.01, 28.38, 17.57. HRMS (ESI) found $[\text{M}+\text{H}]^+$ 421.0908, $\text{C}_{23}\text{H}_{22}\text{N}_2\text{OBr}$ requires 421.0910.

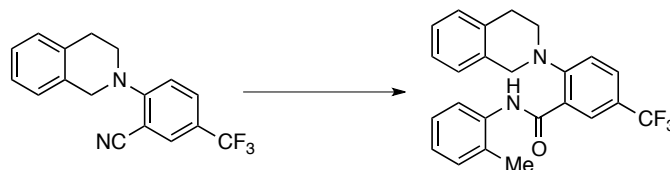
2-(3,4-dihydroisoquinolin-2(1H)-yl)-5-(trifluoromethyl)benzonitrile (2.38p)



Subjection of 1,2,3,4-tetrahydroisoquinoline (4.62 g, 34.7 mmol) and 2-fluoro-5-(trifluoromethyl)benzonitrile (3.12 g, 16.5 mmol) to General Procedure E gave the title compound (4.89 g, 16.17 mmol, 98 % yield) as a yellow oil after purification by column chromatography on silica gel using Hex/EtOAc as eluent (20:1). ^1H NMR (500 MHz, CDCl_3) δ 7.83 (s, 1H), 7.68 (d, $J = 9.9$ Hz, 1H), 7.27 - 7.21 (m, 3H), 7.21 - 7.14 (m, 1H), 7.12 (d, $J = 8.9$ Hz, 1H), 4.57 (s, 2H),

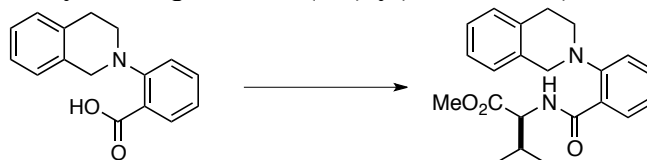
3.84 (t, $J = 5.8$ Hz, 2H), 3.13 (t, $J = 5.8$ Hz, 2H). ^{13}C NMR (126 MHz, CDCl_3) δ 156.43, 134.40, 132.91, 132.38, 132.34, 130.44, 130.41, 128.91, 126.98, 126.41, 126.35, 118.06, 117.40, 101.80, 51.73, 49.82, 29.14. HRMS (ESI) found $[\text{M}+\text{H}]^+$ 303.1103, $\text{C}_{17}\text{H}_{14}\text{N}_2\text{F}_3$ requires 303.1104.

2-(3,4-dihydroisoquinolin-2(1H)-yl)-*N*-(*o*-tolyl)-5-(trifluoromethyl)benzamide (2.6p)



Subjection of nitrile **S7p** (0.320 g, 1.06 mmol) to General Procedure F gave the title compound (0.100 g, 0.243 mmol, 23 % yield) as a yellow oil after purification by column chromatography on silica gel using Hex/EtOAc as eluent (9:1). ^1H NMR (500 MHz, CDCl_3) δ 10.98 (s, 1H), 8.57 (s, 1H), 8.14 (d, $J = 8.1$ Hz, 1H), 7.74 (d, $J = 7.6$ Hz, 1H), 7.41 (d, $J = 8.4$ Hz, 1H), 7.28 - 7.20 (m, 3H), 7.20 - 7.09 (m, 3H), 7.06 (app t, $J = 7.3$ Hz, 1H), 4.39 (s, 2H), 3.51 (t, $J = 5.9$ Hz, 2H), 3.00 (t, $J = 5.9$ Hz, 2H), 2.01 (s, 3H). ^{13}C NMR (126 MHz, CDCl_3) δ 163.37, 153.35, 136.16, 133.22, 133.04, 130.45, 129.54, 129.51, 129.09, 129.01, 128.99, 128.96, 128.28, 127.18, 126.74, 126.56, 126.37, 124.70, 122.38, 121.05, 55.12, 52.09, 28.15, 17.52. HRMS (ESI) found $[\text{M}+\text{H}]^+$ 411.1677, $\text{C}_{24}\text{H}_{22}\text{N}_2\text{O}_1\text{F}_3$ requires 411.1679.

(*S*)-methyl 2-(2-(3,4-dihydroisoquinolin-2(1H)-yl)benzamido)-3-methylbutanoate (2.17)



Subjection of 2-(3,4-dihydroisoquinolin-2(1H)-yl)benzoic acid (0.500 g, 1.97 mmol) to General Procedure D gave the title compound (0.662 g, 1.81 mmol, 92 % yield) as a white solid after recrystallization from hot EtOH. ^1H NMR (500 MHz, CDCl_3) δ 10.59 (d, $J = 8.3$ Hz, 1H), 8.29 (d, $J = 7.8$ Hz, 1H), 7.62 - 7.40 (m, 1H), 7.38 - 7.29 (m, 2H), 7.24 - 7.12 (m, 3H), 7.06 (d, $J = 7.2$ Hz, 1H), 4.64 (t, $J = 6.6$ Hz, 1H), 4.26 (d, $J = 15.4$ Hz, 1H), 4.13 (d, $J = 15.1$ Hz, 1H), 3.59 (s, 3H), 3.51 - 3.35 (m, 2H), 3.22 (dd, $J = 14.5, 7.7$ Hz, 1H), 3.16 - 2.97 (m, 1H), 1.94 (h, $J = 7.1$ Hz, 1H), 0.79 (d, $J = 6.8$ Hz, 3H), 0.63 (d, $J = 6.9$ Hz, 3H). ^{13}C NMR (126 MHz, CDCl_3) δ 172.40, 166.18, 151.71, 134.06, 133.71, 132.46, 131.77, 128.86, 127.68, 126.69, 126.44, 125.97, 125.44, 121.70, 57.94, 57.41, 51.77, 50.21, 30.77, 29.21, 19.00, 17.80. HRMS (ESI) found $[\text{M}+\text{H}]^+$ 367.2081, $\text{C}_{22}\text{H}_{26}\text{N}_2\text{O}_3$ requires 367.2016.

Synthesis of Products

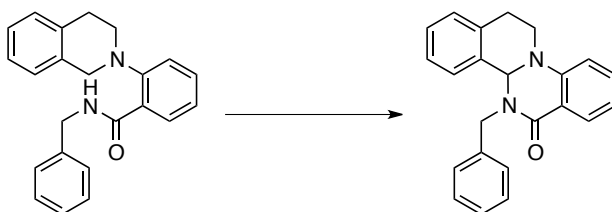
General Procedure G: Asymmetric Amidation

To the catalyst **2.11** (0.005 mmol) in a 2 dram (15 X 60 mm) vial equipped with a Teflon stir bar (1/2" X 5/16") were added substrate **2.6** (0.1 mmol), Na_3PO_4 (0.24 mmol), 4-acetamido-2,2,6,6-tetramethyl-1-oxopiperidinium tetrafluoroborate (**2.8**, 0.22 mmol), and *p*-xylene (4 mL) in succession. The vial was fitted with a screw cap and the reaction mixture was stirred rapidly at room temperature for 48 h with the vial standing on the stir plate. After this time, the reaction mixture was diluted with saturated aqueous Na_2SO_3 (2 mL) and the contents were shaken

vigorously. This mixture was extracted with EtOAc (3 X 2 mL) and the organic extracts were dried with Na₂SO₄ and concentrated *in vacuo*. The crude residue was purified by flash column chromatography. Due to the heterogeneous nature of the reaction mixture, it is essential that fast and efficient stirring be maintained in order to achieve reliable results.

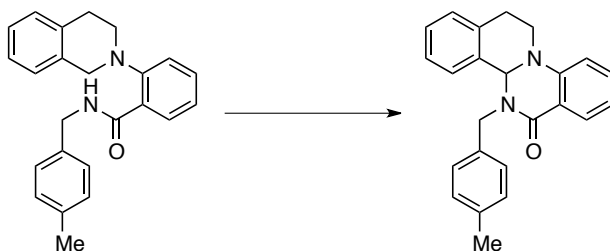
Preparation of reagents: Crystalline 4-acetamido-2,2,6,6-tetramethyl-1-oxopiperidinium tetrafluoroborate was ground with a mortar and pestle into a fine, light-yellow powder prior to use. Anhydrous Na₃PO₄ was ground with a mortar and pestle and dried at 80 °C under vacuum for 30 min prior to use.

5-benzyl-12,13-dihydro-4bH-isoquinolino[2,1-a]quinazolin-6(5H)-one (2.7a)



Subjection of **2.6a** (34 mg, 0.1 mmol) to General Procedure G gave the title compound (28 mg, 0.083 mmol, 83 % yield) as a white powder after purification by column chromatography on silica gel using Hex/EtOAc as eluent (4:1). ¹H NMR (500 MHz, CDCl₃) δ 7.98 (d, *J* = 6.7 Hz, 1H), 7.36 (app t, *J* = 7.8 Hz, 1H), 7.34 - 7.24 (m, 6H), 7.24 - 7.16 (m, 2H), 7.04 (d, *J* = 7.0 Hz, 1H), 6.91 (d, *J* = 8.5 Hz, 1H), 6.88 (app t, *J* = 7.5 Hz, 1H), 5.82-5.71 (m, 1H), 5.69 (s, 1H), 4.39 (d, *J* = 15.3 Hz, 1H), 4.11 - 3.96 (m, 1H), 3.53 (ddd, *J* = 14.0, 11.0, 5.7 Hz, 1H), 3.21 - 3.02 (m, 1H), 2.73 (dd, *J* = 16.3, 4.8 Hz, 1H). ¹³C NMR (126 MHz, CDCl₃) δ 163.45, 147.45, 137.23, 134.75, 133.37, 129.48, 129.22, 129.04, 128.63, 128.25, 127.63, 127.45, 126.20, 125.88, 119.41, 113.65, 109.08, 71.67, 49.64, 44.58, 29.73. HRMS (ESI) found [M+H]⁺ 341.1649, C₂₃H₂₁N₂O requires 341.1648. HPLC (Chiralpak IC column, 75:25 hexanes/isopropanol, 1 mL/min); t_r = 18.8 min (minor), 22.5 min (major); 84 % ee.

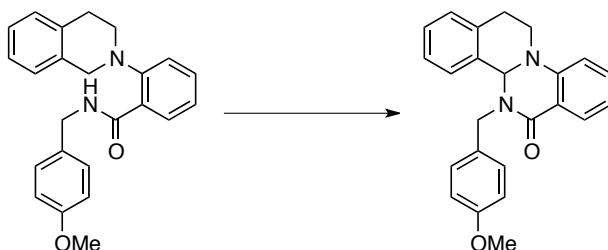
5-(4-methylbenzyl)-12,13-dihydro-4bH-isoquinolino[2,1-a]quinazolin-6(5H)-one (2.7b)



Subjection of **2.6b** (36 mg, 0.1 mmol) to General Procedure G gave the title compound (29 mg, 0.081 mmol, 81 % yield) as a white powder after purification by column chromatography on silica gel using Hex/EtOAc as eluent (4:1). ¹H NMR (500 MHz, CDCl₃) δ 7.98 (d, *J* = 7.3 Hz, 1H), 7.35 (app t, *J* = 7.7 Hz, 1H), 7.33 - 7.26 (m, 1H), 7.26 - 7.17 (m, 4H), 7.17 - 7.10 (m, 2H), 7.04 (d, *J* = 6.9 Hz, 1H), 6.95 - 6.84 (m, 2H), 5.92 - 5.71 (m, 1H), 5.68 (s, 1H), 4.31 (d, *J* = 14.9 Hz, 1H), 4.03 (dd, *J* = 13.3, 5.0 Hz, 1H), 3.53 (ddd, *J* = 14.6, 11.3, 5.7 Hz, 1H), 3.21 - 3.09 (m, 1H), 2.73 (dd, *J* = 16.9, 4.4 Hz, 1H), 2.35 (s, 3H). ¹³C NMR (126 MHz, CDCl₃) δ 163.34, 151.19, 147.36,

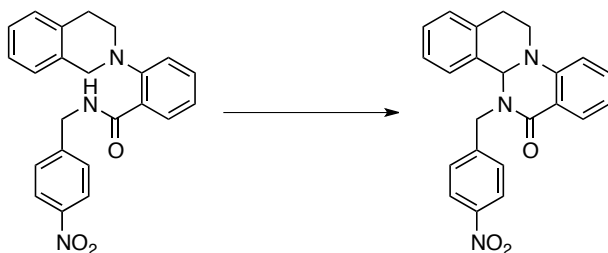
137.15, 134.72, 134.14, 133.34, 132.11, 131.62, 129.45, 129.34, 129.24, 129.14, 128.18, 127.85, 127.72, 126.19, 121.00, 119.29, 71.52, 50.48, 44.57, 24.08, 21.16. **HRMS** (ESI) found $[M+H]^+$ 355.1804, $C_{24}H_{23}N_2O$ requires 355.1805. **HPLC** (Chiralpak IC column, 70:30 hexanes/isopropanol, 1 mL/min); t_r = 19.9 min (minor), 28.5 min (major); 87 % ee.

5-(4-methoxybenzyl)-12,13-dihydro-4bH-isoquinolino[2,1-a]quinazolin-6(5H)-one (2.7c)



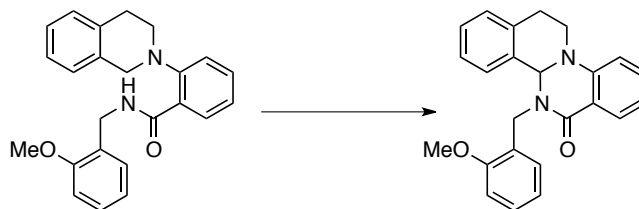
Subjection of **2.6c** (37 mg, 0.1 mmol) to General Procedure G gave the title compound (33 mg, 0.089 mmol, 89 % yield) as a white powder after purification by column chromatography on silica gel using Hex/EtOAc as eluent (4:1). **1H NMR** (500 MHz, $CDCl_3$) δ 7.98 (d, J = 7.4 Hz, 1H), 7.35 (app t, J = 7.3 Hz, 1H), 7.32 - 7.11 (m, 5H), 7.04 (d, J = 7.0 Hz, 2H), 6.92 - 6.82 (m, 4H), 5.83 - 5.49 (m, 2H), 4.32 (d, J = 14.5 Hz, 1H), 4.06 - 3.96 (m, 1H), 3.80 (s, 3H), 3.52 (ddd, J = 16.3, 12.8, 5.7 Hz, 1H), 3.23 - 3.04 (m, 1H), 2.73 (dd, J = 17.0, 4.2 Hz, 1H). **^{13}C NMR** (151 MHz, $CDCl_3$) δ 163.31, 158.99, 147.34, 134.73, 133.27, 129.38, 129.27, 129.16, 129.08, 128.15, 126.76, 126.14, 125.86, 119.31, 113.98, 113.55, 71.37, 55.23, 48.88, 44.53, 24.33. **HRMS** (ESI) found $[M+H]^+$ 371.1756, $C_{24}H_{22}N_2O_2$ requires 371.1754. **HPLC** (Chiralpak IC column, 70:30 hexanes/isopropanol, 1 mL/min); t_r = 23.2 min (minor), 28.6 min (major); 86 % ee.

5-(4-nitrobenzyl)-12,13-dihydro-4bH-isoquinolino[2,1-a]quinazolin-6(5H)-one (2.7d)



Subjection of **2.6d** (37 mg, 0.1 mmol) to General Procedure G gave the title compound (35 mg, 0.090 mmol, 90 % yield) as a yellow powder after purification by column chromatography on silica gel using Hex/EtOAc as eluent (3:2). **1H NMR** (500 MHz, $CDCl_3$) δ 8.14 (d, J = 8.4 Hz, 2H), 8.00 (d, J = 7.6 Hz, 1H), 7.47 - 7.34 (m, 3H), 7.28 - 7.17 (m, 3H), 7.07 (d, J = 7.0 Hz, 1H), 7.00 - 6.87 (m, 2H), 5.74 (s, 1H), 5.66 - 5.34 (m, 1H), 4.61 (d, J = 16.5 Hz, 1H), 4.02 - 3.92 (m, 1H), 3.58 - 3.45 (m, 1H), 3.13 - 2.97 (m, 1H), 2.82 - 2.73 (m, 1H). **^{13}C NMR** (126 MHz, $CDCl_3$) δ 163.92, 147.87, 147.26, 145.19, 135.15, 133.74, 129.53, 129.30, 128.73, 128.56, 128.15, 126.37, 123.79, 123.51, 120.06, 118.69, 114.38, 72.15, 48.56, 44.66, 25.41. **HRMS** (ESI) found $[M+H]^+$ 386.1501, $C_{23}H_{20}N_3O_3$ requires 386.1499. **HPLC** (Chiralpak IC column, 70:30 hexanes/isopropanol, 1 mL/min); t_r = 30.8 min (minor), 39.9 min (major); 88 % ee.

5-(2-methoxybenzyl)-12,13-dihydro-4*bH*-isoquinolino[2,1-*a*]quinazolin-6(5*H*)-one (2.7e)



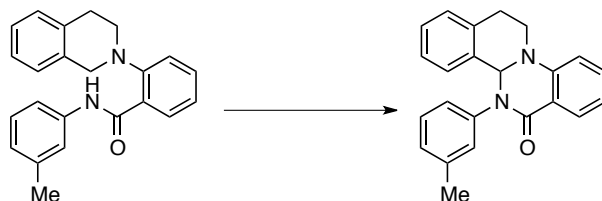
Subjection of **2.6e** (37 mg, 0.1 mmol) to General Procedure G gave the title compound (30 mg, 0.081 mmol, 81 % yield) as a white powder after purification by column chromatography on silica gel using Hex/EtOAc as eluent (1:1). **¹H NMR** (500 MHz, CDCl₃) δ 7.94 (d, *J* = 7.7 Hz, 1H), 7.50 (d, *J* = 7.4 Hz, 1H), 7.37 - 7.30 (m, 2H), 7.25 (d, *J* = 7.5 Hz, 1H), 7.17 (app p, *J* = 7.2 Hz, 2H), 7.03 (d, *J* = 6.8 Hz, 1H), 6.96 (app t, *J* = 7.5 Hz, 1H), 6.90 (d, *J* = 8.5 Hz, 1H), 6.88 (d, *J* = 8.5 Hz, 1H), 6.82 (app t, *J* = 7.5 Hz, 1H), 5.82 (s, 1H), 5.68 (d, *J* = 15.7 Hz, 1H), 4.48 (d, *J* = 15.7 Hz, 1H), 4.17 (dd, *J* = 14.4, 6.3 Hz, 1H), 3.82 (s, 3H), 3.62 (ddd, *J* = 14.5, 11.8, 5.8 Hz, 1H), 3.25 (ddd, *J* = 17.9, 11.0, 6.6 Hz, 1H), 2.74 (dd, *J* = 17.0, 5.3 Hz, 1H). **¹³C NMR** (126 MHz, CDCl₃) δ 164.54, 163.28, 157.36, 147.19, 134.36, 133.24, 129.37, 129.16, 128.92, 128.48, 127.97, 126.18, 125.62, 125.26, 120.79, 119.00, 118.34, 113.06, 110.16, 72.60, 55.29, 45.75, 44.66, 23.99. **HRMS** (ESI) found [M+H]⁺ 371.1756, C₂₄H₂₃N₂O₂ requires 371.1754. **HPLC** (Chiralpak IC column, 75:25 hexanes/isopropanol, 1 mL/min); t_r = 24.1 min (minor), 28.4 min (major); 94 % ee.

5-phenyl-12,13-dihydro-4*bH*-isoquinolino[2,1-*a*]quinazolin-6(5*H*)-one (2.7f)



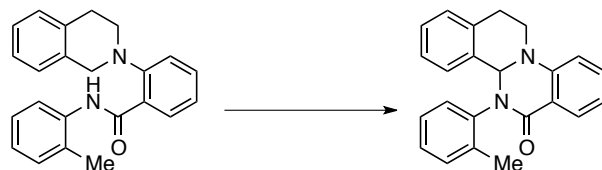
Subjection of **2.6f** (33 mg, 0.1 mmol) to General Procedure G gave the title compound (28 mg, 0.086 mmol, 86 % yield) as a white powder after purification by column chromatography on silica gel using Hex/EtOAc as eluent (4:1). **¹H NMR** (500 MHz, CDCl₃) δ 8.03 (d, *J* = 7.7 Hz, 1H), 7.52 (d, *J* = 7.9 Hz, 2H), 7.44 - 7.31 (m, 4H), 7.23 (app t, *J* = 7.4 Hz, 1H), 7.17 (app t, *J* = 7.4 Hz, 1H), 7.13 - 7.05 (m, 2H), 7.01 (d, *J* = 8.3 Hz, 1H), 6.90 (app t, *J* = 7.5 Hz, 1H), 6.19 (s, 1H), 4.26 (dd, *J* = 14.0, 6.2 Hz, 1H), 3.75 (ddd, *J* = 14.4, 11.3, 5.8 Hz, 1H), 3.32 (ddd, *J* = 17.5, 11.1, 6.9 Hz, 1H), 2.86 (dd, *J* = 17.1, 5.0 Hz, 1H). **¹³C NMR** (126 MHz, CDCl₃) δ 162.80, 147.40, 141.67, 135.66, 134.38, 133.77, 129.91, 129.14, 128.87, 128.19, 127.21, 126.16, 125.87, 125.01, 119.67, 119.16, 114.06, 75.34, 45.09, 24.58. **HRMS** (ESI) found [M+H]⁺ 327.1492, C₂₂H₁₉N₂O₁ requires 327.1492. **HPLC** (Chiralpak IA column, 70:30 hexanes/isopropanol, 1 mL/min); t_r = 10.1 min (minor), 15.6 min (major); 63 % ee.

5-(*m*-tolyl)-12,13-dihydro-4*bH*-isoquinolino[2,1-*a*]quinazolin-6(5*H*)-one (2.7g)



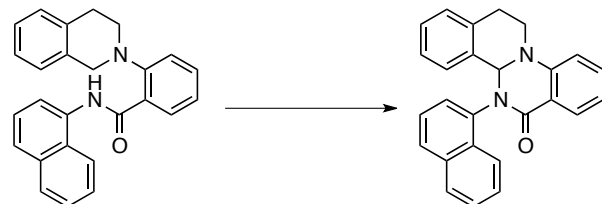
Subjection of **2.6g** (34 mg, 0.1 mmol) to General Procedure G gave the title compound (31 mg, 0.091 mmol, 91 % yield) as a white powder after purification by column chromatography on silica gel using Hex/EtOAc as eluent (4:1). **¹H NMR** (500 MHz, CDCl₃) δ 8.01 (d, *J* = 7.0 Hz, 1H), 7.46 - 7.35 (m, 3H), 7.34 - 7.26 (m, 2H), 7.18 (app t, *J* = 7.3 Hz, 1H), 7.11 (app t, *J* = 7.4 Hz, 1H), 7.06 (d, *J* = 7.0 Hz, 2H), 7.00 (d, *J* = 8.3 Hz, 1H), 6.89 (app t, *J* = 7.5 Hz, 1H), 6.17 (s, 1H), 4.27 (dd, *J* = 14.4, 6.1 Hz, 1H), 3.76 (ddd, *J* = 14.5, 11.5, 5.9 Hz, 1H), 3.32 (ddd, *J* = 17.6, 11.1, 6.9 Hz, 1H), 2.85 (dd, *J* = 17.1, 5.2 Hz, 1H), 2.39 (s, 3H). **¹³C NMR** (126 MHz, CDCl₃) δ 162.78, 147.32, 141.73, 138.74, 135.94, 134.34, 133.72, 129.89, 129.13, 128.70, 128.15, 127.14, 126.71, 126.16, 125.67, 121.81, 119.58, 119.17, 113.94, 75.45, 45.09, 24.42, 21.52. **HRMS** (ESI) found [M+H]⁺ 341.1647, C₂₃H₂₁N₂O requires 341.1648. **HPLC** (Chiralpak IC column, 70:30 hexanes/isopropanol, 1 mL/min); t_r = 17.4 min (minor), 48.0 min (major); 60 % ee.

5-(*o*-tolyl)-12,13-dihydro-4*bH*-isoquinolino[2,1-*a*]quinazolin-6(5*H*)-one (2.7h)



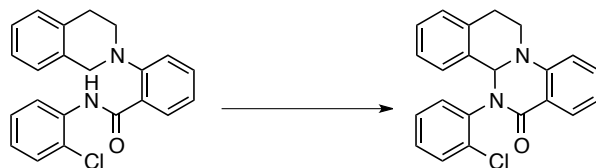
Subjection of **2.6h** (34 mg, 0.1 mmol) to General Procedure G gave the title compound (22 mg, 0.065 mmol, 65 % yield) as a white powder after purification by column chromatography on silica gel using Hex/EtOAc as eluent (4:1). **¹H NMR** (500 MHz, CDCl₃, major rotamer) δ 8.08 (d, *J* = 7.7 Hz, 1H), 7.46 (app t, *J* = 7.7 Hz, 1H), 7.23 - 7.10 (m, 4H), 7.10 - 7.04 (m, 4H), 7.03 - 6.96 (m, 2H), 6.00 (s, 1H), 4.16 - 4.06 (m, 1H), 3.61 (ddd, *J* = 13.7, 9.1, 5.9 Hz, 1H), 3.36 - 3.19 (m, 1H), 3.03 - 2.89 (m, 1H), 2.44 (s, 3H). **¹³C NMR** (126 MHz, CDCl₃) δ 162.90, 148.62, 139.53, 136.40, 134.67, 133.58, 133.50, 130.94, 129.69, 128.83, 128.28, 128.19, 127.65, 127.42, 126.30, 125.88, 120.58, 120.38, 115.72, 74.10, 44.98, 26.62, 18.91. **HRMS** (ESI) found [M+H]⁺ 341.1648, C₂₃H₂₁N₂O requires 341.1648. **HPLC** (Chiralpak IA column, 70:30 hexanes/isopropanol, 1 mL/min); t_r = 8.5 min (minor), 10.8 min (major); 91 % ee.

5-(naphthalen-1-yl)-12,13-dihydro-4*bH*-isoquinolino[2,1-*a*]quinazolin-6(5*H*)-one (2.7i)



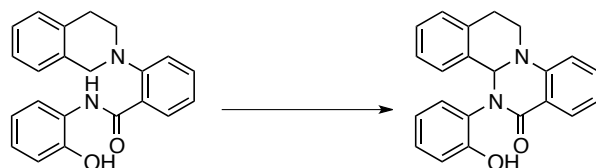
Subjection of **2.6i** (38 mg, 0.1 mmol) to General Procedure G gave the title compound (26 mg, 0.069 mmol, 69 % yield) as a white powder after purification by column chromatography on silica gel using Hex/EtOAc as eluent (4:1). $^1\text{H NMR}$ (500 MHz, CDCl_3) δ 8.25 (d, $J = 8.3$ Hz, 1H), 8.12 (d, $J = 7.7$ Hz, 1H), 7.91 (d, $J = 8.0$ Hz, 1H), 7.80 (d, $J = 8.1$ Hz, 1H), 7.61 (app t, $J = 7.6$ Hz, 1H), 7.58 - 7.52 (m, 2H), 7.49 (app t, $J = 7.8$ Hz, 1H), 7.43 (app t, $J = 7.7$ Hz, 1H), 7.25 (d, $J = 7.7$ Hz, 1H), 7.17 - 7.04 (m, 3H), 7.02 (app t, $J = 7.5$ Hz, 1H), 6.91 (app t, $J = 7.7$ Hz, 1H), 6.21 (s, 1H), 4.22 (ddd, $J = 12.2, 6.3, 3.7$ Hz, 1H), 3.66 (ddd, $J = 14.0, 9.9, 5.6$ Hz, 1H), 3.32 (ddd, $J = 16.2, 9.9, 6.2$ Hz, 1H), 2.99 - 2.87 (m, 1H). $^{13}\text{C NMR}$ (126 MHz, CDCl_3) δ 163.48, 148.54, 137.30, 134.70, 134.46, 133.70, 130.48, 129.92, 128.91, 128.73, 128.15, 128.10, 127.15, 127.13, 127.02, 126.14, 125.79, 125.24, 123.46, 120.44, 119.91, 115.39, 74.58, 45.06, 26.09. **HRMS** (ESI) found $[\text{M}+\text{Na}]^+$ 399.1472, $\text{C}_{26}\text{H}_{22}\text{N}_2\text{O}_1\text{Na}_1$ requires 399.1468. **HPLC** (Chiralpak IA column, 70:30 hexanes/isopropanol, 1 mL/min); $t_r = 13.7$ min (minor), 16.5 min (major); 82 % ee.

5-(2-chlorophenyl)-12,13-dihydro-4bH-isoquinolino[2,1-a]quinazolin-6(5H)-one (2.7j)



Subjection of **2.6j** (36 mg, 0.1 mmol) to General Procedure G gave the title compound (15 mg, 0.042 mmol, 42 % yield) as a white powder after purification by column chromatography on silica gel using Hex/EtOAc as eluent (4:1). $^1\text{H NMR}$ (500 MHz, CDCl_3) δ 8.16 (d, $J = 6.9$ Hz, 1H), 7.52 (app t, $J = 7.6$ Hz, 1H), 7.46 (d, $J = 7.6$ Hz, 1H), 7.19 - 7.07 (m, 6H), 7.07 - 6.95 (m, 2H), 6.95 - 6.75 (m, 3H), 6.24 (s, 1H), 4.03 - 3.89 (m, 1H), 3.54 (dd, $J = 12.1, 6.4$ Hz, 1H), 3.31 - 3.15 (m, 1H), 3.11 (dd, $J = 14.2, 7.8$ Hz, 1H). $^{13}\text{C NMR}$ (126 MHz, CDCl_3) δ 164.55, 163.52, 149.59, 137.32, 134.91, 134.52, 133.63, 131.06, 130.75, 129.83, 129.61, 129.16, 128.73, 128.52, 127.09, 125.87, 121.84, 121.27, 118.06, 72.44, 45.44, 28.65. **HRMS** (ESI) found $[\text{M}-\text{H}]^-$ 359.0945 $\text{C}_{22}\text{H}_{16}\text{N}_2\text{OCl}$ requires 359.0946. **HPLC** (Chiralpak IA column, 70:30 hexanes/isopropanol, 1 mL/min); $t_r = 8.0$ min (minor), 12.5 min (major); 87 % ee.

5-(2-hydroxyphenyl)-12,13-dihydro-4bH-isoquinolino[2,1-a]quinazolin-6(5H)-one (2.7k)



Subjection of **2.6k** (34 mg, 0.1 mmol) to General Procedure G gave the title compound (13 mg, 0.038 mmol, 38 % yield) as a white powder after purification by column chromatography on silica gel using Hex/EtOAc as eluent (4:1). $^1\text{H NMR}$ (300 MHz, CDCl_3) δ 8.35 (br s, 1H), 7.98 (d, $J = 7.8$ Hz, 1H), 7.48 - 7.33 (m, 2H), 7.33 - 6.74 (m, 9H), 6.32 (s, 1H), 4.31 (dd, $J = 14.4, 6.6$ Hz, 1H), 3.75 (ddd, $J = 14.4, 12.4, 5.5$ Hz, 1H), 3.31 (ddd, $J = 18.0, 11.9, 6.8$ Hz, 1H), 2.77 (dd, $J = 17.2, 5.0$ Hz, 1H). $^{13}\text{C NMR}$ (126 MHz, CDCl_3) δ 164.76, 152.02, 147.84, 134.70, 133.76, 130.18, 129.04, 128.64, 128.32, 128.28, 126.63, 126.52, 126.41, 125.44, 121.43, 120.84, 119.70, 117.39, 113.64, 44.95, 29.72, 24.19. **HRMS** (ESI) found $[\text{M}+\text{H}]^+$ 343.1439, $\text{C}_{22}\text{H}_{19}\text{N}_2\text{O}_2$ requires

343.1441. **HPLC** (Chiralpak IA column, 70:30 hexanes/isopropanol, 1 mL/min); t_r = 8.8 min (minor), 10.8 min (major); 80 % ee.

5-(tert-butyl)-12,13-dihydro-4bH-isoquinolino[2,1-a]quinazolin-6(5H)-one (2.7i)



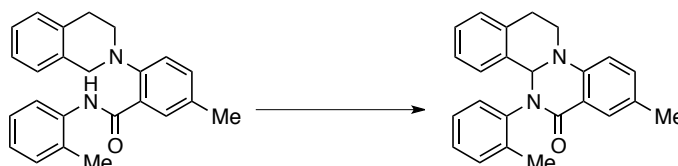
Subjection of **2.6i** (31 mg, 0.1 mmol) to General Procedure G gave the title compound (25 mg, 0.082 mmol, 82 % yield) as a white powder after purification by column chromatography on silica gel using Hex/EtOAc as eluent (4:1). $^1\text{H NMR}$ (300 MHz, CDCl_3) δ 7.79 (d, J = 7.8 Hz, 0H), 7.47 - 7.32 (m, 1H), 7.25 (app t, J = 7.7 Hz, 1H), 7.19 - 7.04 (m, 2H), 7.01 - 6.92 (m, 1H), 6.85 (d, J = 8.2 Hz, 1H), 6.74 (app t, J = 7.5 Hz, 0H), 5.93 (s, 1H), 4.24 (dd, J = 14.8, 7.3 Hz, 1H), 3.77 (ddd, J = 14.9, 11.8, 6.3 Hz, 1H), 3.26 (ddd, J = 18.7, 11.8, 7.5 Hz, 1H), 2.72 (dd, J = 17.3, 6.1 Hz, 1H), 1.71 (s, 9H). $^{13}\text{C NMR}$ (126 MHz, CDCl_3) δ 163.90, 146.71, 138.08, 134.17, 132.78, 129.16, 129.12, 127.64, 126.31, 126.00, 120.86, 119.04, 112.95, 70.62, 58.19, 45.33, 29.47, 23.53. **HRMS** (ESI) found $[\text{M}+\text{H}]^+$ 307.1805, $\text{C}_{20}\text{H}_{23}\text{N}_2\text{O}$ requires 307.1805. **HPLC** (Chiralpak IA column, 95:05 hexanes/isopropanol, 1 mL/min); t_r = 21.4 min (minor), 22.8 min (major); 73 % ee.

5-cyclohexyl-12,13-dihydro-4bH-isoquinolino[2,1-a]quinazolin-6(5H)-one (2.7m)



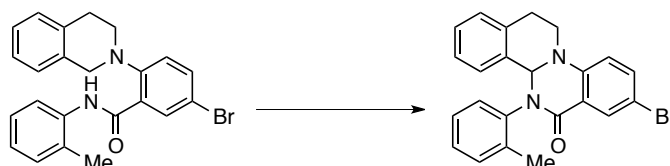
Subjection of **2.6m** (34 mg, 0.1 mmol) to General Procedure G gave the title compound (32 mg, 0.094 mmol, 94 % yield) as a white powder after purification by column chromatography on silica gel using Hex/EtOAc as eluent (9:1). $^1\text{H NMR}$ (500 MHz, CDCl_3) δ 7.86 (d, J = 7.7 Hz, 1H), 7.36 (d, J = 7.2 Hz, 1H), 7.28 (app t, J = 8.3 Hz, 1H), 7.16 - 7.07 (m, 2H), 6.99 (d, J = 7.1 Hz, 1H), 6.87 (d, J = 8.3 Hz, 1H), 6.78 (app t, J = 7.5 Hz, 1H), 5.68 (s, 1H), 4.69 (br s, 1H), 4.24 (dd, J = 14.7, 7.3 Hz, 1H), 3.81 (ddd, J = 14.7, 11.5, 6.5 Hz, 1H), 3.28 (ddd, J = 18.3, 11.4, 7.5 Hz, 1H), 2.80 (dd, J = 17.3, 6.3 Hz, 1H), 2.24 - 2.13 (m, 1H), 2.12 - 1.97 (m, 1H), 1.96 - 1.81 (m, 2H), 1.80 - 1.66 (m, 2H), 1.62 - 1.41 (m, 3H), 1.21 - 1.07 (m, 1H). $^{13}\text{C NMR}$ (126 MHz, CDCl_3) δ 163.33, 146.94, 134.27, 133.04, 129.40, 129.01, 127.77, 126.47, 125.81, 119.48, 119.05, 113.08, 99.77, 68.78, 54.50, 44.84, 32.42, 30.79, 25.92, 25.90, 25.53. **HRMS** (ESI) found $[\text{M}+\text{H}]^+$ 333.1963, $\text{C}_{22}\text{H}_{25}\text{N}_2\text{O}$ requires 333.1961. **HPLC** (Chiralpak IA column, 80:20 hexanes/isopropanol, 1 mL/min); t_r = 12.2 min (minor), 15.6 min (major); 80 % ee.

8-methyl-5-(o-tolyl)-12,13-dihydro-4bH-isoquinolino[2,1-a]quinazolin-6(5H)-one (2.7n)



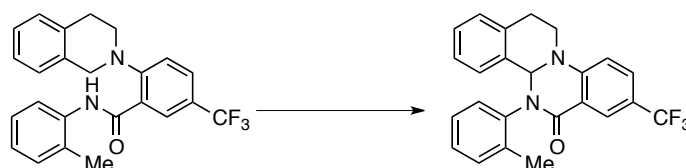
Subjection of **2.6n** (36 mg, 0.1 mmol) to General Procedure G gave the title compound (26 mg, 0.073 mmol, 73 % yield) as a white powder after purification by column chromatography on silica gel using Hex/EtOAc as eluent (4:1). **¹H NMR** (300 MHz, CDCl₃) δ 7.87 (s, 1H), 7.19 - 7.07 (m, 5H), 7.07 - 6.93 (m, 5H), 5.95 (s, 1H), 4.08 - 3.91 (m, 1H), 3.54 (ddd, *J* = 13.6, 8.2, 6.0 Hz, 1H), 3.28 - 3.11 (m, 1H), 3.07 - 2.88 (m, 1H), 2.40 (s, 3H), 2.31 (s, 3H). **¹³C NMR** (126 MHz, CDCl₃) δ 164.54, 162.97, 146.54, 139.47, 136.54, 134.59, 134.40, 130.86, 130.63, 129.57, 128.80, 128.24, 128.14, 127.83, 127.34, 126.28, 125.74, 120.77, 116.73, 74.09, 45.14, 26.72, 20.60, 18.91. **HRMS** (ESI) found [M+H]⁺ 355.1806, C₂₄H₂₃N₂O requires 355.1805. **HPLC** (Chiralpak IA column, 80:20 hexanes/isopropanol, 1 mL/min); t_r = 11.1 min (minor), 13.4 min (major); 90 % ee.

8-bromo-5-(*o*-tolyl)-12,13-dihydro-4*bH*-isoquinolino[2,1-*a*]quinazolin-6(5*H*)-one (2.7o)



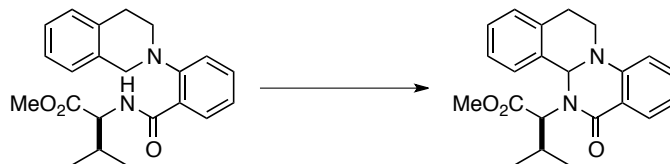
Subjection of **2.6o** (42 mg, 0.1 mmol) to General Procedure G gave the title compound (23 mg, 0.055 mmol, 55 % yield) as a white powder after purification by column chromatography on silica gel using Hex/EtOAc as eluent (4:1). **¹H NMR** (300 MHz, CDCl₃) δ 8.14 (s, 1H), 7.48 (dd, *J* = 8.6, 2.5 Hz, 1H), 7.23 - 6.96 (m, 8H), 6.90 (d, *J* = 8.7 Hz, 1H), 5.93 (s, 1H), 4.04 (ddd, *J* = 13.4, 6.5, 4.1 Hz, 1H), 3.59 (ddd, *J* = 13.5, 9.8, 5.7 Hz, 1H), 3.22 (ddd, *J* = 16.0, 9.6, 6.2 Hz, 1H), 3.05 - 2.83 (m, 1H), 2.38 (s, 3H). **¹³C NMR** (126 MHz, CDCl₃) δ 164.52, 161.67, 147.41, 139.36, 136.20, 134.45, 133.52, 132.23, 131.08, 128.93, 128.40, 128.00, 127.61, 127.49, 126.43, 126.06, 121.68, 117.17, 112.80, 74.28, 45.03, 26.30, 18.88. **HRMS** (ESI) found [M+H]⁺ 419.0755, C₂₃H₂₀N₂O₁Br₁ requires 419.0754. **HPLC** (Chiralpak IA column, 80:20 hexanes/isopropanol, 0.75 mL/min); t_r = 20.5 min (major), 21.8 min (minor); 93 % ee.

5-(*o*-tolyl)-8-(trifluoromethyl)-12,13-dihydro-4*bH*-isoquinolino[2,1-*a*]quinazolin-6(5*H*)-one (2.7p)



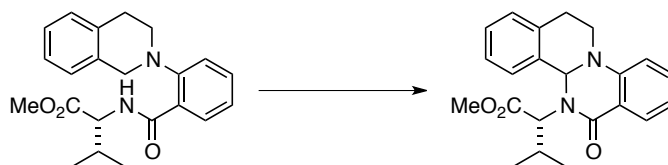
Subjection of **2.6p** (41 mg, 0.1 mmol) to General Procedure G gave the title compound (28 mg, 0.069 mmol, 69 % yield) as a white powder after purification by column chromatography on silica gel using Hex/EtOAc as eluent (4:1). **¹H NMR** (500 MHz, CDCl₃) δ 8.33 (s, 1H), 7.64 (d, *J* = 8.5 Hz, 1H), 7.32 (dd, *J* = 12.4, 7.9 Hz, 2H), 7.24 - 7.16 (m, 3H), 7.16 - 7.03 (m, 4H), 6.00 (s, 1H), 4.25 - 4.12 (m, 1H), 3.80 - 3.63 (m, 1H), 3.31 (ddd, *J* = 16.9, 11.1, 6.6 Hz, 1H), 2.94 (ddd, *J* = 16.3, 4.8, 2.6 Hz, 1H), 2.42 (s, 3H). **¹³C NMR** (126 MHz, CDCl₃) δ 164.64, 161.87, 150.52, 139.48, 135.96, 134.49, 133.88, 131.18, 130.20, 130.17, 128.98, 128.52, 127.97, 127.74, 127.44 (q, *J* = 3.8 Hz), 127.20, 126.50, 126.28, 118.86, 114.16, 74.37, 44.95, 26.25, 18.85. **HRMS** (ESI) found [M+H]⁺ 409.1525, C₂₄H₂₀N₂O₁F₃ requires 409.1522. **HPLC** (Chiralpak IC column, 80:20 hexanes/isopropanol, 1 mL/min); t_r = 21.1 min (minor), 23.9 min (major); 90 % ee.

(2*S*)-methyl 3-methyl-2-(6-oxo-12,13-dihydro-4*bH*-isoquinolino[2,1-*a*]quinazolin-5(6*H*)-yl)butanoate (2.18)



Subjection of **2.6q** (36 mg, 0.1 mmol) to General Procedure G gave the title compound (32 mg, 0.088 mmol, 88 % yield) as a 7:1 mixture of diastereomers in favor of diastereomer 1. The two diastereomers were separable by column chromatography on silica gel using Hex/EtOAc as eluent (10:1).

(2*R*)-methyl 3-methyl-2-(6-oxo-12,13-dihydro-4*bH*-isoquinolino[2,1-*a*]quinazolin-5(6*H*)-yl)butanoate (2.20)



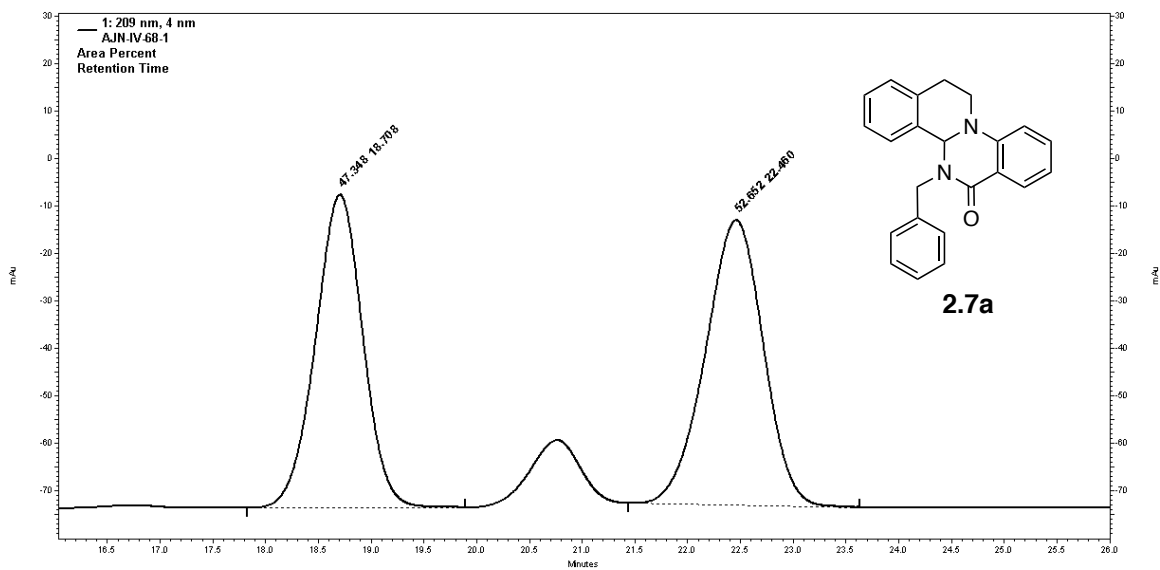
Subjection of **2.6r** (36 mg, 0.1 mmol) to General Procedure G gave the title compound (33 mg, 0.091 mmol, 91 % yield) as a 3:1 mixture of diastereomers in favor of diastereomer 2. The two diastereomers were separable by column chromatography on silica gel using Hex/EtOAc as eluent (10:1).

Diastereomer # 1

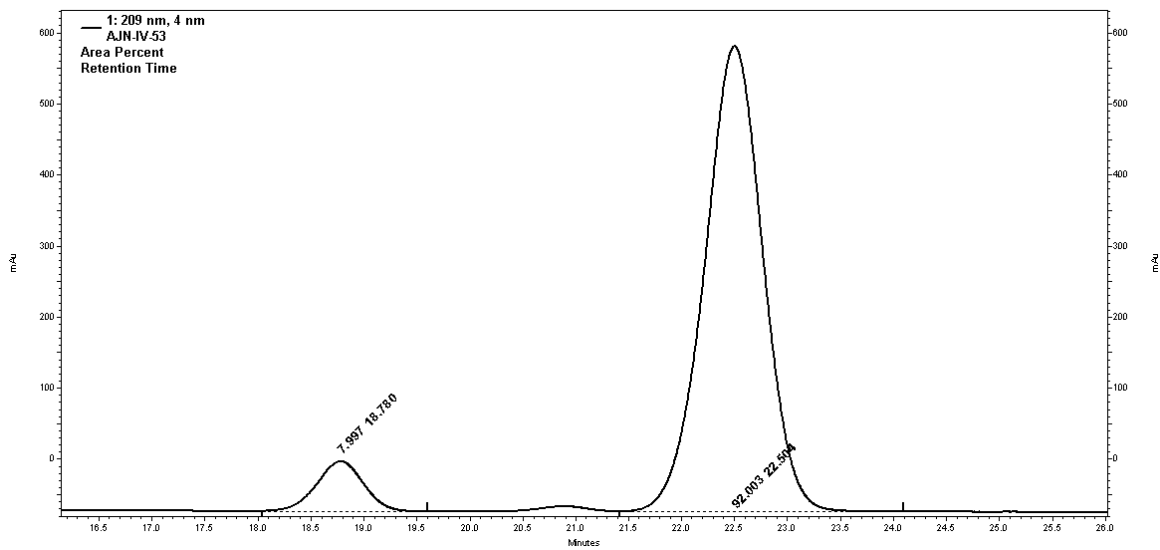
¹H NMR (500 MHz, CDCl₃) δ 7.88 (d, *J* = 7.7 Hz, 1H), 7.31 (app t, *J* = 7.7 Hz, 1H), 7.16 - 6.95 (m, 4H), 6.91 (d, *J* = 8.3 Hz, 1H), 6.80 (app t, *J* = 7.0 Hz, 1H), 6.02 (s, 1H), 5.34 (br s, 1H), 4.32 - 4.16 (m, 1H), 3.86-3.69 (m, 1H), 3.75 (s, 3H), 3.24 (ddd, *J* = 17.9, 11.2, 7.4 Hz, 1H), 2.89 - 2.74 (m, 1H), 2.50 - 2.25 (m, 1H), 1.11 - 0.88 (m, 6H). **¹³C NMR** (126 MHz, CDCl₃) δ 171.48, 164.54, 147.41, 134.24, 133.56, 129.91, 129.18, 127.85, 125.70, 119.15, 118.47, 113.48, 69.11, 62.16, 52.00, 44.78, 30.11, 19.45, 19.09. **HRMS** (ESI) found [M+H]⁺ 365.1861, C₂₂H₂₅N₂O₃ requires 365.1860.

Diastereomer # 2

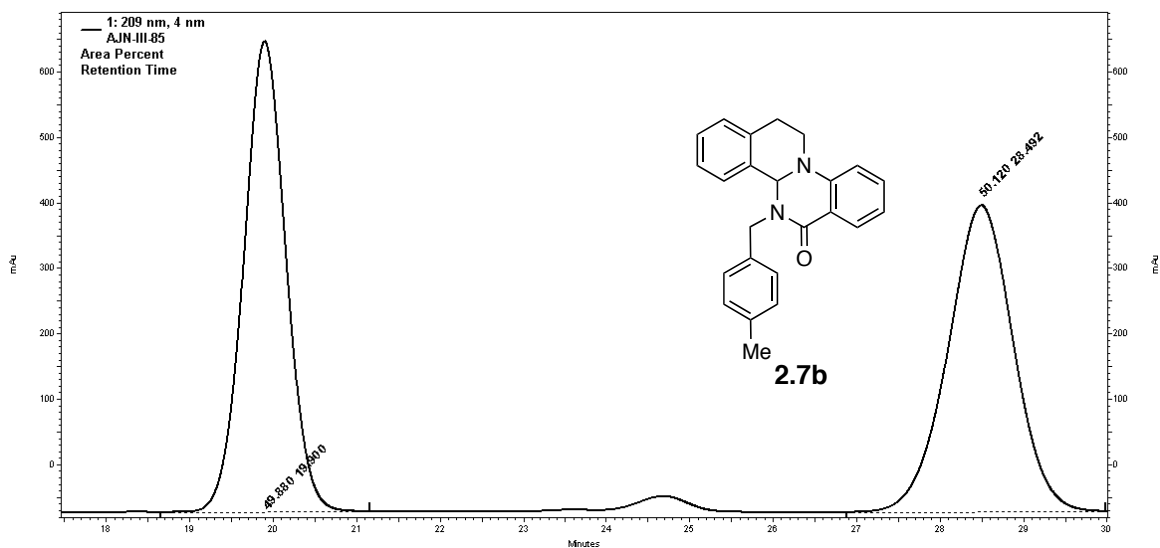
¹H NMR (500 MHz, CDCl₃) δ 7.85 (d, *J* = 8.0 Hz, 2H), 7.35 (app t, *J* = 7.8 Hz, 1H), 7.25 - 7.15 (m, 2H), 7.15 - 7.00 (m, 1H), 6.95 (d, *J* = 8.1 Hz, 1H), 6.90 - 6.74 (m, 1H), 5.81 (s, 1H), 4.33 - 4.08 (m, 1H), 4.06 - 3.76 (m, 4H), 3.72 - 3.58 (m, 1H), 3.32 (ddd, *J* = 17.5, 11.2, 6.9 Hz, 1H), 2.81 (dd, *J* = 18.8, 5.7 Hz, 1H), 2.70 - 2.54 (m, 1H), 1.18 (d, *J* = 6.7 Hz, 3H), 1.13 (d, *J* = 6.7 Hz, 3H). **¹³C NMR** (126 MHz, CDCl₃) δ 170.60, 164.59, 163.37, 147.58, 134.67, 133.45, 129.40, 129.23, 126.26, 119.58, 73.74, 66.41, 52.12, 45.22, 29.73, 29.25, 20.67, 19.93. **HRMS** (ESI) found [M+H]⁺ 365.1862, C₂₂H₂₅N₂O₃ requires 365.1860.



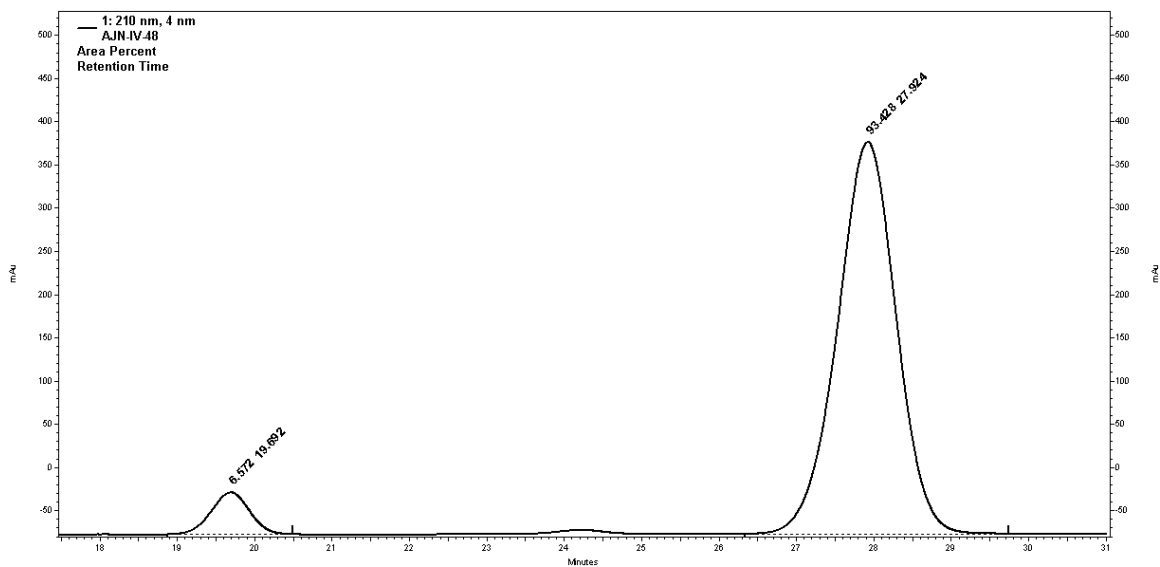
Peak #1	Retention Time (min)	Area Percent
1	18.8	47.34
2	22.5	52.65



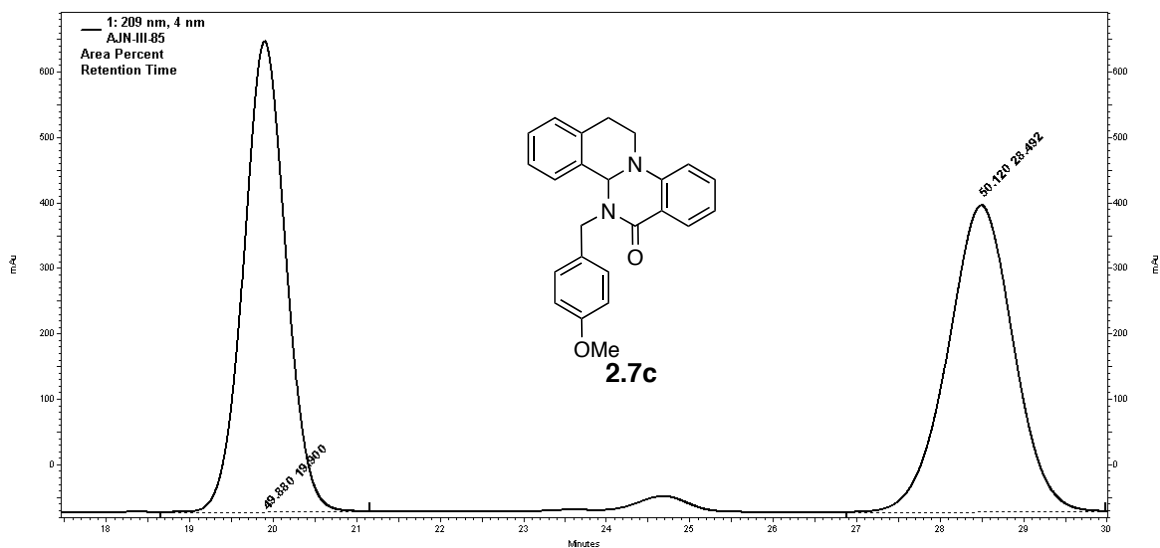
Peak #1	Retention Time (min)	Area Percent
1	18.7	8.00
2	22.5	92.00



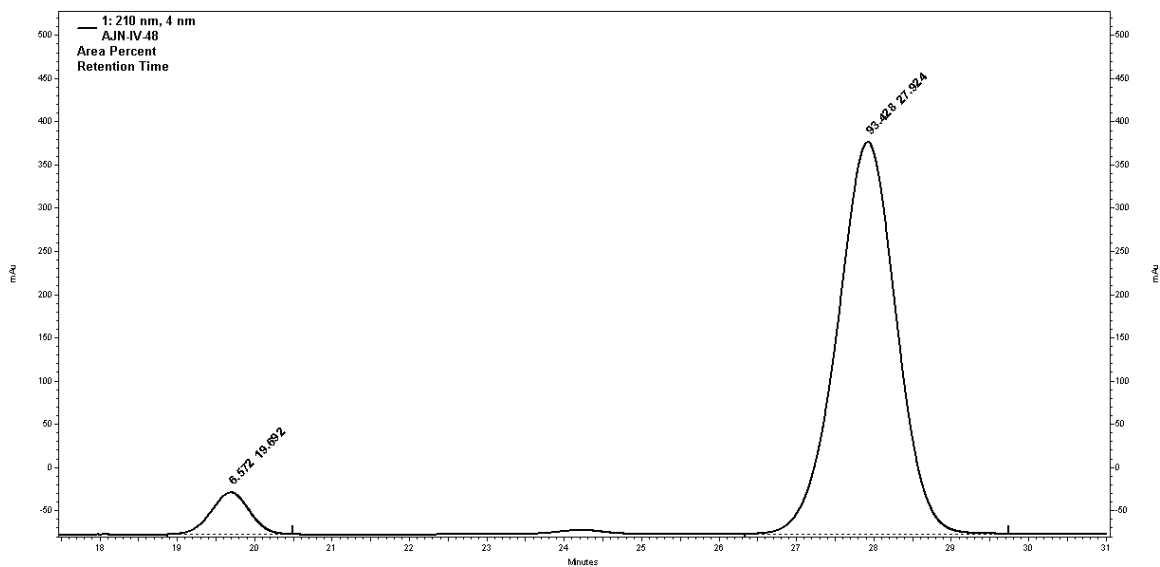
Peak #1	Retention Time (min)	Area Percent
1	19.9	49.88
2	28.5	50.12



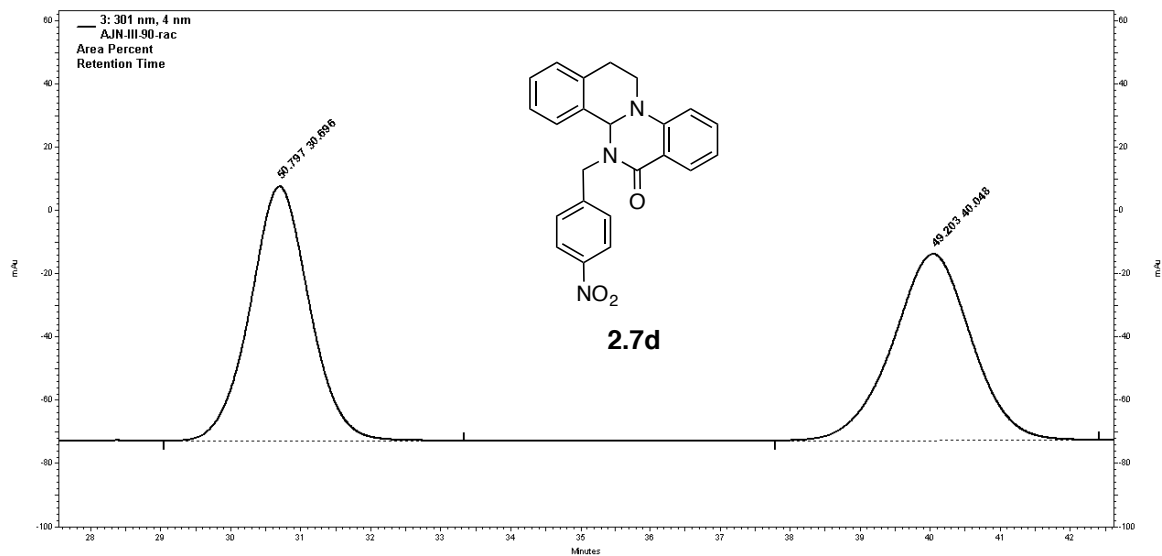
Peak #1	Retention Time (min)	Area Percent
1	19.7	6.57
2	27.9	93.43



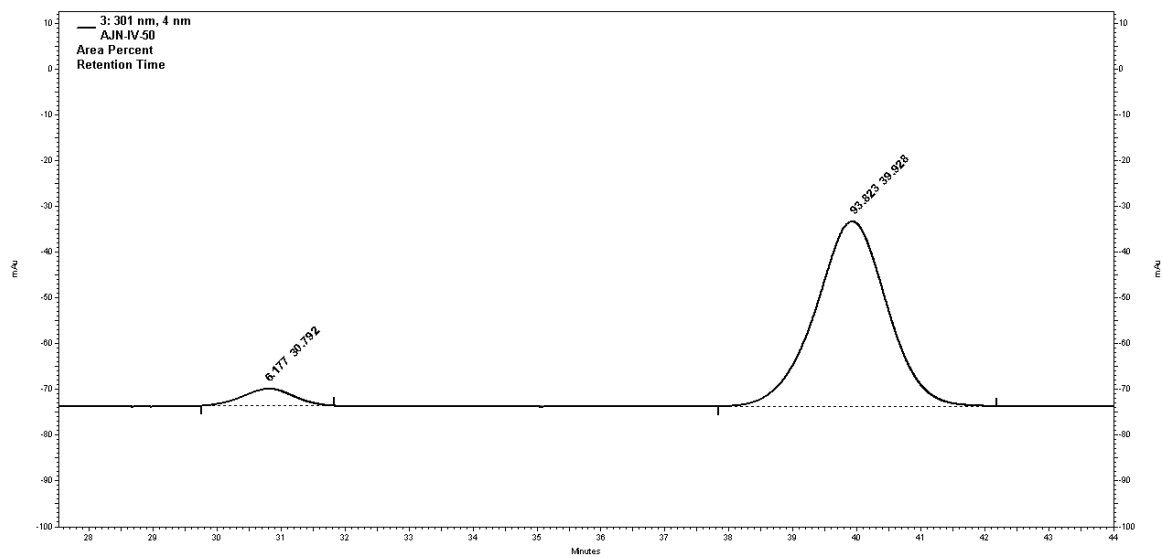
Peak #1	Retention Time (min)	Area Percent
1	19.9	49.88
2	28.5	50.12



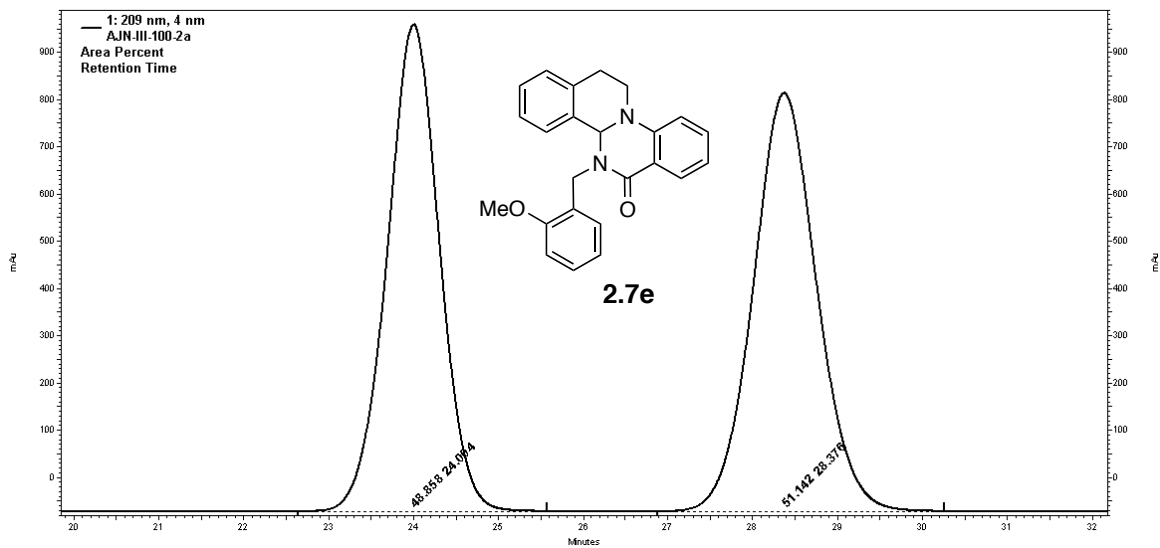
Peak #1	Retention Time (min)	Area Percent
1	19.7	6.57
2	27.9	93.43



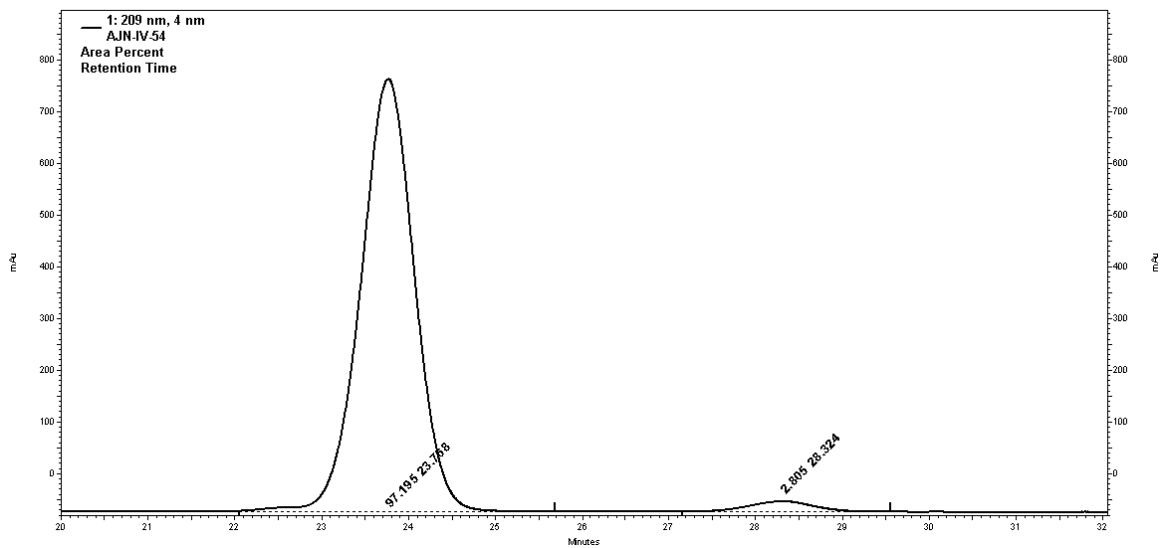
Peak #1	Retention Time (min)	Area Percent
1	30.7	50.80
2	40.0	49.20



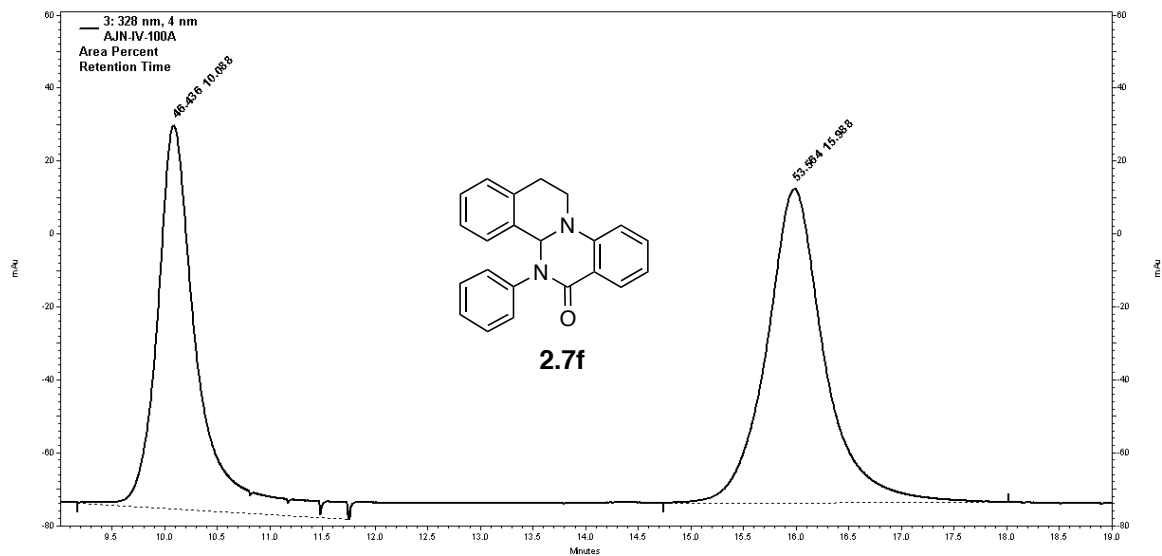
Peak #1	Retention Time (min)	Area Percent
1	30.8	6.18
2	39.9	93.82



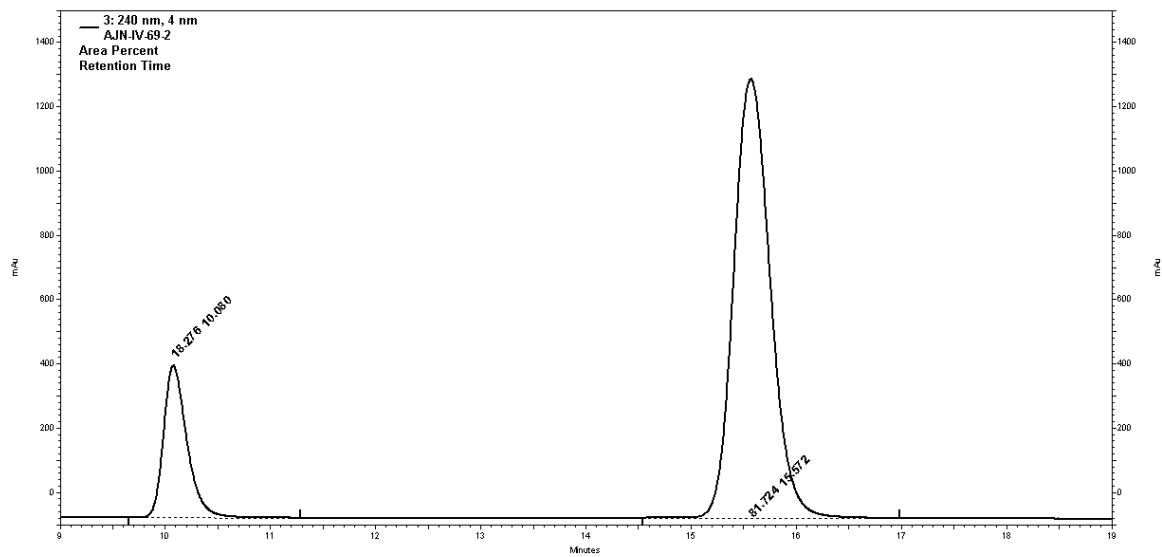
Peak #1	Retention Time (min)	Area Percent
1	24.1	48.86
2	28.4	51.14



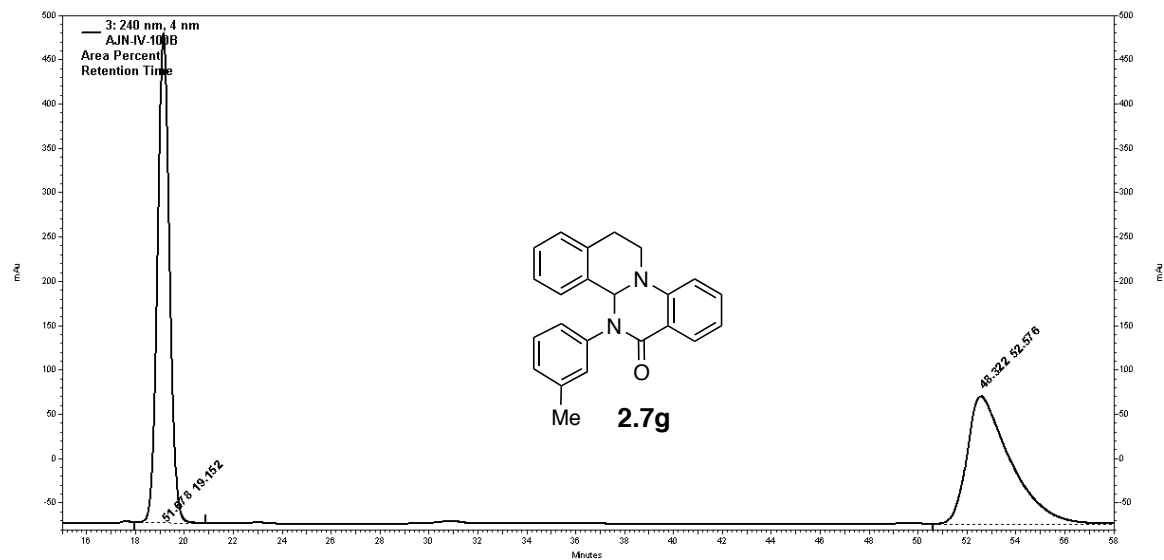
Peak #1	Retention Time (min)	Area Percent
1	23.8	97.20
2	28.3	2.80



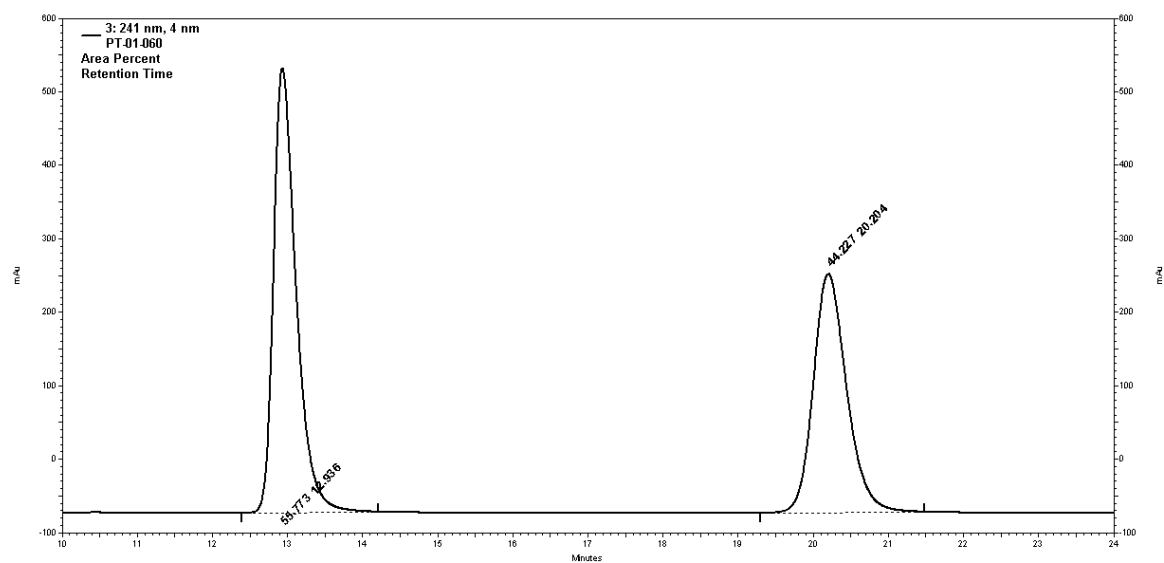
Peak #1	Retention Time (min)	Area Percent
1	10.1	46.43
2	16.0	53.56



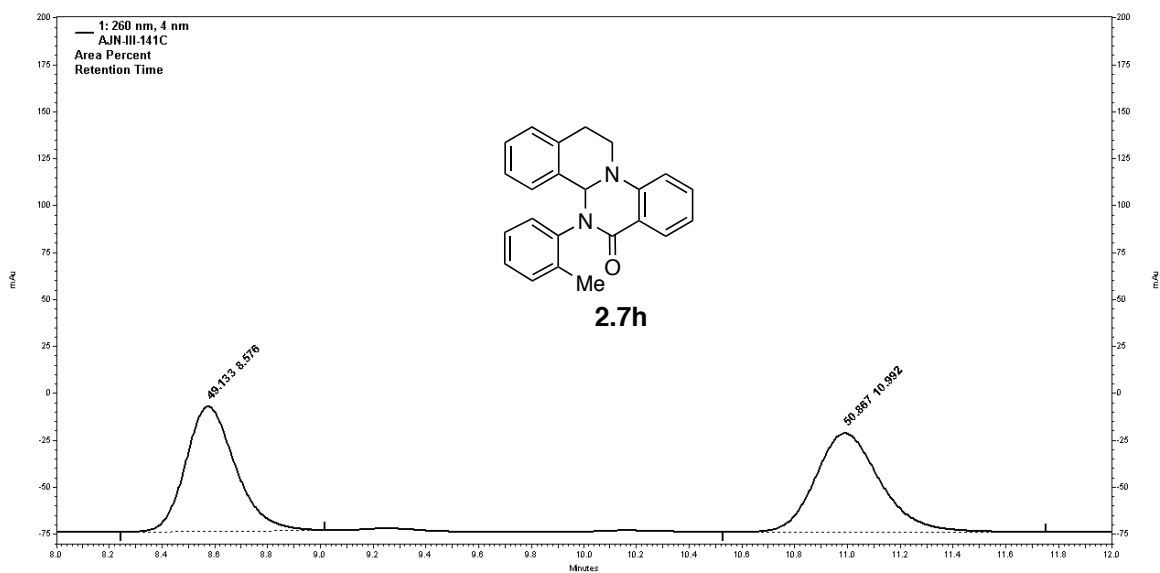
Peak #1	Retention Time (min)	Area Percent
1	10.1	18.28
2	15.6	81.72



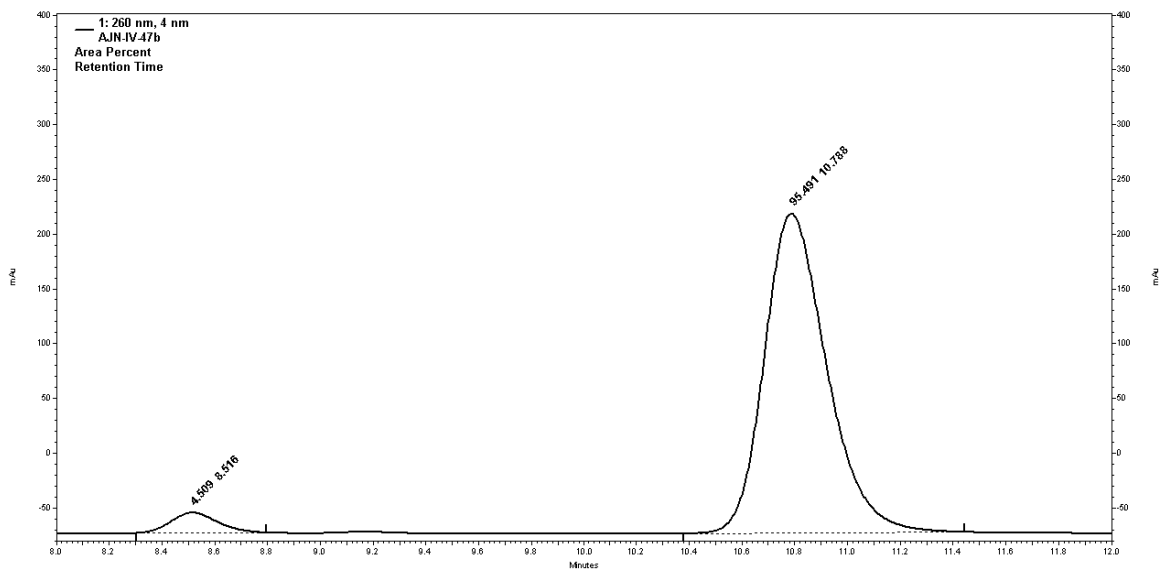
Peak #1	Retention Time (min)	Area Percent
1	19.2	51.68
2	52.6	48.32



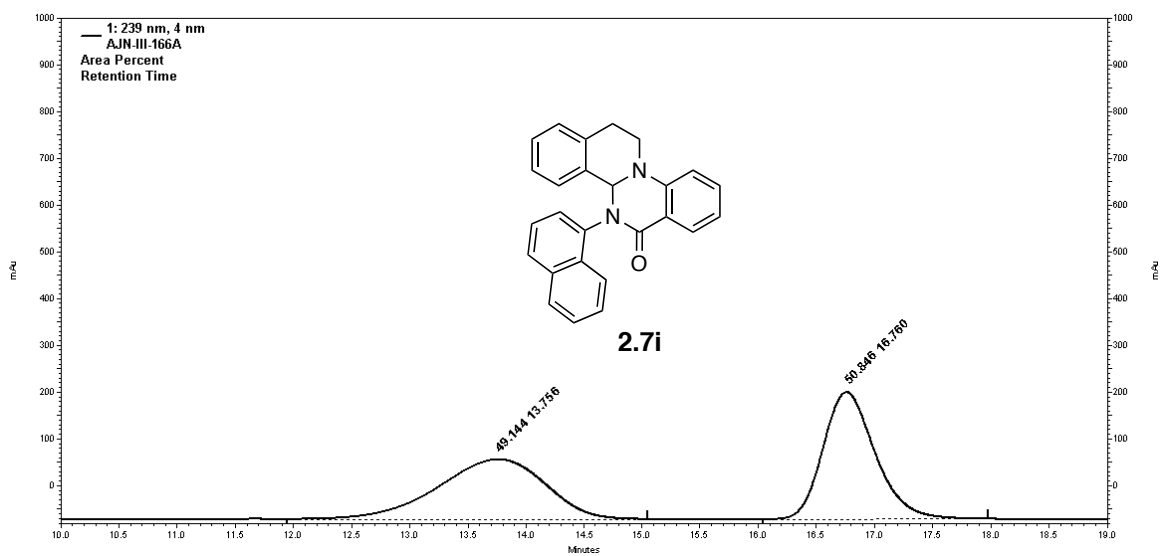
Peak #1	Retention Time (min)	Area Percent
1	17.4	79.76
2	48.0	20.24



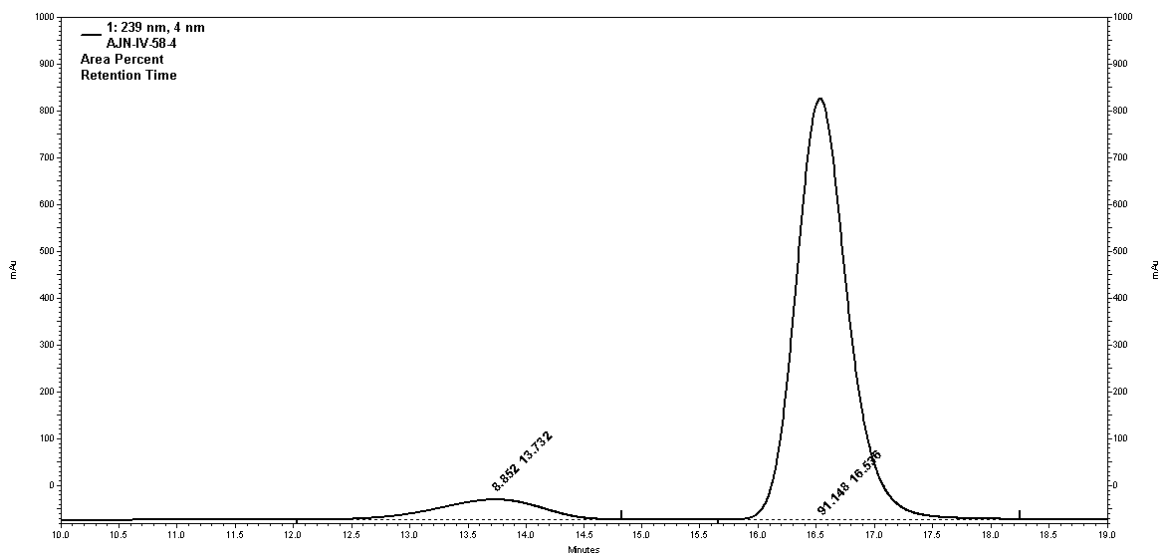
Peak #1	Retention Time (min)	Area Percent
1	8.6	49.13
2	11.0	50.87



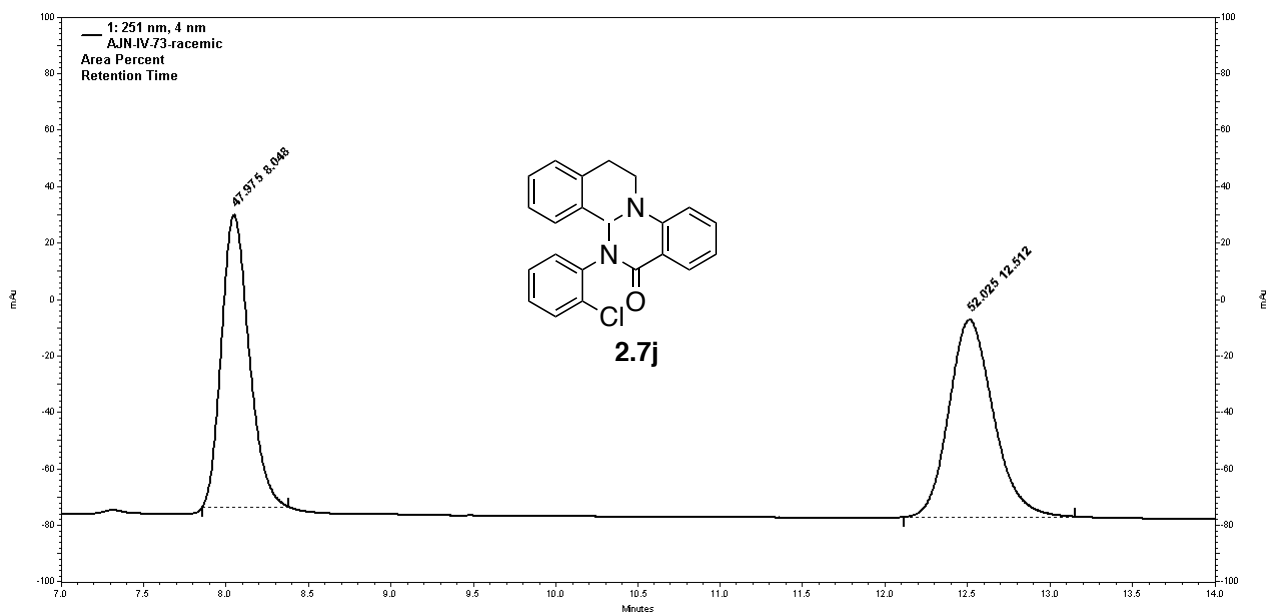
Peak #1	Retention Time (min)	Area Percent
1	8.5	4.51
2	10.8	95.49



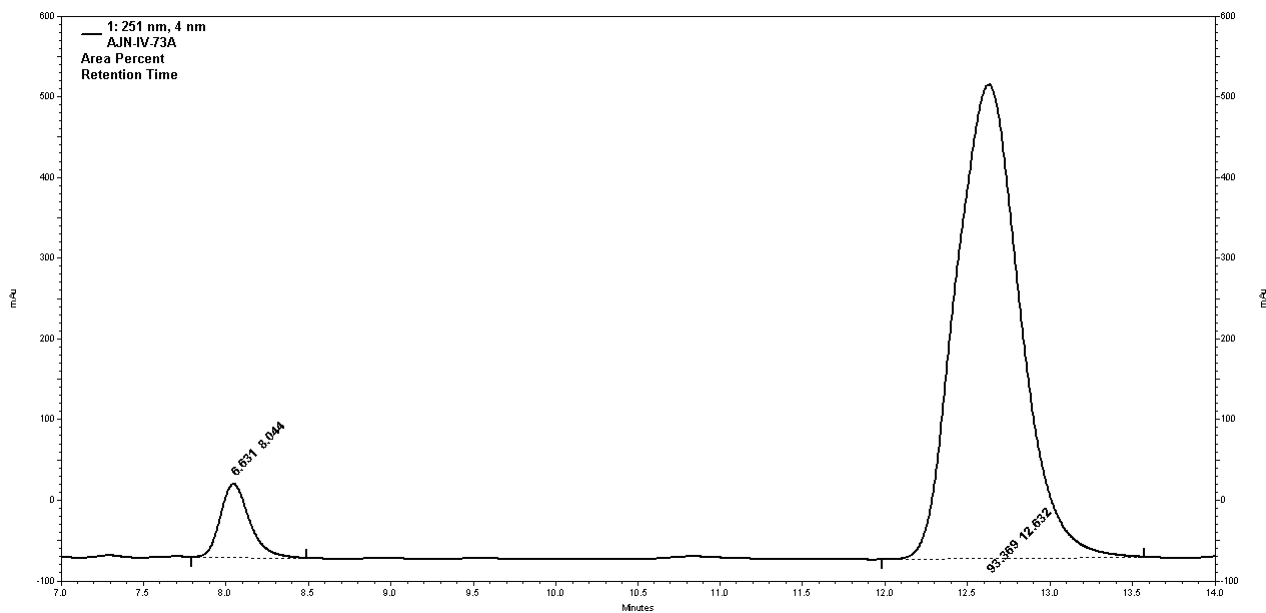
Peak #1	Retention Time (min)	Area Percent
1	13.8	49.14
2	16.8	50.85



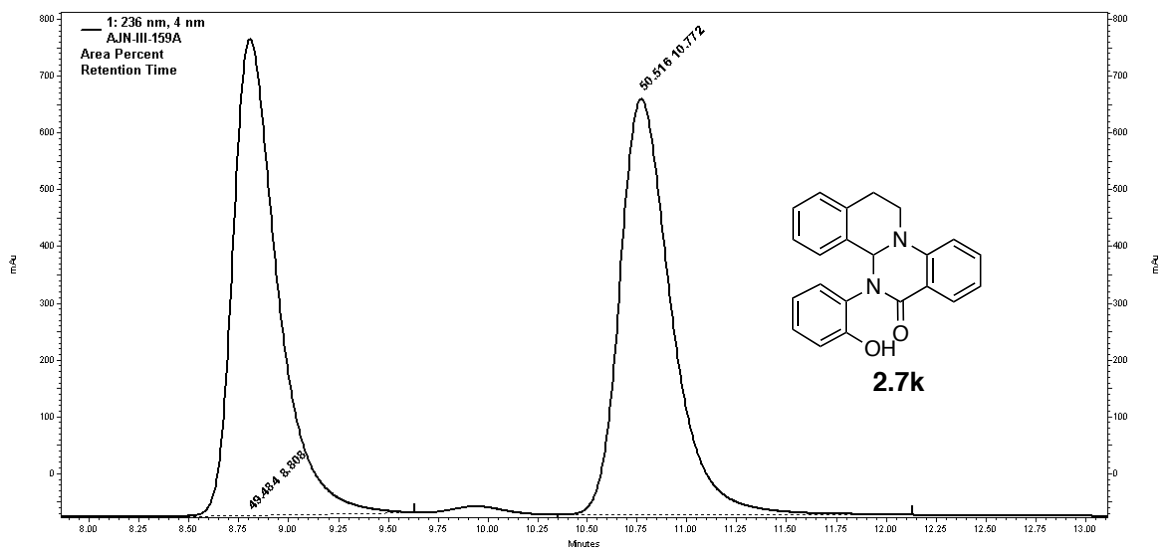
Peak #1	Retention Time (min)	Area Percent
1	13.7	8.85
2	16.5	91.15



Peak #1	Retention Time (min)	Area Percent
1	8.0	48.98
2	12.5	52.03

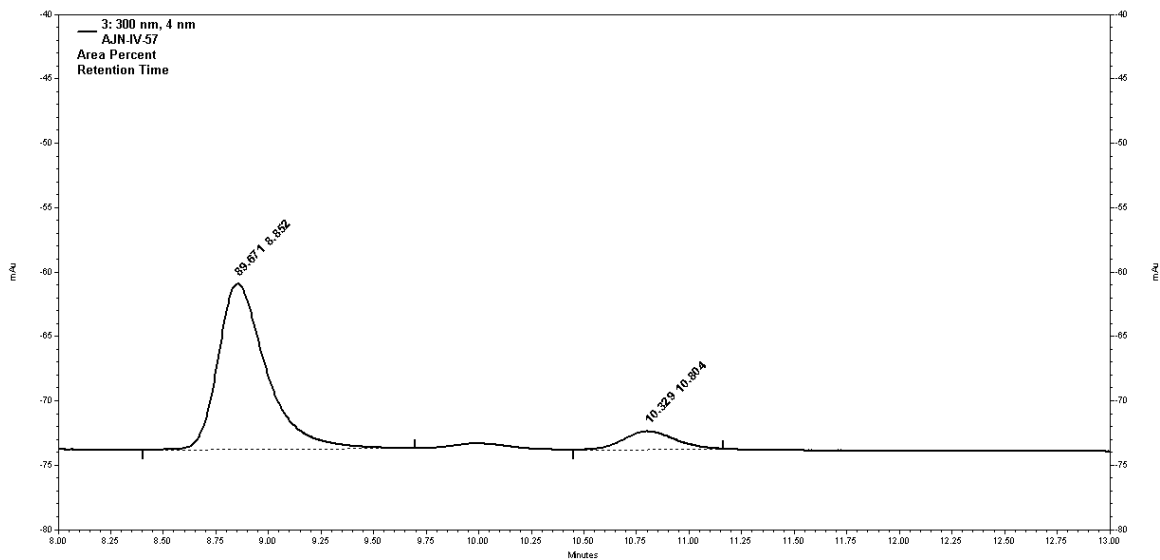


Peak #1	Retention Time (min)	Area Percent
1	8.0	6.63
2	12.6	93.37

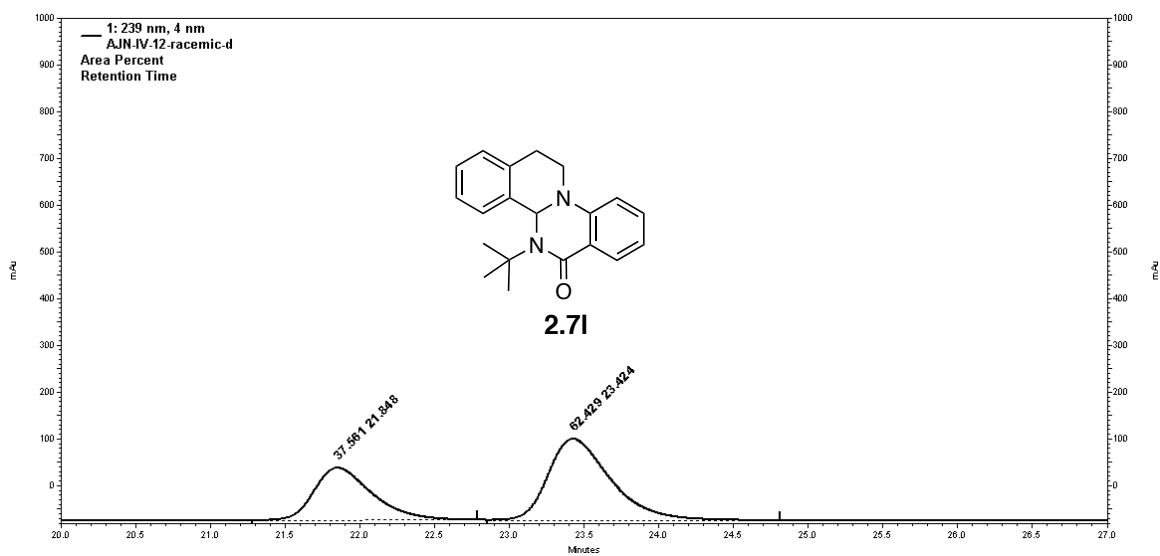


Peak #1	Retention Time (min)	Area Percent
1	8.8	49.48
2	10.8	50.52

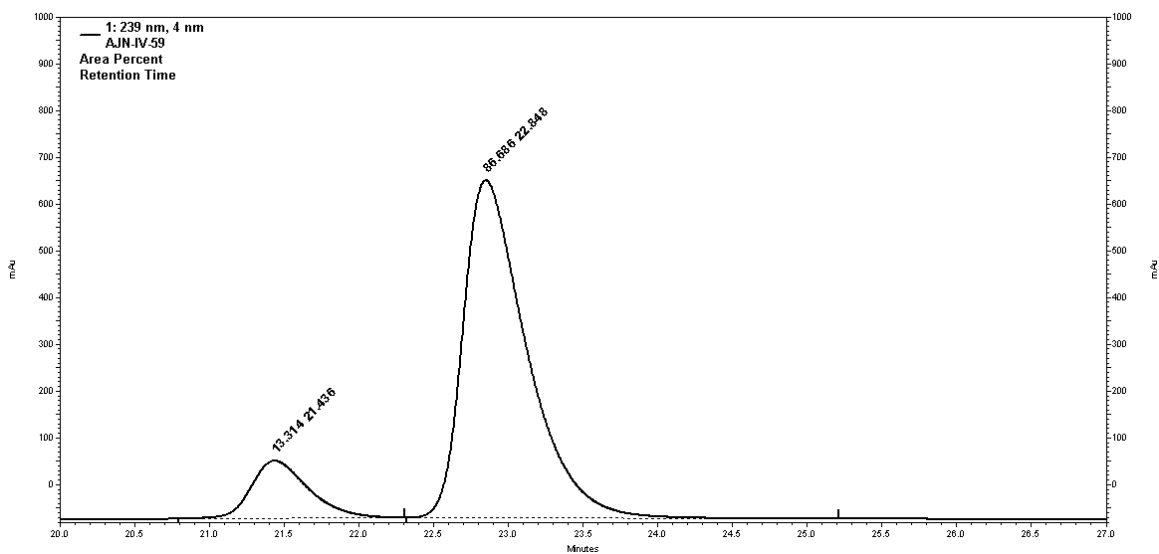
15



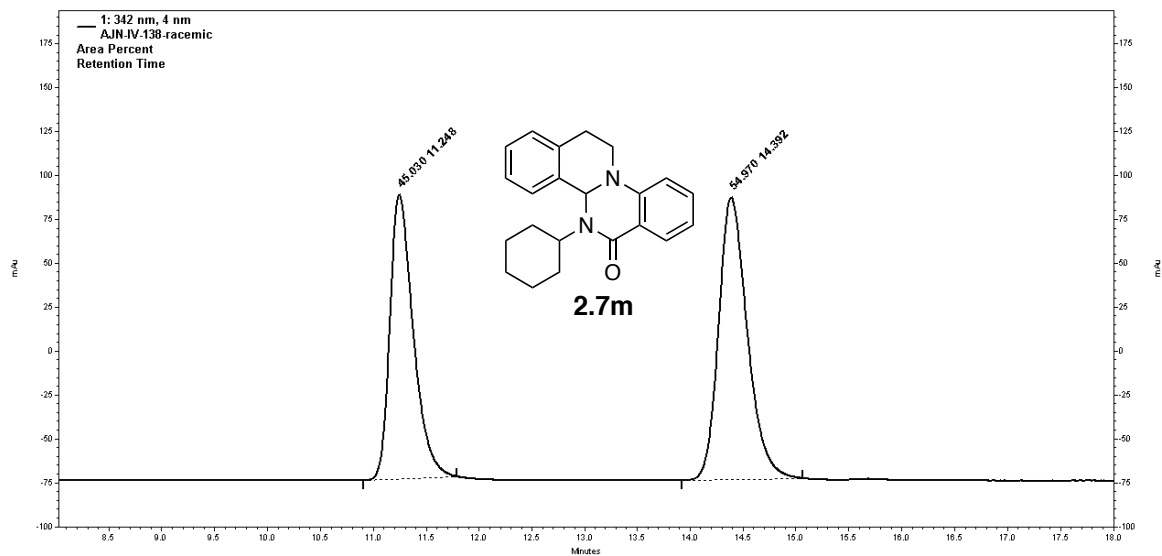
Peak #1	Retention Time (min)	Area Percent
1	8.9	89.67
2	10.8	10.33



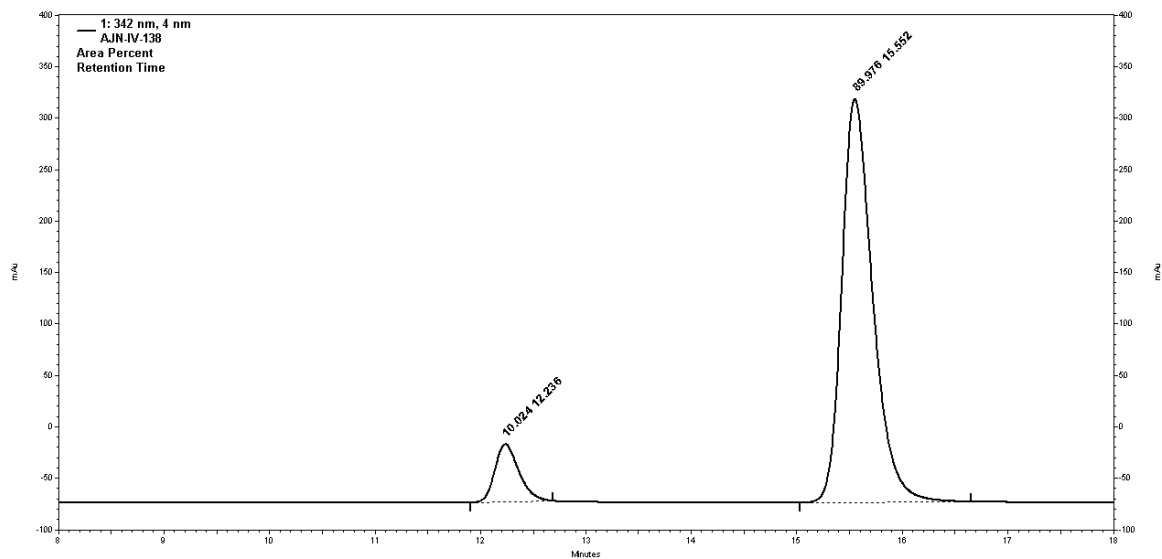
Peak #1	Retention Time (min)	Area Percent
1	21.8	37.56
2	23.4	62.43



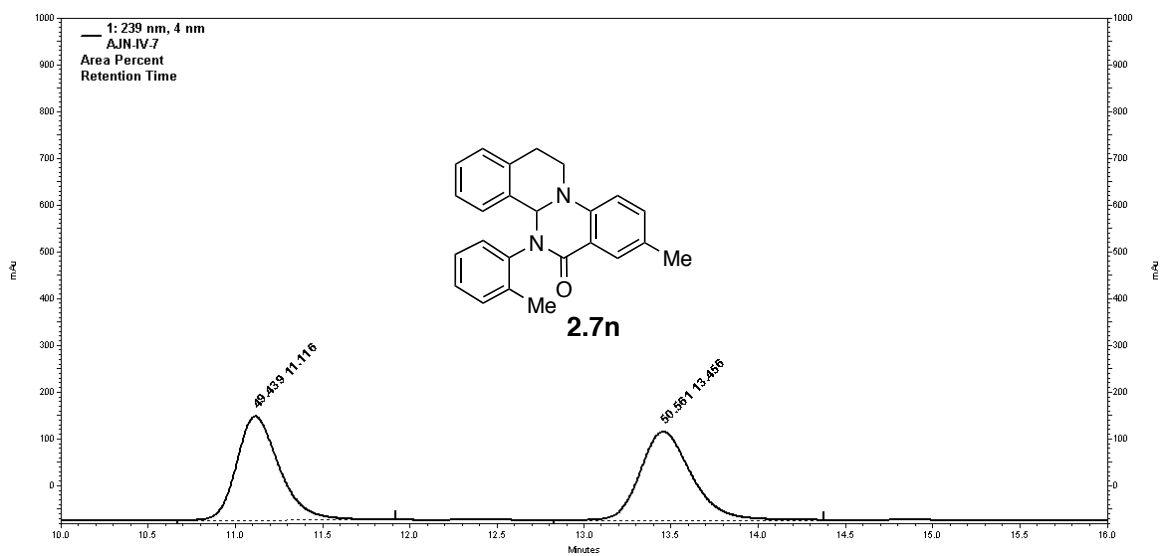
Peak #1	Retention Time (min)	Area Percent
1	21.4	13.31
2	22.8	86.61



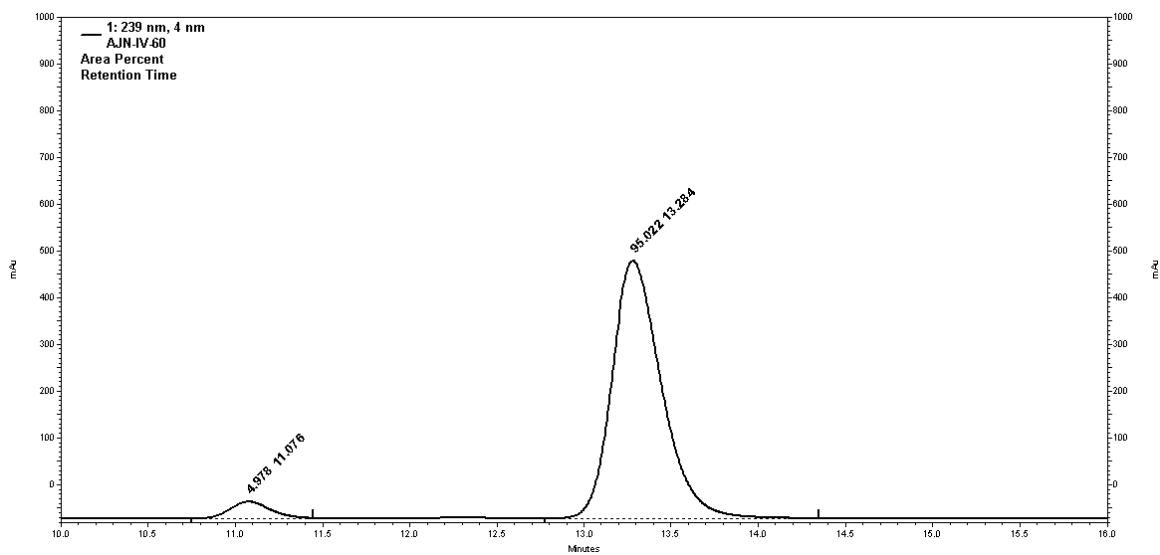
Peak #1	Retention Time (min)	Area Percent
1	11.2	45.03
2	14.4	54.97



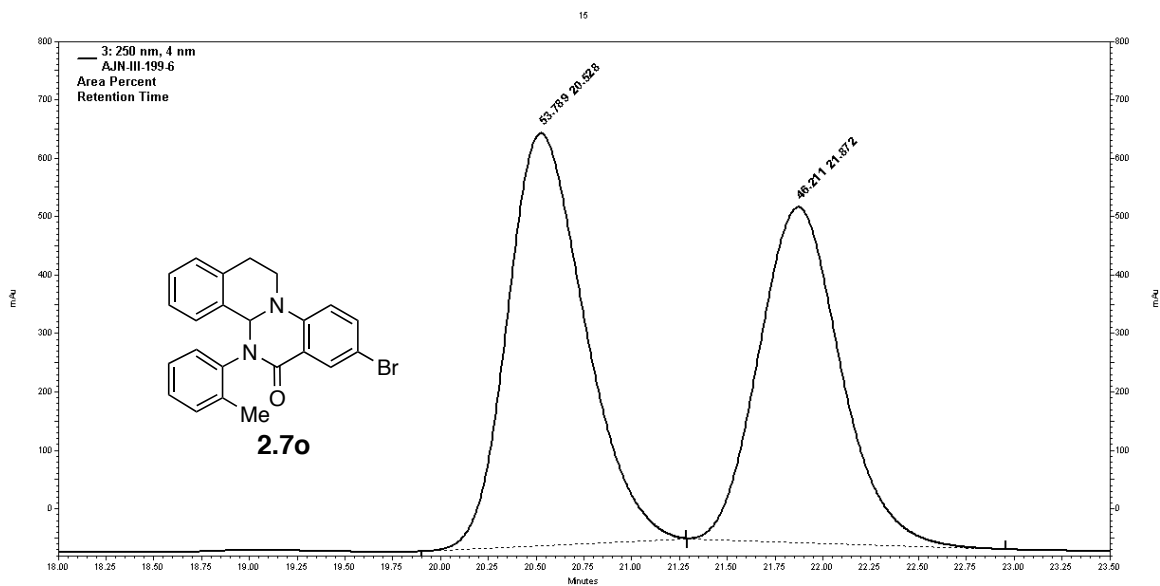
Peak #1	Retention Time (min)	Area Percent
1	12.2	10.02
2	15.6	89.98



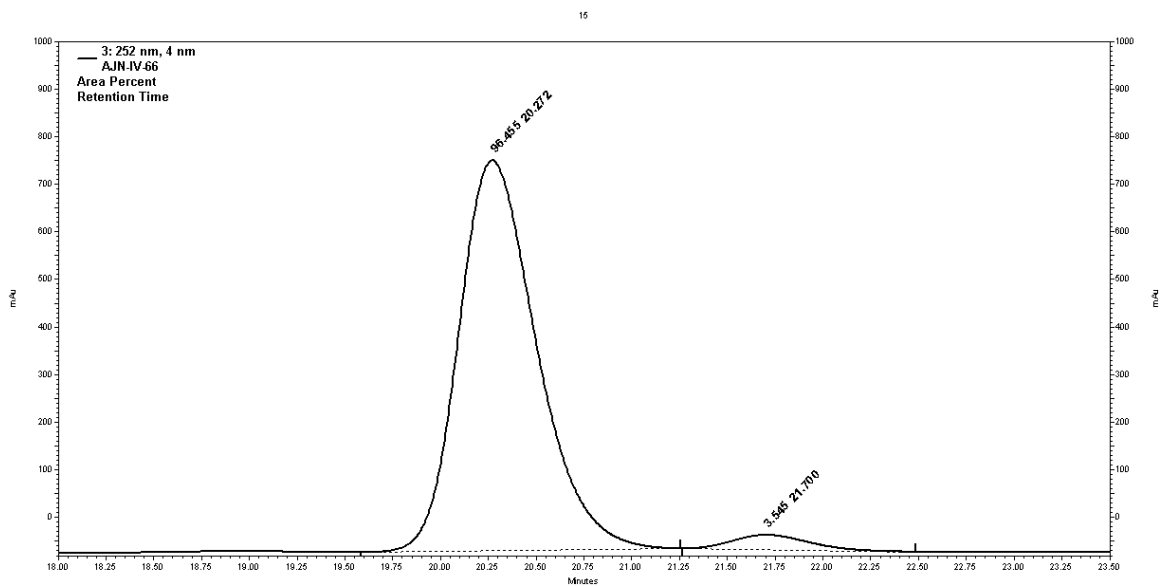
Peak #1	Retention Time (min)	Area Percent
1	11.1	49.44
2	13.5	50.56



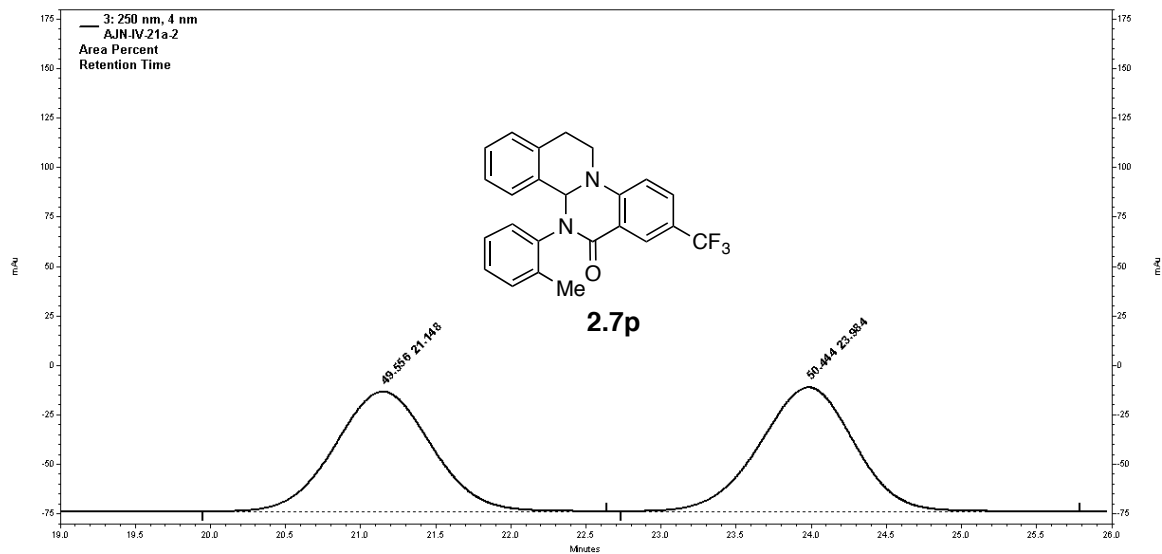
Peak #1	Retention Time (min)	Area Percent
1	11.1	4.98
2	13.3	95.02



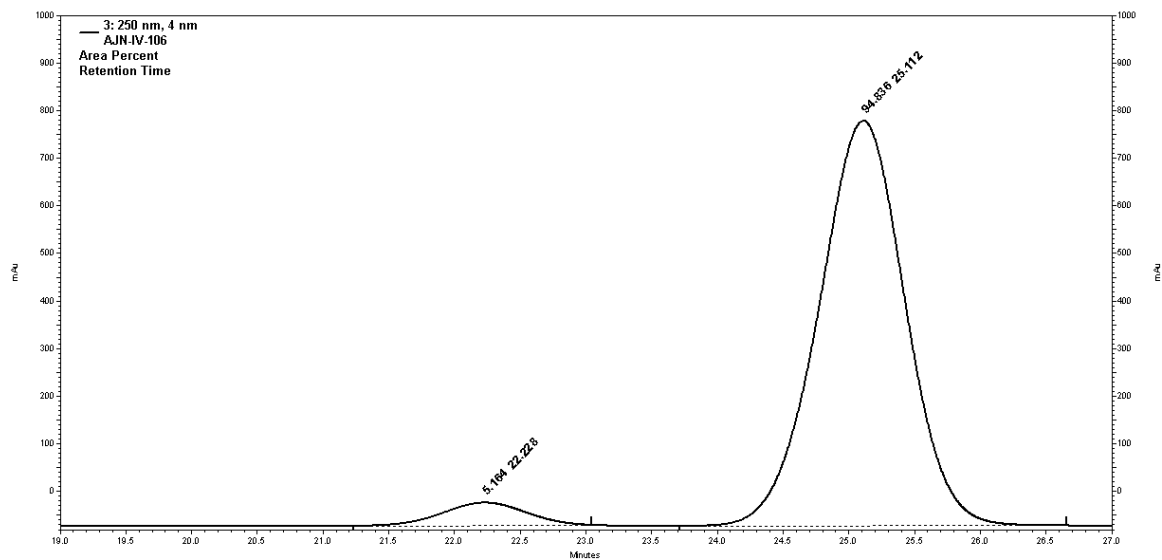
Peak #1	Retention Time (min)	Area Percent
1	20.5	53.79
2	21.9	46.21



Peak #1	Retention Time (min)	Area Percent
1	20.3	96.46
2	21.7	3.54



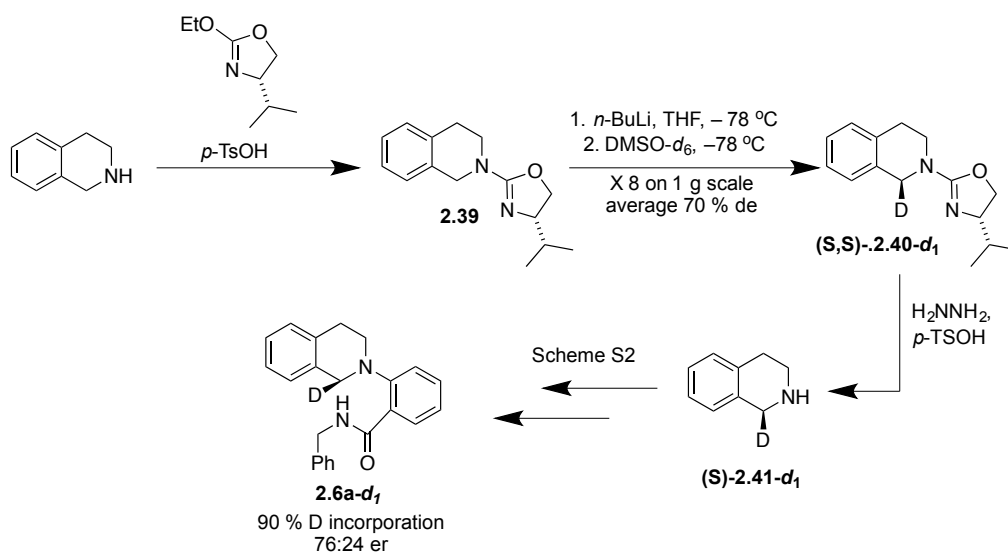
Peak #1	Retention Time (min)	Area Percent
1	21.1	49.56
2	24.0	50.44



Peak #1	Retention Time (min)	Area Percent
1	22.2	5.16
2	25.1	94.84

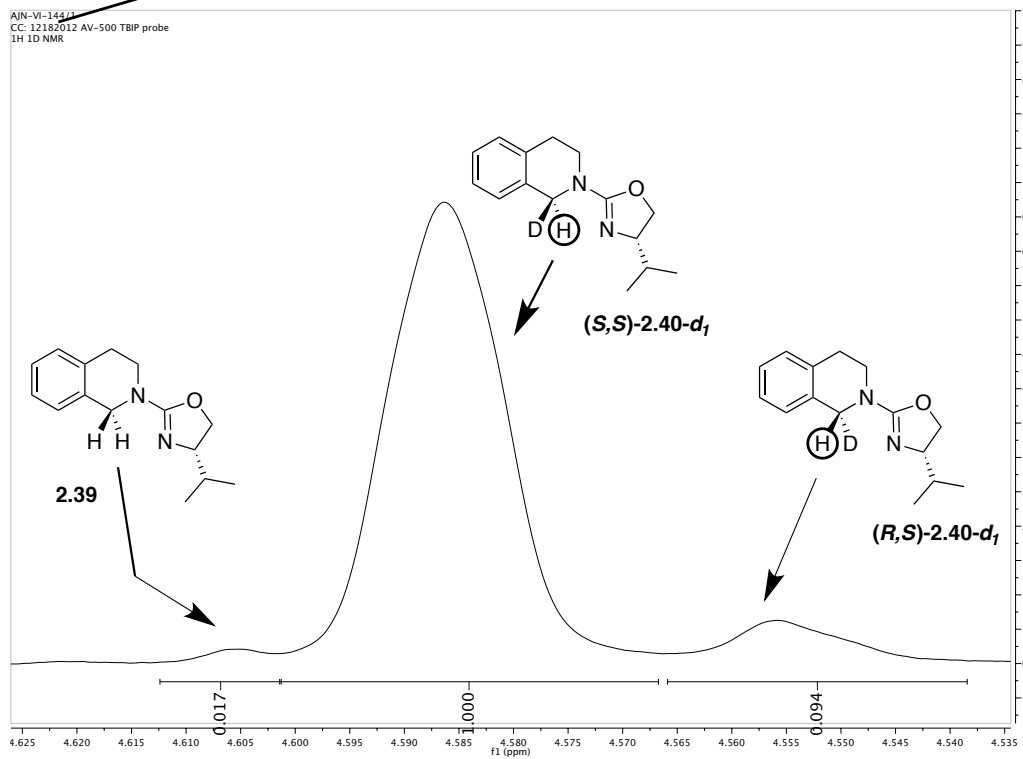
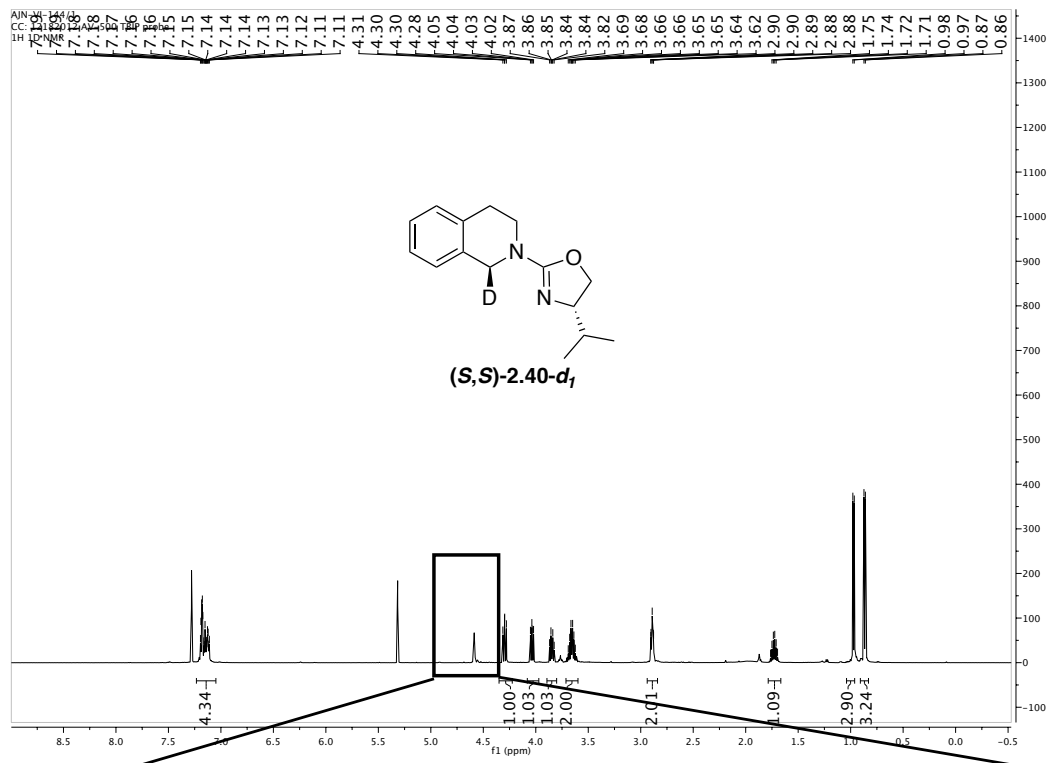
Kinetic Isotope Effect (KIE) Experiments

Enantioenriched substrate **2.6a-d₁** was prepared from the corresponding deuterated tetrahydroisoquinoline ((*S*)-**2.41-d₁**) according to reaction sequence depicted in Scheme 2.8 (*vide supra*). (*S*)-**2.41-d₁** in turn, was prepared by the method of Gawley and coworkers,¹¹² as shown in Scheme 2.9. It was determined that extent of both diastereomeric excess (de) and deuterium incorporation in the formation of intermediate (*S,S*)-**2.40-d₁** were highly dependent on the experimental conditions employed. The following procedure was found to give fairly reproducible results:

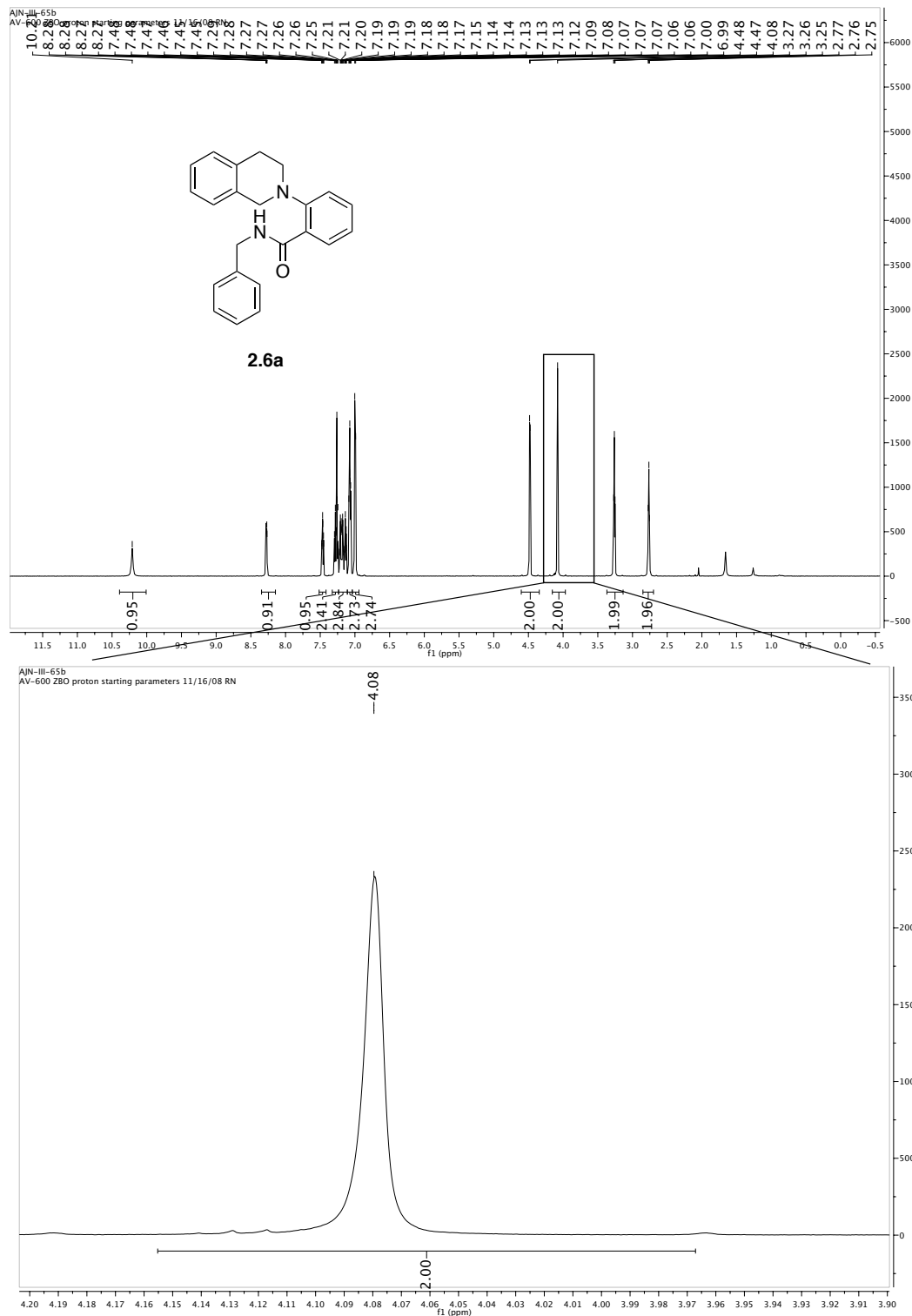


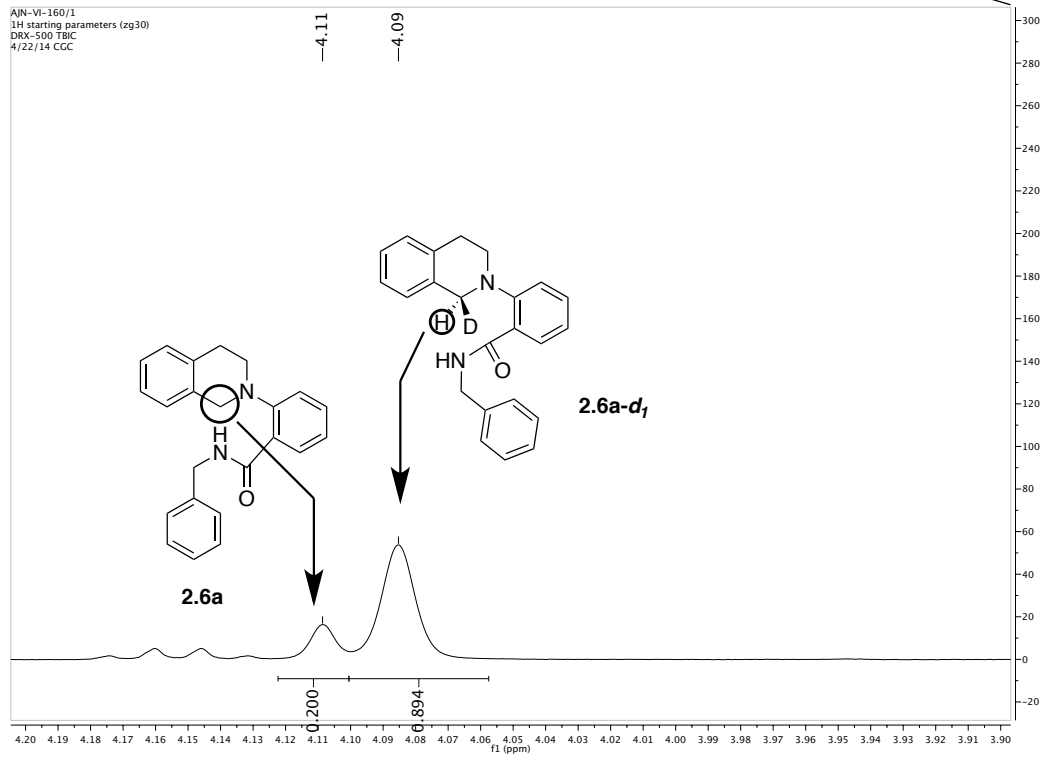
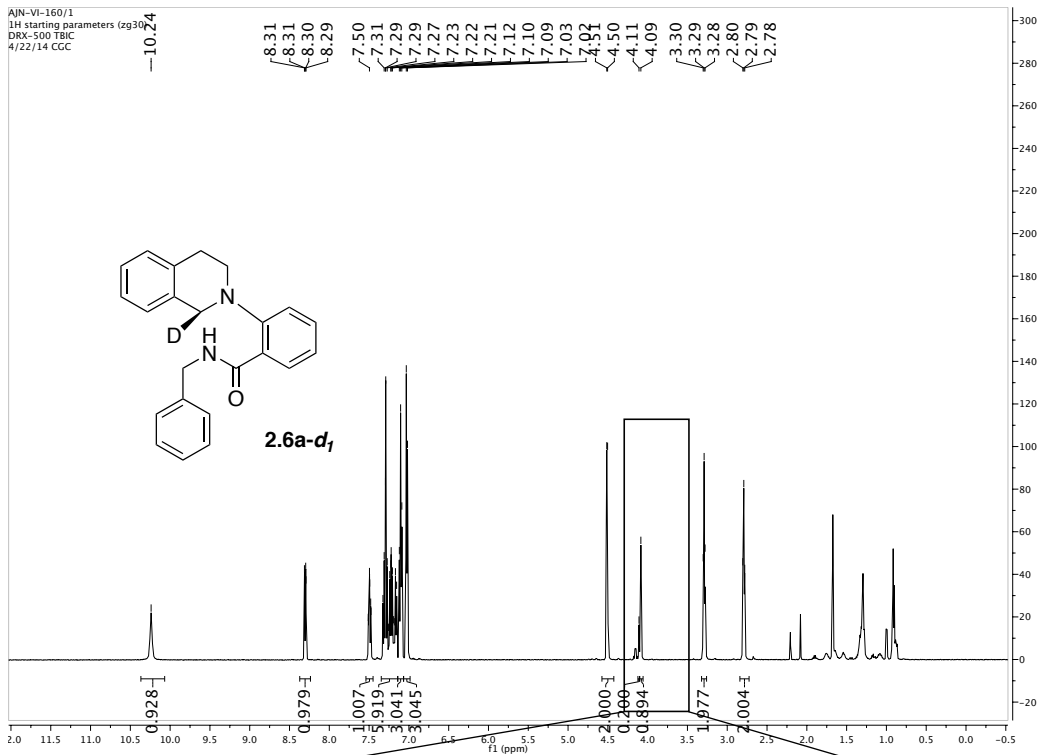
Scheme 2.9. Synthesis of substrate **2.6a-d₁**

A 250-mL flame-dried round bottomed flask equipped with a magnetic stir bar was charged with (*S*)-2-(3,4-dihydroisoquinolin-2(1*H*)-yl)-4-isopropyl-4,5-dihydrooxazole (**2.39**, 1.00 g, 4.09 mmol) and THF (40 mL) under an atmosphere of N₂. The resulting solution was cooled to -78 °C and allowed to stir for 30 min. *n*-Butyllithium (4.91 mmol, 2.5 M solution in hexanes, 1.96 mL) was added *via* syringe over 10 min in such a way that it ran slowly down the sides of the round-bottomed flask prior to entering the reaction mixture. The resulting red-orange mixture was stirred at -78 °C for 2 h at which point DMSO-*d*₆ (0.939 mL, 12.27 mmol) was added dropwise over the course of 10 min directly to the reaction mixture at -78 °C. The mixture was allowed to warm slowly to room temperature and quenched by the addition of H₂O (20 mL), extracted with EtOAc, dried (Na₂SO₄) and concentrated *in vacuo*. This procedure was repeated eight times, resulting in a total of 7.82 g of (*S,S*)-**2.40-d₁** (98% combined yield) with an average de of 70% and >99% D incorporation. The diastereomeric excess and extent of deuterium incorporation of (*S,S*)-**2.40-d₁** were readily determined by ¹H NMR analysis in CDCl₃ as previously reported by Gawley and coworkers.¹¹² An example spectrum is provided below. The singlets at 4.61, 4.59 and 4.56 correspond to **2.39**, (*S,S*)-**2.40-d₁** and (*R,S*)-**2.40-d₁** respectively. This example corresponds to a sample with 83% de and >99% D incorporation.

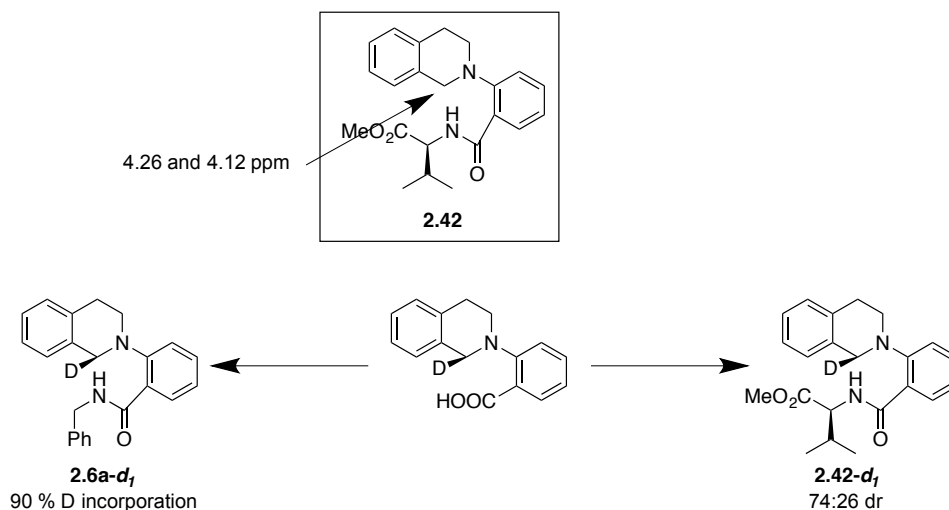


During the course of the synthesis of **2.6a-d₁**, deuterium content was eroded somewhat from that in **(S,S)-2.40-d₁** (i.e. from > 99 % to 90 % D incorporation). The extent of deuterium incorporation in **2.6a-d₁** was readily determined by ¹H NMR analysis by integrating the singlets at 4.08 and 4.06 ppm which correspond to **2.6a** and **2.6a-d₁** respectively. Spectra are provided below of **2.6a** and **2.6a-d₁** with 90 % D incorporation.





Given the extent of deuterium erosion over the course of the synthesis of **2.6a-d₁** (from >99 % in (*S,S*)-**2.40-d₁** to 90 % in **2.6a-d₁**), it was necessary to determine its enantiomeric excess, as it was presumably different from that of (*S,S*)-**2.40-d₁**. This was accomplished by the formation of *L*-Valine methyl ester derived compound **2.42-d₁** (Scheme 2.10), as the resonances corresponding to the indicated protons in **2.42** were previously shown to be well resolved doublets in the ¹H NMR spectrum in CDCl₃ (4.26 and 4.12 ppm).



Scheme 2.10. Determination of er of **2.6a-d₁**

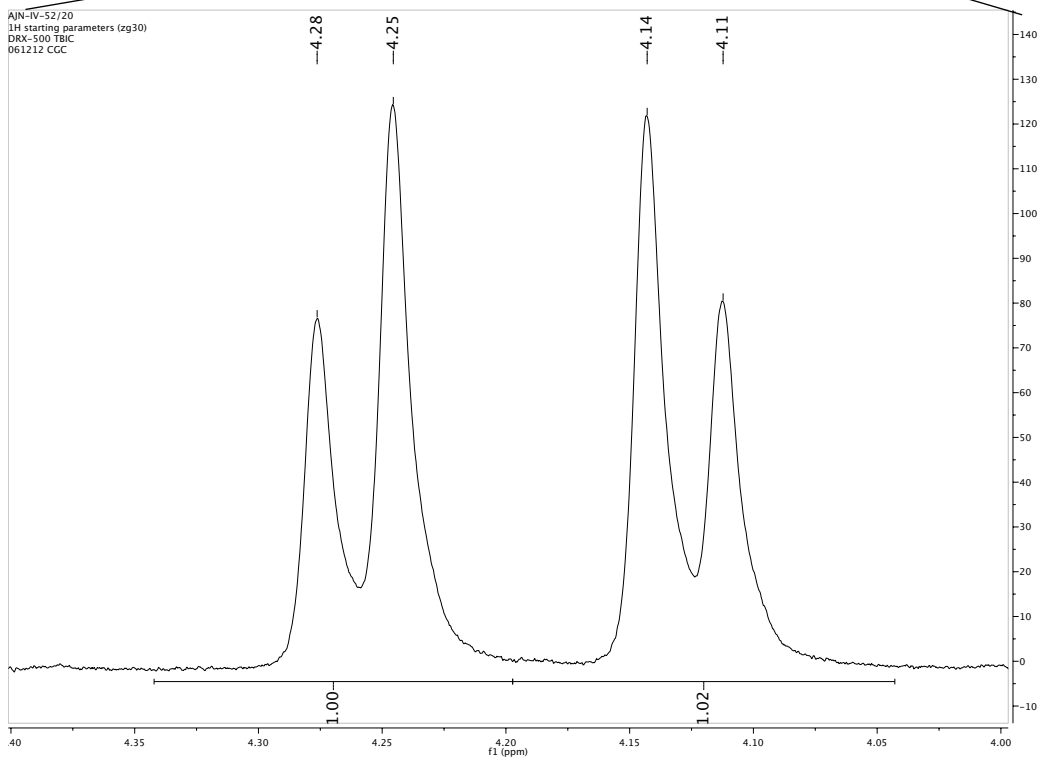
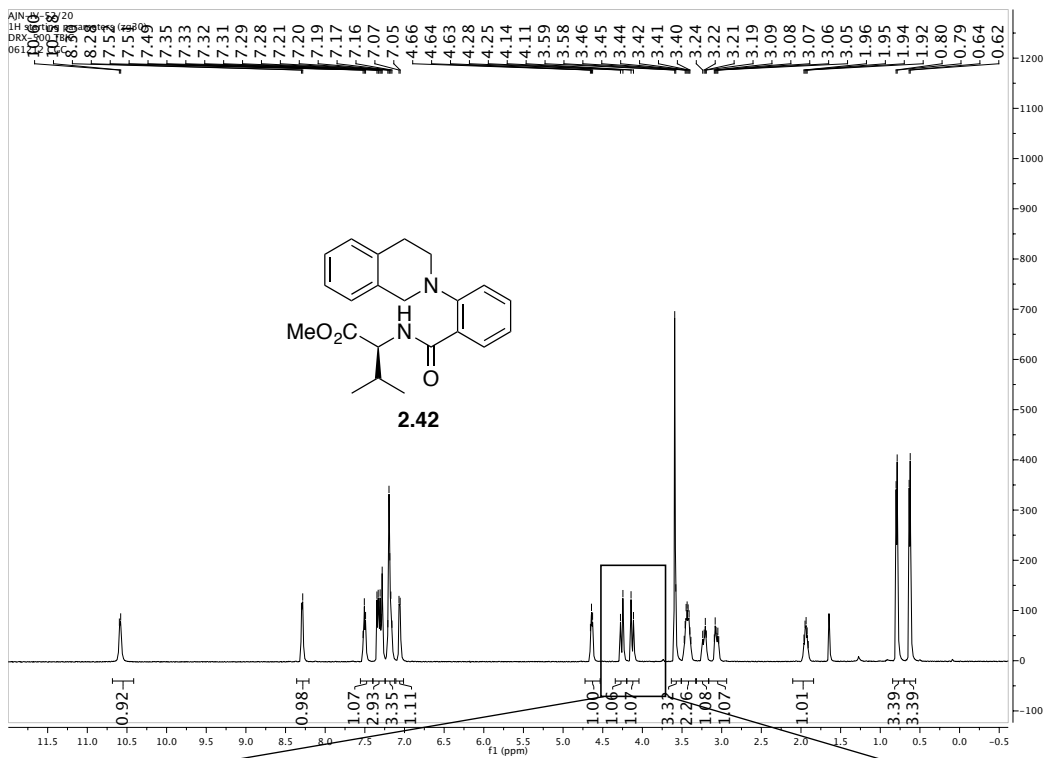
Integration of the corresponding resonances in the spectrum of **2.42-d₁** along with the knowledge of the extent of deuterium incorporation (from **2.6a-d₁** *vide supra*) allows for determination of the diastereomeric excess of **2.42-d₁** according to Equation 2.2:

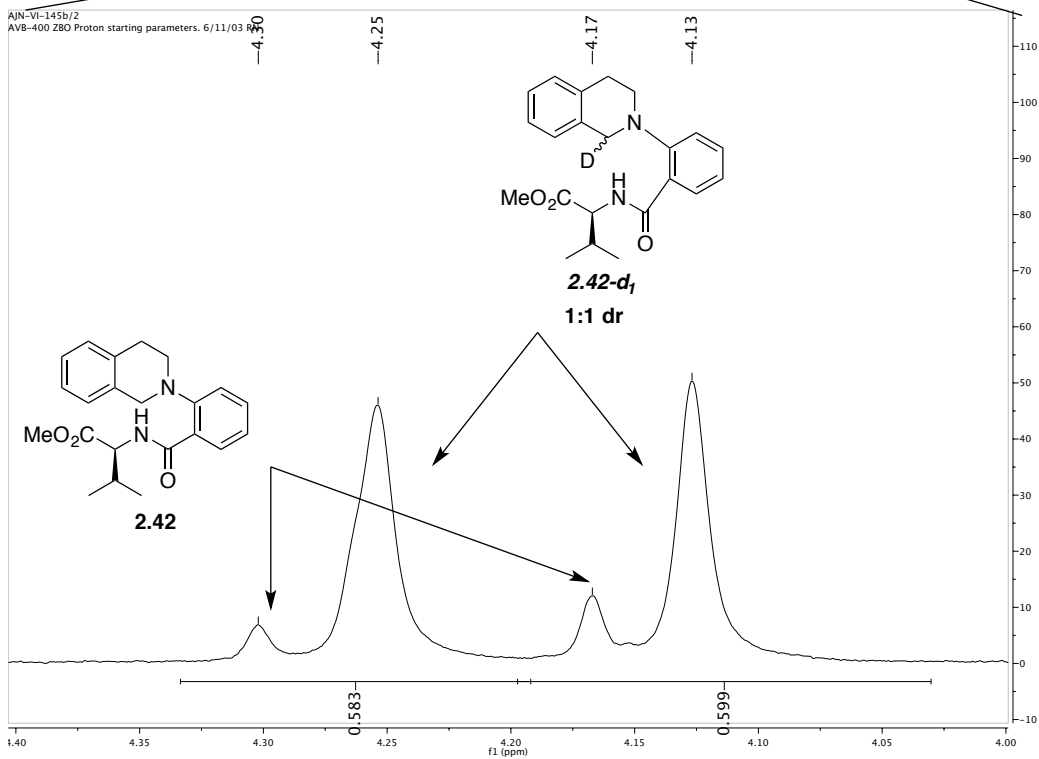
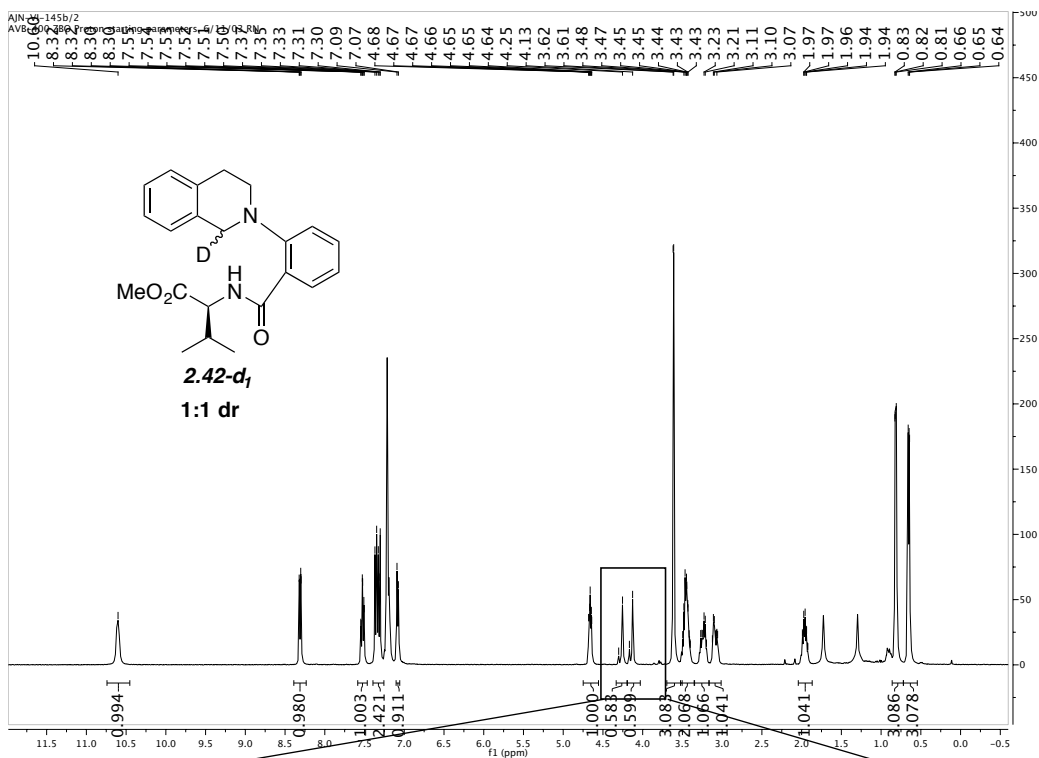
$$de = 100 * \frac{\text{integral}_{\text{major}} - \text{integral}_{\text{minor}}}{(\text{fractional D incorporation}) * (\text{integral}_{\text{major}} + \text{integral}_{\text{minor}})} \quad (\text{Eq. 2.2})$$

Applying this equation to the data from the spectra shown below results in a calculated de of 48 % (74:26 dr).

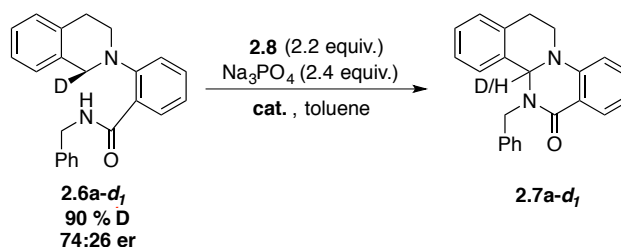
$$de = 100 * \frac{0.7853 - 0.3144}{(0.90) * (0.7853 + 0.3144)} = 47.6$$

Spectra of **2.42**, **2.42-d₁** with 1:1 dr (0 % de) and **2.42-d₁** with 76:24 dr (48 % de) are provided below. Assuming that no racemization occurs in the final peptide coupling step to form **2.6a-d₁** (see Scheme 2.10), this latter value also corresponds to the enantiomeric excess of **2.6a-d₁**.





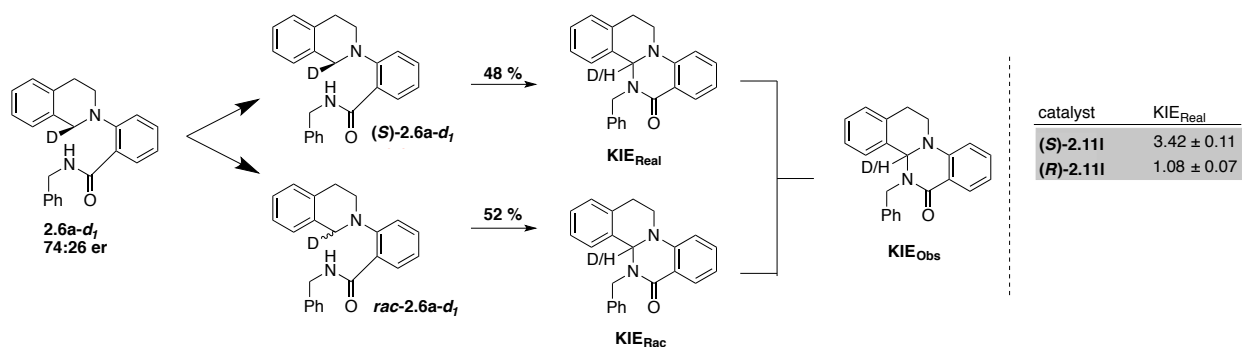
Having established the extent of deuterium incorporation and enantiomeric excess of **2.6a-d₁**, kinetic isotope effects were determined by ¹H NMR analysis. Each reaction was run in triplicate on 0.025 mmol scale as described above. Each sample was analyzed with an AV-500 MHz NMR spectrometer using 5 scans and a delay time of 15.0 sec. Isotope effects were determined from ¹H NMR spectra of **2.7a-d₁** in DMSO-*d*₆ by integration of the aminal resonance at 5.99 ppm relative to the diastereotopic tetrahydroisoquinoline methylene multiplet centered at 3.66 ppm. As these two protons should be present in a 1:1 ratio in **2.7a**, it was assumed that any deviation was due to the presence of **2.7a-d₁**, as it would lack the resonance at 5.99 ppm. The raw data obtained directly from the spectra is presented in Table 2.3 as KIE_{Obs.}. Considering that **2.6a-d₁** contained 10 % of un-deuterated **2.6a**, only 90 % of the resonance at 5.99 ppm was assumed to have arisen from **2.6a-d₁**, resulting in a KIE value modified from that from the raw data. This value is presented in Table 2.3 as KIE_{Corrected}, along with the average value for KIE_{Corrected} for each catalyst employed.



Entry	Catalyst	Trial	KIE _{Obs}	KIE _{Corrected}	
1	(S)-2.111	1	2.62 ± 0.10	3.04 ± 0.13	
2	(S)-2.111	2	2.36 ± 0.08	2.75 ± 0.11	Avg. = 2.81 ± 0.07
3	(S)-2.111	3	2.28 ± 0.08	2.65 ± 0.11	
4	(R)-2.111	1	1.43 ± 0.04	1.71 ± 0.06	
5	(R)-2.111	2	1.42 ± 0.04	1.70 ± 0.07	
6	(R)-2.111	3	1.39 ± 0.04	1.67 ± 0.06	

Table 2.3. Kinetic isotope effect data

Because **2.6a-d₁** existed as a 76:24 mixture of enantiomers, an additional calculation was necessary to determine the “real” KIE values for theoretically enantiopure (S)-**2.6a-d₁**. This was accomplished by treating **2.6a-d₁** as a 52:48 mixture of racemic and enantiopure material (Scheme 2.11) and treating the value of KIE_{Corrected} (Table 2.3) as a composite of the KIE’s from each (KIE_{rac} and KIE_{real} respectively). By solving the system of equations 2.3-2.5, the “real” KIE’s for the matched and mismatched scenarios can be extracted (equations 2.6 and 2.7 respectively). These are the values reported in the main text and reproduced below in Scheme 2.11.



Scheme 2.11. Determination of KIE_{Real}

$$\text{KIE}_{\text{corrected (S cat)}} = \frac{1}{2}\text{KIE}_{\text{rac}} + \frac{1}{2}\text{KIE}_{\text{real (S cat)}} \quad (\text{Eq. 2.3})$$

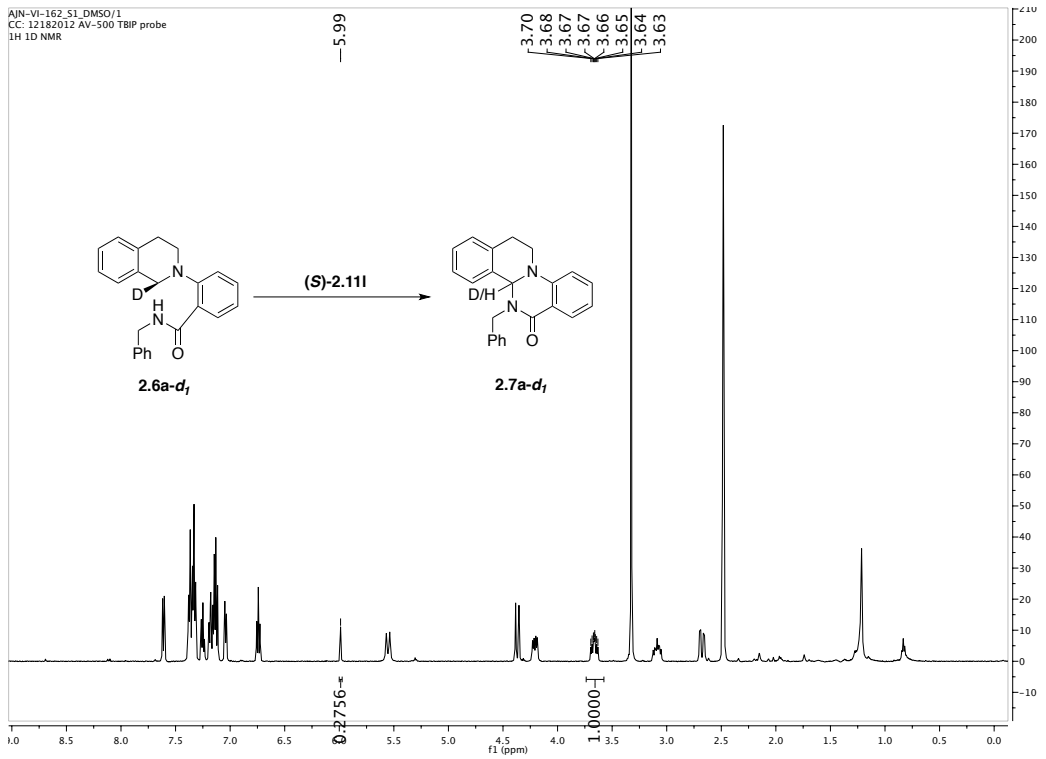
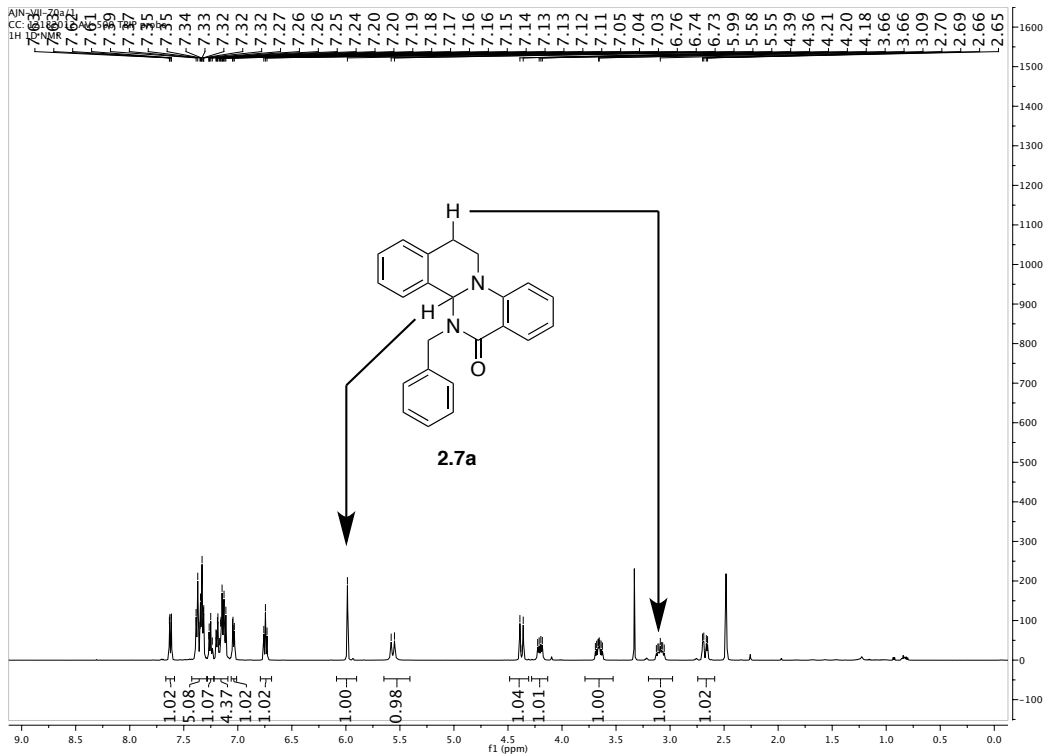
$$\text{KIE}_{\text{corrected(R cat)}} = \frac{1}{2}\text{KIE}_{\text{rac}} + \frac{1}{2}\text{KIE}_{\text{real(R cat)}} \quad (\text{Eq. 2.4})$$

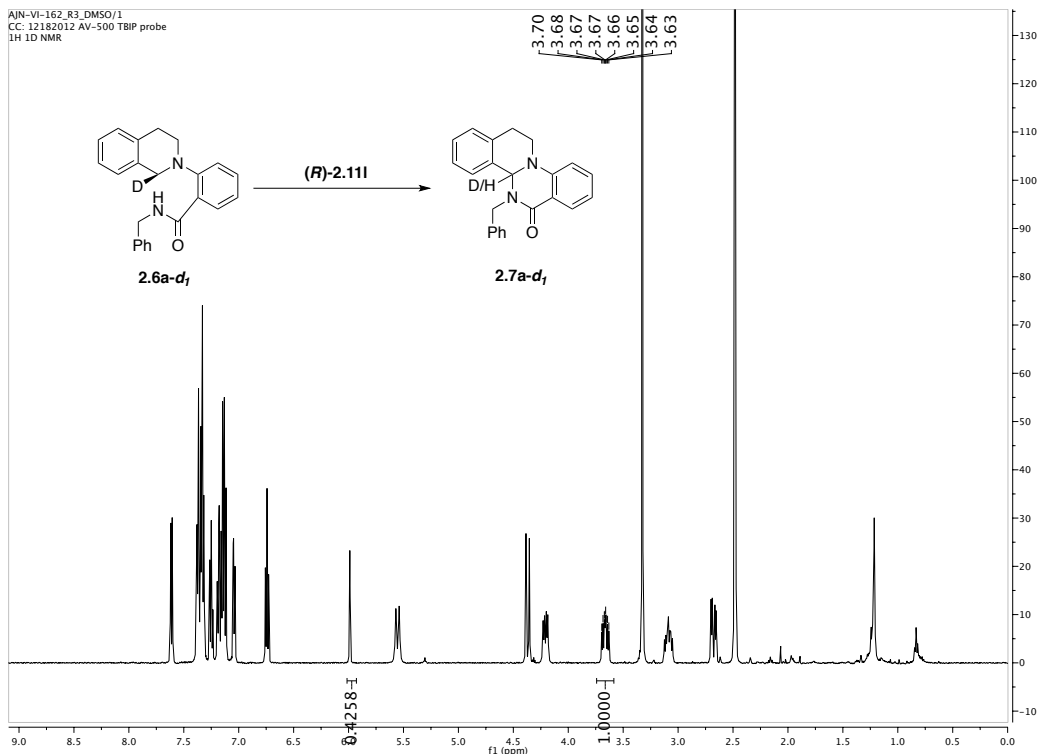
$$\text{KIE}_{\text{rac}} = \frac{1}{2}\text{KIE}_{\text{real (R cat)}} + \frac{1}{2}\text{KIE}_{\text{real (S cat)}} \quad (\text{Eq. 2.5})$$

$$\text{KIE}_{\text{real (S cat)}} = \frac{74}{48} * \text{KIE}_{\text{corrected (S cat)}} - \frac{26}{48} * \text{KIE}_{\text{corrected (R cat)}} \quad (\text{Eq. 2.6})$$

$$\text{KIE}_{\text{real (R cat)}} = \frac{74}{48} * \text{KIE}_{\text{corrected(R cat)}} - \frac{26}{48} * \text{KIE}_{\text{corrected (S cat)}} \quad (\text{Eq. 2.7})$$

Example spectra are provided for **2.7a**, **2.7a-d₁** obtained using (*S*)-**2.111** as the catalyst, and **2.7a-d₁** obtained using (*R*)-**2.111** as catalyst (Table 2.3, entries 1 and 5 respectively).





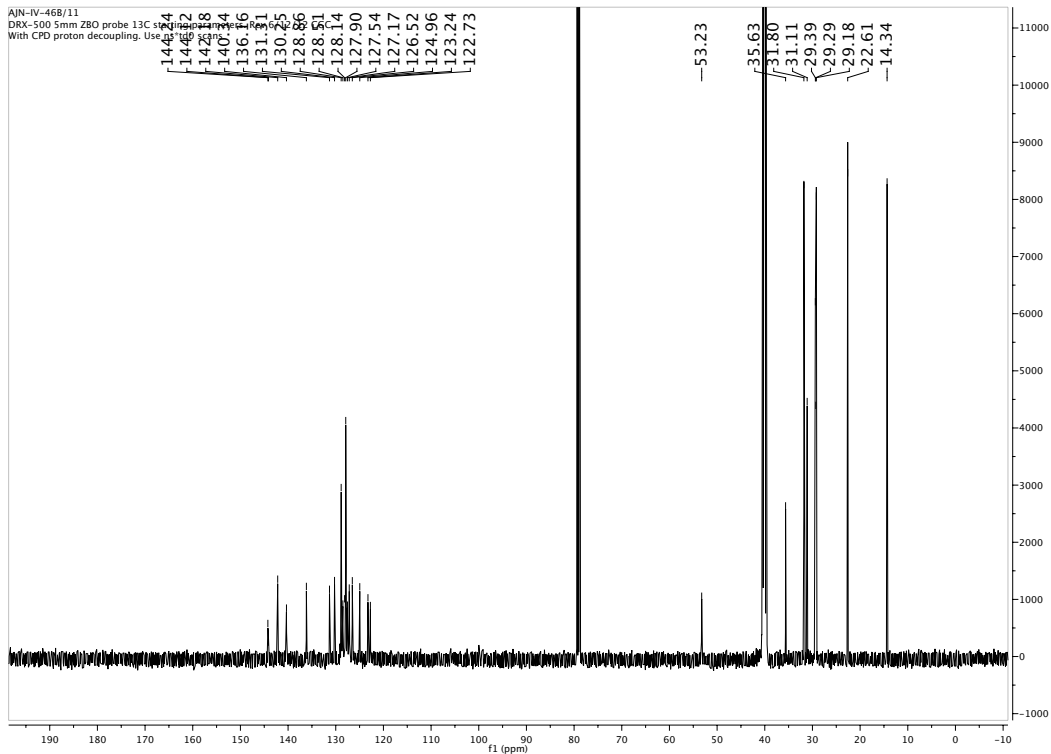
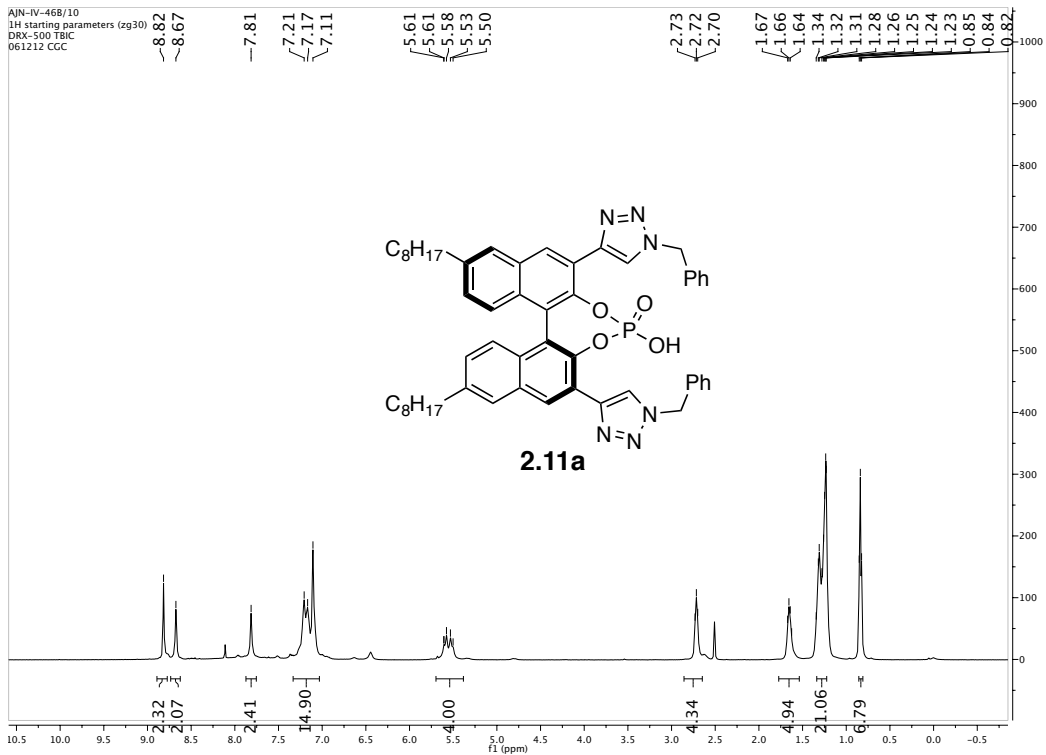
References and Notes

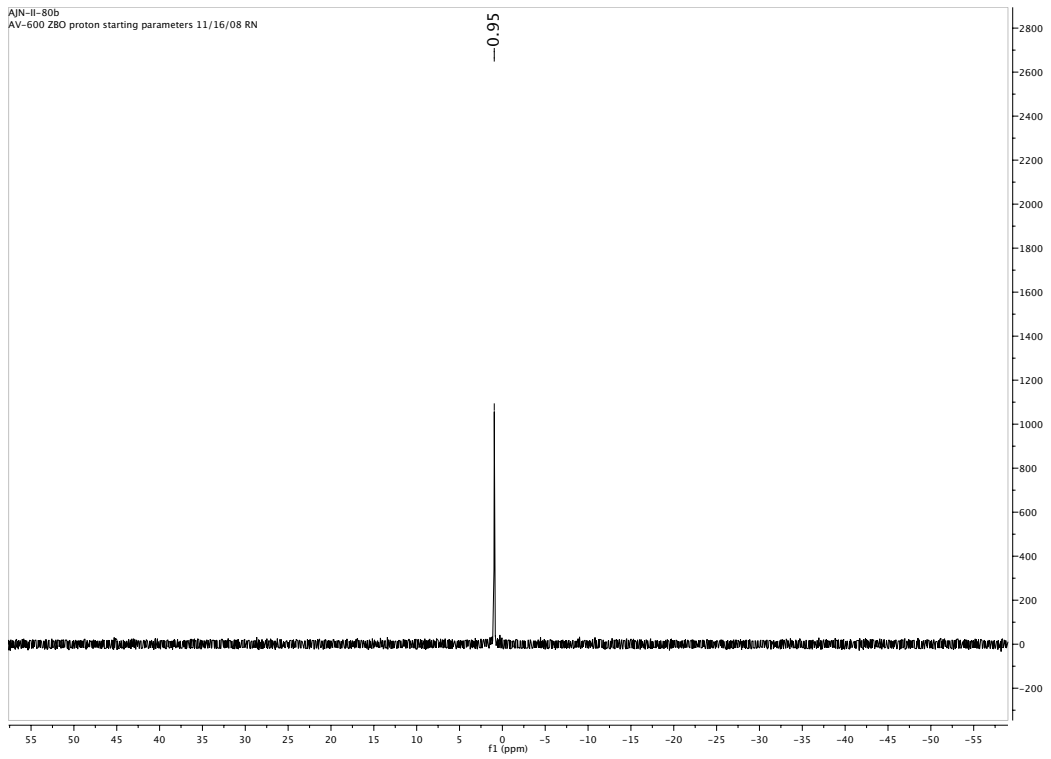
- (1) Shapiro, N.; Toste, F. *Synlett* **2010**, 2010, 675.
- (2) Phipps, R. J.; Hamilton, G. L.; Toste, F. D. *Nat. Chem.* **2012**, 4 (8), 603.
- (3) Mahlau, M.; List, B. *Angew. Chem. Int. Ed.* **2013**, 52 (2), 518.
- (4) Brak, K.; Jacobsen, E. N. *Angew. Chem. Int. Ed.* **2013**, 52 (2), 534.
- (5) Fleischmann, M.; Drettwan, D.; Sugiono, E.; Rueping, M.; Gschwind, R. M. *Angew. Chem. Int. Ed.* **2011**, 50 (28), 6364.
- (6) Mukherjee, S.; List, B. *J. Am. Chem. Soc.* **2007**, 129 (37), 11336.
- (7) Rueping, M.; Antonchick, A. P.; Brinkmann, C. *Angew. Chem. Int. Ed.* **2007**, 46 (36), 6903.
- (8) Liao, S.; List, B. *Angew. Chem. Int. Ed.* **2010**, 49 (3), 628.
- (9) Jiang, G.; Halder, R.; Fang, Y.; List, B. *Angew. Chem. Int. Ed.* **2011**, 50 (41), 9752.
- (10) Rauniyar, V.; Wang, Z. J.; Burks, H. E.; Toste, F. D. *J. Am. Chem. Soc.* **2011**, 133 (22), 8486.
- (11) Chai, Z.; Rainey, T. J. *J. Am. Chem. Soc.* **2012**, 134 (8), 3615.
- (12) Zbieg, J. R.; Yamaguchi, E.; McInturff, E. L.; Krische, M. J. *Science* **2012**, 336 (6079), 324.
- (13) Ohmatsu, K.; Ito, M.; Kunieda, T.; Ooi, T. *Nat. Chem.* **2012**, 4 (6), 473.
- (14) Wang, X.; List, B. *Angew. Chem. Int. Ed.* **2008**, 47 (6), 1119.
- (15) Hamilton, G. L.; Kanai, T.; Toste, F. D. *J. Am. Chem. Soc.* **2008**, 130 (45), 14984.
- (16) Rueping, M.; Uria, U.; Lin, M.-Y.; Atodiresi, I. *J. Am. Chem. Soc.* **2011**, 133 (11), 3732.
- (17) Akiyama, T. *Chem Rev* **2007**, 107 (12), 5744.
- (18) Terada, M. *Curr. Org. Chem.* **2011**, 15 (13), 2227.
- (19) Terada, M. *Synthesis* **2010**, 2010 (12), 1929.

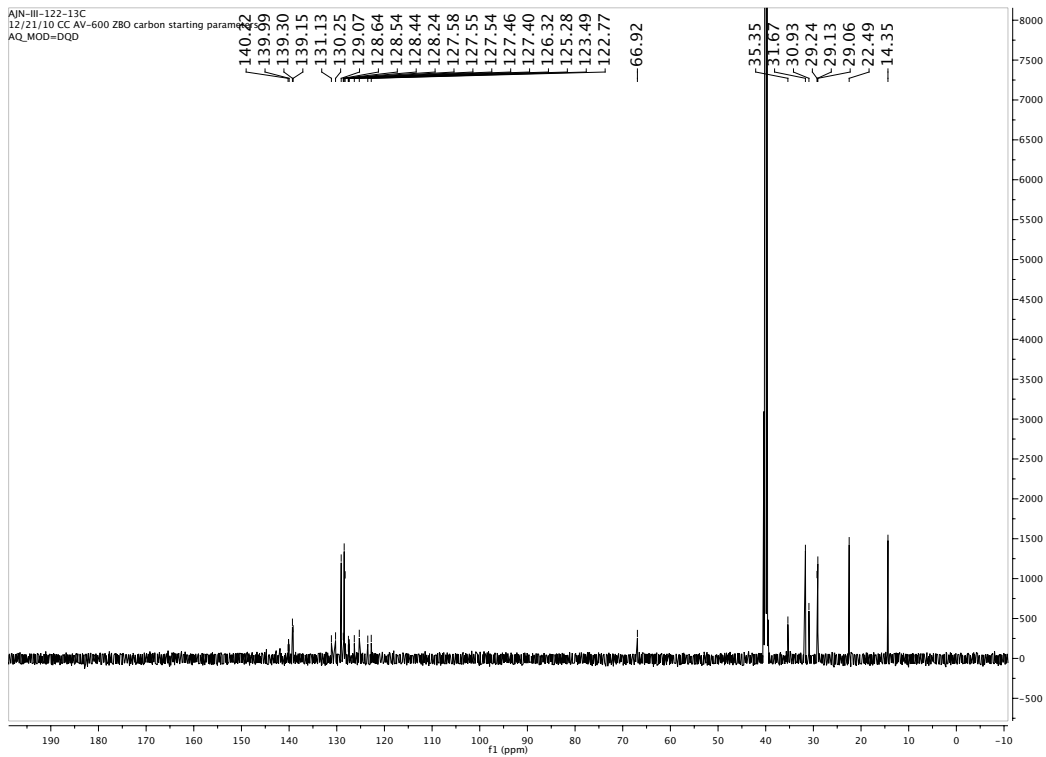
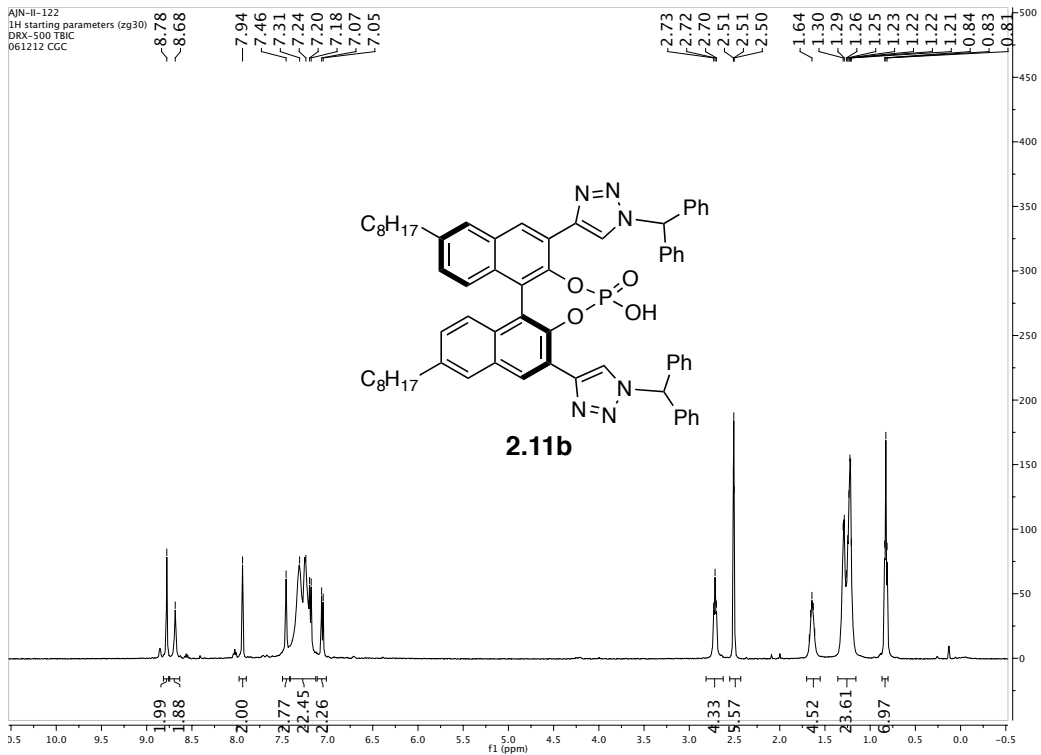
- (20) Parmar, D.; Sugiono, E.; Raja, S.; Rueping, M. *Chem. Rev.* **2014**, *114* (18), 9047.
- (21) Akiyama, T.; Itoh, J.; Yokota, K.; Fuchibe, K. *Angew. Chem. Int. Ed.* **2004**, *43* (12), 1566.
- (22) Uraguchi, D.; Terada, M. *J. Am. Chem. Soc.* **2004**, *126* (17), 5356.
- (23) Mayer, S.; List, B. *Angew. Chem. Int. Ed.* **2006**, *45* (25), 4193.
- (24) Tiago Menezes Correia, J. *Synlett* **2015**, *26* (03), 416.
- (25) Hamilton, G. L.; Kang, E. J.; Mba, M.; Toste, F. D. *Science* **2007**, *317* (5837), 496.
- (26) Shirakawa, S.; Maruoka, K. *Angew. Chem. Int. Ed.* **2013**, *52* (16), 4312.
- (27) Tan, J.; Yasuda, N. *Org. Process Res. Dev.* **2015**.
- (28) Hughes, D. L.; Dolling, U. H.; Ryan, K. M.; Schoenewaldt, E. F.; Grabowski, E. J. J. *J. Org. Chem.* **1987**, *52* (21), 4745.
- (29) Rauniyar, V.; Lackner, A. D.; Hamilton, G. L.; Toste, F. D. *Science* **2011**, *334* (6063), 1681.
- (30) Purser, S.; Moore, P. R.; Swallow, S.; Gouverneur, V. *Chem. Soc. Rev.* **2008**, *37* (2), 320.
- (31) Bobbio, C.; Gouverneur, V. *Org. Biomol. Chem.* **2006**, *4* (11), 2065.
- (32) Shibata, N.; Ishimaru, T.; Nakamura, S.; Toru, T. *J. Fluor. Chem.* **2007**, *128* (5), 469.
- (33) Ma, J.-A.; Cahard, D. *Chem. Rev.* **2008**, *108* (9), PR1.
- (34) Cahard, D.; Xu, X.; Couve-Bonnaire, S.; Pannecoucke, X. *Chem. Soc. Rev.* **2010**, *39* (2), 558.
- (35) Lectard, S.; Hamashima, Y.; Sodeoka, M. *Adv. Synth. Catal.* **2010**, *352* (16), 2708.
- (36) Valero, G.; Companyó, X.; Rios, R. *Chem. – Eur. J.* **2011**, *17* (7), 2018.
- (37) Ye, Z.; Zhao, G. *Chim. Int. J. Chem.* **2011**, *65* (12), 902.
- (38) Yang, X.; Wu, T.; Phipps, R. J.; Toste, F. D. *Chem. Rev.* **2015**, *115* (2), 826.
- (39) Banks, R. E. *J. Fluor. Chem.* **1998**, *87* (1), 1.
- (40) Nyffeler, P. T.; Durón, S. G.; Burkart, M. D.; Vincent, S. P.; Wong, C.-H. *Angew. Chem. Int. Ed.* **2005**, *44* (2), 192.
- (41) Stavber, Stojan. *Acta Chim Slov* **2005**, *52*, 13.
- (42) Stavber, S. *Molecules* **2011**, *16* (8), 6432.
- (43) Phipps, R. J.; Hiramatsu, K.; Toste, F. D. *J. Am. Chem. Soc.* **2012**, *134* (20), 8376.
- (44) Wang, Y.-M.; Wu, J.; Hoong, C.; Rauniyar, V.; Toste, F. D. *J. Am. Chem. Soc.* **2012**, *134* (31), 12928.
- (45) Honjo, T.; Phipps, R. J.; Rauniyar, V.; Toste, F. D. *Angew. Chem. Int. Ed.* **2012**, *51* (38), 9684.
- (46) Phipps, R. J.; Toste, F. D. *J. Am. Chem. Soc.* **2013**, *135* (4), 1268.
- (47) Shunatona, H. P.; Früh, N.; Wang, Y.-M.; Rauniyar, V.; Toste, F. D. *Angew. Chem. Int. Ed.* **2013**, *52* (30), 7724.
- (48) Wu, J.; Wang, Y.-M.; Drljevic, A.; Rauniyar, V.; Phipps, R. J.; Toste, F. D. *Proc. Natl. Acad. Sci.* **2013**, *110* (34), 13729.
- (49) Yang, X.; Phipps, R. J.; Toste, F. D. *J. Am. Chem. Soc.* **2014**, *136* (14), 5225.
- (50) Liu, H.; Jiang, G.; Pan, X.; Wan, X.; Lai, Y.; Ma, D.; Xie, W. *Org. Lett.* **2014**, *16* (7), 1908.
- (51) Romanov-Michailidis, F.; Guénée, L.; Alexakis, A. *Angew. Chem. Int. Ed.* **2013**, *52* (35), 9266.
- (52) Romanov-Michailidis, F.; Guénée, L.; Alexakis, A. *Org. Lett.* **2013**, *15* (22), 5890.
- (53) Romanov-Michailidis, F.; Pupier, M.; Guénée, L.; Alexakis, A. *Chem. Commun.* **2014**, *50* (88), 13461.
- (54) Romanov-Michailidis, F.; Pupier, M.; Besnard, C.; Bürgi, T.; Alexakis, A. *Org. Lett.* **2014**, *16* (19), 4988.

- (55) Romanov-Michailidis, F.; Romanova-Michaelides, M.; Pupier, M.; Alexakis, A. *Chem. – Eur. J.* **2015**, *21* (14), 5561.
- (56) Egami, H.; Asada, J.; Sato, K.; Hashizume, D.; Kawato, Y.; Hamashima, Y. *J. Am. Chem. Soc.* **2015**, *137* (32), 10132.
- (57) Bobbitt, J. M.; Brückner, C.; Merbouh, N. In *Organic Reactions*; John Wiley & Sons, Inc., Ed.; John Wiley & Sons, Inc.: Hoboken, NJ, USA, 2010.
- (58) García Mancheño, O.; Stopka, T. *Synthesis* **2013**, *45* (12), 1602.
- (59) Richter, H.; García Mancheño, O. *Eur. J. Org. Chem.* **2010**, *2010* (23), 4460.
- (60) Richter, H.; García Mancheño, O. *Org. Lett.* **2011**, *13* (22), 6066.
- (61) Wertz, S.; Kodama, S.; Studer, A. *Angew. Chem. Int. Ed.* **2011**, *50* (48), 11511.
- (62) Li, C.-J. *Acc. Chem. Res.* **2009**, *42* (2), 335.
- (63) Scheuermann, C. J. *Chem. – Asian J.* **2010**, *5* (3), 436.
- (64) Yeung, C. S.; Dong, V. M. *Chem. Rev.* **2011**, *111* (3), 1215.
- (65) Boess, E.; Schmitz, C.; Klusmann, M. *J. Am. Chem. Soc.* **2012**, *134* (11), 5317.
- (66) Simón, L.; Goodman, J. M. *J. Org. Chem.* **2011**, *76* (6), 1775.
- (67) Uraguchi, D.; Sorimachi, K.; Terada, M. *J. Am. Chem. Soc.* **2004**, *126* (38), 11804.
- (68) Cheng, X.; Vellalath, S.; Goddard, R.; List, B. *J. Am. Chem. Soc.* **2008**, *130* (47), 15786.
- (69) Bachu, P.; Akiyama, T. *Chem. Commun.* **2010**, *46* (23), 4112.
- (70) Shapiro, N. D.; Rauniyar, V.; Hamilton, G. L.; Wu, J.; Toste, F. D. *Nature* **2011**, *470* (7333), 245.
- (71) Čorić, I.; List, B. *Nature* **2012**, *483* (7389), 315.
- (72) Doyle, A. G.; Jacobsen, E. N. *Chem. Rev.* **2007**, *107* (12), 5713.
- (73) Knowles, R. R.; Lin, S.; Jacobsen, E. N. *J. Am. Chem. Soc.* **2010**, *132* (14), 5030.
- (74) Knowles, R. R.; Jacobsen, E. N. *Proc. Natl. Acad. Sci.* **2010**, *107* (48), 20678.
- (75) Uyeda, C.; Jacobsen, E. N. *J. Am. Chem. Soc.* **2011**, *133* (13), 5062.
- (76) Lin, S.; Jacobsen, E. N. *Nat. Chem.* **2012**, *4* (10), 817.
- (77) Halpern, J. *Science* **1982**, *217* (4558), 401.
- (78) Seeman, J. I. *Chem. Rev.* **1983**, *83* (2), 83.
- (79) Bess, E. N.; Sigman, M. S. In *Asymmetric Synthesis II*; Christmann, thias, Bräse, S., Eds.; Wiley-VCH Verlag GmbH & Co. KGaA, 2012; pp 363–370.
- (80) Beckendorf, S.; Mancheño, O. *Synthesis* **2012**, *44* (14), 2162.
- (81) Recsei, C.; McErlean, C. S. P. *Tetrahedron* **2012**, *68* (2), 464.
- (82) Kolb, H. C.; Finn, M. G.; Sharpless, K. B. *Angew. Chem. Int. Ed.* **2001**, *40* (11), 2004.
- (83) Törnøe, C. W.; Christensen, C.; Meldal, M. *J. Org. Chem.* **2002**, *67* (9), 3057.
- (84) Rostovtsev, V. V.; Green, L. G.; Fokin, V. V.; Sharpless, K. B. *Angew. Chem. Int. Ed.* **2002**, *41* (14), 2596.
- (85) Hein, J. E.; Fokin, V. V. *Chem. Soc. Rev.* **2010**, *39* (4), 1302.
- (86) Hua, Y.; Flood, A. H. *Chem. Soc. Rev.* **2010**, *39* (4), 1262.
- (87) Juriček, M.; Kouwer, P. H. J.; Rowan, A. E. *Chem. Commun.* **2011**, *47* (31), 8740.
- (88) Kumar, A.; Pandey, P. S. *Org. Lett.* **2008**, *10* (2), 165.
- (89) Leigh, D. A.; Robertson, C. C.; Slawin, A. M. Z.; Thomson, P. I. T. *J. Am. Chem. Soc.* **2013**.
- (90) Asmus, S.; Beckendorf, S.; Zurro, M.; Mück-Lichtenfeld, C.; Fröhlich, R.; García Mancheño, O. *Chem. – Asian J.* **2014**, n/a.
- (91) Kolb, H. C.; Sharpless, K. B. *Drug Discov. Today* **2003**, *8* (24), 1128.
- (92) Brik, A.; Alexandratos, J.; Lin, Y.-C.; Elder, J. H.; Olson, A. J.; Wlodawer, A.; Goodsell, D. S.; Wong, C.-H. *ChemBioChem* **2005**, *6* (7), 1167.

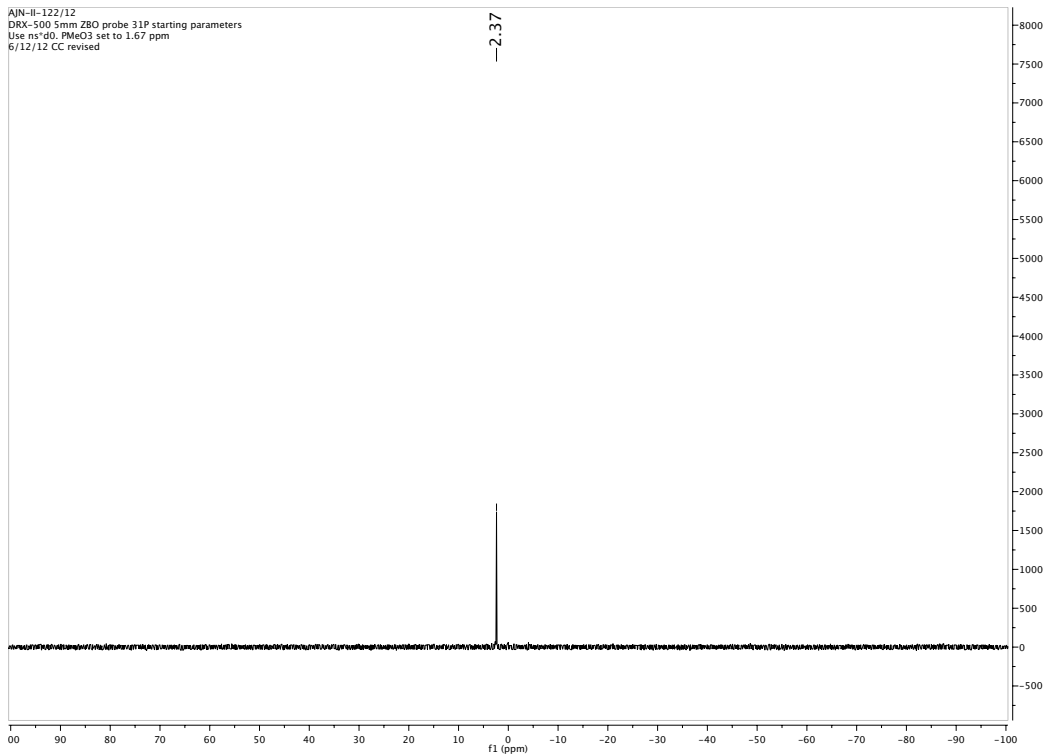
- (93) Valverde, I. E.; Mindt, T. L. *Chim. Int. J. Chem.* **2013**, *67* (4), 262.
- (94) Thirumurugan, P.; Matosiuk, D.; Jozwiak, K. *Chem. Rev.* **2013**.
- (95) Li, N.; Chen, X.-H.; Song, J.; Luo, S.-W.; Fan, W.; Gong, L.-Z. *J. Am. Chem. Soc.* **2009**, *131* (42), 15301.
- (96) Bartók, M. *Chem. Rev.* **2010**, *110* (3), 1663.
- (97) Jiang, J.; Xu, H.-D.; Xi, J.-B.; Ren, B.-Y.; Lv, F.-P.; Guo, X.; Jiang, L.-Q.; Zhang, Z.-Y.; Hu, W.-H. *J. Am. Chem. Soc.* **2011**, *133* (22), 8428.
- (98) Escorihuela, J.; Burguete, M. I.; Luis, S. V. *Chem. Soc. Rev.* **2013**.
- (99)
- (100) Hoffmann, S.; Seayad, A. M.; List, B. *Angew. Chem. Int. Ed.* **2005**, *44* (45), 7424.
- (101) Čorić, I.; Müller, S.; List, B. *J. Am. Chem. Soc.* **2010**, *132* (49), 17370.
- (102) Li, G.; Liang, Y.; Antilla, J. C. *J. Am. Chem. Soc.* **2007**, *129* (18), 5830.
- (103) Li, L.; Zhu, A.; Yao, H.; Wei, Y.; Yang, D.; Li, J.; Zhang, G. *J. Chem. Res.* **2010**, *34* (9), 511.
- (104) Prakash, G. K. S.; Stephenson, M. A.; Shih, J. G.; Olah, G. A. *J. Org. Chem.* **1986**, *51* (16), 3215.
- (105) Tao, C.-Z.; Cui, X.; Li, J.; Liu, A.-X.; Liu, L.; Guo, Q.-X. *Tetrahedron Lett.* **2007**, *48* (20), 3525.
- (106) Liu, Q.; Tor, Y. *Org. Lett.* **2003**, *5* (14), 2571.
- (107) Danjo, H.; Hirata, K.; Noda, M.; Uchiyama, S.; Fukui, K.; Kawahata, M.; Azumaya, I.; Yamaguchi, K.; Miyazawa, T. *J. Am. Chem. Soc.* **2010**, *132* (44), 15556.
- (108) Wayne Craig, G.; Eberle, M.; Irminger, B.; Laime, Y.; Schückenböhmer, A.; Müller, P. *Heterocycles* **2007**, *71* (9), 1967.
- (109) Cabildo, P.; Claramunt, R. M.; Forfar, I.; Elguero, J. *Tetrahedron Lett.* **1994**, *35* (1), 183.
- (110) Asano, K.; Matsubara, S. *Org. Lett.* **2010**, *12* (21), 4988.
- (111) Yoshida, H.; Morishita, T.; Ohshita, J. *Org. Lett.* **2008**, *10* (17), 3845.
- (112) Rein, K.; Goicoechea-Pappas, M.; Anklekar, T. V.; Hart, G. C.; Smith, G. A.; Gawley, R. E. *J. Am. Chem. Soc.* **1989**, *111* (6), 2211.



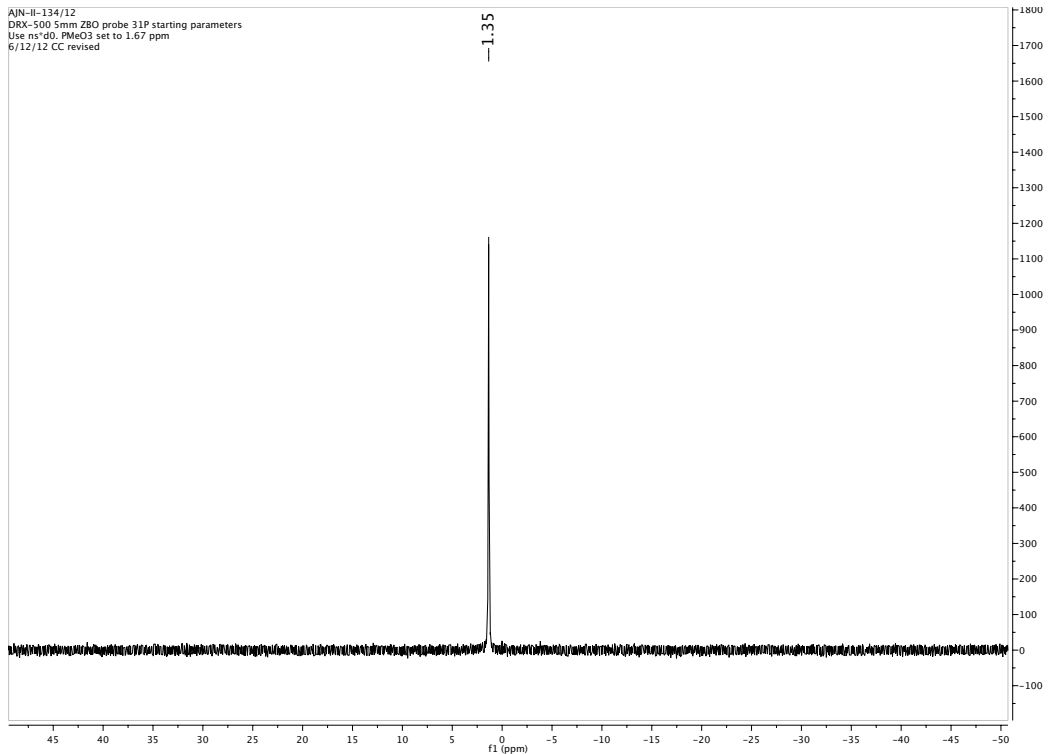


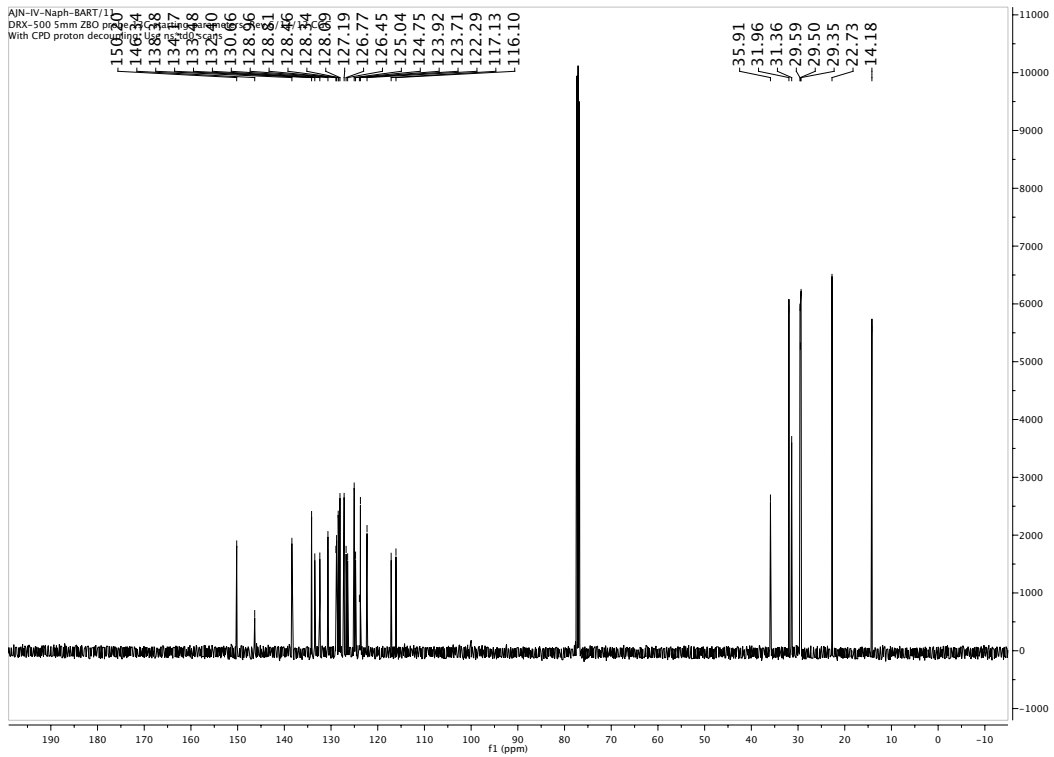
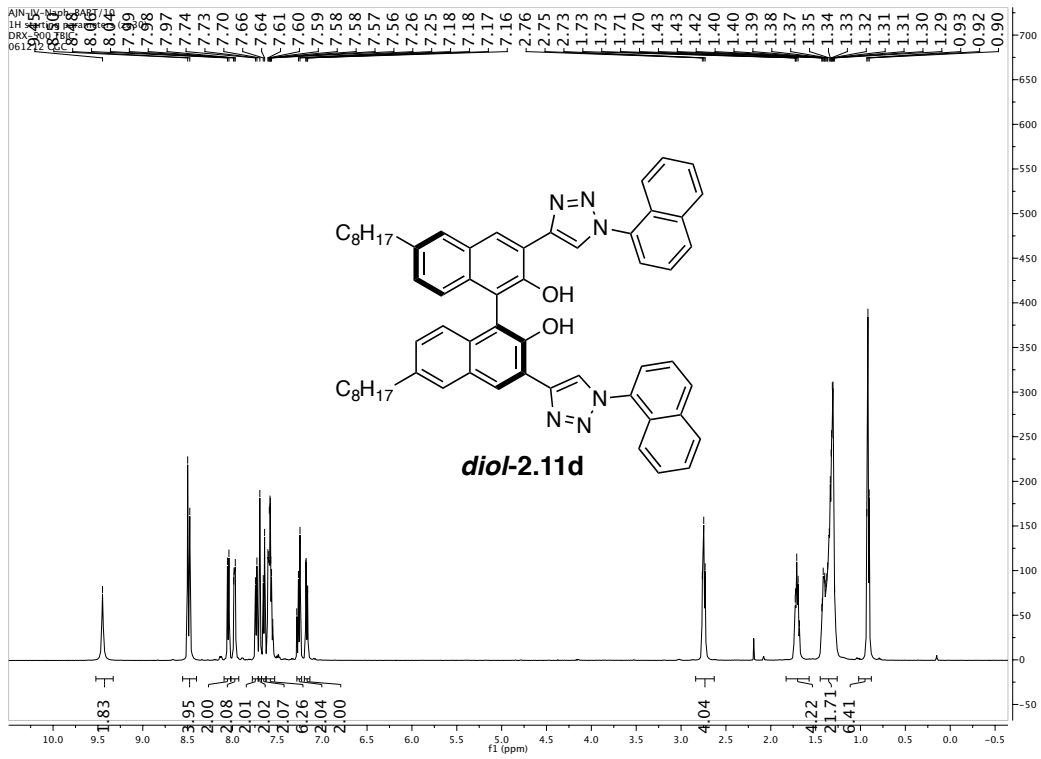


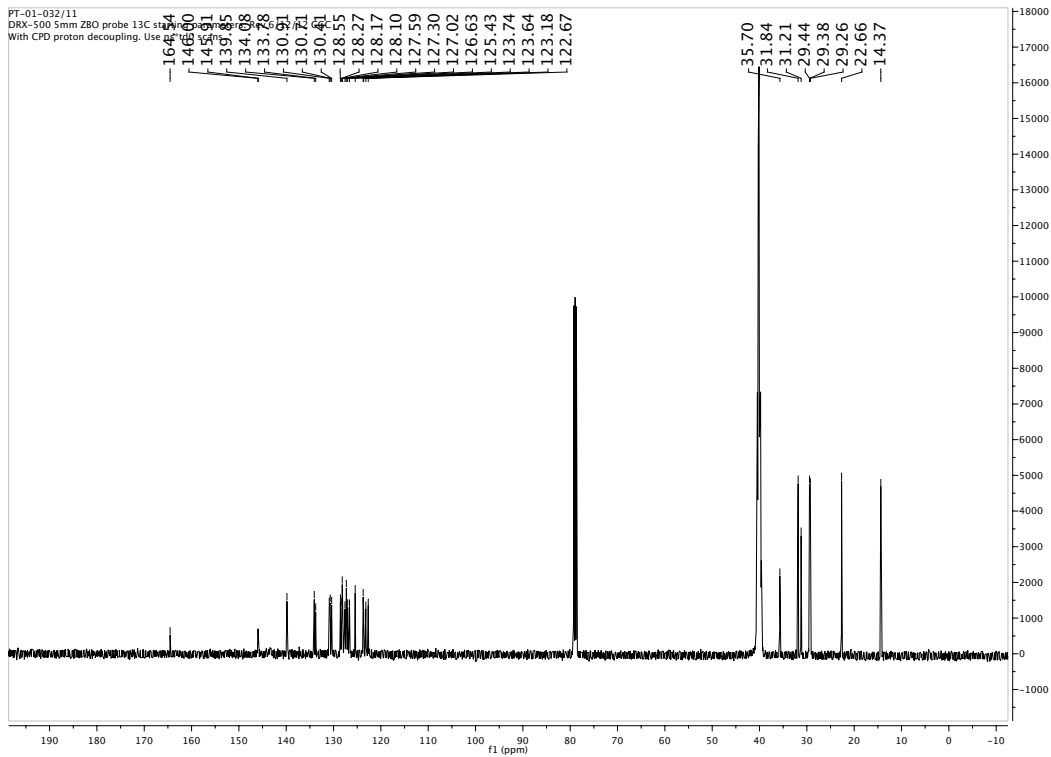
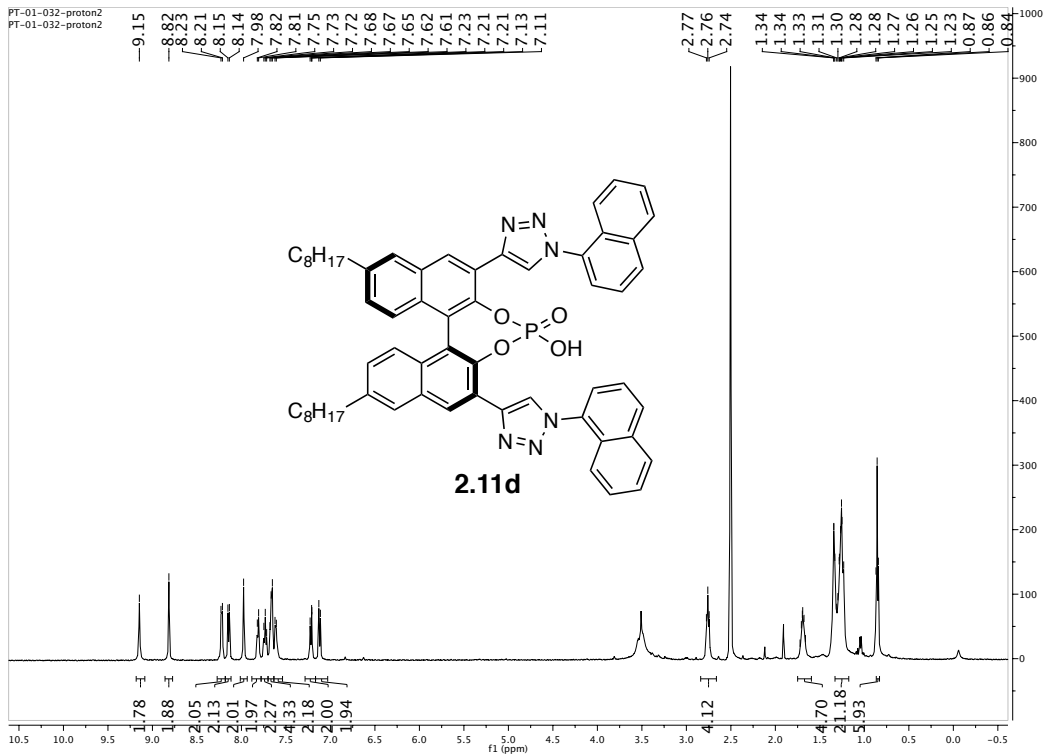
AIN-II-122/12
DRX-500 5mm Z80 probe 31P starting parameters
Use ns=50, PMeO3 set to 1.67 ppm
6/12/12 CC revised

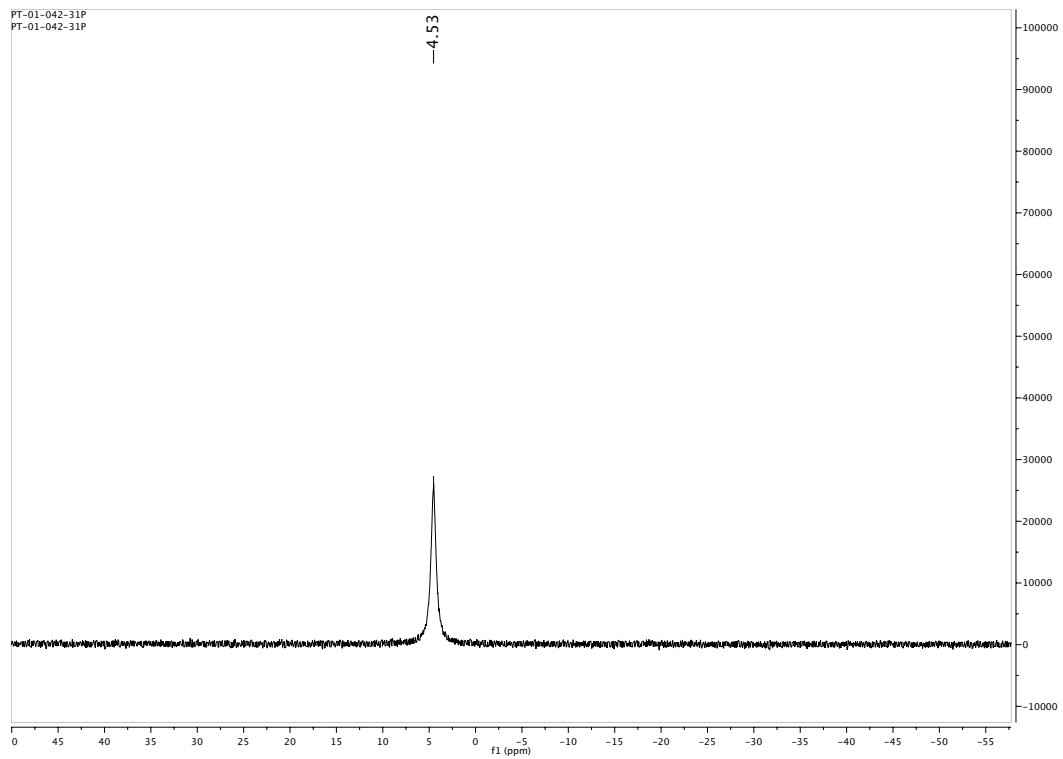


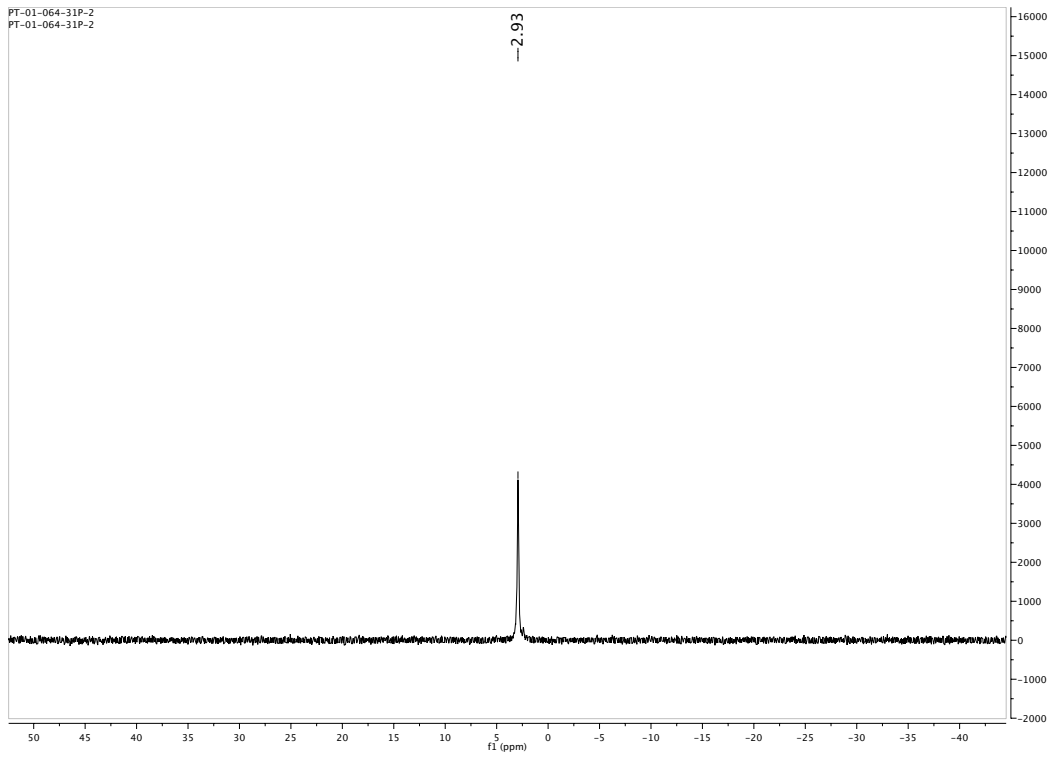
AIN-II-134/12
DRX-500 5mm Z80 probe 31P starting parameters
Use ns=50, PMeO3 set to 1.67 ppm
6/12/12 CC revised

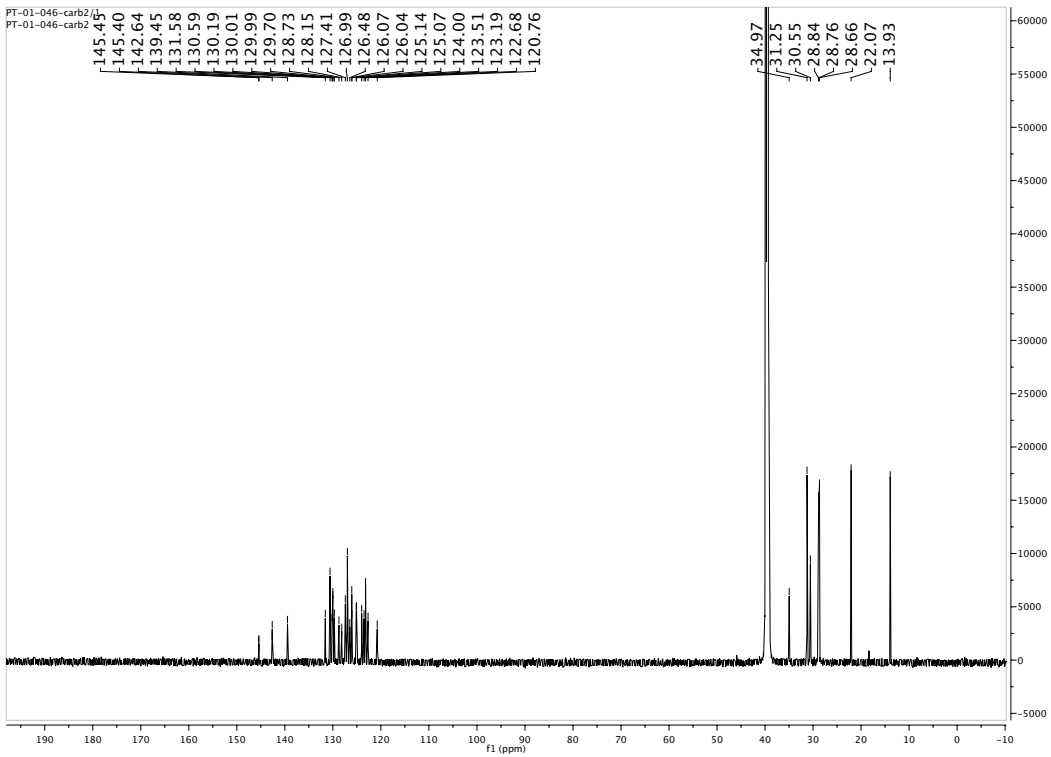
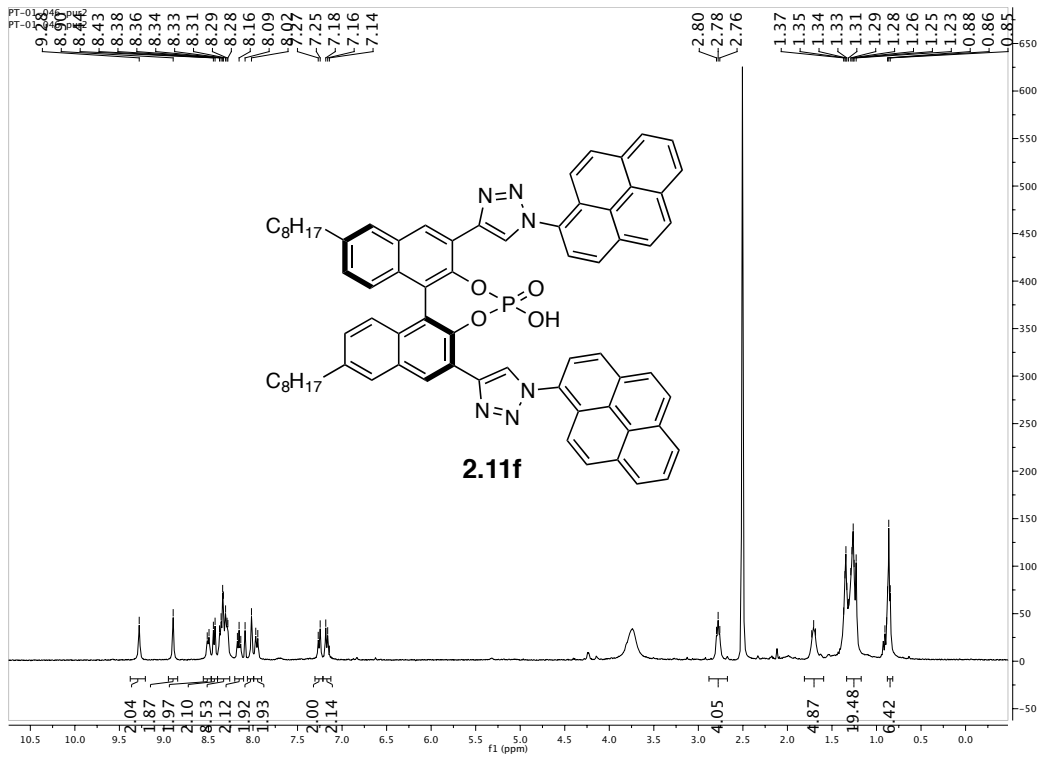


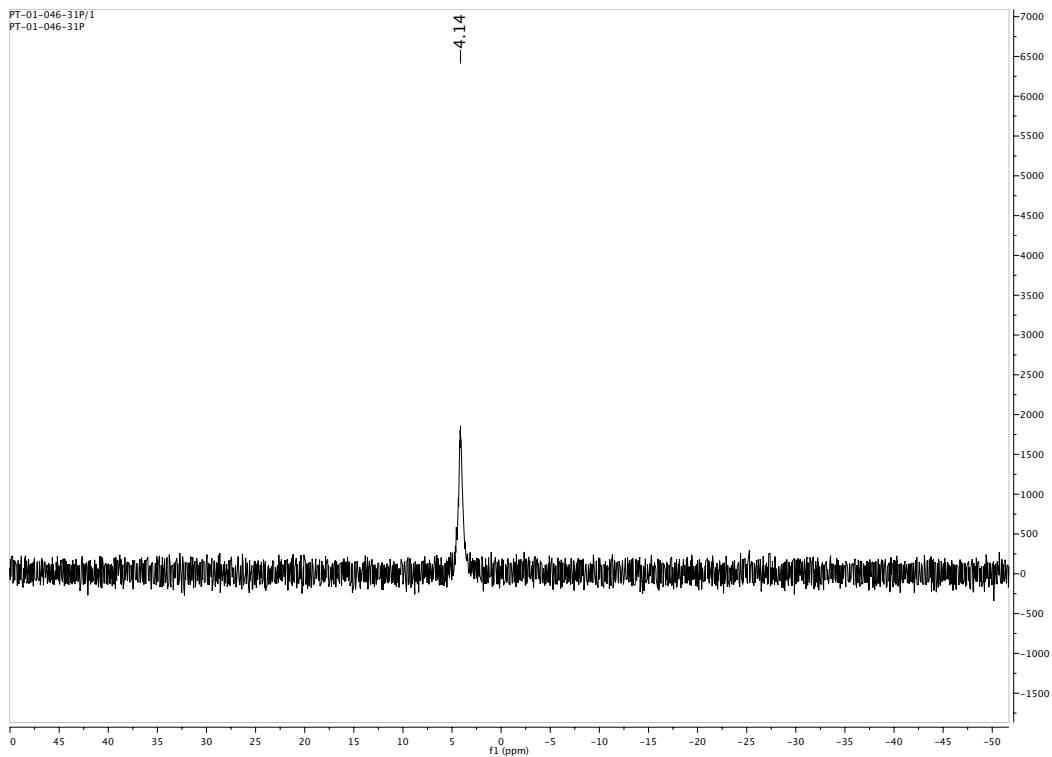


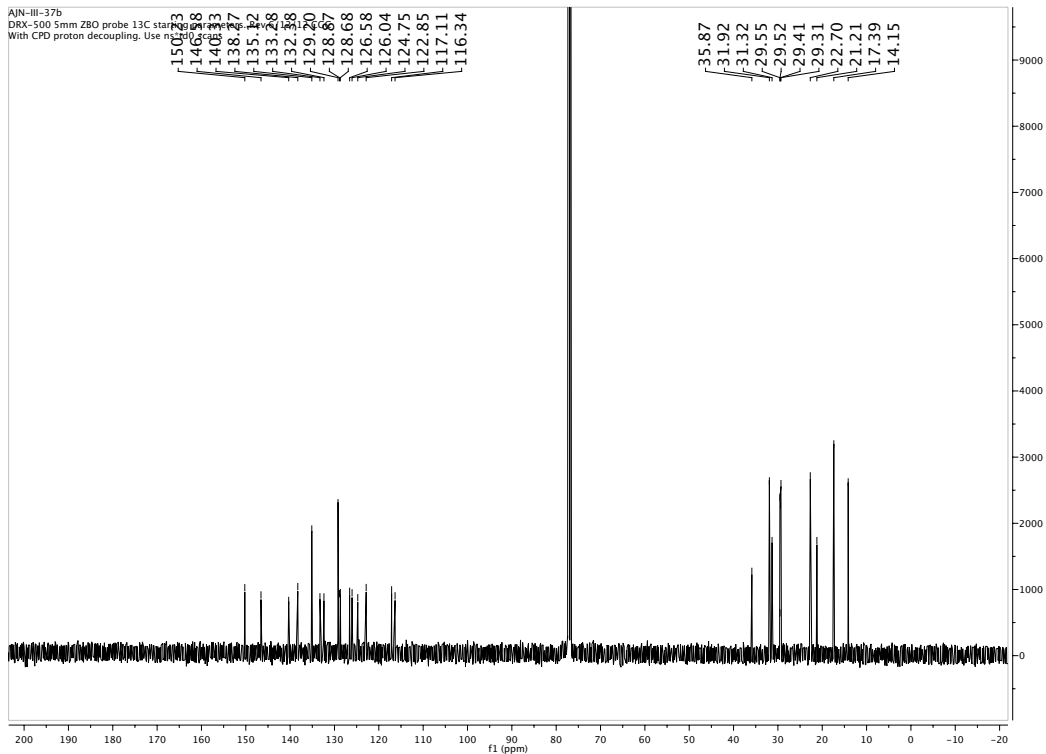
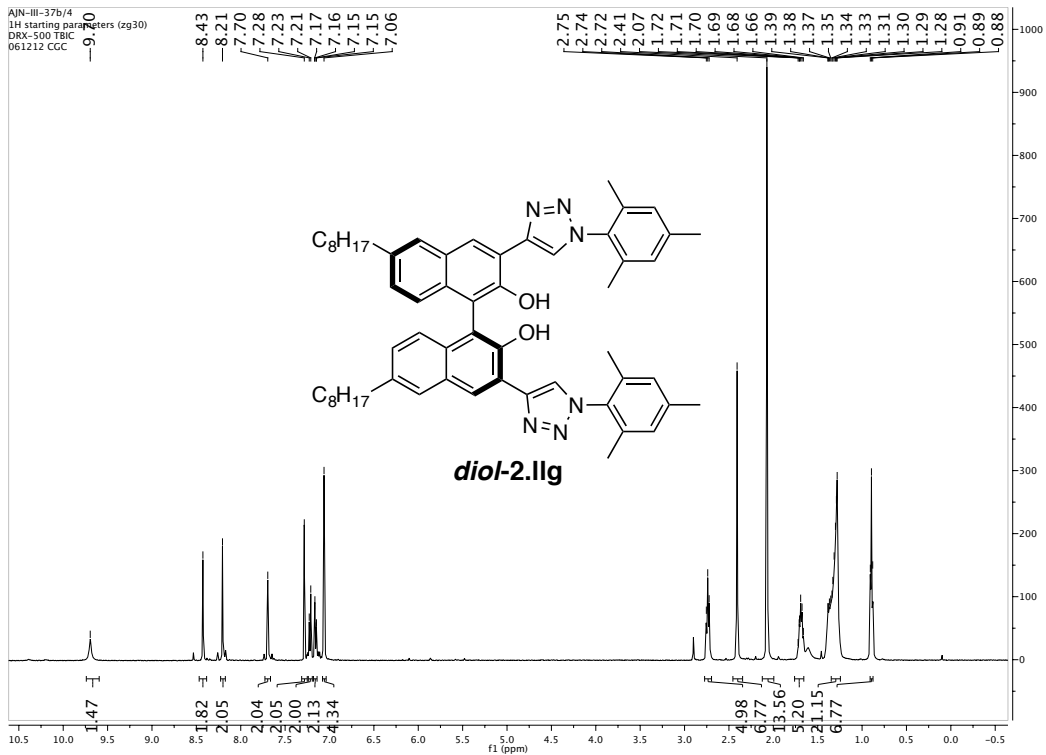


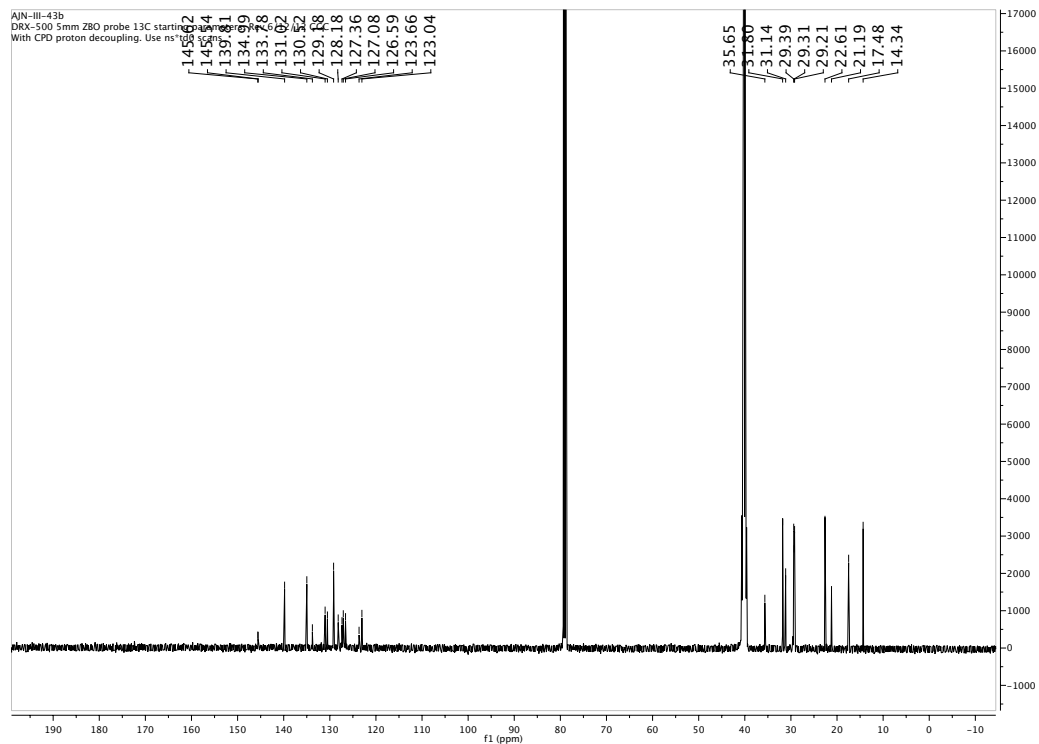
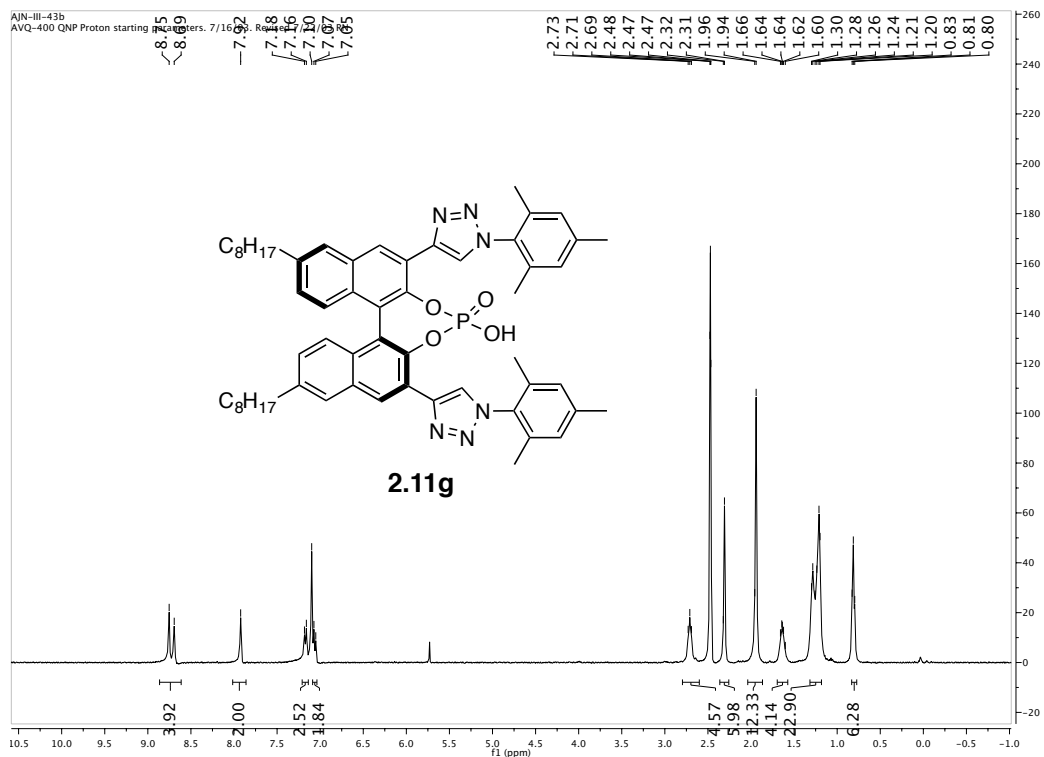


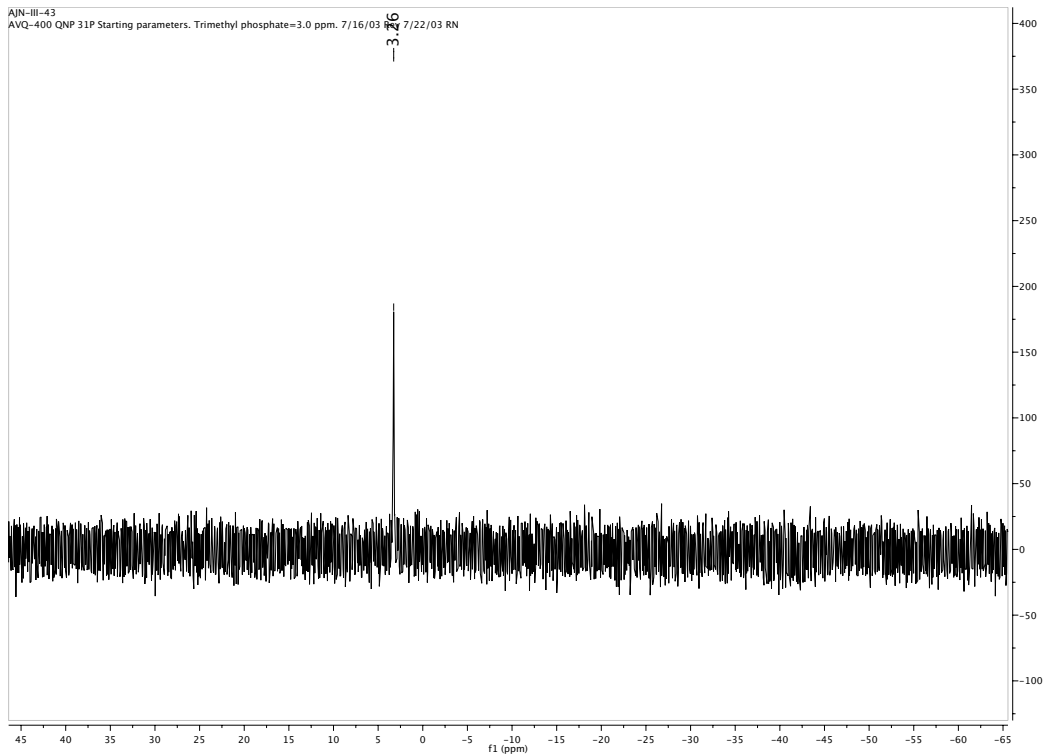


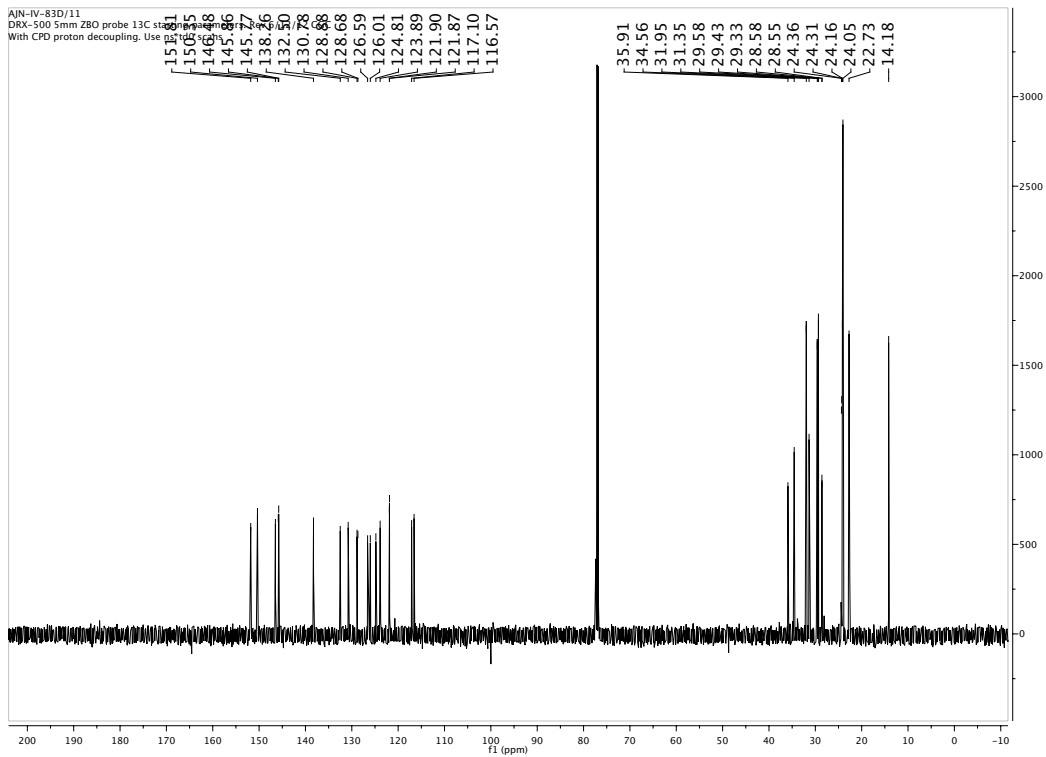
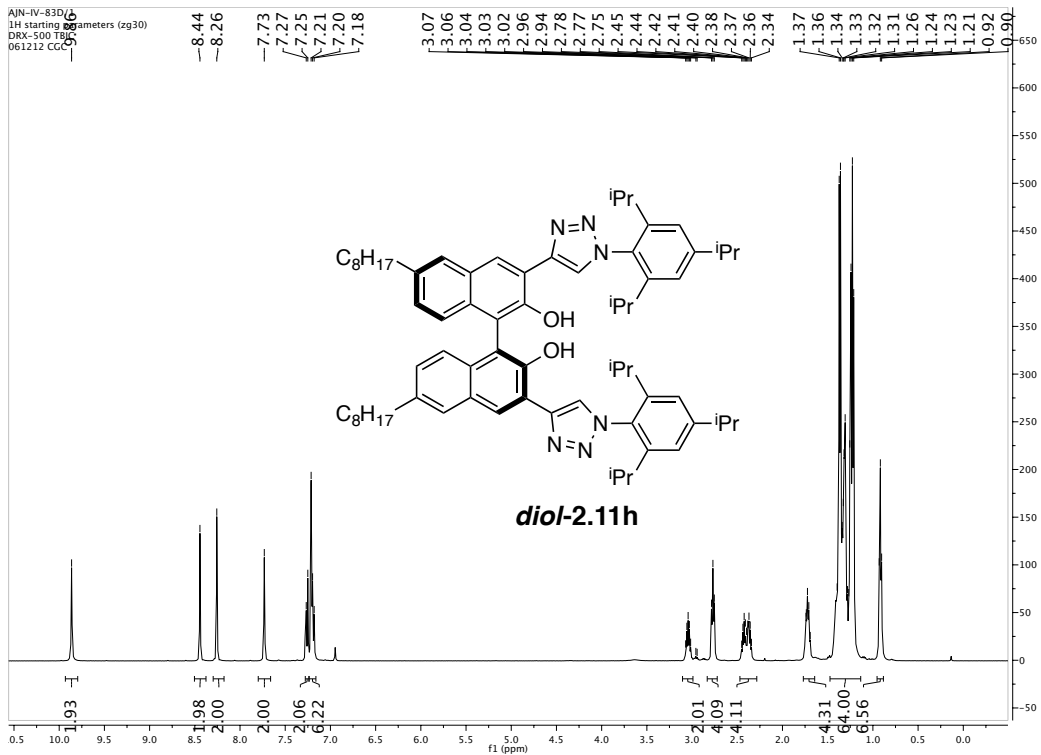


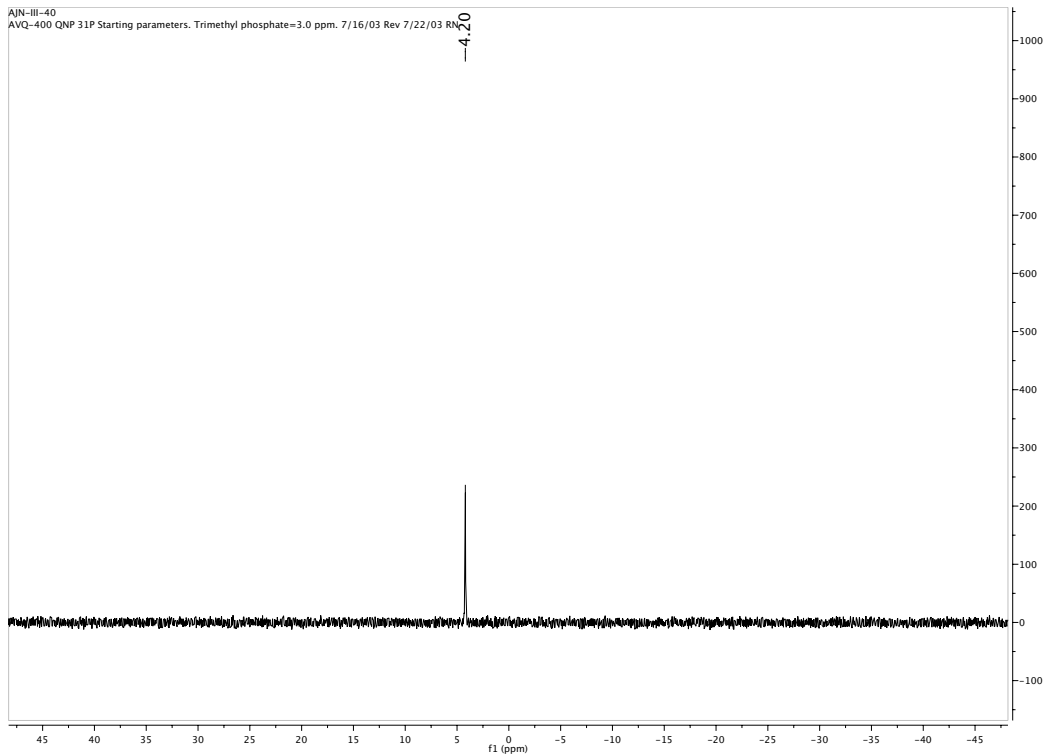


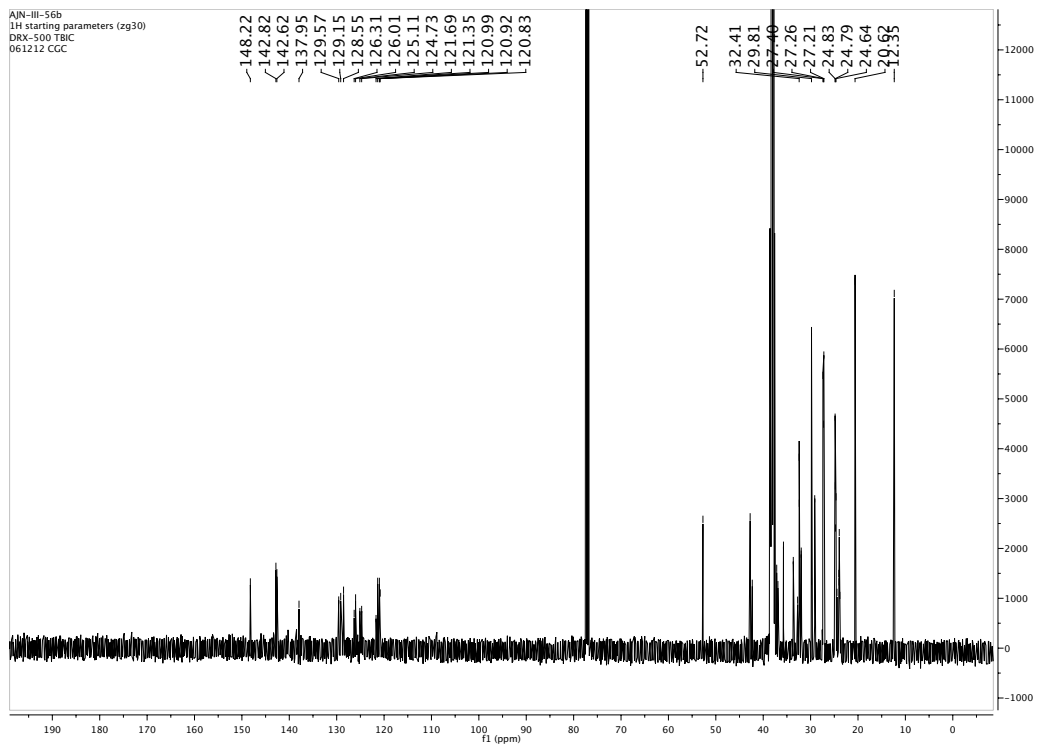
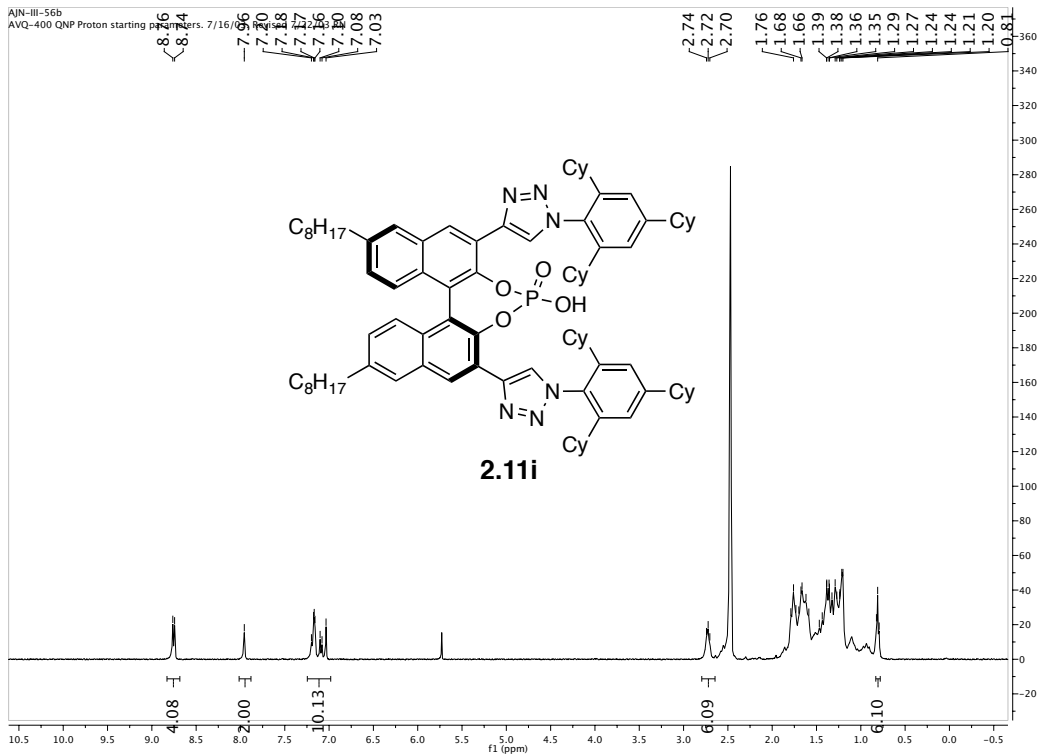


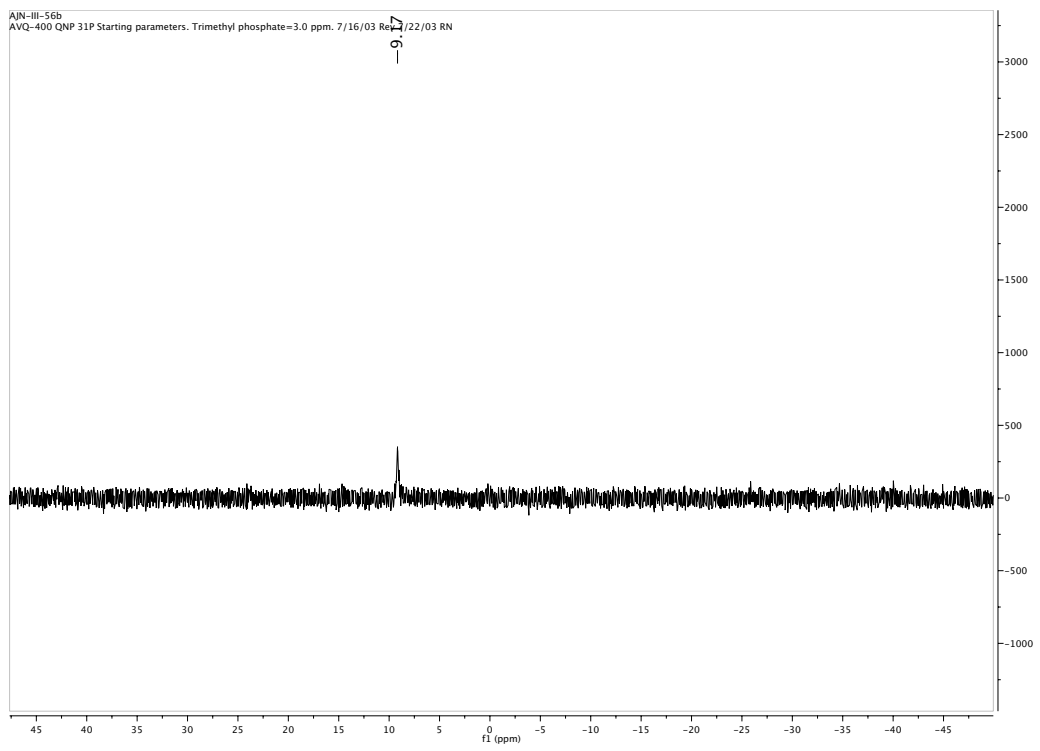


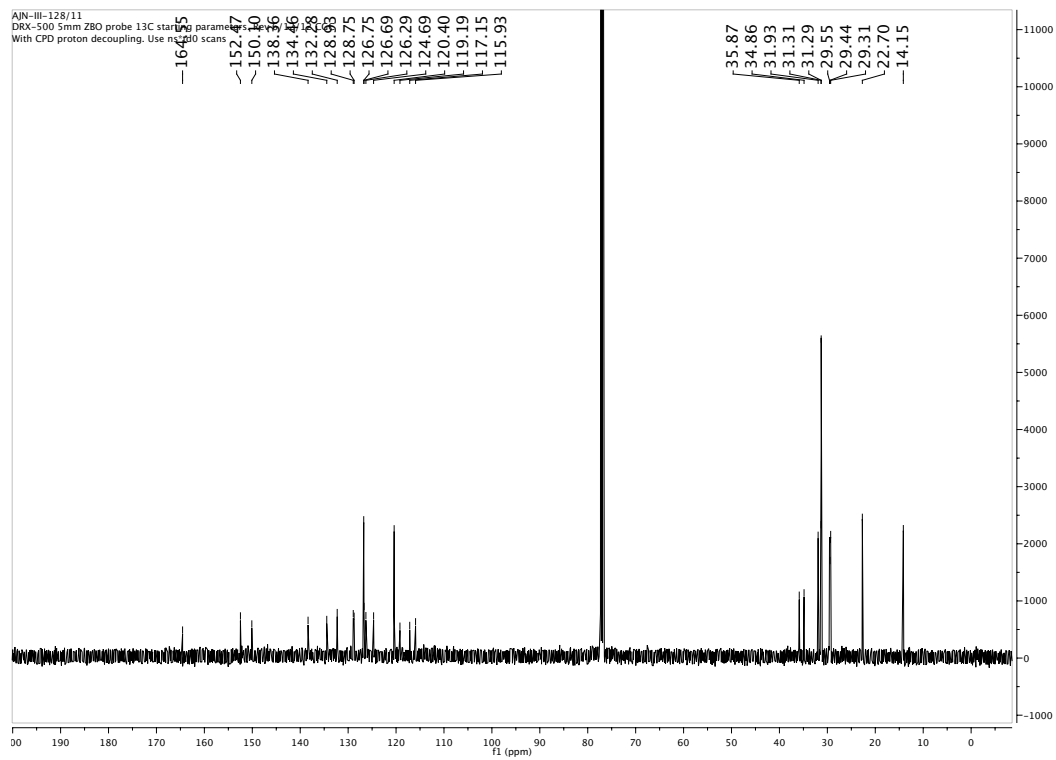
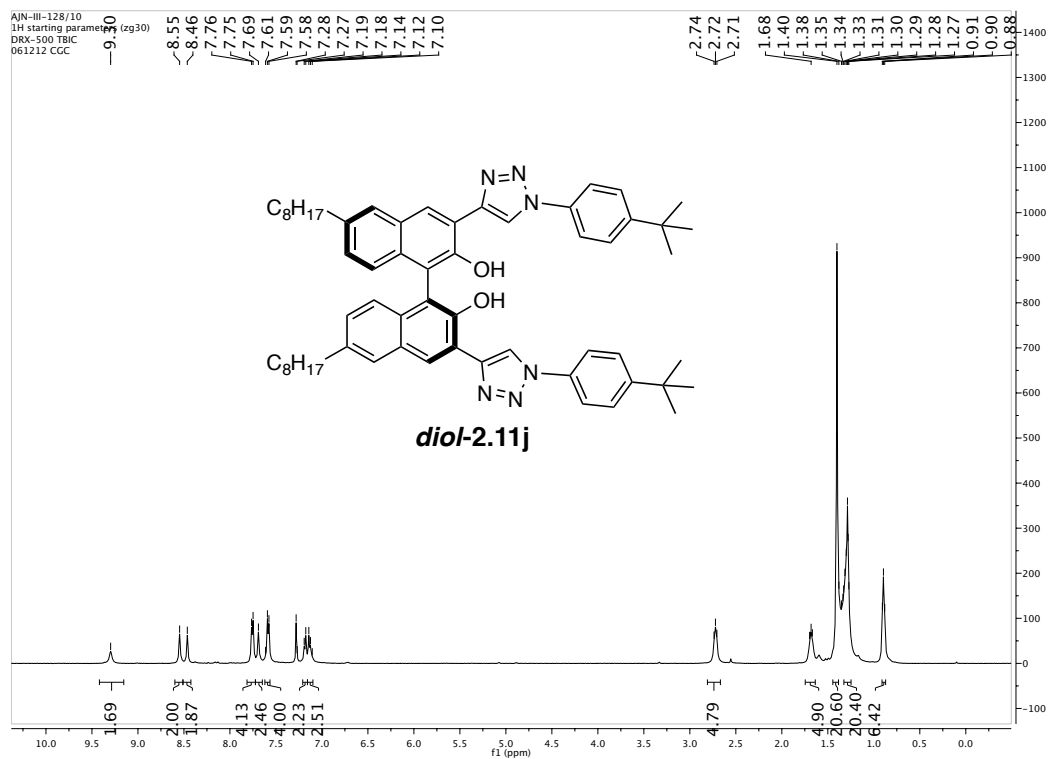


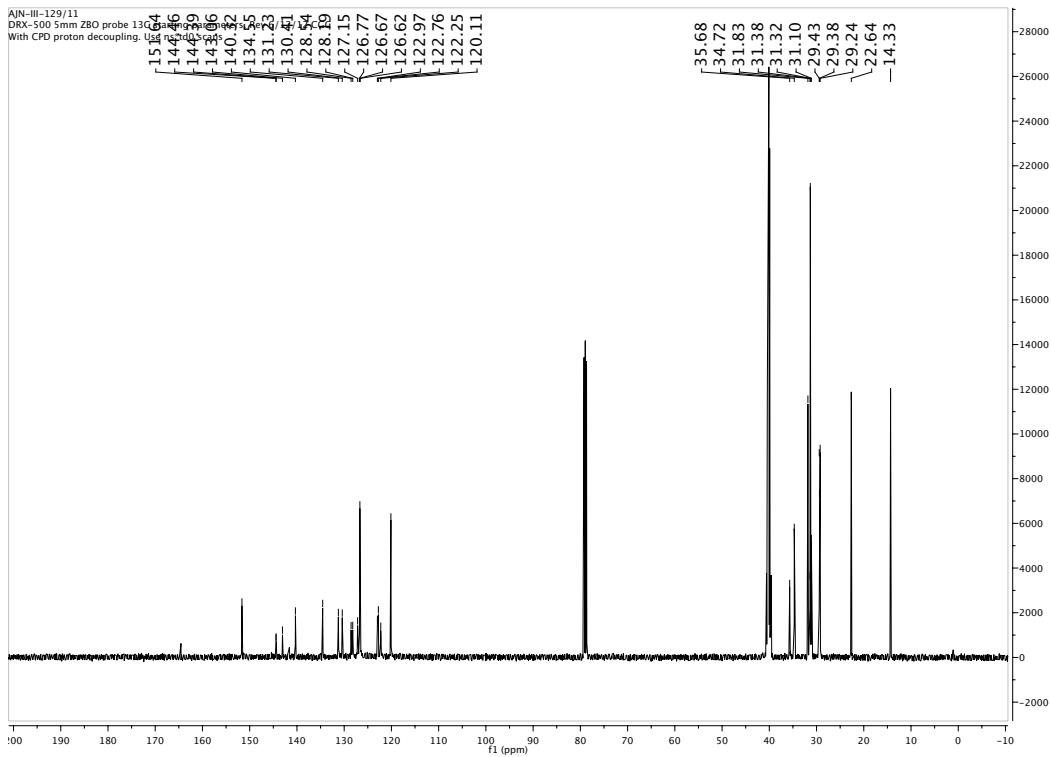
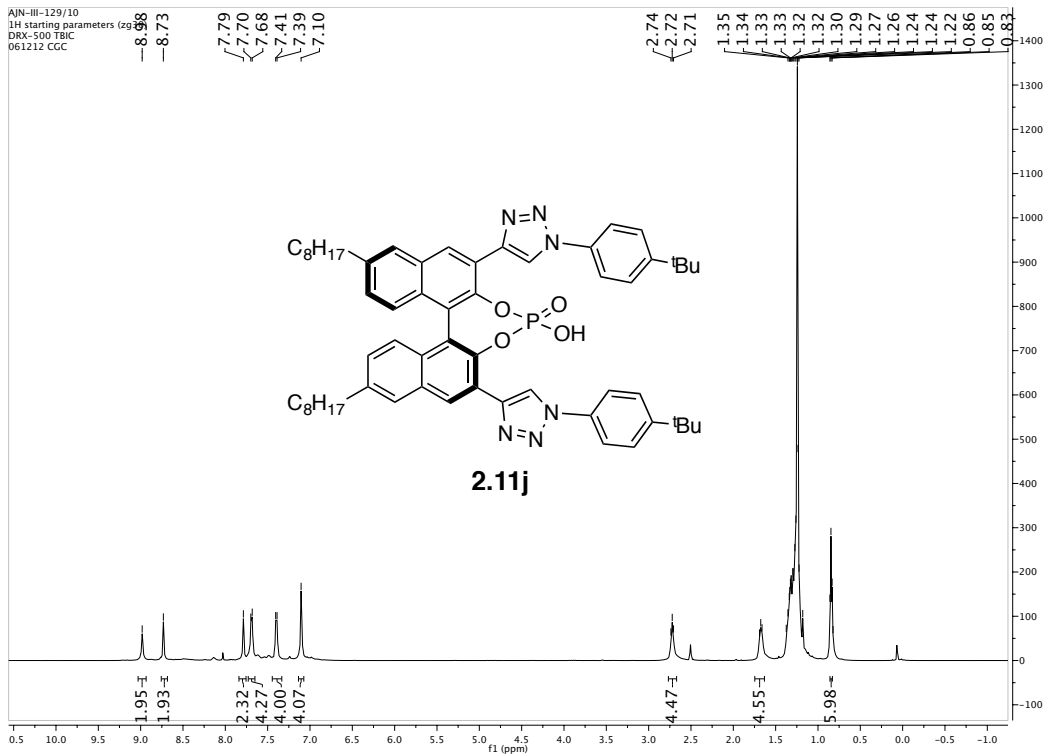




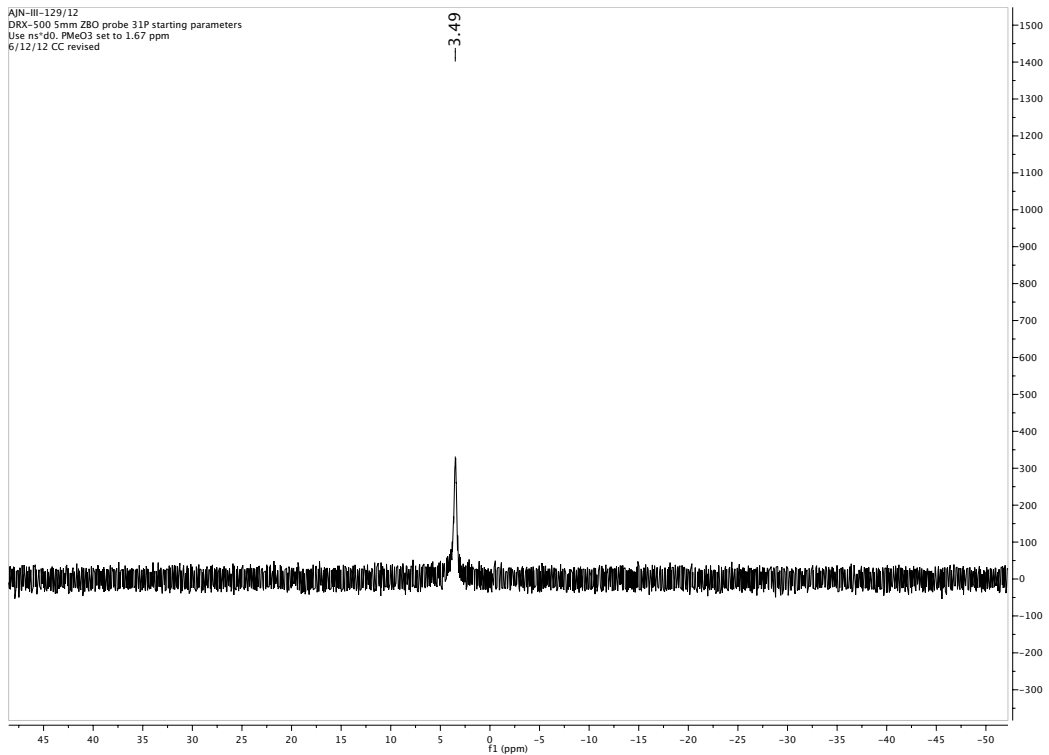


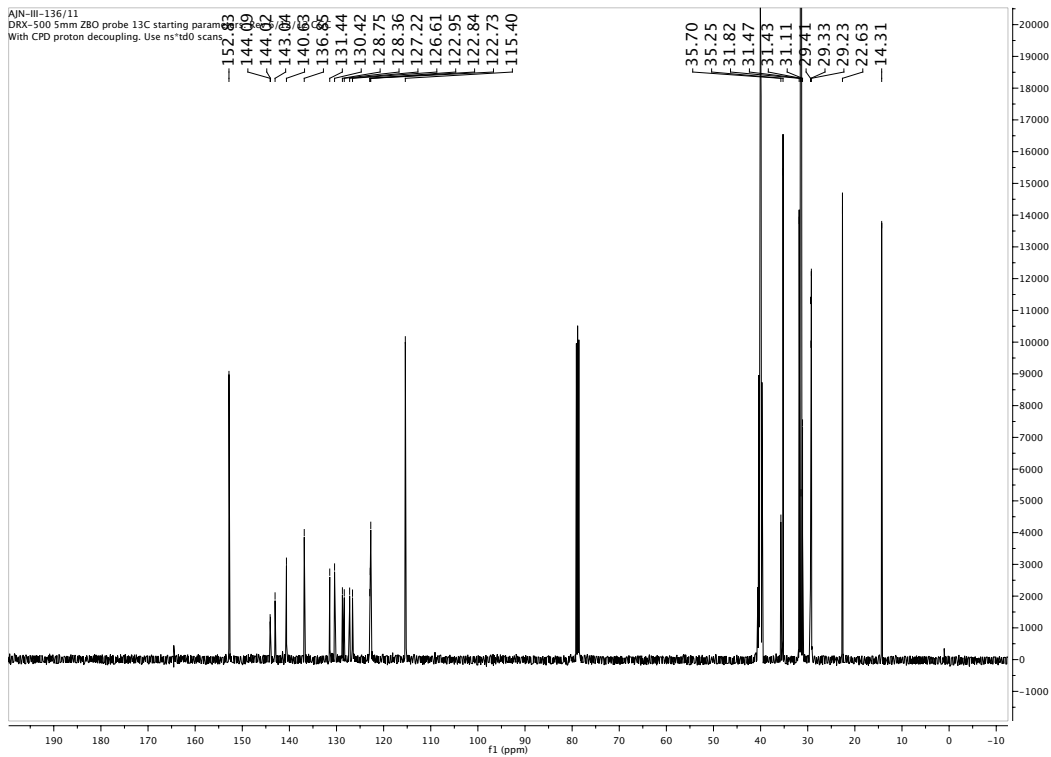
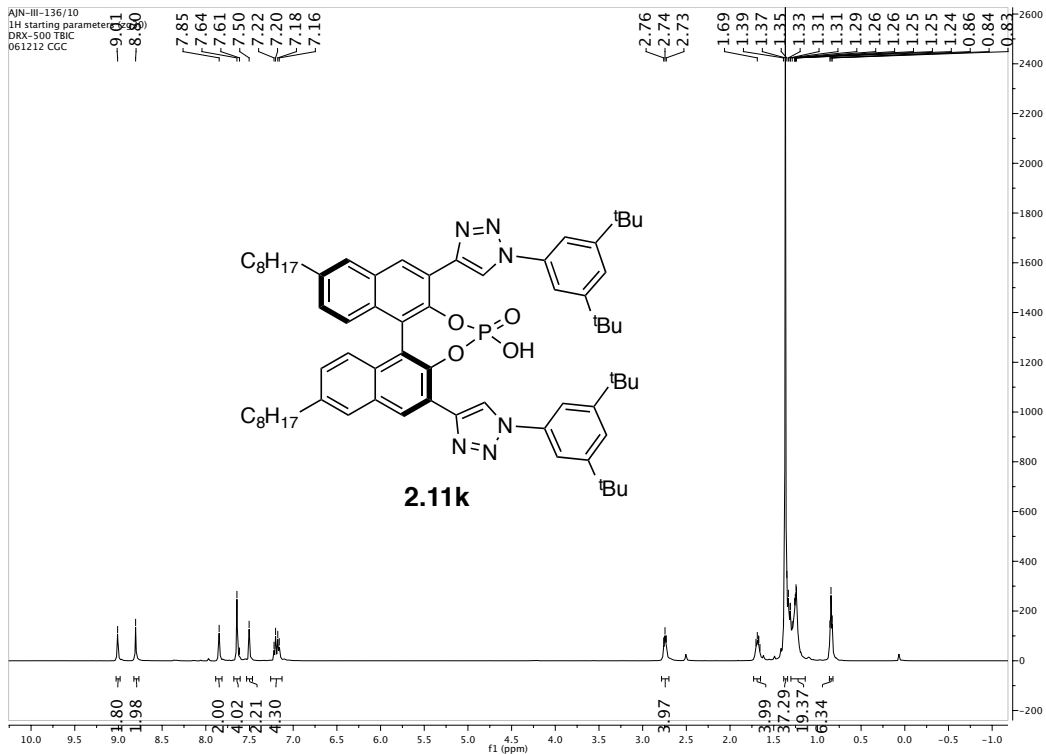




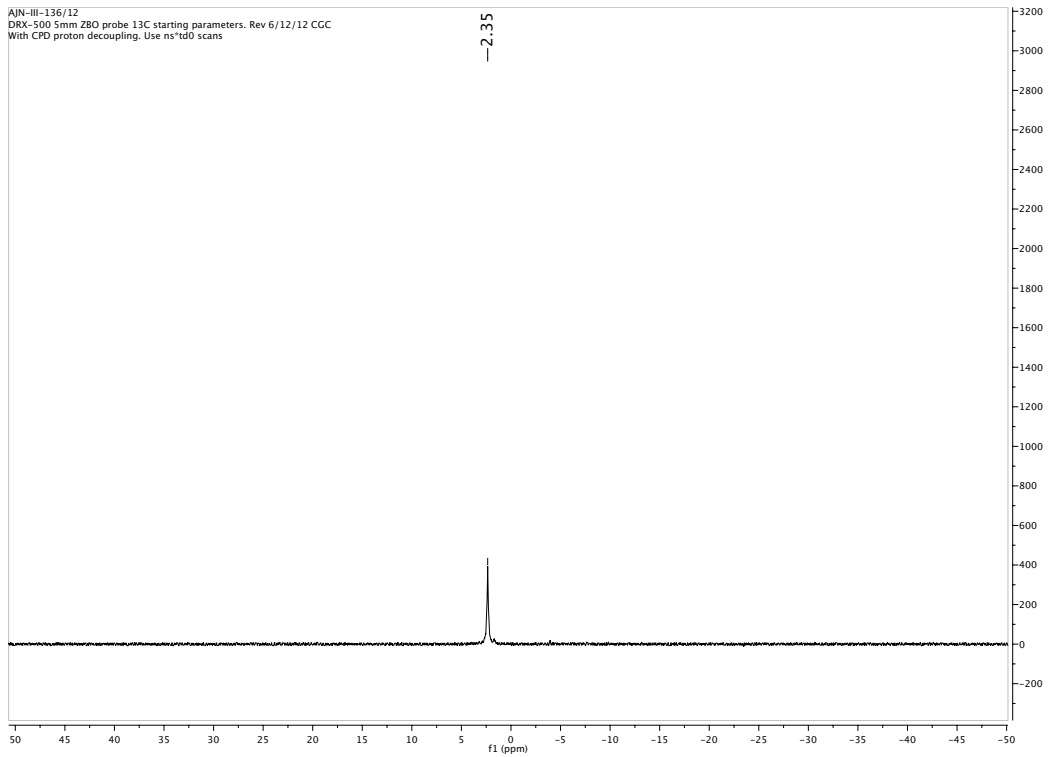


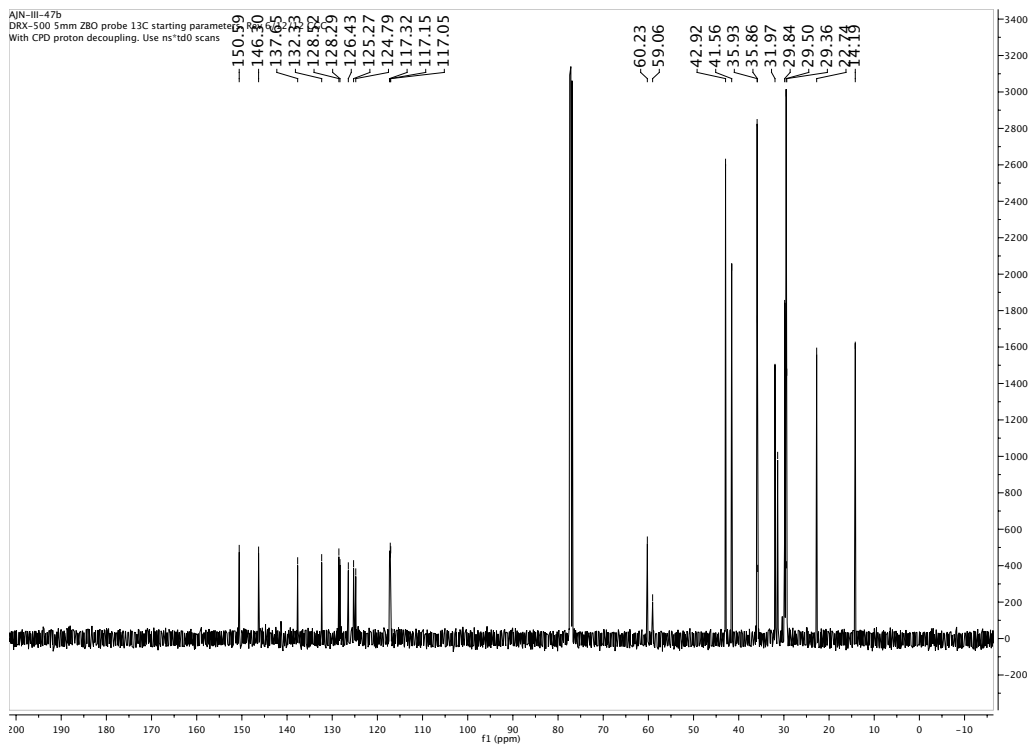
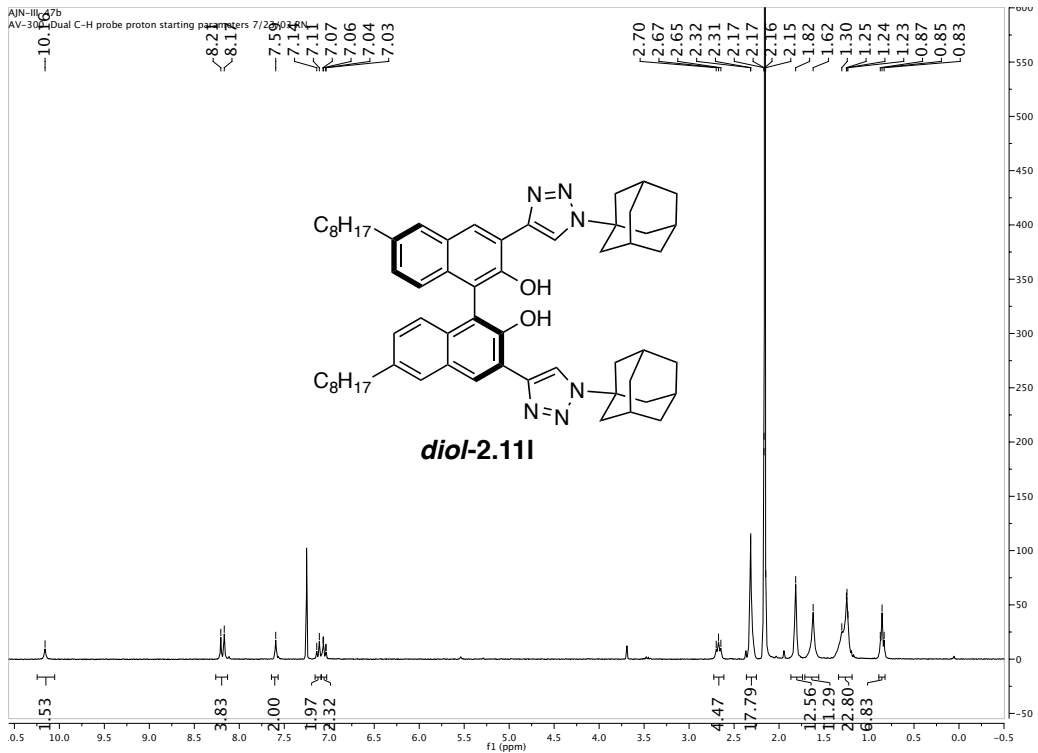
AIN-III-129/12
DRX-500 5mm Z80 probe 31P starting parameters
Use ns=10, PMeO3 set to 1.67 ppm
6/12/12 CC revised

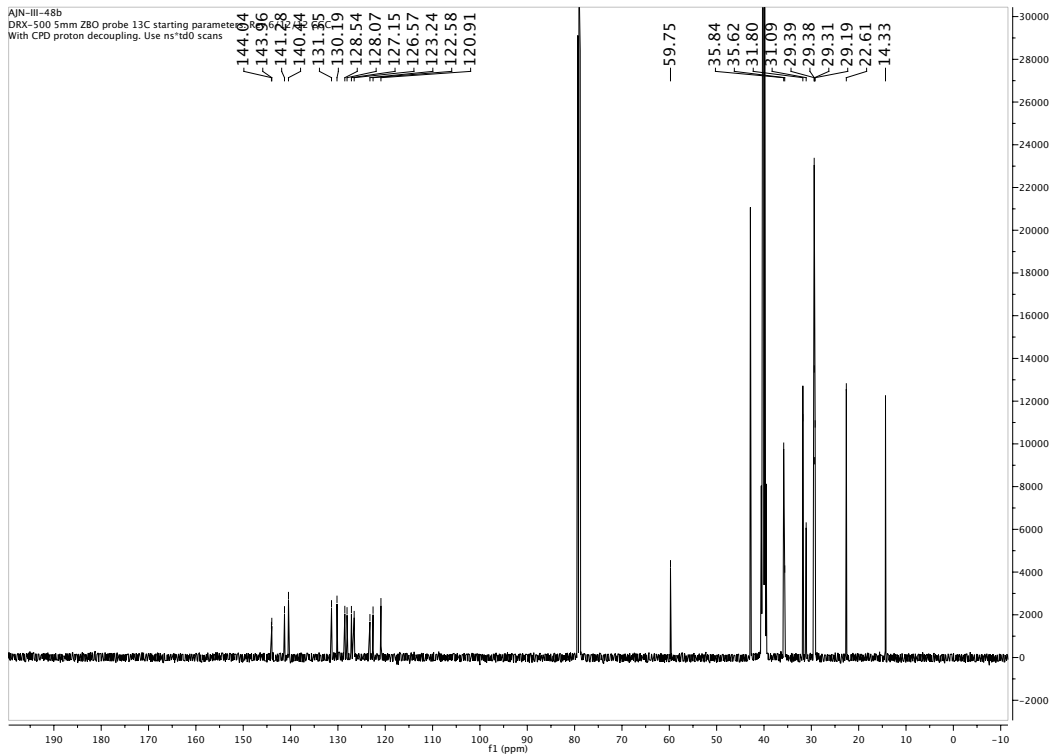
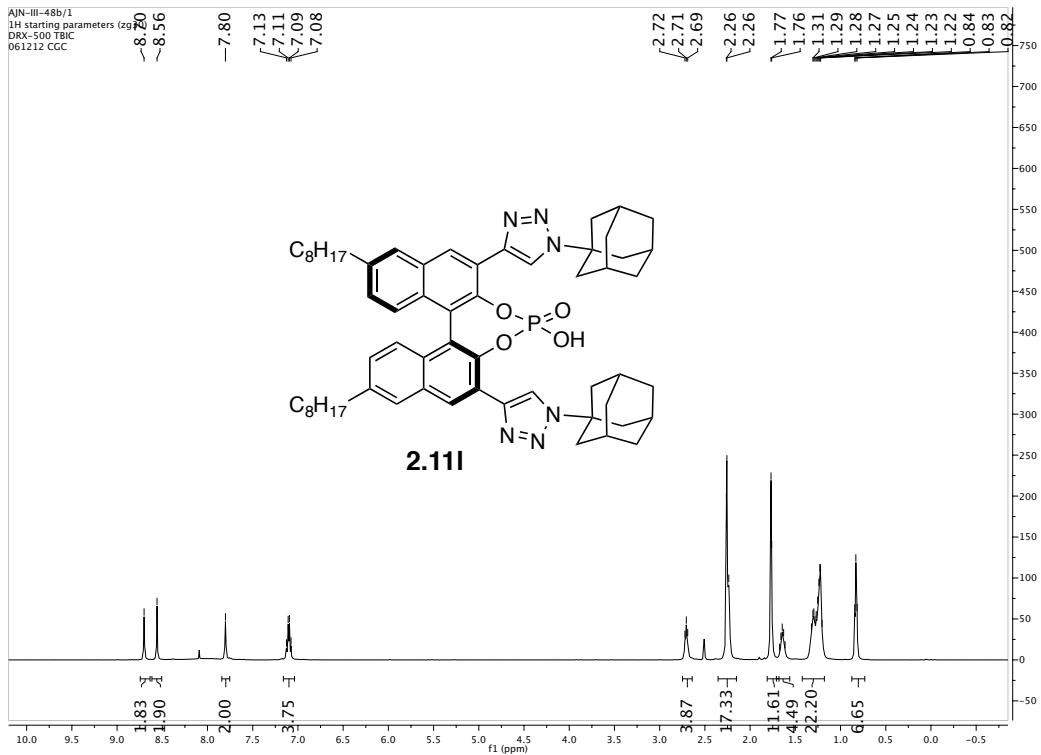




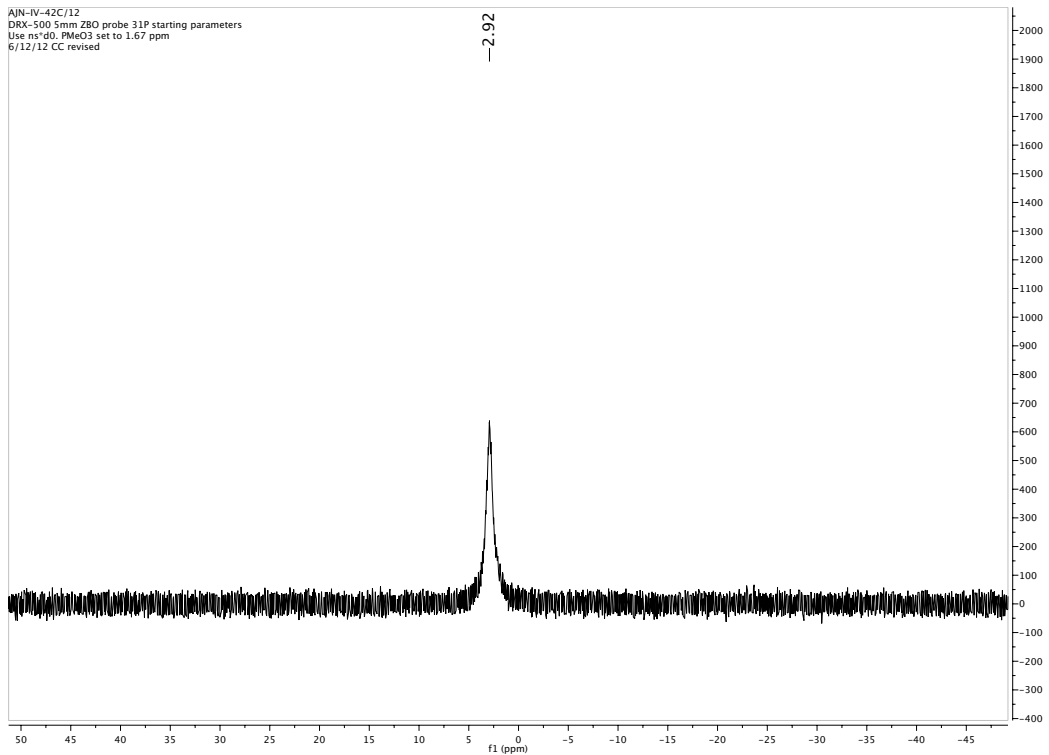
AIN-III-136/12
DRX-500 5mm Z80 probe 13C starting parameters. Rev 6/12/12 CGC
With CPD proton decoupling. Use ns1d0 scans

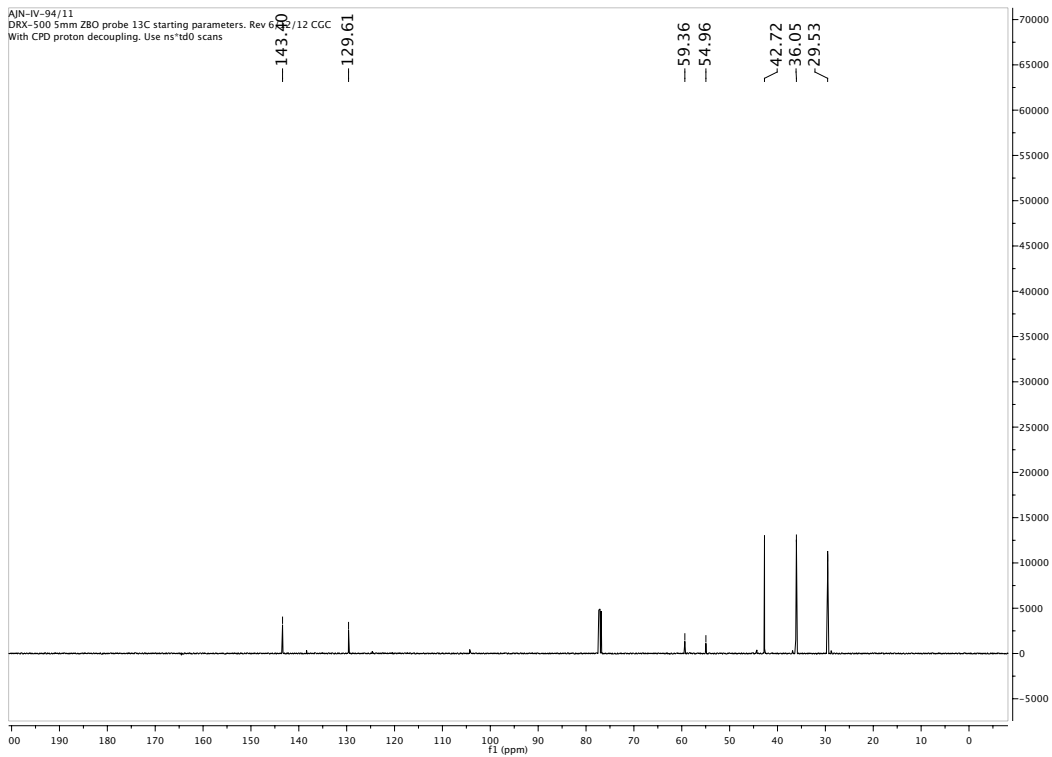
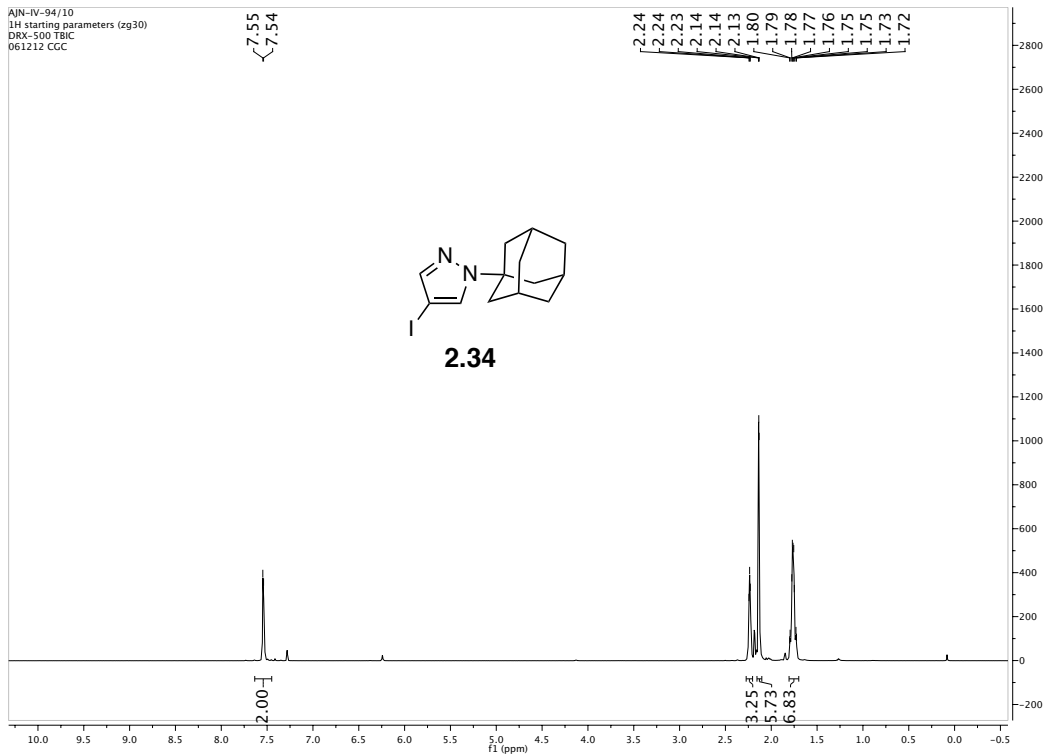


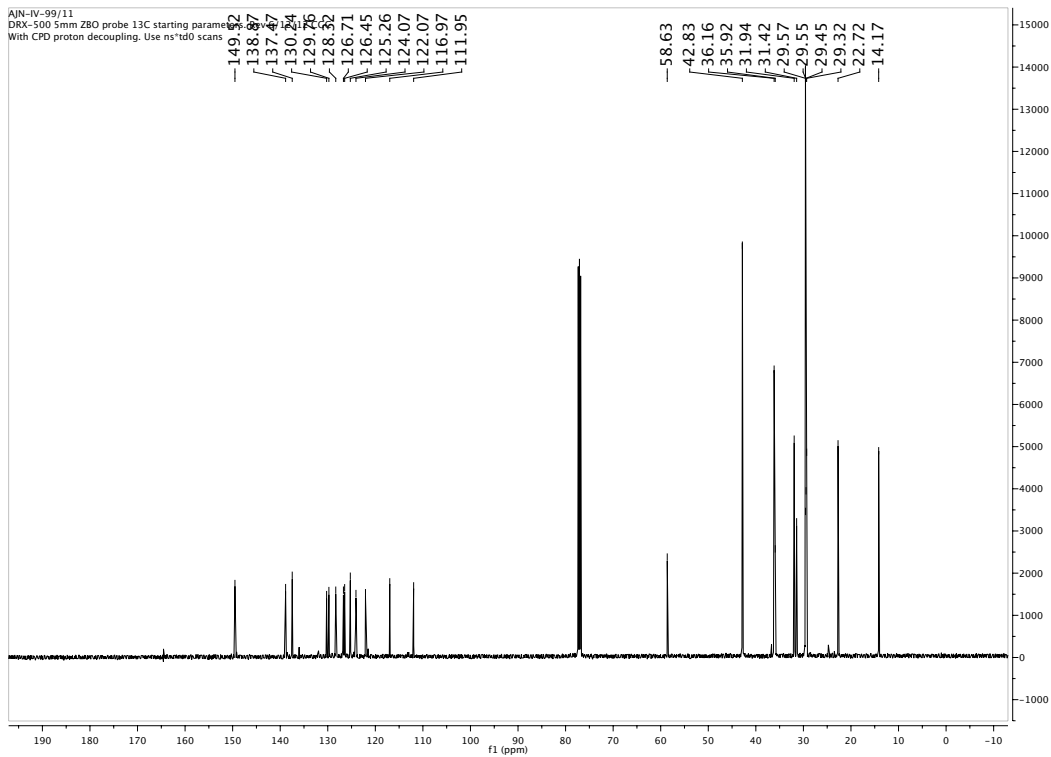
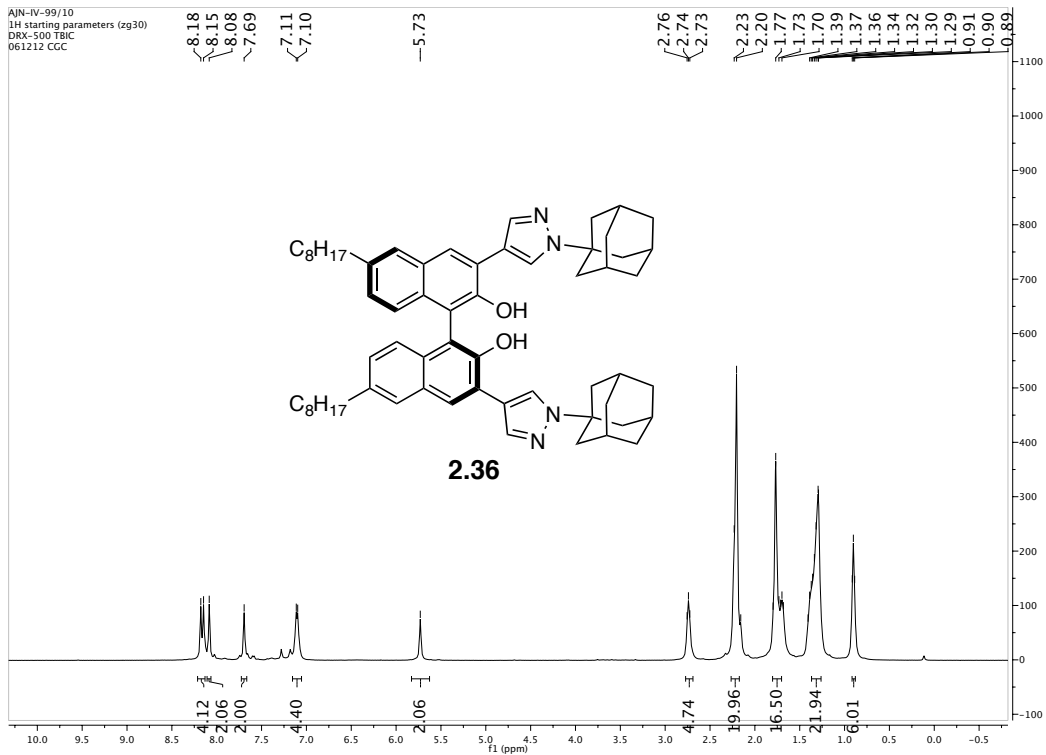


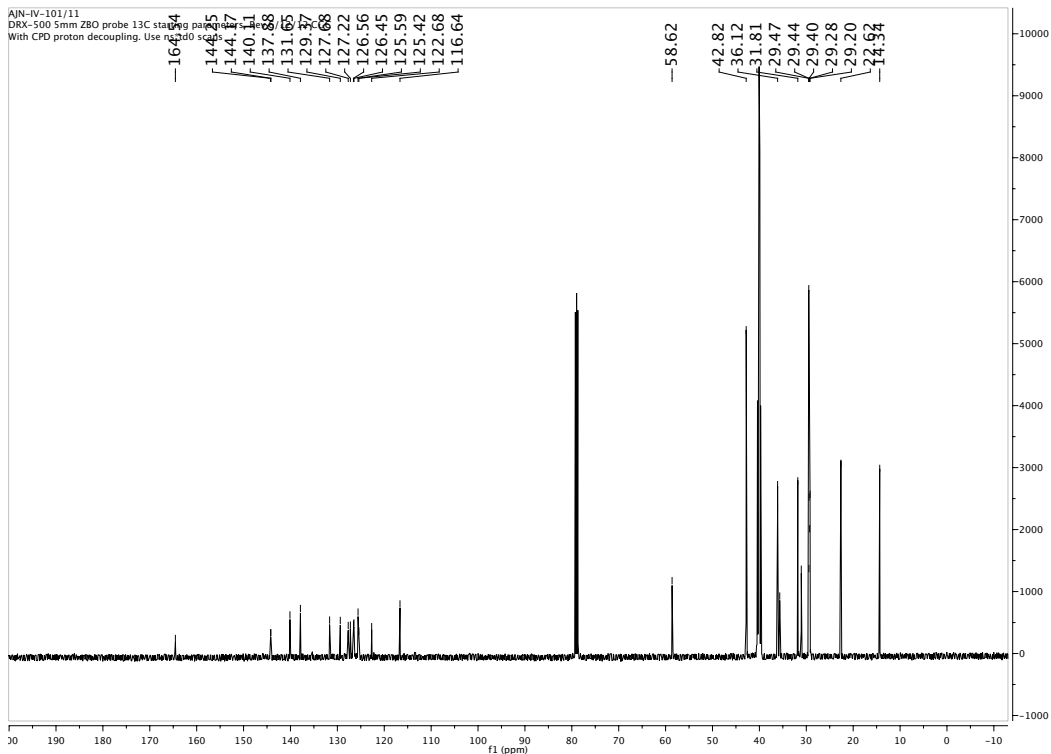
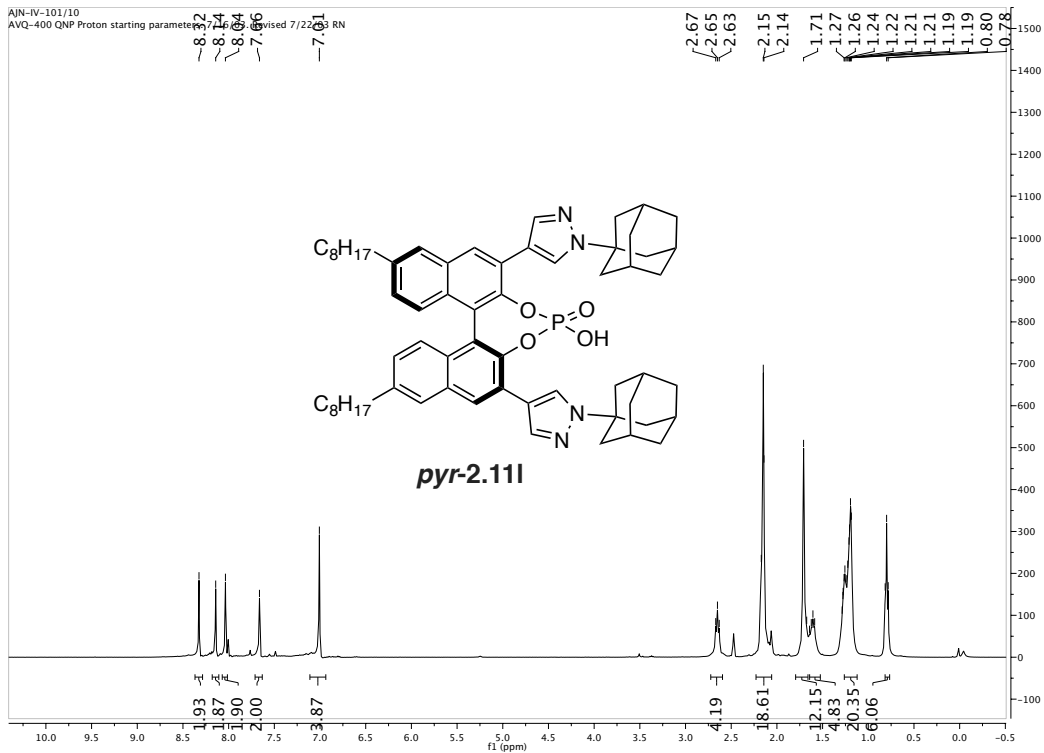


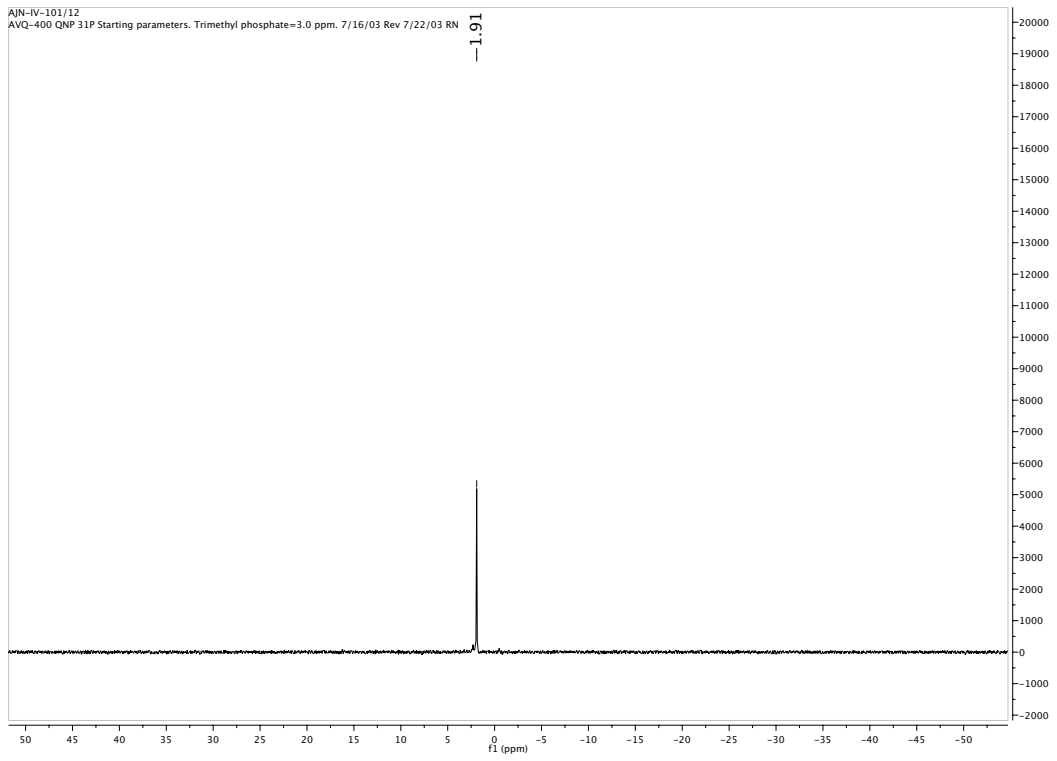
AIN-IV-42C/12
DRX-500 5mm Z80 probe 31P starting parameters
Use ns=10, PMeO3 set to 1.67 ppm
6/12/12 CC revised

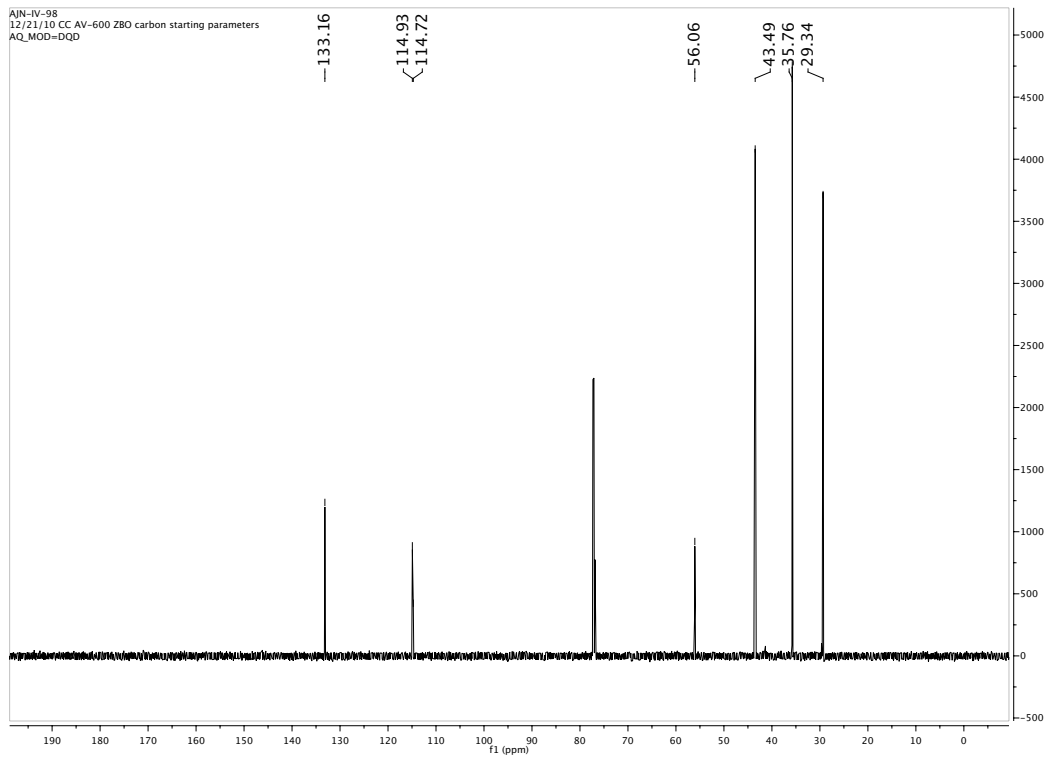
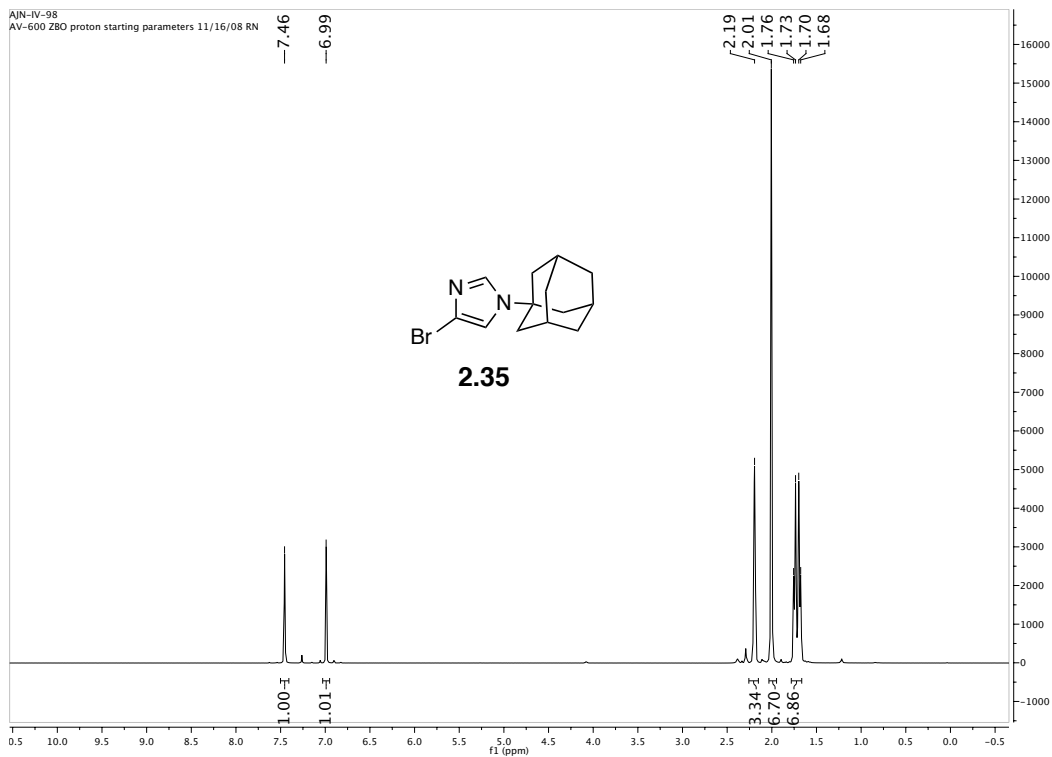


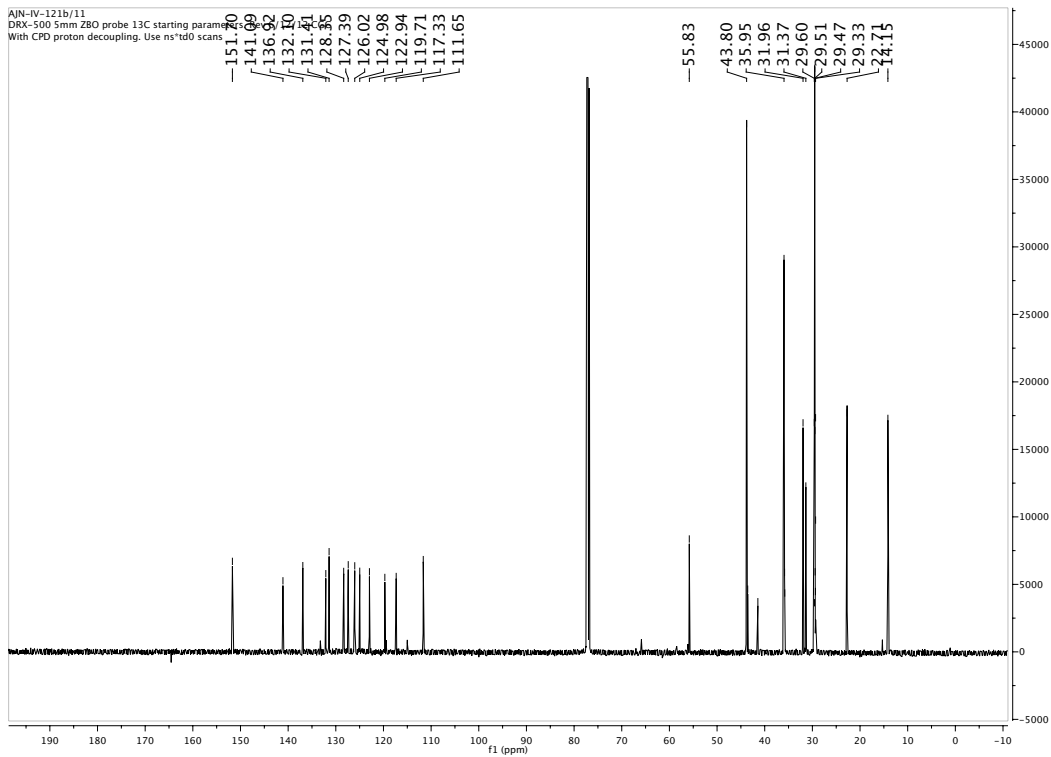
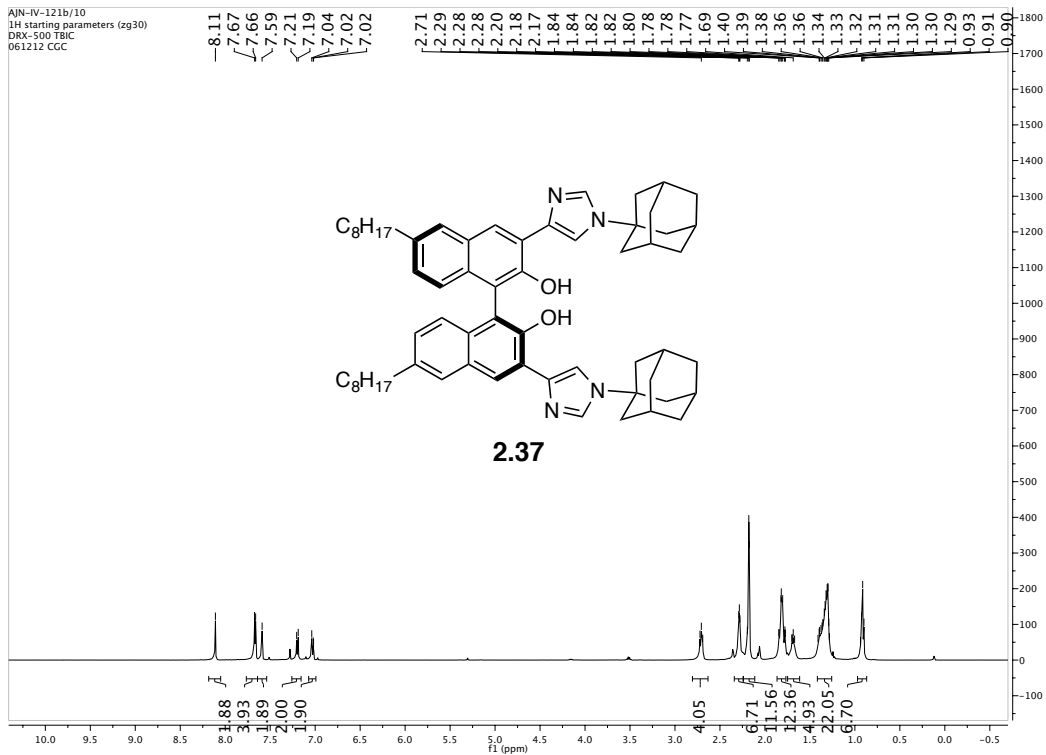


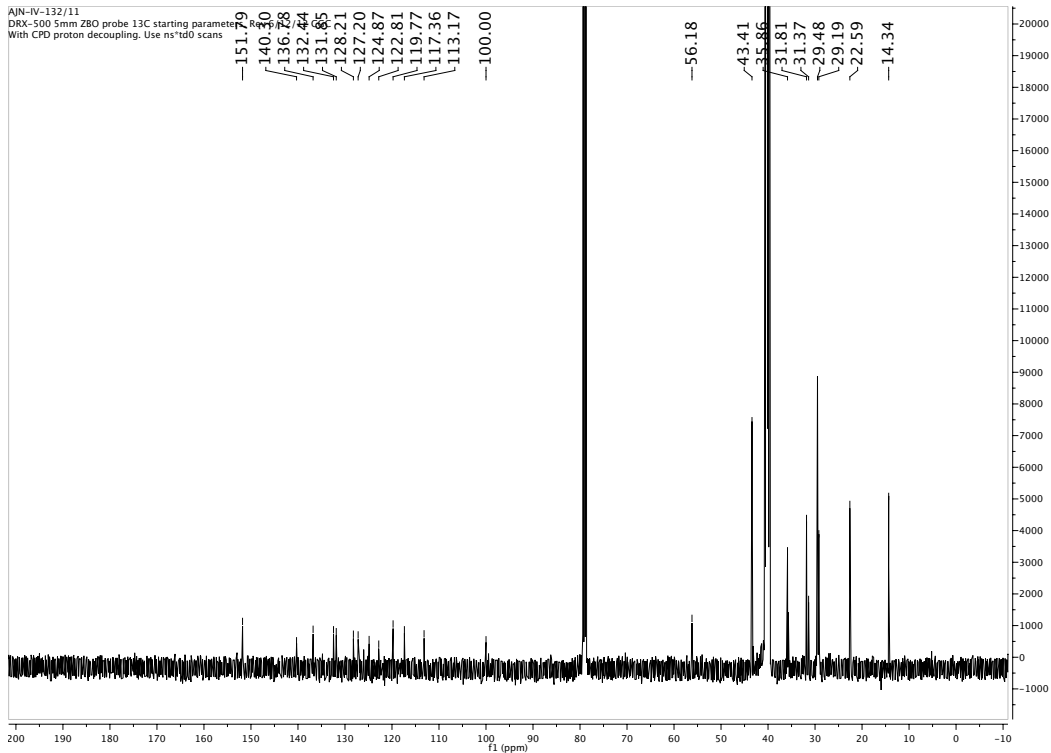
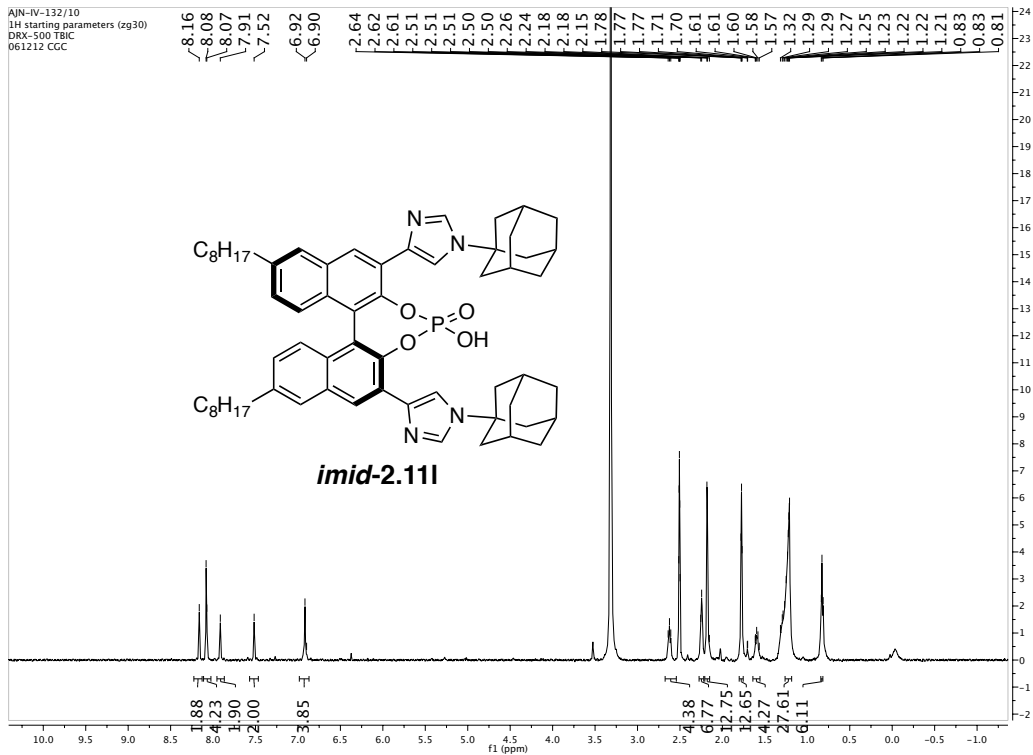




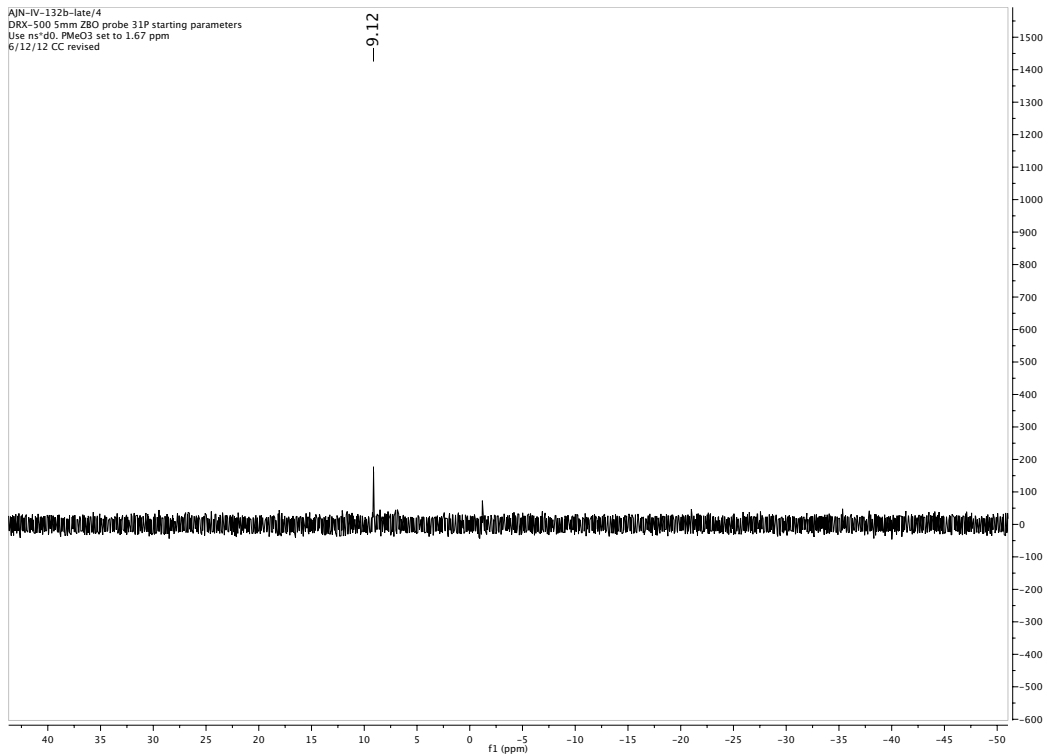


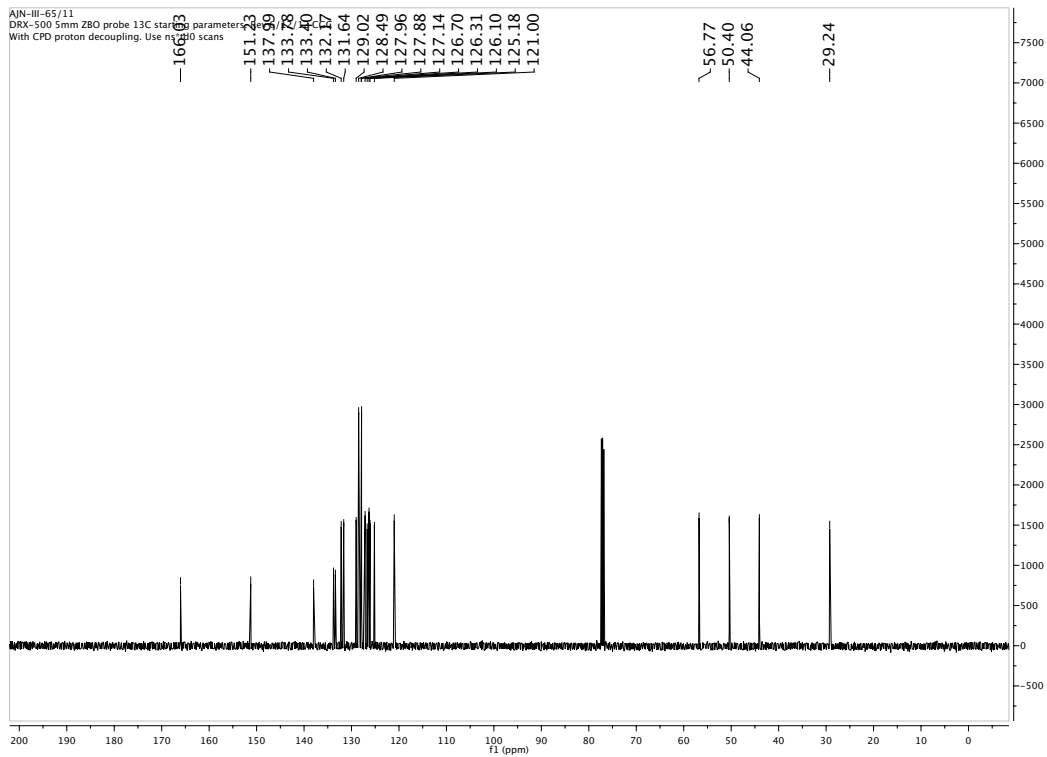
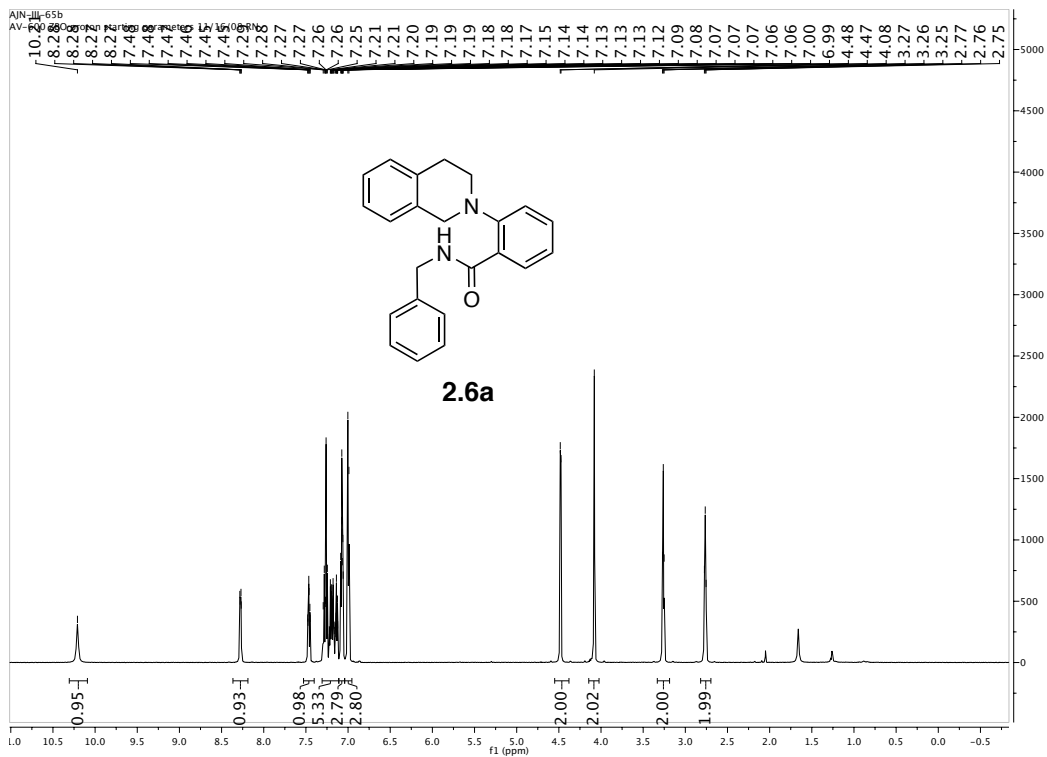


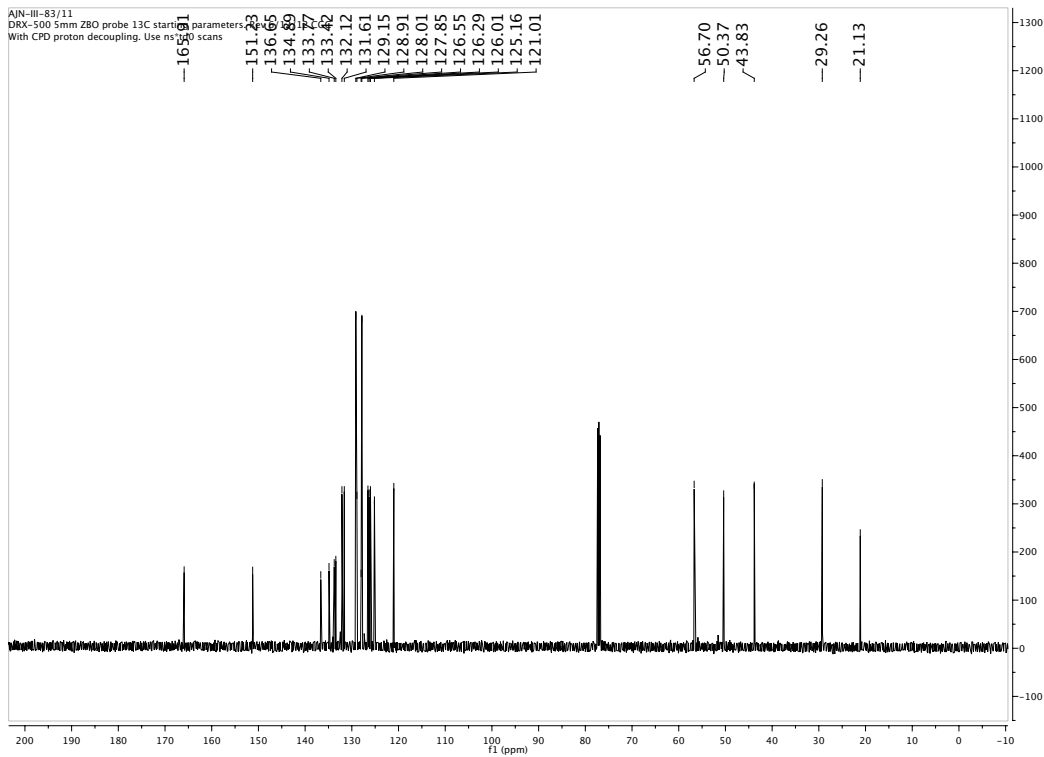
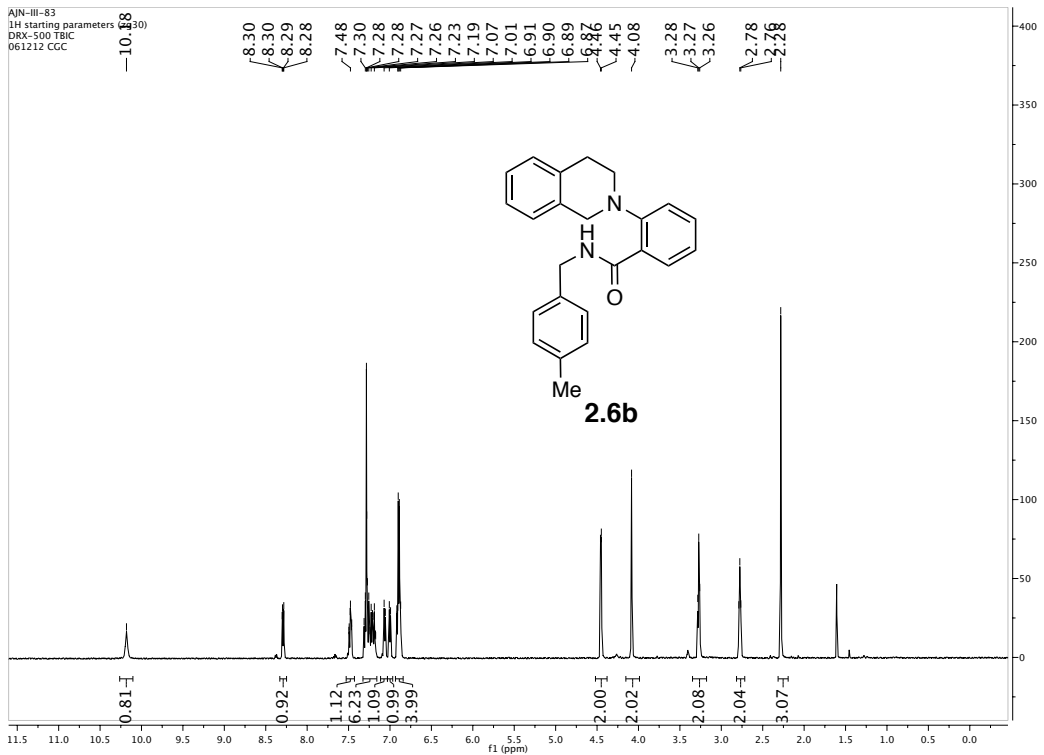


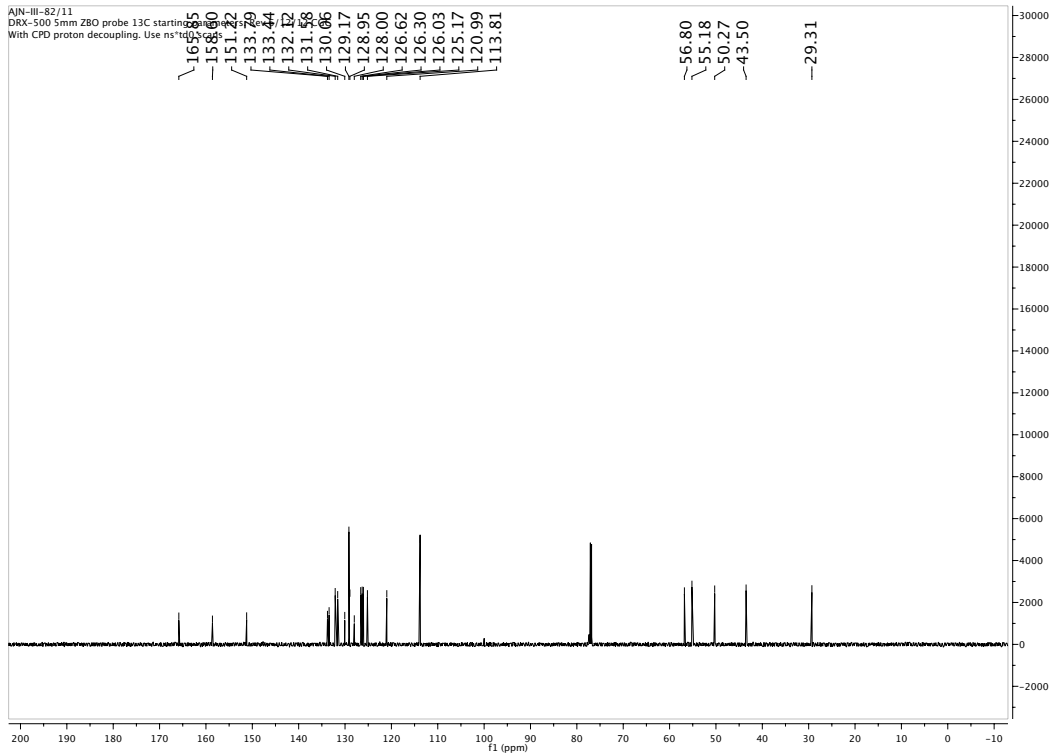
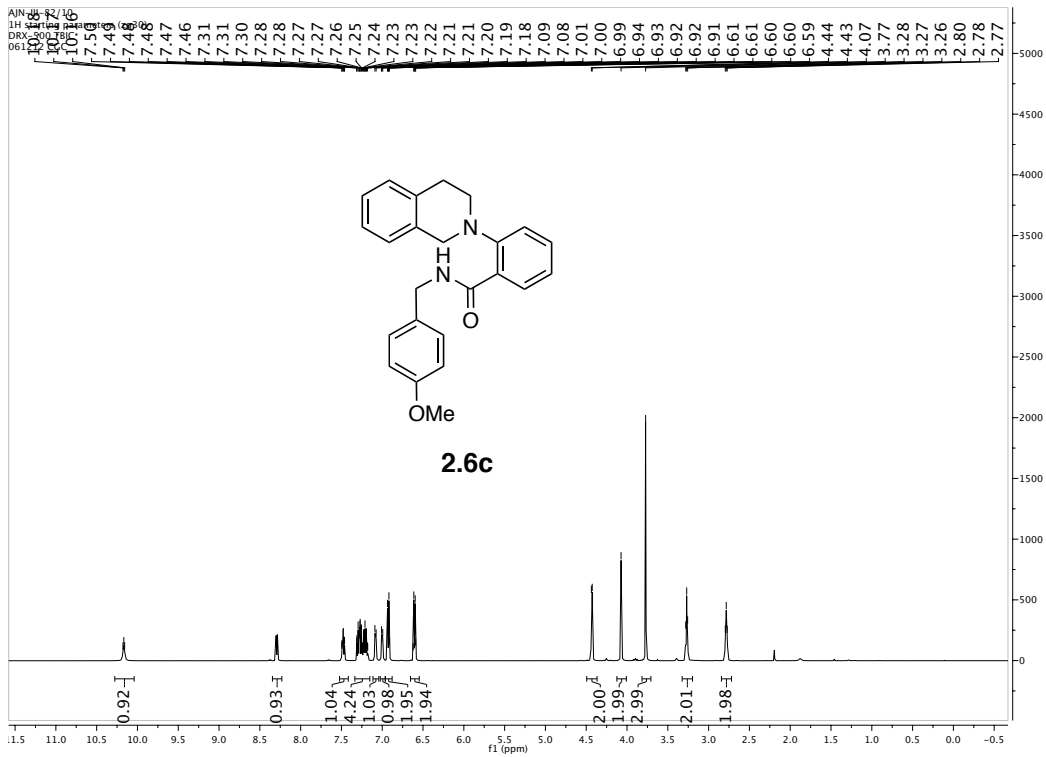


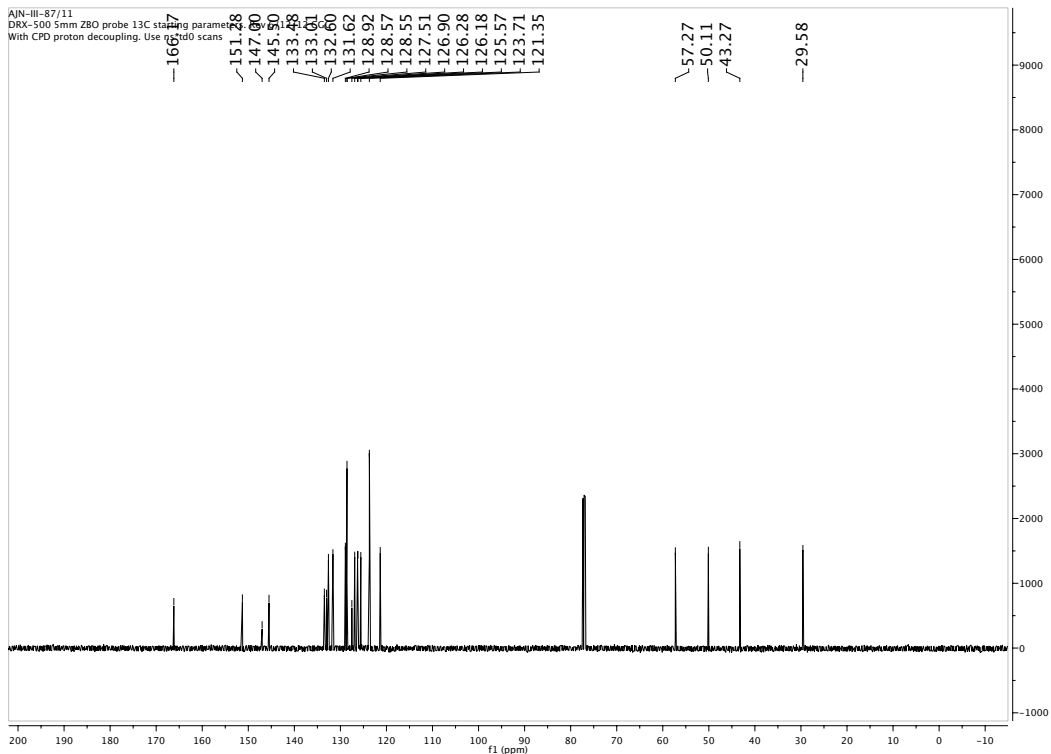
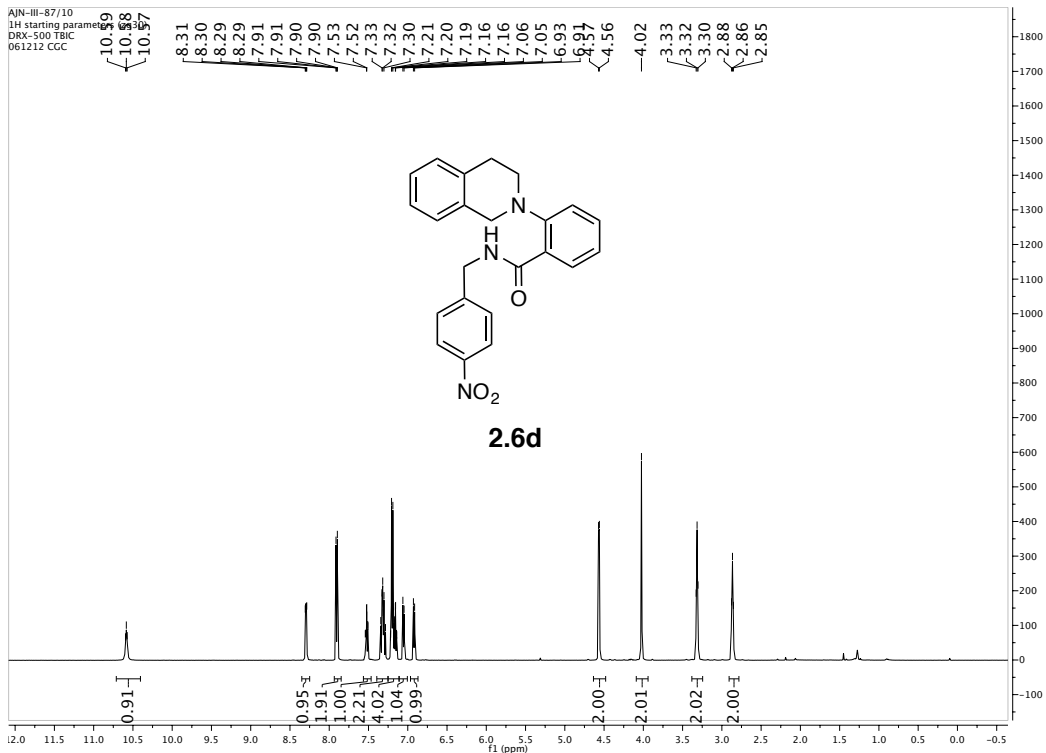
AIN-IV-132b-late/4
DRX-500 5mm Z80 probe 31P starting parameters
Use ns=40, PMeOS set to 1.67 ppm
6/12/12 CC revised

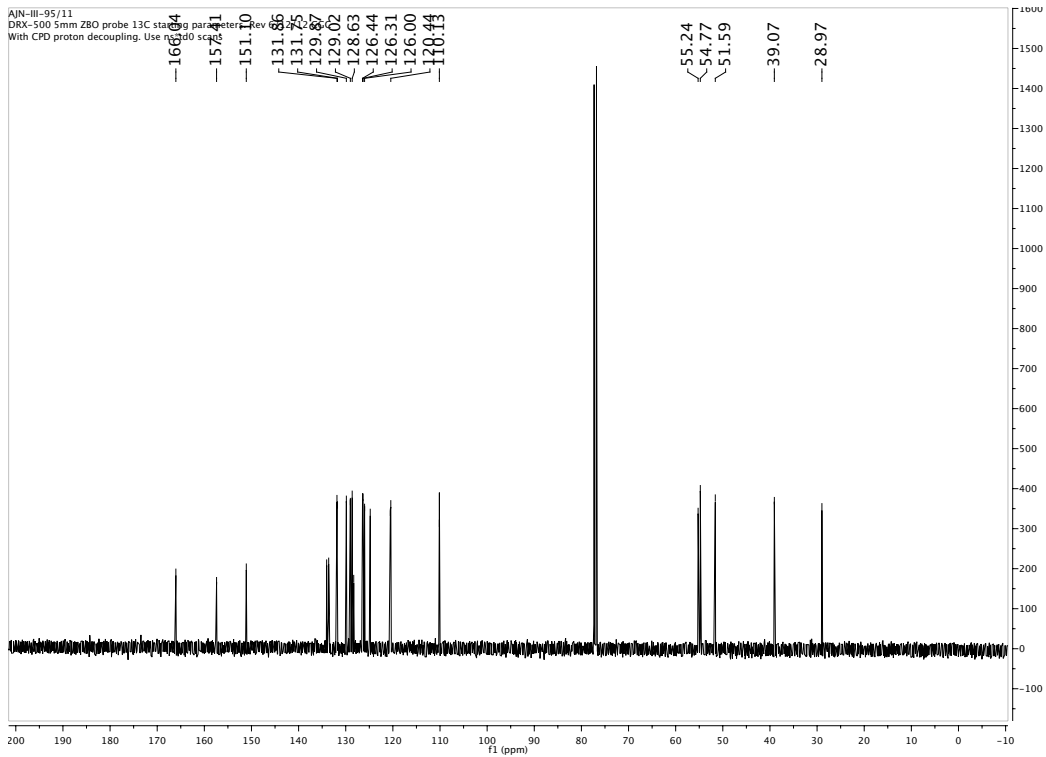
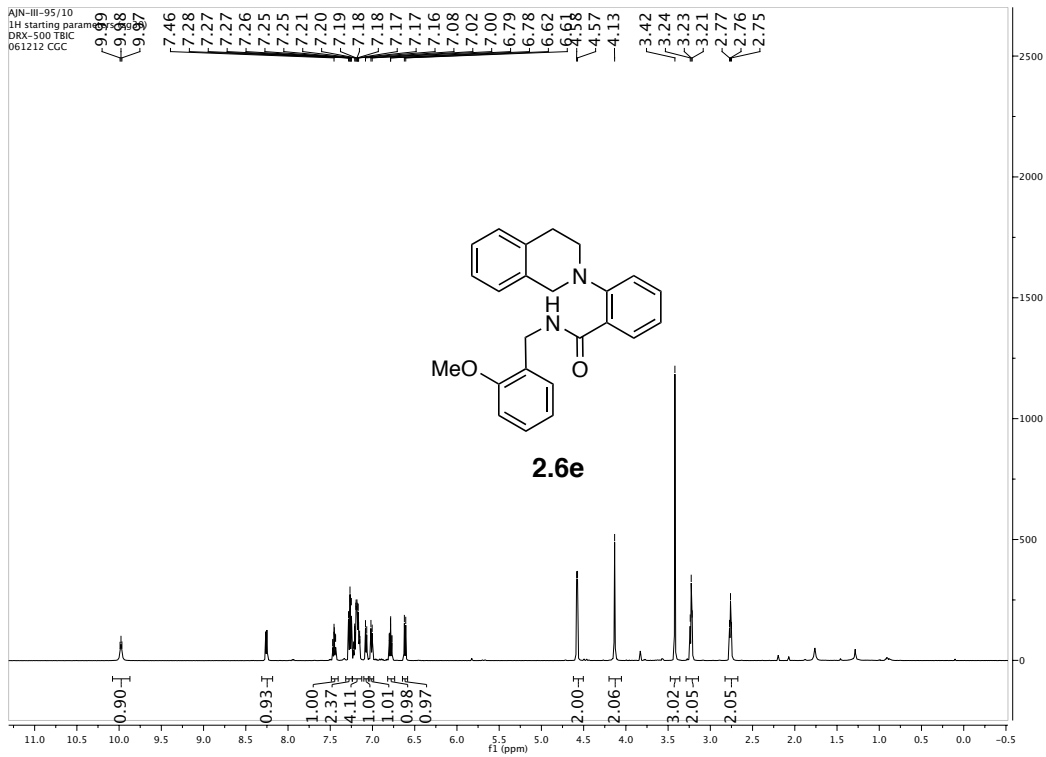


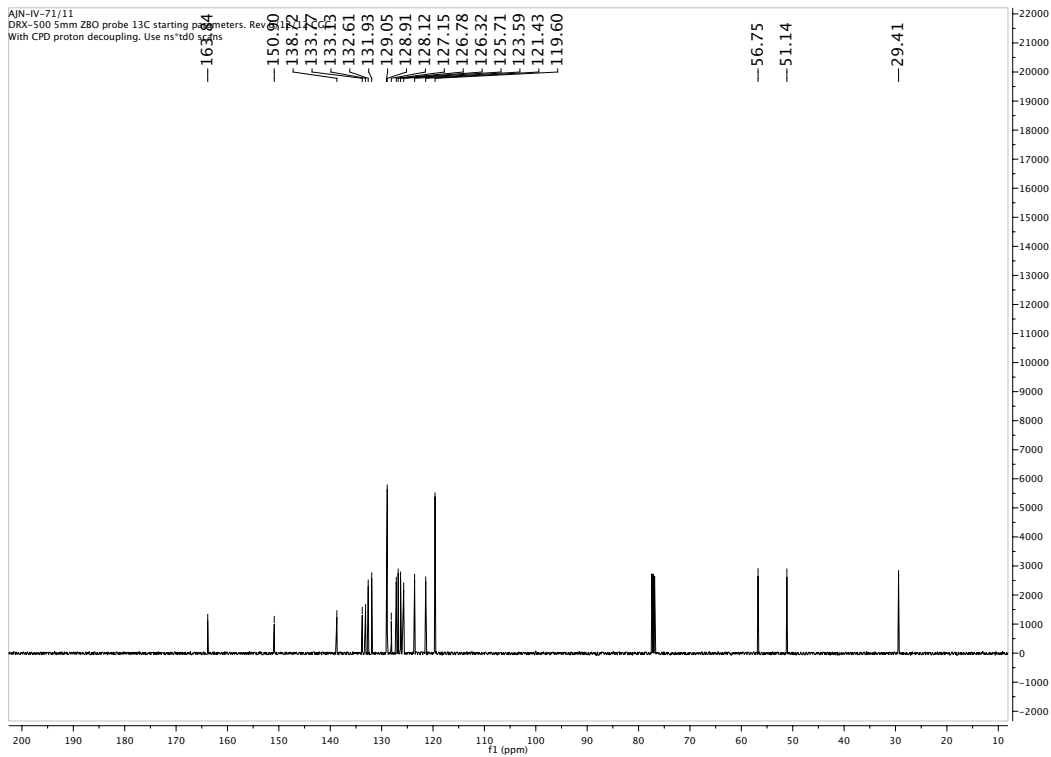
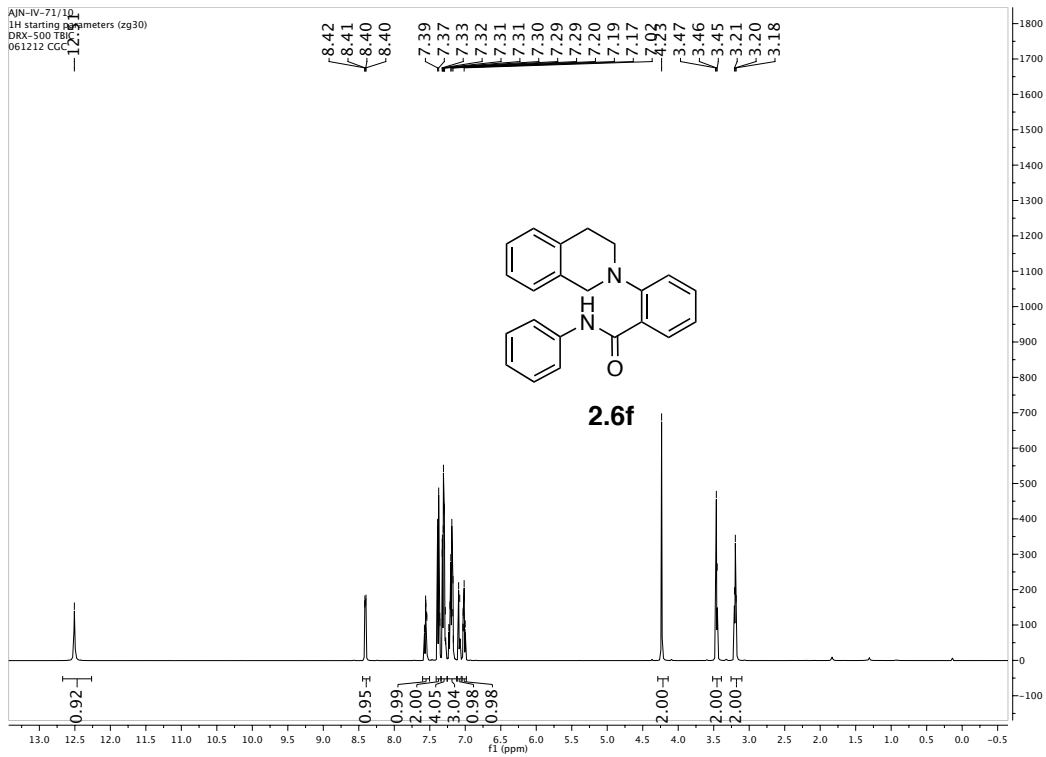


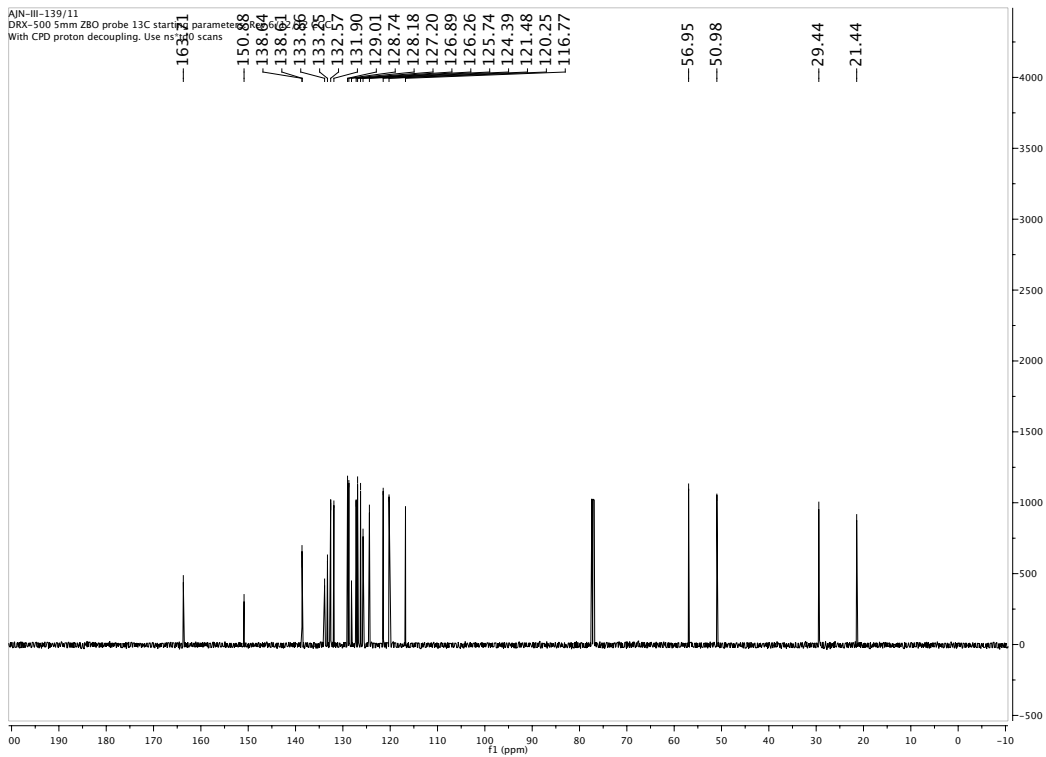
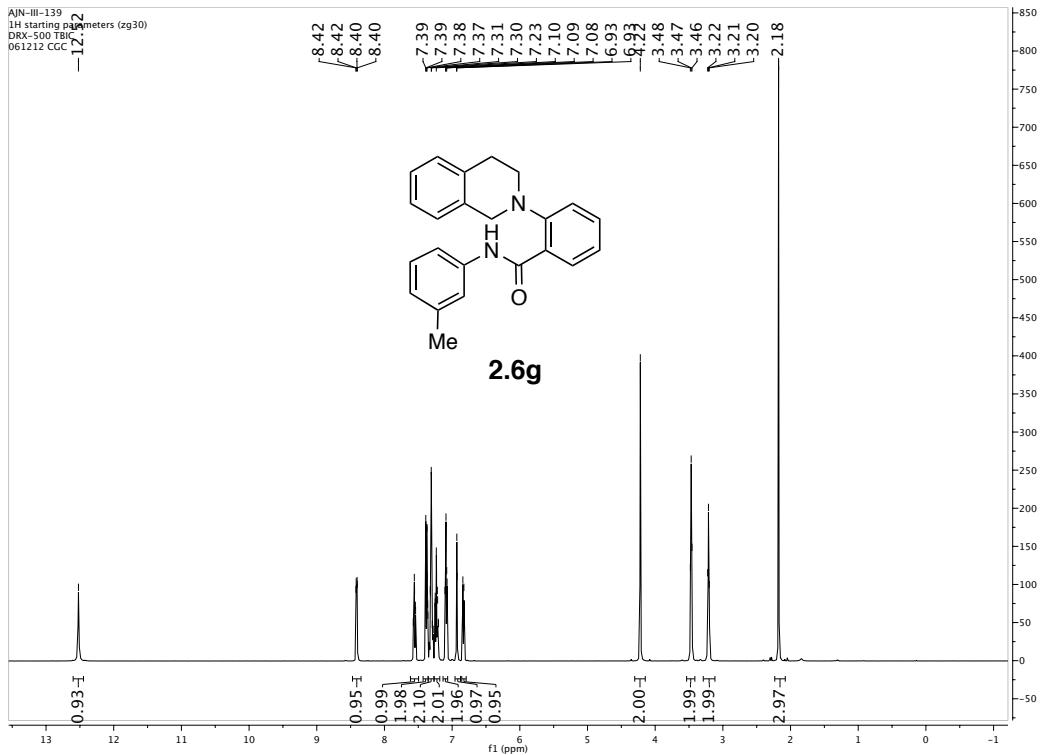


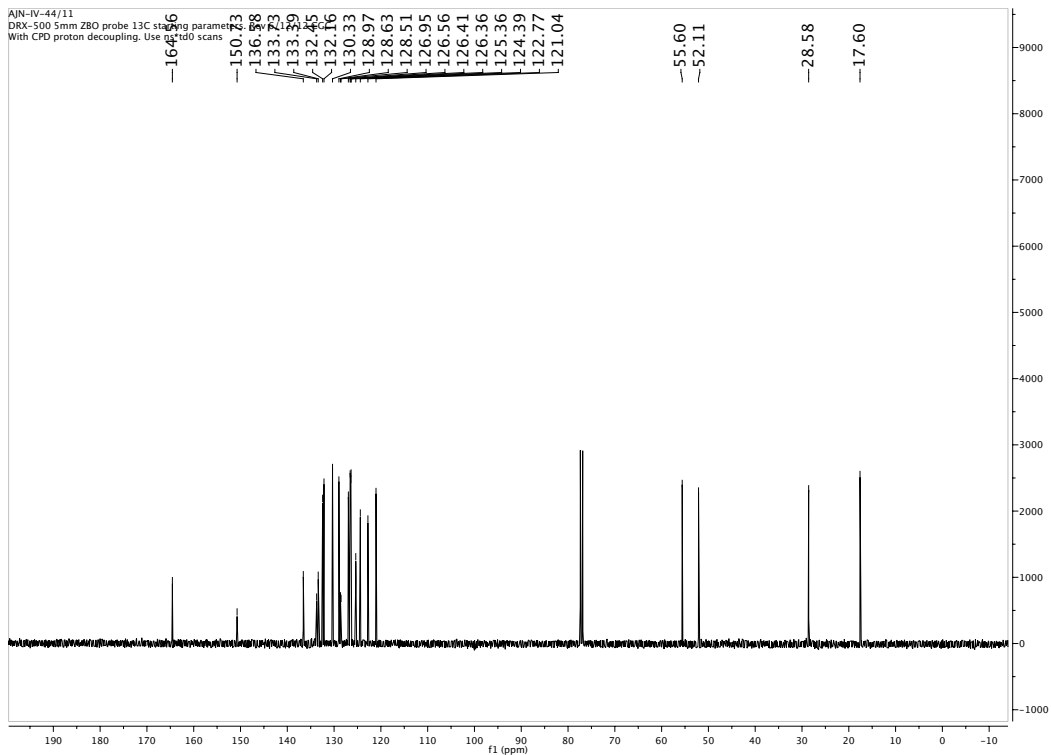
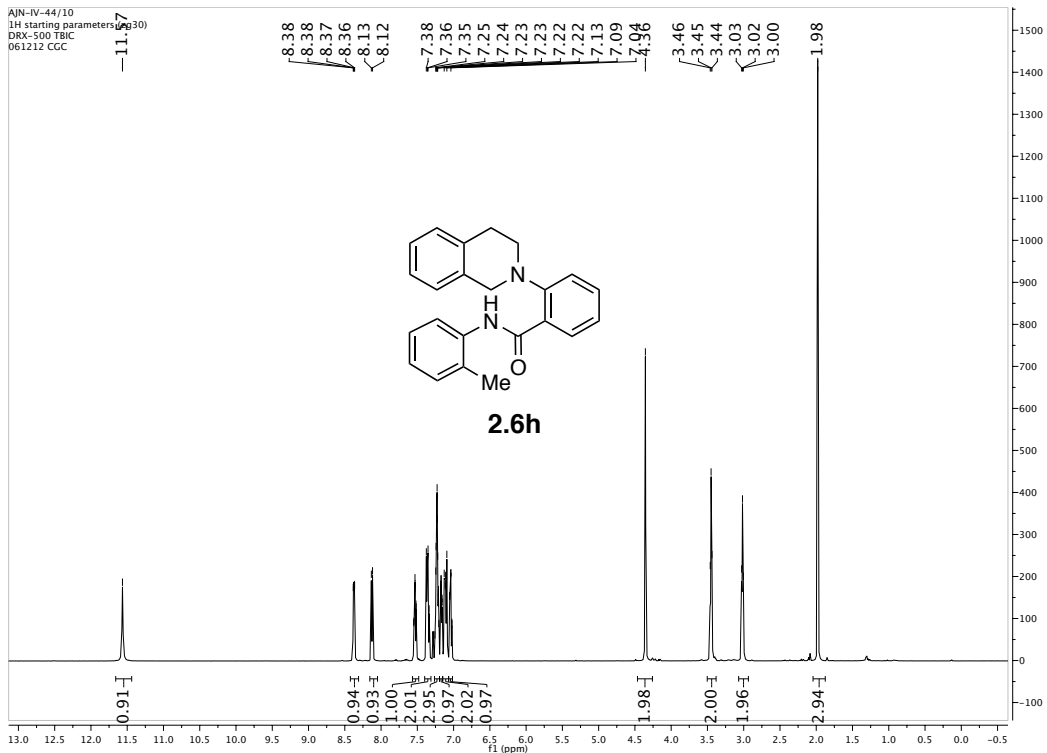


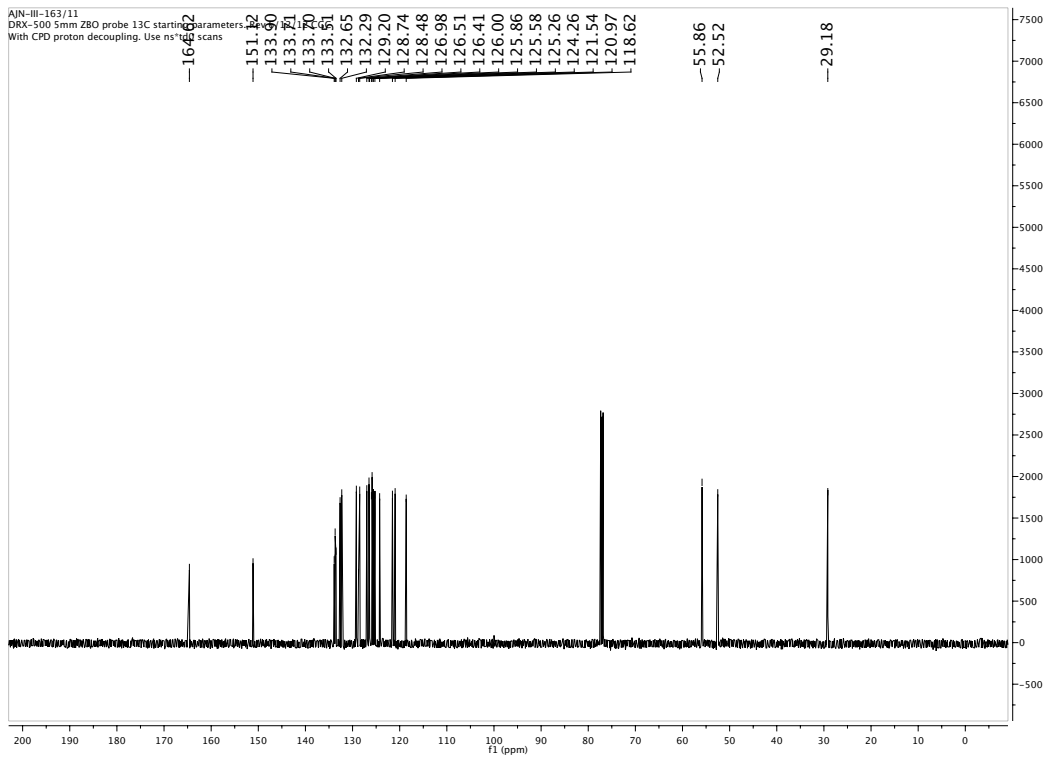
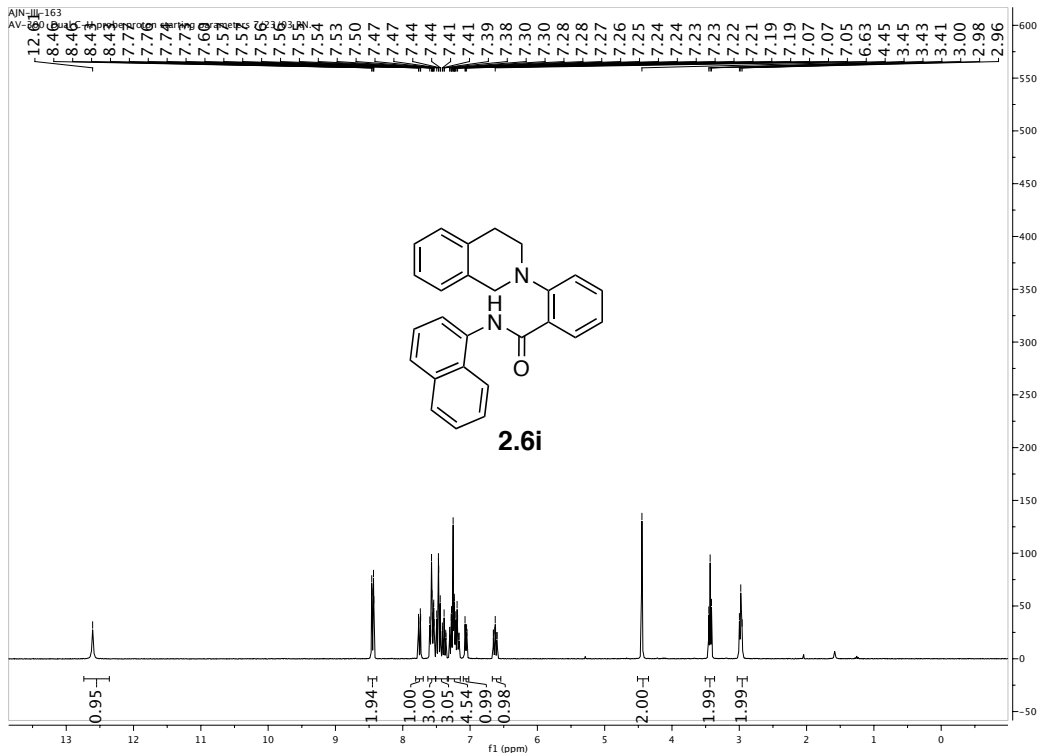


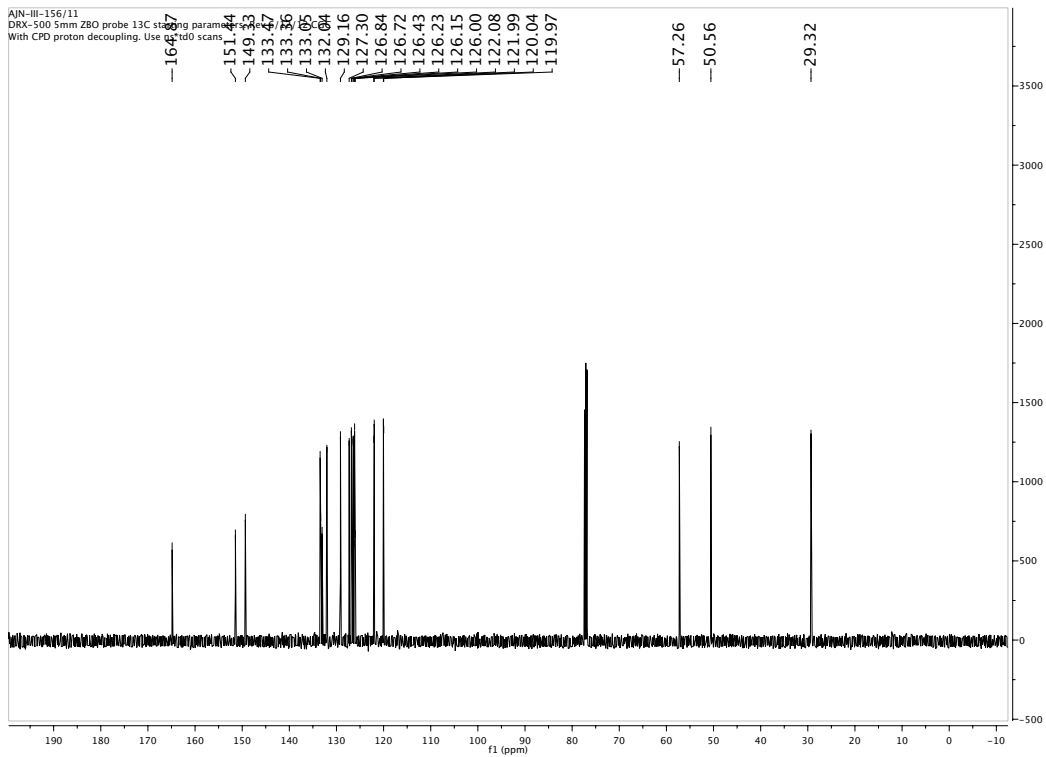
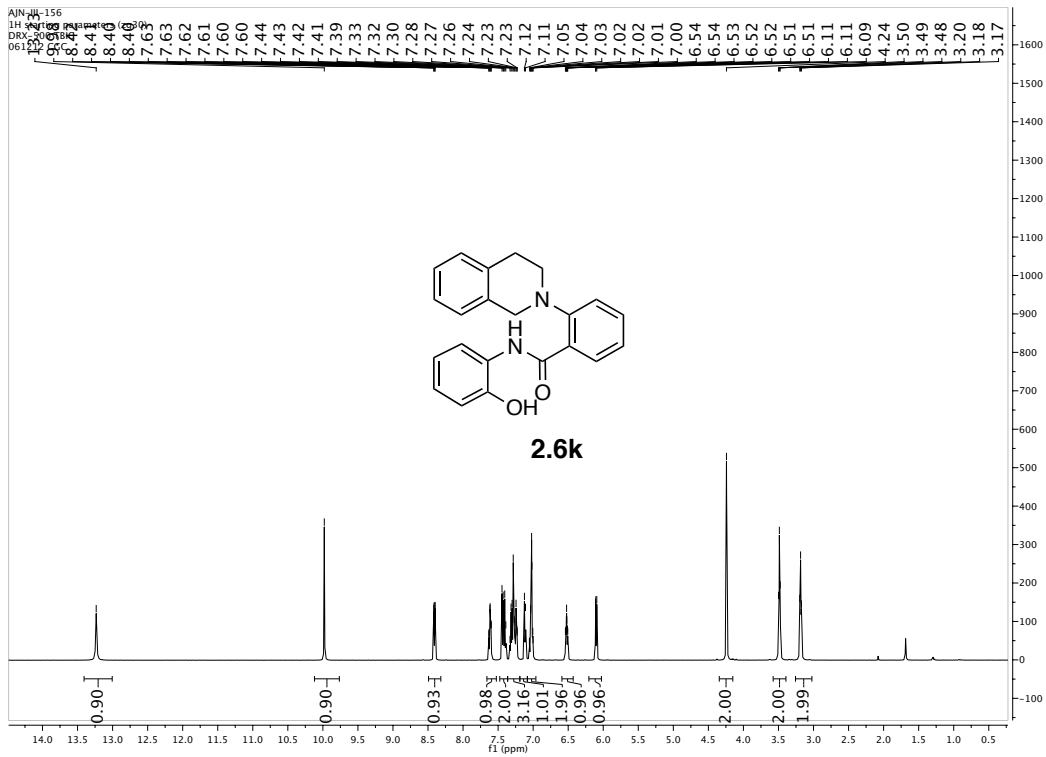


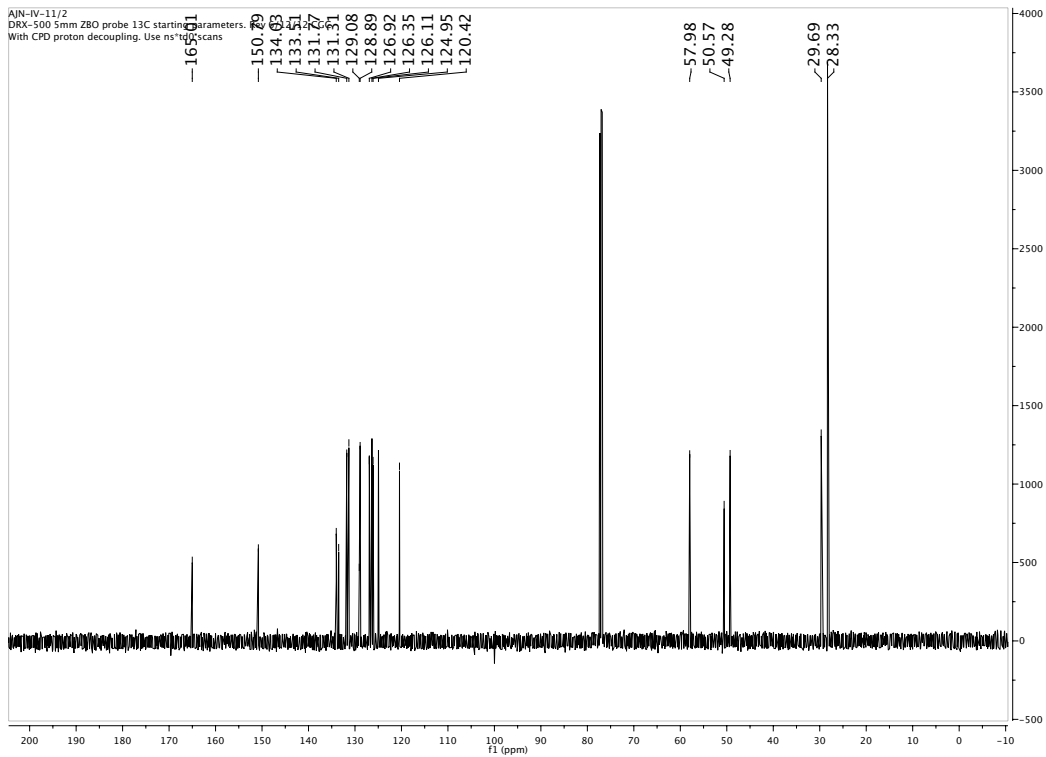
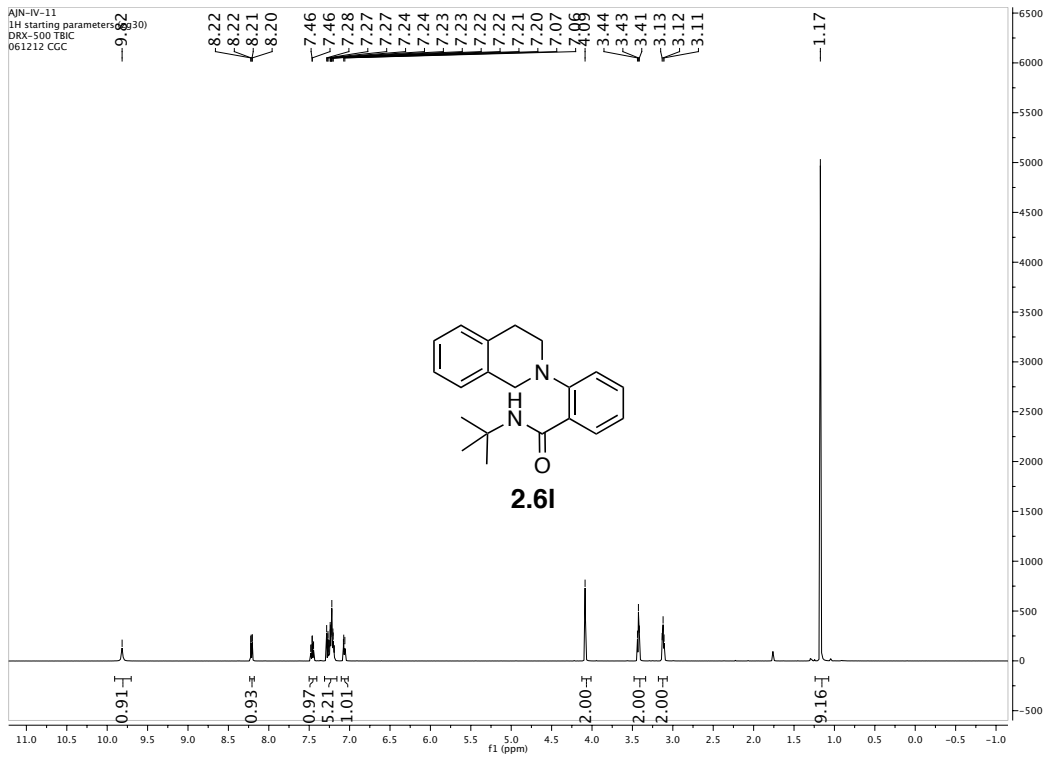


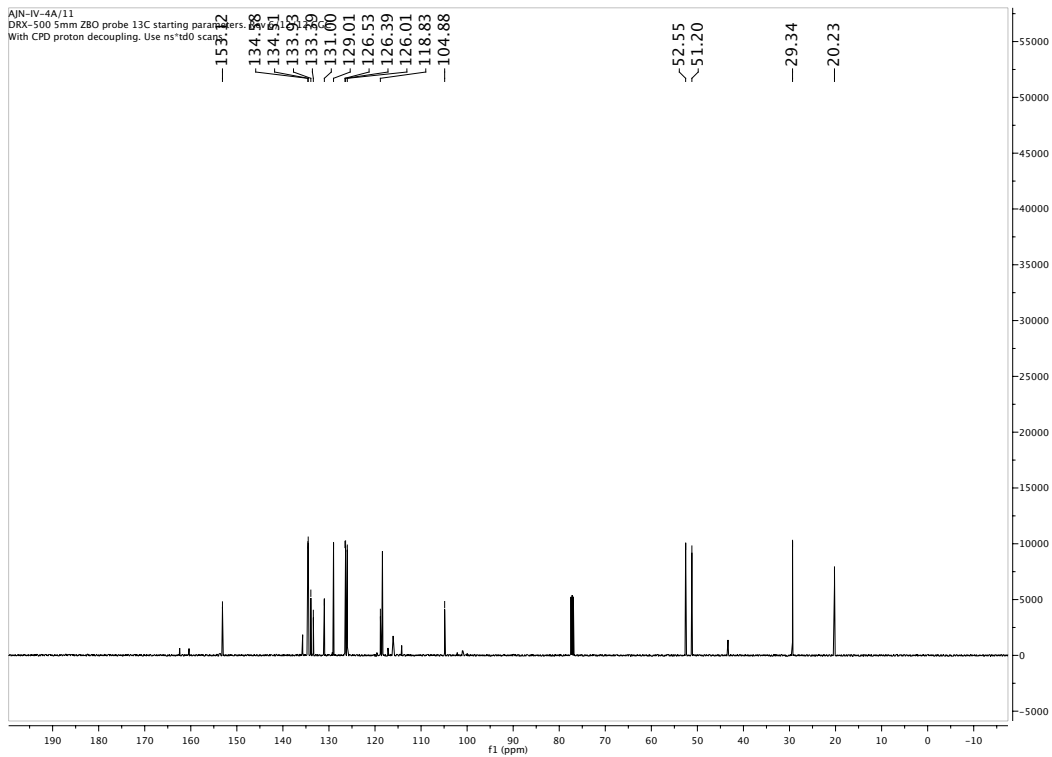
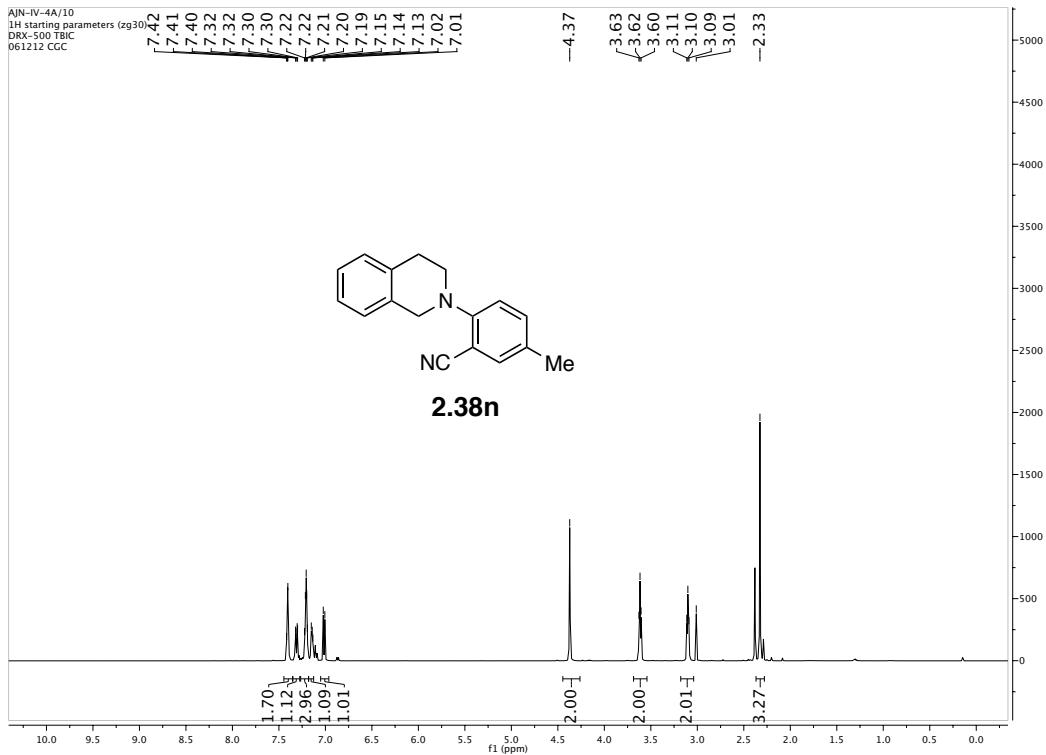


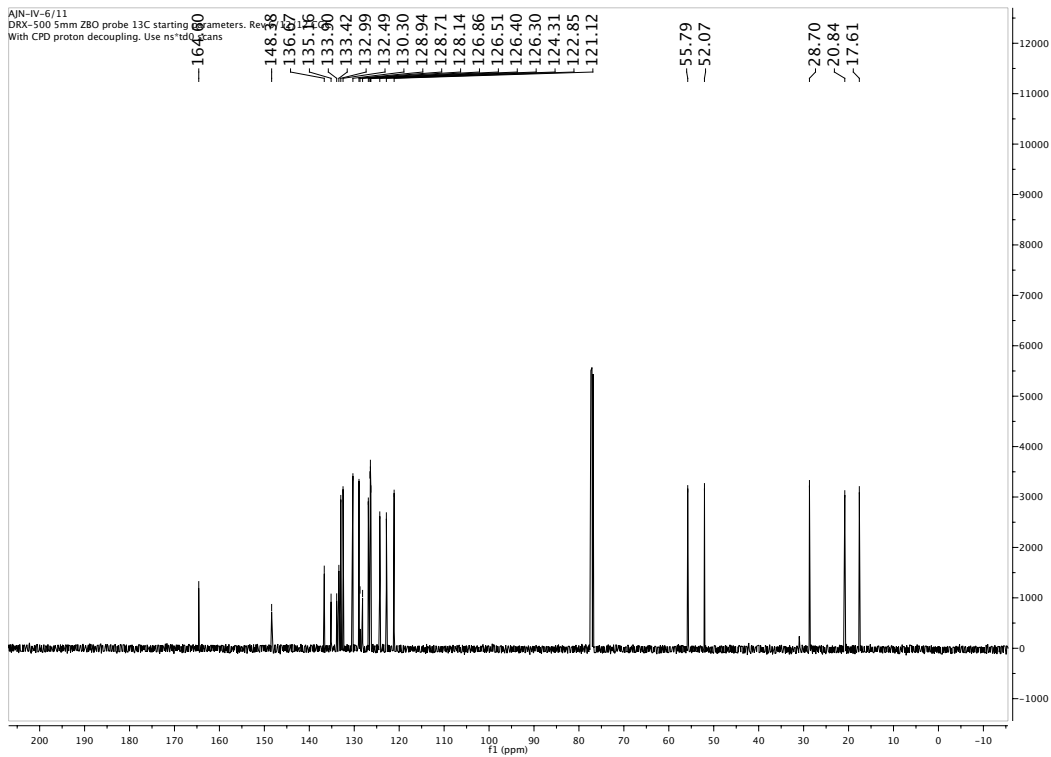
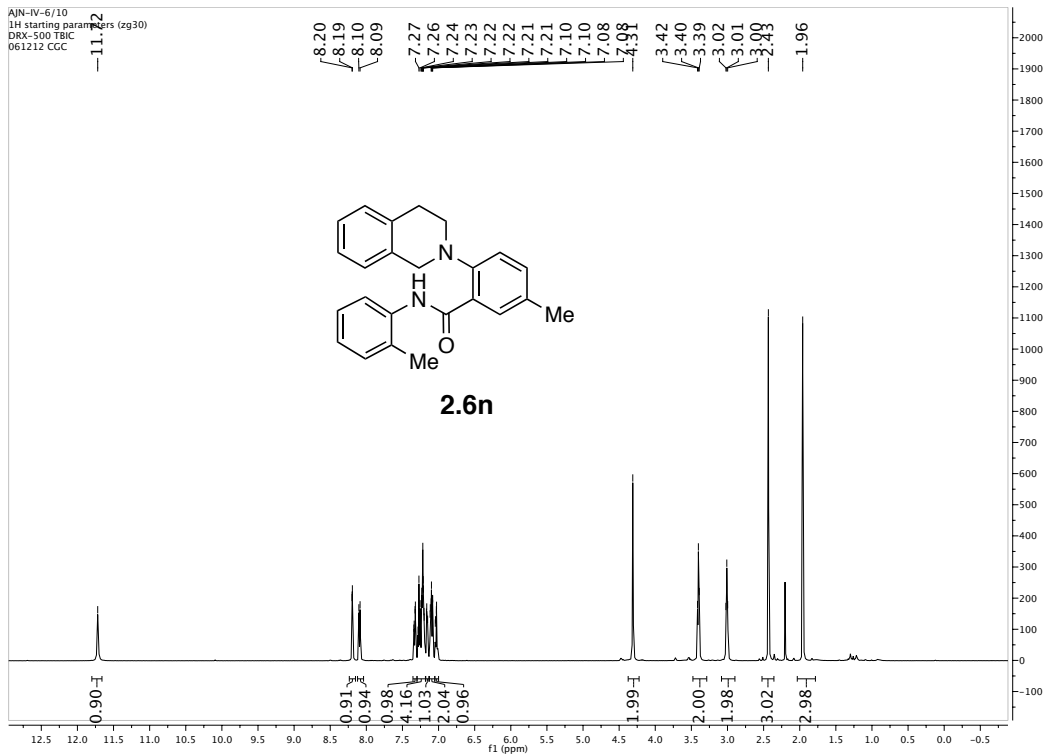


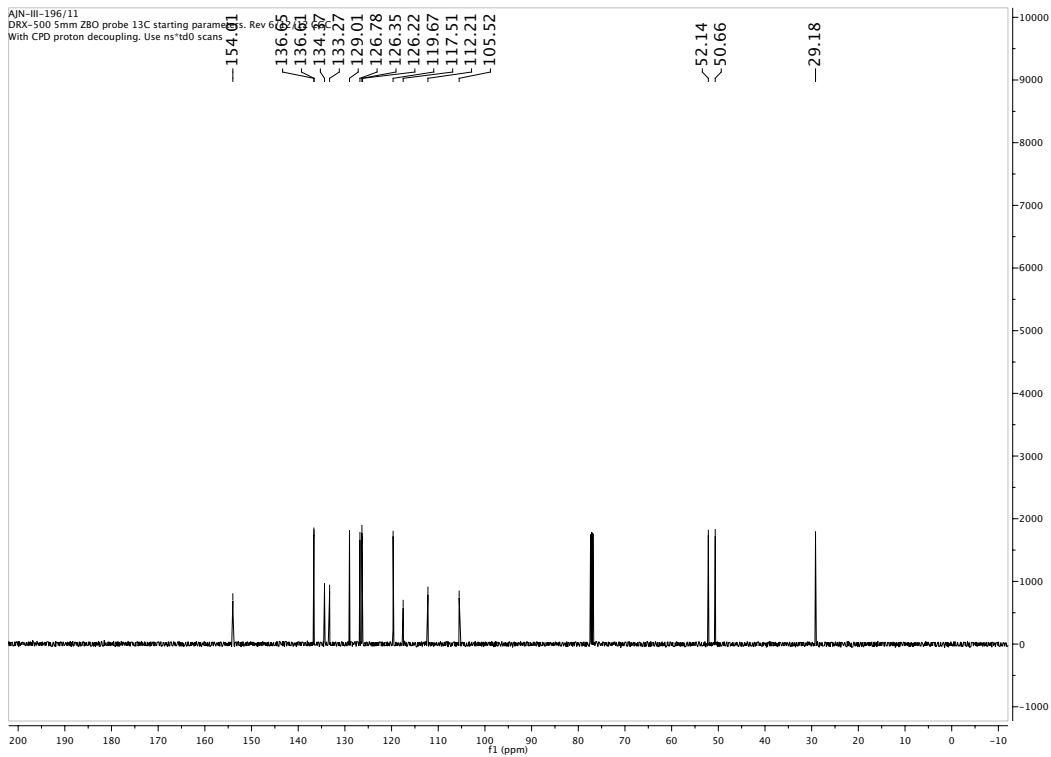
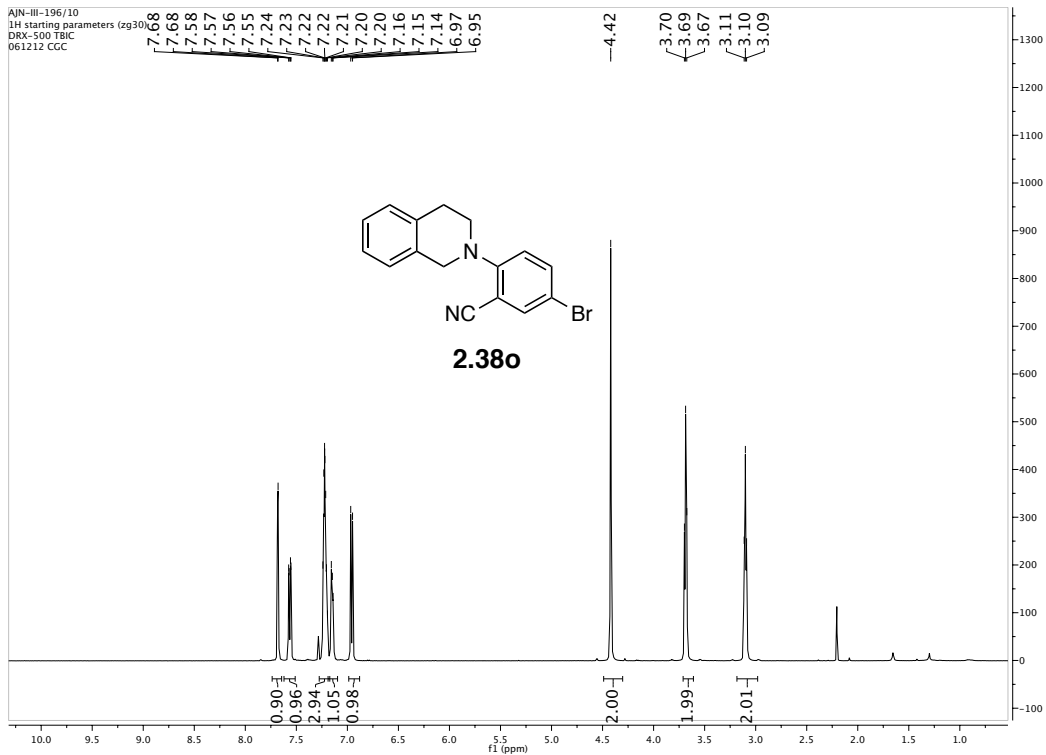


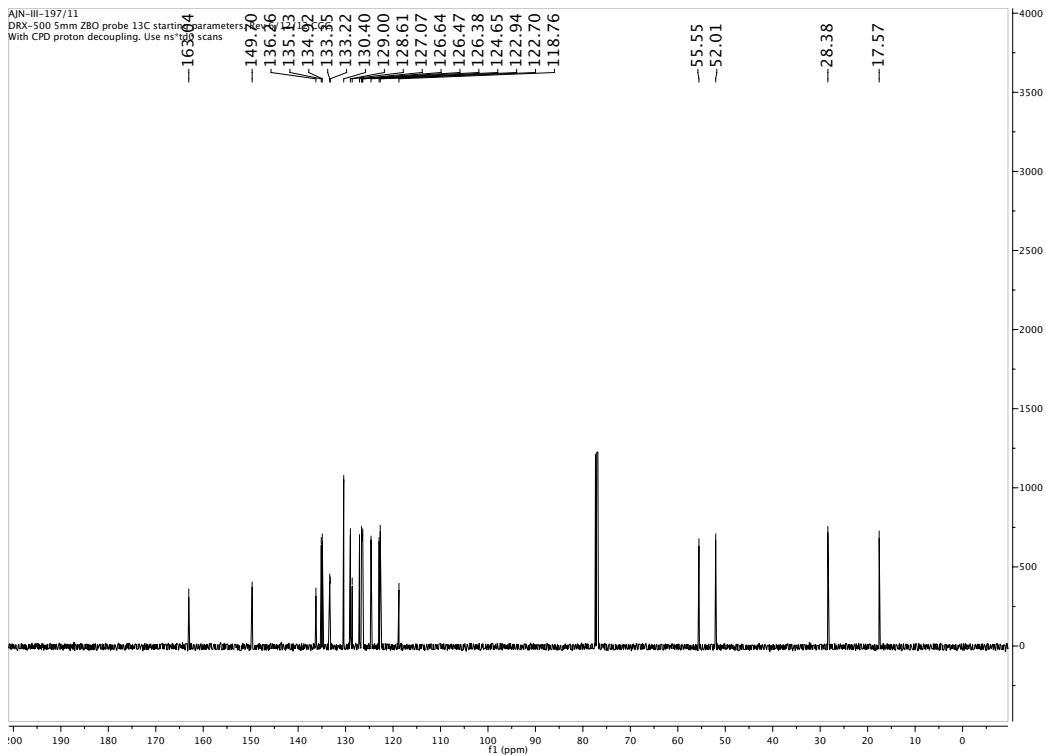
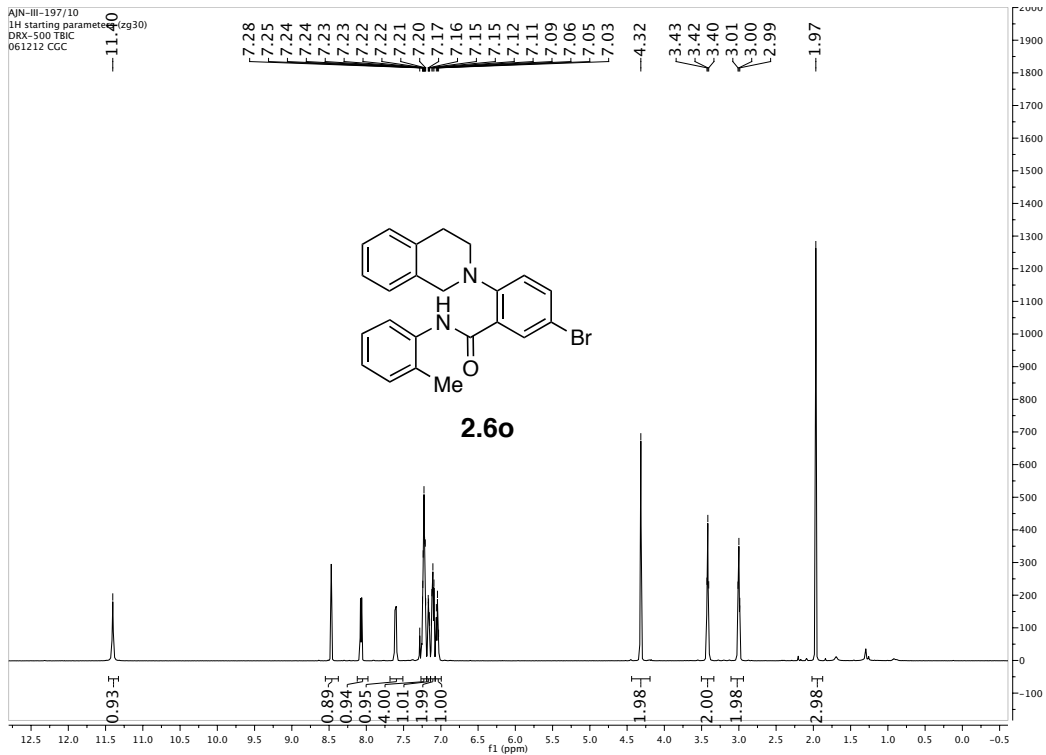


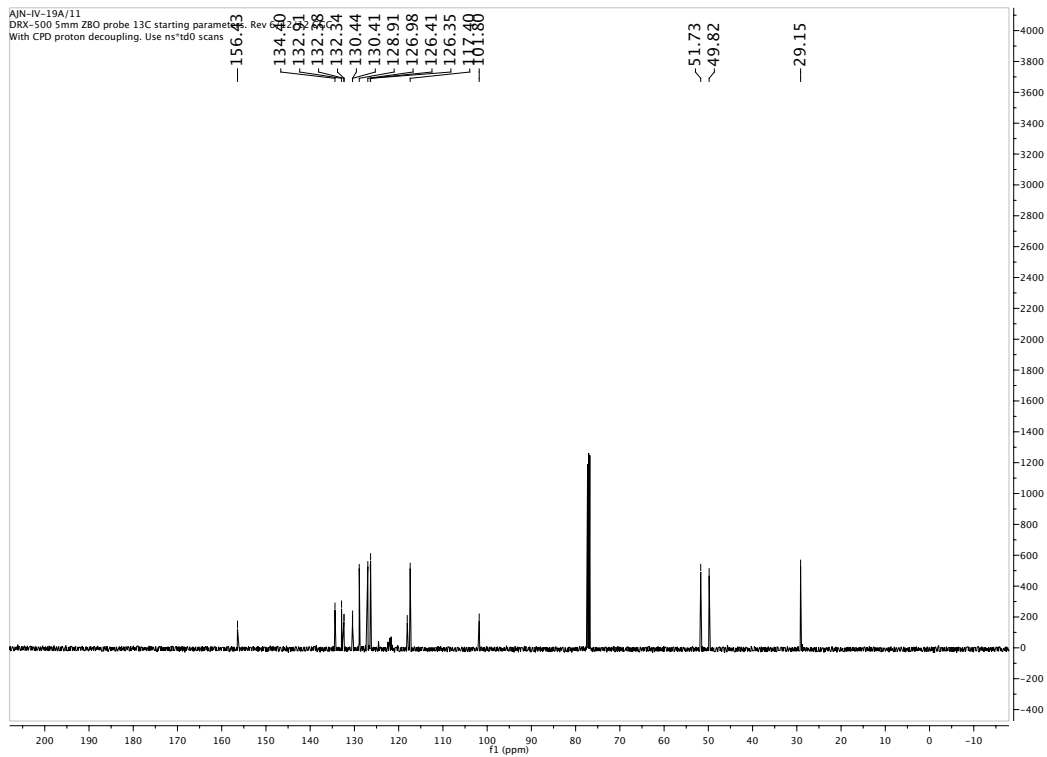
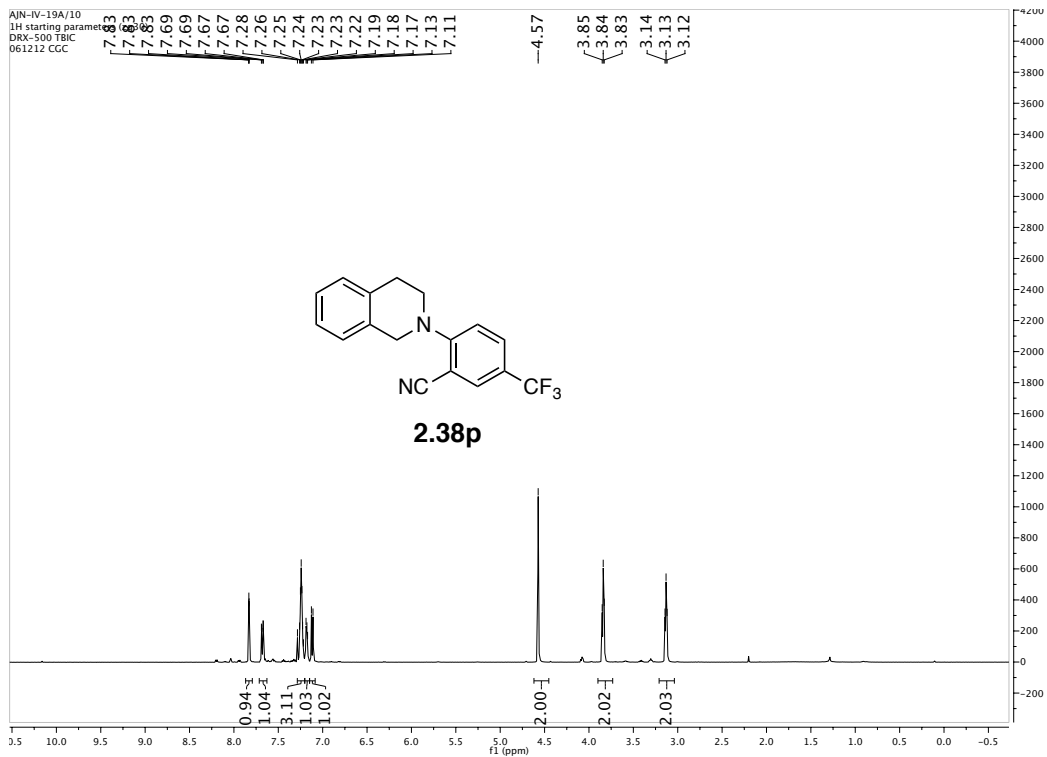


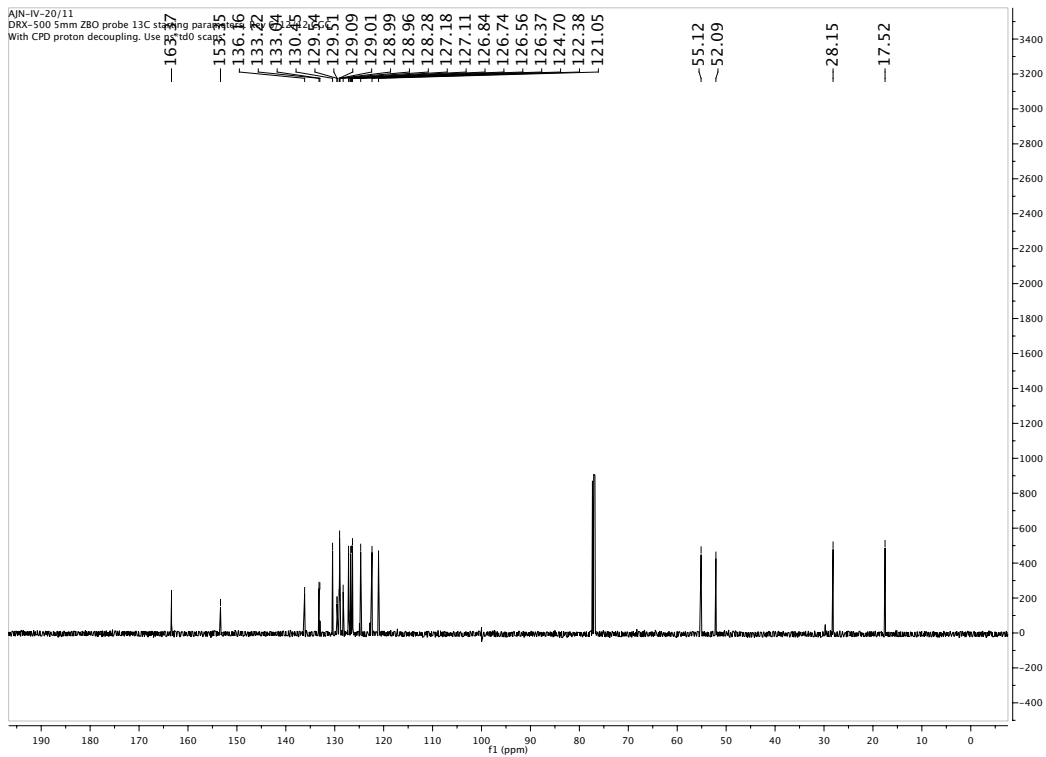
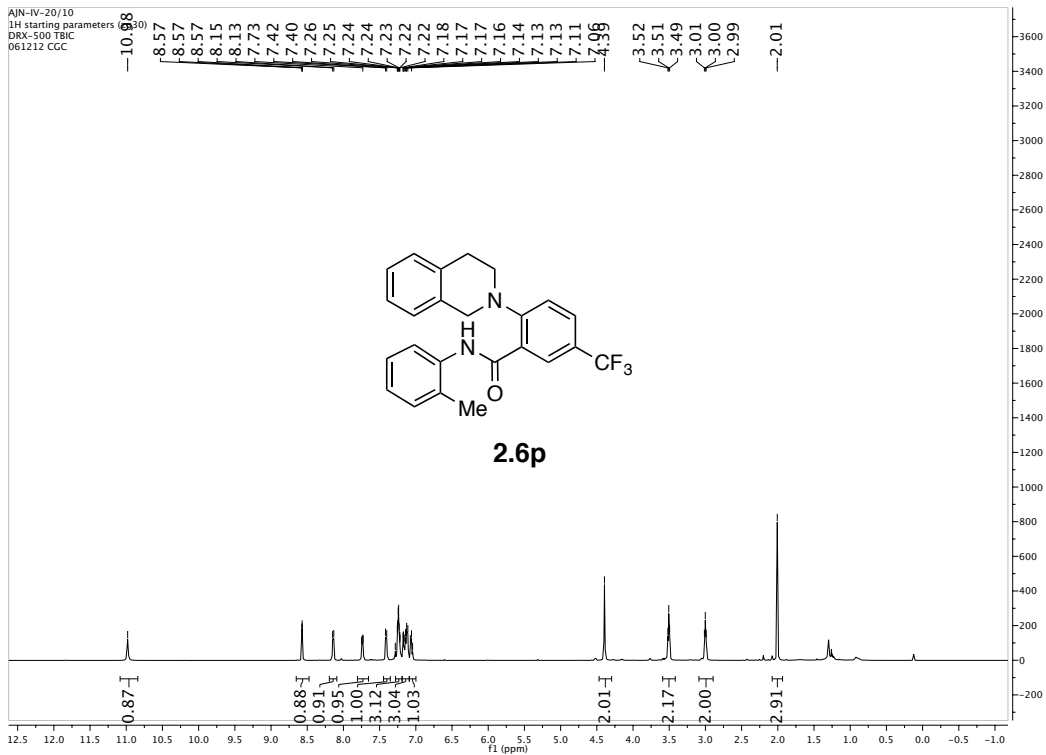


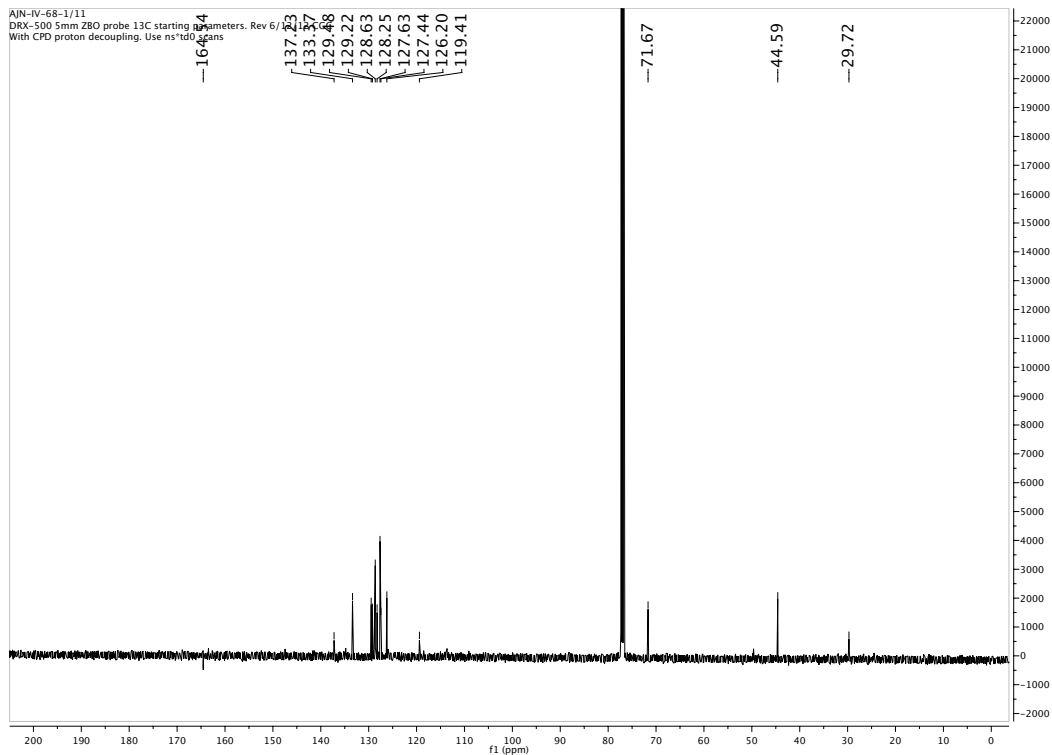
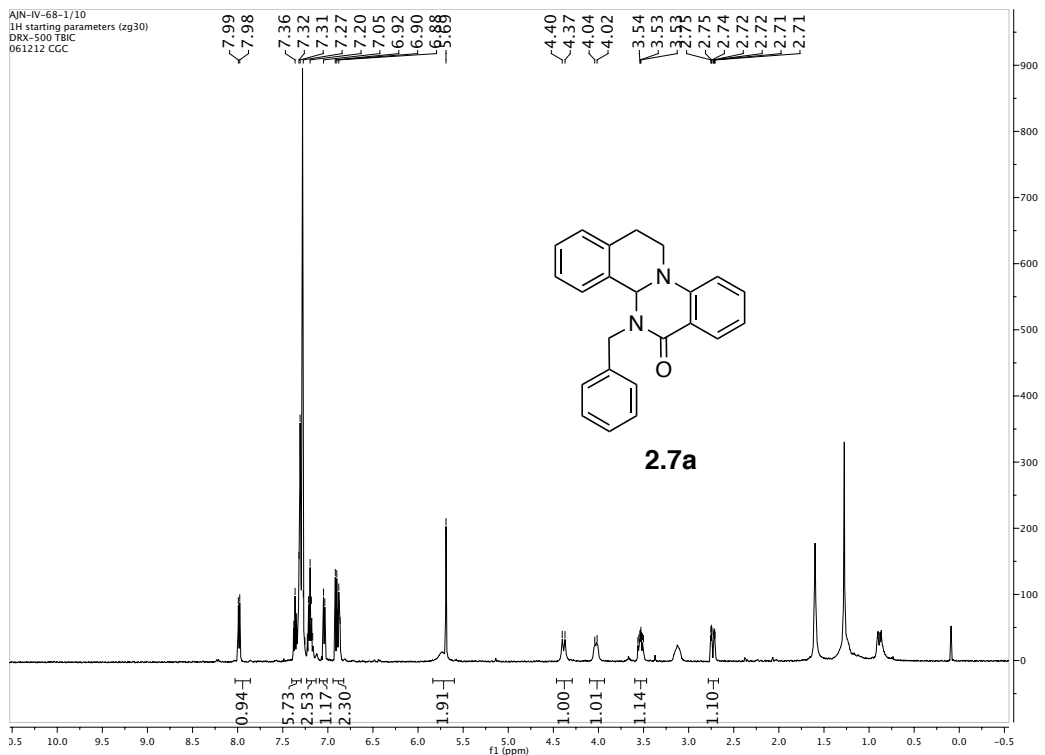




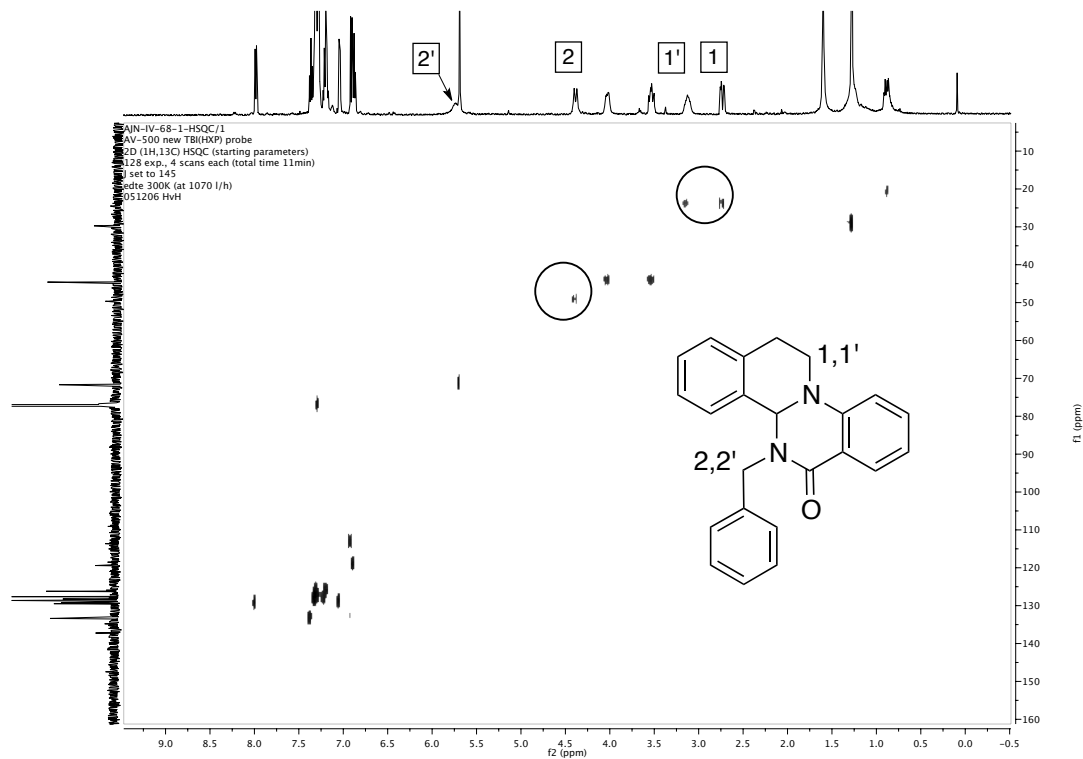


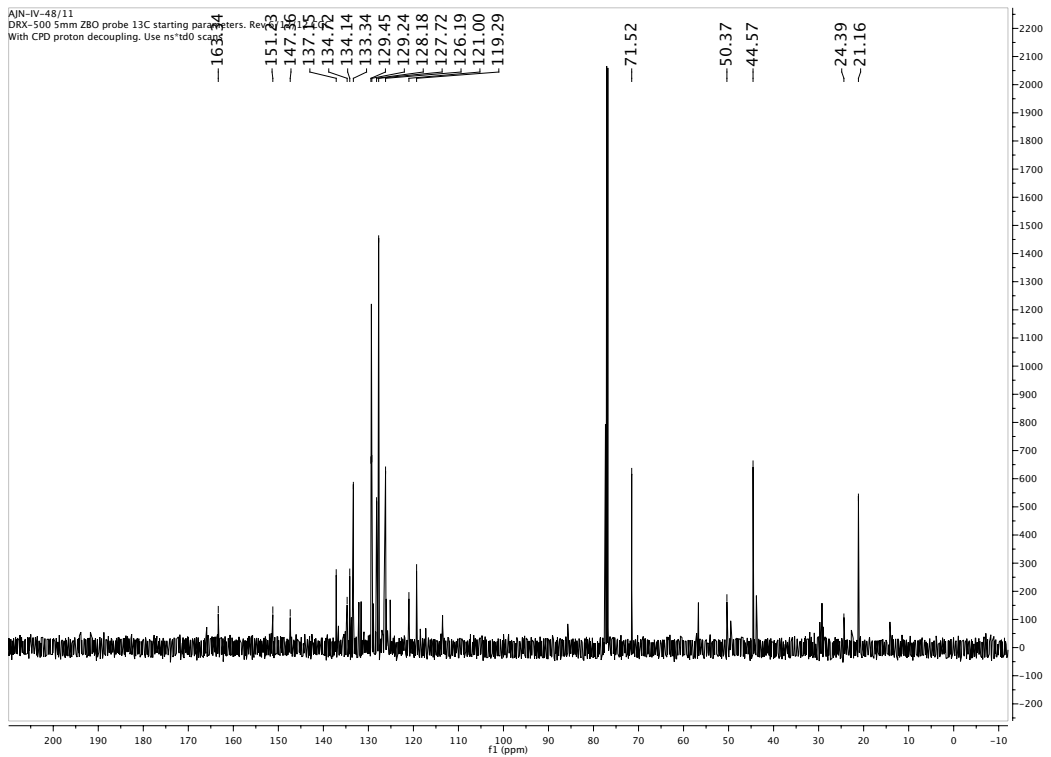
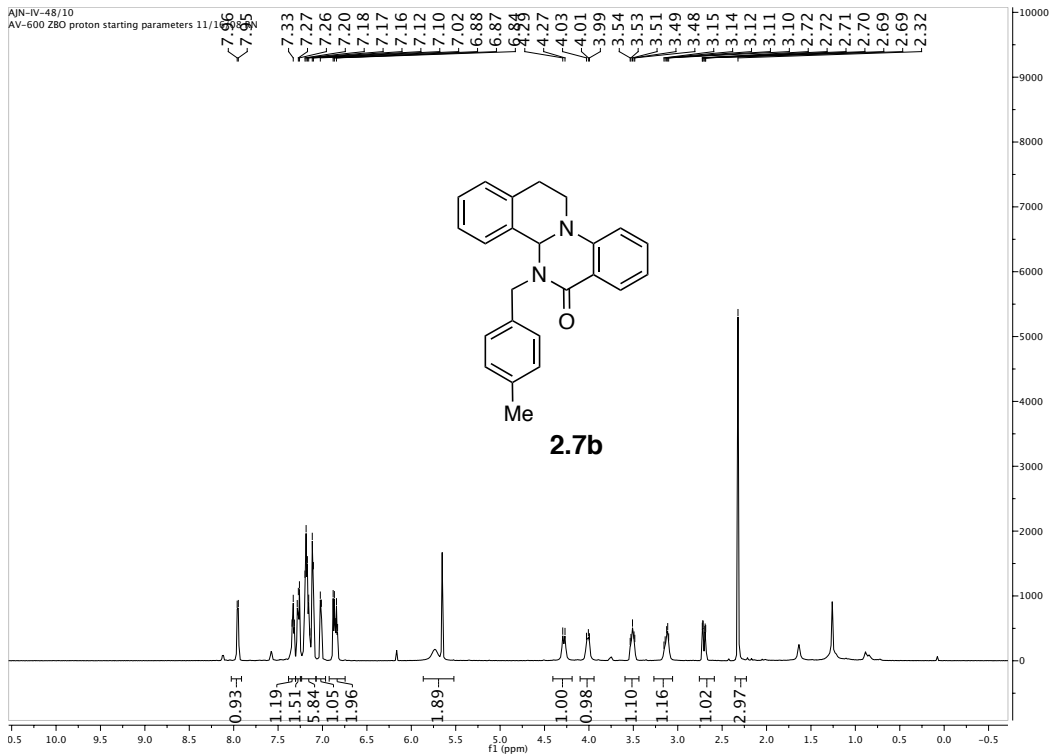




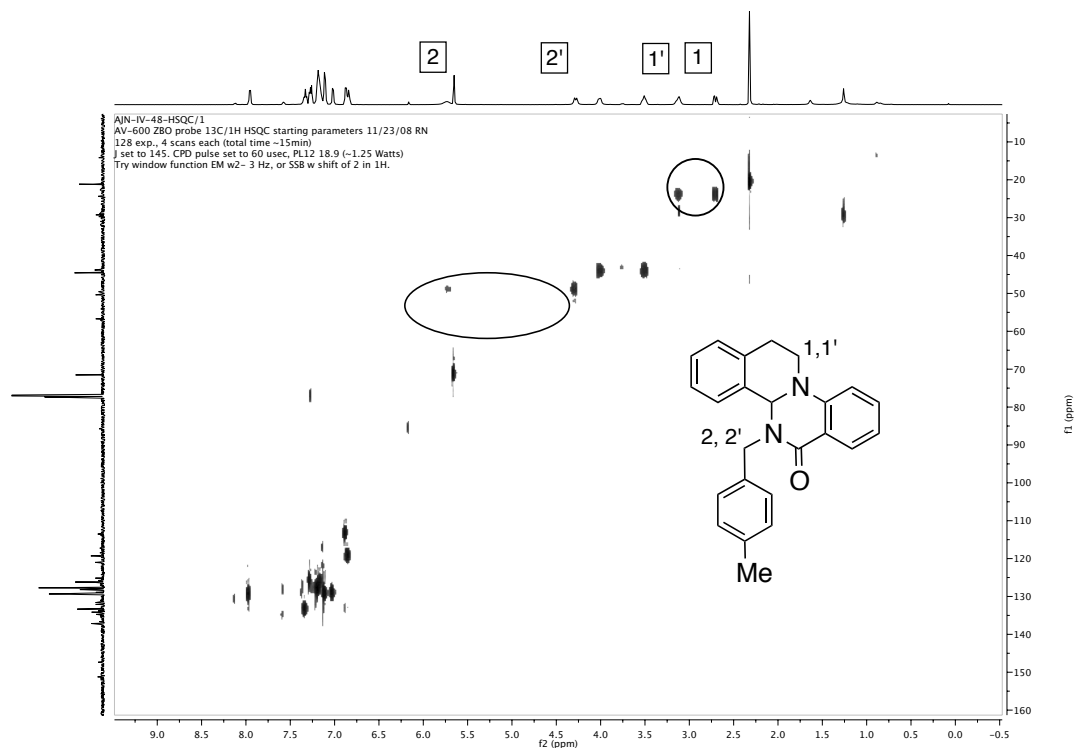


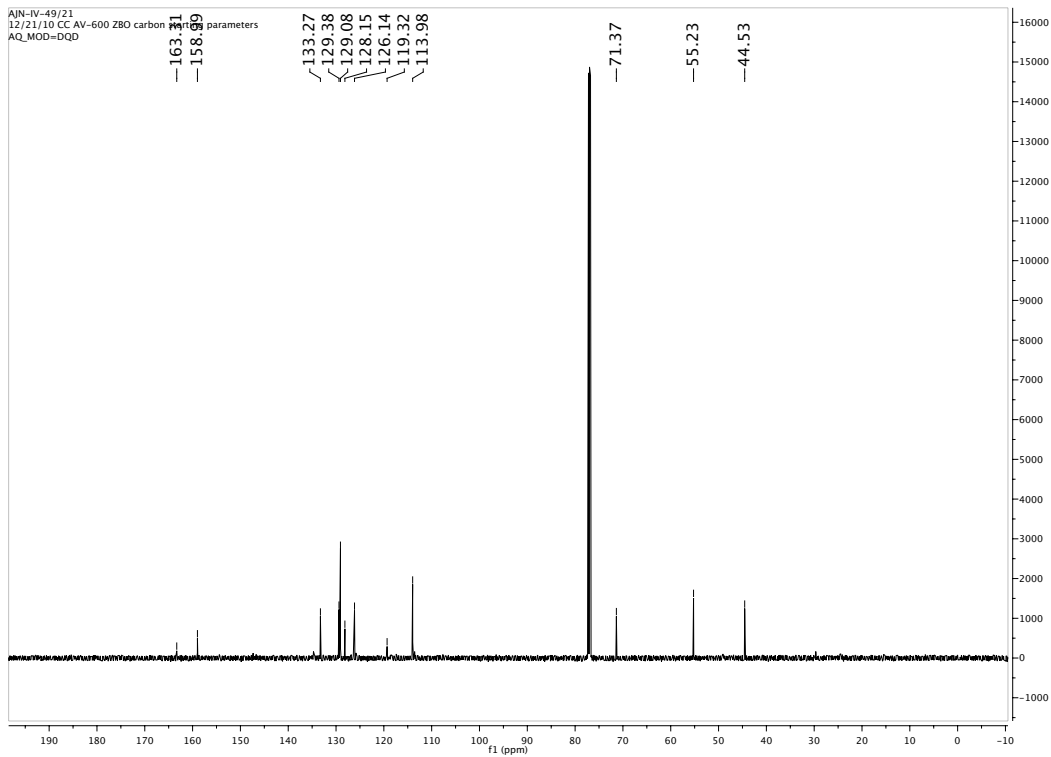
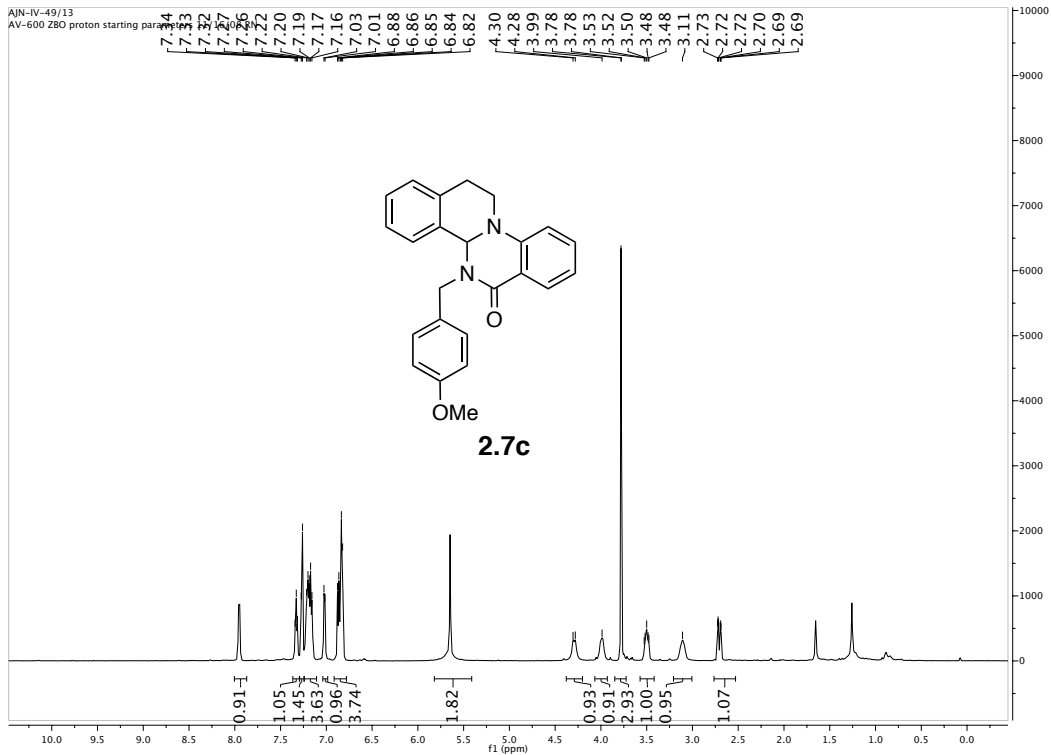
Only three of the five expected alkyl carbons show significant resonances in the ^{13}C NMR spectrum above. HSQC confirms that the remaining two carbons are present and correlate with diastereotopic sets 1,1' and 2,2', corresponding to tetrahydroisoquinoline methylene and benzylic protons respectively.



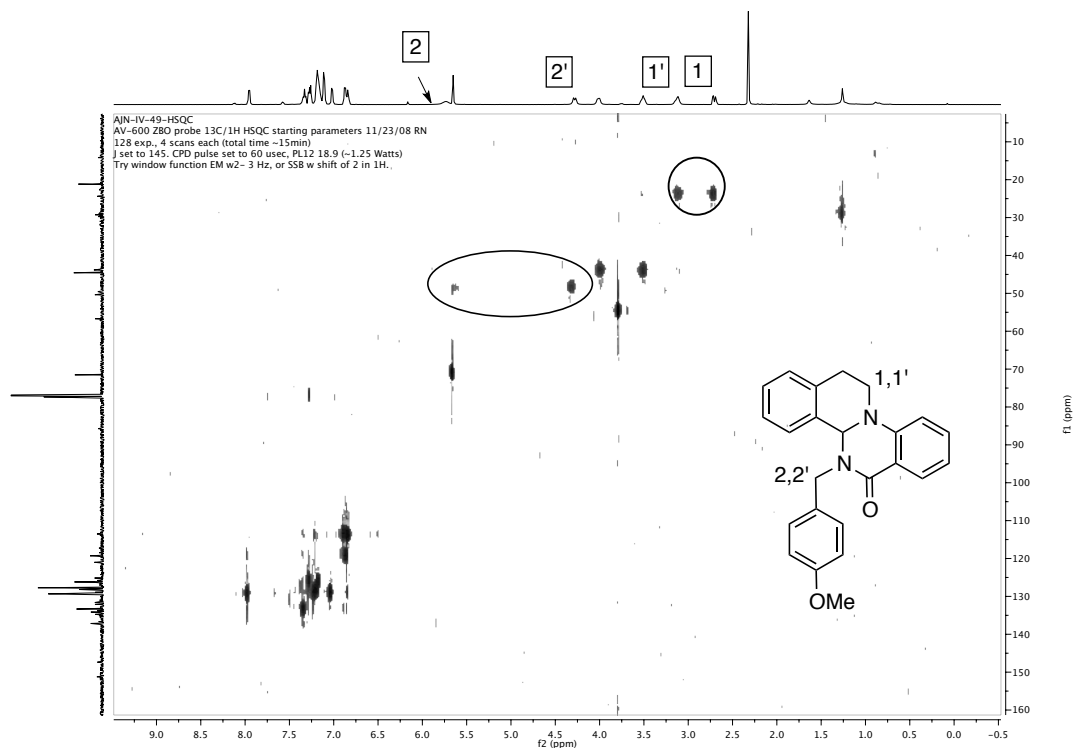


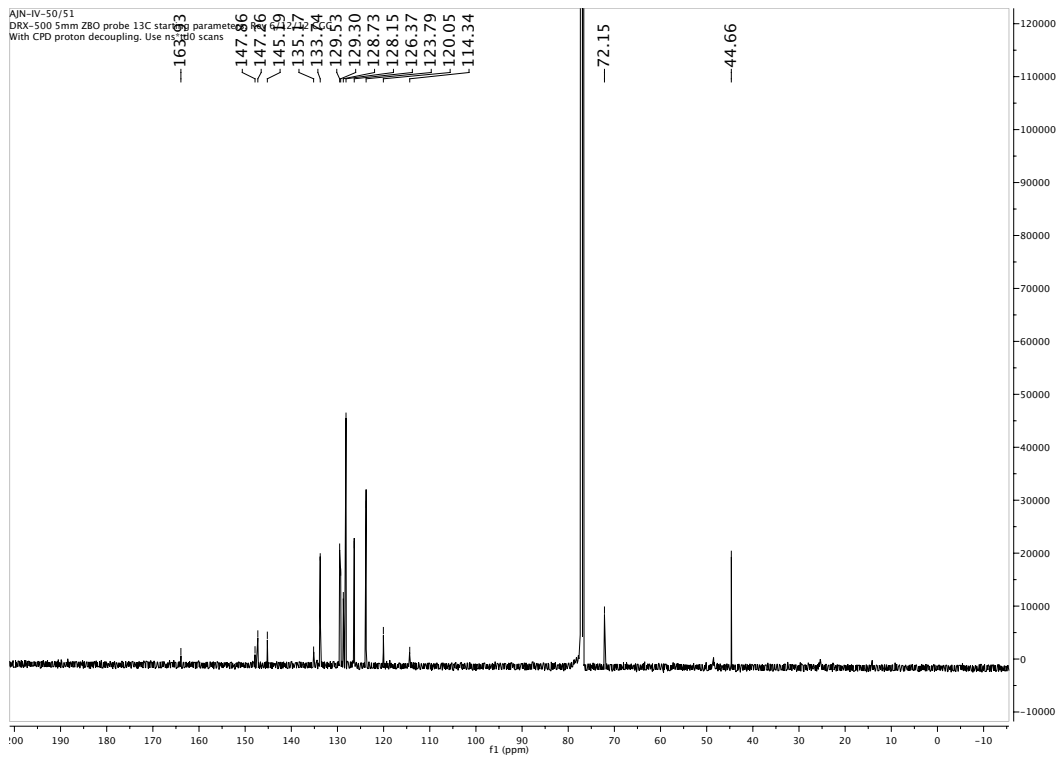
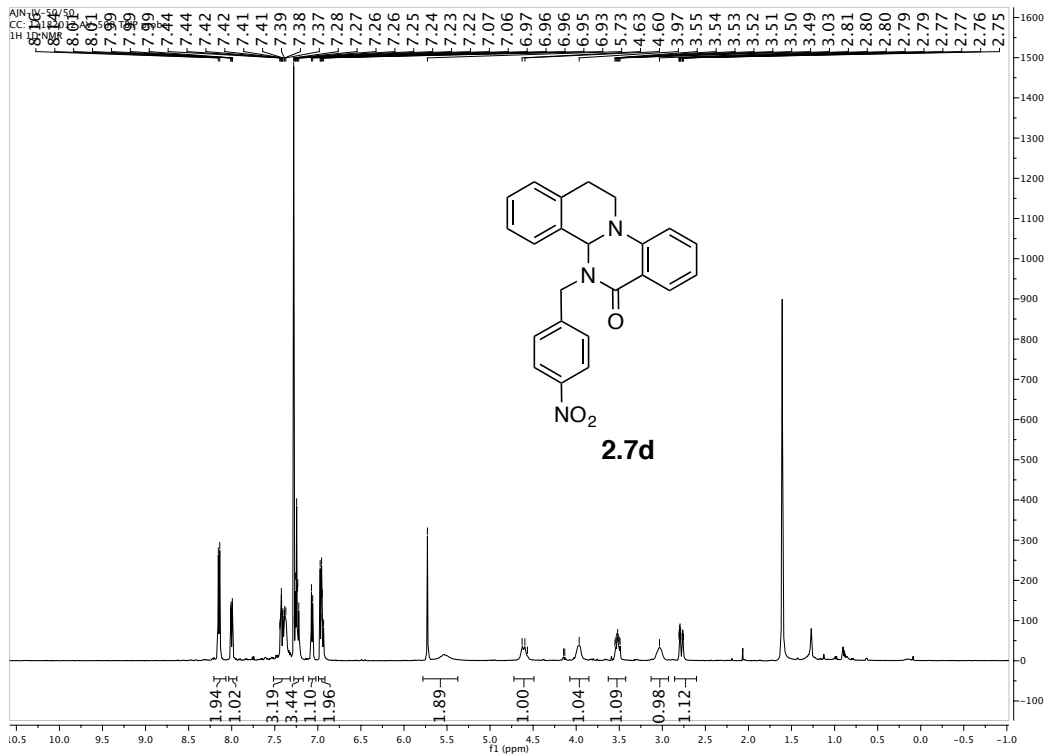
Only three of the five expected alkyl carbons show significant resonances in the ^{13}C NMR spectrum above. HSQC confirms that the remaining two carbons are present and correlate with diastereotopic sets 1,1' and 2,2', corresponding to tetrahydroisoquinoline methylene and benzylic protons respectively.



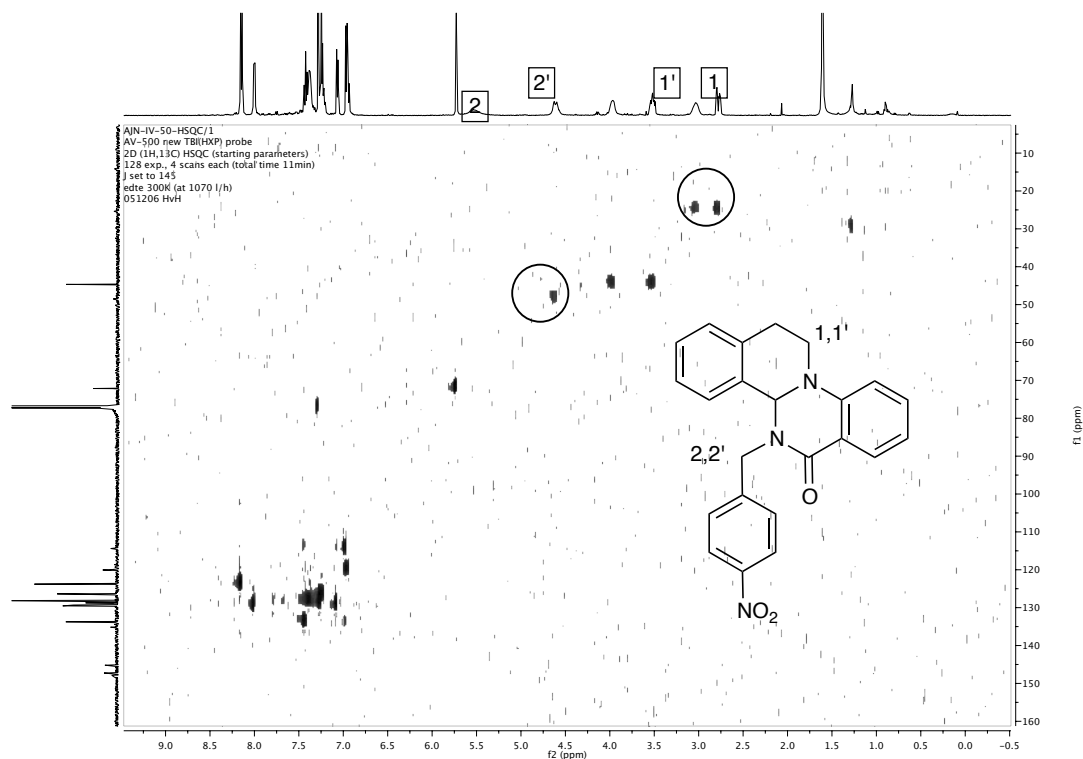


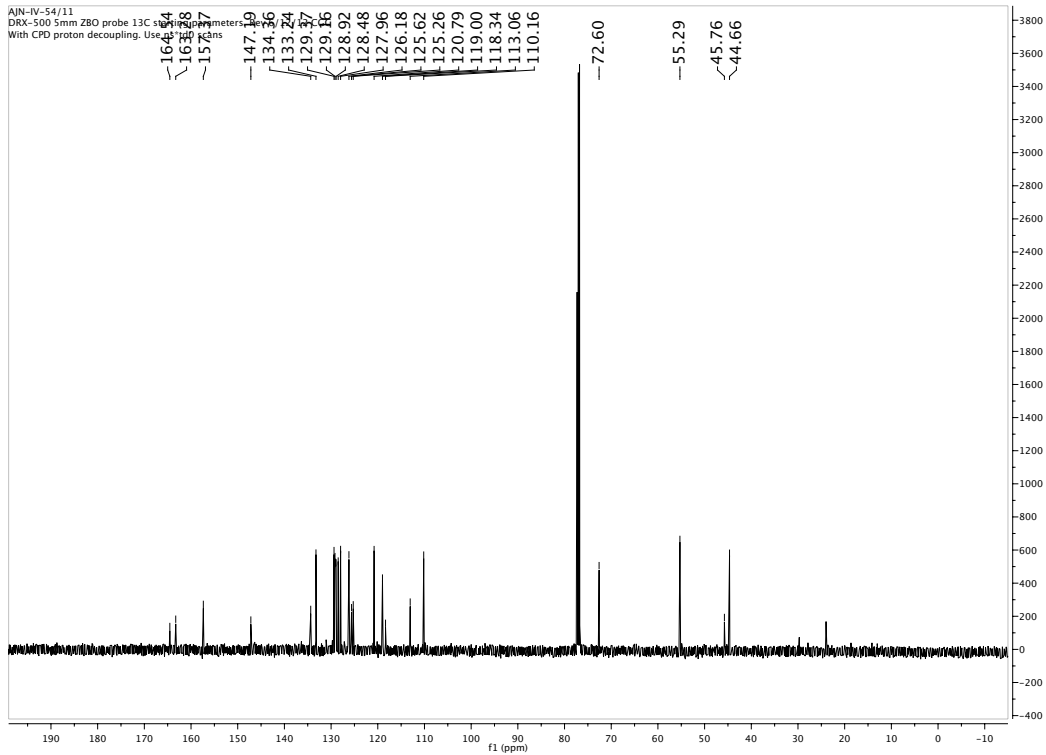
Only three of the five expected alkyl carbons show significant resonances in the ^{13}C NMR spectrum above. HSQC confirms that the remaining two carbons are present and correlate with diastereotopic proton sets 1,1' and 2,2', corresponding to tetrahydroisoquinoline methylene and benzylic protons respectively.



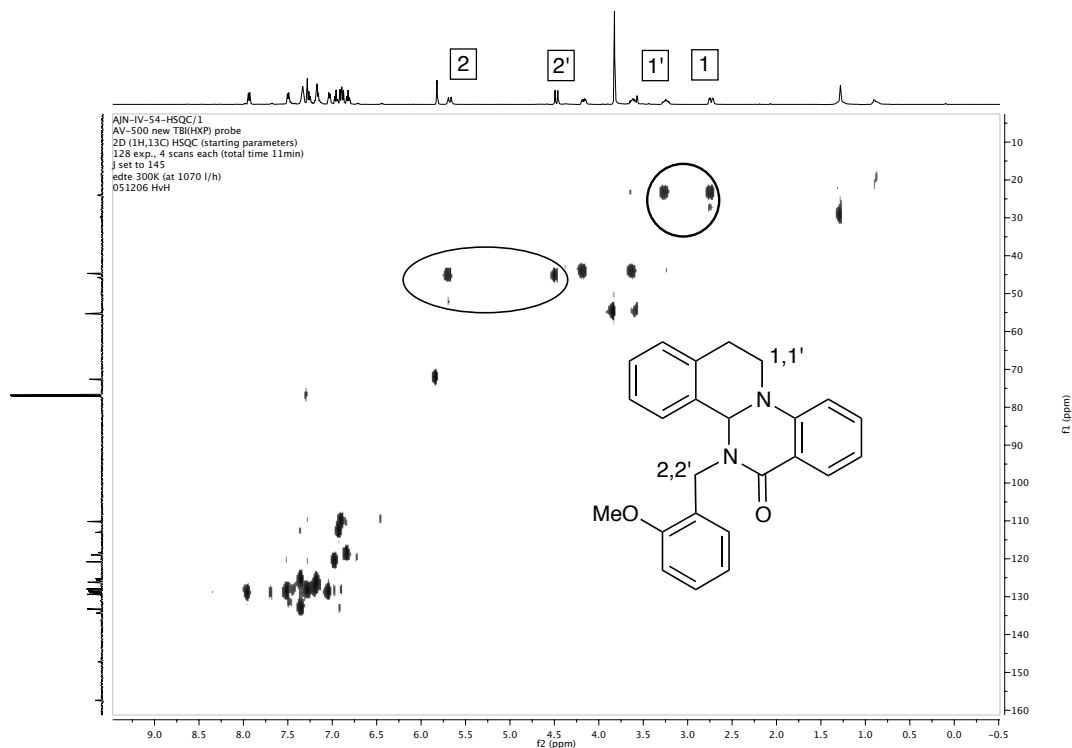


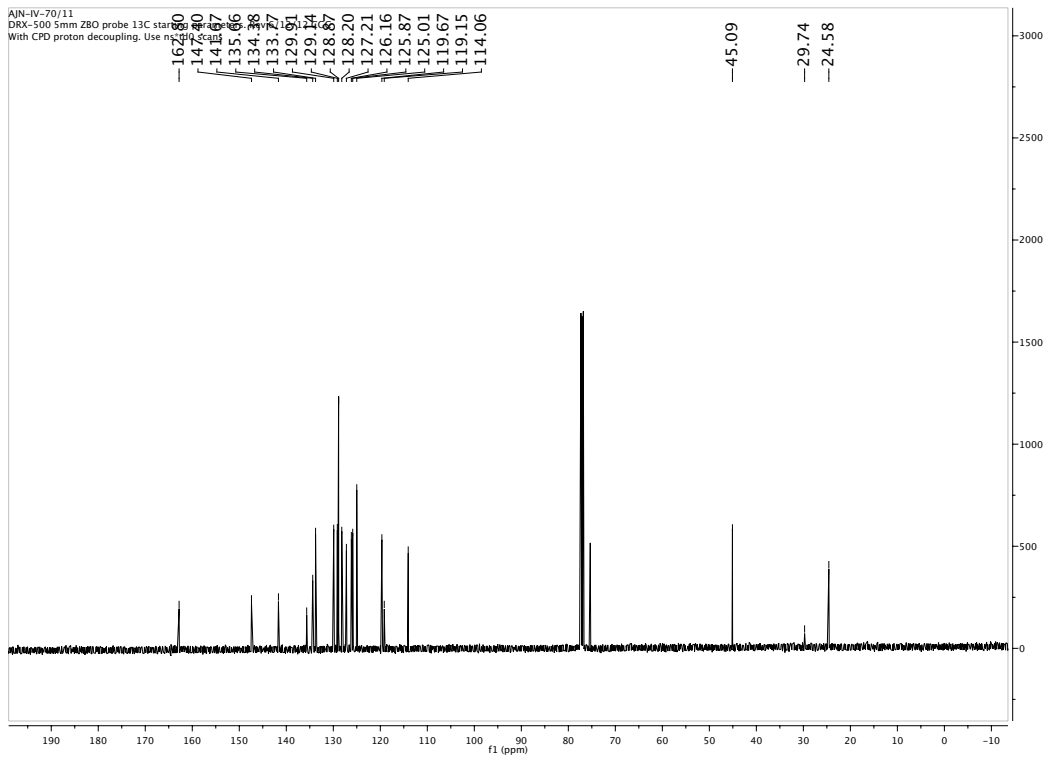
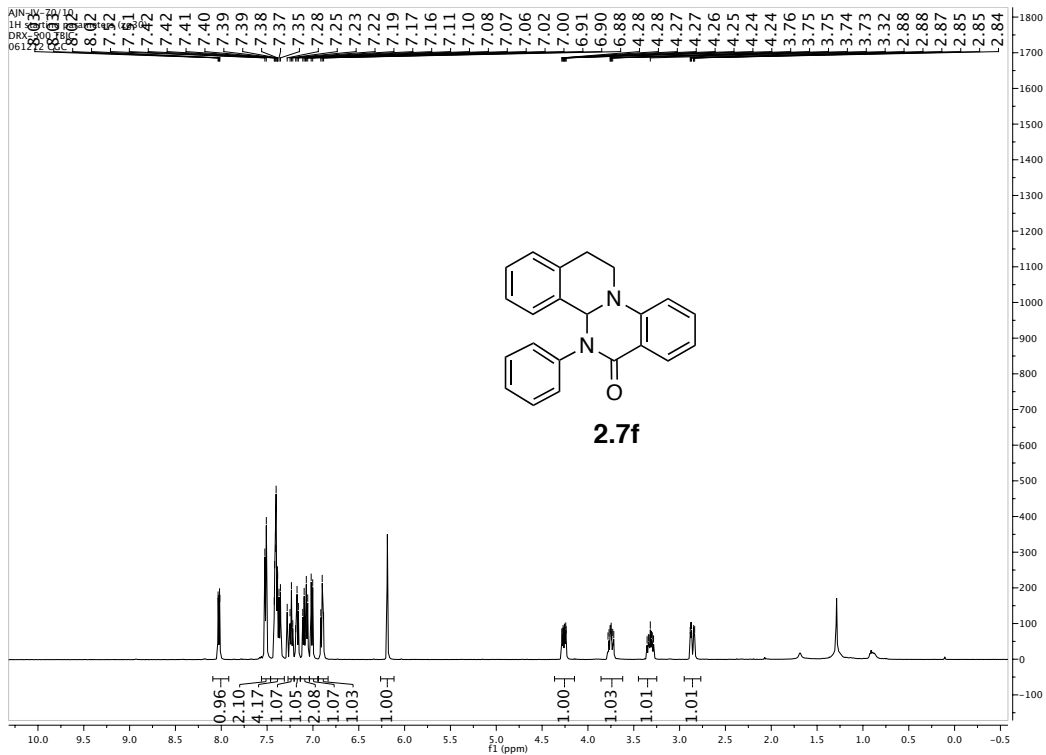
Only two of the four expected alkyl carbons show significant resonances in the ^{13}C NMR spectrum above. HSQC confirms that the remaining two carbons are present and correlate with diastereotopic proton sets 1,1' and 2,2', corresponding to tetrahydroisoquinoline methylene and benzylic protons respectively.

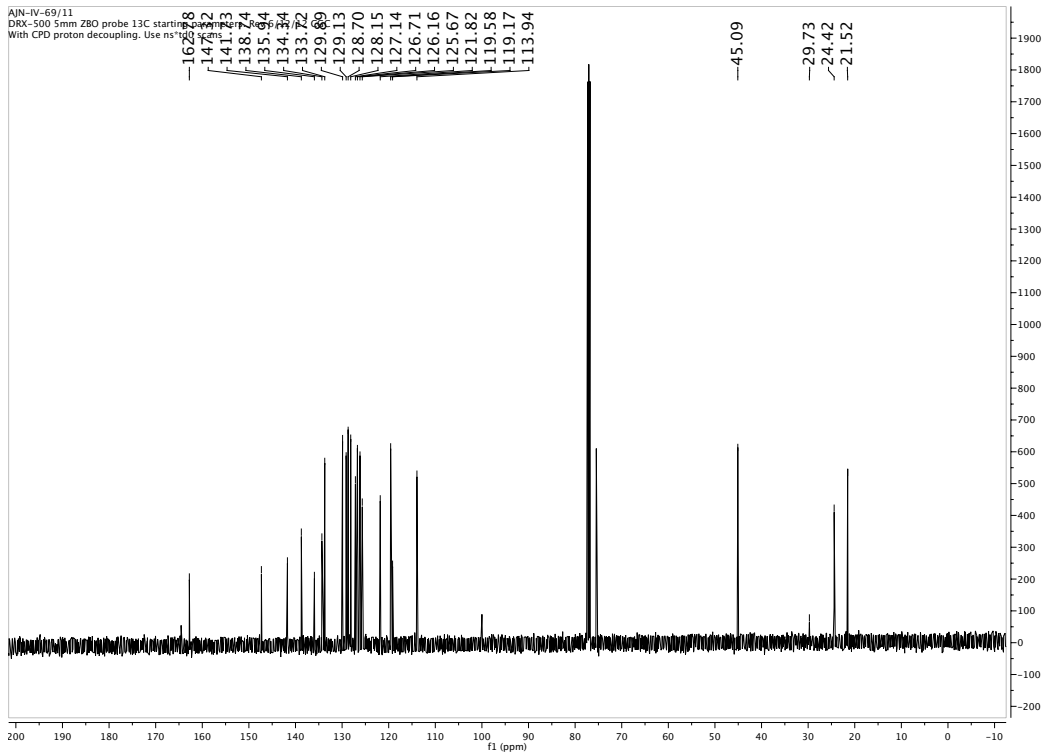
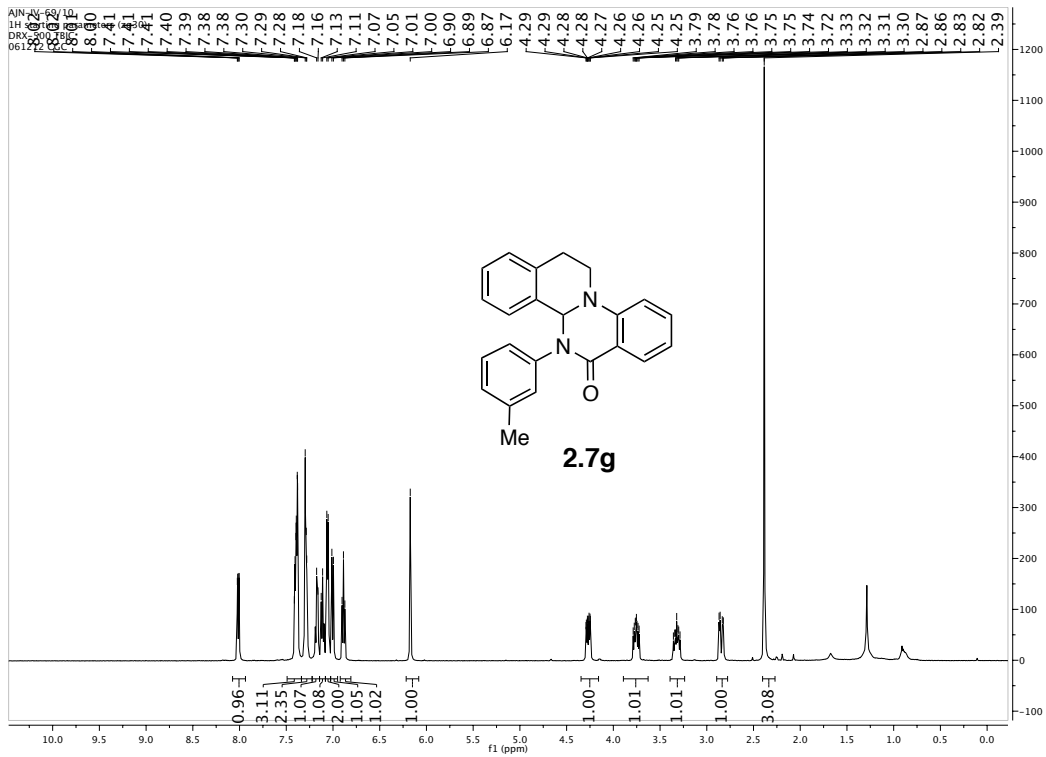


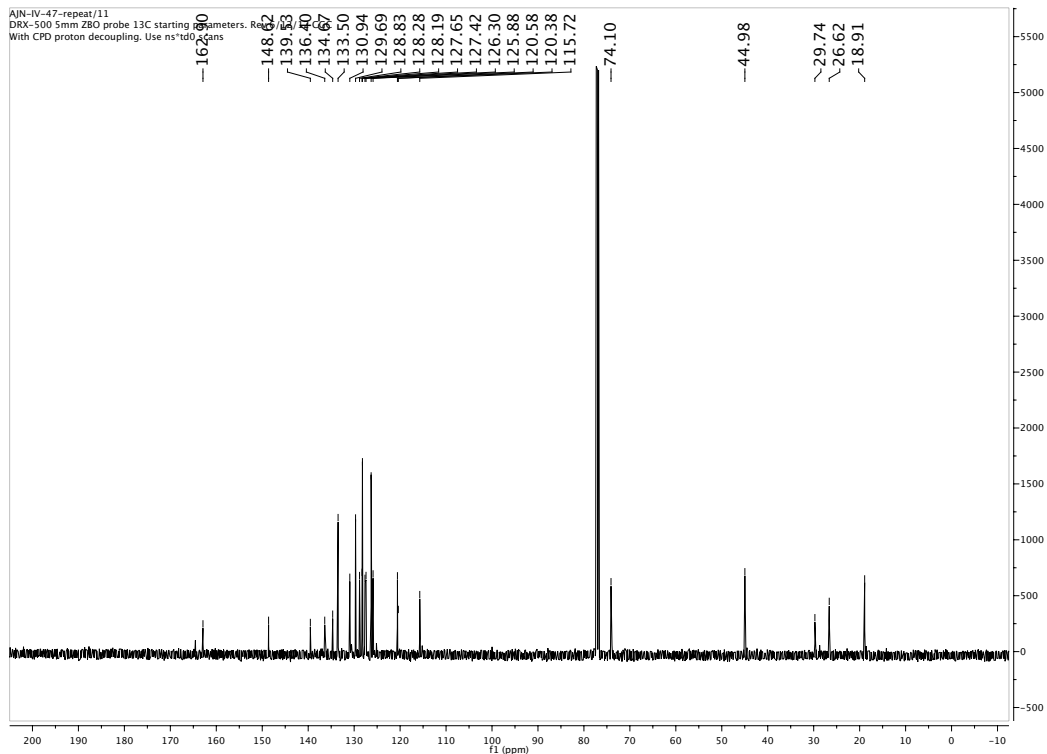
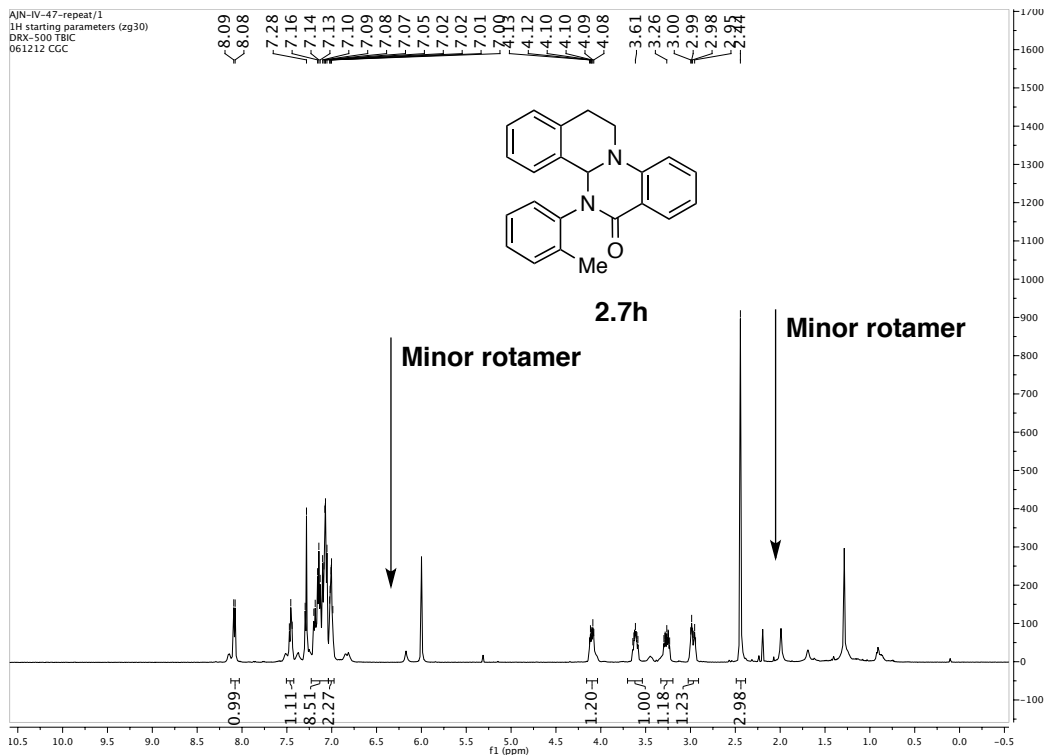


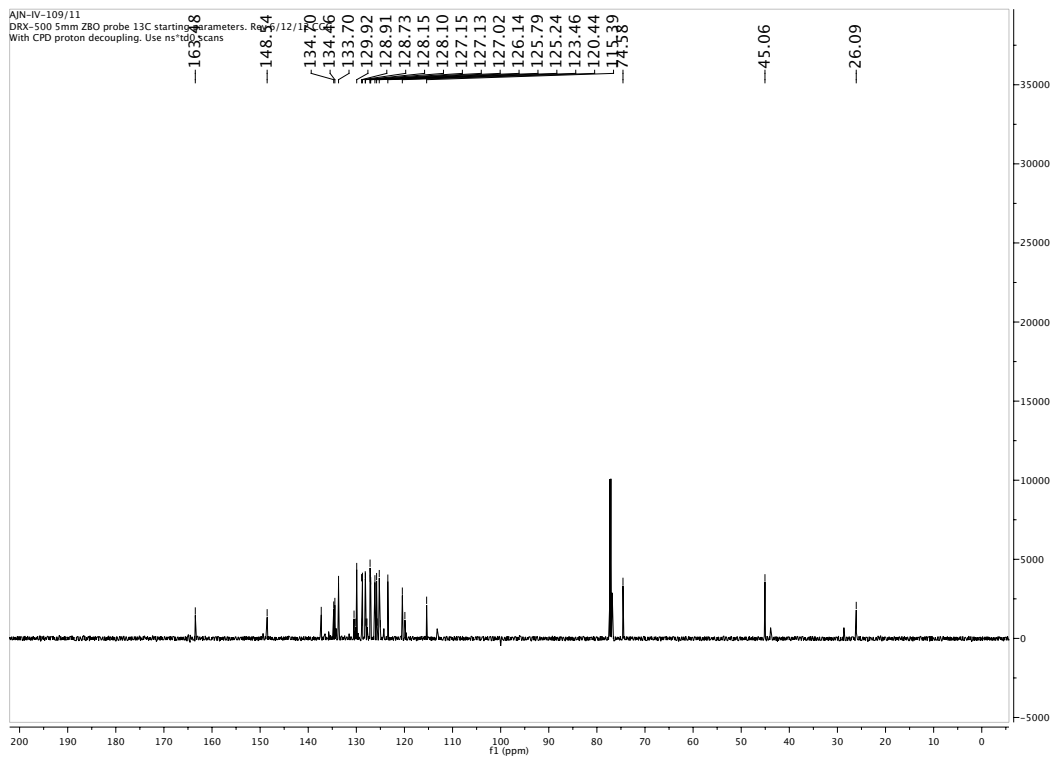
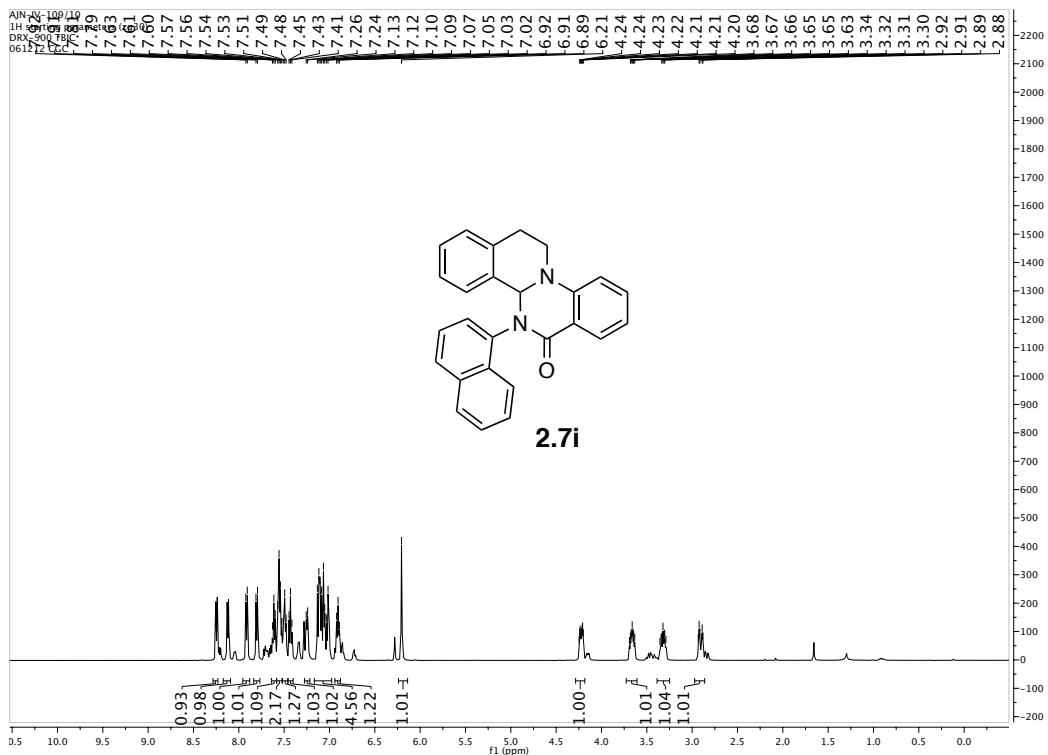
Only three of the five expected alkyl carbons show significant resonances in the ^{13}C NMR spectrum above. HSQC confirms that the remaining two carbons are present and correlate with diastereotopic proton sets 1,1' and 2,2', corresponding to tetrahydroisoquinoline methylene and benzylic protons respectively.

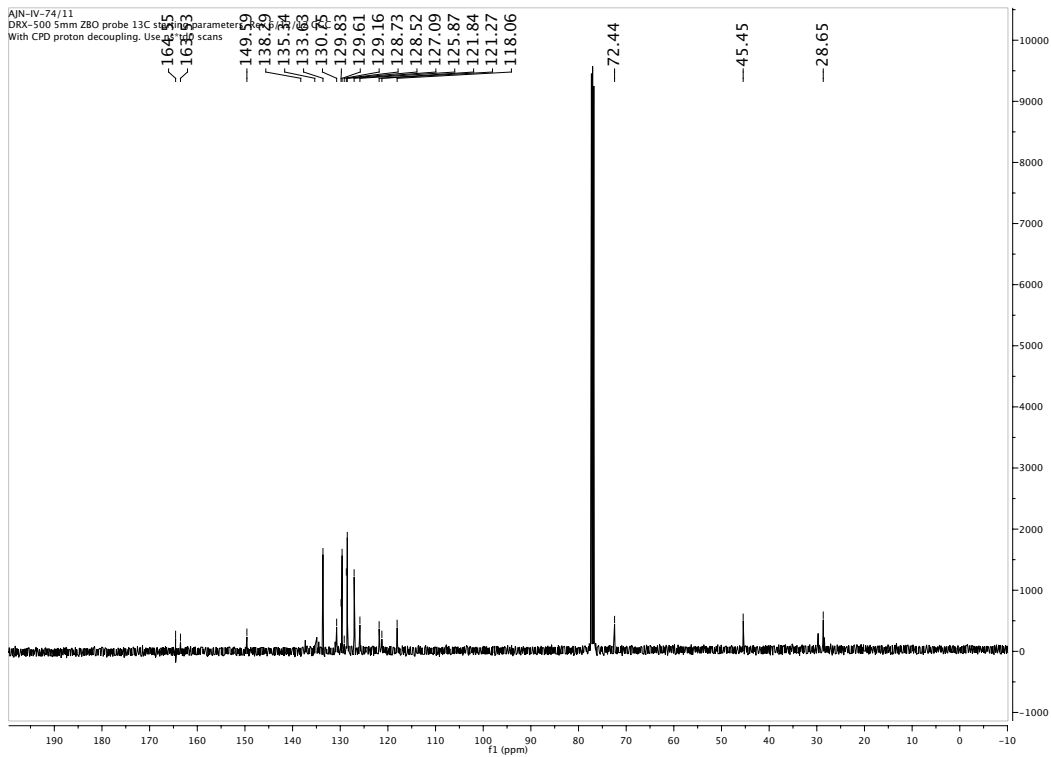
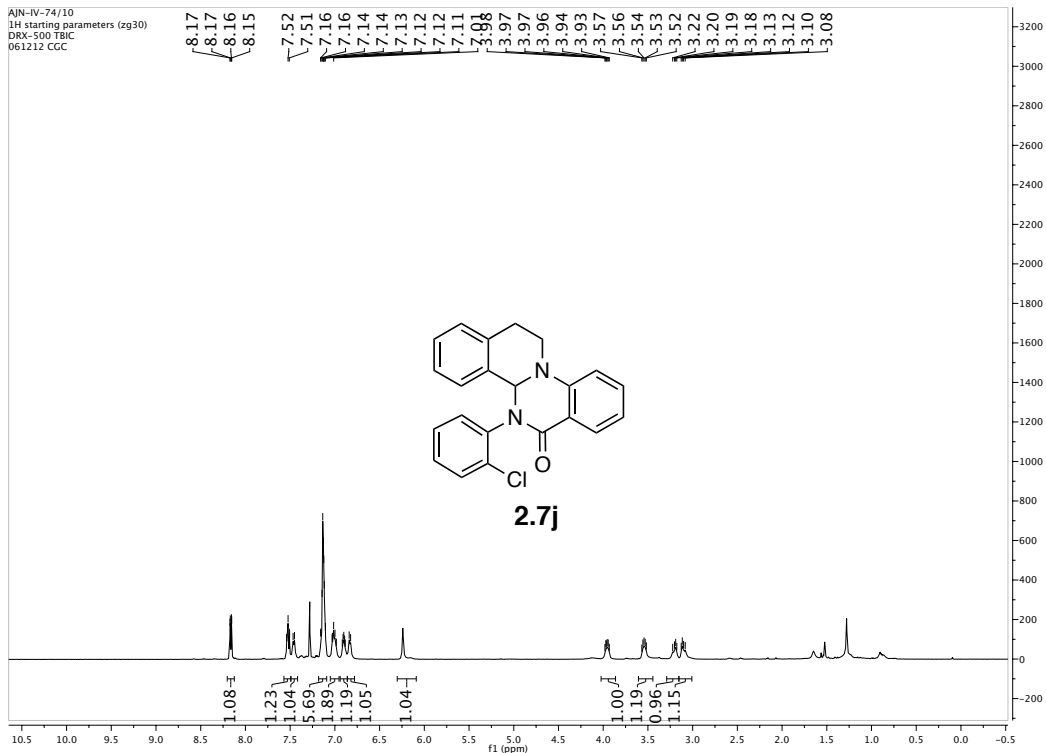


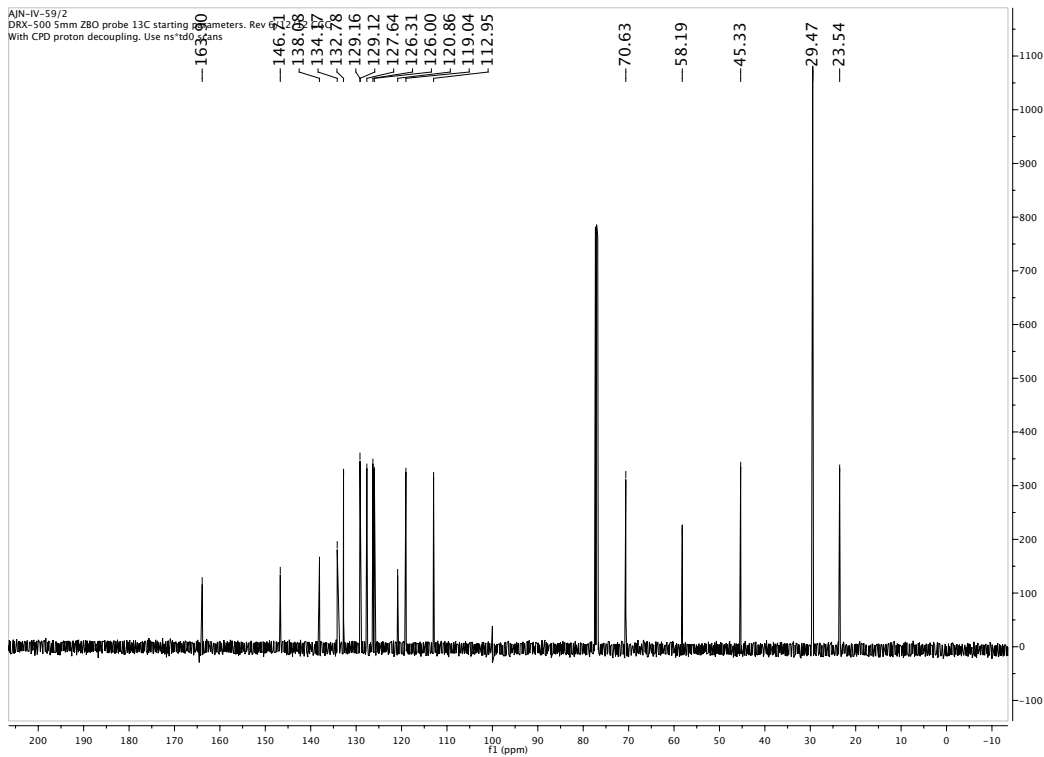
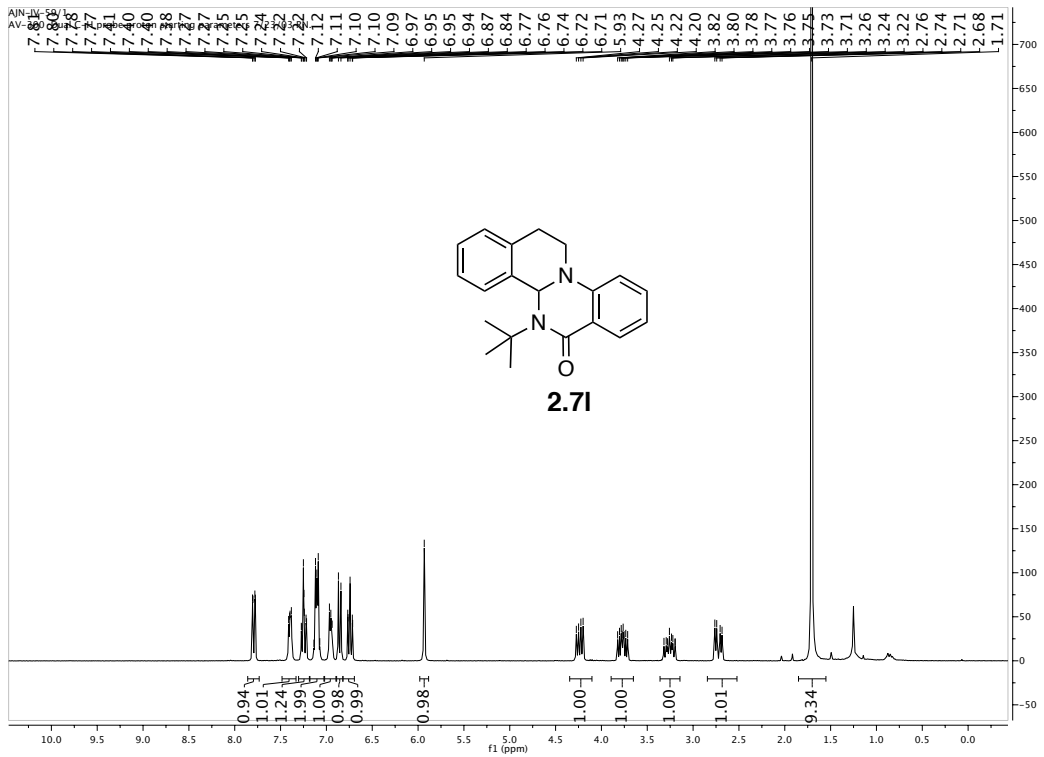


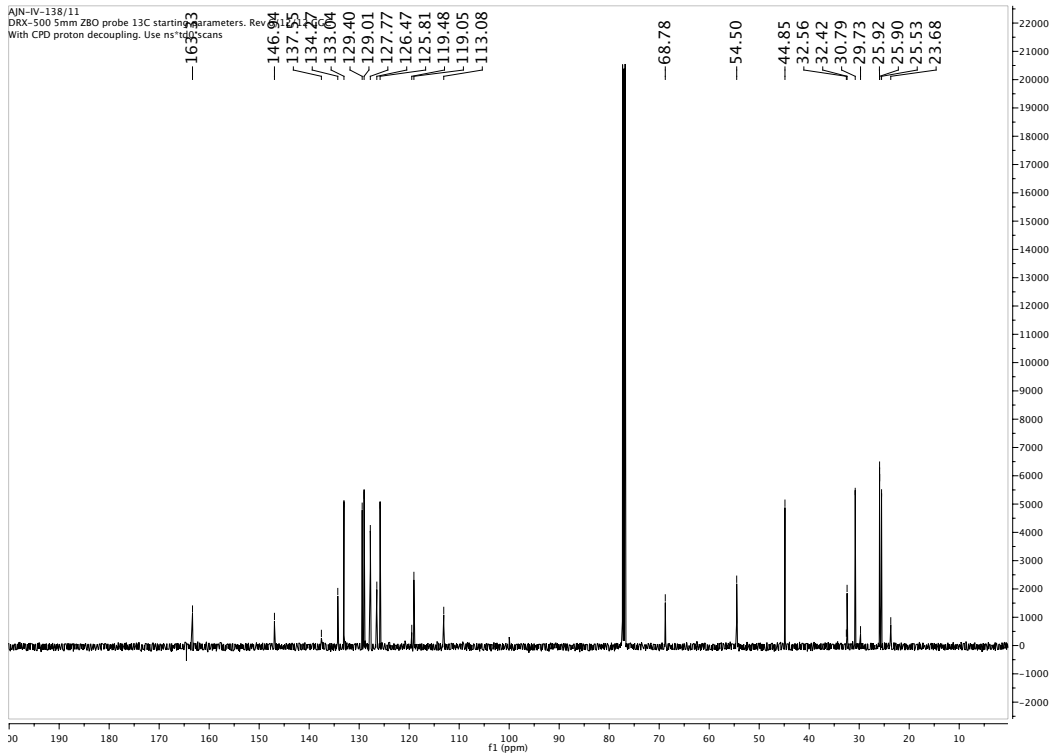
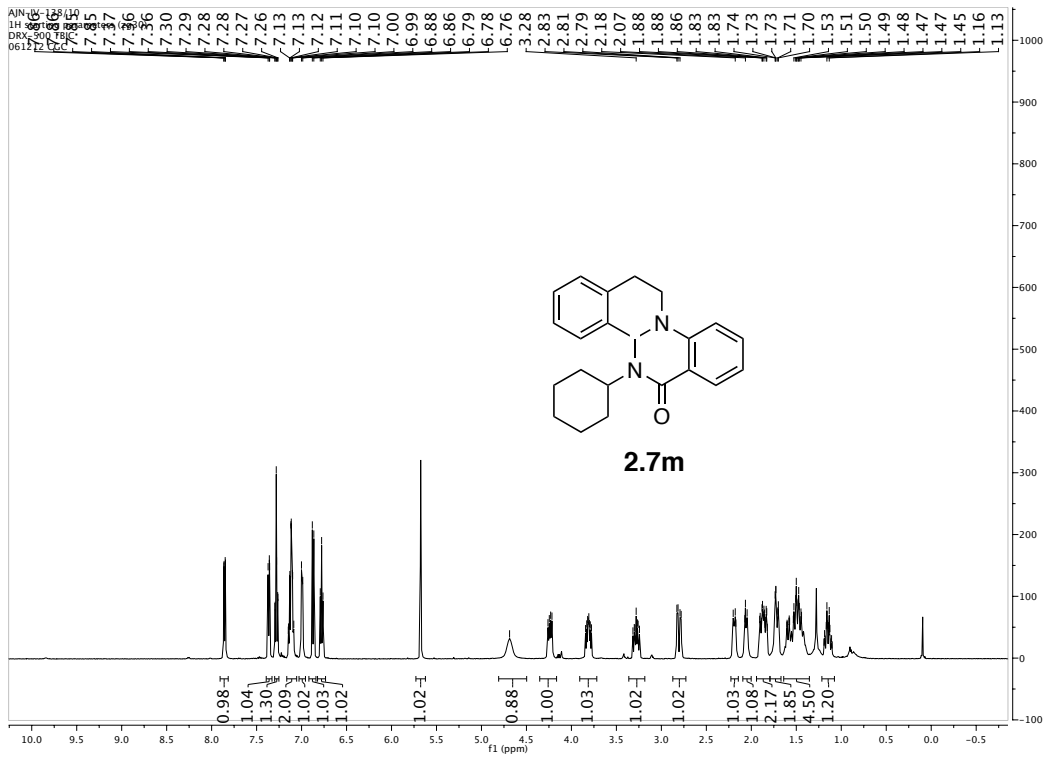


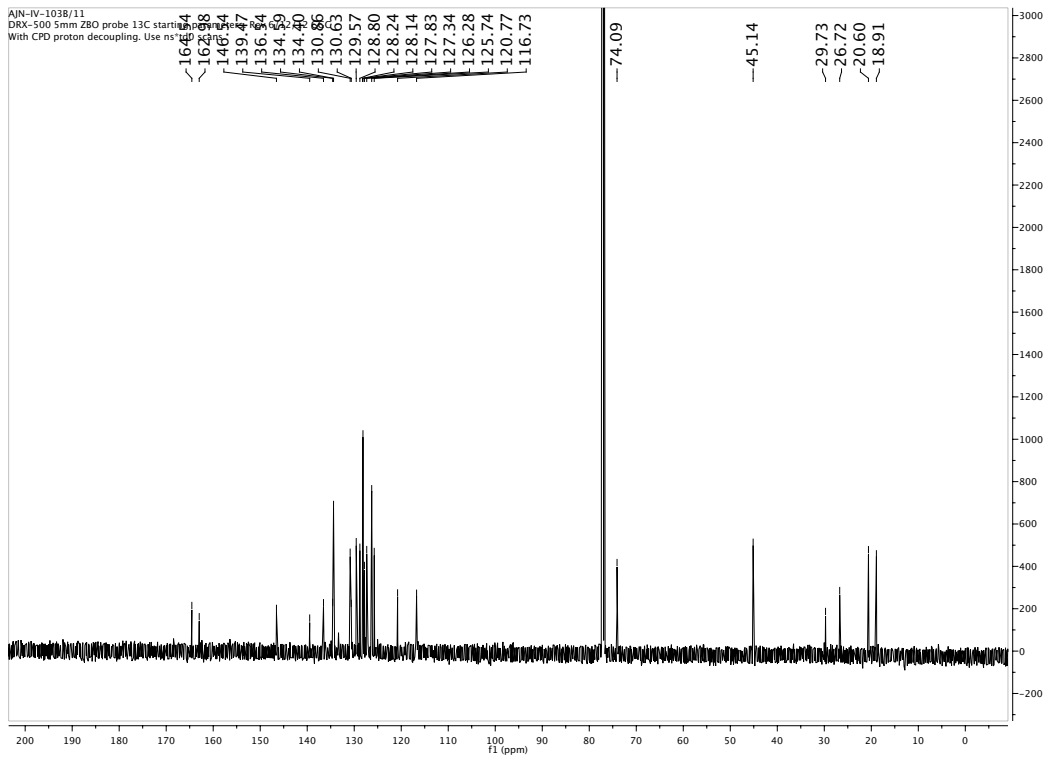
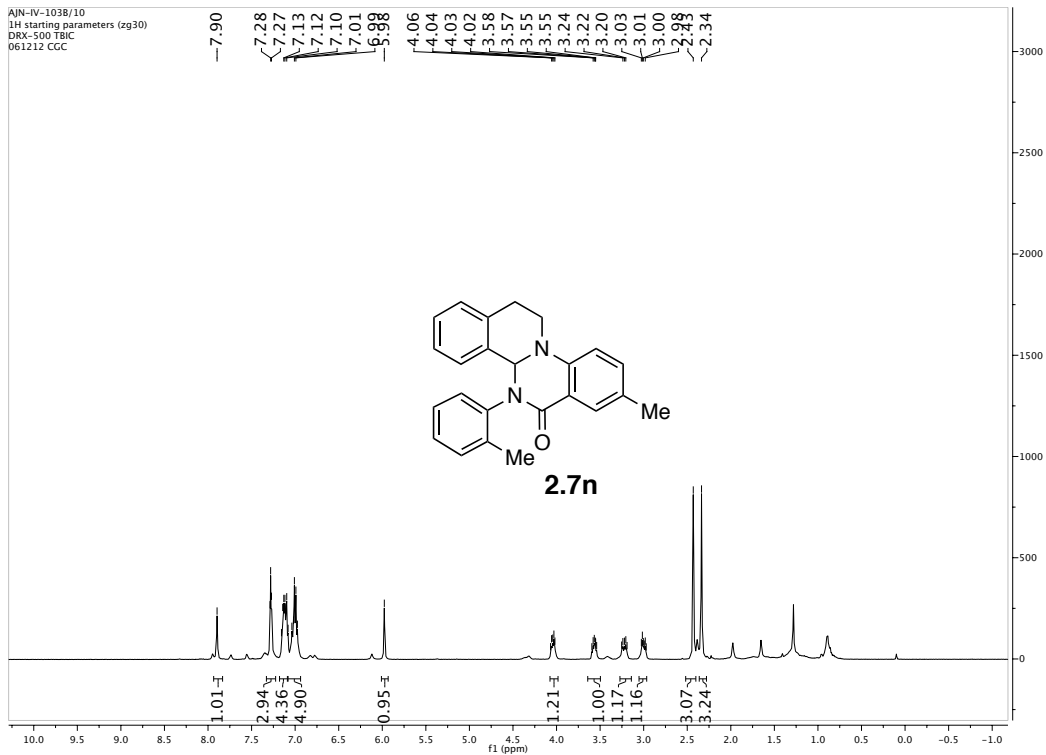


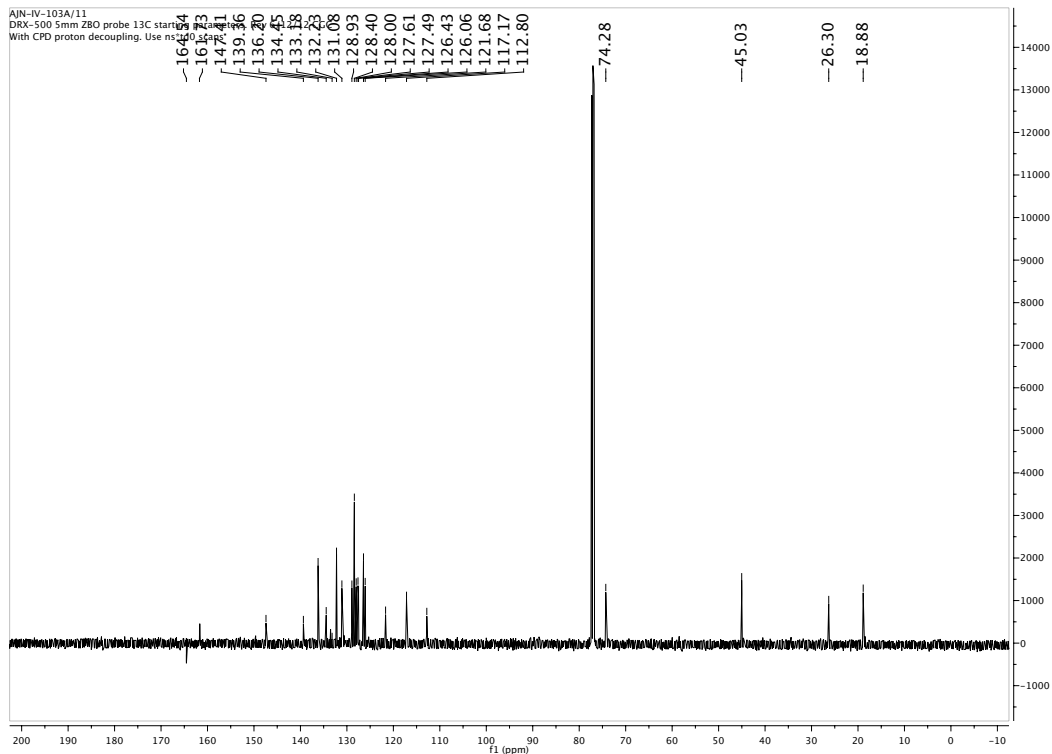
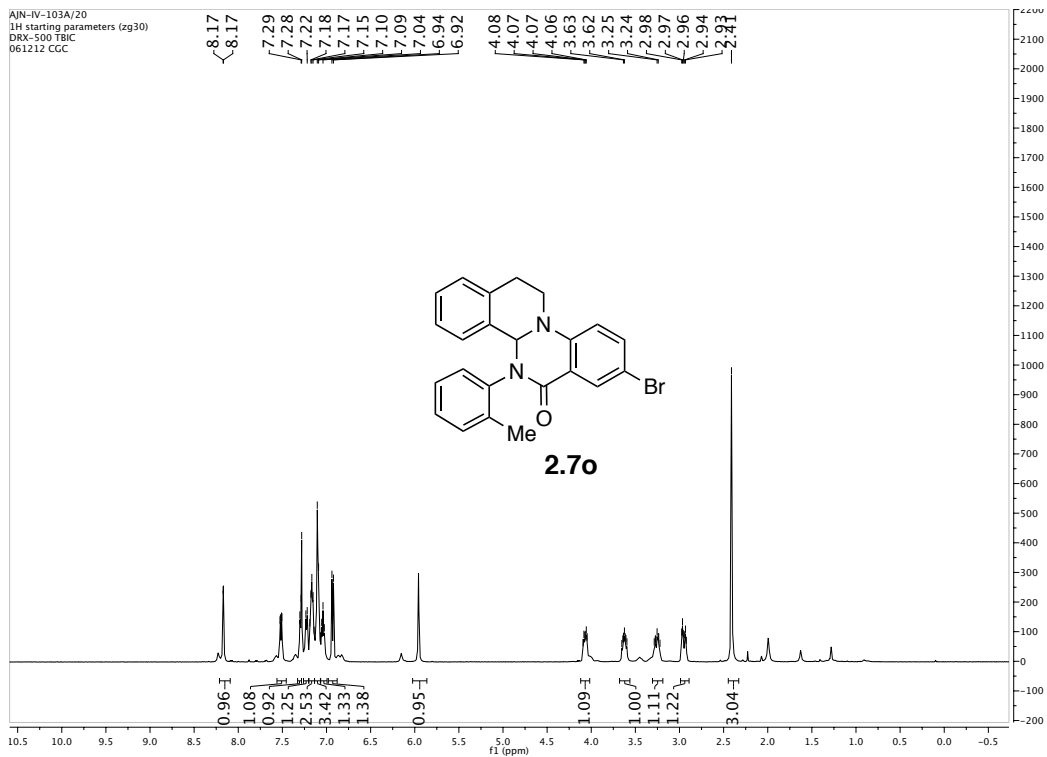


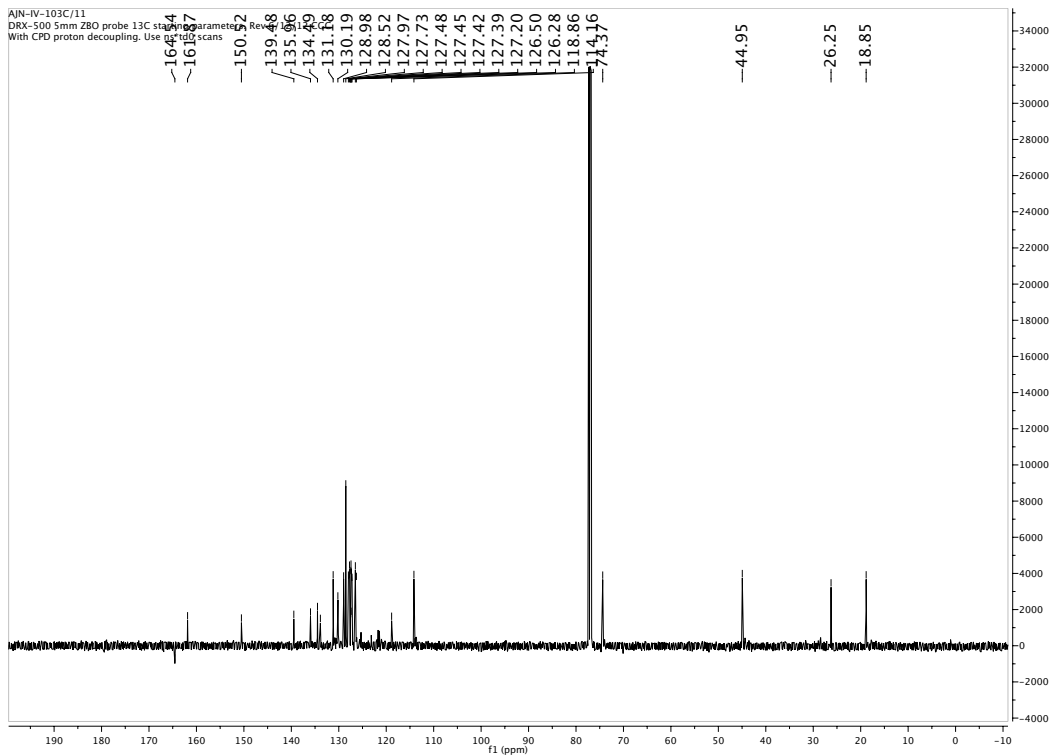
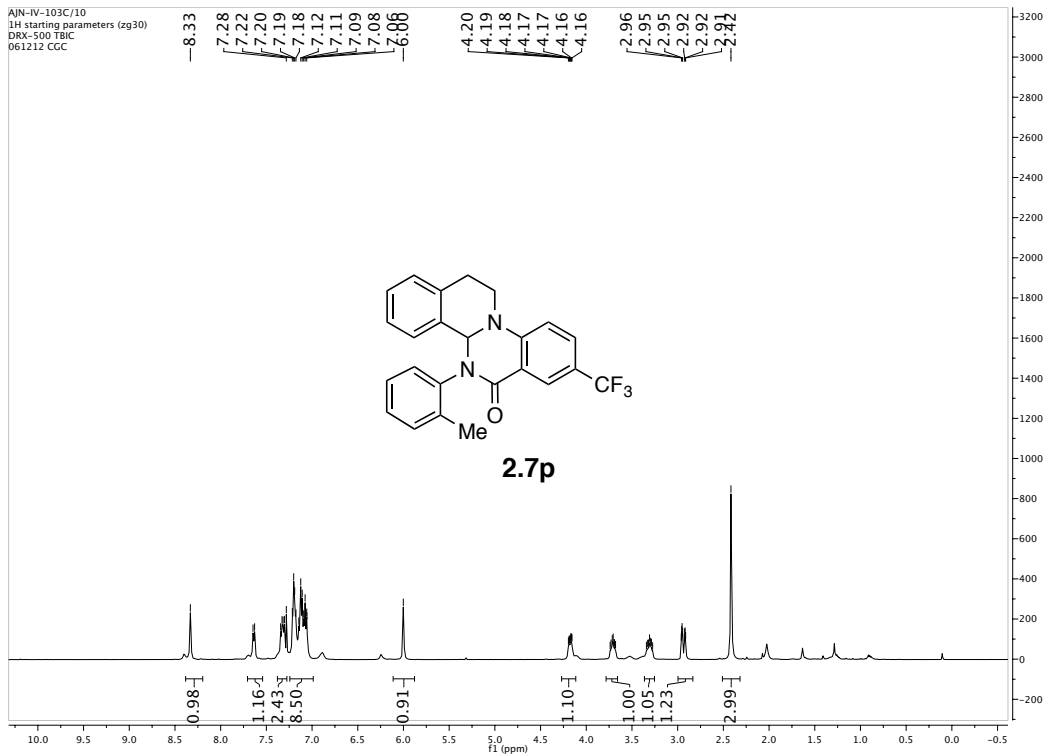


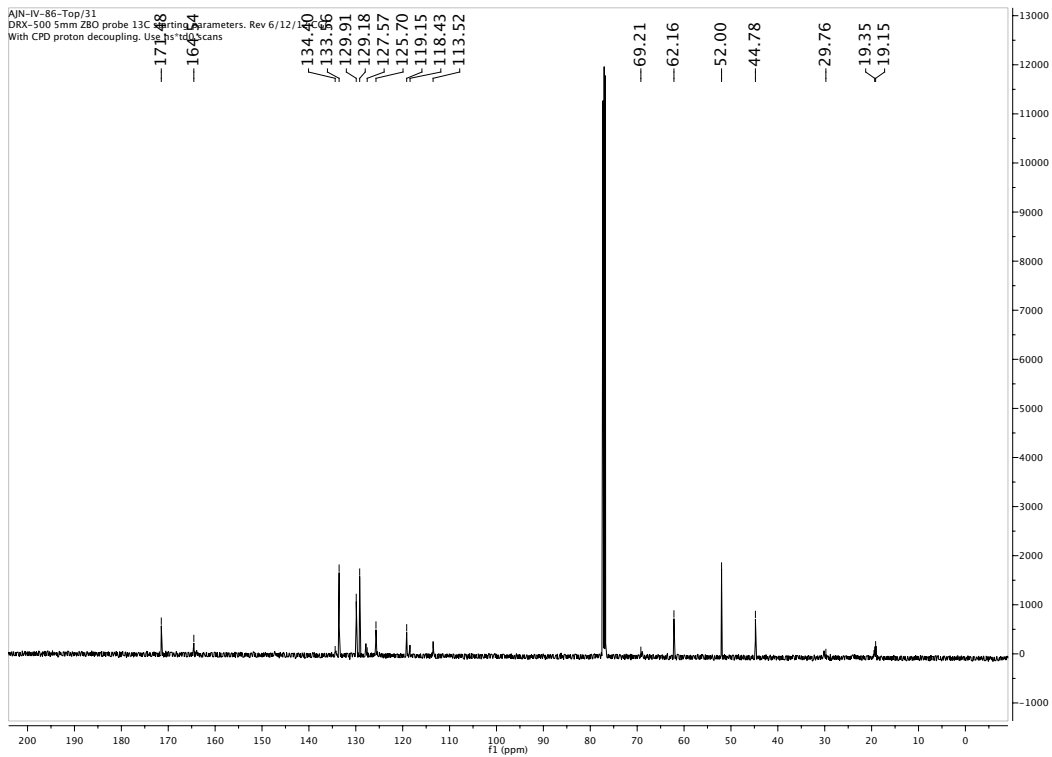
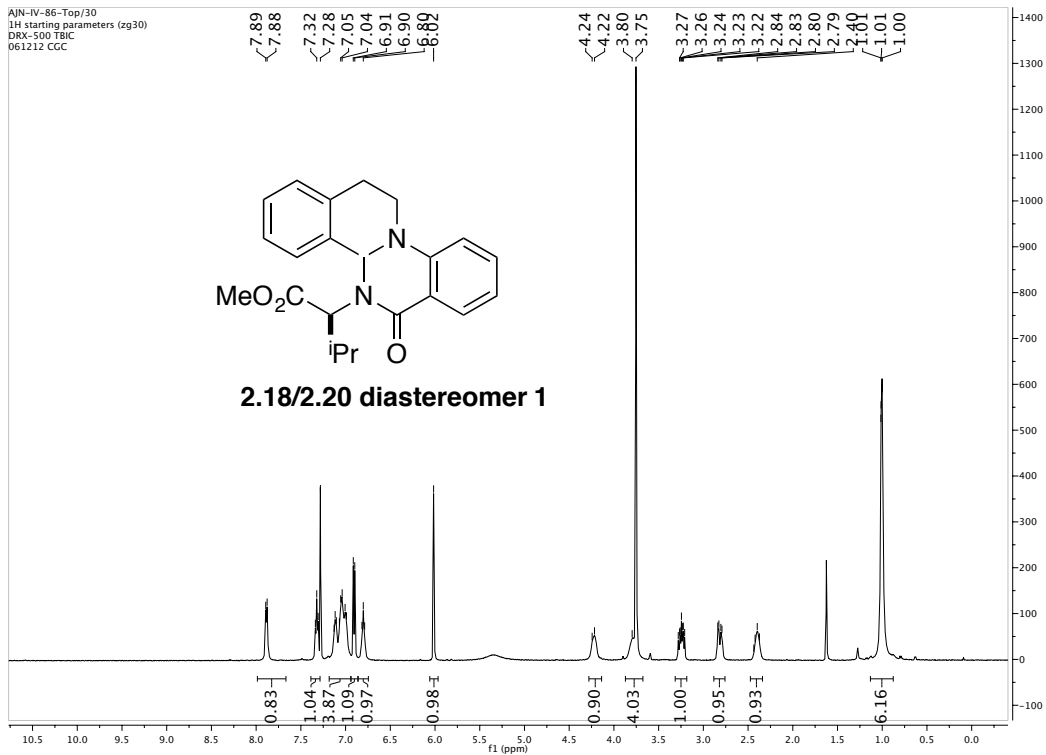


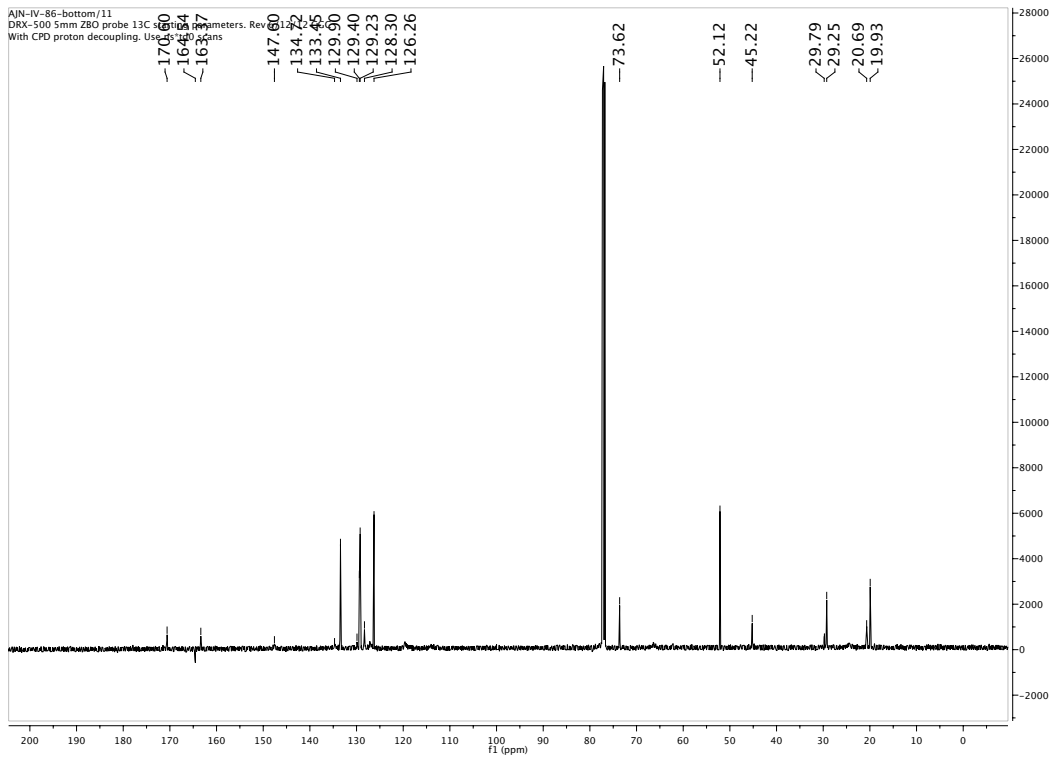
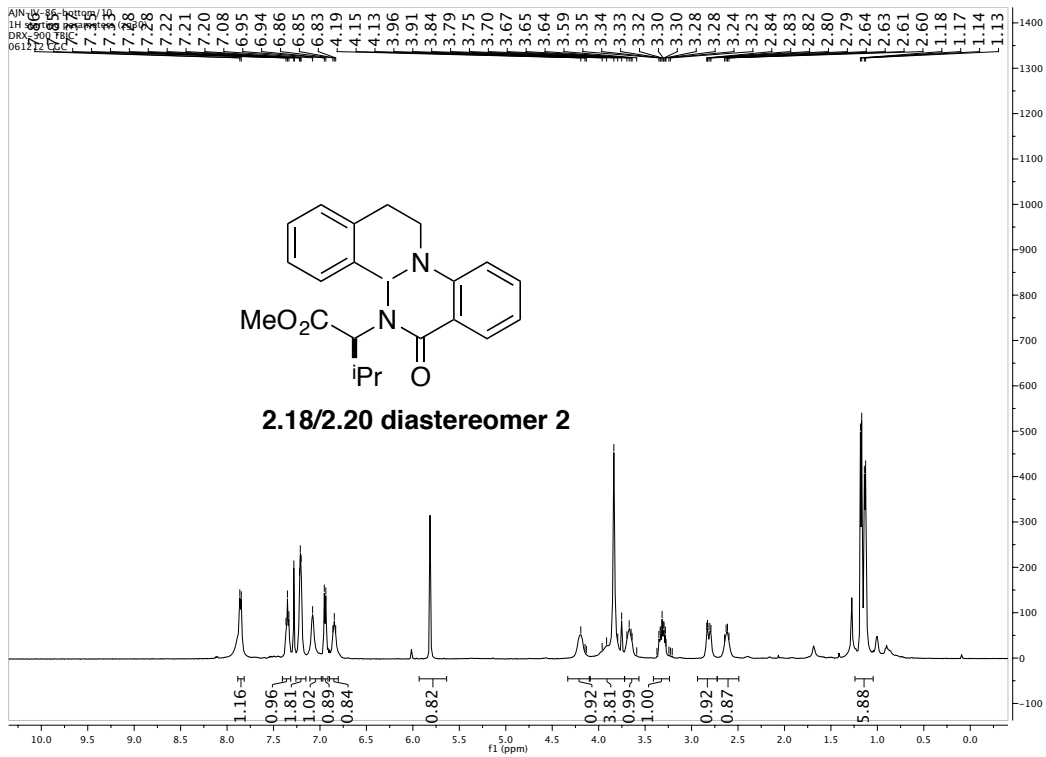












Chapter 3

Development of a Data-Intensive Method for Mechanistic Elucidation using Structurally Diverse Enantioselectivity Datasets

Portions of this chapter were adapted with permission from (Milo, A.*; Neel, A. J.* , Toste, F. D; Sigman, M. S. *Science* **2015**, *347*, 737. “A Data-Intensive Approach to Mechanistic Elucidation Applied to Chiral Anion Catalysis). Copyright (2015) The American Association for the Advancement of Science.

Chapter 3. Development of a Data-Intensive Method for Mechanistic Elucidation using Structurally Diverse Enantioselectivity Datasets

Introduction

The *de novo* design of chemo-, regio-, and stereo-selective catalysts remains an ongoing challenge in the field of organic synthesis. Even in instances where the overall mechanism of a transformation (i.e. the relative ordering of bond-breaking and bond-making events) is well understood, the origin of selectivity can remain undefined. In the case of enantioselective catalysis, the key challenge lies in recognizing the influence that catalyst and substrate structural features have on product enantiomeric excess (ee) due to interactions at the transition state (TS). This issue, while essential for the rational development of superior catalysts, is exacerbated in situations where seemingly minor perturbations to the catalyst or substrate structures have a profound, and often non-intuitive, influence on enantioselectivity.

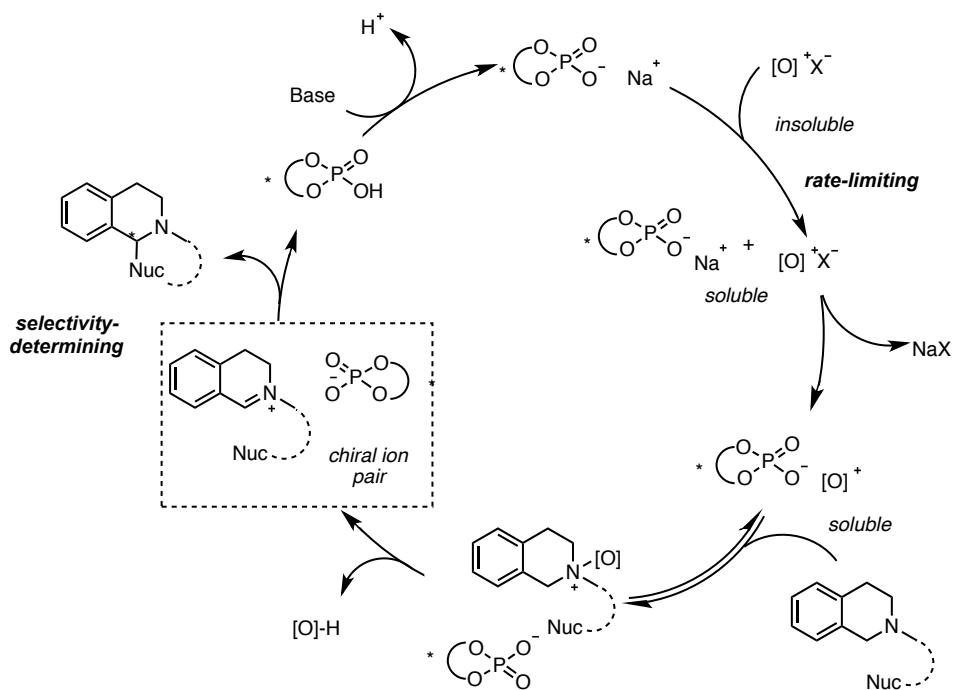
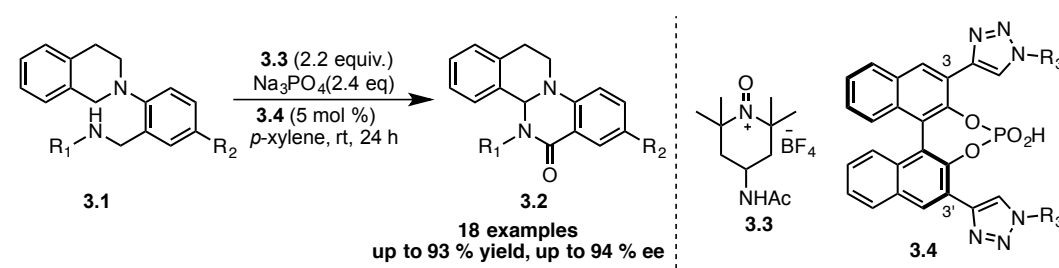


Figure 3.1. Summary of triazolyl PA-catalyzed CDC reaction

This phenomenon is exemplified by the work presented in Chapter 2, in which a novel class of chiral BINOL-based phosphoric acids (PAs) was developed containing 1,2,3-triazoles at the 3 and 3' positions (Figure 3.1).¹ These catalysts were “rationally designed” in the sense that

the triazole substituents were expected to be capable of undergoing attractive, noncovalent interactions²⁻⁶ with a substrate at the TS. We proposed that this feature would afford an alternative to the more conventional strategy of installing bulky groups at these positions whose proposed function is to occupy chiral space, forcing the substrate into conformations within the active site that minimize unfavorable steric interactions with the catalyst.⁷ Although use of the triazole-containing catalysts did indeed lead to improvement in the observed enantioselectivities of the cross dehydrogenative coupling (CDC) products under study (Figure 3.1), the specific role of triazole substituents remained ambiguous.

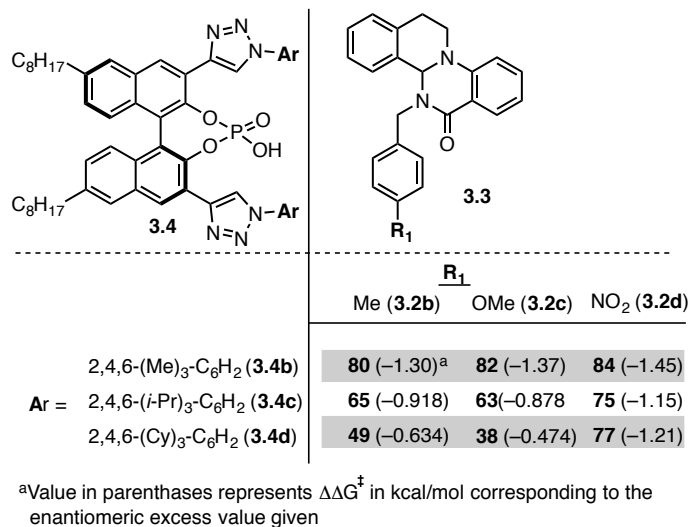


Figure 3.2. Subset of nonintuitive enantioselectivity trends from asymmetric CDC reaction

Particularly vexing was the subtle interplay observed between the structures of the reacting components, with even minor perturbations to the catalyst or substrate structures often resulting in significant and unpredictable variations in enantioselectivity. Figure 3.2 demonstrates this phenomenon for the subset of catalysts bearing a 2,4,6-trisubstituted aryl group on the triazole ring (**3.4b-d**) for a series of N-benzylated products (**3.2b-d**). For example, considering only mesityl-substituted catalyst **3.4b**, it appeared that the observed ee was relatively insensitive to substituent identity at the 4-position of the substrate benzyl group (R₁, 80-84 % ee). However, upon moving to structurally analogous 2,4,6-(*i*-Pr)₃-substituted catalyst **3.4c**, greater variance was observed (63-75 % ee) with a change in the relative ordering (i.e. **3.2d**>**3.2b**>**3.2c**). The trend completely breaks down for 2,4,6-(Cy)₃-substituted analogue **3.4d**. The structural origins of these data were impossible to discern upon inspection and as a result, the examination of multiple catalysts (**3.4**) for each substrate (**3.1**) was often necessary to achieve the desired outcome.

Although not ideal from the standpoint of catalyst generality, we wondered if the nonintuitive relationship between substrate and catalyst structures and enantioselectivity might serve as the foundation for a novel approach to mechanistic investigation. Assuming that the conditions of the Curtin-Hammett principle are satisfied,^{8,9} a product's observed enantioenrichment can be related to the free energy difference between the competing diastereomeric TSs leading to either enantiomer ($\Delta\Delta G^{\ddagger} = -RT\ln([S]/[R])$ in kcal/mol, Figure 3.3). Thus, enantioselectivity represents a relative rate measurement that is sensitive to the structural

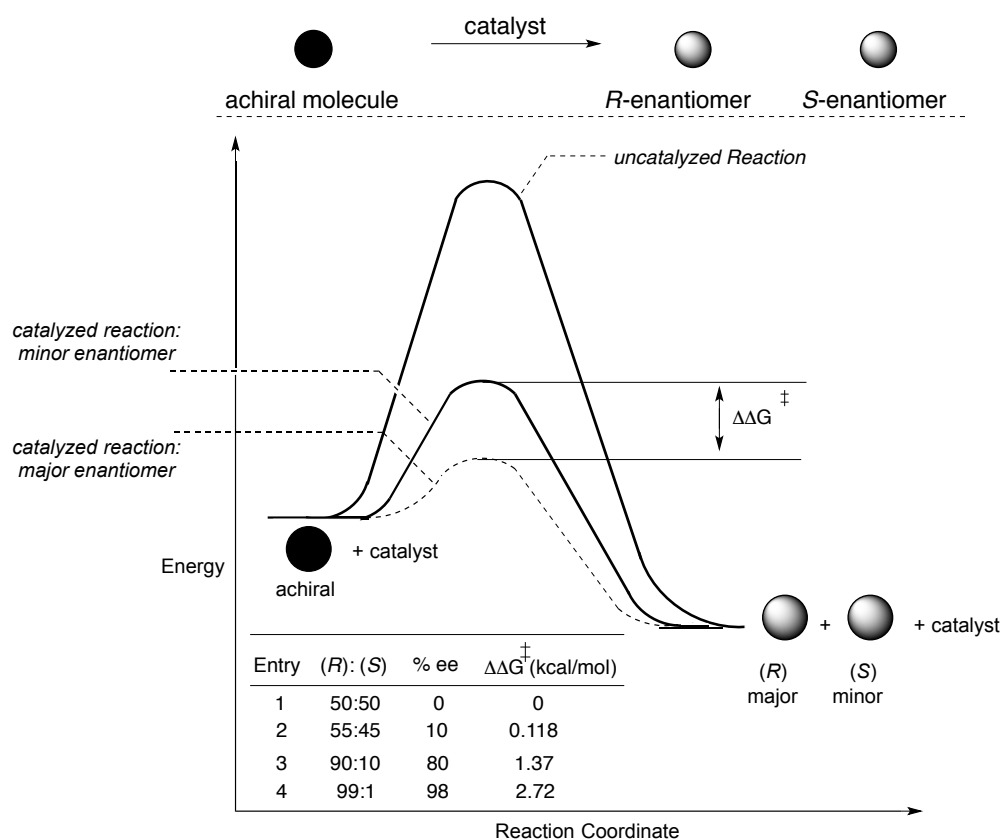


Figure 3.3. Example reaction coordinate diagram depicting energy difference between competing diastereomeric TS's required for asymmetric induction

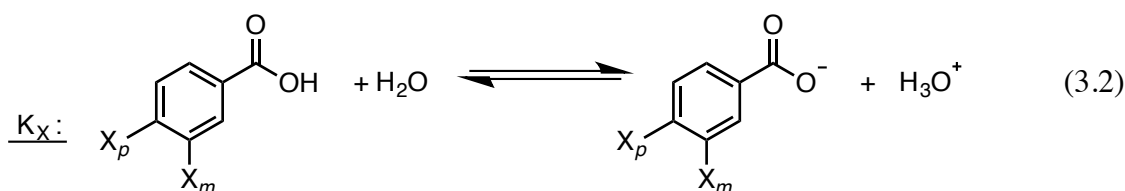
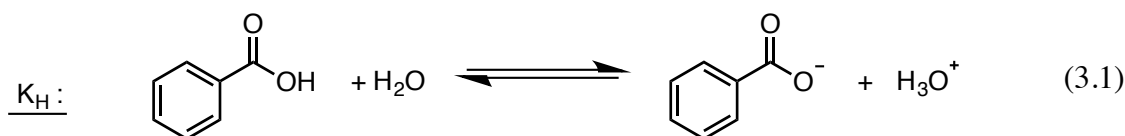
features of each reacting component. Considered from this perspective, every selectivity value obtained in the course of data collection bears specific structural information regarding the TS interactions underlying asymmetric catalysis. We thus hypothesized that, given a dataset of enantiomeric excess values that is highly variable as a function of catalyst and substrate structure, relevant information could be extracted that would shed light on the interactions responsible for asymmetric induction. With this goal in mind, we established a collaboration with the group of Professor Matthew Sigman at the University of Utah given its expertise in the development of structure-selectivity relationships in asymmetric catalysis. Prior to describing the results of this collaboration in detail, a summary of relevant background information is required.

Background

Quantitative structure activity relationships (QSARs) are mathematical models that relate a response of interest (e.g. drug activity, binding, reaction rate, etc.) to parameters that describe molecular structure.¹⁰ In building such relationships, scientists typically endeavor to predict the performance of molecules that have yet to be tested. The subset of QSARs that has seen the most extensive use in physical organic chemistry is the linear free energy relationship (LFER), which relates the free energy (ΔG) of a reaction of interest to that of a standard reaction whose sensitivity to molecular structure is known.¹¹ What distinguishes the LFER approach from the QSAR one at large is that the former is typically employed as a tool to support or refute a mechanistic hypothesis, not as a means to predict new examples. One reason that LFERs have proven to be such useful

mechanistic tools is that the parameters employed are fundamentally mechanistic in origin, as they are derived from free energy measurements and thus directly linked to reactant stability/reactivity.

Of the many parameters used in LFERs, Hammett σ constants were the first developed and have seen the most extensive use.¹² These values represent proportionality constants, relating the thermodynamic acidity of *meta* (σ_m) or *para*-(σ_p) substituted benzoic acid derivatives and the parent compound (eq. 3.1-3.3) and are used to describe the ability of a substituent to stabilize negative charge. The equilibrium constant or rate of a new reaction of interest can be measured and plotted against σ . A linear correlation suggests that this new reaction is sensitive to substituent effects in a manner that is relatable to the ionization of benzoic acid.



$$\log\left(\frac{K_X}{K_H}\right) = \sigma_x \quad (3.3)$$

$$\log\left(\frac{K_{X_new}}{K_{H_new}}\right) = \rho\sigma_x \quad (3.4)$$

According to the Hammett equation (eq. 3.4), the slope (ρ) of the resulting plot contains information regarding the sensitivity of the new reaction to substitution relative to the standard reaction. For example, if the rate of the new reaction is being studied, a positive slope suggests that this process is accelerated by electron withdrawing substituents and therefore that the TS must contain greater anionic character than the ground state. Similarly, a slope of $\rho > 1$ suggests that the new reaction is more sensitive to substitution than the ionization of benzoic acid, whereas a slope of $0 < \rho < 1$ implies the opposite. Importantly, the assumption underlying any LFER is that the *trends* in how substituents affect the standard reaction will hold across a wide range of otherwise unrelated reactions. It is this feature that allows the *rates* of new reactions to be correlated with the *equilibrium* constants of a standard reaction.

As enantiomeric excess values represent relative rates that reflect the free energy difference between competing diastereomeric transition states ($\Delta\Delta G^\ddagger$), LFERs can be constructed relating catalyst or reactant structure to enantioselectivity.¹³ A beautiful example from Jacobsen and coworkers is shown in Figure 3.4 in which Hammett σ -constants were used to quantify the electronic effect on enantioselectivity in the asymmetric epoxidation of olefins catalyzed by substituted Mn(III)-salen complexes.^{14,15} This LFER led to the proposal that the position of the enantiodetermining TS along the reaction coordinate depends on the electronic nature of the salen ligand, demonstrating the power of simple correlations to provide detailed mechanistic insight.

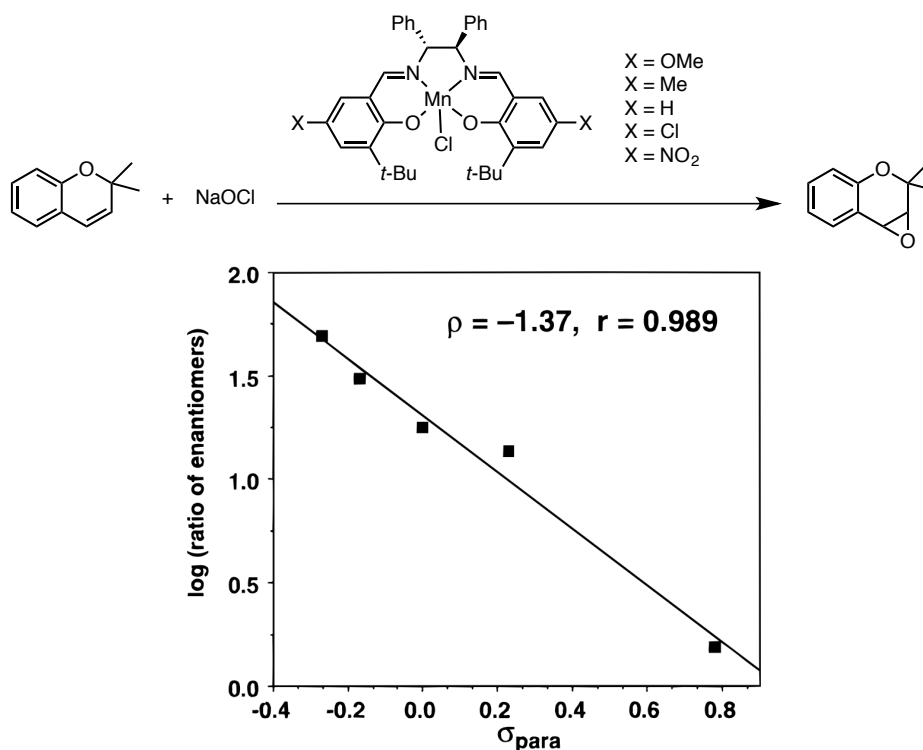


Figure 3.4. LFER correlating ee of asymmetric epoxidation to Hammett σ constant (ref 14)

Similarly to the electronic effects described by σ , substituent steric effects can be described quantitatively for use in LFERs.¹¹ Sigman and coworkers were the first to apply this approach to the quantification of steric effects in asymmetric catalysis.¹⁶ Using the asymmetric Nozaki-Hiyama-Kishi (NHK) allylation of aldehydes depicted in Figure 3.5 as a test case, the authors found a linear correlation between a parameter (ν) describing the steric effect of the substituent (**G**) on the chiral oxazoline ligand and the log of the enantiomeric ratio (er) of several aldehydes and ketones.

The value ν was developed by Charton^{17–20} and is a modification of the parameter E_s developed by Taft²¹ based on the acid-catalyzed hydrolysis rates of methyl esters (eq. 3.5-3.6). As positive charge is maintained from the ground state to the TS, any variation in rate is presumed to arise from a steric effect of the substituent R. Charton recognized a correlation between the values obtained by Taft and the Van der Waals radii of the substituents, conferring a more intuitive nature to the parameter ν . Enantioselectivity could be effectively modeled by a single steric parameter in this NHK allylation reaction (Figure 3.5) which was taken as evidence that ligand steric bulk was the primary determinant of enantioselectivity.

The example LFERs highlighted thus far have involved chiral ligands where the isolated steric or electronic effect of substitution at a single position was analyzed. However, chiral ligands are often designed with modularity in mind and thus possess multiple sites that can be modified, raising the question of how to correlate simultaneous changes at more than one position to selectivity. To address this issue, Harper and Sigman described the use of multivariate LFERs in which the free energy of a reaction is correlated with a linear combination of multiple parameters that describe changes at multiple positions.²²

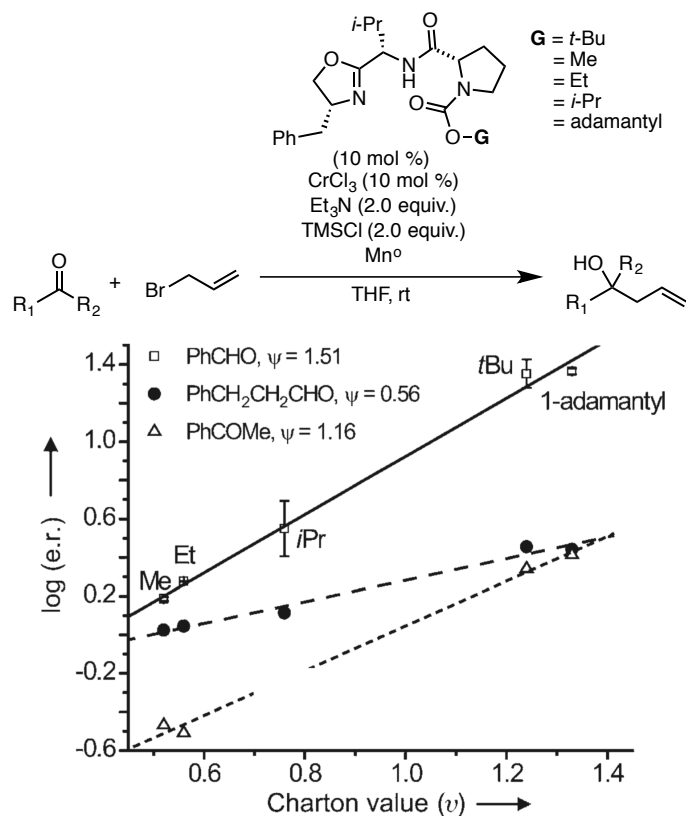
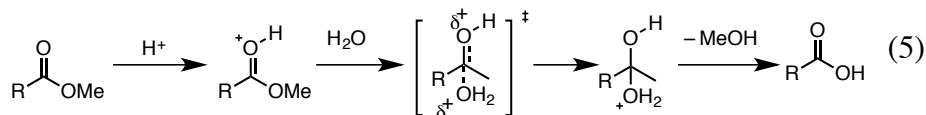


Figure 3.5. LFER correlating ee of asymmetric NHK allylation with Taft-Charton steric parameter (ν) (ref 16)



$$\log\left(\frac{k_x}{k_{Me}}\right) = \delta E_s \quad (6)$$

As shown in Figure 3.6, a matrix of nine quinolone-proline ligands that were systematically varied with respect to electronics and sterics at positions **E** and **S** (as judged by their respective σ and ν values) were evaluated in the NHK propargylation of acetophenone. Application of standard linear regression techniques resulted in an LFER containing five terms (eq. 3.7).

The parameters **E** and **S** represent normalized values of σ and ν respectively; therefore, the coefficients in eq. 3.7 describe the relative extent to which each parameter models the variance in $\Delta\Delta G^\ddagger$. Notably, the largest coefficient in eq. 3.7 is for a cross term (3.79 ES), highlighting the cooperative effect of ligand steric and electronic properties in determining product enantiomeric excess. A surface representing eq. 3.7 is shown in Figure 3.7, demonstrating the optimal ligand with the quinoline-proline structure (**E** = OMe, **S** = *t*-Bu) was likely identified.

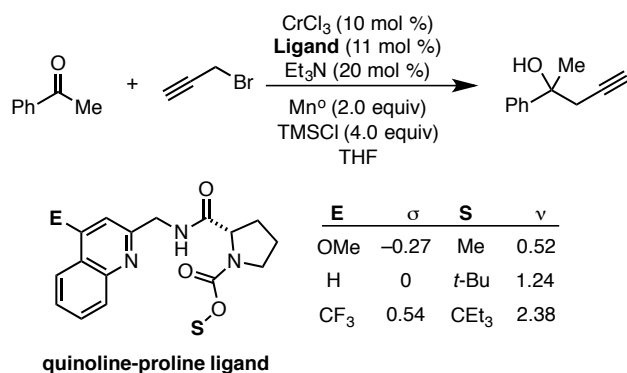


Figure 3.6. Systematically modified ligand library for evaluation in NHK propargylation (ref 22).

$$\Delta\Delta G^\ddagger = -1.20 + 1.22 E + 2.84 S - 0.85 S^2 - 3.79 ES + 1.25 ES^2 \quad (3.7)$$

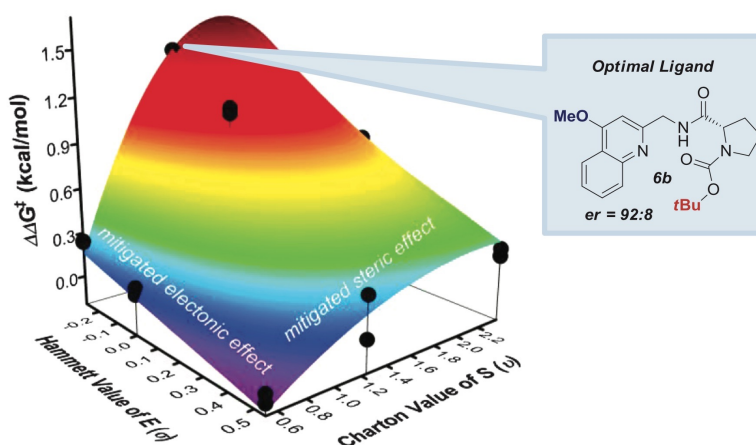


Figure 3.7. Three-dimensional surface illustrating interplay of steric and electronic effects in NHK propargylation (ref 22).

Harper and Sigman have also demonstrated that multivariate LFERs can be applied to the description of multifaceted steric effects.²³ Although the aforementioned Taft-Charton steric parameters (ν) had been effective for modeling substituents that could be approximated as spherical (e.g. *t*-Bu), they proved less so for those where this assumption was not valid (e.g. CH₂*t*-Bu, Figure 3.9, left). The authors addressed this limitation by implementing the Sterimol parameters developed by Verloop and coworkers²⁴ that treat substituents as asymmetric and describe different directional aspects

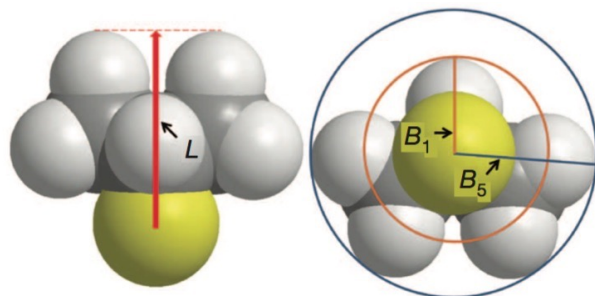


Figure 3.8. Pictorial representation of Sterimol parameters B_1 , B_5 , and L (ref 23).

As shown in Figure 3.8, the minimal (B_1) and maximal (B_5) width and length (L) of a substituent along the primary bond axis can be described separately, allowing for a more sophisticated characterization of substituent shape. The effectiveness of moving from Taft-Charton (ν) to Sterimol values for describing steric effects of non-spherical substituents is illustrated in Figure 3.9 for the desymmetrization of *bis*-phenols (**3.5**) catalyzed by tetrapeptide catalyst **3.6**.²³

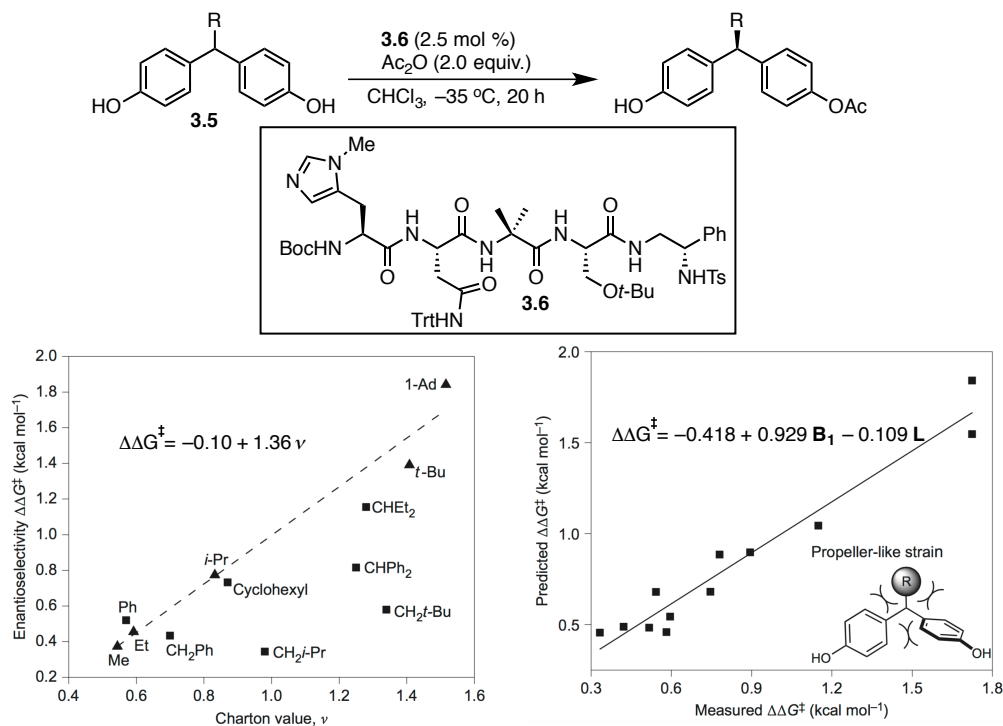


Figure 3.9. Comparison of ability of Taft-Charton (left) and Sterimol (right) parameters to correlate with *ee* in desymmetrization of *bis*-phenols (ref 23).

The parameters discussed thus far (i.e. σ , ν /Sterimol) were developed for the explicit purpose of describing isolated electronic and steric effects respectively. For example, *ortho*-substituted aryl rings are typically not used in Hammett studies, as such substituents introduce a

steric perturbation that may obfuscate the electronic effect being analyzed. However, for many enantioselective catalyst systems (and organic reactions in general), these effects cannot be decoupled. In fact, a molecule's steric and electronic properties may often act in a synergistic fashion, precluding the correlation between the $\Delta\Delta G^\ddagger$ of a reaction of interest and any single parameter.

A creative approach to this limitation was recently developed by Milo and Sigman.²⁵ Recognizing that the unique structural features of any molecule are imbedded in its vibrational modes, it was hypothesized that infrared (IR) vibrational frequencies (ν) and intensities (i) might serve as useful parameters for correlating selectivity. As individual IR ν and i values are often difficult to discern from experimental spectra, it was proposed that computationally-derived values would allow for the detailed comparison of analogous ν and i among structurally related molecules. Although a large number of such values exist for a given molecule, discretion can be exercised in selecting ν and i corresponding to molecular regions presumed to be of mechanistic relevance (such as aryl rings observed to experimentally impact selectivity or bonds undergoing bond breaking/making) and whose magnitudes are observed to be sensitive to substitution. An example of this approach is shown in Figure 3.10 for the same desymmetrization reaction presented previously in Figure 3.9.

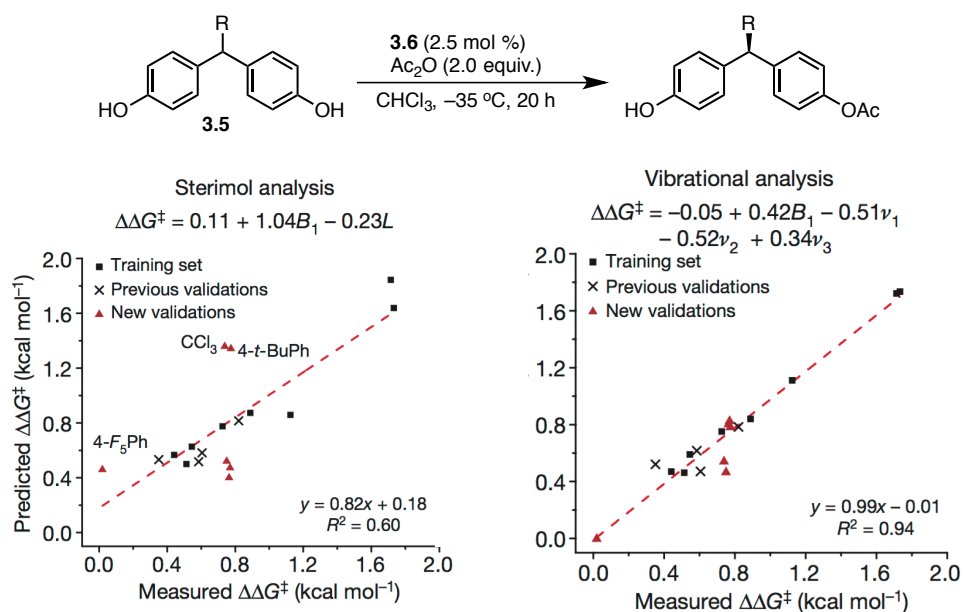


Figure 3.10. Improvement of correlation between predicted and measured ee upon switching from steric (left) to vibrational (right) analysis (ref 25).

As steric effects were the focus of the previous study (*vide supra*), major electronic changes to R had been explicitly avoided. When such alterations were included (e.g. R = F₅Ph or CCl₃, triangles, Figure 3.10, left), they were poorly predicted by a Sterimol analysis. To assess the potential of the vibrational approach for improving this correlation, six computationally-derived IR frequencies were selected that were identifiable across the entire training set of *bis*-phenol substrates and whose values were observed to be sensitive to the identity of R. Regression analysis produced a much more predictive model (Figure 3.10, right) that contained three of the selected

vibrational parameters (ν_1 , ν_2 , and ν_3) and a single Sterimol value (B_1). Among other hypotheses, it was proposed that the vibrational parameters may serve as electronic corrections to steric effects, affording an improved correlation. Illustrations of the relevant vibrational modes are shown in Figure 3.11 and data for *bis*-phenols containing several different substituents, along with their relative magnitudes and ranges are presented in Table 3.1.

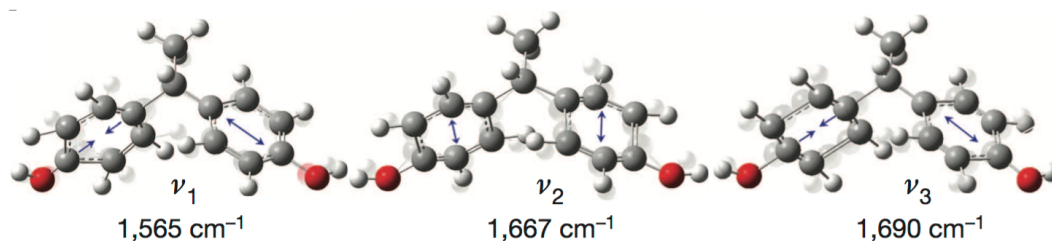


Figure 3.11. *Bis*-phenol vibrational modes relevant for modeling enantioselectivity in peptide-catalyzed desymmetrization (ref 25).

Table 3.1. Selected values of parameters used for modeling of *bis*-phenol desymmetrization (ref 25).

R	CMe ₃	CCl ₃	Ph	F ₅ Ph	<i>p</i> - <i>t</i> -BuPh	Range
$\Delta\Delta G^\ddagger$	1.73	0.74	0.51	0.02	0.77	—
B_1	2.92	2.58	1.77	1.77	2.86	—
ν_1	1536.6	1567.3	1564.6	1565.5	1565.1	4.0 cm ⁻¹
ν_2	1665.3	1667.1	1667.4	1668.6	1668.0	3.4 cm ⁻¹
ν_3	1688.9	1690.4	1688.8	1689.3	1689.3	2.2 cm ⁻¹

Collectively, the examples presented above outline the evolution of strategies for modeling the variance in a reaction's enantioselectivity from simple single variable LFERs to multivariate correlations with molecular descriptors capable of representing multifaceted structural aspects. Given this foundation, we were in a position to address the complexity of our triazolyl PA-catalyzed CDC reaction. Specifically, the challenges of this system can be summarized as follows: 1) enantioselectivity was sensitive to substitution at multiple positions on two separate reacting partners (i.e. substrate and catalyst), 2) the nature of association between the catalyst and substrate at the enantiodetermining TS was undefined and 3) noncovalent interactions were likely to be at least partially responsible for asymmetric induction, a situation that had not been explicitly addressed using structure-selectivity relationships in asymmetric catalysis. With these challenges in mind, we set out to develop a strategy to extract information regarding the structural origins of enantioselectivity from a diverse dataset of enantioselectivity values.

Results and Discussion

Experimental Design

Figure 3.12 outlines our experimental plan. Initially, substrate and catalyst libraries would be designed that varied at positions of interest with respect to their steric and electronic properties. Simultaneously, molecular descriptors would be collected describing these multifaceted structural perturbations. Experimental enantiomeric excess values would then be collected for each catalyst-substrate combination, affording a diverse dataset. Different organization and analysis strategies would next be explored, seeking meaningful correlations, akin to free energy relationships,

between experimental enantioselectivity data and the molecular descriptors. Based on the nature of the derived models and the resulting chemical intuition, mechanistic hypotheses could be developed that could be tested using new catalysts and/or substrates specifically tailored to probe these hypotheses. Agreement between the predicted and observed results both numerically and intuitively would provide support for the proposed mechanism whereas disagreement would serve as refutation and would call for a reevaluation. In this way, this approach is no different from a traditional mechanistic analysis in which testable hypotheses are generated and experiments performed to support or refute them. The novelty in this proposed strategy lies in its ability to report on mechanistic details within regions of catalytic cycles that have traditionally been difficult to interrogate, such as the present case wherein the selectivity determining step occurs after the rate limiting step (*vide supra*).

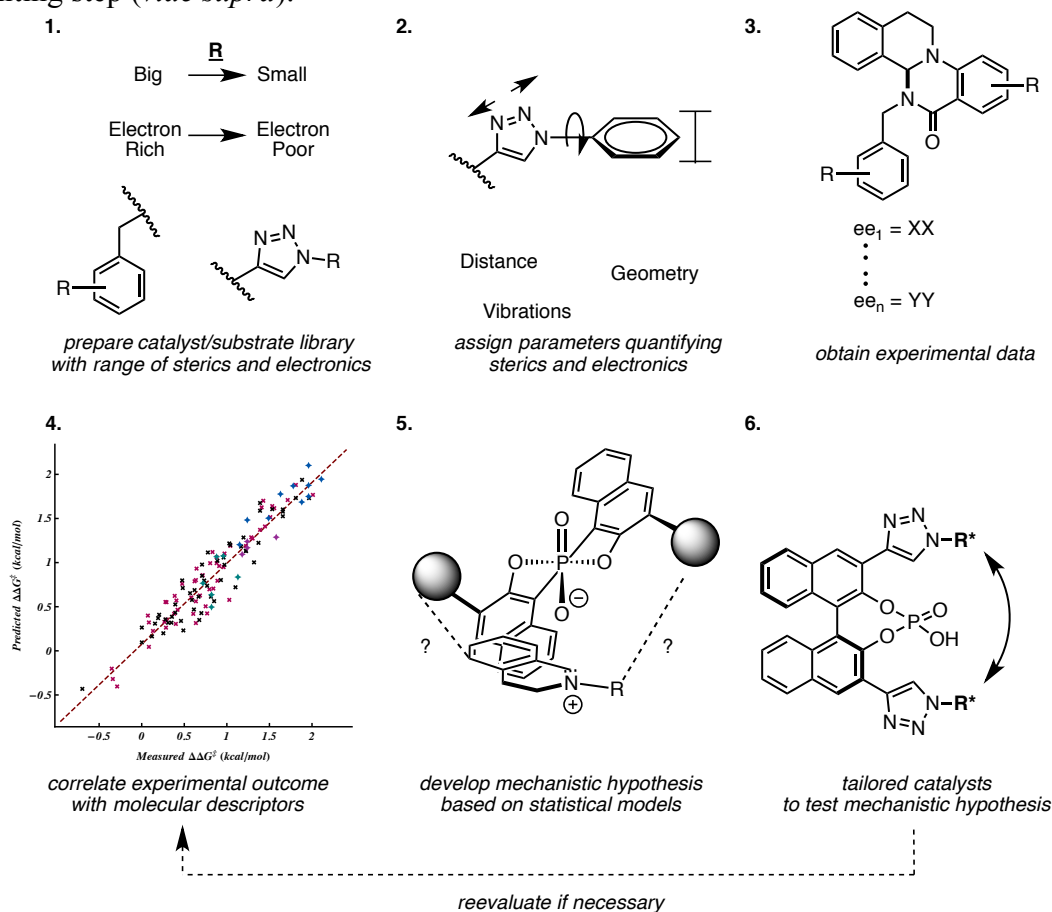


Figure 3.12. Outline of strategy for studying origin of enantioselectivity

Library Design and Parameter Selection

Although we had already obtained certain data that demonstrated the subtle interplay between substrate and catalyst structure (e.g. Figure 3.2),¹ we decided to take a more systematic approach to data collection with the aim of obtaining the largest range of enantioselectivities possible. To this end, a library of twelve N-benzyl substrates was prepared, five from our previous study (3.1a-e) and seven new examples (3.1f-l). The members of this library were designed to cover sufficient steric and electronic space at positions noted to affect selectivity. Using σ_m and B_1 as proxies for electronic and steric effects respectively, substrates 3.1 were varied at the N-

benzyl 4- (Me, OMe, NO₂), and 2- (OMe, Me, Br, *i*-Pr, 2,6-(Me)₂) positions and the distal aniline 4-position (Ph, Br, *i*-Pr). Similarly, nine N-aryl triazolyl catalysts (**3.4**) were prepared that included members with 2,4,6- (Me, *i*-Pr, Cy), 4-(H, OMe, NEt₂, SO₂Me), and 2,6- (OMe, F) substitution patterns. Adamantyl-substituted catalysts **3.4e**, *pyr*-**3.4**, and *imid*-**3.4** were also included to allow for exploration of the nitrogen deletion results from Chapter 2 (*vide infra*).

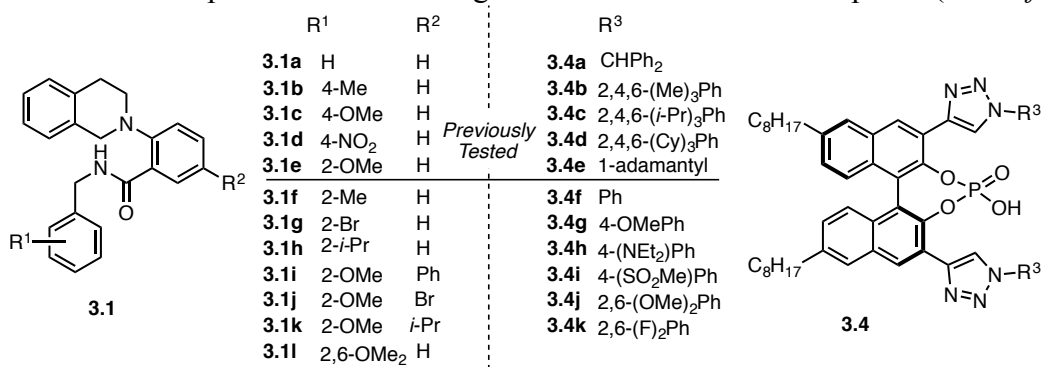


Figure 3.13. Substrate and catalyst libraries used for modeling

Simultaneously, a diverse array of molecular descriptors was collected to describe the structural features of each catalyst and substrate, including Sterimol parameters (B₁, B₅, L), distance measurements from geometry optimized structures, and computationally-derived vibrational frequencies and intensities (*vide supra*). For the substrates, gas phase ground state energy minimization and vibrational frequency calculation were carried out for all members of the library using density functional theory (DFT, see Experimental Section for details). Vibrational modes clearly identifiable across the whole series and deemed potentially relevant for describing structural modification were selected. The specific descriptors along with their associated ranges are displayed in Figure 3.14. As substitution on the N-benzyl and distal aniline rings (ring 3 and ring 2 respectively) had been observed to influence selectivity, three vibrational modes primarily centered on these rings were selected, along with Sterimol values. Additionally, vibrational modes involving the C-H, N-H, amide bond, and C=O moieties were chosen as potential descriptors. Finally, Sterimol values across the entire substrate, along with apparent charge on the amide nitrogen atom and the distance between the amide nitrogen and tetrahydroisoquinoline C-H were tabulated. In total, thirty-three descriptors were collected for the substrate library.

Given the computational cost required for the complete catalyst structures, vibrational frequency and intensity calculations were conducted on truncated triazole rings anchored with a bromine atom at the C4 position (Figure 3.15). As the triazole moiety is the major feature of each catalyst modulated throughout the library, and considering that the trends from one catalyst to the next were more important than the absolute value of any one structure, this choice was deemed acceptable. Full geometry optimized structures of catalysts were employed for the measurements of various distances. The full set of molecular descriptors used for catalyst modeling is presented in Figure 3.15, along with their respective ranges. Seven vibrational modes centered on the triazole ring were deemed potentially relevant along with one describing the attached aryl ring. Two example vibrational modes (ν_{N-NI} and ν_{RingD}) for catalyst **3.4f** are shown in Figure 3.16. Sterimol values were also selected. Finally, the distances between various atoms in the complete catalyst scaffold were measured. Twenty-two parameters were collected overall to define the catalyst structure.

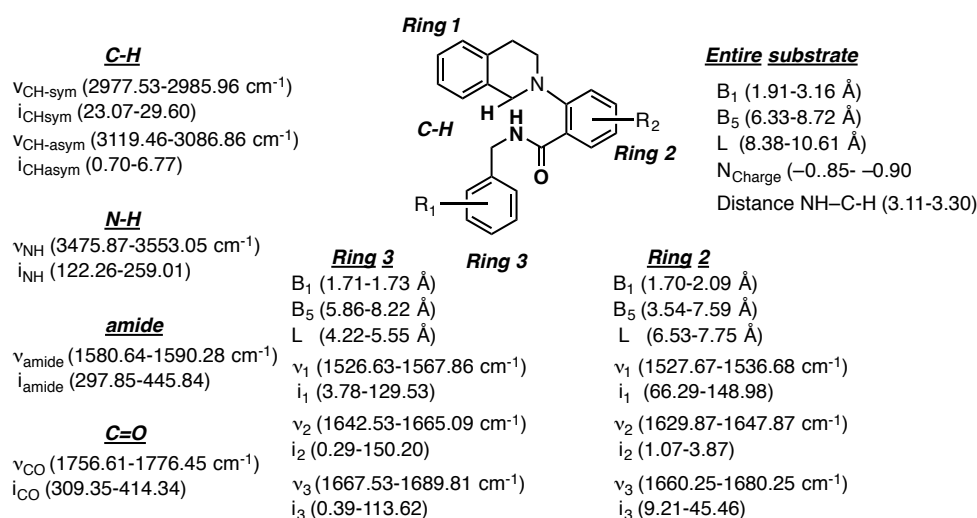


Figure 3.14. Substrate molecular descriptors used for modeling

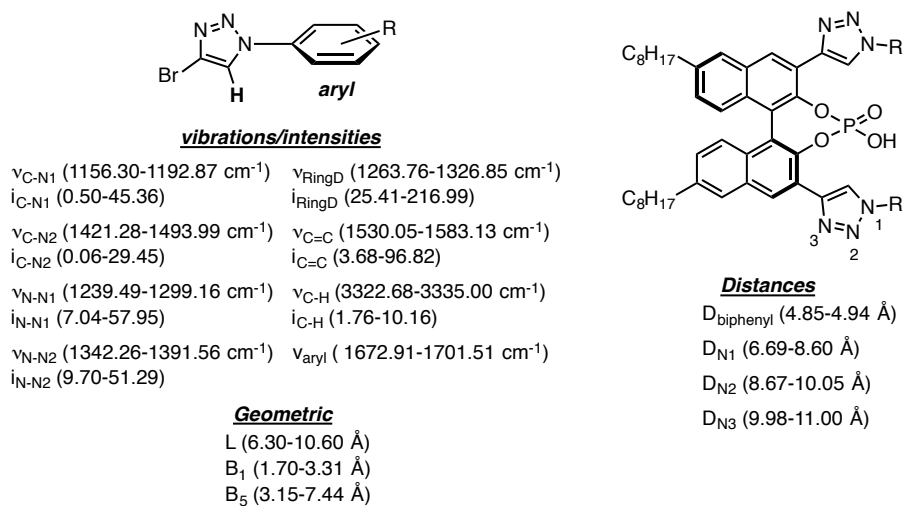


Figure 3.15. Catalyst molecular descriptors used for modeling

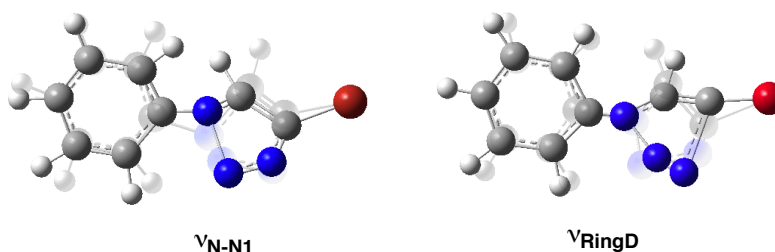
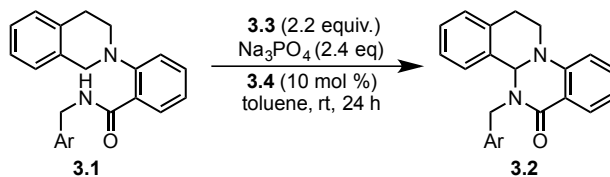


Figure 3.16. Example catalyst vibrational frequencies

Having prepared the appropriate libraries and parameterized them accordingly, the enantioselectivity of each substrate (**3.1a-l**) and catalyst (**3.4a-k**) combination was determined in duplicate using the conditions outlined in Scheme 1. Additionally, *pyr-3.4e* was tested in

combination with **3.1a-c**, **3.1e**, and **3.1i-k** for a total of 278 independent measurements of enantioselectivity (see Experimental Section for a complete summary of these experiments), spanning a range of -54 to 94 % ee (2.8 kcal/mol). With these values in hand, different subsets of the data were analyzed with the goal of producing correlations that would elucidate the TS interactions governing asymmetric induction.

Scheme 1. Reaction conditions used for data collection



Modeling Catalyst Heterocyclic Rings

One of the more intriguing observations presented in Chapter 2 was that isosteric pyrazolyl and imidazolyl catalysts *pyr-3.4e* and *imid-3.4e* respectively afforded **3.2** with significantly diminished enantiomeric excess relative to their triazolyl counterpart (**3.4e**, Figure 3.17). This result suggested that the selectivity improvement afforded by the triazolyl catalysts was likely due to an interaction other than hydrogen bonding (e.g. π - π , cation/anion- π , etc) as originally hypothesized. Given the clear importance of the catalyst heterocyclic ring in enantioselectivity determination, we initially sought to understand this subset of results obtained using catalysts **3.4e**, *pyr-3.4e*, and *imid-3.4e*.

Accordingly, using linear regression techniques, the correlation depicted in Figure 3.18 was identified from a training set of ten different substrate-catalyst combinations (Figure. 3.18, black diamonds and Table 3.2, unhighlighted entries). Of the large number of steric and vibrational terms initially investigated as molecular descriptors, four discrete vibrational parameters were sufficient to produce a correlation with enantioselectivity: one catalyst descriptor (ν_{Y-N} , a stretching frequency on the heterocyclic ring), and two substrate descriptors (the stretching frequency of the amide C=O bond, $\nu_{C=O}$, and stretching frequency/intensity of the C-H bond undergoing oxidation, ν/i_{C-H} , Figure. 3.18). A cross-term between the catalyst and substrate descriptors improves the overall quality of the model ($\nu_{Y-N} \times i_{C-H}$), suggesting a synergistic structural effect. The model was evaluated by plotting measured *vs.* predicted $\Delta\Delta G^\ddagger$ values, and as a validation of its robustness, the enantioselectivities of ten catalyst-substrate combinations not included in the training set were well-predicted (Figure. 3.18 red diamonds, and Table 3.2, highlighted entries). A slope approaching unity and intercept approaching zero over the training and validation sets indicate an accurate and predictive model, while the R^2 value of 0.89 demonstrates a high degree of precision. The largest coefficient in this normalized model belongs to the heterocyclic ring vibrational frequency (0.40 ν_{Y-N}), signifying its substantial role in the quantification of enantioselectivity.

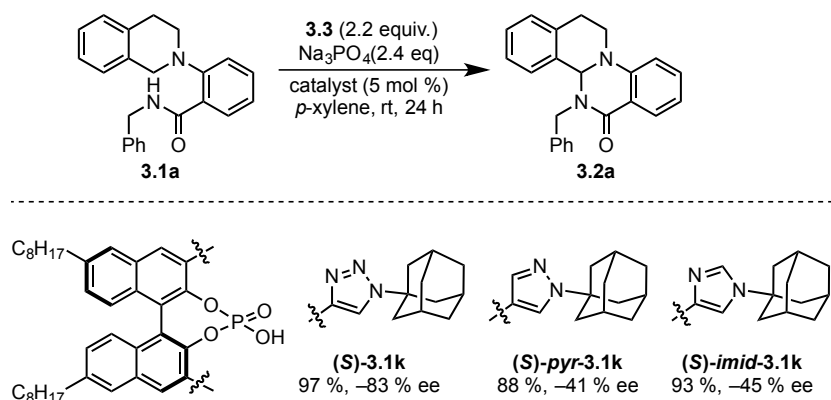


Figure 3.17. Nitrogen deletion experiments

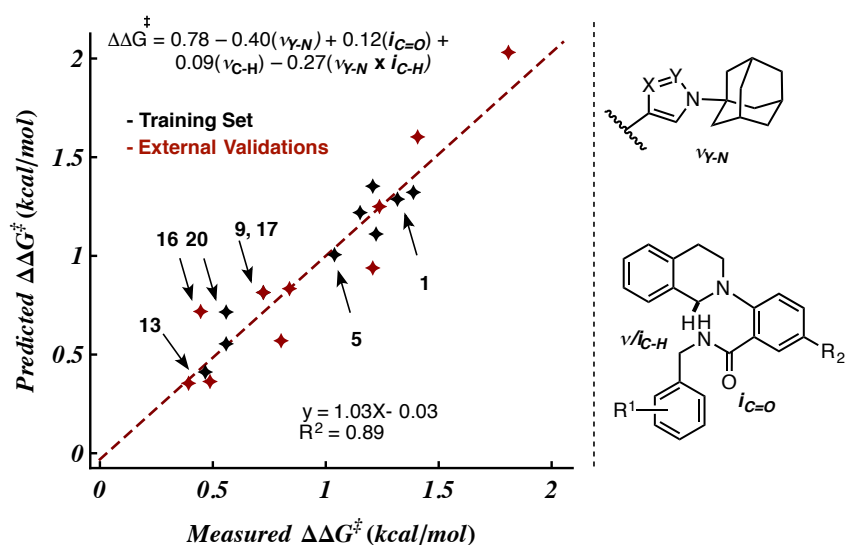


Figure 3.18. Mathematical correlation of normalized catalyst and substrate vibrational parameters to enantioselectivity and associated measured vs. predicted $\Delta\Delta G^\ddagger$ plot.

This model was capable of predicting results whose origins are not obvious upon inspection. For example, comparison of the reaction outcomes employing **3.4e** and *pyr-3.4e* with substrate **3.1a** (Table 3.2, entries 1 vs 13, Figure 3.18) may lead to the conclusion that *pyr-3.4e* generally affords inferior selectivity. Indeed, experimental results for several additional substrates supported this notion, and were accurately predicted by the model (e.g., 2-OMe benzyl substrate **3.1e**, entries 5 vs 16). However, with substrate **3.1i** ($R_1 = 2\text{-OMe}$, $R_2 = \text{Ph}$, entries 9 vs 17), the triazolyl and pyrazolyl PAs afforded the product with similar levels of enantioselectivity. This counterintuitive result was precisely predicted, indicating that the divergent enantioselectivity displayed by **3.4e**, compared to *pyr-3.4e* and *imid-3.4e*, was adequately addressed by the model.

The correlation in Figure 3.18 served as a proof of concept, establishing the capacity of the chosen parameters to describe subtle aspects of this system. However, the ultimate goal of this approach was to discern underlying mechanistic phenomena. This objective could not be achieved using merely the above correlation, as it was produced using a small subset of data, in which the catalyst heterocyclic rings bore the same substituent (i.e. adamantyl). We hypothesized that the complete dataset contained invaluable information to this end, as it was produced using

strategically modified catalysts and substrates with substituents intentionally introduced to probe subtle effects. In accordance with a data-intensive strategy, none of the measured enantioselectivity values (139 catalyst-substrate combinations) was discarded, because even low enantioselectivity carried information regarding the catalyst-substrate interactions at the origin of asymmetric induction.

Table 3.2. Predicted and measured enantioselectivities for adamantyl-substituted catalysts

entry	substrate	catalyst		predicted %ee ($\Delta\Delta G^\ddagger$) ^a	measured %ee ($\Delta\Delta G^\ddagger$)	
		R ¹	R ²			
1	3.1a	H	H	3.4e	79 (1.27)	81 (1.32)
2	3.1b	4-Me	H	3.4e	78 (1.23)	78 (1.24)
3	3.1c	4-OMe	H	3.4e	73 (1.10)	78 (1.22)
4	3.1d	4-NO ₂	H	3.4e	77 (1.20)	75 (1.15)
5	3.1e	2-OMe	H	3.4e	68 (0.99)	70 (1.04)
6	3.1f	2-Me	H	3.4e	94 (2.02)	91 (1.81)
7	3.1g	2-Br	H	3.4e	80 (1.31)	83 (1.39)
8	3.1h	2- <i>i</i> Pr	H	3.4e	87 (1.59)	83 (1.41)
9	3.1i	2-OMe	Ph	3.4e	59 (0.80)	55 (0.72)
10	3.1j	2-OMe	Br	3.4e	60 (0.82)	61 (0.84)
11	3.1k	2-OMe	<i>i</i> -Pr	3.4e	65 (0.92)	77 (1.21)
12	3.1l	2,6-(OMe) ₂	H	3.4e	82 (1.34)	77 (1.21)
13	3.1a	H	H	pyr-3.4e	32 (0.40)	37 (0.47)
14	3.1b	4-Me	H	pyr-3.4e	28 (0.34)	32 (0.39)
15	3.1c	4-OMe	H	pyr-3.4e	29 (0.35)	39 (0.49)
16	3.1e	2-OMe	H	pyr-3.4e	53 (0.70)	36 (0.45)
17	3.1i	2-OMe	Ph	pyr-3.4e	59 (0.80)	55 (0.72)
18	3.1j	2-OMe	Br	pyr-3.4e	43 (0.54)	44 (0.56)
19	3.1k	2-OMe	<i>i</i> -Pr	pyr-3.4e	44 (0.55)	59 (0.80)
20	3.1a	H	H	imid-3.4e	53 (0.70)	44 (0.56)

^a $\Delta\Delta G^\ddagger$ in kcal/mol

Modeling of individual substrates and catalysts

Prior to producing a global, predictive model for the full dataset, we considered that a series of focused correlations, coupled with an evaluation of overall trends, might serve to reveal fundamental features of the system. To this end, for each individual substrate (**3.1a-l**), a model was produced relating its observed enantioselectivity values for the entire set of catalysts with parameters describing the catalyst structure (12 models in total, see Experimental Section for complete summary). The same strategy was applied to all aryl-substituted triazole catalysts (**3.4b-d**, **3.4f-k**) using parameters describing the substrate structure (9 models total, see Experimental Section for complete summary). This organizational scheme was viewed as a means to facilitate the identification of catalyst features that were important for particular substrate types and vice versa. An example is shown in Figure 3.19 for substrate **3.1f**.

The model in Figure 3.19 demonstrates that the range of ee values obtained for **3.1f** (23-93 % ee) across the entire library of catalysts could be modeled using only two triazole vibrational parameters (ν_{N-N1} , ν_{RingD}) and a cross term between them. Notably, every substrate of this type (i.e. 2-substituted benzyl, **3.1a**, **3.1e-k**) could be modeled using these same molecular descriptors (Figure 3.20). Substrates substituted at the benzylic 4-positions (**3.1b-d**) required significantly more complex models (Figure 3.20, *vide infra*). Although we felt that a crucial aspect of the system was captured by these individual models, the mechanistic interpretation of

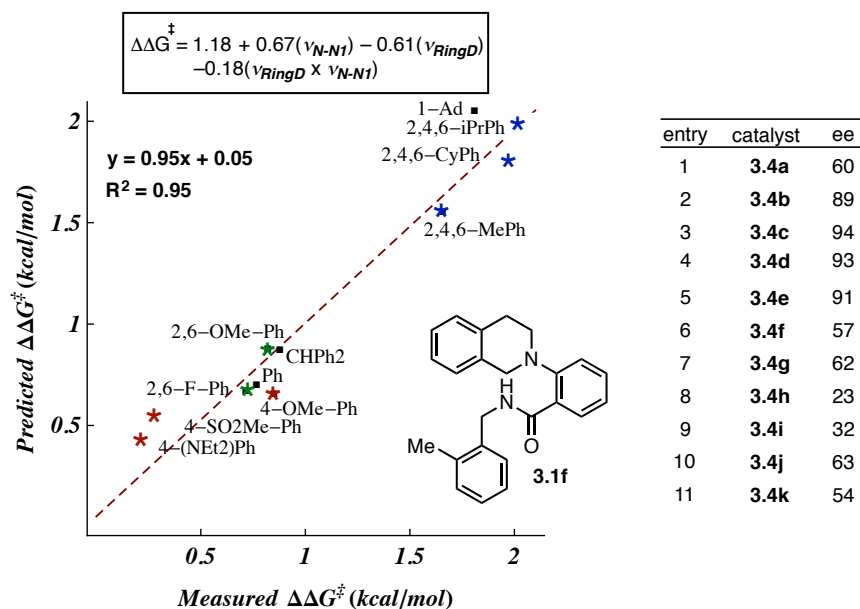


Figure 3.19. Example mathematical correlation of catalyst vibrational parameters to enantioselectivity for a single substrate with 11 catalysts and associated predicted vs. measured $\Delta\Delta G^\ddagger$ plot.

the molecular descriptors required (in particular v_{N-N1} and v_{RingD}) remained challenging at this juncture. To assist in this process, we sought a visualization scheme that would allow for the inspection of all of the data simultaneously.

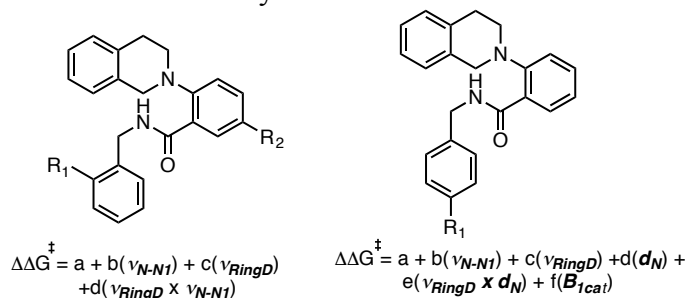


Figure 3.20. General form of initial substrate models

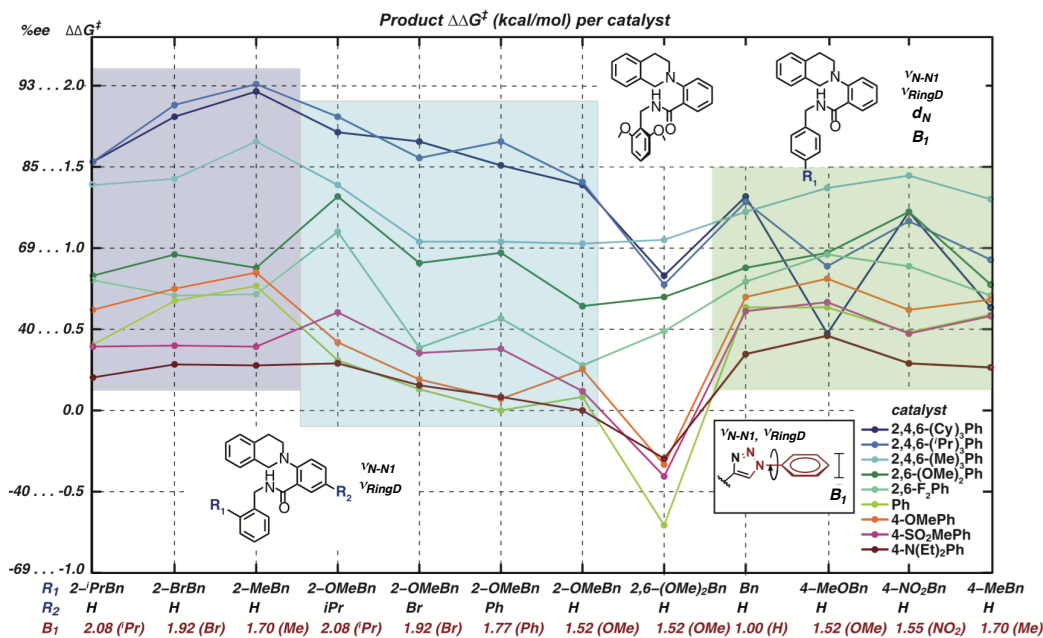


Figure 3.21. Graphical representation of catalyst structure-selectivity trends as a function of substrate.

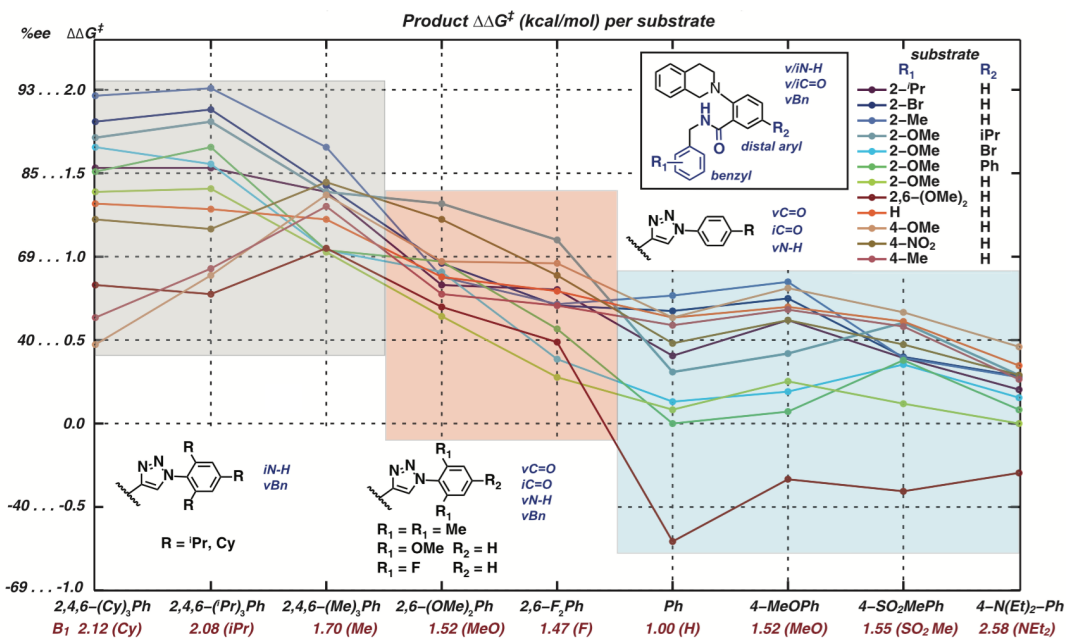


Figure 3.22. Graphical representation of substrate structure-selectivity trends as a function of catalyst.

Trend Analysis

We elected to present the information gained from the aforementioned individual models alongside multiple observed enantioselectivity results, organized according to trends in catalyst or substrate structural features. Demonstrating this visualization technique, the enantioselectivity trend for each catalyst (Figure 3.21, each line represents a catalyst) was plotted as a function of the substrates (each x axis tick-line represents a substrate), and vice versa (Figure 3.22). The plots were arranged according to which positions were modified on the catalyst or substrate structures, and the corresponding substituent's Sterimol B_1 value. For example, in the purple frame in Figure 3.21, 2-substituted benzyl substrates are displayed from the largest to smallest substituent. The catalyst molecular descriptors required for correlating each subset of substrates are also depicted (Figure 3.21), along with the substrate descriptors for each subset of catalysts (Figure 3.22). For example, the catalyst molecular descriptors used as parameters for the correlation of enantioselectivity obtained for 2-substituted benzyl substrates are presented below the blue frame in Figure 3.21 (ν_{N-N} , ν_{RingD}).

Analysis of this systematic data arrangement suggested that the reaction was mainly under catalyst control as catalyst features affected enantioselectivity in a more considerable and systematic manner (Figure 3.22), while, for each substrate, the spread of observed enantioselectivity was broader (Figure 3.21). Additionally, it appeared that catalyst performance correlated with the aryl substitution pattern in the order 2,4,6 > 2,6 > 4 (Figure 3.22, grey, orange, and blue frames, respectively). This latter feature in particular suggested that perhaps the torsion angle between the triazole and its attached aryl ring might be influencing selectivity, as this metric is expected to be greater (i.e. closer to 90°) for 2,6-disubstituted aryl groups than their 4-substituted analogues. We thus hypothesized that the triazole vibrational modes previously noted to be good predictors of enantioselectivity (ν_{N-N} , ν_{RingD} , Figure 3.20), might be related to this angle.

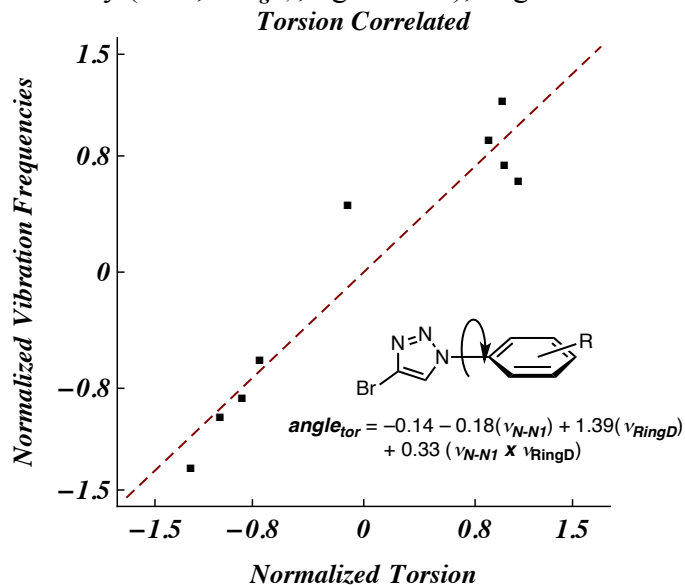
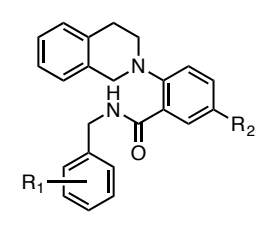


Figure 3.23. Mathematical correlation of torsion angle to catalyst vibrational frequencies

Indeed, testing this hypothesis revealed an excellent correlation between torsion angle and the triazole vibrational modes ($R^2 = 0.91$, Figure 3.23). The torsion angle represents a steric effect, yet also contains information concerning the conjugation between the triazole ring and its substituent. The vibrational frequency can serve as a correction to both of these effects, as it takes

into account non-additive features of the substituents' charge and mass distribution. Reevaluation of the previously-developed substrate models (e.g. Figure 3.19) revealed that inclusion of torsion angle as a parameter led to significantly simplified models across the entire substrate library. These new models are summarized in Table 3.3. Specifically, the enantioselectivities of all substrates with 2-substituted benzyl groups could be modeled using only two parameters (ν_{N-N1} and \angle_{tor}) whereas their 4-substituted counterparts (**3.1b** and **3.1c**) were effectively described by these same two descriptors in addition to a Sterimol B_1 term.

Table 3.3. Summary of simplified substrate models using torsion angle as a parameter



‡
 $\Delta\Delta G = a + b(\nu_{N-N1}) + c(\angle_{tor}) + d(B_1)$

Substrate	R ₁	R ₂	coefficient			goodness-of-fit
			ν_{N-N1}	\angle_{tor}	B_1	
3.1a	H	H	0.11	-0.25	0	R ² = 0.90
3.1b	4-Me-Bn	H	0.18	-0.27	-0.27	R ² = 0.80
3.1c	4-OMe-Bn	H	0.12	-0.28	-0.33	R ² = 0.80
3.1d	4-NO ₂ -Bn	H	0	-0.39	0	R ² = 0.88
3.1e	2-OMe-Bn	H	0.21	-0.43	0	R ² = 0.96
3.1i	2-OMe-Bn	Ph	0.10	-0.56	0	R ² = 0.92
3.1j	2-OMe-Bn	Br	0.16	-0.49	0	R ² = 0.90
3.1k	2-OMe-Bn	<i>i</i> -Pr	0.05	-0.56	0	R ² = 0.95
3.1f	2-Me-Bn	H	0.36	-0.42	0	R ² = 0.96
3.1g	2-Br-Bn	H	0.27	-0.42	0	R ² = 0.95
3.1h	2- <i>i</i> -Pr-Bn	H	0.20	-0.40	0	R ² = 0.96
3.1l	2,6-(OMe) ₂ -Bn	H	0.03	-0.63	0	R ² = 0.91

Similar interactions with the triazole ring should still be present for these 4-benzyl substrates, but the presence of a B_1 term suggested an additional steric interaction between the substrate and catalyst substituents, avoided in the case where hydrogen occupied the 4-benzyl position. This claim is supported by the lower enantioselectivities observed for substrates with larger 4-benzyl substituents, especially using catalysts with larger 2,6-groups. Thus, the lack of the catalyst B_1 term in the models describing 2- relative to 4-benzyl substrates, and their overall higher enantioselectivities, were thought to arise from a better accommodation of the former substrates' shapes in the catalyst active site (*vide infra*).

Trend Interpretation

Based on the following observations, we propose that a π interaction^{26–32} is established between the catalyst triazole and substrate benzyl rings at the enantiodetermining TS, the strength of which is modulated by local steric and electronic features of both interacting partners: 1) catalyst heterocycle identity was experimentally shown to be intimately involved in asymmetric induction due to interactions beyond hydrogen bonding (Figures 3.17 and 3.18), 2) catalysts with 2,6-disubstituted aryl groups generally afforded the products in higher enantiomeric excess than their 4-substituted counterparts, and 3) the torsion angle between the catalyst triazole and its aryl substituent had the largest coefficient of any molecular descriptor employed during model development (Figure 3.23 and Table 3.3).

For a given pair of molecules undergoing a “ π -stacking” interaction with an optimum geometry, the energetic stabilization becomes greater with the introduction of a heteroatom into one of the partners.^{29,31,33} Although the presence of a heteroatom in a π -system reduces the system's polarizability, and thus its ability to benefit from dispersion interactions, the reduced

spatial extent of the π -electron cloud leads to diminished repulsion with the other ring, overcompensating for the former effect.³³ Furthermore, the introduction of a permanent dipole upon inclusion of a heteroatom results in increased dipole-induced dipole interactions with the unsubstituted partner. Consequently, for π -interactions with a large electrostatic component (such as those involving heteroatom-substituted partners), the relative orientation between two interacting partners can be significant, with even minor perturbations (e.g. a change in the dipole moment of one or both partners) resulting in a significant loss in stabilization.^{33,34} Collectively, the variations in enantioselectivity as a function of catalyst heterocycle identity are consistent with this view of the nature of π -interactions.

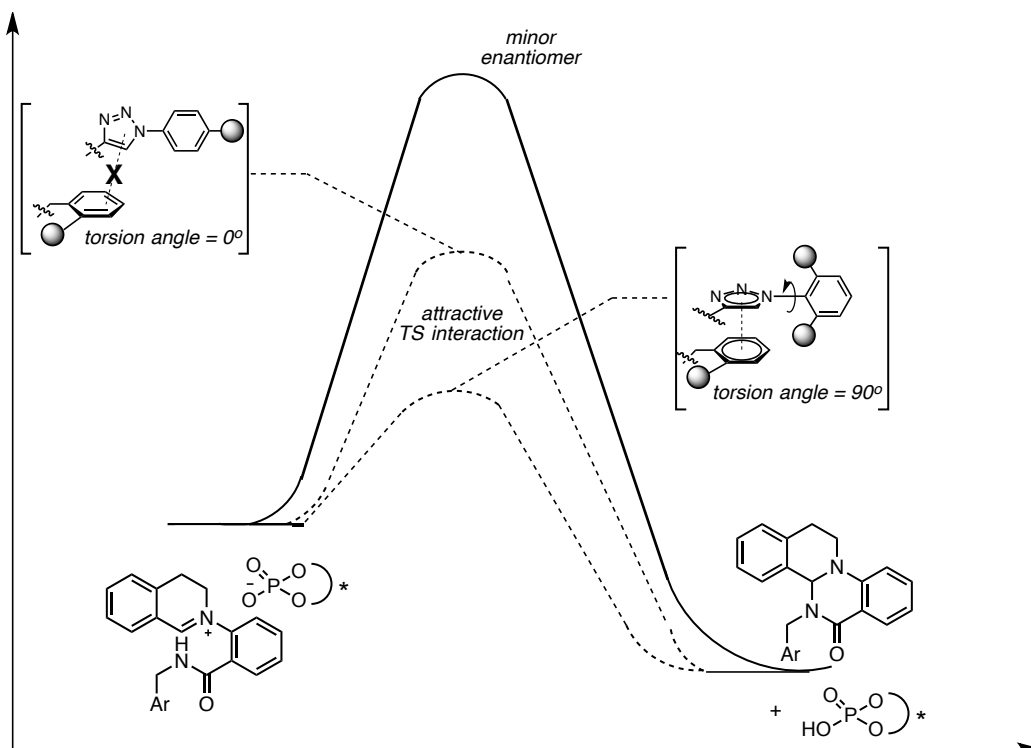


Figure 3.24. Qualitative depiction of data interpretation

We believe that the torsion angle between triazole and its substituent reflects the orientation at which the triazole can engage the substrate at the enantiodetermining TS. In cases in which the catalyst triazole is favorably positioned to engage the nucleophilic substrate benzyl group during the enantiodetermining nucleophilic addition, a lower energy pathway becomes available (Figure 3.24), which is absent for the diastereomeric TS lacking this stabilizing interaction. This view is consistent with a mechanistic picture in which attractive, noncovalent interactions stabilize one diastereomeric TS, as opposed to the more commonly proposed situation in which steric repulsion selectively disfavors one pathway. Rigorous kinetics experiments to support or refute this hypothesis were precluded for these reactions given their heterogeneity, which was a prerequisite for the desired reactivity, and due to the fact that the selectivity-determining step occurred after the rate-limiting step (presumably oxidant dissolution, see Figure 3.1 and Chapter 2).

Based on our results, the most favorable TS triazole orientation appeared to be predicted for catalysts with torsion angles closer to 90° (i.e. 2,6-disubstituted: Ar = -2,4,6-(Me) (**3.4b**),

2,4,6-*(i*-Pr)₃ (**3.4c**), 2,4,6-(Cy)₃ (**3.4d**), 2,6-(F)₂ (**3.4k**) and 2,6-(OMe)₂ (**3.4j**) which led to higher observed enantioselectivities (Figure 3.22, grey and orange frames). In contrast, catalysts with reduced torsion angles (Ar = Ph (**3.4f**), 4-(NEt₂)-Ph (**3.4h**), 4-(OMe)-Ph (**3.4g**), and 4-(SO₂Me)-Ph (**3.4i**)) that did not introduce the proposed directional and steric effects, led to diminished enantioselectivities overall (Figure 3.21, blue frame). Correspondingly, substrates with elongated 4-substituents (R = Me (**3.1b**) and OMe (**3.1c**)) led to lower enantioselectivities using catalysts with large substituents at the 2,6-position (Figure 3.21, green frame, blue lines). For these substrates, the steric repulsion exerted by the large catalyst 2,6-substituents precluded the putative stabilizing TS π interaction, resulting in diminished enantioselectivities. This additional steric interaction for 4-substituted substrates was reflected in the more complex models initially required to describe them (Figure 3.20), as well as the presence of a Sterimol B₁ term in their revised models (Table 3.3).

Comprehensive Model and Probes of Mechanistic Hypotheses

Based on these hypotheses, we set out to design a series of new catalysts to specifically probe the putative interactions. To facilitate catalyst development, a predictive model (Figure 3.25) was generated for the entire substrate set with the aryl-substituted catalysts (**3.4b-d** and **3.4f-k**). This model contains 108 combinations (9 catalysts times 12 substrates) from the initial library of experiments, where half were used as a training set (Figure 3.25, black squares) and the other half as external validations (red crosses). New catalysts were proposed to address hypotheses raised by the focused models and trend analysis, and their enantioselectivities were predicted prior to synthesis by the comprehensive model (Figure 3.25).

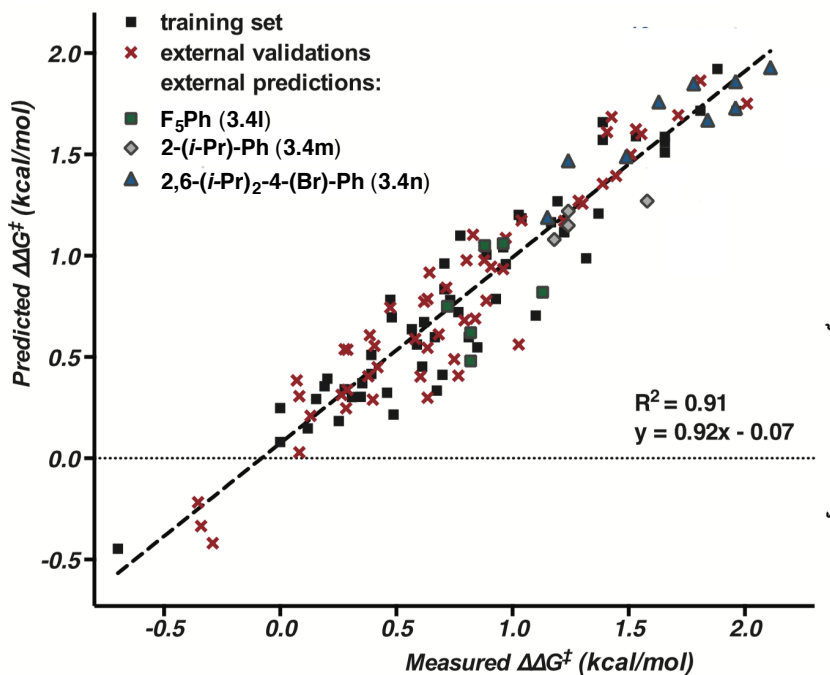
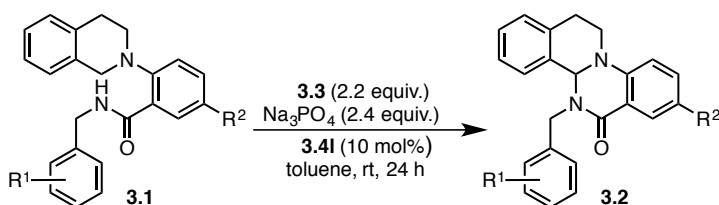


Figure 3.25. Predicted vs. measured $\Delta\Delta G^\ddagger$ plot for normalized global model relating enantioselectivity to both catalyst and substrate structural features.

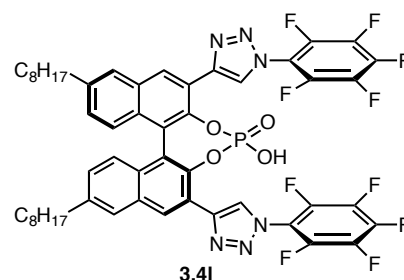
First, to probe whether the aryl substituent on the triazole ring played a primarily steric role, rather than directly engaging the substrate in a π interaction, perfluorophenyl catalyst **3.4l**

was designed and evaluated. Substituent local sterics and charge distribution have been shown to strongly affect π interactions.^{28,29,35–42} Therefore, we expected that if enantioselectivity were predominantly dependent on the aryl substituent directly engaging as a partner in a π interaction (as opposed to taking an ancillary role in π interactions involving the triazole), perfluorophenyl catalyst **3.4i** would deviate significantly from its 2,6-(F)₂-Ph (**3.4k**) or 2,6-(MeO)₂-Ph (**3.4j**) counterparts. However, all three catalysts behaved similarly with respect to the magnitude and sign of enantioselectivity (entries 1-9, Table 3.4). This result was well predicted by the model (Figure 3.25) and is consistent with the hypothesis that the main function of the aryl substituent is steric.

Table 3.4. Hypothesis-driven external validation using catalyst **3.4i**



entry	catalyst Ar	substrate R ₁ R ₂	predicted %ee ($\Delta\Delta G^\ddagger$)	measured %ee ($\Delta\Delta G^\ddagger$)
1	F ₅ Ph (3.4i)	3.1a 4-H H	60 (0.82)	74 (1.13)
2	F ₅ Ph (3.4i)	3.1b 4-Me H	72 (1.06)	67 (0.96)
3	F ₅ Ph (3.4i)	3.1i 2-OMe Ph	56 (0.75)	54 (0.72)
4	2,6-F ₂ Ph (3.4k)	3.1a 4-H H	52 (0.68)	58 (0.79)
5	2,6-F ₂ Ph (3.4k)	3.1b 4-Me H	66 (0.96)	54 (0.71)
6	2,6-F ₂ Ph (3.4k)	3.1i 2-OMe Ph	50 (0.64)	44 (0.57)
7	2,6-MeO ₂ Ph (3.4j)	3.1a 4-H H	68 (0.98)	63 (0.88)
8	2,6-MeO ₂ Ph (3.4j)	3.1b 4-Me H	73 (1.10)	58 (0.78)
9	2,6-MeO ₂ Ph (3.4j)	3.1i 2-OMe Ph	67 (0.96)	67 (0.97)

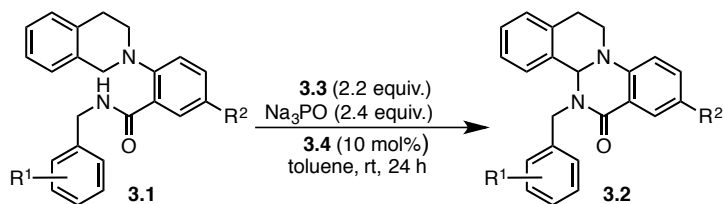


Next, catalyst **3.4m**, bearing a single isopropyl group at the 2-position of the triazole aryl substituent was prepared to probe the hypothesis that steric repulsion existed between larger catalyst 2,6-substituents and elongated substrate 4-substituents. We anticipated that an isopropyl group would induce the torsion necessary to enforce the proposed benzyl-triazole π interaction, while avoiding a direct steric interaction between the substrate benzyl 4-position and the catalyst aryl 2,6-substituents. Indeed, for all 4-substituted substrates tested (entries 1-3, Table 3.5), **3.4m** provided the corresponding product in higher enantioselectivity than **3.4c**, which bears isopropyl groups at both *ortho* positions of the triazole aryl substituent (entries 4-6, Table 3.5). For 4-NO₂-Bn substrate **3.1d**, the 2-*i*Pr catalyst **3.4m** resulted in the highest enantioselectivity observed to date (entry 3, Table 3.5), as predicted by the model.

Finally, in order to evaluate the capacity to obtain improved enantioselectivity as a result of a data-intensive approach, and the hypothesis that torsion led to enhanced enantioselectivity for the 2-substituted substrates, several proposed catalysts were evaluated using the model in Figure 3.25. Catalyst **3.4n** was selected as it is synthetically feasible, accommodates a torsion angle close to 90°, and was predicted to give improved enantioselectivity for all substrates bearing hydrogen at the 4-benzyl position. This prediction was verified in practice for all eight substrates evaluated, affording the highest enantioselectivities observed to date (Table 3.6, entries 1-8). These results support the claim that the orientation of the triazole ring coupled with its R group's steric

constraints can be strategically manipulated to fine tune the noncovalent interactions underlying enantioselectivity

Table 3.5. Hypothesis-driven external validation using catalyst **3.4m**



entry	catalyst		substrate		predicted %ee ($\Delta\Delta G^\ddagger$)	measured %ee ($\Delta\Delta G^\ddagger$)
	Ar		R ₁	R ₂		
1	2- <i>i</i> PrPh (3.4m)		3.1b 4-Me	H	77 (1.22)	78 (1.24)
2	2- <i>i</i> PrPh (3.4m)		3.1c 4-OMe	H	75 (1.15)	78 (1.24)
3	2- <i>i</i> PrPh (3.4m)		3.1d 4-NO ₂	H	79 (1.27)	87 (1.58)
4	2,4,6- <i>i</i> Pr ₃ Ph (3.4c)		3.1b 4-Me	H	58 (0.79)	66 (0.93)
5	2,4,6- <i>i</i> Pr ₃ Ph (3.4c)		3.1c 4-OMe	H	58 (0.78)	63 (0.89)
6	2,4,6- <i>i</i> Pr ₃ Ph (3.4c)		3.1d 4-NO ₂	H	76 (1.17)	76 (1.17)

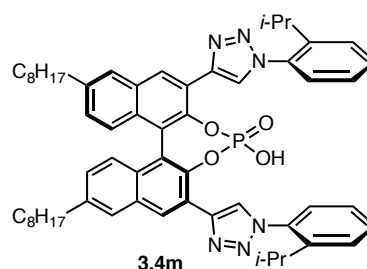
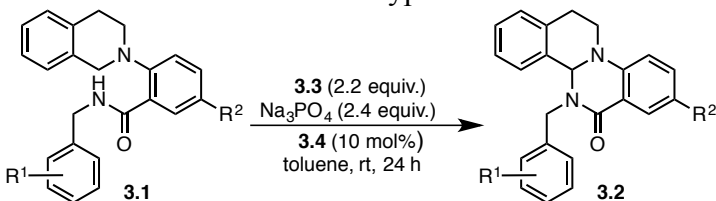
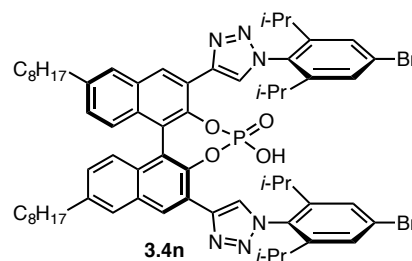


Table 3.6. Hypothesis-driven external validation using catalyst **3.4n**



entry	catalyst		substrate		predicted %ee ($\Delta\Delta G^\ddagger$)	measured %ee ($\Delta\Delta G^\ddagger$)
	Ar		R ₁	R ₂		
1	2,6- <i>i</i> Pr ₂ -4-BrPh (3.4n)		3.1a 4-H	H	85 (1.49)	85 (1.49)
2	2,6- <i>i</i> Pr ₂ -4-BrPh (3.4n)		3.1e 2-OMe	H	90 (1.76)	88 (1.63)
3	2,6- <i>i</i> Pr ₂ -4-BrPh (3.4n)		3.1f 2-Me	H	93 (1.93)	95 (2.11)
4	2,6- <i>i</i> Pr ₂ -4-BrPh (3.4n)		3.1g 2-Br	H	94 (2.09)	93 (1.96)
5	2,6- <i>i</i> Pr ₂ -4-BrPh (3.4n)		3.1h 2- <i>i</i> Pr	H	92 (1.86)	93 (1.96)
6	2,6- <i>i</i> Pr ₂ -4-BrPh (3.4n)		3.1j 2-MeO	Br	90 (1.73)	93 (1.96)
7	2,6- <i>i</i> Pr ₂ -4-BrPh (3.4n)		3.1k 2-MeO	<i>i</i> Pr	92 (1.85)	91 (1.78)
8	2,6- <i>i</i> Pr ₂ -4-BrPh (3.4n)		3.1k 2-MeO	Ph	89 (1.67)	92 (1.84)



Conclusion

The information presented in this chapter demonstrates the complementary manner in which classical physical organic techniques and modern data analysis strategies can be merged toward a more complete mechanistic assessment. This approach is based on the use of empirical data, which is often a prerequisite for a rational reaction optimization process, to concomitantly conduct a mechanistic investigation. Information of this sort that could be used for an in-depth analysis is often omitted from reports in the field of catalysis, as only results leading to the desired outcomes are generally presented and pursued. Yet, as high-throughput, automated methods for reaction development are now common,^{43–49} data analysis strategies could be applied in parallel to optimization procedures, allowing for simultaneous mechanistic and structural analysis.

Creatively collecting and organizing data to examine proposed hypotheses affords improved generalizations, particularly as datasets become larger and more complex. This idea holds true for the analysis of reaction trends by parameters that reflect structural modification. Indeed, the focused catalyst and substrate models, and their organization according to fundamental, quantitative, physical organic trends, provided non-intuitive insights regarding interactions involved in enantioselectivity determination. Although this approach is general for the prediction and study of chemical reaction outcomes, its application to the triazolyl-PA catalyzed CDC reaction reported herein represents a particularly challenging case because it employs weak, non-covalent interactions for the induction of enantioselectivity. These interactions are typically in the energy range required to distinguish a highly enantioselective reaction from its racemic counterpart (2-3 kcal/mol), providing seemingly endless approaches to rational catalyst design. However, controlling non-covalent interactions represents a notable challenge in the design of catalytic systems due to multiple energetically accessible orientations. Complemented with rigorous experimental analysis, the disclosed data-intensive approach is suited to addressing such intricacies, and holds potential for the analysis of increasingly complicated catalytic systems streamlining both reaction and catalyst development.

A necessary caveat that has not been explicitly acknowledged hitherto is that the mechanism underlying asymmetric induction need be the same for each member of the data set. If this assumption is not met, not all members of the data set are directly comparable. Addressing such situations with an eye towards generalizing the methodology presented herein will be the subject matter of Chapter 4.

Experimental Section

General Information

Unless otherwise noted, all reagents were purchased from commercial suppliers and used without further purification. Enantioselective cross-dehydrogenative coupling (CDC) reactions were run in 1 dram (15 X 45 mm) vials equipped with a screw cap and stirred using a magnetic Teflon stir bar (8 mm), placed on the surface of a magnetic stir plate. Due to the heterogeneous nature of these reactions, it was important that fast and efficient stirring be maintained over the course of the reaction in order to obtain reproducible results. Tetrahydrofuran, dichloromethane, diethyl ether, toluene, triethylamine and N,N-dimethylformamide were purified by passage through an activated alumina column under argon. Thin-layer chromatography (TLC) analysis of reaction mixtures was performed using Merck silica gel 60 F254 TLC plates, and visualized under UV or by staining with ceric ammonium molybdate or KMNO₄. Column chromatography was performed on Merck Silica Gel 60 Å, 230 X 400 mesh. Nuclear magnetic resonance (NMR) spectra were recorded using Bruker AV-600, AV-500, DRX-500, AVQ-400, and AVB-400 spectrometers. ¹H and ¹³C chemical shifts are reported in ppm downfield of tetramethylsilane and referenced to residual solvent peak (CHCl₃; δH = 7.26 ppm and δC = 77.0 ppm, DMSO; δH = 2.50 and δC = 39.5 ppm). Multiplicities are reported using the following abbreviations: s = singlet, d = doublet, t = triplet, q = quartet, app t = apparent triplet, m = multiplet, dm = doublet of multiplets, br = broad resonance. Solvent abbreviations are reported as follows: EtOAc = ethyl acetate, hex = hexanes, DCM = dichloromethane, Et₂O = diethyl ether, MeOH = methanol, THF = tetrahydrofuran, DMF = N,N-dimethylformamide, Et₃N = triethylamine. Mass spectral data were obtained from the Micro-Mass/Analytical Facility operated by the College of Chemistry, University of California, Berkeley. Enantiomeric excesses were measured on a Shimadzu VP

Series Chiral HPLC using Chiralpak IA or IC columns. The syntheses of triazolyl phosphoric acids **3.4a**, **3.4b**, **3.4c**, **3.4d**, and **3.4e**¹ have been previously reported. **Caution:** Although we have not experienced any problems during the preparation and handling of the azides reported herein, appropriate safety precautions should be taken due to the explosive nature of organic azides, including the use of a blast shield during any manipulations involving azides. All azides were synthesized from the corresponding anilines and used directly without purification.

Materials and Methods

Computations

Geometry optimizations and frequency calculations were carried out using Gaussian 09 software, Revision D.01.⁵⁰ The functional used for DFT calculation is M06-2x, which was previously benchmarked for thermodynamic and kinetic accuracy of main group elements, and for non-covalent interactions.^{51,52} A triple zeta potential basis-set (TZVP)^{53,54} was chosen based on Zhao and Truhlar's evaluation of the M06-2x functional for organic molecules, indicating that a triple zeta quality is generally more quantitative.⁵¹ As this study seeks correlations, we opted not to incorporate scaling factors for vibrational terms.⁵⁵ This simplification was justified by the assumption that a constant scaling factor would neither change the descriptive parameters identified, nor the relationship between them. Sterimol values were calculated for the geometry optimized structures using Molecular Modeling Pro[®].

Modeling

Towards probing the effects of catalyst and substrate substitution patterns on enantioselectivity, it was first necessary to define an experimental space that effectively sampled the molecular properties responsible for enantioselectivity. To this end, a library of catalysts and substrates was designed with varied steric and electronic properties at positions noted to affect enantioselectivity (Figure 3.13). The selected catalyst and substrate structures were synthetically accessible and spread a range of B_1 (the Sterimol minimal width) and Hammett σ_{para} values at each substrate and catalyst modulated position. These two parameters were proposed as straightforward design elements because B_1 describes the steric constraint proximal to the modulated aryl rings and the σ_{para} values represent a standard electronic measurement in aryl rings.

For the initially designed training and validation sets, twelve substrates were targeted with modifications at the 2 (Br, H, Me, ¹Pr) and 4 (NO₂, H, Me, OMe) positions of the benzyl ring and the 4-position (Br, Ph, H, ⁱPr) of the distal aryl ring attached to the tetrahydroisoquinoline. An eleven-membered catalyst library was similarly prepared, utilizing N-aryl triazoles with 2,6- (F, H, OMe), 4- (SO₂Me, H, OMe, NEt₂) and 2,4,6- (H, Me, ¹Pr, *c*-C₆H₁₁) substitution patterns, along with two additional substituents (CHPh₂, 1-adamantyl) previously noted to give high enantioselectivity.

Next, parameters had to be identified capable of mathematically relating these structural perturbations to enantioselectivity. Therefore, a combination of Sterimol parameters, various length measurements from geometry optimized structures, and computationally-derived vibrational frequencies and intensities were pursued as these measurements were thought to be descriptive of the structural features influencing asymmetric induction (Figures 3.14 and 3.15). For this purpose, gas-phase ground-state energy minimization and vibrational frequency calculations were carried out for all studied substrates. Any vibrational modes and length measurements clearly identifiable across the entire substrate series, and deemed relevant to describing the particular structural modifications in the dataset, were selected as possible terms for

model development. For example, vibrational frequencies and intensities involving bond forming atoms such as the amide N–H stretch or the tetrahydroisoquinoline C–H stretch, the distances between these nitrogen and carbon atoms, aryl ring stretching vibrations, the amide C=O stretch.

For measurements of relevant molecular distances, a geometry minimization was carried out over the triazolyl PA catalysts' structure not including the C₈H₁₇ side chains. Infrared vibration calculations were carried out on truncated substituted triazoles in which the binaphthyl portion, which remained structurally invariant throughout the entire catalyst series, was replaced with an anchoring bromine atom. Similar to the substrate series, vibrations deemed as potentially relevant descriptors were selected for parameterization. For example, since the triazole ring was considered crucial for the observed selectivity, vibrational parameters that describe this ring were selected. Given the lack of mechanistic information, a relatively large number of descriptors were initially selected for model development; 33 for the substrates (one charge, 10 steric, 22 vibrational) and 23 for the catalysts (7 steric, 15 vibrational, and the torsion angle between the triazole and aryl rings).

Having defined the structural space to be sampled and the parameterization framework accordingly, enantioselectivities were measured for all substrate-catalyst combinations (Figure 3.28). Using these data, linear regression algorithms were implemented to relate relevant substrate and catalyst parameters to enantioselectivity, represented as $\Delta\Delta G^\ddagger$, which is the energy difference, in kcal/mol, between the diastereomeric transition states leading to opposite enantiomers. A number of different models were constructed by this process to explore different aspects of the system, as detailed below.

The parameter sets for the studied substrates and catalysts are presented in Tables 3.7 and 3.9, respectively. Model development involved 4 stepwise regression algorithms that assess the significance of each parameter by applying statistical criteria. In order to realize this assessment, each set of parameter values was normalized by subtracting its respective mean and dividing by its standard deviation. The 4 stepwise regression algorithms are built in MATLAB[®] (version 7.14.0.739, R2012a) statistical toolbox and add or remove normalized parameters from an initial model according to a p-value threshold.⁵⁶ Additional suggestions for models were inputted manually based on the results of the 4 preliminary algorithm results or based on additional mechanistic hypotheses. A linear fit was performed to probe each manually suggested model's statistical probability, and each suggestion was examined as an initial model for stepwise regression to seek a more effective model.

By modeling each substrate *vs.* all the catalysts and vice versa, several statistically probable parameters were identified, and a limited set of parameters was proposed for the model in Figure 3.25 (marked in yellow in Tables 3.7 and 3.9, normalized in Tables 3.8 and 3.10). For the models in Figures 3.18 and 3.25, an external validation was carried out in order to determine the predictive nature of the proposed model for substrates that are not included in the training set. In addition to the initial external validation, for Figure 3.25, predictions were carried out for several proposed catalysts, which serve as supplementary external validations.

Table 3.7 depicts the parameters that describe each substrate. Sterimol values (L – length of the substituent B1 – minimal width of substituent perpendicular to L, and B5 – maximal width of substituent perpendicular to L), followed by vibration frequencies and intensities centered on certain bonds. Particular vibrational modes were selected as they were thought to reflect the structural changes within the experimental space, and were reliably accessible across the data set. The substrate parameters in Table 3.7 were used to identify the models shown in Figure 3.26, in which each measured *vs.* predicted $\Delta\Delta G^\ddagger$ plot represents the enantioselectivity obtained for each

catalyst with every substrate in the initially designed library (each catalyst and substrates **3.1a-l**). The catalyst parameters in Table 3.9 were used to identify the models shown in Figure 3.27, in which each plot represents the enantioselectivity obtained for each substrate with every catalyst in the initially designed library (each substrate and catalysts **3.4a-k**). To identify significant models, each of the parameters was normalized and linear regression algorithms were applied as described above. In Tables 3.8 and 3.10 are the normalized parameter sets that were found to be important for correlating selectivity in the individual models. The normalized parameter values in these two tables were used to obtain the predictive model in Figure 3.25, for which the measured *vs.* predicted $\Delta\Delta G^\ddagger$ values are presented in Table 3.11.

Table 3.7. Parameters used for substrates **3.1**

<i>entry</i>	<i>substrate</i>		<i>rings 2 & 3</i>		
	<i>R1</i>	<i>R2</i>	<i>23B₁</i>	<i>23B₅</i>	<i>23L</i>
2a	H	H	1.92	7.27	8.38
2b	4-Me	H	1.94	8.33	9.04
2c	4-MeO	H	2.01	8.72	8.56
2d	4-NO ₂	H	2.06	7.09	10.06
2e	2-MeO	H	1.87	7.53	8.69
2f	2-MeO	Ph	2.48	7.53	10.61
2g	2-MeO	Br	1.88	7.53	8.68
2h	2-MeO	iPr	3.16	7.51	8.68
2i	2-Me	H	1.88	7.07	8.74
2j	2-Br	H	2.17	6.33	9.67
2k	2-iPr	H	1.91	8.44	8.86
2l	2,6-MeO	H	2.26	8.54	8.98
			1	2	3

<i>entry</i>	<i>ring 3</i>			<i>ring 2 (removing ring 1)</i>		
	<i>3B₁</i>	<i>3B₅</i>	<i>3L</i>	<i>2B₁</i>	<i>2B₅</i>	<i>2L</i>
2a	1.72	5.93	5.05	1.70	3.58	6.53
2b	1.72	7.29	5.55	1.70	3.58	6.53
2c	1.72	8.22	5.18	1.70	3.57	6.53
2d	1.71	7.70	5.23	1.70	3.54	6.53
2e	1.71	5.87	4.98	1.70	3.61	6.54
2f	1.72	5.86	4.99	1.87	7.59	7.75
2g	1.71	5.86	5.00	1.70	5.04	6.54
2h	1.72	5.87	4.98	2.09	5.54	6.97
2i	1.72	5.90	4.80	1.70	3.61	6.54
2j	1.70	6.34	4.22	1.70	3.59	6.53
2k	1.73	6.24	4.67	1.70	3.61	6.54
2l	1.70	5.92	5.52	1.70	3.60	6.53

	4	5	6	7	8	9
--	---	---	---	---	---	---

entry	vibrational terms					
	ν_{1ring2}	i_{1ring2}	ν_{1ring3}	i_{1ring3}	ν_{amide}	i_{amide}
2a	1535.18	75.67	1543.62	9.96	1584.03	328.54
2b	1535.87	78.10	1564.74	15.46	1583.32	332.63
2c	1535.20	75.31	1567.86	129.53	1584.04	326.99
2d	1535.20	71.31	1544.97	4.18	1583.80	297.85
2e	1534.21	70.62	1550.70	61.12	1583.15	384.15
2f	1532.53	127.17	1549.31	64.29	1586.28	445.84
2g	1527.67	148.98	1549.09	64.41	1585.69	404.65
2h	1548.19	66.29	1548.91	84.64	1584.39	422.11
2i	1533.97	68.38	1541.65	10.91	1585.20	369.51
2j	1533.14	72.86	1526.62	5.43	1586.67	419.04
2k	1535.44	68.16	1543.61	11.28	1590.28	367.02
2l	1536.68	79.73	1541.14	3.78	1580.64	385.60
	10	11	12	13	14	15

entry	vibrational terms					
	ν_{2ring2}	i_{2ring2}	ν_{2ring3}	i_{2ring3}	ν_{3ring2}	i_{3ring2}
2a	1646.75	2.93	1657.03	1.83	1672.51	44.38
2b	1646.69	2.81	1649.47	1.60	1672.42	44.63
2c	1646.31	3.20	1653.39	5.36	1672.25	45.46
2d	1647.87	3.74	1642.53	150.20	1672.94	39.13
2e	1645.58	2.25	1662.37	8.18	1671.43	33.86
2f	1629.87	2.80	1662.80	7.84	1677.74	9.82
2g	1632.42	1.07	1662.92	8.40	1660.25	9.21
2h	1638.74	3.23	1662.87	8.35	1680.25	10.08
2i	1643.96	1.45	1652.37	0.36	1671.38	30.65
2j	1645.49	2.86	1643.41	4.10	1672.42	33.00
2k	1645.32	1.80	1652.46	0.29	1672.08	34.14
2l	1646.99	3.87	1665.09	39.94	1672.41	35.38
	16	17	18	19	20	21

entry	vibrational terms					
	ν_{3ring3}	i_{3ring3}	$\nu_{C=O}$	$i_{C=O}$	$\nu_{CH_{sym}}$	$i_{CH_{sym}}$
2a	1677.88	5.33	1760.28	331.36	2981.70	28.88
2b	1689.81	1.46	1761.82	327.31	2982.78	27.98
2c	1687.77	47.67	1761.19	320.57	2982.34	28.13
2d	1674.14	23.32	1771.71	309.35	2985.96	23.07
2e	1676.14	21.58	1772.67	392.10	2979.40	29.60

2f	1675.11	30.84	1773.09	343.62	2979.66	28.52
2g	1675.00	26.16	1776.45	349.88	2980.77	28.49
2h	1674.20	26.54	1771.37	360.72	2977.53	28.71
2i	1677.95	0.39	1761.74	379.96	2980.36	29.29
2j	1667.53	1.50	1774.09	414.34	2982.65	28.74
2k	1677.54	0.95	1756.67	374.97	2981.46	26.75
2l	1673.57	113.62	1765.55	400.62	2981.36	27.95
	22	23	24	25	26	27

<i>entry</i>	<i>vibrational terms</i>				<i>charge</i>	<i>distance</i>
	νCH_{asym}	iCH_{asym}	νNH	iNH	N_{APT}	$dN-CH$
2a	3118.43	2.97	3523.15	199.06	-0.85	3.12
2b	3114.11	3.05	3522.12	188.21	-0.85	3.15
2c	3109.80	2.50	3525.55	179.07	-0.85	3.16
2d	3086.86	4.70	3511.74	172.41	-0.86	3.30
2e	3096.45	0.79	3508.11	235.57	-0.87	3.13
2f	3095.69	0.70	3515.73	217.11	-0.89	3.13
2g	3094.11	0.76	3513.40	227.64	-0.88	3.13
2h	3096.33	1.09	3501.63	239.08	-0.89	3.14
2i	3119.46	6.77	3488.15	259.01	-0.87	3.11
2j	3106.34	1.87	3475.87	242.09	-0.90	3.26
2k	3100.43	5.01	3484.99	242.87	-0.87	3.12
2l	3115.85	1.90	3553.05	122.26	-0.86	3.15
	28	29	30	31	32	33

Table 3.8. Normalized reduced parameter set used for substrates

<i>entry</i>	<i>substrate</i>		<i>vibrational terms</i>			
	<i>R1</i>	<i>R2</i>	ν_{3ring3}	i_{3ring3}	$\nu C=O$	$iC=O$
2a	H	H	0.08	-0.58	-0.97	-0.81
2b	4-Me	H	2.12	-0.70	-0.74	-0.94
2c	4-MeO	H	1.77	0.79	-0.83	-1.14
2d	4-NO ₂	H	-0.56	0.00	0.75	-1.49
2e	2-MeO	H	-0.21	-0.05	0.89	1.05
2f	2-MeO	Ph	-0.39	0.25	0.96	-0.44
2g	2-MeO	Br	-0.41	0.10	1.46	-0.24
2h	2-MeO	iPr	-0.54	0.11	0.70	0.09
2i	2-Me	H	0.10	-0.73	-0.75	0.68
2j	2-Br	H	-1.68	-0.70	1.11	1.73
2k	2-iPr	H	0.03	-0.72	-1.52	0.53
2l	2,6-MeO	H	-0.65	2.91	-0.18	1.31
			22	23	24	25

<i>entry</i>	<i>vibrational term</i>			
	νCH_{asym}	iCH_{asym}	νNH	iNH
2a	1.21	0.06	0.70	-0.38
2b	0.81	0.10	0.65	-0.65
2c	0.41	-0.18	0.81	-0.87
2d	-1.70	0.94	0.17	-1.04
2e	-0.81	-1.05	0.00	0.52
2f	-0.88	-1.10	0.36	0.07
2g	-1.03	-1.06	0.25	0.33
2h	-0.83	-0.90	-0.30	0.61
2i	1.30	1.99	-0.92	1.10
2j	0.10	-0.50	-1.49	0.68
2k	-0.45	1.09	-1.07	0.70
2l	0.97	-0.48	2.09	-2.28
	28	29	30	31

Table 3.9. Parameters used for catalysts **3.4**

<i>entry</i>	<i>catalyst</i>	<i>vibrational terms</i>				
		$\nu C-N$	$iC-N$	$\nu N-N_I$	$iN-N_I$	<i>vringD</i>
1a	CHPh ₂	1138.19	0.50	1247.24	10.15	1282.16
1b	2,4,6-Me ₃ Ph	1168.29	2.72	1258.88	15.11	1286.31
1c	2,4,6-iPr ₃ Ph	1156.30	0.96	1261.66	17.82	1284.03
1d	2,4,6-Cy ₃ Ph	1171.99	3.03	1261.23	12.58	1285.51
1e	1-Ad	1162.40	2.14	1266.95	19.31	1287.55
1f	Ph	1192.74	15.94	1252.34	8.00	1290.80
1g	4-MeOPh	1191.20	45.36	1253.36	18.11	1292.28
1j	2,6-MeO ₂ Ph	1176.50	15.49	1239.49	32.12	1263.76
1h	4-NEt ₂ Ph	1192.87	13.63	1250.35	12.00	1292.77
1k	2,6-F ₂ Ph	1186.36	10.95	1247.76	18.46	1286.34
1i	4-SO ₂ MePh	1191.43	26.89	1246.58	7.65	1286.70
<i>imid-1e</i>	1-Ad-imidazole	1167.01	6.35	1299.16	57.95	1289.11
<i>pyr-1e</i>	1-Ad-pyrazole	1167.69	7.19	1287.98	7.04	1326.85
1l	F ₅ Ph			1240.47		1271.68
1m	26-iPr-4-BrPh			1258.07		1279.69
1n	2-iPrPh			1256.37		1290.25
		1	2	3	4	5

<i>entry</i>	<i>vibrational terms</i>					
	<i>iringD</i>	<i>vN-N₂</i>	<i>iN-N₂</i>	<i>vC=N</i>	<i>iC=N</i>	<i>vC=C</i>
1a	74.56	1357.44	45.10	1501.51	35.77	1553.63
1b	56.40	1370.23	34.29	1463.71	5.25	1545.63
1c	25.41	1372.87	36.66	1477.10	10.52	1536.79
1d	32.29	1367.50	27.82	1480.23	11.51	1536.01
1e	84.91	1353.58	10.52	1476.82	29.45	1553.38
1f	123.78	1384.59	27.60	1475.13	17.91	1551.39
1g	216.99	1378.24	21.74	1472.41	0.09	1553.97
1j	34.81	1344.93	51.29	1463.69	20.62	1530.05
1h	84.65	1382.15	20.20	1493.99	0.82	1555.69
1k	56.18	1391.37	21.79	1471.98	11.13	1560.57
1i	160.72	1391.56	20.00	1491.96	20.11	1553.52
<i>imid-1e</i>	148.84	1357.82	26.49	1421.28	0.06	1562.02
<i>pyr-1e</i>	19.76	1342.26	9.70	1473.16	27.14	1583.13
1l						
1m						
1n						
	6	7	8	9	10	11
<i>entry</i>	<i>vibrational terms</i>				<i>distances</i>	
	<i>iC=C</i>	<i>vC-H</i>	<i>iC-H</i>	<i>aryl-ring stretch</i>	<i>dbiphenyl</i>	<i>dN₁[*]</i>
1a	16.95	3324.94	6.38		4.94	7.09
1b	93.34	3325.18	7.49	1679.86	4.86	8.51
1c	93.99	3325.21	7.66	1673.84	4.87	8.55
1d	84.29	3326.74	6.67	1673.07	4.94	7.07
1e	26.61	3328.87	4.12		4.93	6.69
1f	84.47	3333.69	7.70	1677.89	4.86	8.56
1g	95.19	3330.82	7.34	1692.58	4.86	8.55
1j	55.02	3335.00	6.81	1662.99	4.85	8.48
1h	77.35	3333.04	7.27	1683.29	4.85	8.54
1k	56.44	3330.47	10.16	1701.51	4.87	8.58
1i	96.82	3334.34	8.84	1672.91	4.86	8.60
<i>imid-1e</i>	27.45	3323.58	1.76		4.92	6.69
<i>pyr-1e</i>	3.68	3322.68	2.47		4.92	7.28
1l				1720.08		
1m				1647.8		
1n				1661.62		
	12	13	14	15	16	17

<i>entry</i>	<i>distances</i>	<i>Sterimol</i>	<i>torsion</i>
--------------	------------------	-----------------	----------------

	dN_2^*	dN_3 (on R) *	<i>L</i>	<i>B1</i>	<i>B5</i>	<i>dihedral</i>
1a	8.74	10.09	6.04	2.08	6.14	
1b	9.96	10.02	7.28	1.99	4.53	104.51
1c	10.01	10.05	8.53	3.31	5.76	91.77
1d	8.67	9.98	10.60	3.31	7.44	97.17
1e	8.70	10.83	6.30	3.31	3.68	
1f	10.01	10.05	6.27	1.77	3.15	149.77
1g	10.01	10.06	8.51	1.90	3.16	146.84
1j	9.92	10.00	6.26	2.01	5.50	101.27
1h	10.00	10.05	9.28	2.30	4.56	149.41
1k	10.05	10.09	6.44	1.70	3.81	120.76
1i	10.03	10.03	8.59	2.03	3.59	152.36
<i>imid-1e</i>	8.80	11.00	6.31	3.31	3.67	
<i>pyr-1e</i>	9.27	10.73	6.30	3.31	3.69	
1l			6.98	1.77	3.82	121.21
1m			7.98	2.91	5.76	89.83
1n			6.26	1.95	5.81	68.19
	18	19	20	21	22	23

* distance (Å) between each couple of nitrogen atoms on the two adjacent triazole rings.

Table 3.10. Normalized reduced parameter set used for aryl triazole catalysts

<i>entry</i>	<i>catalyst</i>	<i>vibrational terms</i>		<i>Sterimol</i>		<i>torsion</i>
		$\nu N-N_1$	<i>vringD</i>	<i>L (cat)</i>	<i>B1 (cat)</i>	<i>dihedral</i>
1b	2,4,6-Me ₃ Ph	0.89	0.25	-0.34	-0.43	-0.41
1c	2,4,6-iPr ₃ Ph	1.26	-0.02	0.56	1.80	-0.86
1d	2,4,6-Cy ₃ Ph	1.20	0.15	2.04	1.80	-0.67
1f	Ph	0.02	0.76	-1.06	-0.81	1.19
1g	4-MeOPh	0.15	0.93	0.54	-0.59	1.08
1j	2,6-MeO ₂ Ph	-1.69	-2.35	-1.06	-0.40	-0.52
1h	4-NEt ₂ Ph	-0.25	0.99	1.09	0.09	1.18
1k	2,6-F ₂ Ph	-0.59	0.25	-0.93	-0.93	0.16
1i	4-SO ₂ MePh	-0.75	0.29	0.60	-0.37	1.28
1l	F ₅ Ph	-1.56	-1.44	-0.55	-0.81	0.18
1m	26-iPr-4-BrPh	0.78	-0.52	0.17	1.13	-0.93
1n	2iPrPh	0.55	0.70	-1.06	-0.50	-1.69
		3	5	20	21	23

Table 3.11. Measured vs. predicted $\Delta\Delta G^\ddagger$ values (black represents training set, red represents external validations, and blue represents external predictions)

	measured $\Delta\Delta G^\ddagger$	predicted $\Delta\Delta G^\ddagger$	catalyst	substrate
	1.22	1.12	2,4,6-Me ₃ Ph	Bn
	1.19	1.27	2,4,6-Cy ₃ Ph	"
	0.70	0.41	4-MeOPh	"
	0.35	0.30	4-NEt ₂ Ph	"
	0.61	0.45	4-SO ₂ MePh	"
	0.93	0.79	2,4,6-iPr ₃ Ph	4-Me-Bn
	0.59	0.56	Ph	"
	0.78	1.10	2,6-MeO ₂ Ph	"
	0.71	0.96	2,6-F ₂ Ph	"
	1.37	1.21	2,4,6-Me ₃ Ph	4-MeO-Bn
	0.47	0.78	2,4,6-Cy ₃ Ph	"
	0.81	0.60	4-MeOPh	"
	0.46	0.32	4-NEt ₂ Ph	"
	0.67	0.60	4-SO ₂ MePh	"
	1.17	1.17	2,4,6-iPr ₃ Ph	4-NO ₂ -Bn
	0.48	0.70	Ph	"
	1.22	1.12	2,6-MeO ₂ Ph	"
	0.89	1.01	2,6-F ₂ Ph	"
	1.03	1.20	2,4,6-Me ₃ Ph	2-MeO-Bn
	1.39	1.57	2,4,6-Cy ₃ Ph	"
	0.25	0.18	4-MeOPh	"
	0.00	0.08	4-NEt ₂ Ph	"
	0.12	0.15	4-SO ₂ MePh	"
	1.66	1.51	2,4,6-iPr ₃ Ph	2-MeO-Bn_Ph
	0.00	0.25	Ph	"
	0.97	0.96	2,6-MeO ₂ Ph	"
	0.57	0.64	2,6-F ₂ Ph	"
	1.04	1.18	2,4,6-Me ₃ Ph	2-MeO-Bn_Br
	1.66	1.59	2,4,6-Cy ₃ Ph	"
	0.19	0.36	4-MeOPh	"
	0.15	0.29	4-NEt ₂ Ph	"
	0.35	0.37	4-SO ₂ MePh	"
	measured $\Delta\Delta G^\ddagger$	predicted $\Delta\Delta G^\ddagger$	catalyst	substrate
	1.81	1.72	2,4,6-iPr ₃ Ph	2-MeO-Bn_iPr
	0.31	0.30	Ph	"
	1.32	0.99	2,6-MeO ₂ Ph	"

	1.10	0.70	2,6-F ₂ Ph	"
	1.66	1.56	2,4,6-Me ₃ Ph	2-Me-Bn
	1.96	1.72	2,4,6-Cy ₃ Ph	"
	0.85	0.55	4-MeOPh	"
	0.28	0.34	4-NEt ₂ Ph	"
	0.39	0.42	4-SO ₂ MePh	"
	1.88	1.92	2,4,6-iPr ₃ Ph	2-Br-Bn
	0.67	0.33	Ph	"
	0.96	1.04	2,6-MeO ₂ Ph	"
	0.71	0.83	2,6-F ₂ Ph	"
	1.39	1.66	2,4,6-Me ₃ Ph	2-iPrBn
	1.53	1.59	2,4,6-Cy ₃ Ph	"
	0.62	0.67	4-MeOPh	"
	0.20	0.39	4-NEt ₂ Ph	"
	0.39	0.51	4-SO ₂ MePh	"
	0.77	0.72	2,4,6-iPr ₃ Ph	26-MeOBn
	-0.70	-0.45	Ph	"
	0.73	0.78	2,6-MeO ₂ Ph	"
	0.49	0.22	2,6-F ₂ Ph	"
	1.28	1.27	2,4,6-iPr ₃ Ph	Bn
	0.63	0.30	Ph	"
	0.88	0.98	2,6-MeO ₂ Ph	"
	0.79	0.68	2,6-F ₂ Ph	"
	1.30	1.26	2,4,6-Me ₃ Ph	4-MeBn
	0.63	0.79	2,4,6-Cy ₃ Ph	"
	0.68	0.61	4-MeOPh	"
	0.26	0.31	4-NEt ₂ Ph	"
	0.58	0.59	4-SO ₂ MePh	"
	0.89	0.78	2,4,6-iPr ₃ Ph	4-MeOBn
	0.63	0.55	Ph	"
	0.97	1.09	2,6-MeO ₂ Ph	"
	0.96	0.93	2,6-F ₂ Ph	"
	measured $\Delta\Delta G^\ddagger$	predicted $\Delta\Delta G^\ddagger$	catalyst	substrate
	1.45	1.39	2,4,6-Me ₃ Ph	4-NO ₂ Bn
	1.22	1.17	2,4,6-Cy ₃ Ph	"
	0.62	0.77	4-MeOPh	"
	0.29	0.54	4-NEt ₂ Ph	"

	0.47	0.74	4-SO ₂ MePh	"
	1.41	1.61	2,4,6-iPr ₃ Ph	2-MeO-Bn
	0.08	0.03	Ph	"
	0.64	0.92	2,6-MeO ₂ Ph	"
	0.28	0.54	2,6-F ₂ Ph	"
	1.04	1.17	2,4,6-Me ₃ Ph	2-MeO-Bn_Ph
	1.51	1.50	2,4,6-Cy ₃ Ph	"
	0.07	0.38	4-MeOPh	"
	0.08	0.31	4-NEt ₂ Ph	"
	0.38	0.40	4-SO ₂ MePh	"
	1.55	1.60	2,4,6-iPr ₃ Ph	2-MeO-Bn_Br
	0.13	0.21	Ph	"
	0.91	0.95	2,6-MeO ₂ Ph	"
	0.39	0.61	2,6-F ₂ Ph	"
	1.39	1.36	2,4,6-Me ₃ Ph	2-MeO-Bn_iPr
	1.71	1.69	2,4,6-Cy ₃ Ph	"
	0.42	0.45	4-MeOPh	"
	0.29	0.34	4-NEt ₂ Ph	"
	0.60	0.40	4-SO ₂ MePh	"
	2.01	1.75	2,4,6-iPr ₃ Ph	2-Me-Bn
	0.77	0.41	Ph	"
	0.88	1.05	2,6-MeO ₂ Ph	"
	0.72	0.84	2,6-F ₂ Ph	"
	1.43	1.69	2,4,6-Me ₃ Ph	2-Br-Bn
	1.81	1.86	2,4,6-Cy ₃ Ph	"
	0.75	0.49	4-MeOPh	"
	0.28	0.25	4-NEt ₂ Ph	"
	0.40	0.29	4-SO ₂ MePh	"
	1.53	1.62	2,4,6-iPr ₃ Ph	2-iPr-Bn
	0.41	0.56	Ph	"
	0.83	1.10	2,6-MeO ₂ Ph	"
	0.80	0.98	2,6-F ₂ Ph	"
	measured $\Delta\Delta G^\ddagger$	predicted $\Delta\Delta G^\ddagger$	catalyst	substrate
	1.03	0.56	2,4,6-Me ₃ Ph	26-MeO-Bn
	0.84	0.69	2,4,6-Cy ₃ Ph	"
	-0.34	-0.34	4-MeOPh	"
	-0.29	-0.42	4-NEt ₂ Ph	"

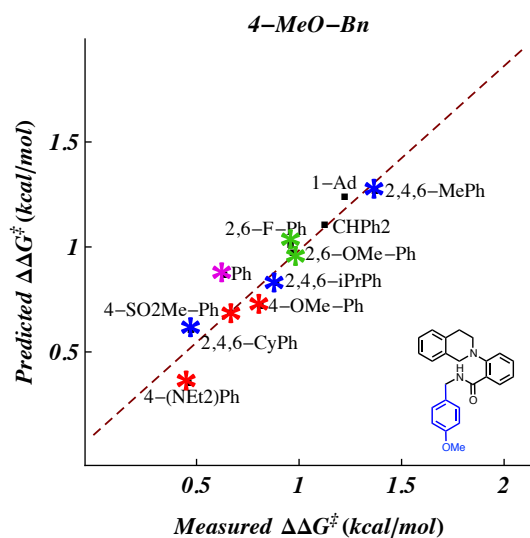
	-0.35	-0.22	4-SO ₂ MePh	"
	1.13	0.82	F ₃ Ph	Bn
	0.96	1.06	"	4-Me-Bn
	0.88	1.05	"	4-MeO-Bn
	0.82	0.62	"	2-MeO-Bn
	0.72	0.75	"	2-MeO-Bn_Ph
	0.82	0.48	"	26-MeO-Bn
	1.49	1.49	26-iPr-4-BrPh	Bn
	1.15	1.19	"	4-Me-Bn
	1.24	1.47	"	4-NO ₂ -Bn
	1.63	1.76	"	2-MeO-Bn
	1.96	1.73	"	2-MeO-Bn_Br
	1.78	1.85	"	2-MeO-Bn_iPr
	1.84	1.67	"	2-MeO-Bn_Ph
	2.11	1.93	"	2-Me-Bn
	1.96	2.09	"	2-Br-Bn
	1.96	1.86	"	2-iPr-Bn
	1.18	1.08	2iPrPh	Bn
	1.24	1.22	"	4-Me-Bn
	1.24	1.15	"	4-MeO-Bn
	1.58	1.27	"	4-NO ₂ -Bn

Table 3.12. $\Delta\Delta G^\ddagger$ values used as inputs for modeling

<i>catalyst</i>		<i>substrate</i>	<i>S1</i>	<i>S2</i>	<i>S3</i>	<i>S4</i>	<i>S5</i>	<i>S6</i>
		<i>R1 --></i>	H	4-Me	4-MeO	4-NO ₂	2-MeO	2-MeO
		<i>R2 --></i>	H	H	H	H	H	Ph
C1	CHPh ₂		0.99	1.00	1.13	0.54	0.52	0.63
C2	2,4,6-Me ₃ Ph		1.22	1.30	1.37	1.45	1.03	1.04
C3	2,4,6-iPr ₃ Ph		1.28	0.93	0.89	1.17	1.41	1.66
C4	2,4,6-Cy ₃ Ph		1.19	0.63	0.47	1.22	1.39	1.51
C5	1-Ad		1.32	1.24	1.22	1.15	1.04	0.72
C6	Ph		0.63	0.59	0.63	0.48	0.08	0.00
C7	4-MeOPh		0.70	0.68	0.81	0.62	0.25	0.07
C8	2,6-MeO ₂ Ph		0.88	0.78	0.97	1.22	0.64	0.97
C9	4-NEt ₂ Ph		0.35	0.26	0.46	0.29	0.00	0.08

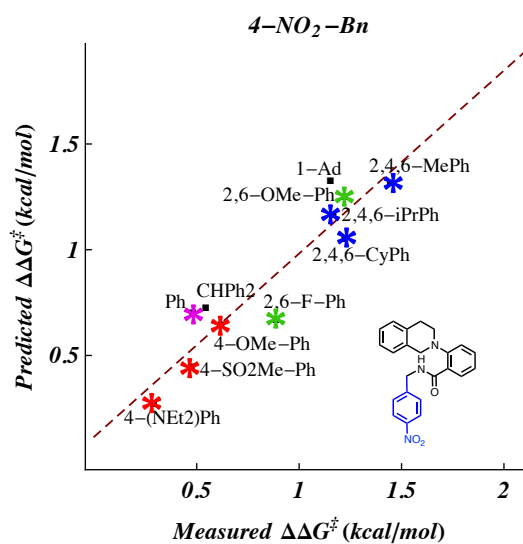
C10	2,6-F ₂ Ph		0.79	0.71	0.96	0.89	0.28	0.57
C11	4-SO ₂ MePh		0.61	0.58	0.67	0.47	0.12	0.38
C12h	1-Ad-pyrazole		0.57	0.39	0.49		0.45	0.73
C13h	1-Ad-imidazole		0.52					
catalyst		substrate	S7	S8	S9	S10	S11	S12
		R1 -->	2-MeO	2-MeO	2-Me	2-Br	2-iPr	26-MeO
		R2 -->	Br	iPr	H	H	H	H
C1	CHPh ₂		0.50	1.24	0.82	0.92	0.88	0.77
C2	2,4,6-Me ₃ Ph		1.04	1.39	1.66	1.43	1.39	1.05
C3	2,4,6-iPr ₃ Ph		1.55	1.81	2.01	1.88	1.53	0.78
C4	2,4,6-Cy ₃ Ph		1.66	1.71	1.96	1.81	1.53	0.83
C5	1-Ad		0.84	1.21	1.81	1.39	1.41	1.19
C6	Ph		0.13	0.31	0.77	0.67	0.41	0.71
C7	4-MeOPh		0.19	0.37	0.85	0.75	0.62	0.33
C8	2,6-MeO ₂ Ph		0.91	1.32	0.88	0.96	0.83	-0.70
C9	4-NEt ₂ Ph		0.15	0.29	0.28	0.28	0.20	0.30
C10	2,6-F ₂ Ph		0.39	1.10	0.72	0.71	0.80	-0.49
C11	4-SO ₂ MePh		0.35	0.60	0.39	0.40	0.39	0.41
C12h	1-Ad-pyrazole		0.56	0.80				
C13h	1-Ad-imidazole							

$$\begin{aligned} \Delta\Delta G^\ddagger &= 1.05 + 0.35 \text{vN=N} \\ &- 0.67 \text{vRingD} + 0.24 \text{d N} \\ &- 0.98 \text{vRingD} : \text{d N} \\ &\text{R}^2 = 0.95 \\ &\text{y} = 0.95\text{x} + 0.04 \end{aligned}$$

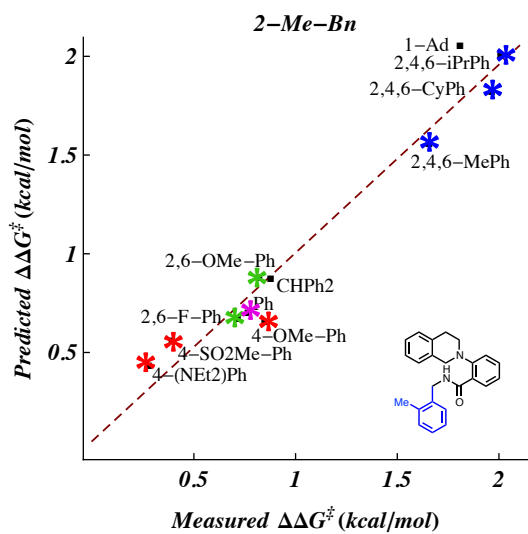


$$\begin{aligned} \Delta\Delta G^\ddagger &= 1.03 + 0.37 \text{vN=N} \\ &- 0.77 \text{vRingD} + 0.45 \text{d N} \\ &- 1.15 \text{vRingD} : \text{d N} - 0.36 \text{cat B}_1 \\ &\text{R}^2 = 0.88 \\ &\text{y} = 0.88\text{x} + 0.11 \end{aligned}$$

$$\begin{aligned} \Delta\Delta G^\ddagger &= 1.06 + 0.40 \text{vN=N} \\ &- 1.05 \text{vRingD} + 0.59 \text{d N} \\ &- 1.76 \text{vRingD} : \text{d N} - 0.29 \text{cat B}_1 \\ &\text{R}^2 = 0.94 \\ &\text{y} = 0.94\text{x} + 0.05 \end{aligned}$$



$$\begin{aligned} \Delta\Delta G^\ddagger &= 0.86 + 0.60 \text{vN=N} \\ &- 0.45 \text{vRingD} - 0.08 \text{d N} \\ &- 0.23 \text{cat B}_1 \\ &\text{R}^2 = 0.87 \\ &\text{y} = 0.87\text{x} + 0.11 \end{aligned}$$



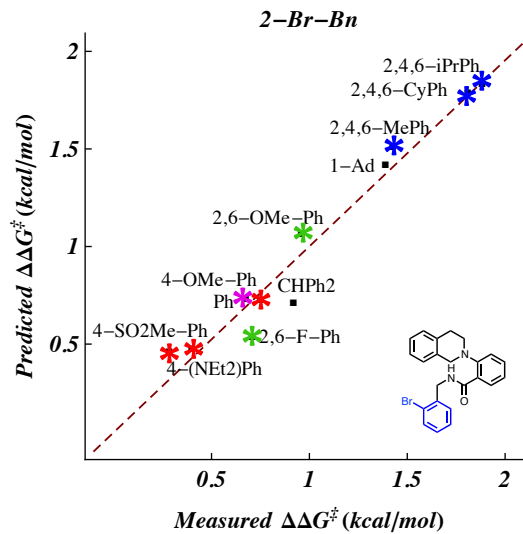
$$\Delta\Delta G^\ddagger = 1.18 + 0.67 \nu N=N$$

$$- 0.61 \nu \text{RingD}$$

$$- 0.18 \nu \text{RingD} : \nu N=N$$

$$R^2 = 0.95$$

$$y = 0.95x + 0.05$$



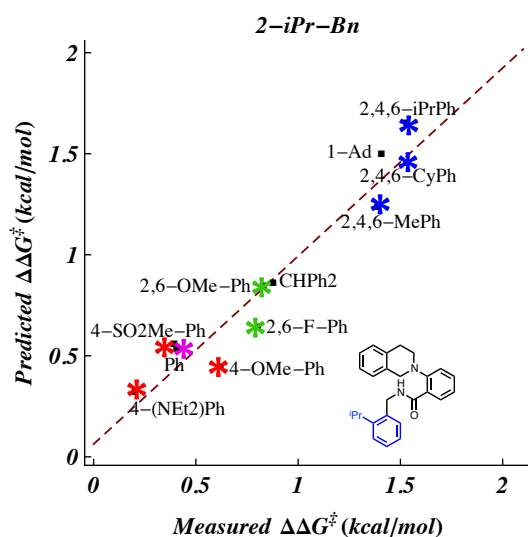
$$\Delta\Delta G^\ddagger = 1.13 + 0.52 \nu N=N$$

$$- 0.69 \nu \text{RingD}$$

$$- 0.26 \nu \text{RingD} : \nu N=N$$

$$R^2 = 0.95$$

$$y = 0.95x + 0.05$$



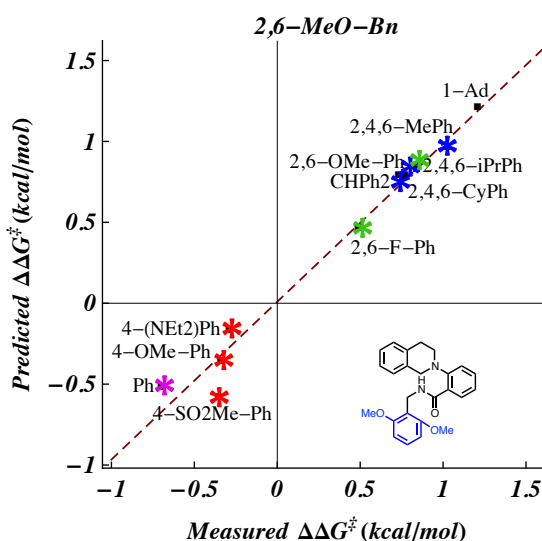
$$\Delta\Delta G^\ddagger = 1.02 + 0.47 \nu N=N$$

$$- 0.65 \nu \text{RingD}$$

$$- 0.25 \nu \text{RingD} : \nu N=N$$

$$R^2 = 0.93$$

$$y = 0.93x + 0.06$$



$$\Delta\Delta G^\ddagger = 1.13 + 0.51 \nu N=N$$

$$- 0.34 \nu \text{RingD}$$

$$2.45 \nu N=N : \nu \text{RingD}$$

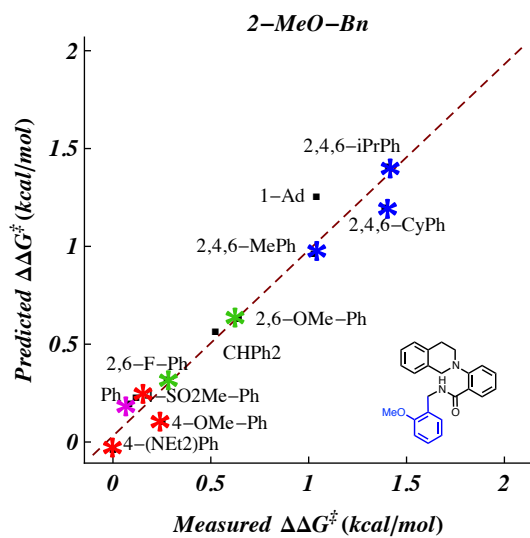
$$- 1.64 \nu N=N : d N$$

$$- 1.39 \nu \text{RingD} : \text{cat } B_1$$

$$- 0.25 \text{cat } B_1$$

$$R^2 = 0.98$$

$$y = 0.98x + 0.01$$



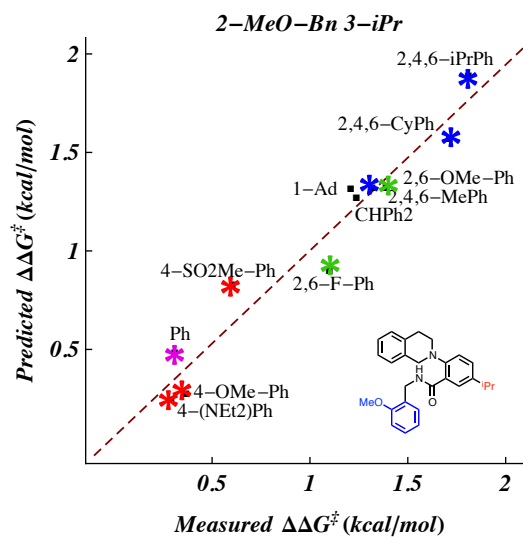
$$\Delta\Delta G^\ddagger = 0.73 + 0.50 \nu N=N$$

$$- 0.71 \nu \text{RingD}$$

$$- 0.26 \nu N=N : \nu \text{RingD}$$

$$R^2 = 0.95$$

$$y = 0.95x + 0.03$$



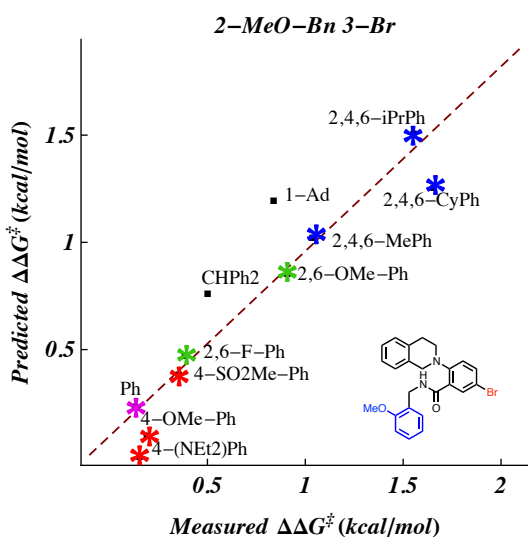
$$\Delta\Delta G^\ddagger = 1.24 + 0.37 \nu N=N$$

$$- 1.08 \nu \text{RingD}$$

$$- 0.49 \nu N=N : \nu \text{RingD}$$

$$R^2 = 0.94$$

$$y = 0.94x + 0.06$$



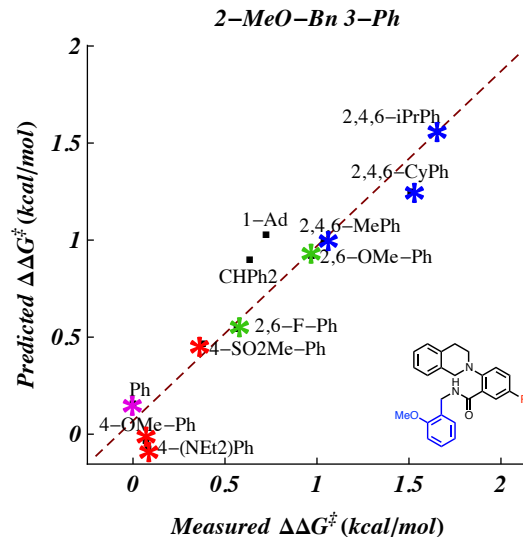
$$\Delta\Delta G^\ddagger = 0.79 + 0.59 \nu N=N$$

$$- 0.71 \nu \text{RingD} + 0.20 d N$$

$$- 0.22 \nu N=N : \nu \text{RingD}$$

$$R^2 = 0.86$$

$$y = 0.86x - 0.10$$



$$\Delta\Delta G^\ddagger = 0.90 + 0.39 \nu N=N$$

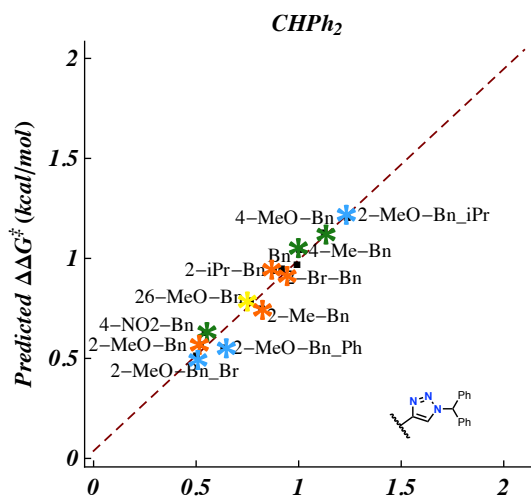
$$- 1.06 \nu \text{RingD}$$

$$- 0.48 \nu N=N : \nu \text{RingD}$$

$$R^2 = 0.90$$

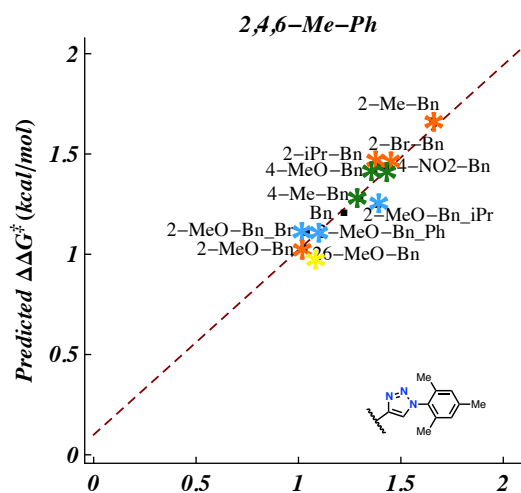
$$y = 0.90x - 0.07$$

Figure 3.26. Individual models and plots for substrates **3.1**



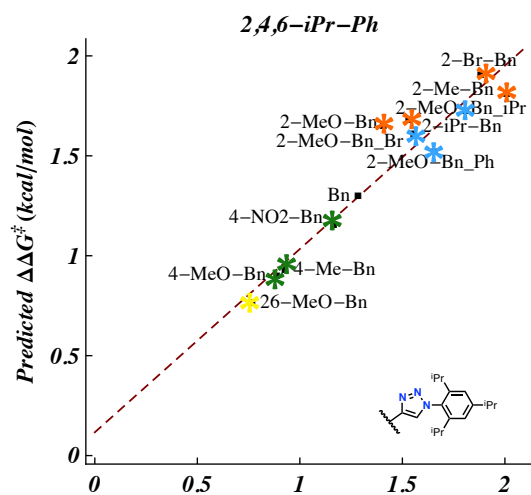
Measured $\Delta\Delta G^\ddagger$ (kcal/mol)

$$\begin{aligned} \Delta\Delta G^\ddagger = & 0.92 - 0.31 \text{ vC=O} \\ & + 0.19 \text{ vC=O} : \text{iC=O} \\ & - 0.44 \text{ vN-H} \\ & - 0.49 \text{ vC=O} : \text{vN-H} \\ & + 0.55 \text{ iC=O} : \text{vN-H} \\ & - 0.41 \text{ vR}_3 : \text{iN-H} \\ & \text{R}^2 = 0.95 \\ & \text{y} = 0.95\text{x} + 0.03 \end{aligned}$$



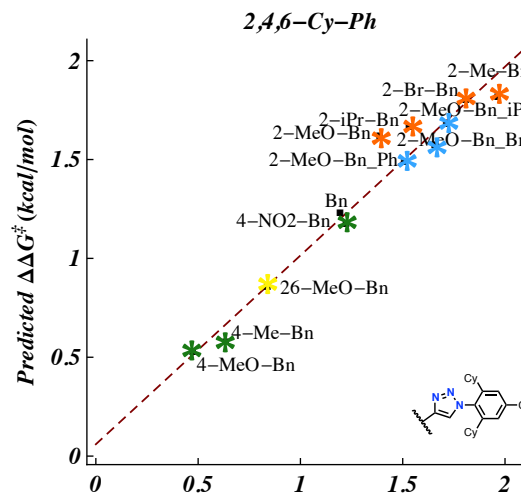
Measured $\Delta\Delta G^\ddagger$ (kcal/mol)

$$\begin{aligned} \Delta\Delta G^\ddagger = & 1.39 + 0.11 \text{ vR}_3 \\ & - 0.27 \text{ vC=O} + 0.22 \text{ iC=O} \\ & - 0.60 \text{ vC=O} : \text{iC=O} - 0.1 \text{ vN-H} \\ & - 0.60 \text{ vC=O} : \text{vN-H} \\ & \text{R}^2 = 0.92 \\ & \text{y} = 0.92\text{x} + 0.10 \end{aligned}$$



Measured $\Delta\Delta G^\ddagger$ (kcal/mol)

$$\begin{aligned} \Delta\Delta G^\ddagger = & 1.41 - 0.14 \text{ vR}_3 \\ & + 0.33 \text{ iN-H} \\ & \text{R}^2 = 0.92 \\ & \text{y} = 0.92\text{x} + 0.12 \end{aligned}$$



Measured $\Delta\Delta G^\ddagger$ (kcal/mol)

$$\begin{aligned} \Delta\Delta G^\ddagger = & 1.34 - 0.25 \text{ vR}_3 \\ & + 0.32 \text{ iN-H} \\ & \text{R}^2 = 0.95 \\ & \text{y} = 0.95\text{x} + 0.06 \end{aligned}$$

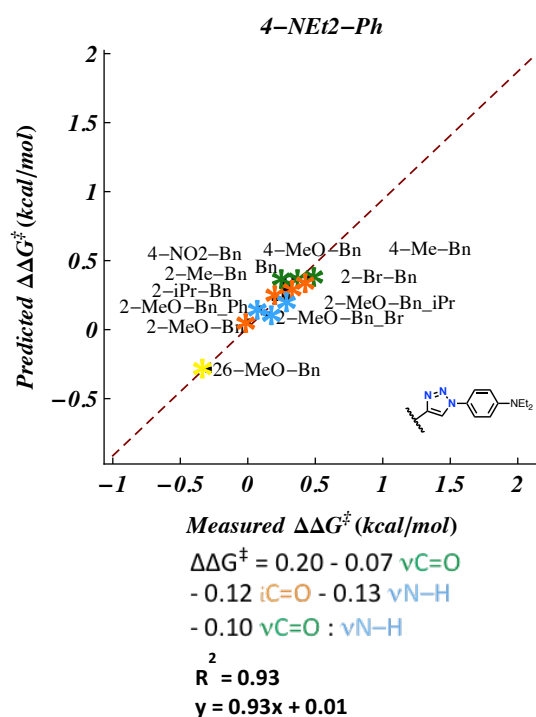
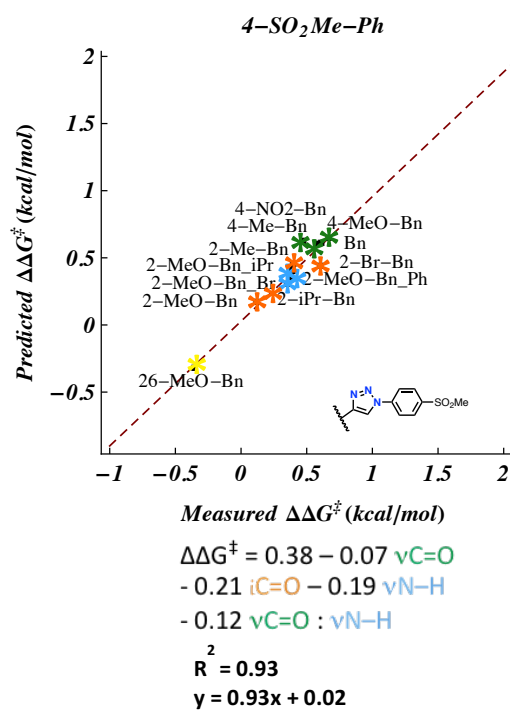
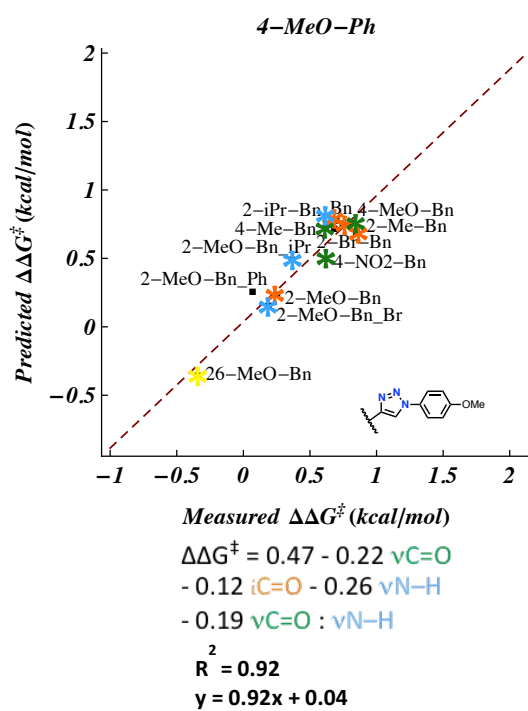
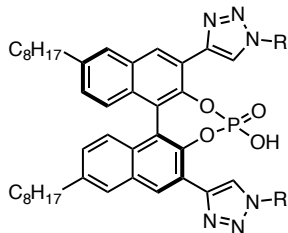
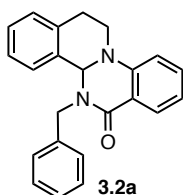


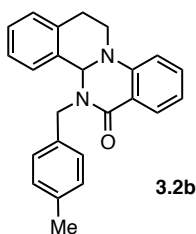
Figure 3.27. Individual models and plots for catalysts **3.4**



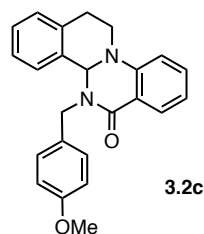
- 3.4a:** R = CHPh₂ **3.4h:** R = 4-(NEt₂)Ph
3.4b: R = 2,4,6-(Me)₃Ph **3.4i:** R = 4-(SO₂Me)-Ph
3.4c: R = 2,4,6-(iPr)₃Ph **3.4j:** R = 2,6-(OMe)₂Ph
3.4d: R = 2,4,6-(Cy)₃Ph **3.4k:** R = 2,6-(F)₂Ph
3.4e: R = adamantyl **3.4l:** R = F5Ph
3.4f: R = Ph **3.4m:** R = 2-iPr
3.4g: R = 4-OMe-Ph **3.4n:** R = 2,6-(iPr)₂-4-Br-Ph



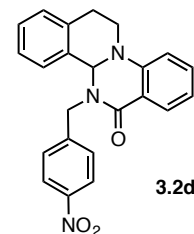
cat	ee ₁	ee ₂
3.4a	68	69
3.4b	77	78
3.4c	79	80
3.4d	76	77
3.4e	80	81
3.4f	49	49
3.4g	53	53
3.4h	28	29
3.4i	48	47
3.4j	63	63
3.4k	58	59
3.4l	74	74
3.4m	--	--
3.4n	85	84
pyr-3.4e	37	38



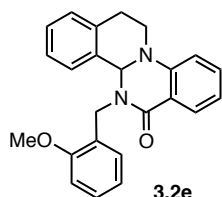
cat	ee ₁	ee ₂
3.4a	70	68
3.4b	81	79
3.4c	67	64
3.4d	47	51
3.4e	77	79
3.4f	45	47
3.4g	52	52
3.4h	22	22
3.4i	45	46
3.4j	58	57
3.4k	53	54
3.4l	67	64
3.4m	78	74
3.4n	75	75
pyr-3.4e	32	32



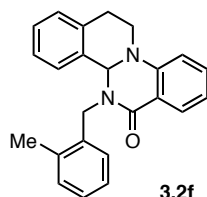
cat	ee ₁	ee ₂
3.4a	74	74
3.4b	82	82
3.4c	63	64
3.4d	38	38
3.4e	78	77
3.4f	49	49
3.4g	60	59
3.4h	37	37
3.4i	50	52
3.4j	68	67
3.4k	67	67
3.4l	63	71
3.4m	78	77
3.4n	--	--
pyr-3.4e	39	39



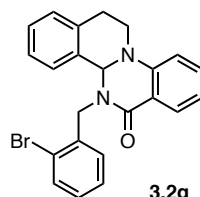
cat	ee ₁	ee ₂
3.4a	43	43
3.4b	84	84
3.4c	76	75
3.4d	77	78
3.4e	75	75
3.4f	39	38
3.4g	48	48
3.4h	25	23
3.4i	38	38
3.4j	77	78
3.4k	65	62
3.4l	--	--
3.4m	87	86
3.4n	--	--
pyr-3.4e	--	--



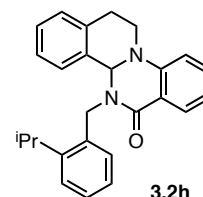
cat	ee ₁	ee ₂
3.4a	43	40
3.4b	68	72
3.4c	84	82
3.4d	83	82
3.4e	70	71
3.4f	6	8
3.4g	21	21
3.4h	0	0
3.4i	10	10
3.4j	49	50
3.4k	24	22
3.4l	60	60
3.4m	--	--
3.4n	88	87
pyr-3.4e	36	36



cat	ee ₁	ee ₂
3.4a	63	57
3.4b	88	89
3.4c	93	94
3.4d	92	94
3.4e	91	91
3.4f	57	57
3.4g	62	61
3.4h	23	23
3.4i	33	31
3.4j	63	63
3.4k	53	55
3.4l	--	--
3.4m	--	--
3.4n	95	95
pyr-3.4e	--	--



cat	ee ₁	ee ₂
3.4a	65	65
3.4b	83	84
3.4c	92	92
3.4d	89	93
3.4e	81	84
3.4f	51	52
3.4g	56	56
3.4h	23	24
3.4i	33	32
3.4j	67	67
3.4k	53	54
3.4l	--	--
3.4m	--	--
3.4n	93	93
pyr-3.4e	--	--



cat	ee ₁	ee ₂
3.4a	71	66
3.4b	85	84
3.4c	91	88
3.4d	90	88
3.4e	84	82
3.4f	32	34
3.4g	48	48
3.4h	17	17
3.4i	33	31
3.4j	62	59
3.4k	59	59
3.4l	--	--
3.4m	--	--
3.4n	93	91
pyr-3.4e	--	--

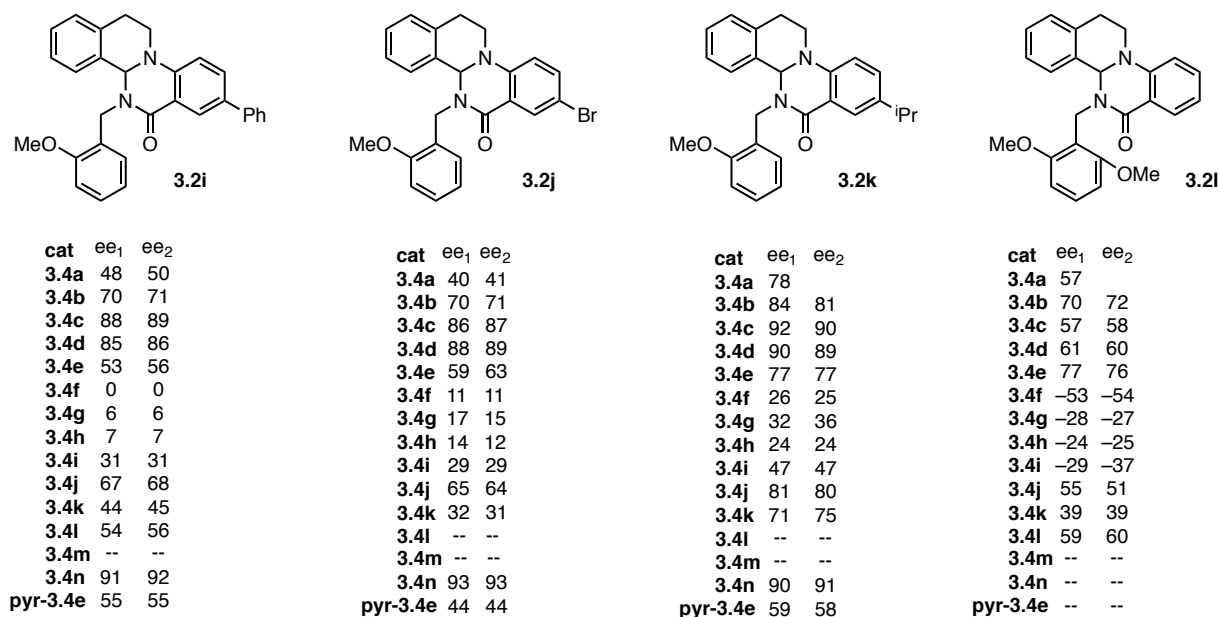
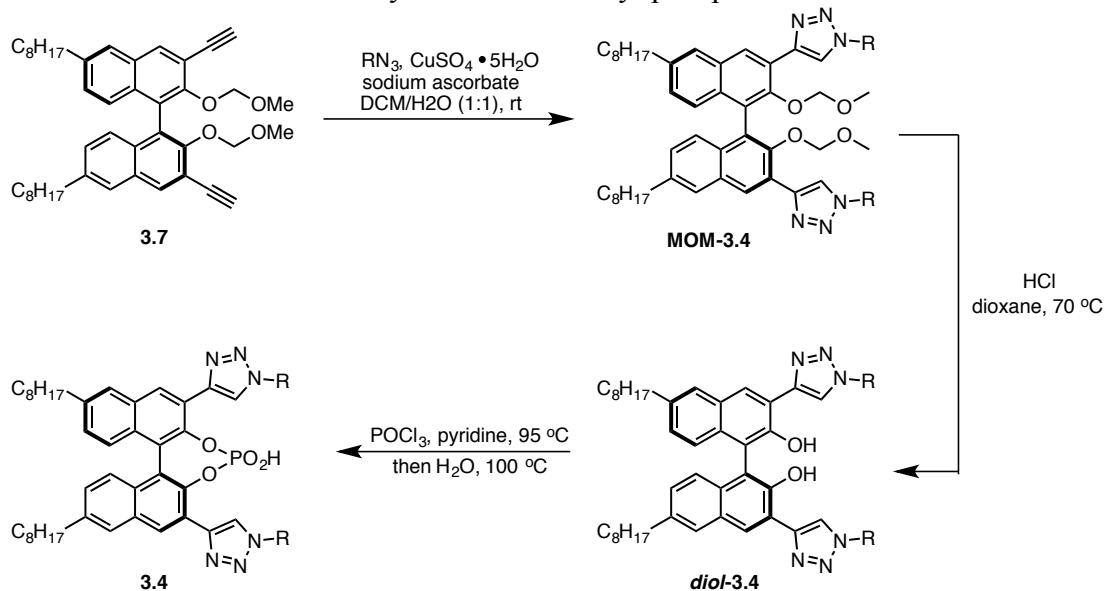


Figure 3.28. Enantioselectivity data for all catalyst-substrate combinations

Synthesis and characterization of catalysts

Scheme 3.1. Synthesis of triazolyl phosphoric acids **3.4**



Phosphoric acid catalysts **3.4f-n** were prepared according to the general reaction sequence depicted in Scheme 3.1.

Synthesis of aryl azides: 1-Azido-4-methoxybenzene and 2-azido-1,3-dimethoxybenzene were prepared according to the method of Goddard-Borger.⁵⁷ All other azides were prepared from the corresponding aniline according to the following procedure: The appropriate aniline (5 mmol) was dissolved in water (5 mL) and conc. HCl (1.5 mL) and the resulting mixture was cooled to 0

°C. NaNO₂ (6 mmol) was slowly added and the resulting suspension was vigorously stirred for 1.5 h at which point NaN₃ (7.5 mmol) was carefully added. The reaction mixture was allowed to warm to room temperature, extracted with EtOAc, dried (Na₂SO₄) and concentrated *in vacuo* to afford the crude azide which was used immediately without further purification.

General Procedure A: Synthesis of MOM-protected *bis*-triazoles MOM-3.4f–MOM-3.4n:

A 25-mL round-bottomed flask was charged with *bis*-alkyne **3.7** (0.500 g, 0.772 mmol), azide (2.32 mmol) and DCM (4 mL) under an atmosphere of N₂. Copper (II) sulfate pentahydrate (0.038 g, 0.154 mmol) and sodium L-ascorbate (0.061 g, 0.308 mmol) were weighed into separate 1-dram vials and each was dissolved in 2 mL H₂O. These solutions were then added to the rapidly-stirred DCM solution containing *bis*-alkyne **3.7** and azide in rapid succession. The reaction mixture was allowed to stir at room temperature under an atmosphere of N₂ and the progress of the reaction was monitored by TLC analysis. If incomplete conversion or remaining mono-triazole product (intermediate polarity between *bis*-alkyne and *bis*-triazole) was observed after 12 h, additional portions of copper sulfate pentahydrate (0.019 g, 0.077 mmol) and sodium L-ascorbate (0.030, 0.154 mmol) were added every hour until complete conversion was observed. The crude reaction mixture was dissolved in EtOAc (20 mL) and the aqueous layer was separated. The organic phase was washed with H₂O (20 mL) and brine (20 mL), dried (Na₂SO₄) and concentrated *in vacuo*. The crude residue was purified by flash chromatography on silica gel using EtOAc/Hex as eluent.

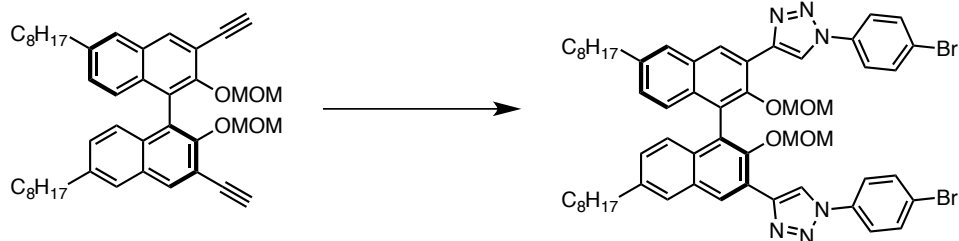
General Procedure B: Synthesis of diols *diol*-3.4f–*diol*-3.4n:

Methoxymethyl-protected *bis*-triazole (**MOM-3.4**) was dissolved in 1,4-dioxane (0.05 M) and concentrated HCl (2 mL) was added to the magnetically stirred solution. The reaction mixture was heated at 70 °C for 2 h at which point it was allowed to cool to room temperature and concentrated *in vacuo*. The residue was dissolved in DCM (20 mL) and washed with saturated aqueous Na₂SO₄ (20 mL) and brine (20 mL), dried (Na₂SO₄) and concentrated *in vacuo*. The crude residue was purified by flash chromatography using EtOAc/Hex as eluent.

General Procedure C: Synthesis of phosphoric acids 3.4f-n

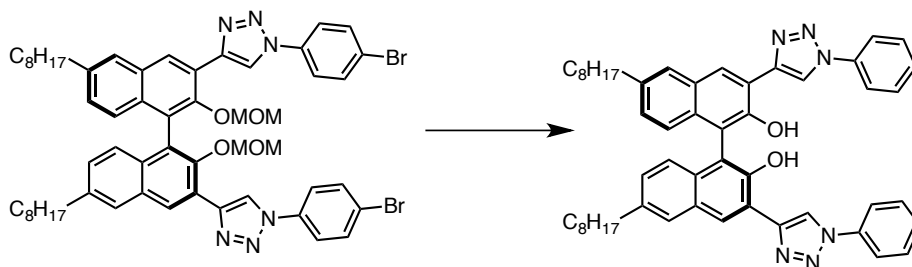
To a magnetically stirred solution of triazolyl diol (*diol*-**3.4**) in pyridine (0.05 M) was added phosphorus (V) oxychloride (2 equiv) and the reaction mixture was heated at 95 °C for 12 h under an atmosphere of N₂. After cooling to room temperature, H₂O (5 mL) was added and the reaction mixture was stirred at 100 °C for 5 h. After cooling to room temperature, the reaction mixture was dissolved in DCM (10 mL) and washed with 3 N HCl (3 X 10 mL) and brine (10 mL), dried (Na₂SO₄) and concentrated *in vacuo*. If necessary, the product was purified by flash chromatography on silica gel using DCM/MeOH as eluent.

(S)-4,4'-(2,2'-bis(methoxymethoxy)-6,6'-dioctyl-[1,1'-binaphthalene]-3,3'-diyl)bis(1-(4-bromophenyl)-1*H*-1,2,3-triazole) (MOM-3.4f)



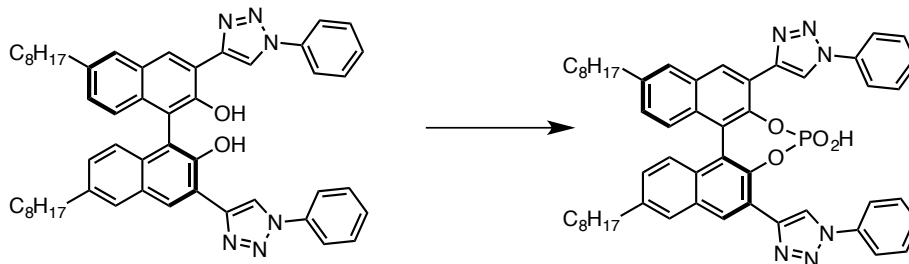
Subjection of *bis*-alkyne **3.7** (1.14 g, 1.76 mmol) and 4-bromophenyl azide (1.05 g, 5.29 mmol) to General Procedure A gave the title compound (1.58 g, 1.51 mmol, 86 % yield) as an amorphous orange solid after purification by column chromatography on silica gel using Hex/EtOAc as eluent (20:1 to 9:1). $^1\text{H NMR}$ (500 MHz, CDCl_3) δ 9.00 (s, 2H), 8.83 (s, 2H), 7.85 (s, 2H), 7.75 (d, J = 6.5 Hz, 4H), 7.70 (d, J = 6.5 Hz, 4H), 7.24 (d, J = 8.5 Hz, 2H), 7.22 (d, J = 8.5 Hz, 2H), 4.65 (d, J = 5.0 Hz, 2H), 4.42 (d, J = 5.0 Hz, 2H), 2.80 (t, J = 7.8 Hz, 4H), 2.74 (s, 6H), 1.80 – 1.67 (m, 4H), 1.46 – 1.25 (m, 20H), 0.91 (t, J = 6.6 Hz, 6H). $^{13}\text{C NMR}$ (126 MHz, CDCl_3) δ 149.0, 144.4, 140.5, 136.1, 133.0, 132.3, 131.22, 129.1, 128.2, 127.1, 125.9, 125.7, 123.6, 122.3, 121.8, 121.0, 98.8, 57.1, 35.9, 31.9, 31.2, 29.5, 29.5, 29.3, 22.7, 14.2. **HRMS** (ESI) found $[\text{M}+\text{H}]^+$ 1041.3284, $\text{C}_{56}\text{H}_{63}\text{N}_6\text{O}_4\text{Br}_2$ requires 1041.3272.

(S)-6,6'-dioctyl-3,3'-bis(1-phenyl-1*H*-1,2,3-triazol-4-yl)-[1,1'-binaphthalene]-2,2'-diol (diol-3.4f)



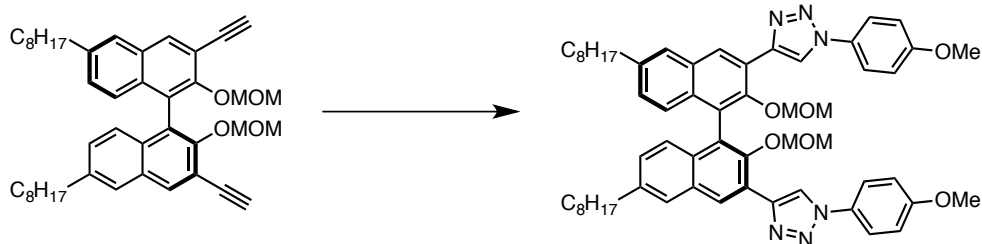
A 100-mL round bottomed flask was charged with **MOM-3.4f** (0.820 g, 0.786 mmol), 15 % palladium on carbon (0.110 g), EtOAc (10 mL) and MeOH (15 mL). The reaction mixture was stirred at room temperature under H_2 (1 atm). The reaction was judged to be complete in 2 h by TLC analysis, at which point the mixture was filtered through Celite, washed with saturated aqueous NaHCO_3 (20 mL), extracted with DCM (2 X 20 mL), dried (Na_2SO_4) and concentrated *in vacuo*. The title compound (0.458 g, 0.575 mmol, 73 % yield) was obtained after column chromatography on silica gel using Hex/EtOAc as eluent (9:1). $^1\text{H NMR}$ (500 MHz, CDCl_3) δ 9.26 (s, 1H), 8.56 (s, 2H), 8.42 (s, 2H), 7.82 (d, J = 7.8 Hz, 4H), 7.63 (s, 2H), 7.55 (t, J = 7.6 Hz, 4H), 7.48 (t, J = 7.5 Hz, 2H), 7.17 (d, J = 8.6 Hz, 2H), 7.11 (d, J = 8.6 Hz, 2H), 2.69 (t, J = 7.7 Hz, 4H), 1.70 - 1.63 (m, 4H), 1.40 - 1.27 (m, 20H), 0.90 (t, J = 6.7 Hz, 6H). $^{13}\text{C NMR}$ (126 MHz, CDCl_3) δ 150.1, 146.8, 138.4, 136.8, 132.2, 129.8, 129.0, 128.9, 128.8, 126.7, 126.4, 124.6, 120.7, 119.3, 117.07, 115.9, 35.9, 31.9, 31.31, 29.6, 29.5, 29.3, 22.7, 14.2. **HRMS** (ESI) found $[\text{M}-\text{H}]^-$ 795.4365, $\text{C}_{52}\text{H}_{55}\text{N}_6\text{O}_2$ requires 795.4392.

(11*bS*)-4-hydroxy-9,14-dioctyl-2,6-bis(1-phenyl-1*H*-1,2,3-triazol-4-yl)dinaphtho[2,1-*d*:1',2'-*f*][1,3,2]dioxaphosphepine 4-oxide (3.4f)



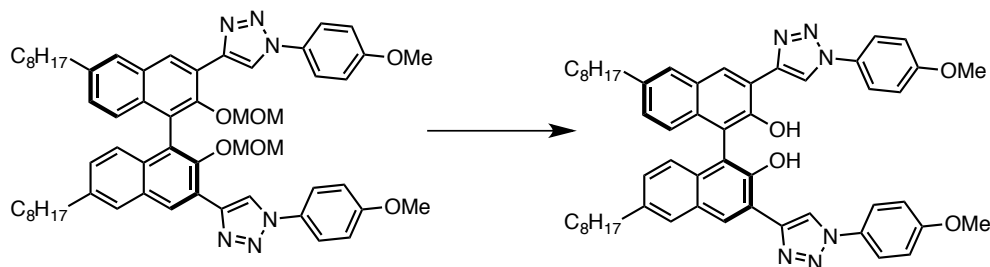
Subjection of **diol-3.4f** (0.458 g, 0.575 mmol) to General Procedure C gave the title compound (0.454 g, 0.528 mmol, 92 % yield) as a beige powder after purification by column chromatography on silica gel using DCM/MeOH as eluent (40:1 to 20:1). $^1\text{H NMR}$ (500 MHz, CDCl_3 :DMSO- d_6 2:1) δ 8.89 (s, 2H), 8.69 (s, 2H), 7.77 (d, $J = 7.7$ Hz, 4H), 7.72 (s, 2H), 7.42 (t, $J = 7.8$ Hz, 4H), 7.32 (t, $J = 7.4$ Hz, 2H), 7.08 (d, $J = 9.0$ Hz, 2H), 7.05 (d, $J = 9.0$ Hz, 2H), 2.71 (t, $J = 7.8$ Hz, 4H), 1.75 - 1.54 (m, 4H), 1.42 - 1.08 (m, 20H), 0.82 (t, $J = 6.6$ Hz, 6H). $^{13}\text{C NMR}$ (126 MHz, CDCl_3 :DMSO- d_6 2:1) δ 143.7 (d, $J = 9.5$ Hz), 143.0, 140.6, 136.9, 131.3, 130.3, 129.8, 128.7, 128.7, 128.4, 127.1, 126.6, 122.6, 122.4, 121.9, 120.4, 35.7, 31.8, 31.1, 29.4, 29.4, 29.2, 22.6, 14.2. $^{31}\text{P NMR}$ (202 MHz, CDCl_3 :DMSO- d_6 2:1) δ 2.8. **HRMS** (ESI) found $[\text{M}-\text{H}]^-$ 857.3921, $\text{C}_{52}\text{H}_{54}\text{N}_6\text{O}_4\text{P}$ requires 857.3950.

(S)-4,4'-(2,2'-bis(methoxymethoxy)-6,6'-dioctyl-[1,1'-binaphthalene]-3,3'-diyl)bis(1-(4-methoxyphenyl)-1H-1,2,3-triazole) (MOM-3.4g)



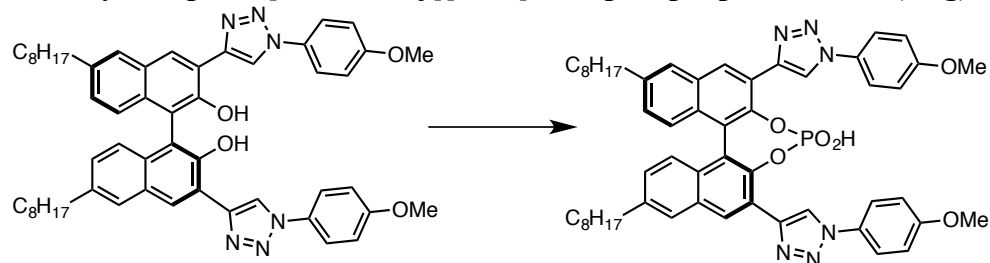
Subjection of *bis*-alkyne **3.7** (0.335 g, 0.518 mmol) and 4-methoxyphenyl azide (0.232 g, 1.56 mmol) to General Procedure A gave the title compound (0.400 g, 0.423 mmol, 82 % yield) as an amorphous solid after purification by column chromatography on silica gel using Hex/EtOAc as eluent (9:1). $^1\text{H NMR}$ (500 MHz, CDCl_3) δ 8.98 (s, 2H), 8.74 (s, 2H), 7.83 (s, 2H), 7.74 (d, $J = 9.0$ Hz, 4H), 7.24 (d, $J = 8.5$ Hz, 2H), 7.20 (d, $J = 8.5$ Hz, 2H), 7.05 (d, $J = 9.0$ Hz, 4H), 4.67 (d, $J = 4.9$ Hz, 2H), 4.42 (d, $J = 4.9$ Hz, 2H), 3.89 (s, 6H), 2.78 (t, $J = 7.8$ Hz, 4H), 2.70 (s, 6H), 1.77 - 1.68 (m, 4H), 1.44 - 1.27 (m, 20H), 0.90 (t, $J = 6.4$ Hz, 6H). $^{13}\text{C NMR}$ (126 MHz, CDCl_3) δ 159.8, 149.0, 144.0, 140.4, 132.2, 131.2, 130.6, 128.9, 128.0, 127.0, 126.0, 125.8, 124.0, 122.0, 121.4, 114.8, 98.7, 57.1, 55.7, 35.9, 31.9, 31.2, 29.5, 29.5, 29.3, 22.7, 14.2. **HRMS** (ESI) found $[\text{M}+\text{H}]^+$ 945.5281, $\text{C}_{58}\text{H}_{69}\text{N}_6\text{O}_6$ requires 945.5273.

(S)-3,3'-bis(1-(4-methoxyphenyl)-1H-1,2,3-triazol-4-yl)-6,6'-dioctyl-[1,1'-binaphthalene]-2,2'-diol (diol-3.4g)



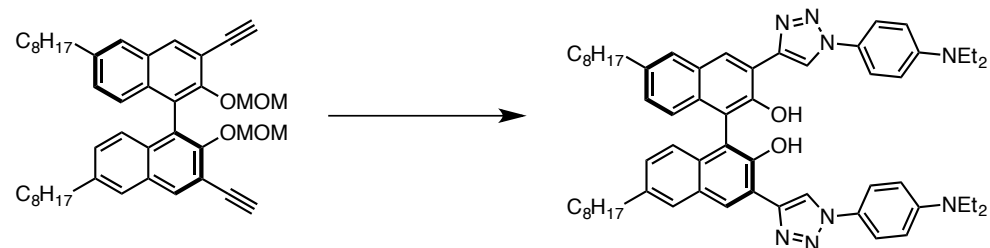
Subjection of **MOM-3.4g** (0.350 g, 0.370 mmol) to General Procedure B gave the title compound (0.277 g, 0.323 mmol, 87 % yield) as a beige powder after purification by column chromatography on silica gel using Hex/EtOAc as eluent (9:1). $^1\text{H NMR}$ (400 MHz, CDCl_3) δ 9.39 (s, 1H), 8.51 (s, 2H), 8.45 (s, 2H), 7.77 (s, 2H), 7.74 (s, 2H), 7.70 (s, 2H), 7.20 (d, 2H), 7.15 (d, 2H), 7.12 – 7.04 (m, 4H), 3.92 (s, 6H), 2.74 (t, $J = 7.6$ Hz, 4H), 1.81 – 1.66 (m, 4H), 1.50 – 1.24 (m, 20H), 0.91 (t, $J = 6.8$ Hz, 6H). $^{13}\text{C NMR}$ (101 MHz, CDCl_3) δ 160.0, 150.2, 146.8, 138.3, 132.3, 130.2, 128.8, 128.7, 126.7, 126.2, 124.7, 122.3, 119.4, 117.1, 116.1, 114.8, 55.6, 35.9, 31.9, 31.3, 29.6, 29.5, 29.3, 22.7, 14.2. **HRMS** (ESI) found $[\text{M}+\text{H}]^+$ 857.4760, $\text{C}_{54}\text{H}_{61}\text{N}_6\text{O}_4$ requires 857.4749.

(4*R*,11*S*)-4-hydroxy-2,6-bis(1-(4-methoxyphenyl)-1*H*-1,2,3-triazol-4-yl)-9,14-dioctyldinaphtho[2,1-*d*:1',2'-*f*][1,3,2]dioxaphosphepine 4-oxide (3.4g)



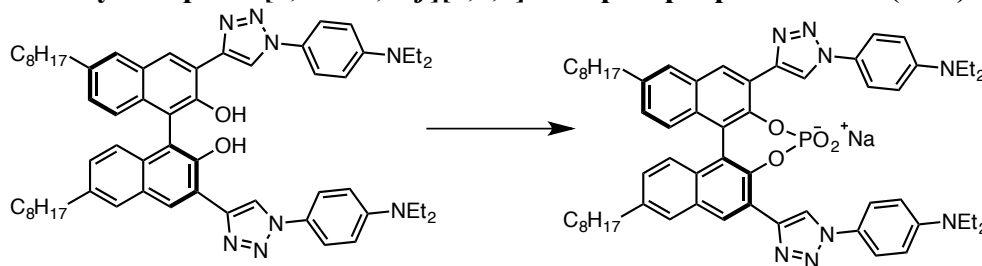
Subjection of **diol-3.4g** (0.267 g, 0.312 mmol) to General Procedure C gave the title compound (0.263 g, 0.286 mmol, 92 % yield) as a beige powder after purification by column chromatography on silica gel using DCM/MeOH as eluent (40:1 to 20:1). $^1\text{H NMR}$ (400 MHz, 2:1 CDCl_3 : $\text{DMSO-}d_6$) δ 9.02 (s, 2H), 8.72 (s, 2H), 7.92 (s, 2H), 7.75 (d, $J = 8.5$ Hz, 4H), 7.24 – 6.97 (m, 8H), 3.78 (s, 6H), 2.70 (t, $J = 7.7$ Hz, 4H), 1.77 – 1.53 (m, 4H), 1.42 – 1.08 (m, 20H), 0.81 (t, $J = 6.4$ Hz, 6H). $^{13}\text{C NMR}$ (126 MHz, 1:1 CDCl_3 : $\text{DMSO-}d_6$) δ 159.6, 143.8 (d, $J = 9.0$ Hz), 142.7, 140.4, 131.3, 130.3, 130.2, 128.6, 128.1, 127.2, 126.5, 122.6, 122.5, 122.0, 121.9, 114.9, 55.6, 35.7, 31.8, 31.1, 29.5, 29.4, 29.3, 22.7, 14.4. $^{31}\text{P NMR}$ (162 MHz, 2:1 CDCl_3 : $\text{DMSO-}d_6$) δ 3.3. **HRMS** (ESI) found $[\text{M}+\text{H}]^+$ 919.4334, $\text{C}_{54}\text{H}_{60}\text{N}_6\text{O}_6\text{P}$ requires 919.4306.

(*S*)-3,3'-bis(1-(4-(diethylamino)phenyl)-1*H*-1,2,3-triazol-4-yl)-6,6'-dioctyl-[1,1'-binaphthalene]-2,2'-diol (diol-3.4h)



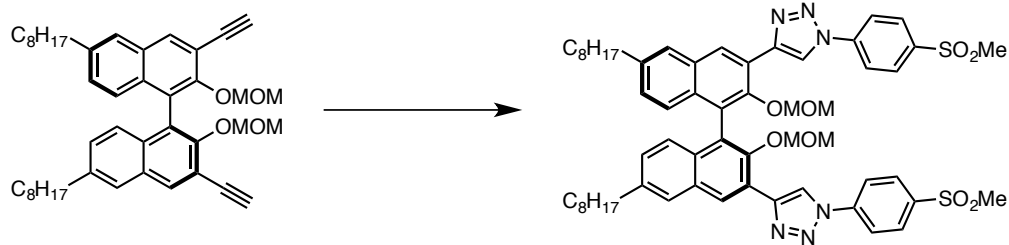
Subjection of *bis*-alkyne **3.7** (0.500 g, 0.772 mmol) to General Procedure A resulted in no detectable conversion after 48 h as judged by TLC analysis. Thus, the temperature of the reaction was transferred to a round-bottomed flask fitted with a reflux condenser and heated at 100 °C for ca. 1h at which point full conversion was observed. Upon inspection of the resulting ¹H NMR spectrum, it was noted that in addition to the desired cycloaddition reaction, the methoxymethyl groups had been fully removed, resulting in the direct formation of *diol*-**3.4h** from **3.7**. Flash chromatography on silica gel using Hex/EtOAc as eluent (9:1 to 1:1) afforded the product (0.280 g, 0.298 mmol, 39 % yield) as an off-white powder. ¹H NMR (400 MHz, CDCl₃) δ 9.88 (s, 1H), 8.43 (s, 2H), 8.38 (s, 2H), 7.68 (s, 2H), 7.62 (d, *J* = 9.1 Hz, 4H), 7.23 (d, *J* = 10.0 Hz, 2H), 7.14 (d, *J* = 10.0 Hz, 2H), 6.77 (d, *J* = 9.1 Hz, 4H), 3.44 (q, *J* = 7.1 Hz, 8H), 2.74 (t, *J* = 7.7 Hz, 4H), 1.79 – 1.61 (m, 4H), 1.44 – 1.29 (m, 20H), 1.24 (t, *J* = 7.1 Hz, 12H), 0.93 (t, *J* = 6.7 Hz, 6H). ¹³C NMR (101 MHz, CDCl₃) δ 150.4, 148.2, 146.8, 138.1, 132.3, 128.7, 126.6, 125.9, 125.5, 124.8, 122.3, 118.9, 117.3, 116.4, 111.6, 44.6, 35.9, 32.0, 31.3, 29.6, 29.5, 29.3, 22.7, 14.2, 12.5. HRMS (ESI) found [M+H]⁺ 939.6027, C₆₀H₇₅N₈O₂ requires 939.6008.

(11*bS*)-2,6-bis(1-(4-(diethylamino)phenyl)-1*H*-1,2,3-triazol-4-yl)-4-hydroxy-9,14-dioctyldinaphtho[2,1-*d*:1',2'-*f*][1,3,2]dioxaphosphepine 4-oxide (3.4h)



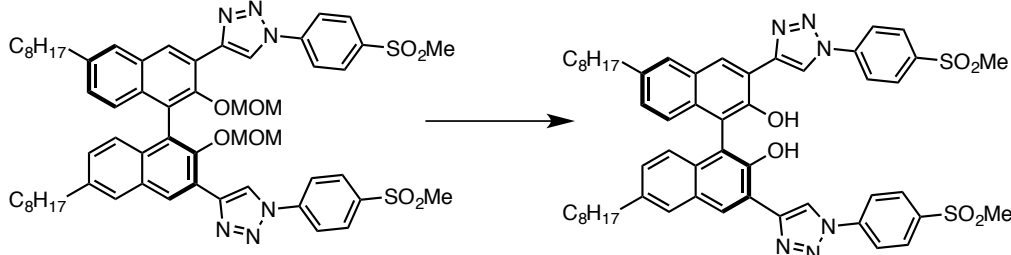
Subjection of *diol*-**3.4h** (0.272 g, 0.290 mmol) to General Procedure C gave the title compound (0.122 g, 0.122 mmol, 42 % yield) as a beige powder after precipitation from DCM with MeCN. As the phosphoric acid appeared to undergo extensive self-aggregation in solution, it was quantitatively deprotonated by stirring with Na₂CO₃ (10 equiv) in DCM/DMSO (1:1) overnight prior to spectroscopic analysis. ¹H NMR (500 MHz, CDCl₃) δ 9.19 (s, 2H), 8.67 (s, 2H), 7.92 (s, 2H), 7.59 (d, *J* = 8.6 Hz, 4H), 7.17 (d, *J* = 8.6 Hz, 2H), 7.08 (d, *J* = 8.7 Hz, 2H), 6.87 (d, *J* = 9.0 Hz, 4H), 3.42 (q, *J* = 7.0 Hz, 8H), 2.74 (t, *J* = 7.7 Hz, 4H), 1.75 – 1.59 (m, 4H), 1.41 – 1.20 (m, 20H), 1.14 (t, *J* = 7.0 Hz, 12H), 0.86 (t, *J* = 6.9 Hz, 6H). ¹³C NMR (126 MHz, CDCl₃) δ 147.8, 146.2 (d, *J* = 10.1 Hz), 143.4, 139.5, 130.8, 130.7, 127.9, 127.3, 126.9, 126.6, 125.8, 124.0, 123.2, 122.9, 122.2, 111.7, 44.5, 31.8, 31.2, 31.0, 29.4, 29.3, 29.2, 22.6, 14.3, 12.6. ³¹P NMR (162 MHz, DMSO) δ 4.9. HRMS (ESI) found [M+Na]⁺ 1023.5415, C₆₀H₇₃N₈O₄Na₁P requires 1023.5385.

(S)-4,4'-(2,2'-bis(methoxymethoxy)-6,6'-dioctyl-[1,1'-binaphthalene]-3,3'-diyl)bis(1-(4-(methylsulfonyl)phenyl)-1H-1,2,3-triazole) (MOM-3.4i)



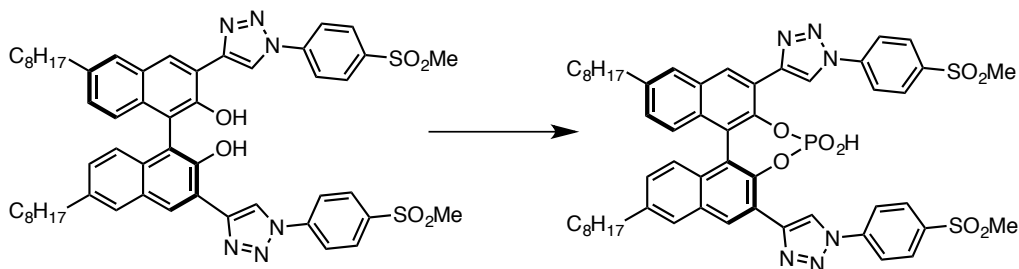
Subjection of *bis*-alkyne **3.7** (0.330 g, 0.509 mmol) and 4-(methylsulfonyl)phenyl azide (0.301 g, 1.53 mmol) to General Procedure A gave the title compound (0.360 g, 0.346 mmol, 68 % yield) as an orange-white powder after purification by column chromatography on silica gel using Hex/EtOAc as eluent (1:1). $^1\text{H NMR}$ (600 MHz, CDCl_3) δ 8.98 (s, 1H), 8.93 (s, 2H), 8.13 (d, J = 8.3 Hz, 4H), 8.07 (d, J = 8.4 Hz, 4H), 7.83 (s, 2H), 7.23 (app q, J = 9.0 Hz, 4H), 4.63 (d, J = 5.0 Hz, 2H), 4.41 (d, J = 5.2 Hz, 2H), 3.11 (s, 6H), 2.87 – 2.66 (m, 10H), 1.77 – 1.63 (m, 4H), 1.49 – 1.15 (m, 20H), 0.86 (t, J = 6.7 Hz, 6H). $^{13}\text{C NMR}$ (151 MHz, CDCl_3) δ 149.0, 144.8, 140.7, 140.6, 140.3, 132.3, 131.1, 129.5, 129.2, 128.3, 127.1, 125.8, 125.6, 123.2, 120.9, 120.5, 98.8, 57.2, 44.5, 35.8, 31.8, 31.1, 29.4, 29.4, 29.2, 22.6, 14.1. **HRMS** (ESI) found $[\text{M}+\text{H}]^+$ 1041.4654, $\text{C}_{58}\text{H}_{69}\text{N}_6\text{O}_8\text{S}_2$ requires 1041.4613.

(S)-3,3'-bis(1-(4-(methylsulfonyl)phenyl)-1H-1,2,3-triazol-4-yl)-6,6'-dioctyl-[1,1'-binaphthalene]-2,2'-diol (*diol*-3.4i)



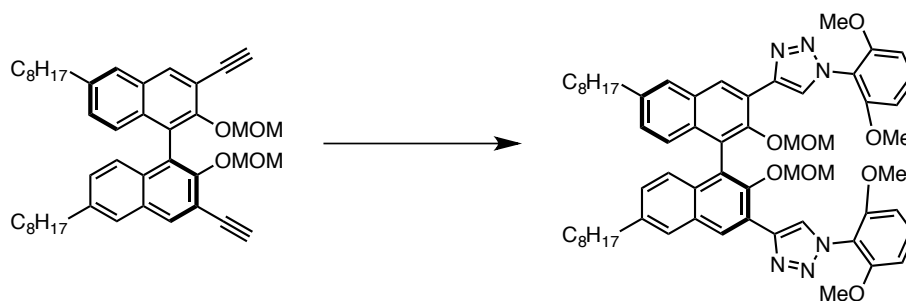
Subjection of **MOM-3.4i** (0.350 g, 0.336 mmol) to General Procedure B gave the title compound (0.259 g, 0.271 mmol, 81 % yield) as a white solid after purification by column chromatography on silica gel using Hex/EtOAc as eluent (1:1 to 1:3). $^1\text{H NMR}$ (300 MHz, CDCl_3) δ 8.88 (s, 2H), 8.62 (s, 2H), 8.33 (s, 2H), 8.14 – 7.83 (m, 8H), 7.55 (s, 2H), 7.16 – 7.02 (m, 4H), 3.07 (s, 6H), 2.65 (t, J = 7.8 Hz, 4H), 1.74 – 1.56 (m, 4H), 1.45 – 1.15 (m, 20H), 0.86 (t, J = 6.6 Hz, 6H). $^{13}\text{C NMR}$ (101 MHz, CDCl_3) δ 149.8, 146.9, 140.3, 140.2, 138.6, 132.2, 129.2, 129.2, 128.6, 126.7, 124.5, 120.9, 119.6, 116.4, 115.9, 44.5, 35.8, 31.9, 31.2, 29.6, 29.3, 22.7, 14.1. **HRMS** (ESI) found $[\text{M}+\text{H}]^+$ 953.4120, $\text{C}_{54}\text{H}_{61}\text{N}_6\text{O}_6\text{S}_2$ requires 953.4089.

(11b*S*)-4-hydroxy-2,6-bis(1-(4-(methylsulfonyl)phenyl)-1*H*-1,2,3-triazol-4-yl)-9,14-dioctyldinaphtho[2,1-*d*:1',2'-*f*][1,3,2]dioxaphosphepine 4-oxide (3.4i)



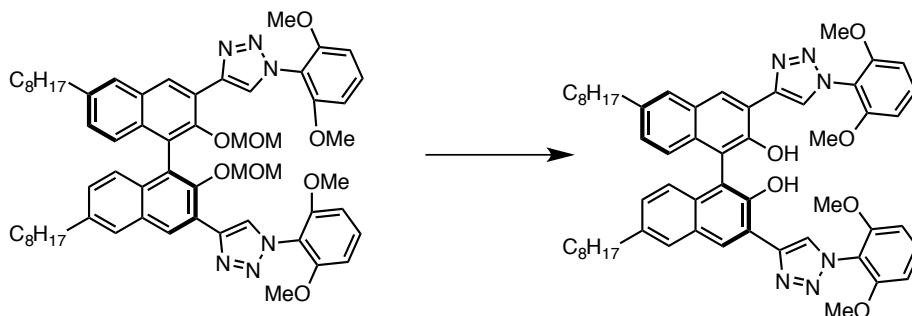
Subjection of *diol-3.4i* (0.259 g, 0.272 mmol) to General Procedure C gave the title compound (0.231 g, 0.227 mmol, 83 % yield) as a beige powder. $^1\text{H NMR}$ (500 MHz, $\text{DMSO-}d_6$) δ 9.47 (s, 2H), 8.74 (s, 2H), 8.35 – 8.08 (m, 8H), 7.97 (s, 2H), 7.22 (d, $J = 8.5$ Hz, 2H), 7.10 (d, $J = 7.8$ Hz, 2H), 3.32 (s, 6H), 2.74 (br s, 4H), 1.78 – 1.52 (m, 4H), 1.44 – 1.07 (m, 20H), 0.84 (br s, $J = 14.6$, 6.6 Hz, 6H). $^{13}\text{C NMR}$ (126 MHz, 1:1 CDCl_3 : $\text{DMSO-}d_6$) δ 143.6 (d, $J = 9.5$ Hz), 143.1, 141.7, 140.1, 140.0, 131.0, 130.0, 129.2, 128.5, 127.7, 127.1, 126.2, 122.2, 121.6, 121.4, 120.3, 44.3, 35.8, 31.9, 31.1, 29.6, 29.5, 29.3, 22.7, 14.4. $^{31}\text{P NMR}$ (202 MHz, $\text{DMSO-}d_6$) δ 4.3. **HRMS** (ESI) found $[\text{M}+\text{H}]^+$ 1015.3686, $\text{C}_{54}\text{H}_{60}\text{N}_6\text{O}_8\text{P}_1\text{S}_2$ requires 1015.3646.

(*S*)-4,4'-(2,2'-bis(methoxymethoxy)-6,6'-dioctyl-[1,1'-binaphthalene]-3,3'-diyl)bis(1-(2,6-dimethoxyphenyl)-1*H*-1,2,3-triazole) (MOM-3.4j)



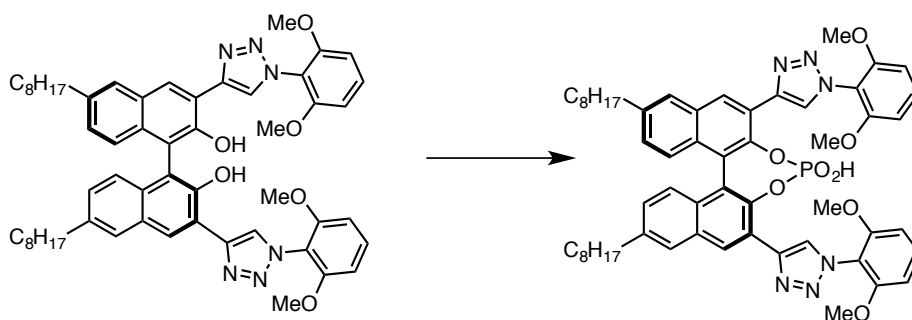
Subjection of *bis-alkyne 3.7* (0.500 g, 0.772 mmol) and 2,6-dimethoxyphenyl azide (0.414 g, 2.32 mmol) to General Procedure A gave the title compound (0.326 g, 0.324 mmol, 42 % yield) as a white powder after purification by column chromatography on silica gel using Hex/EtOAc as eluent (4:1 to 1.5:1). $^1\text{H NMR}$ (600 MHz, CDCl_3) δ 8.93 (s, 2H), 8.36 (s, 2H), 7.78 (s, 2H), 7.39 (t, $J = 8.5$ Hz, 2H), 7.21 (d, $J = 8.6$ Hz, 2H), 7.15 (d, $J = 8.6$ Hz, 2H), 6.67 (d, $J = 8.5$ Hz, 4H), 4.66 (d, $J = 4.9$ Hz, 2H), 4.43 (d, $J = 4.9$ Hz, 2H), 3.76 (s, 12H), 2.75 (t, $J = 7.7$ Hz, 4H), 2.59 (s, 6H), 1.70 (t, $J = 7.4$ Hz, 4H), 1.43 - 1.17 (m, 20H), 0.87 (t, $J = 6.3$ Hz, 6H). $^{13}\text{C NMR}$ (151 MHz, CDCl_3) δ 155.9, 149.2, 142.5, 140.0, 132.1, 131.2, 131.2, 128.4, 127.9, 126.9, 126.8, 126.0, 125.7, 124.5, 115.4, 104.3, 98.3, 56.6, 56.1, 35.8, 31.8, 31.1, 29.5, 29.4, 29.2, 22.6, 14.1. **HRMS** (ESI) found $[\text{M}+\text{H}]^+$ 1005.5507, $\text{C}_{60}\text{H}_{73}\text{N}_6\text{O}_8$ requires 1005.5484.

(S)-3,3'-bis(1-(2,6-dimethoxyphenyl)-1*H*-1,2,3-triazol-4-yl)-6,6'-dioctyl-[1,1'-binaphthalene]-2,2'-diol (*diol-3.4j*)



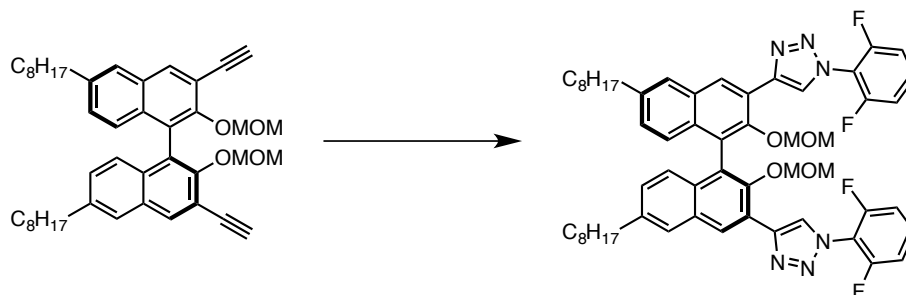
Subjection of **MOM-3.4j** (0.326 g, 0.324 mmol) to General Procedure B gave the title compound (0.235 g, 0.256 mmol, 79 % yield) as a white powder after purification by column chromatography on silica gel using Hex/EtOAc as eluent (1.5:1 to 1:1). ¹H NMR (600 MHz, CDCl₃) δ 10.05 (s, 2H), 8.33 (s, 2H), 8.21 (s, 2H), 7.65 (s, 2H), 7.42 (t, *J* = 8.4 Hz, 2H), 7.21 (d, *J* = 8.6 Hz, 2H), 7.12 (d, *J* = 8.6 Hz, 2H), 6.69 (d, *J* = 8.4 Hz, 4H), 3.79 (s, 12H), 2.71 (t, *J* = 7.7 Hz, 4H), 1.68 (t, *J* = 7.5 Hz, 4H), 1.42 - 1.25 (m, 20H), 0.88 (t, *J* = 7.1 Hz, 6H). ¹³C NMR (151 MHz, CDCl₃) δ 155.9, 150.4, 146.0, 137.9, 132.3, 131.7, 128.6, 128.5, 126.5, 125.7, 124.8, 124.3, 117.3, 116.6, 115.0, 104.3, 56.2, 35.9, 31.9, 31.3, 29.5, 29.4, 29.2, 22.7, 14.1. HRMS (ESI) found [M+H]⁺ 917.4988, C₅₆H₆₅N₆O₆ requires 917.4960.

(1*bS*)-2,6-bis(1-(2,6-dimethoxyphenyl)-1*H*-1,2,3-triazol-4-yl)-4-hydroxy-9,14-dioctyldinaphtho[2,1-*d*:1',2'-*f*][1,3,2]dioxaphosphine 4-oxide (3.4j**)**



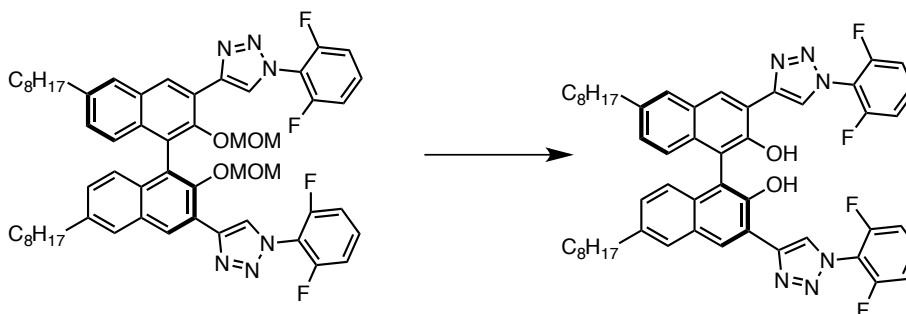
Subjection of **diol-3.4j** (0.235 g, 0.256 mmol) to General Procedure C gave the title compound (0.209 g, 0.213 mmol, 83 % yield) as a beige powder after purification by column chromatography on silica gel using DCM/MeOH as eluent (40:1 to 20:1). ¹H NMR (500 MHz, DMSO-*d*₆) δ 8.75 (s, 2H), 8.62 (s, 2H), 7.95 (s, 2H), 7.55 (t, *J* = 8.5 Hz, 2H), 7.20 (d, *J* = 8.9 Hz, 2H), 7.06 (d, *J* = 8.9 Hz, 2H), 6.91 (d, *J* = 8.7 Hz, 4H), 3.75 (s, 12H), 2.75 (t, *J* = 7.6 Hz, 4H), 1.76 - 1.59 (m, 4H), 1.35 - 1.22 (m, 20H), 0.85 (t, *J* = 6.4 Hz, 6H). ¹³C NMR (126 MHz, 1:1 CDCl₃:DMSO-*d*₆) δ 155.7, 144.0 (d, *J* = 9.7 Hz), 141.3, 140.6, 131.9, 131.5, 130.3, 128.6, 127.9, 127.5, 127.2, 126.6, 123.2, 122.7, 115.1, 104.8, 56.5, 35.7, 31.8, 31.2, 29.4, 29.4, 29.2, 22.7, 14.4. ³¹P NMR (202 MHz, DMSO-*d*₆) δ 3.5. HRMS (ESI) found [M+H]⁺ 979.4541, C₅₆H₆₄N₆O₈P requires 979.451.

(S)-4,4'-(2,2'-bis(methoxymethoxy)-6,6'-dioctyl-[1,1'-binaphthalene]-3,3'-diyl)bis(1-(2,6-difluorophenyl)-1*H*-1,2,3-triazole) (MOM-3.4k)



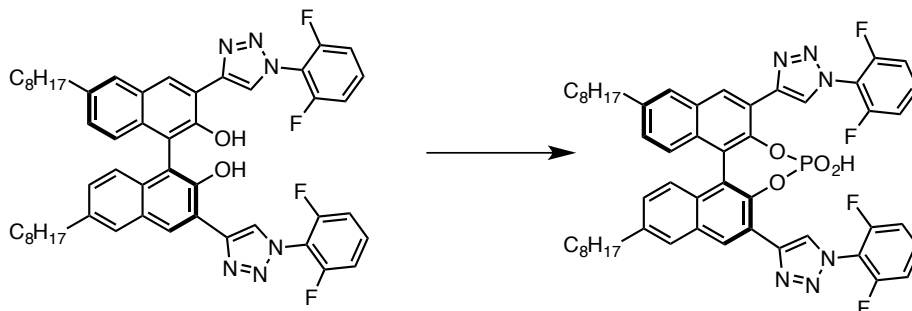
Subjection of *bis*-alkyne **3.7** (0.500 g, 0.772 mmol) and 2,6-difluorophenyl azide (0.360 g, 2.32 mmol) to General Procedure A gave the title compound (0.625 g, 0.653 mmol, 85 % yield) as a light orange amorphous solid after purification by column chromatography on silica gel using Hex/EtOAc as eluent (9:1 to 4:1). $^1\text{H NMR}$ (400 MHz, CDCl_3) δ 9.00 (s, 2H), 8.63 (s, 2H), 7.83 (s, 2H), 7.59 - 7.43 (m, 2H), 7.36 - 7.06 (m, 8H), 4.64 (d, $J = 5.1$ Hz, 2H), 4.44 (d, $J = 5.1$ Hz, 2H), 2.79 (t, $J = 7.8$ Hz, 4H), 2.70 (s, 6H), 1.82 - 1.66 (m, 4H), 1.48 - 1.20 (m, 20H), 0.90 (t, $J = 6.8$ Hz, 6H). $^{13}\text{C NMR}$ (101 MHz, CDCl_3) δ 157.0 (dd, $J = 308, 2.5$ Hz), 149.3, 143.5, 140.3, 132.3, 131.3 (t, $J = 9.4$ Hz), 131.1, 128.9, 128.2, 127.0, 125.9, 125.9, 125.5, 123.6, 115.4 (t, $J = 15.4$ Hz), 112.5 (dd, $J = 19.5, 3.6$ Hz), 98.7, 56.9, 35.9, 31.9, 31.1, 29.5, 29.4, 29.3, 22.7, 14.11. $^{19}\text{F NMR}$ (376 MHz, CDCl_3) δ -118.0 (app t, $J = 6.4$ Hz). **HRMS** (ESI) found $[\text{M}+\text{H}]^+$ 957.4690, $\text{C}_{56}\text{H}_{61}\text{N}_6\text{O}_4\text{F}_4$ requires 957.4685.

(S)-3,3'-bis(1-(2,6-difluorophenyl)-1*H*-1,2,3-triazol-4-yl)-6,6'-dioctyl-[1,1'-binaphthalene]-2,2'-diol (*diol*-3.4k)



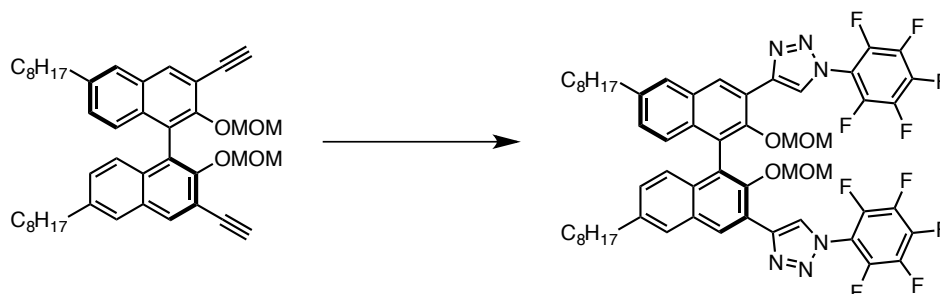
Subjection of **MOM-1k** (0.575 g, 0.590 mmol) to General Procedure B gave the title compound (0.468 g, 0.538 mmol, 91 % yield) as a brownish solid after purification by column chromatography on silica gel using Hex/EtOAc as eluent (1.5:1). $^1\text{H NMR}$ (300 MHz, CDCl_3) δ 8.56 (s, 2H), 8.49 (s, 2H), 8.41 (s, 2H), 7.70 (s, 2H), 7.51 (tt, $J = 8.5, 6.0$ Hz, 2H), 7.22 - 7.09 (m, 8H), 2.71 (t, $J = 12.5$ Hz, 4H), 1.78 - 1.46 (m, 4H), 1.42 - 1.15 (m, 20H), 0.86 (t, $J = 6.7$ Hz, 6H). $^{13}\text{C NMR}$ (126 MHz, CDCl_3) δ 156.9 (dd, $J = 260, 2.5$ Hz), 149.8, 145.7, 138.7, 132.2, 131.6 (t, $J = 9.5$ Hz), 129.2, 128.9, 126.9, 126.9, 124.6, 124.2, 117.1, 115.3, 115.2 (t, $J = 15.2$ Hz), 112.7 (dd, $J = 19.5, 3.6$ Hz), 35.9, 31.9, 31.3, 29.6, 29.5, 29.3, 22.7, 14.2. $^{19}\text{F NMR}$ (470 MHz, CDCl_3) δ -118.7 (app t, $J = 6.1$ Hz). **HRMS** (ESI) found $[\text{M}+\text{H}]^+$ 869.4170, $\text{C}_{52}\text{H}_{53}\text{N}_6\text{O}_2\text{F}_4$ requires 869.4161.

(11b*S*)-2,6-bis(1-(2,6-difluorophenyl)-1*H*-1,2,3-triazol-4-yl)-4-hydroxy-9,14-dioctyldinaphtho[2,1-*d*:1',2'-*f*][1,3,2]dioxaphosphepine 4-oxide (3.4k)



Subjection of *diol-3.4k* (0.418 g, 0.481 mmol) to General Procedure C gave the title compound (0.408 g, 0.438 mmol, 91 % yield) as a beige powder. $^1\text{H NMR}$ (500 MHz, 1:1 CDCl_3 : $\text{DMSO-}d_6$) δ 8.84 (s, 2H), 8.78 (s, 2H), 7.85 (s, 2H), 7.62 (tt, $J = 8.6, 6.1$ Hz, 2H), 7.29 (t, $J = 8.3$ Hz, 4H), 7.17 (s, 4H), 2.74 (t, $J = 7.7$ Hz, 4H), 1.81 – 1.57 (m, 4H), 1.38 – 1.14 (m, 20H), 0.83 (t, $J = 6.7$ Hz, 6H). $^{13}\text{C NMR}$ (151 MHz, 1:1 CDCl_3 : $\text{DMSO-}d_6$) δ 156.7 (dd, $J = 255, 2.7$ Hz), 143.7 (d, $J = 9.7$ Hz), 142.4, 140.8, 132.0 (t, $J = 9.5$ Hz), 131.4, 130.4, 128.8, 128.5, 127.1, 126.6, 126.6, 122.6, 122.2, 115.0 (t, $J = 15.4$ Hz), 112.8 (dd, $J = 19.4, 3.2$ Hz), 35.6, 31.7, 31.0, 29.3, 29.2, 29.1, 22.5, 14.2. $^{19}\text{F NMR}$ (470 MHz, 1:1 CDCl_3 : $\text{DMSO-}d_6$) δ -119.6 (app t, $J = 6.6$ Hz). $^{31}\text{P NMR}$ (162 MHz, 1:1 CDCl_3 : $\text{DMSO-}d_6$) δ 3.1. **HRMS** (ESI) found $[\text{M}+\text{H}]^+$ 931.3732, $\text{C}_{52}\text{H}_{52}\text{N}_6\text{O}_4\text{F}_4\text{P}$ requires 931.3718.

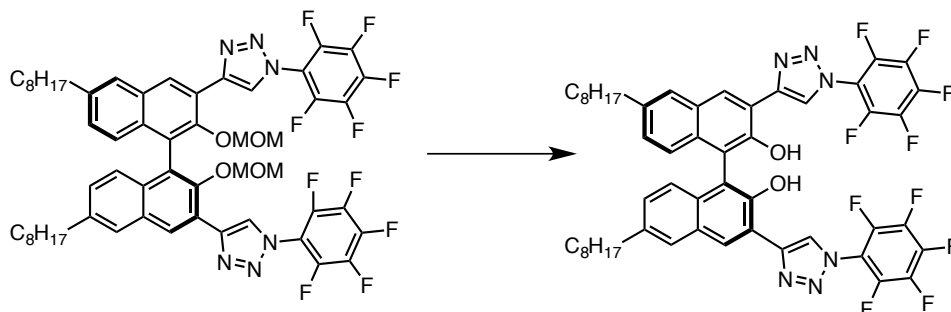
(*S*)-4,4'-(2,2'-bis(methoxymethoxy)-6,6'-dioctyl-[1,1'-binaphthalene]-3,3'-diyl)bis(1-(perfluorophenyl)-1*H*-1,2,3-triazole) (MOM-3.4l)



A 50-mL round bottomed flask was charged with *bis*-alkyne **3.7** (0.500 g, 0.772 mmol), pentafluorophenyl azide (0.646 g, 3.09 mmol), *N,N*-diisopropylethylamine (5 mL) and MeCN (15 mL). To this magnetically stirred solution was added copper (I) iodide (0.103 g, 0.540 mmol) and the reaction mixture was allowed to stir at room temperature under an atmosphere of N_2 for 15 h at which point TLC analysis indicated complete consumption of the starting material. The reaction mixture was partitioned between DCM and H_2O and the organic phase was separated. The aqueous phase was extracted with DCM (2 X 20 mL), the combined organics washed with H_2O (20 mL) and brine (20 mL), dried (Na_2SO_4) and concentrated *in vacuo*. The title compound (0.580 g, 0.545 mmol, 71 % yield) was obtained after purification by column chromatography on silica gel using Hex/EtOAc as eluent (40:1 to 20:1). $^1\text{H NMR}$ (500 MHz, CDCl_3) δ 9.00 (s, 2H), 8.67 (s, 2H), 7.84 (s, 2H), 7.27 – 7.21 (m, 4H), 4.60 (d, $J = 5.1$ Hz, 2H), 4.42 (d, $J = 5.1$ Hz, 2H), 2.80 (t, $J = 7.8$ Hz, 4H), 2.73 (s, 6H), 1.83 – 1.70 (m, 4H), 1.49 – 1.25 (m, 20H), 0.91 (t, $J = 6.6$ Hz, 6H). $^{13}\text{C NMR}$ (126 MHz, CDCl_3) δ 149.2, 144.1, 142.4 (dm, $J = 258$ Hz), 142.3 (dm, $J = 259$ Hz), 140.6, 138.1 (dm, $J = 259$ Hz), 132.4, 131.1, 129.3, 128.5, 127.1, 125.9, 125.6, 125.4, 123.0, 113.3 –

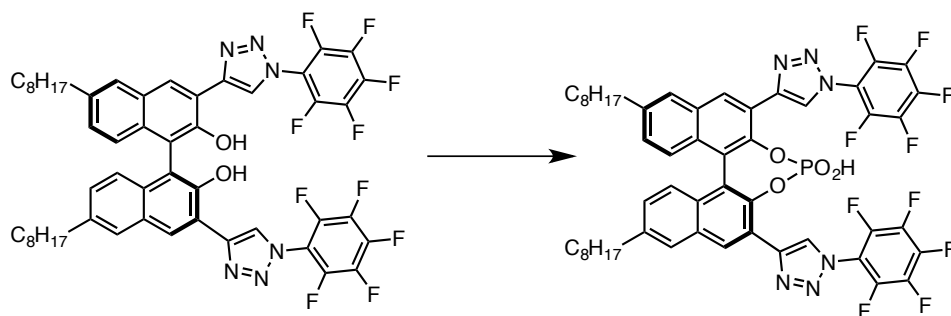
112.9 (m), 98.8, 57.1, 35.9, 31.9, 31.2, 29.5, 29.5, 29.3, 22.7, 14.1. ^{19}F NMR (470 MHz, CDCl_3) δ -145.3 – -145.6 (m), -149.9 (t, $J = 21.4$ Hz), -159.1 – -159.6 (m). HRMS (ESI) found $[\text{M}+\text{H}]^+$ 1065.4161, $\text{C}_{56}\text{H}_{55}\text{N}_6\text{O}_4\text{F}_{10}$ requires 1065.4120.

(S)-6,6'-dioctyl-3,3'-bis(1-(perfluorophenyl)-1H-1,2,3-triazol-4-yl)-[1,1'-binaphthalene]-2,2'-diol (diol-3.4I)



Subjection of **MOM-3.4I** (0.555 g, 0.521 mmol) to General Procedure B gave the title compound (0.424 g, 0.434 mmol, 83 % yield) as an off-white powder after purification by column chromatography on silica gel using Hex/EtOAc as eluent (20:1 to 9:1). ^1H NMR (500 MHz, CDCl_3) δ 8.74 (s, 2H), 8.46 (s, 2H), 7.77 (s, 2H), 7.60 (s, 2H), 7.20 (d, $J = 9.0$ Hz, 2H), 7.15 (d, $J = 9.0$ Hz, 2H), 2.76 (t, $J = 7.7$ Hz, 4H), 1.76 – 1.65 (m, 4H), 1.45 – 1.22 (m, 20H), 0.90 (t, $J = 6.5$ Hz, 6H). ^{13}C NMR (126 MHz, CDCl_3) δ 149.4, 145.4, 142.5 (dm, $J = 258$ Hz), 142.4 (dm, $J = 260$ Hz), 139.1, 138.2 (dm, $J = 258$ Hz), 132.1, 129.5, 129.0, 127.5, 127.0, 124.5, 124.4, 117.0, 114.4, 113.2-112.7 (m), 35.9, 31.9, 31.3, 29.6, 29.5, 29.3, 22.7, 14.2. ^{19}F NMR (470 MHz, CDCl_3) δ -144.9 – -145.6 (m), -149.6 (t, $J = 21.5$ Hz), -158.5 – -159.6 (m). HRMS (ESI) found $[\text{M}-\text{H}]^-$ 975.3435, $\text{C}_{52}\text{H}_{45}\text{N}_6\text{O}_2\text{F}_{10}$ requires 975.3450.

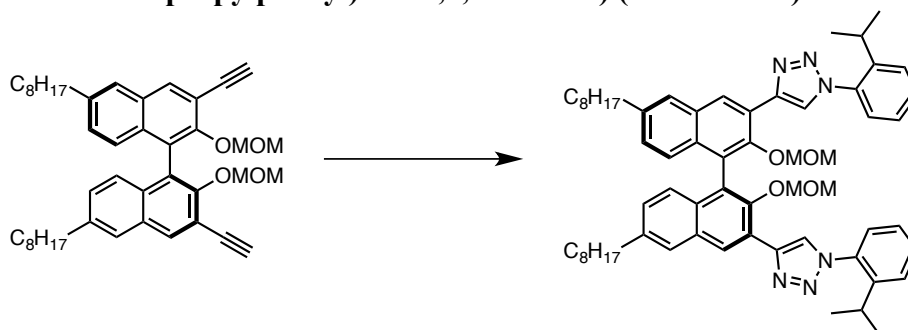
(11bS)-4-hydroxy-9,14-dioctyl-2,6-bis(1-(perfluorophenyl)-1H-1,2,3-triazol-4-yl)dinaphtho[2,1-d:1',2'-f][1,3,2]dioxaphosphepine 4-oxide (3.4I)



Subjection of **diol-3.4I** (0.200 g, 0.205 mmol) to General Procedure C at room temperature gave the title compound (0.198 g, 0.191 mmol, 93 % yield) as a yellow powder after purification by column chromatography on silica gel using DCM/MeOH as eluent (40:1 to 20:1). ^1H NMR (500 MHz, $\text{DMSO}-d_6$) δ 9.18 (s, 2H), 8.81 (s, 2H), 7.98 (s, 2H), 7.24 (d, $J = 8.9$ Hz, 2H), 7.10 (d, $J = 8.8$ Hz, 2H), 2.75 (t, $J = 7.7$ Hz, 4H), 1.77 – 1.60 (m, 4H), 1.44 – 1.18 (m, 20H), 0.86 (t, $J = 6.6$ Hz, 6H). ^{13}C NMR (126 MHz, CDCl_3) δ 144.3 (d, $J = 9.3$ Hz), 142.8, 142.6 (dm, $J = 256.2$ Hz),

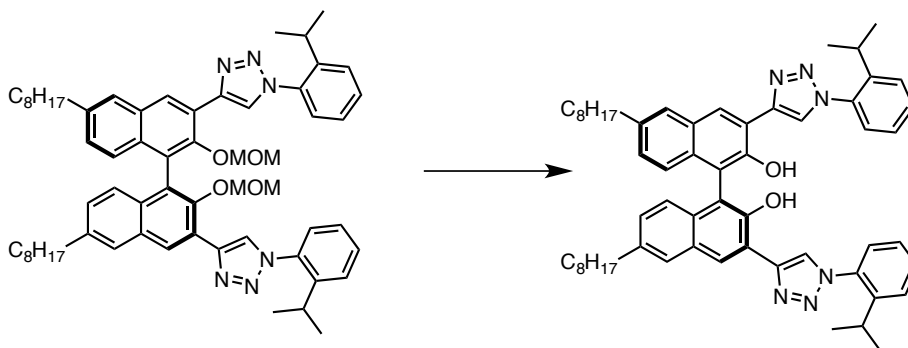
142.0 (dm, $J = 142.02$), 140.4, 138.0 (dm, $J = 258.3$ Hz), 131.1, 130.5, 128.8, 128.2, 127.3, 127.0, 126.6, 122.7, 122.0, 113.3 (m), 35.6, 31.8, 31.1, 29.4, 29.4, 29.3, 22.64 14.3. ^{19}F NMR (470 MHz, C_6D_6) δ -146.6 (app d, $J = 19.9$ Hz), -151.8 (t, $J = 22.5$ Hz), -160.9 (app t, $J = 21.1$ Hz). ^{31}P NMR (202 MHz, CDCl_3) δ 3.5. HRMS (ESI) found $[\text{M}-\text{H}]^-$ 1037.2988, $\text{C}_{52}\text{H}_{44}\text{N}_6\text{O}_4\text{F}_{10}\text{P}$ requires 1037.3007.

(S)-4,4'-(2,2'-bis(methoxymethoxy)-6,6'-dioctyl-[1,1'-binaphthalene]-3,3'-diyl)bis(1-(2-isopropylphenyl)-1H-1,2,3-triazole) (MOM-3.4m)



Subjection of *bis*-alkyne **3.7** (0.500 g, 0.772 mmol) and 2-isopropylphenyl azide (0.373 g, 2.31 mmol) to General Procedure A gave the title compound (0.392 g, 0.404 mmol, 52 % yield) as reddish foam after purification by column chromatography on silica gel using Hex/EtOAc as eluent (9:1). ^1H NMR (500 MHz, CDCl_3) δ 9.03 (s, 2H), 8.55 (s, 2H), 7.83 (s, 2H), 7.58 – 7.49 (m, 4H), 7.39 – 7.31 (m, 4H), 7.26 (d, $J = 8.5$ Hz, 2H), 7.22 (d, $J = 8.5$ Hz, 2H), 4.66 (d, $J = 4.9$ Hz, 2H), 4.45 (d, $J = 4.9$ Hz, 2H), 2.90 (hept, $J = 6.7$ Hz, 2H), 2.80 (t, $J = 7.8$ Hz, 4H), 2.70 (s, 6H), 1.79 – 1.71 (m, 4H), 1.47 – 1.27 (m, 20H), 1.26 – 1.20 (m, 12H), 0.91 (t, $J = 6.6$ Hz, 6H). ^{13}C NMR (126 MHz, CDCl_3) δ 149.1, 144.9, 143.4, 140.3, 135.3, 132.3, 131.2, 130.5, 128.8, 128.0, 127.0, 127.0, 126.6, 126.6, 126.0, 125.7, 125.5, 124.0, 98.6, 56.9, 35.9, 31.9, 31.2, 29.5, 29.5, 29.3, 28.0, 24.0, 23.8, 22.7, 14.2. HRMS (ESI) found $[\text{M}+\text{H}]^+$ 969.6027, $\text{C}_{62}\text{H}_{77}\text{N}_6\text{O}_4$ requires 969.6001.

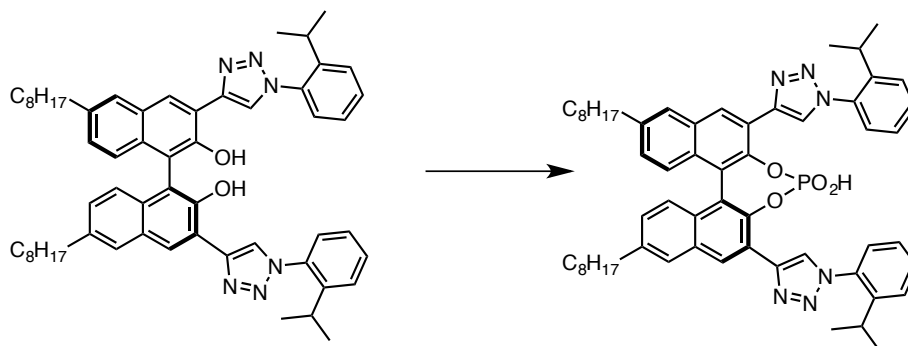
(S)-3,3'-bis(1-(2-isopropylphenyl)-1H-1,2,3-triazol-4-yl)-6,6'-dioctyl-[1,1'-binaphthalene]-2,2'-diol (diol-3.4m)



Subjection of **MOM-1m** (0.342 g, 0.353 mmol) to General Procedure B gave the title compound (0.270 g, 0.307 mmol, 87 % yield) as a yellow powder after purification by column chromatography on silica gel using Hex/EtOAc as eluent (9:1). ^1H NMR (500 MHz, CDCl_3) δ 9.49 (s, 2H), 8.47 (s, 2H), 8.34 (s, 2H), 7.71 (s, 2H), 7.61 – 7.54 (m, 4H), 7.43 – 7.37 (m, 4H), 7.23 (d, $J = 8.5$ Hz, 2H), 7.18 (d, $J = 8.5$ Hz, 2H), 2.86 (hept, $J = 6.9$ Hz, 2H), 2.76 (t, $J = 7.7$ Hz,

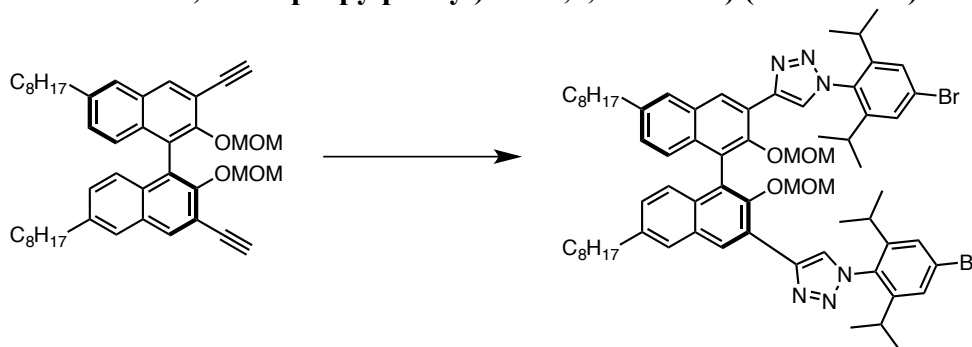
4H), 1.76 – 1.66 (m, 4H), 1.45 – 1.29 (m, 20H), 1.29 – 1.24 (m, 12H), 0.92 (t, $J = 6.6$ Hz, 6H). ^{13}C NMR (126 MHz, CDCl_3) δ 150.2, 146.3, 145.1, 138.4, 135.0, 132.4, 130.8, 128.9, 128.8, 127.0, 126.7, 126.6, 126.3, 124.8, 123.4, 117.1, 116.2, 36.0, 32.0, 31.4, 29.6, 29.5, 29.4, 28.0, 24.0, 22.7, 14.2. HRMS (ESI) found $[\text{M}-\text{H}]^-$ 879.5321, $\text{C}_{58}\text{H}_{67}\text{N}_6\text{O}_2$ requires 879.5331.

(11bS)-4-hydroxy-2,6-bis(1-(2-isopropylphenyl)-1H-1,2,3-triazol-4-yl)-9,14-dioctyldinaphtho[2,1-d':1',2'-f][1,3,2]dioxaphosphepine 4-oxide (3.4m)



Subjection of *diol-3.4m* (0.215 g, 0.244 mmol) to General Procedure C gave the title compound (0.211 g, 0.224 mmol, 92 % yield) as a yellowish powder after purification by column chromatography on silica gel using DCM/MeOH as eluent (40:1). ^1H NMR (500 MHz, DMSO) δ 8.87 (s, 2H), 8.81 (s, 2H), 7.98 (s, 2H), 7.71 – 7.59 (m, 4H), 7.52 – 7.43 (m, 4H), 7.23 (d, $J = 8.6$ Hz, 2H), 7.11 (d, $J = 8.8$ Hz, 2H), 2.84 – 2.66 (m, 6H), 1.78 – 1.60 (m, 4H), 1.38 – 1.21 (m, 20H), 1.17 (d, $J = 6.9$ Hz, 12H), 0.85 (t, $J = 6.6$ Hz, 6H). ^{13}C NMR (126 MHz, 1:1 CDCl_3 : $\text{DMSO}-d_6$) δ 144.7, 144.3 (d, $J = 7.9$ Hz), 142.3, 140.5, 135.3, 131.4, 130.8, 130.4, 128.7, 128.1, 127.2, 127.2, 126.9, 126.7, 126.6, 126.5, 123.0, 122.8, 35.7, 31.8, 31.2, 29.4, 29.3, 29.2, 28.0, 24.1, 24.0, 22.6, 14.4. ^{31}P NMR (202 MHz, 1:1 CDCl_3 : $\text{DMSO}-d_6$) δ 2.6. HRMS (ESI) found $[\text{M}-\text{H}]^-$ 941.4878, $\text{C}_{58}\text{H}_{66}\text{N}_6\text{O}_4\text{P}$ requires 941.4889.

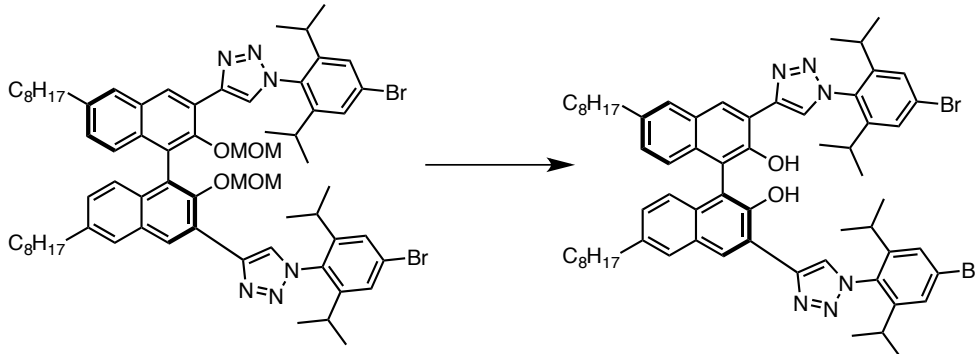
(S)-4,4'-(2,2'-bis(methoxymethoxy)-6,6'-dioctyl-[1,1'-binaphthalene]-3,3'-diyl)bis(1-(4-bromo-2,6-diisopropylphenyl)-1H-1,2,3-triazole) (MOM-3.4n)



Subjection of *bis-alkyne 3.7* (0.500 g, 0.772 mmol) and 2,6-diisopropyl-4-bromophenyl azide (0.762 g, 2.31 mmol) to General Procedure A gave the title compound (0.597 g, 0.493 mmol, 65 % yield) as an off-white foam after purification by column chromatography on silica gel using Hex/EtOAc as eluent (40:1). ^1H NMR (500 MHz, CDCl_3) δ 9.03 (s, 2H), 8.43 (s, 2H), 7.82 (s, 2H), 7.45 (d, $J = 1.5$ Hz, 2H), 7.43 (d, $J = 1.5$ Hz, 2H), 7.23 (d, $J = 9.5$ Hz, 2H), 7.21 (d, $J = 9.5$

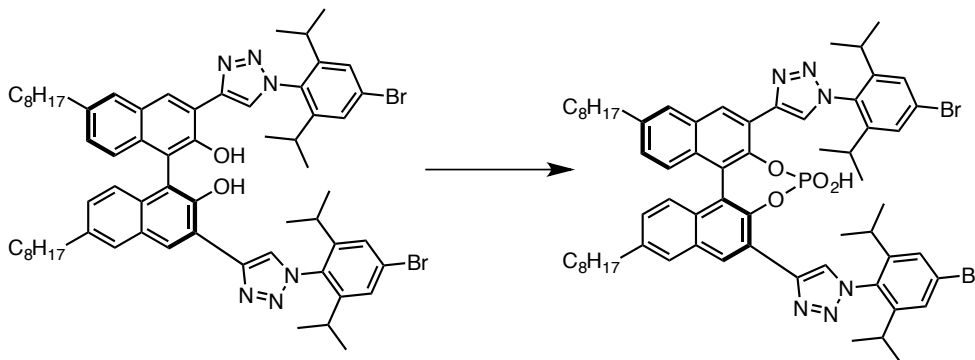
Hz, 2H), 4.65 (d, $J = 4.7$ Hz, 2H), 4.42 (d, $J = 4.8$ Hz, 2H), 2.79 (t, $J = 7.7$ Hz, 4H), 2.66 (s, 6H), 2.39 (hept, $J = 6.8$ Hz, 2H), 2.32 (hept, $J = 6.8$ Hz, 2H), 1.77 – 1.69 (m, 4H), 1.44 – 1.28 (m, 20H), 1.21 (d, $J = 6.8$ Hz, 6H), 1.18 (d, $J = 6.8$ Hz, 6H), 1.15 (d, $J = 6.8$ Hz, 6H), 1.12 (d, $J = 6.9$ Hz, 6H), 0.91 (t, $J = 6.6$ Hz, 6H). ^{13}C NMR (126 MHz, CDCl_3) δ 148.8, 148.4, 148.4, 143.4, 140.4, 132.3, 132.3, 131.2, 128.9, 128.1, 127.3, 127.0, 126.4, 126.2, 125.9, 125.8, 125.3, 123.9, 98.3, 56.8, 35.9, 31.9, 31.1, 29.5, 29.4, 29.3, 28.7, 28.6, 24.2, 24.0, 23.9, 23.7, 22.7, 22.6, 14.2. HRMS (ESI) found $[\text{M}+\text{H}]^+$ 1209.5173, $\text{C}_{68}\text{H}_{87}\text{N}_6\text{O}_4\text{Br}_2$ requires 1209.5150.

(S)-3,3'-bis(1-(4-bromo-2,6-diisopropylphenyl)-1H-1,2,3-triazol-4-yl)-6,6'-dioctyl-[1,1'-binaphthalene]-2,2'-diol (diol-3.4n)



Subjection of intermediate **MOM-1n** (0.400 g, 0.330 mmol) to General Procedure B gave the title compound (0.345 g, 0.307 mmol, 93 % yield) as a beige powder after purification by column chromatography on silica gel using Hex/EtOAc as eluent (40:1 to 20:1). ^1H NMR (500 MHz, CDCl_3) δ 9.53 (s, 2H), 8.48 (s, 2H), 8.23 (s, 2H), 7.73 (s, 2H), 7.50 (d, $J = 2.5$ Hz, 2H), 7.49 (d, $J = 2.5$ Hz, 2H), 7.23 (d, $J = 8.7$ Hz, 2H), 7.19 (d, $J = 8.7$ Hz, 2H), 2.76 (t, $J = 7.7$ Hz, 4H), 2.40 (hept, $J = 6.0$ Hz, 2H), 2.34 (hept, $J = 6.0$ Hz, 2H), 1.79 – 1.66 (m, 4H), 1.42 – 1.29 (m, 20H), 1.24 – 1.18 (m, 24H), 0.91 (t, $J = 6.6$ Hz, 6H). ^{13}C NMR (126 MHz, CDCl_3) δ 150.1, 148.5, 148.4, 146.6, 138.5, 132.5, 132.1, 129.1, 128.7, 127.4, 126.7, 126.5, 126.3, 125.7, 124.7, 123.8, 116.9, 116.3, 35.9, 31.9, 31.3, 29.6, 29.4, 29.3, 28.7, 28.7, 24.2, 24.1, 23.9, 22.7, 22.6, 14.2. HRMS (ESI) found $[\text{M}+\text{H}]^+$ 1121.4622, $\text{C}_{64}\text{H}_{79}\text{N}_6\text{O}_2\text{Br}_2$ requires 1121.4626.

(11bS)-2,6-bis(1-(4-bromo-2,6-diisopropylphenyl)-1H-1,2,3-triazol-4-yl)-4-hydroxy-9,14-dioctyldinaphtho[2,1-d':1',2'-f][1,3,2]dioxaphosphepine 4-oxide (3.4n)

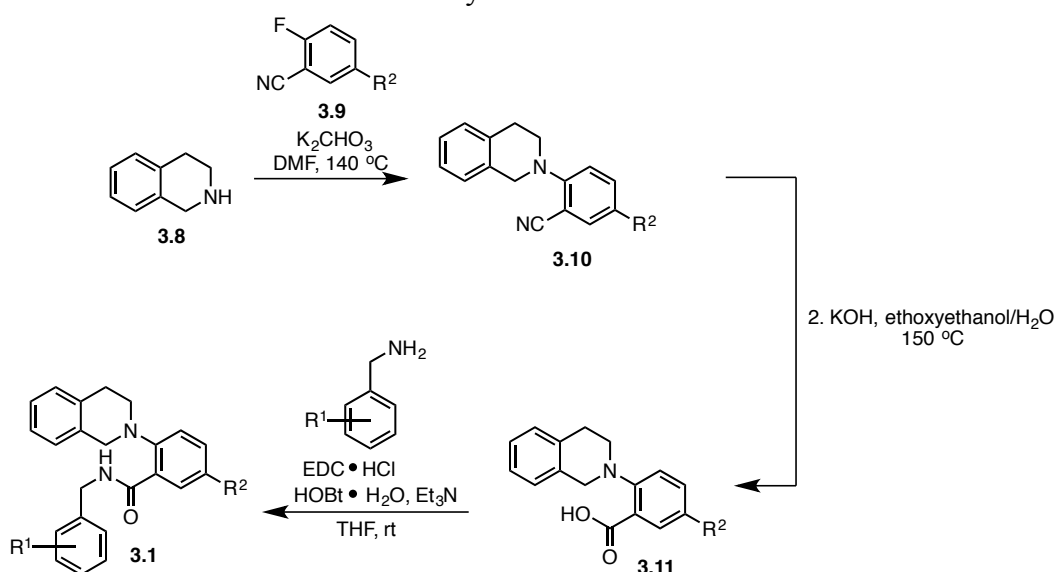


Subjection of **diol-1n** (0.262 g, 0.233 mmol) to General Procedure C gave the title compound (0.254 g, 0.214 mmol, 92 % yield) as a yellowish powder after purification by column

chromatography on silica gel using DCM/MeOH as eluent (40:1). $^1\text{H NMR}$ (500 MHz, 1:1 CDCl_3 : $\text{DMSO}-d_6$) δ 8.84 (s, 2H), 8.81 (s, 2H), 7.99 (s, 2H), 7.63 (s, 2H), 7.62 (s, 2H), 7.24 (d, J = 9.0 Hz, 2H), 7.13 (d, J = 8.7 Hz, 2H), 2.76 (t, J = 7.6 Hz, 4H), 2.30 (hept, J = 6.6 Hz, 2H), 2.21 (hept, J = 6.6 Hz, 2H), 1.77 – 1.60 (m, 4H), 1.42 – 1.19 (m, 20H), 1.17 – 1.07 (m, 24H), 0.85 (t, J = 6.5 Hz, 6H). $^{13}\text{C NMR}$ (126 MHz, 1:1 CDCl_3 : $\text{DMSO}-d_6$) δ 148.7, 148.5, 144.0 (d, J = 9.8 Hz), 142.3, 140.7, 132.5, 131.5, 130.4, 128.8, 128.3, 127.4, 127.3, 127.3, 127.3, 126.7, 125.2, 122.8, 122.7, 35.7, 31.8, 31.1, 29.4, 29.3, 29.2, 28.7, 28.6, 24.1, 24.1, 23.8, 23.6, 22.6, 14.4. $^{31}\text{P NMR}$ (202 MHz, CDCl_3) δ 3.3. **HRMS** (ESI) found $[\text{M}-\text{H}]^-$ 1181.4051, $\text{C}_{64}\text{H}_{76}\text{N}_6\text{O}_4\text{Br}_2\text{P}_1$ requires 1181.4038.

Synthesis and characterization of substrates

Scheme 3.2. Synthesis of substrates **3.1**



Compounds **3.1a-l** were prepared according to the general reaction sequence depicted in Scheme 3.2. Compounds **3.1a-e** were reported in a previous publication.¹

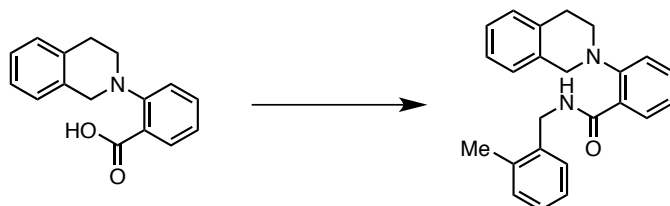
Synthesis of Carboxylic Acids (3.11): A round-bottomed flask was charged with 1,2,3,4-tetrahydroisoquinoline (**S2**, 2.1 equiv.), the appropriate 2-fluorobenzonitrile (**3.9**, 1.0 equiv.), potassium carbonate (2.1 equiv.), and DMF (1 M). The resulting mixture was heated at 140 °C and the reaction's progress was monitored by TLC analysis. Upon completion, the reaction mixture was allowed to cool to room temperature, diluted with EtOAc and washed with saturated aqueous ammonium chloride. The organic phase was washed with distilled H₂O (X 4) and brine, dried (Na_2SO_4) and concentrated *in vacuo*. The crude residue was purified by column chromatography on silica gel using EtOAc/Hex as eluent to afford nitrile **3.10**.

The purified nitrile (**3.10**, 1.0 equiv) was dissolved in ethoxyethanol/H₂O (6:1 v/v, 1.25 M) and freshly-ground KOH (6.0 equiv.) was added. The resulting mixture was heated at 150 °C until a precipitate was observed (typically between 2-3 h). The reaction mixture was allowed to cool to room temperature and the precipitate was collected by filtration using Et₂O. The resulting solid

was dissolved in minimal H₂O, washed with Et₂O, and acidified to pH = 7 using 3 N HCl, resulting in a fine white precipitate which was collected by filtration, washing with H₂O to afford carboxylic acid **3.11**, which was ready for use after drying under high vacuum for ca. 3 h.

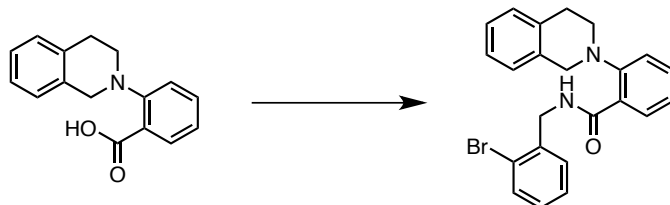
General Procedure D: Synthesis of amide substrates 3.1f-l: The appropriate carboxylic acid (**3.11**, 1 equiv.) was dissolved in THF (0.1 M). To this magnetically stirred solution were added N-(3-dimethylaminopropyl)-N'-ethylcarbodiimide hydrochloride (1.2 equiv.), 1-hydroxybenzotriazole hydrate (1.2 equiv.), triethylamine (1.3 equiv.), and the appropriate primary amine (1.2 equiv.) in succession and the reaction mixture was stirred at room temperature. Upon complete consumption of the starting material, as judged by TLC analysis, the reaction mixture was filtered through silica gel using EtOAc/Hex (1:1) as eluent. The resulting filtrate was concentrated *in vacuo*. The crude residue was purified by column chromatography or recrystallization.

2-(3,4-dihydroisoquinolin-2(1H)-yl)-N-(2-methylbenzyl)benzamide (3.1f)



Subjection of 2-(3,4-dihydroisoquinolin-2(1H)-yl)benzoic acid (0.500 g, 1.97 mmol) to General Procedure D gave the title compound (0.480 g, 1.35 mmol, 68 % yield) as a white powder after recrystallization from hot EtOAc. ¹H NMR (500 MHz, CDCl₃) δ 10.29 (t, *J* = 4.9 Hz, 1H), 8.34 (d, *J* = 7.6 Hz, 1H), 7.49 (app t, 1H), 7.36 - 7.25 (m, 2H), 7.25 - 7.15 (m, 2H), 7.08 (app t, *J* = 7.2 Hz, 1H), 7.05 - 6.88 (m, 5H), 4.52 (d, *J* = 5.0 Hz, 2H), 4.08 (s, 2H), 3.24 (t, *J* = 5.9 Hz, 2H), 2.68 (t, *J* = 5.9 Hz, 2H), 2.13 (s, 3H). ¹³C NMR (126 MHz, CDCl₃) δ 165.8, 151.3, 136.2, 135.9, 133.6, 133.3, 132.2, 131.6, 130.3, 129.1, 128.7, 128.0, 127.5, 126.7, 126.2, 126.1, 126.1, 125.4, 121.3, 56.8, 50.5, 41.8, 29.1, 18.8. HRMS (ESI) found [M+H]⁺ 357.1956, C₂₄H₂₅N₂O requires 357.1961.

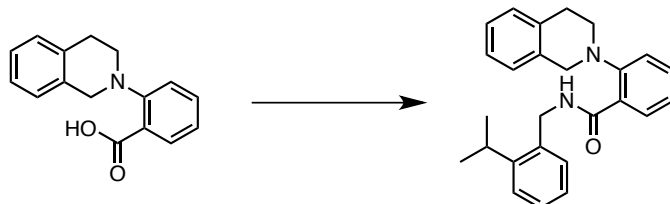
N-(2-bromobenzyl)-2-(3,4-dihydroisoquinolin-2(1H)-yl)benzamide (3.1g)



Subjection of 2-(3,4-dihydroisoquinolin-2(1H)-yl)benzoic acid (0.500 g, 1.97 mmol) to General Procedure D gave the title compound (0.690 g, 1.64 mmol, 83 % yield) as a white powder after purification by column chromatography on silica gel using Hex/EtOAc as eluent (4:1). ¹H NMR (500 MHz, CDCl₃) δ 10.41 (d, *J* = 5.8 Hz, 1H), 8.30 (d, *J* = 6.7 Hz, 1H), 7.53 - 7.44 (m, 1H), 7.34 (d, *J* = 7.9 Hz, 1H), 7.31 - 7.24 (m, 3H), 7.23 - 7.12 (m, 2H), 7.12 - 7.05 (m, 2H), 7.02 (app t, *J* = 7.6 Hz, 1H), 6.97 (d, *J* = 7.3 Hz, 1H), 4.62 (d, *J* = 5.5 Hz, 2H), 4.10 (s, 2H), 3.29 (t, *J* = 5.9 Hz, 2H), 2.88 (t, *J* = 5.9 Hz, 2H). ¹³C NMR (126 MHz, CDCl₃) δ 166.0, 151.3, 137.41 133.8, 133.4,

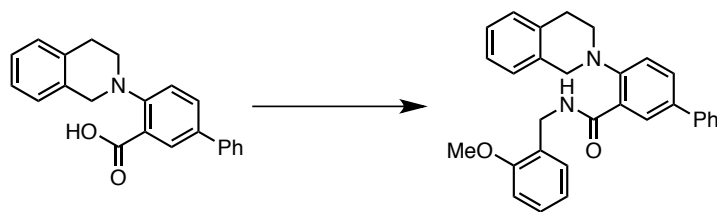
132.6, 132.3, 131.7, 130.5, 129.0, 128.9, 127.9, 127.5, 126.6, 126.3, 126.1, 125.2, 124.0, 121.2, 56.5, 50.7, 43.9, 29.2. **HRMS** (ESI) found $[M+H]^+$ 421.0906, $C_{23}H_{22}N_2OBr$ requires 421.0910.

2-(3,4-dihydroisoquinolin-2(1*H*)-yl)-*N*-(2-isopropylbenzyl)benzamide (3.1h)



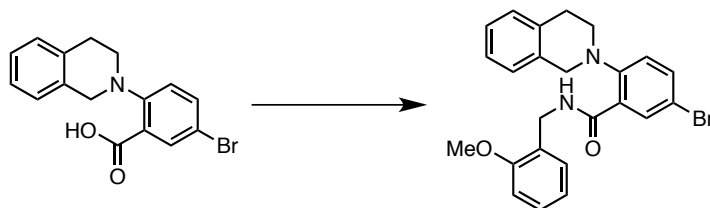
Subjection of 2-(3,4-dihydroisoquinolin-2(1*H*)-yl)benzoic acid (0.500 g, 1.97 mmol) to General Procedure D gave the title compound (0.527 g, 1.38 mmol, 70 % yield) as a clear oil after purification by column chromatography on silica gel using Hex/EtOAc as eluent (9:1). **¹H NMR** (500 MHz, $CDCl_3$) δ 10.18 (t, $J = 4.7$ Hz, 1H), 8.32 (d, $J = 7.8$ Hz, 1H), 7.48 (app t, $J = 8.3$ Hz, 1H), 7.35 - 7.24 (m, 2H), 7.24 - 7.12 (m, 4H), 7.01 (app t, $J = 6.2$ Hz, 2H), 6.92 - 6.81 (m, 2H), 4.59 (d, $J = 5.1$ Hz, 2H), 4.09 (s, 2H), 3.23 (t, $J = 5.9$ Hz, 2H), 3.12 (hept, $J = 6.7$ Hz, 1H), 2.68 (t, $J = 5.9$ Hz, 2H), 1.12 (d, $J = 6.8$ Hz, 6H). **¹³C NMR** (126 MHz, $CDCl_3$) δ 165.7, 151.2, 146.8, 134.6, 133.7, 133.3, 132.1, 131.7, 129.2, 129.1, 127.9, 127.8, 126.6, 126.2, 126.0, 125.9, 125.3, 125.2, 121.1, 56.4, 50.7, 41.0, 29.0, 28.73 23.8. **HRMS** (ESI) found $[M+H]^+$ 385.2266, $C_{26}H_{29}N_2O$ requires 385.2274.

4-(3,4-dihydroisoquinolin-2(1*H*)-yl)-*N*-(2-methoxybenzyl)-[1,1'-biphenyl]-3-carboxamide (3.1i)



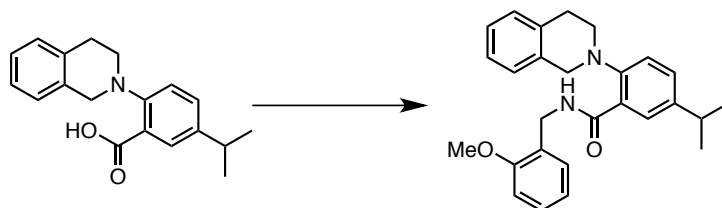
Subjection of 4-(3,4-dihydroisoquinolin-2(1*H*)-yl)-[1,1'-biphenyl]-3-carboxylic acid (1.06 g, 3.22 mmol) to General Procedure D gave the title compound (0.640 g, 1.42 mmol, 44 % yield) as a yellow powder after purification by column chromatography on silica gel using Hex/EtOAc as eluent (9:1 to 4:1). **¹H NMR** (500 MHz, $CDCl_3$) δ 9.96 (t, $J = 5.7$ Hz, 1H), 8.54 (s, 1H), 7.74 - 7.63 (m, 3H), 7.47 (app t, $J = 7.6$ Hz, 2H), 7.42 - 7.30 (m, 2H), 7.26 - 7.14 (m, 4H), 7.10 (d, $J = 7.2$ Hz, 1H), 7.04 (d, $J = 7.3$ Hz, 1H), 6.81 (app t, $J = 7.4$ Hz, 1H), 6.64 (d, $J = 8.2$ Hz, 1H), 4.62 (d, $J = 5.4$ Hz, 2H), 4.18 (s, 2H), 3.43 (s, 3H), 3.27 (t, $J = 5.9$ Hz, 2H), 2.80 (t, $J = 5.8$ Hz, 2H). **¹³C NMR** (126 MHz, $CDCl_3$) δ 166.0, 157.4, 150.2, 139.9, 137.4, 134.0, 133.6, 130.3, 130.1, 129.9, 129.1, 128.8, 128.7, 128.5, 127.4, 127.0, 126.5, 126.4, 126.2, 126.1, 121.0, 120.5, 110.2, 55.2, 54.8, 51.7 39.2, 29.0. **HRMS** (ESI) found $[M+H]^+$ 449.2213, $C_{30}H_{29}N_2O_2$ requires 449.2224.

5-bromo-2-(3,4-dihydroisoquinolin-2(1H)-yl)-N-(2-methoxybenzyl)benzamide (3.1j)



Subjection of 5-bromo-2-(3,4-dihydroisoquinolin-2(1H)-yl)benzoic acid (**4l**) (0.420 g, 1.26 mmol) to General Procedure D gave the title compound (0.411 g, 0.911 mmol, 72 % yield) as a white solid after purification by column chromatography on silica gel using Hex/EtOAc as eluent (4:1). $^1\text{H NMR}$ (500 MHz, CDCl_3) δ 9.83 (t, $J = 5.7$ Hz, 1H), 8.36 (s, 1H), 7.54 (dd, $J = 8.5$, 2.6 Hz, 1H), 7.24 - 7.15 (m, 4H), 7.12 (d, $J = 8.5$ Hz, 1H), 7.07 (d, $J = 7.4$ Hz, 1H), 7.00 (d, $J = 7.4$ Hz, 1H), 6.79 (app t, $J = 7.4$ Hz, 1H), 6.61 (d, $J = 8.6$ Hz, 1H), 4.56 (d, $J = 4.8$ Hz, 2H), 4.10 (s, 2H), 3.41 (s, 3H), 3.19 (t, $J = 5.9$ Hz, 2H), 2.75 (t, $J = 5.9$ Hz, 2H). $^{13}\text{C NMR}$ (126 MHz, CDCl_3) δ 164.6, 157.4, 150.0, 134.6, 134.5, 133.6, 133.4, 130.1, 129.9, 129.1, 128.8, 126.6, 126.3, 126.1, 125.9, 122.4, 120.5, 118.2, 110.2, 55.1, 54.8, 51.7, 39.3, 28.8. **HRMS** (ESI) found $[\text{M}+\text{H}]^+$ 451.1010, $\text{C}_{24}\text{H}_{24}\text{N}_2\text{O}_2\text{Br}$ requires 451.1016.

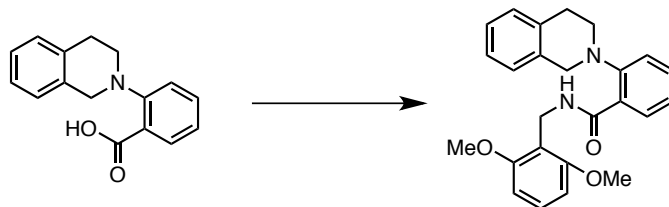
2-(3,4-dihydroisoquinolin-2(1H)-yl)-5-isopropyl-N-(2-methoxybenzyl)benzamide (3.1k)



To a stirred solution of 5-bromo-2-(3,4-dihydroisoquinolin-2(1H)-yl)-N-(2-methoxybenzyl)benzamide (0.350 g, 0.779 mmol) in 1,4-dioxane (4 mL) and water (1 mL) were added isopropenylboronic acid pinacol ester (0.196, 1.16 mmol), palladium (II) acetate (0.004 g, 0.019 mmol), S-Phos (0.016 g, 0.039 mmol), and potassium carbonate (0.322 g, 2.34 mmol). The flask was fitted with a reflux condenser and the reaction mixture was de-gassed (X3) by evacuating for 30 s under high vacuum and backfilling with N_2 . The reaction mixture was allowed to stir at 90°C for 12 h. After cooling to room temperature, the reaction mixture was filtered through Celite, extracted with DCM (2 X 10 mL), washed with brine (1 X 10 mL), dried (Na_2SO_4) and concentrated *in vacuo*. The crude product was transferred to a 25-mL round bottomed flask and dissolved in EtOH (7 mL). To the resulting solution was added 10 % Pd/C (0.030 g). The reaction vessel was evacuated under high vacuum and fitted with a balloon of H_2 . Upon complete reduction of the alkene, as judged by $^1\text{H NMR}$ spectroscopic analysis of aliquots taken every hour (3 hours total), the mixture was filtered through Celite and concentrated *in vacuo*. The crude residue was purified by column chromatography on silica gel using Hex/EtOAc as eluent (9:1) to afford the title compound (0.192 g, 0.465 mmol, 60 % yield over 2 steps). $^1\text{H NMR}$ (500 MHz, CDCl_3) δ 10.15 (t, $J = 5.9$ Hz, 1H), 8.16 (s, 1H), 7.31 (d, $J = 7.9$ Hz, 1H), 7.24 - 7.13 (m, 5H), 7.08 (d, $J = 7.0$ Hz, 1H), 7.00 (d, $J = 7.1$ Hz, 1H), 6.78 (app t, $J = 7.3$ Hz, 1H), 6.61 (d, $J = 8.0$ Hz, 1H), 4.58 (d, $J = 5.2$ Hz, 2H), 4.11 (s, 2H), 3.41 (s, 3H), 3.20 (t, $J = 6.0$ Hz, 2H), 2.97 (sept, $J = 7.1$ Hz, 1H), 2.76 (t, $J = 5.9$ Hz, 2H), 1.29 (d, $J = 6.2$ Hz, 6H). $^{13}\text{C NMR}$ (126 MHz, CDCl_3) δ 166.2, 157.4, 148.9, 145.5, 134.2, 133.7, 129.9, 129.8, 129.7, 129.0, 128.6, 128.0, 126.4, 126.3, 126.0, 120.7,

120.4, 110.1, 55.4, 54.8, 51.6, 39.0, 33.6, 29.1, 23.9. **HRMS** (ESI) found $[M+H]^+$ 415.2375, $C_{27}H_{31}N_2O_2$ requires 415.2380.

2-(3,4-dihydroisoquinolin-2(1*H*)-yl)-*N*-(2,6-dimethoxybenzyl)benzamide (3.11)



Subjection of 2-(3,4-dihydroisoquinolin-2(1*H*)-yl)benzoic acid (0.500 g, 1.97 mmol) to General Procedure D gave the title compound (0.635 g, 1.58 mmol, 80 % yield) as a white powder after purification by column chromatography on silica gel using Hex/EtOAc as eluent (9:1 to 4:1). **¹H NMR** (300 MHz, $CDCl_3$) δ 9.69 (br s, 1H), 8.23 (d, $J = 6.4$ Hz, 1H), 7.40 (m, 1H), 7.25 – 7.17 (m, 2H), 7.17 – 7.03 (m, 3H), 7.02 – 6.91 (m, 2H), 6.31 (d, $J = 8.4$ Hz, 2H), 4.67 (d, $J = 4.6$ Hz, 2H), 4.10 (s, 2H), 3.50 (s, 6H), 3.15 (t, $J = 5.8$ Hz, 2H), 2.62 (t, $J = 5.9$ Hz, 2H). **¹³C NMR** (126 MHz, $CDCl_3$) δ 165.8, 158.5, 151.0, 134.1, 133.7, 131.7, 131.6, 129.0, 128.8, 128.6, 126.3, 126.2, 125.9, 124.6, 120.4, 113.9, 103.6, 55.5, 54.6, 51.9, 32.1, 28.8. **HRMS** (ESI) found $[M+H]^+$ 403.2011, $C_{25}H_{27}N_2O_3$ requires 403.2016.

Synthesis and characterization of products

Amides **3.2a-1** were prepared according to General Procedure F. Compounds **3.2a-e** were reported in a previous publication.¹ It has been previously demonstrated and was re-confirmed that products can be purified by column chromatography on silica gel without erosion of optical activity. However, as crude product mixtures were generally very clean, direct analysis was preferred as it expedited the processing of the large number of reactions required in this study. All reported products were purified by column chromatography or recrystallization prior to characterization.

General Procedure F: for Enantioselective Amidation Reactions

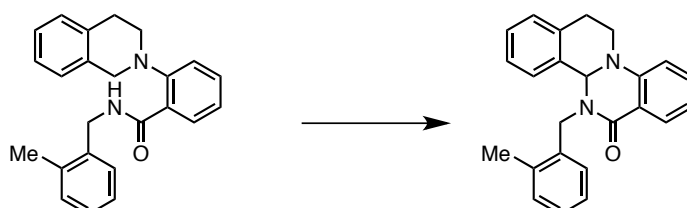
A stock solution of the appropriate substrate (0.025 M in toluene) was prepared. A 1-dram vial was charged with the appropriate catalyst (0.0025 mmol), Na_3PO_4 (9.8 mg, 0.060 mmol), 4-acetamido-2,2,6,6-tetramethyl-1-oxopiperidinium tetrafluoroborate (**3.3**, 16.5 mg, 0.055 mmol) and a 8mm magnetic stir bar. To this vial was added 1 mL of the appropriate stock solution and the reaction mixture was allowed to stir at room temperature. After 24 h, saturated aqueous Na_2SO_3 (1 mL) was added to the reaction mixture followed by extraction with EtOAc (1 mL). Approximately 0.1 mL of the organic layer was removed, diluted with 0.5 mL of a 10:1 IPA/Hex solution, and the enantiomeric excess of the product was analyzed directly by HPLC. Racemic reactions were carried out according to an identical procedure, but omitting catalyst.

Note: Due to the heterogeneous nature of the reaction mixtures, it was essential that fast and efficient stirring be maintained throughout the entire course of the reaction. This was achieved by placing the 1-dram vials containing the reaction mixtures directly onto the surface of the stir plate and utilizing a stir rate of 1500 rpm.

Note: Substrate stock solutions were freshly prepared immediately prior to use, as slow conversion to product was observed after several days in solution.

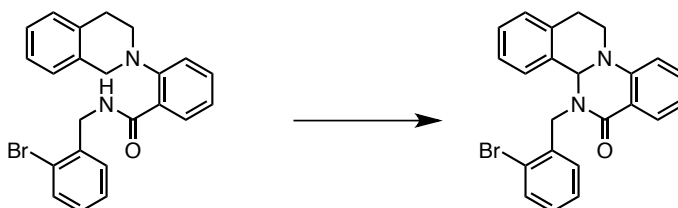
Preparation of reagents: Crystalline 4-acetamido-2,2,6,6-tetramethyl-1-oxopiperidinium tetrafluoroborate was ground with a mortar and pestle into a fine, light-yellow powder prior to use.

5-(2-methylbenzyl)-12,13-dihydro-4*bH*-isoquinolino[2,1-*a*]quinazolin-6(5*H*)-one (3.2f)



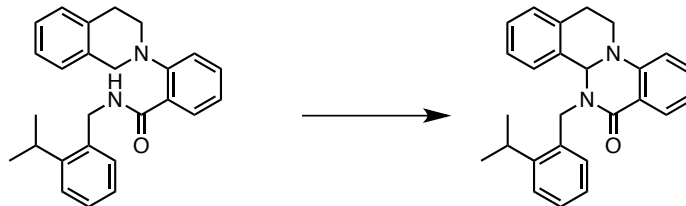
¹H NMR (500 MHz, CDCl₃) δ 7.99 (d, *J* = 7.7 Hz, 1H), 7.43 – 7.31 (m, 3H), 7.26 – 7.14 (m, 5H), 7.05 (d, *J* = 8.3 Hz, 1H), 6.93 (d, *J* = 8.3 Hz, 1H), 6.87 (app t, *J* = 7.5 Hz, 1H), 5.88 (d, *J* = 15.1 Hz, 1H), 5.62 (s, 1H), 4.31 (d, *J* = 15.7 Hz, 1H), 4.13 (dd, *J* = 14.6, 6.6 Hz, 1H), 3.54 (ddd, *J* = 14.3, 11.5, 5.8 Hz, 1H), 3.22 (ddd, *J* = 17.8, 11.0, 6.7 Hz, 1H), 2.73 (dd, *J* = 17.1, 4.6 Hz, 1H), 2.33 (s, 3H). **¹³C NMR** (126 MHz, CDCl₃) δ 163.2, 147.3, 136.5, 136.0, 134.6, 134.5, 133.5, 130.6, 129.6, 129.3, 128.2, 127.6, 127.6, 126.3, 126.3, 125.5, 119.2, 118.2, 113.3, 71.4, 48.2, 44.7, 24.2, 19.3. **HRMS** (ESI) found [M+Na]⁺ 377.1634, C₂₄H₂₂N₂O₁Na requires 377.1624. **HPLC** (Chiralpak IC column, 85:15 hexanes/isopropanol, 0.5 mL/min); t_r = 52.6 min, 55.9 min.

5-(2-bromobenzyl)-12,13-dihydro-4*bH*-isoquinolino[2,1-*a*]quinazolin-6(5*H*)-one (3.2g)



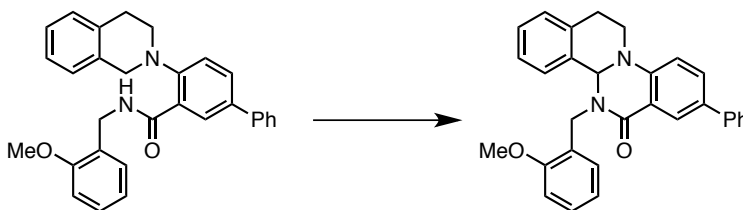
¹H NMR (500 MHz, CDCl₃) δ 7.98 (d, *J* = 7.6 Hz, 1H), 7.57 (app t, *J* = 7.6 Hz, 2H), 7.39 (app t, *J* = 7.8 Hz, 1H), 7.36 – 7.30 (m, 2H), 7.26 – 7.13 (m, 3H), 7.07 (d, *J* = 7.0 Hz, 1H), 6.96 (d, *J* = 8.3 Hz, 1H), 6.88 (app t, *J* = 7.5 Hz, 1H), 5.84 (d, *J* = 16.3 Hz, 1H), 5.76 (s, 1H), 4.47 (d, *J* = 16.3 Hz, 1H), 4.18 (dd, *J* = 14.6, 6.5 Hz, 1H), 3.63 (ddd, *J* = 14.3, 11.5, 5.7 Hz, 1H), 3.27 (ddd, *J* = 17.8, 11.5, 6.7 Hz, 1H), 2.77 (dd, *J* = 17.0, 5.4 Hz, 1H). **¹³C NMR** (126 MHz, CDCl₃) δ 163.4, 147.4, 136.1, 135.5, 134.5, 133.6, 132.8, 129.5, 129.3, 128.9, 128.7, 128.3, 127.9, 126.4, 125.6, 123.1, 119.4, 118.2, 113.5, 72.5, 50.4, 44.7, 24.2. **HRMS** (ESI) found [M+Na]⁺ 441.0585, C₂₃H₁₉N₂O₁Br₁Na₁ requires 441.0573. **HPLC** (Chiralpak IA column, 80:20 hexanes/isopropanol, 1 mL/min); t_r = 12.7 min, 17.6 min.

5-(2-isopropylbenzyl)-12,13-dihydro-4bH-isoquinolino[2,1-a]quinazolin-6(5H)-one (3.2h)



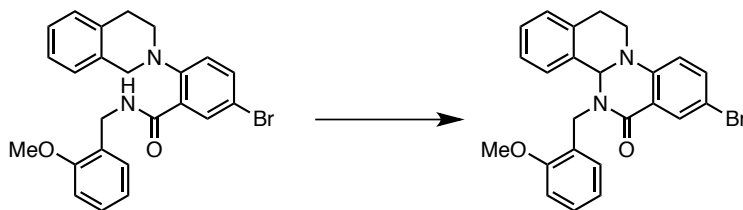
¹H NMR (500 MHz, CDCl₃) δ 7.99 (d, *J* = 7.7 Hz, 1H), 7.43 - 7.30 (m, 5H), 7.23 - 7.15 (m, 3H), 7.05 (d, *J* = 6.9 Hz, 1H), 6.92 (d, *J* = 8.3 Hz, 1H), 6.87 (app t, *J* = 7.5 Hz, 1H), 6.01 (d, *J* = 15.5 Hz, 1H), 5.62 (s, 1H), 4.37 (d, *J* = 15.5 Hz, 1H), 4.12 (dd, *J* = 14.5, 6.7 Hz, 1H), 3.54 (ddd, *J* = 14.3, 11.9, 5.8 Hz, 1H), 3.32 - 3.09 (m, 2H), 2.73 (dd, *J* = 17.0, 5.6 Hz, 1H), 1.25 (d, *J* = 6.5 Hz, 3H), 1.24 (d, *J* = 6.5 Hz, 3H). **¹³C NMR** (126 MHz, CDCl₃) δ 163.2, 147.4, 147.2, 136.0, 134.6, 133.4, 132.8, 129.5, 129.3, 128.1, 128.0, 126.3, 126.01, 125.7, 125.5, 119.2, 118.2, 113.3, 71.1, 47.5, 44.6, 28.6, 24.2, 23.8, 23.7. **HRMS** (ESI) found [M+H]⁺ 383.2114, C₂₆H₂₇N₂O requires 383.2118. **HPLC** (Chiralpak IA column, 85:15 hexanes/isopropanol, 1 mL/min); t_r = 9.9, 11.9 min.

5-(2-methoxybenzyl)-8-phenyl-12,13-dihydro-4bH-isoquinolino[2,1-a]quinazolin-6(5H)-one (3.2i)



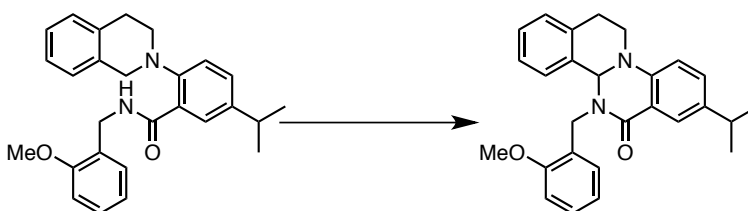
¹H NMR (500 MHz, CDCl₃) δ 8.21 (s, 1H), 7.60 (d, *J* = 8.5 Hz, 1H), 7.58 - 7.47 (m, 3H), 7.43 - 7.34 (m, 3H), 7.28 (app t, *J* = 7.5 Hz, 2H), 7.19 (app p, *J* = 5.2 Hz, 2H), 7.09 - 7.02 (m, 1H), 7.02 - 6.94 (m, 2H), 6.90 (d, *J* = 8.2 Hz, 1H), 5.86 (s, 1H), 5.73 (d, *J* = 15.7 Hz, 1H), 4.51 (d, *J* = 15.7 Hz, 1H), 4.22 (dd, *J* = 14.5, 6.5 Hz, 1H), 3.84 (s, 3H), 3.66 (ddd, *J* = 14.5, 11.7, 5.8 Hz, 1H), 3.30 (ddd, *J* = 18.2, 11.5, 6.8 Hz, 1H), 2.77 (dd, *J* = 17.1, 5.5 Hz, 1H). **¹³C NMR** (126 MHz, CDCl₃) δ 163.2, 157.4, 146.4, 140.1, 136.5, 134.3, 131.9, 131.8, 129.2, 128.9, 128.7, 128.5, 128.1, 127.7, 126.7, 126.4, 126.3, 125.6, 125.2, 120.8, 118.5, 113.5, 110.2, 72.7, 55.3, 46.0, 44.8, 24.1. **HRMS** (ESI) found [M+Na]⁺ 430.1889, C₂₀H₂₆N₂O₂Na requires 469.1886. **HPLC** (Chiralpak IC column, 70:30 hexanes/isopropanol, 1 mL/min); t_r = 27.2 min, 55.6 min.

8-bromo-5-(2-methoxybenzyl)-12,13-dihydro-4bH-isoquinolino[2,1-a]quinazolin-6(5H)-one (3.2j)



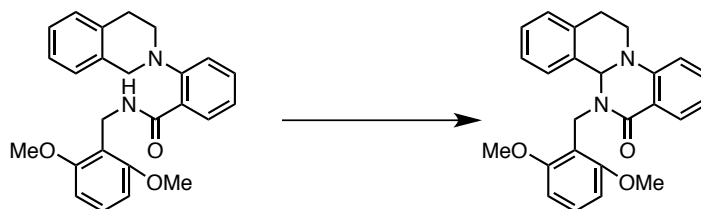
¹H NMR (500 MHz, CDCl₃) δ 8.03 (s, 1H), 7.46 (d, *J* = 7.4 Hz, 1H), 7.40 (dd, *J* = 8.8, 2.5 Hz, 1H), 7.34 - 7.24 (m, 2H), 7.19 (app p, *J* = 7.1 Hz, 2H), 7.04 (d, *J* = 7.2 Hz, 1H), 6.96 (app t, *J* = 7.4 Hz, 1H), 6.89 (d, *J* = 8.1 Hz, 1H), 6.78 (d, *J* = 8.8 Hz, 1H), 5.81 (s, 1H), 5.66 (d, *J* = 15.4 Hz, 1H), 4.47 (d, *J* = 15.6 Hz, 1H), 4.11 (dd, *J* = 14.5, 6.7 Hz, 1H), 3.83 (s, 3H), 3.61 (ddd, *J* = 14.6, 11.8, 5.8 Hz, 1H), 3.21 (ddd, *J* = 18.3, 11.8, 6.8 Hz, 1H), 2.74 (dd, *J* = 17.1, 5.5 Hz, 1H). **¹³C NMR** (126 MHz, CDCl₃) δ 162.1, 157.4, 146.1, 135.9, 134.1, 131.9, 129.3, 129.0, 128.7, 128.2, 126.3, 125.5, 124.9, 120.8, 119.9, 115.0, 111.3, 110.2, 72.6, 55.3, 45.9, 44.8, 23.9. **HRMS** (ESI) found [M+Na]⁺ 471.0684, C₂₄H₂₁N₂O₂BrNa requires 471.0679. **HPLC** (Chiralpak IA column, 75:25 hexanes/isopropanol, 1 mL/min); t_r = 15.6 min, 17.9 min.

8-isopropyl-5-(2-methoxybenzyl)-12,13-dihydro-4*bH*-isoquinolino[2,1-*a*]quinazolin-6(5*H*)-one (3.2k)



¹H NMR (600 MHz, CDCl₃) δ 7.79 (s, 1H), 7.48 (d, *J* = 7.3 Hz, 1H), 7.31 (d, *J* = 7.2 Hz, 1H), 7.23 (app t, *J* = 7.6 Hz, 1H), 7.21 - 7.10 (m, 3H), 7.02 (d, *J* = 7.1 Hz, 1H), 6.93 (app t, *J* = 7.4 Hz, 1H), 6.85 (d, *J* = 7.8 Hz, 1H), 6.82 (d, *J* = 8.4 Hz, 1H), 5.79 (s, 1H), 5.64 (d, *J* = 15.2 Hz, 1H), 4.44 (d, *J* = 15.6 Hz, 1H), 4.12 (dd, *J* = 13.8, 6.1 Hz, 1H), 3.80 (s, 3H), 3.58 (ddd, *J* = 14.8, 11.7, 5.9 Hz, 1H), 3.22 (ddd, *J* = 18.1, 11.3, 6.7 Hz, 1H), 2.80 (sept, *J* = 7.2 Hz, 1H), 2.71 (dd, *J* = 16.8, 5.5 Hz, 1H), 1.17 (d, *J* = 6.7 Hz, 6H). **¹³C NMR** (126 MHz, CDCl₃) δ 164.5, 163.5, 157.3, 145.2, 139.5, 134.5, 131.7, 129.2, 128.9, 128.4, 127.9, 127.0, 126.1, 125.7, 125.4, 120.8, 118.1, 113.2, 110.1, 72.7, 55.3, 45.8, 44.7, 33.2, 24.0, 23.8. **HRMS** (ESI) found [M+H]⁺ 413.2224, C₂₇H₂₉N₂O₂ requires 413.2224. **HPLC** (Chiralpak IA column, 85:15 hexanes/isopropanol, 1 mL/min); t_r = 10.6 min, 13.1 min.

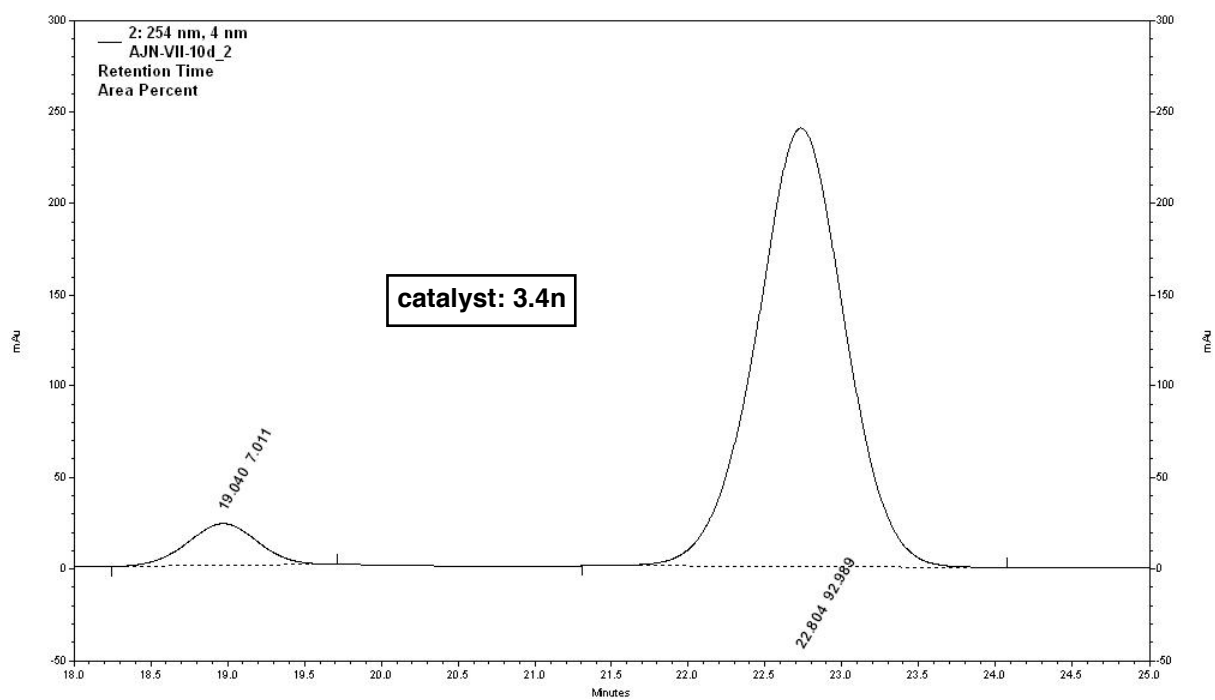
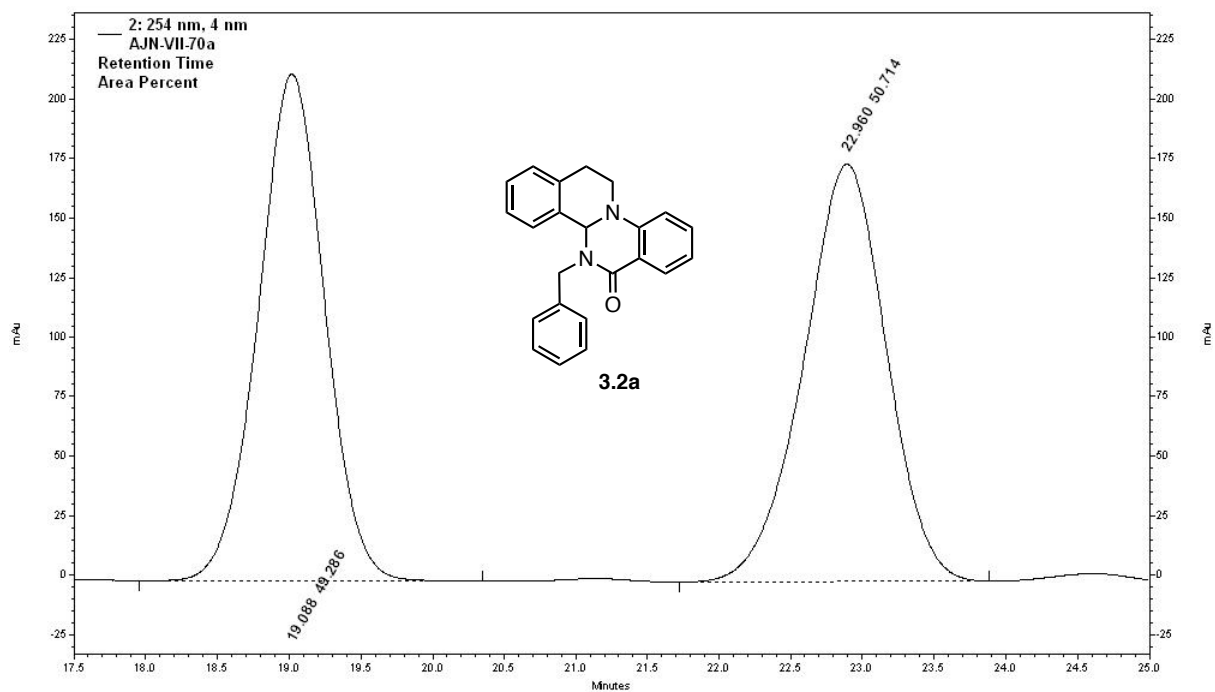
5-(2,6-dimethoxybenzyl)-12,13-dihydro-4*bH*-isoquinolino[2,1-*a*]quinazolin-6(5*H*)-one (3.2l)

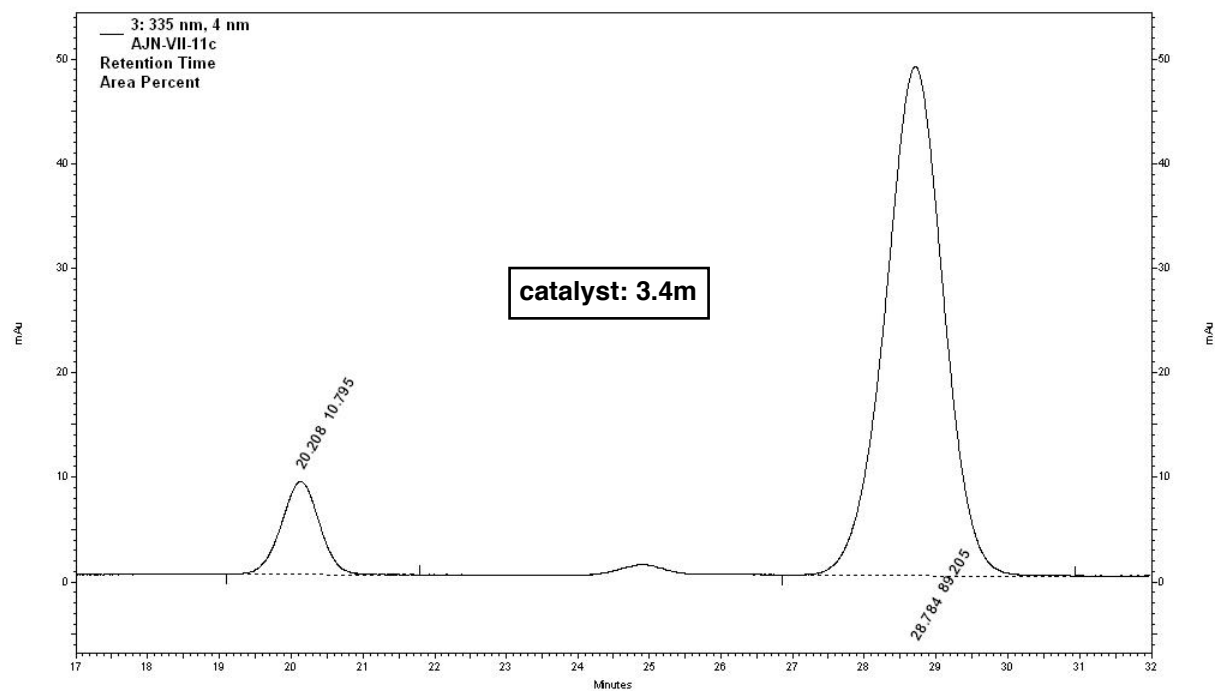
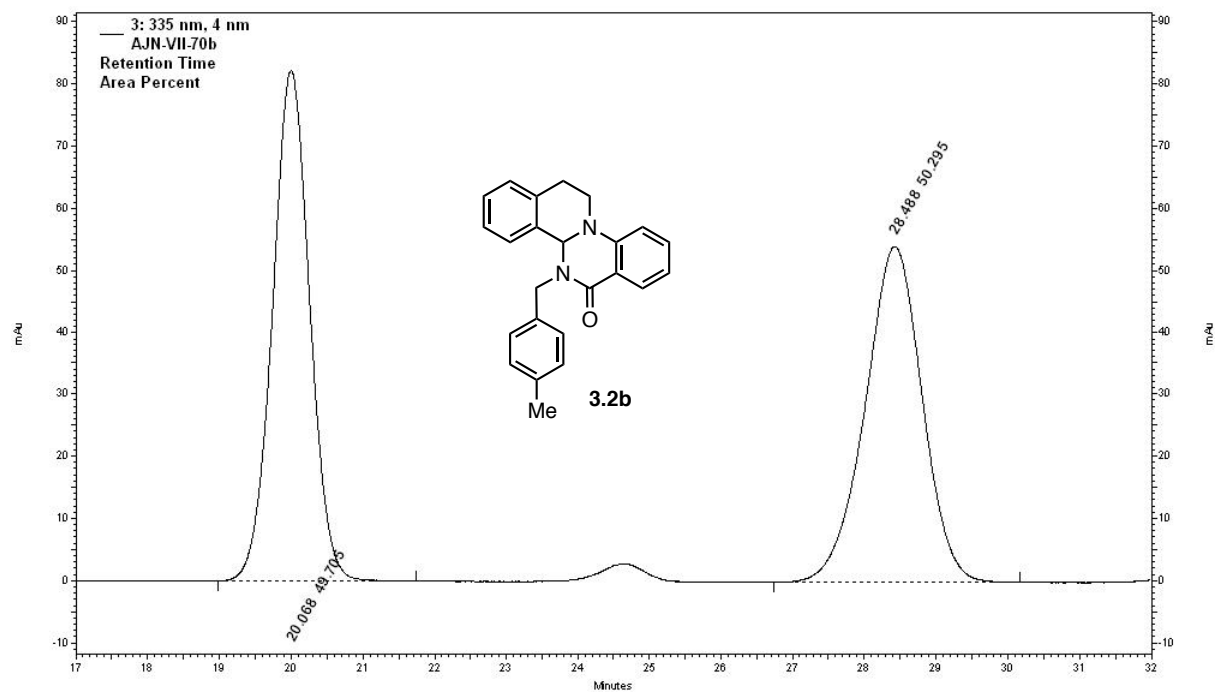


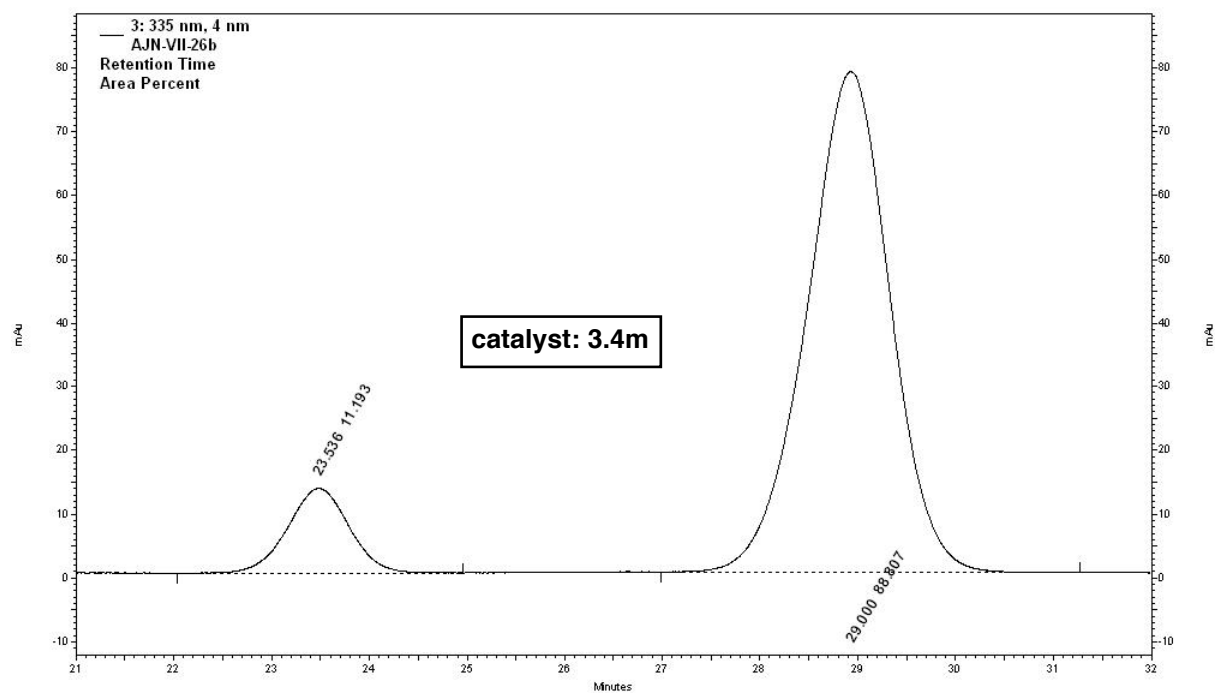
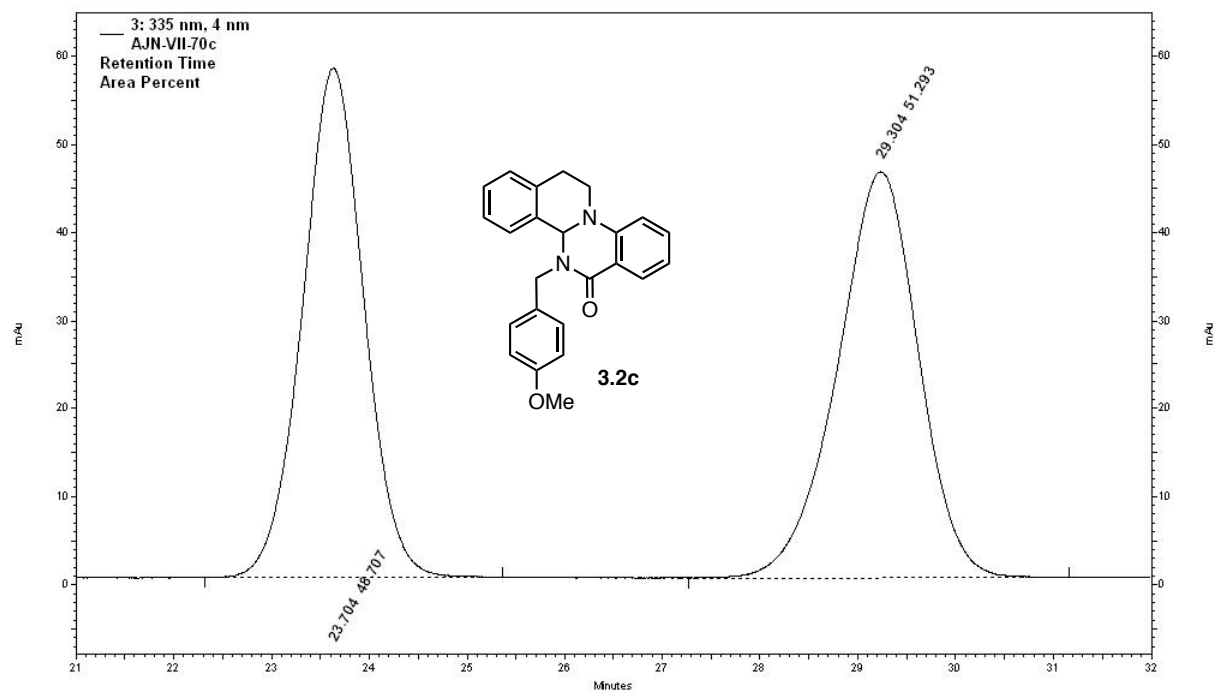
¹H NMR (500 MHz, CDCl₃) δ 7.94 (d, *J* = 7.6 Hz, 1H), 7.52 - 7.40 (m, 1H), 7.34 - 7.21 (m, 2H), 7.19 - 7.09 (m, 2H), 7.04 - 6.91 (m, 1H), 6.83 (d, *J* = 8.2 Hz, 1H), 6.78 (t, *J* = 7.5 Hz, 1H), 6.58 (d, *J* = 8.2 Hz, 2H), 5.77 (d, *J* = 13.8 Hz, 1H), 5.67 (s, 1H), 4.63 (d, *J* = 13.8 Hz, 1H), 4.12 (dd, *J* = 14.9, 6.7 Hz, 1H), 3.77 (s, 6H), 3.51 (ddd, *J* = 14.7, 11.9, 5.9 Hz, 1H), 3.31 - 3.11 (m, 1H), 2.66 (dd, *J* = 17.1, 5.5 Hz, 1H). **¹³C NMR** (126 MHz, CDCl₃) δ 171.2, 163.0, 159.6, 146.9, 134.1, 132.9, 129.4, 129.4, 128.8, 127.5, 126.0, 125.9, 118.6, 118.5, 112.7, 112.6, 103.9, 71.3, 55.9, 44.8, 39.7, 23.8. **HRMS** (ESI) found [M+H]⁺ 401.1862, C₂₅H₂₅N₂O₃ requires 401.1860. **HPLC** (Chiralpak IA column, 75:25 hexanes/isopropanol, 0.5 mL/min); t_r = 16.6 min, 18.2 min.

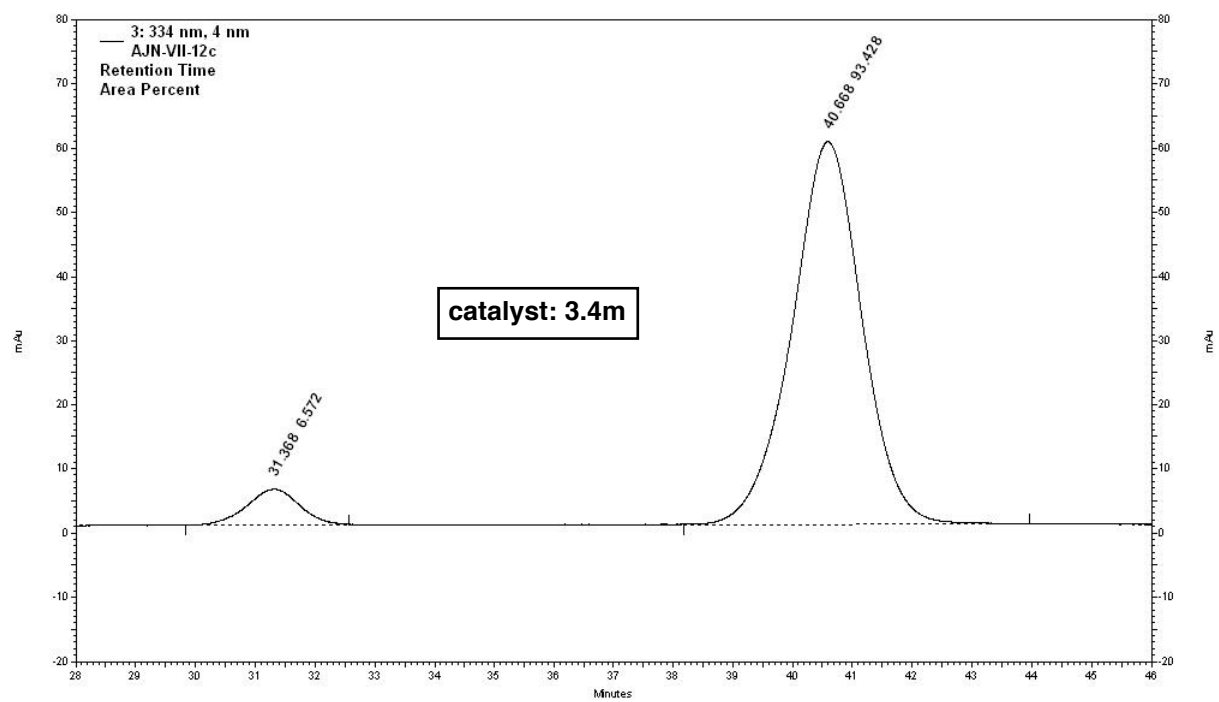
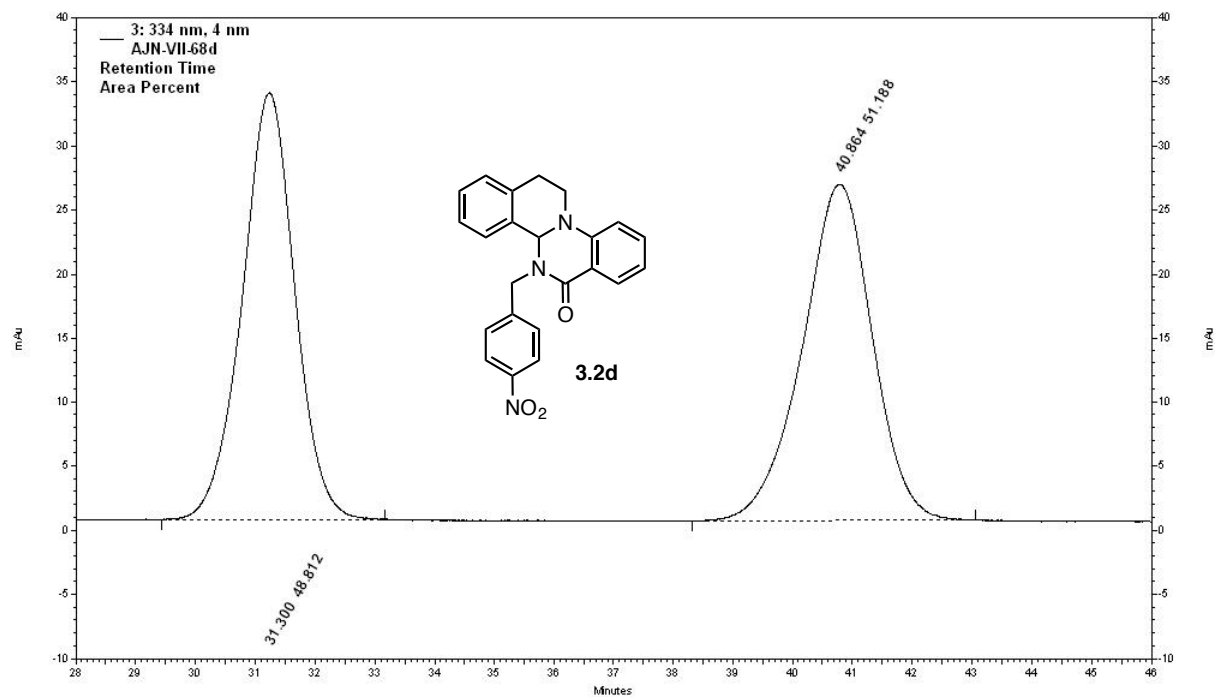
HPLC Traces

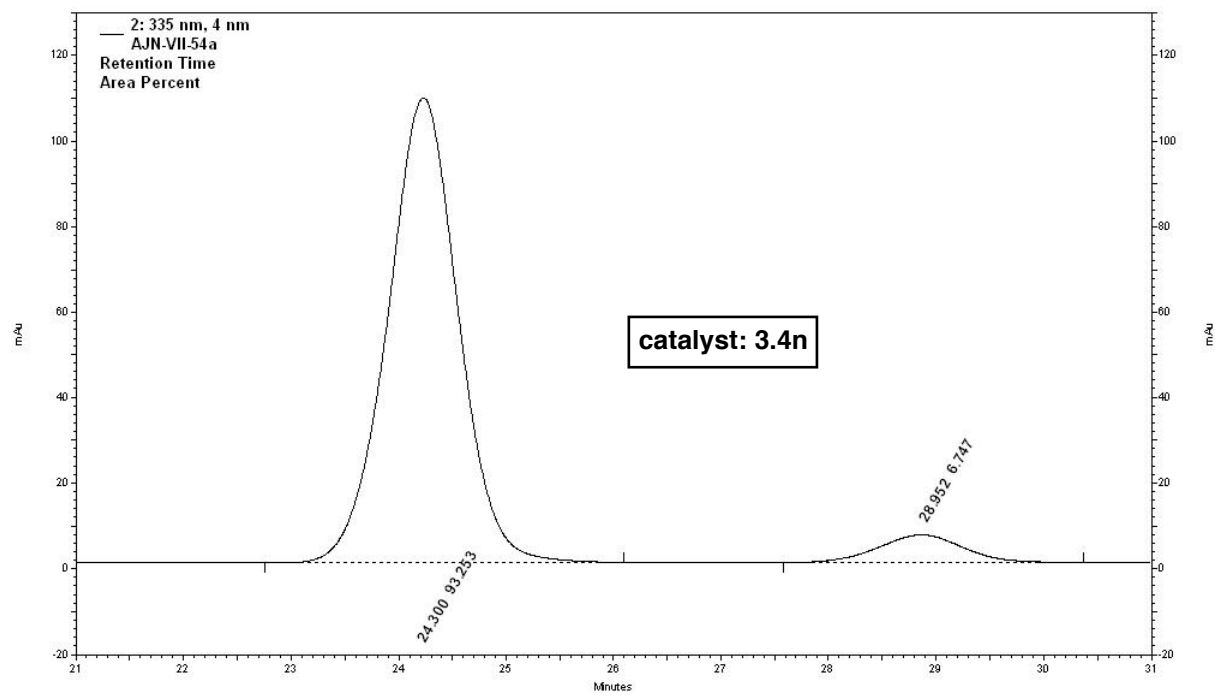
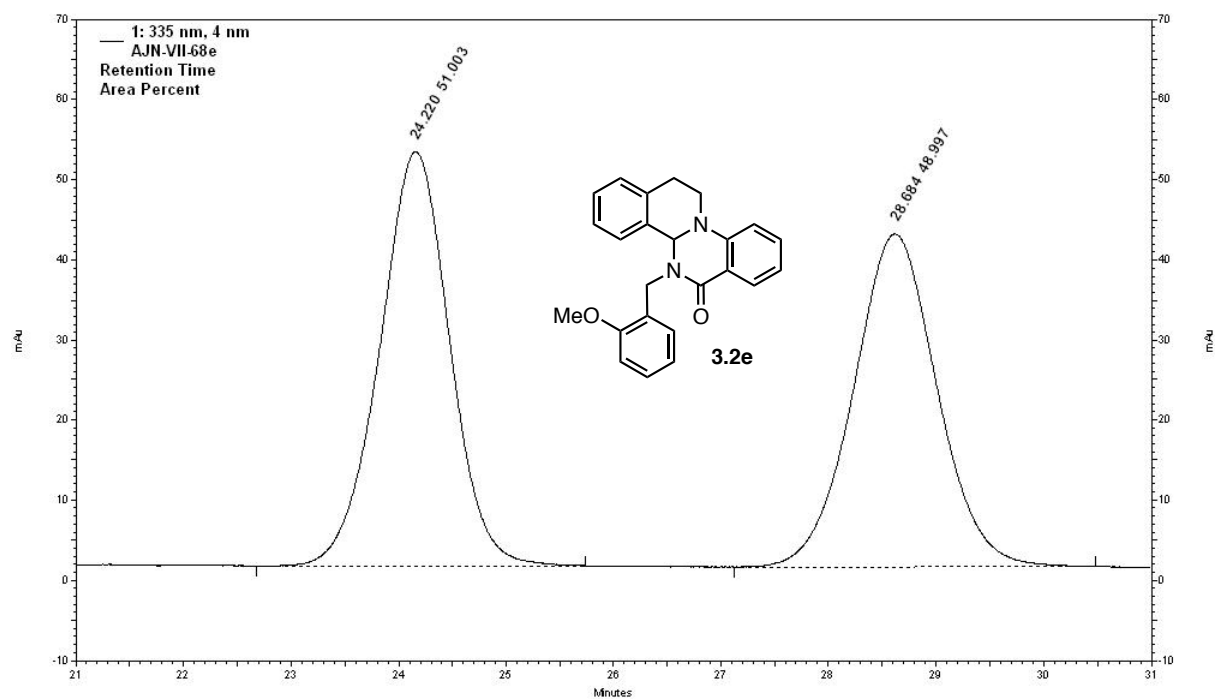
As part of this study, the enantioselectivity of each product **3.2** (12 total) was tested with each catalyst **3.4** (14 triazolyl) a minimum of 2 times for a total of 336 independent outcomes. Additionally, *pyr-3.4e* was tested 2 times with 7 substrates. Thus, only representative HPLC traces are provided, reflecting the results from Figure 5 in the main text, in which new catalysts were prepared to test specific hypotheses (**3.2a-k**). For the substrate that was not used in these experiments (**3.2l**), the trace is provided showing the highest enantioselectivity otherwise obtained. In each case, the catalyst that resulted in the given selectivity is indicated.

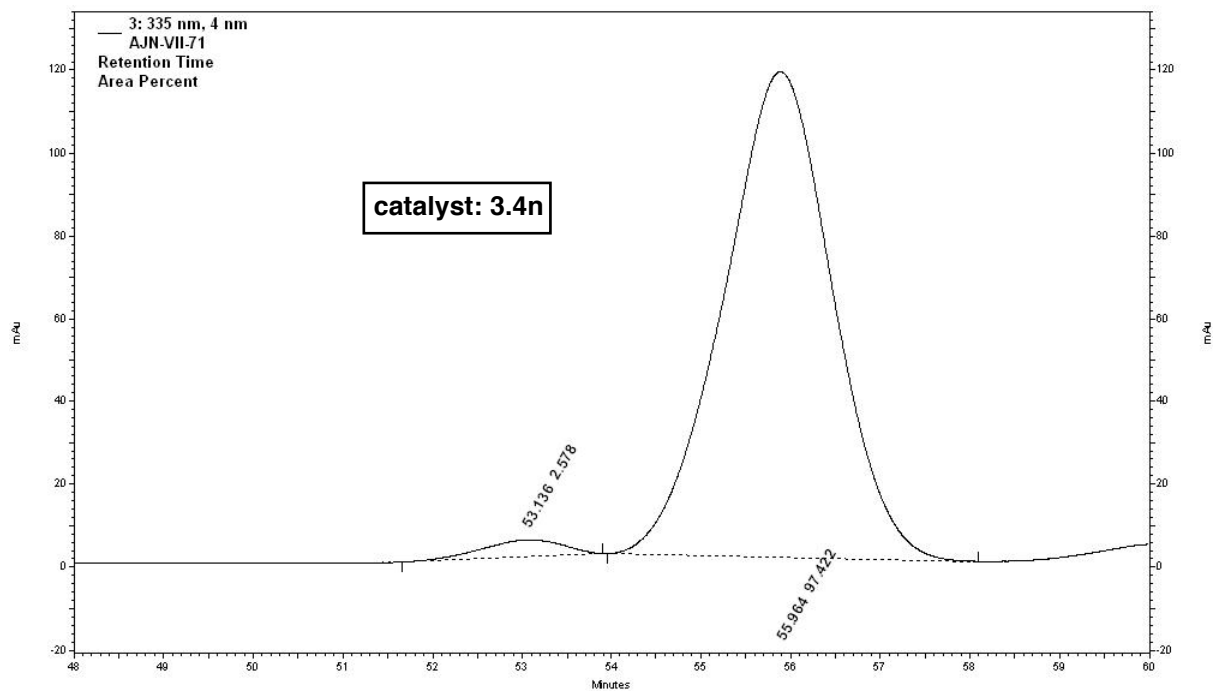
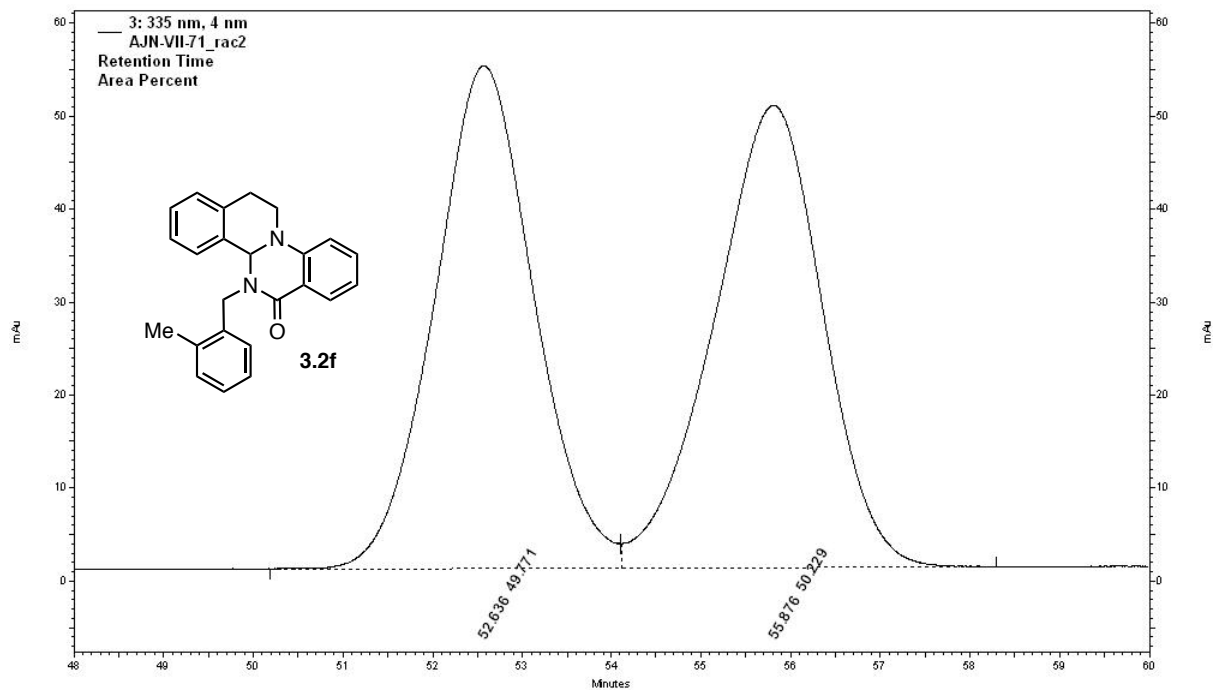


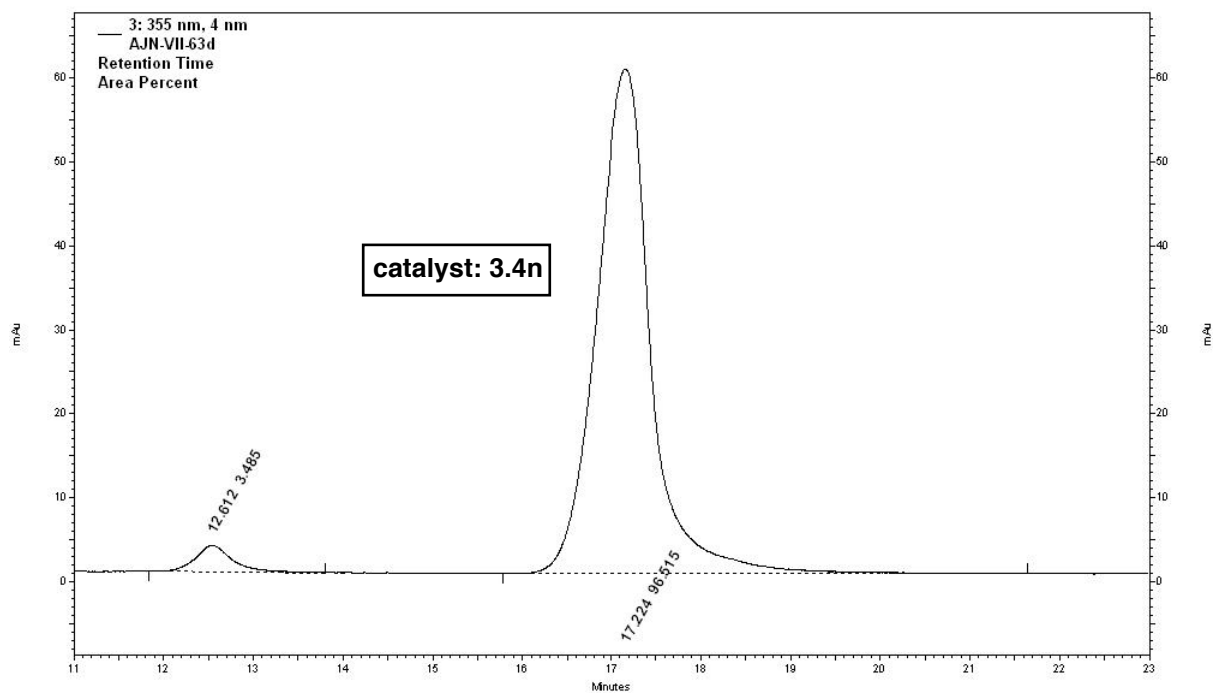
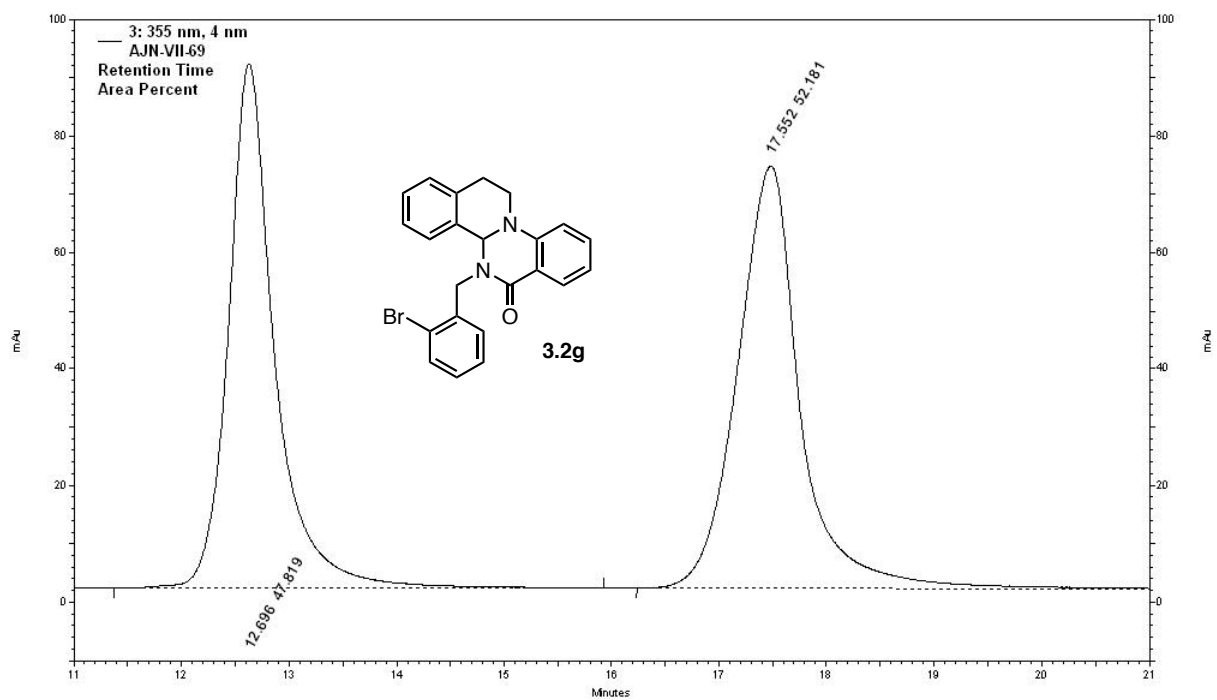


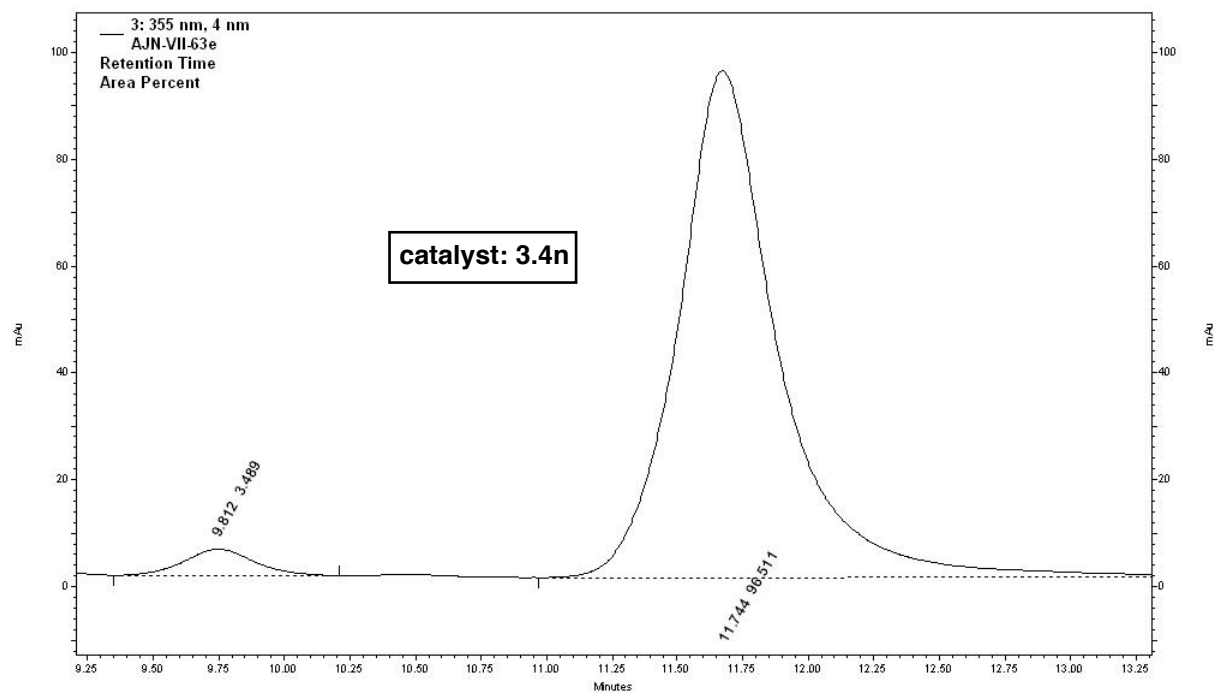
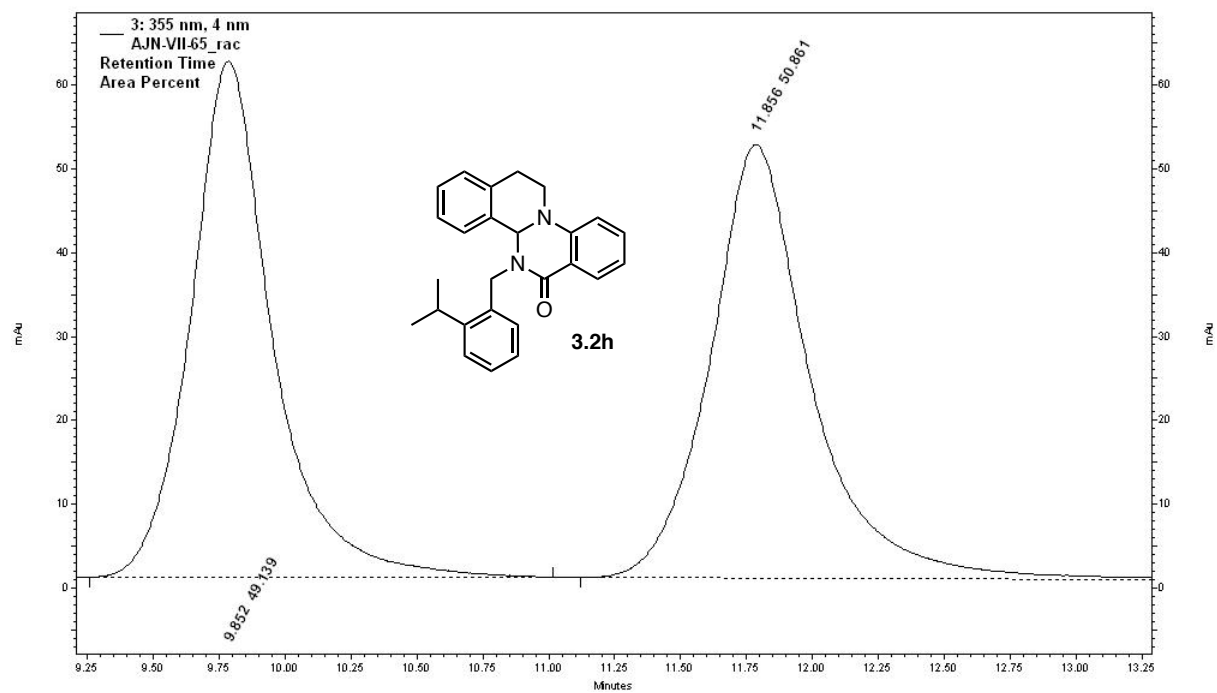


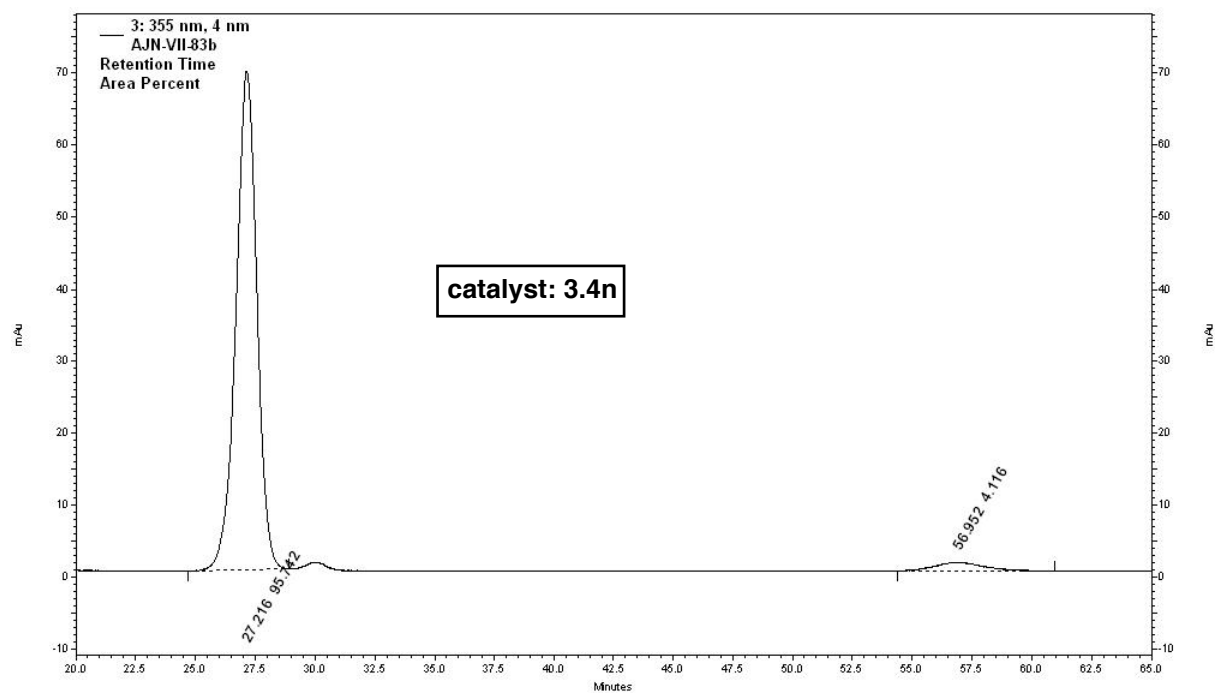
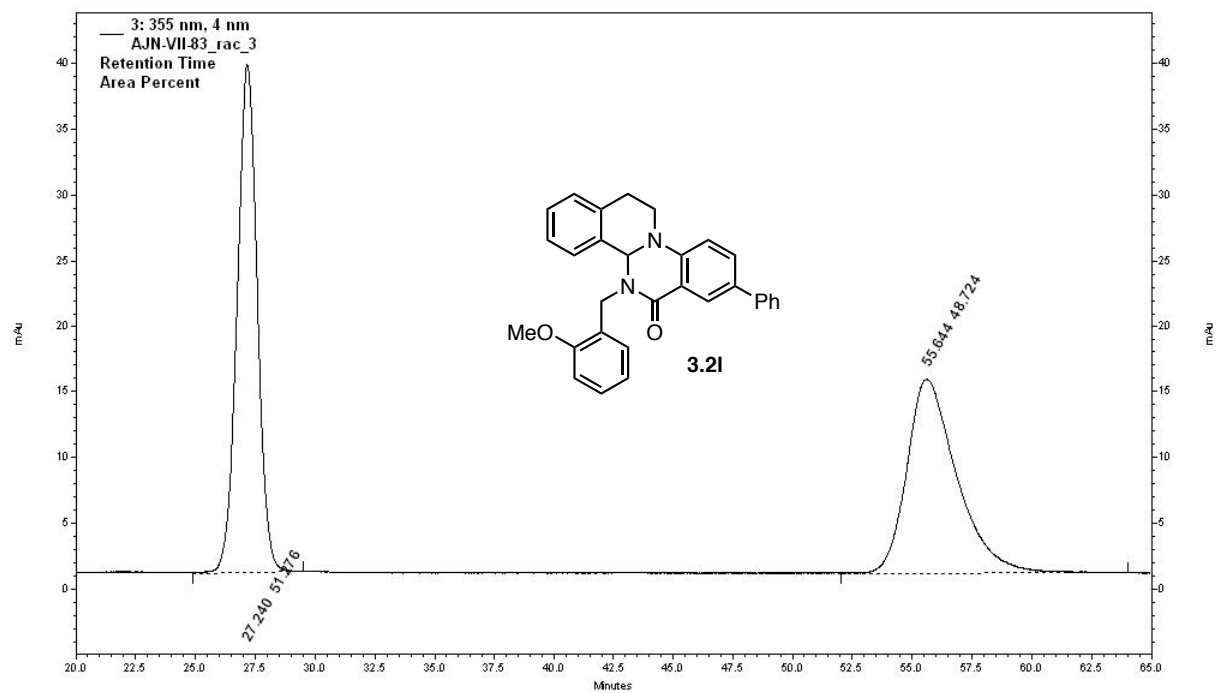


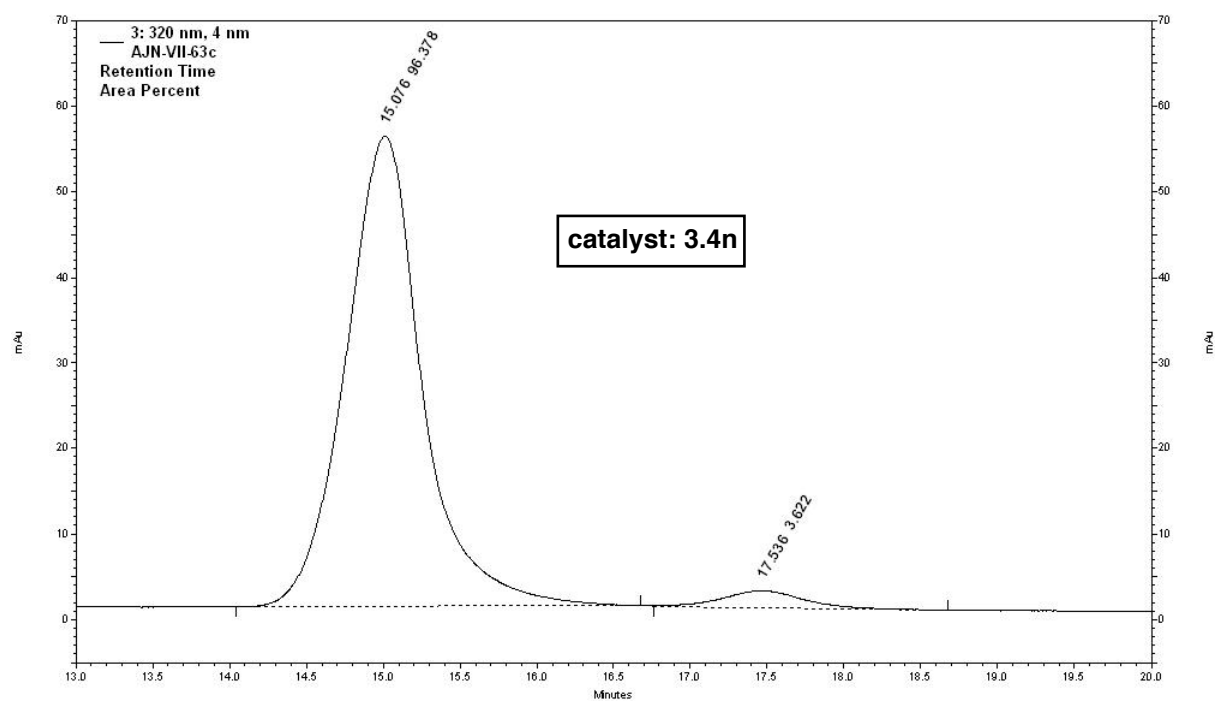
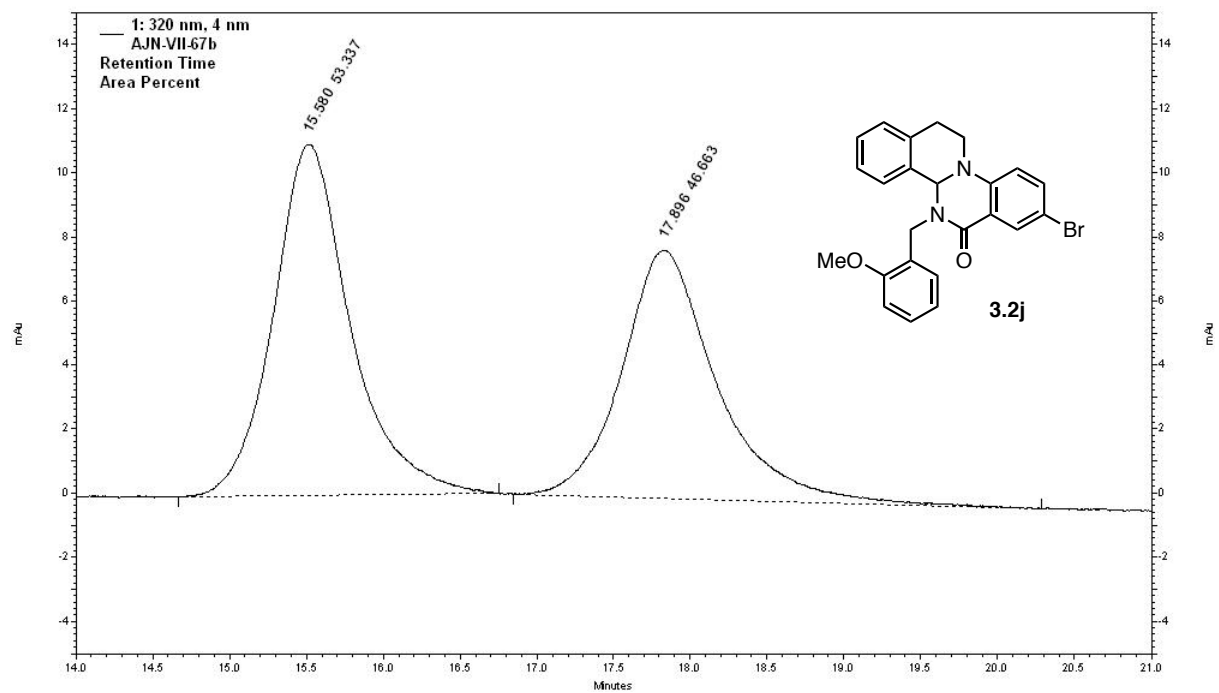


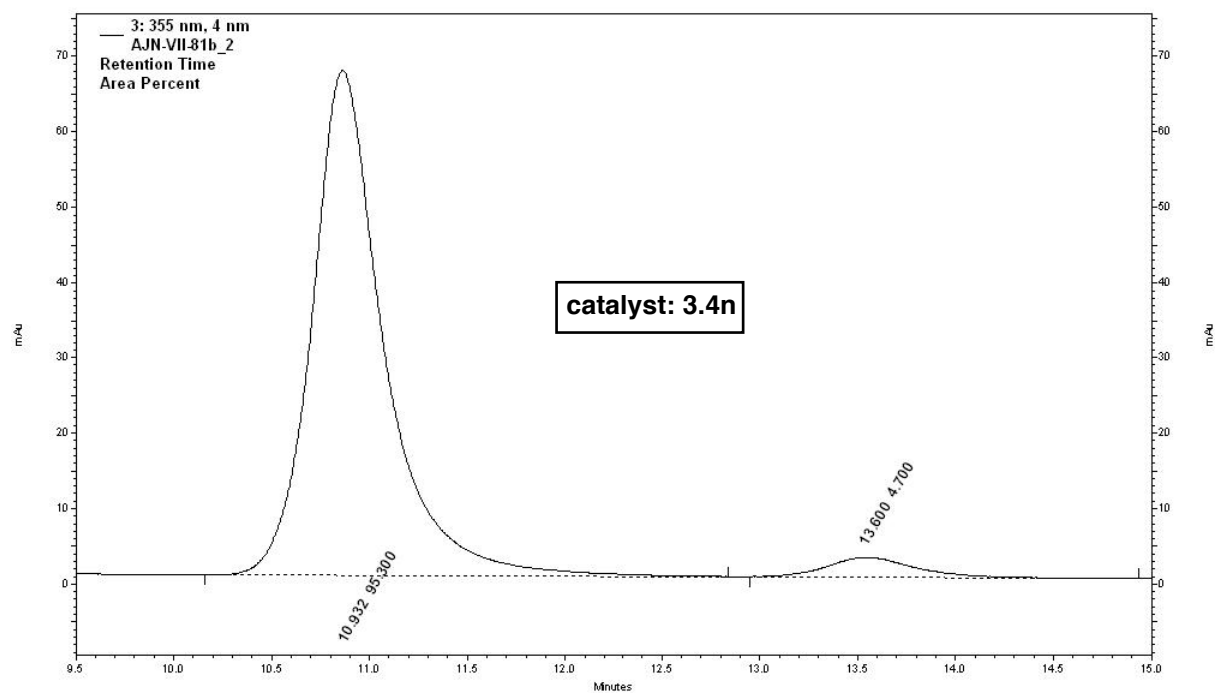
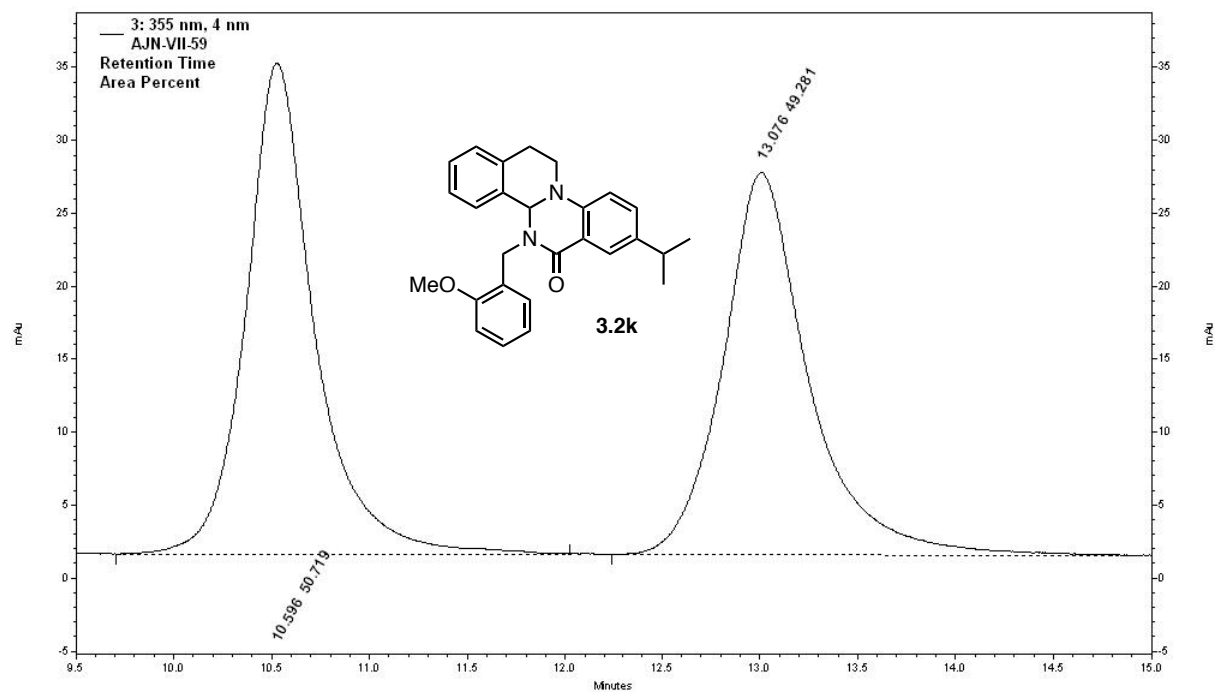


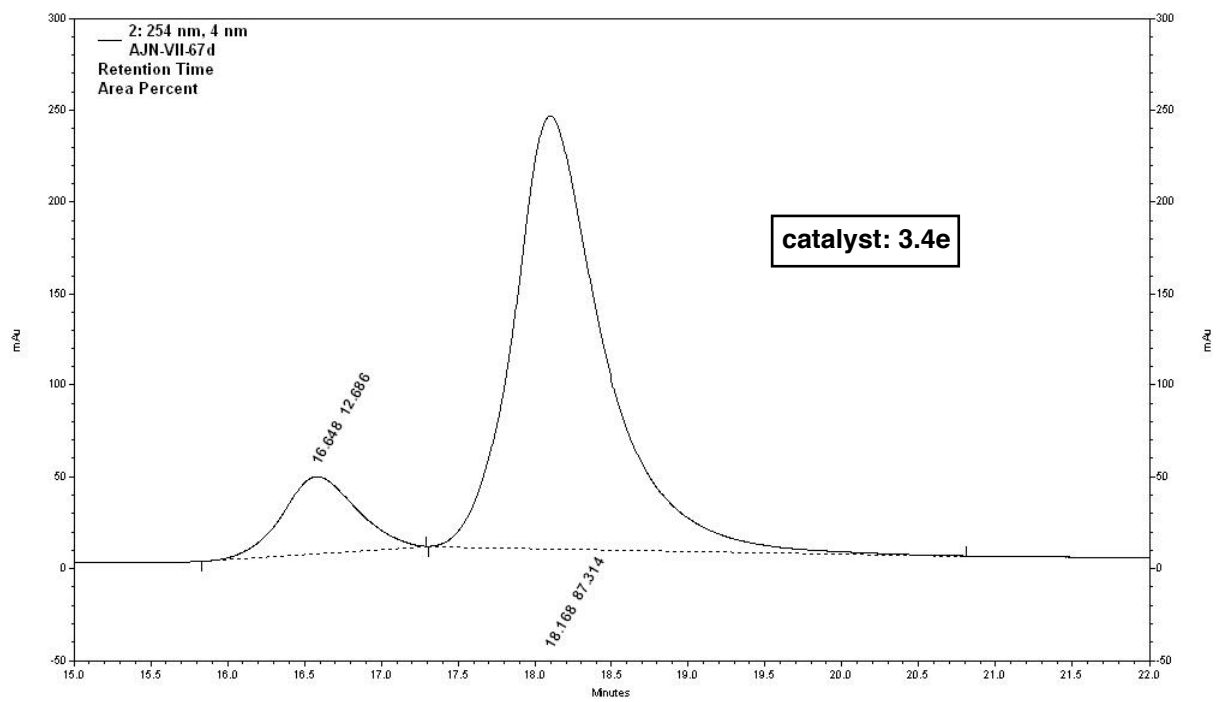
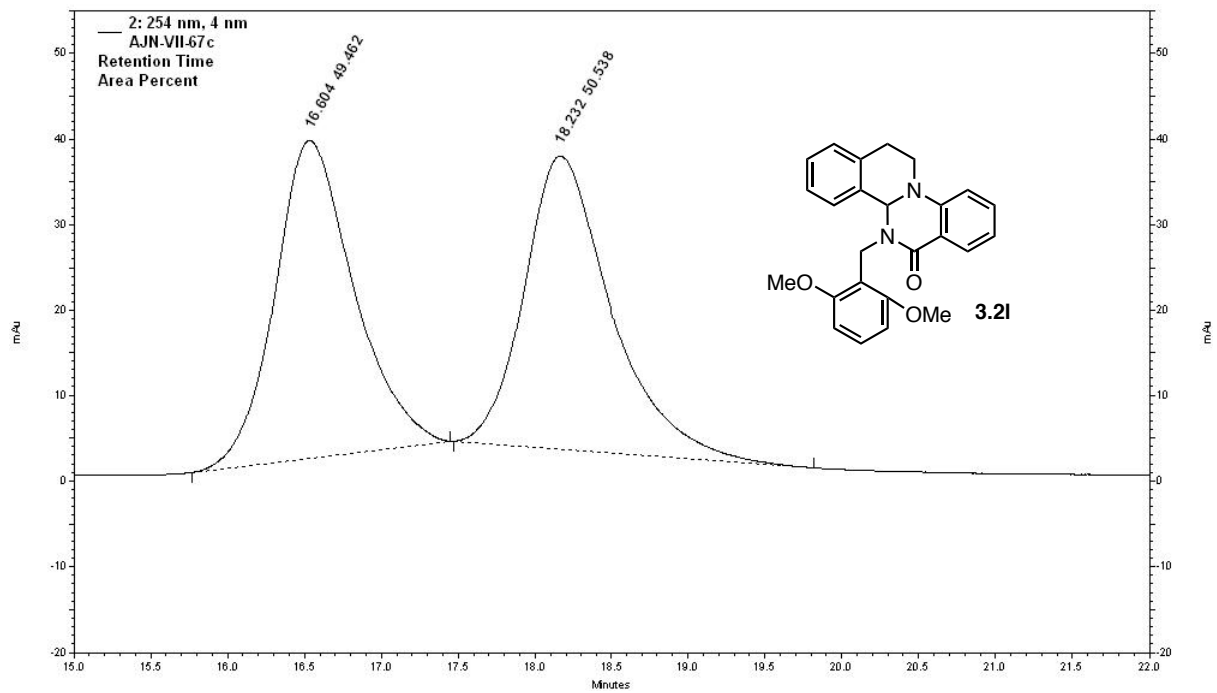










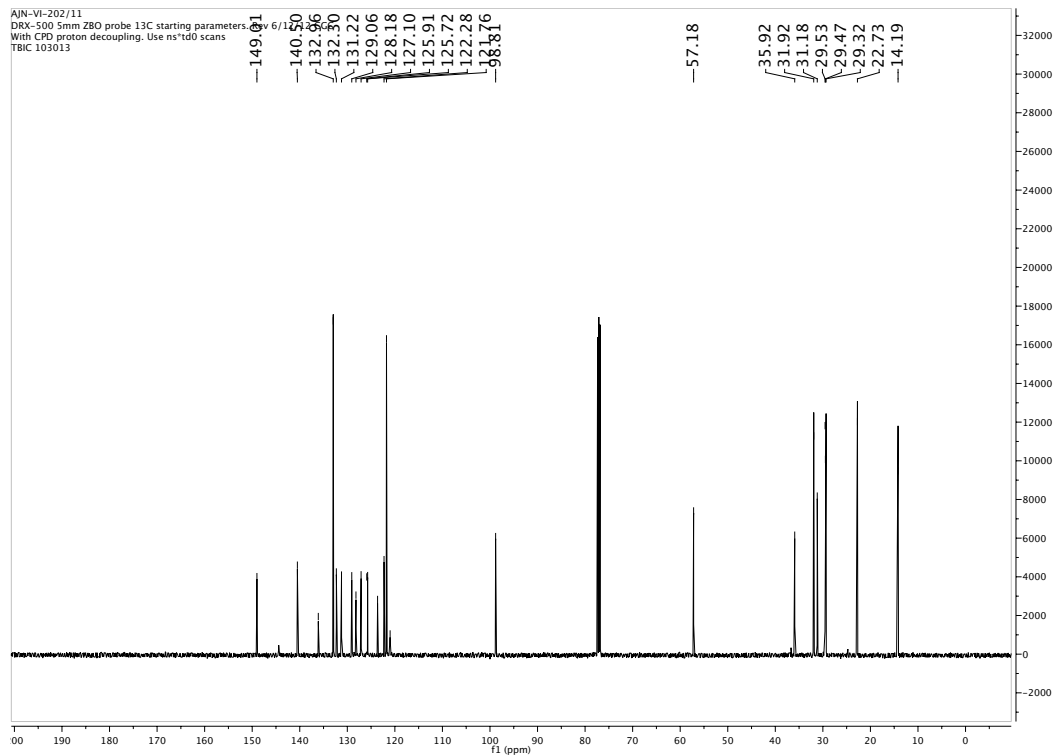
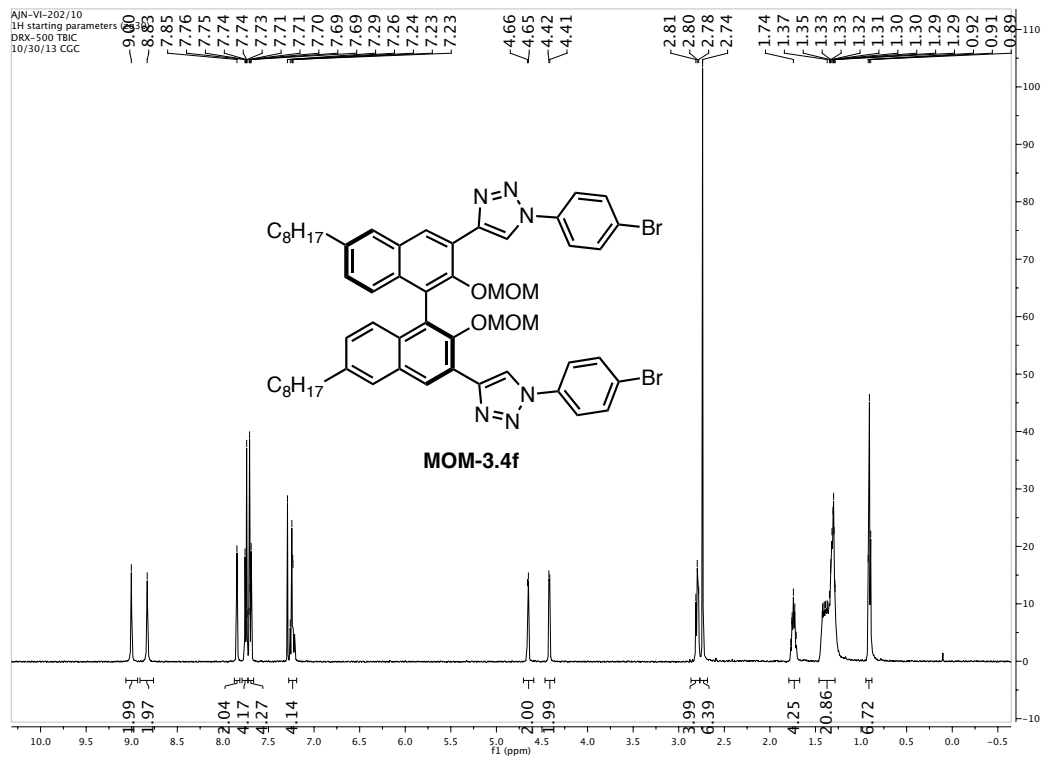


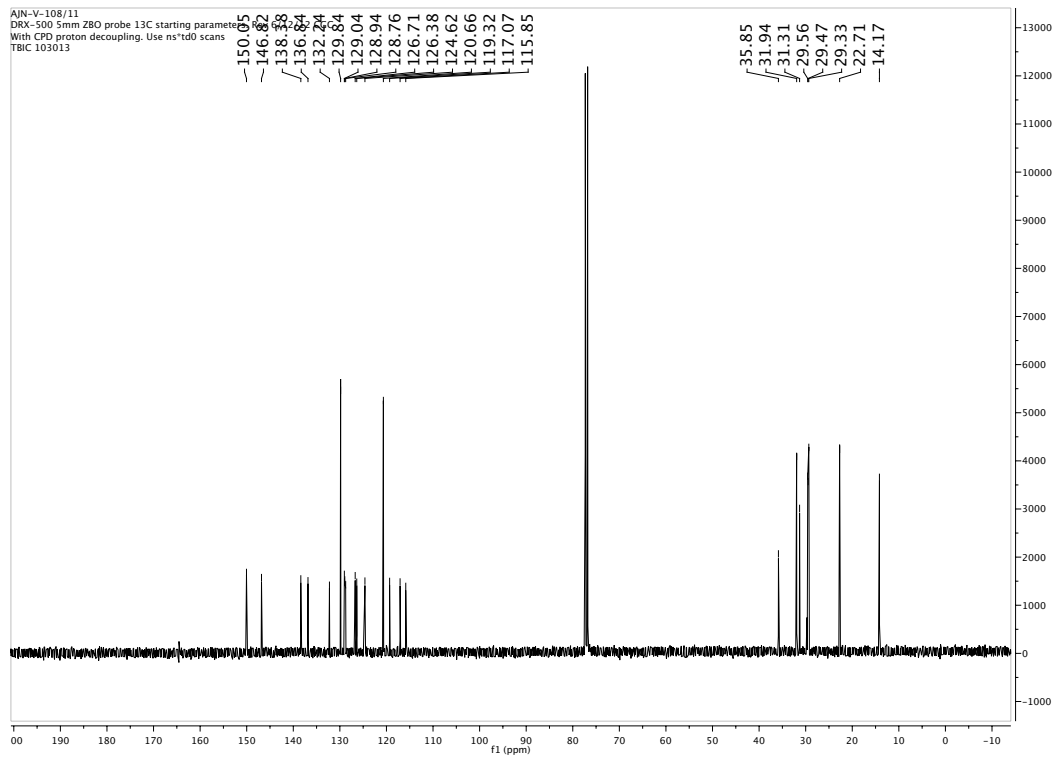
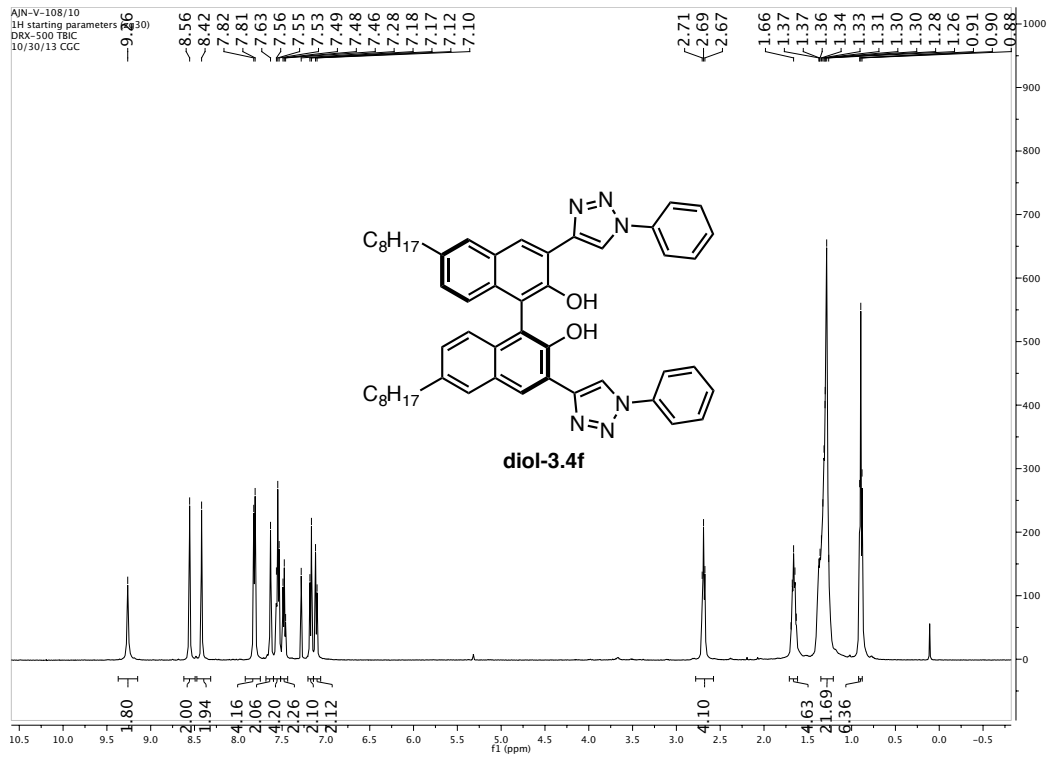
References and Notes

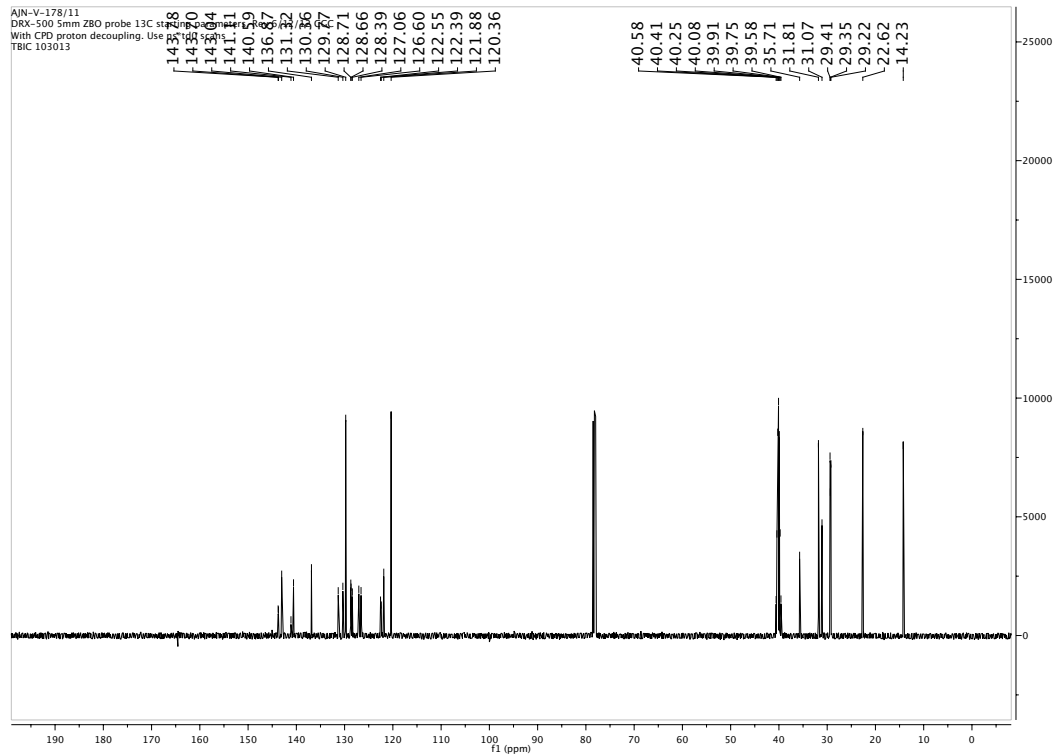
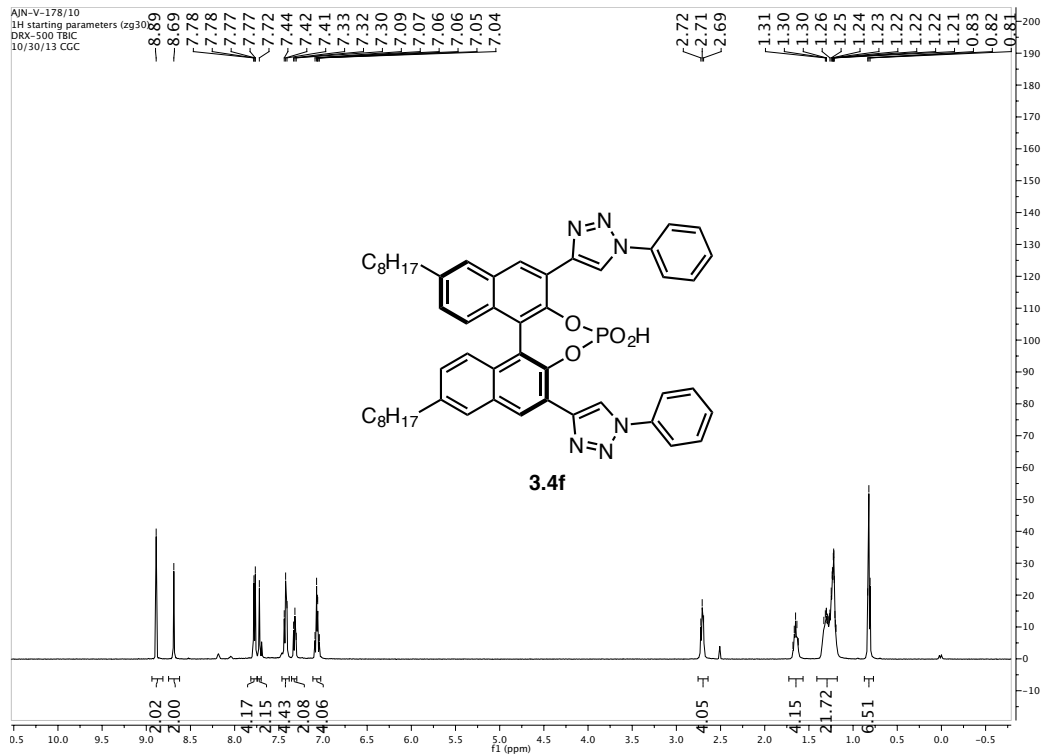
- (1) Neel, A. J.; Hehn, J. P.; Triplet, P. F.; Toste, F. D. *J. Am. Chem. Soc.* **2013**, *135* (38), 14044.
- (2) Doyle, A. G.; Jacobsen, E. N. *Chem. Rev.* **2007**, *107* (12), 5713.
- (3) Knowles, R. R.; Lin, S.; Jacobsen, E. N. *J. Am. Chem. Soc.* **2010**, *132* (14), 5030.
- (4) Knowles, R. R.; Jacobsen, E. N. *Proc. Natl. Acad. Sci.* **2010**, *107* (48), 20678.
- (5) Uyeda, C.; Jacobsen, E. N. *J. Am. Chem. Soc.* **2011**, *133* (13), 5062.
- (6) Lin, S.; Jacobsen, E. N. *Nat. Chem.* **2012**, *4* (10), 817.
- (7) Simón, L.; Goodman, J. M. *J. Org. Chem.* **2011**, *76* (6), 1775.
- (8) Halpern, J. *Science* **1982**, *217* (4558), 401.
- (9) Seeman, J. I. *Chem. Rev.* **1983**, *83* (2), 83.
- (10) *Exploring QSAR*; Leo, A., Hoekman, D. H., Eds.; ACS professional reference book; American Chemical Society: Washington, DC, 1995.
- (11) Anslyn, E. V.; Dougherty, D. A. *Modern physical organic chemistry*; University Science: Sausalito, CA, 2006.
- (12) Hansch, C.; Leo, A.; Taft, R. W. *Chem. Rev.* **1991**, *91* (2), 165.
- (13) Bess, E. N.; Sigman, M. S. In *Asymmetric Synthesis II*; Christmann, thias, Bräse, S., Eds.; Wiley-VCH Verlag GmbH & Co. KGaA, 2012; pp 363–370.
- (14) Jacobsen, E. N.; Zhang, W.; Güler, M. L. *J. Am. Chem. Soc.* **1991**, *113* (17), 6703.
- (15) Palucki, M.; Finney, N. S.; Pospisil, P. J.; Güler, M. L.; Ishida, T.; Jacobsen, E. N. *J. Am. Chem. Soc.* **1998**, *120* (5), 948.
- (16) Miller, J. J.; Sigman, M. S. *Angew. Chem. Int. Ed.* **2008**, *47* (4), 771.
- (17) Charton, M. *J. Am. Chem. Soc.* **1975**, *97* (6), 1552.
- (18) Charton, M. *J. Am. Chem. Soc.* **1975**, *97* (13), 3691.
- (19) Charton, M. *J. Am. Chem. Soc.* **1975**, *97* (13), 3694.
- (20) Charton, M. *J. Org. Chem.* **1976**, *41* (12), 2217.
- (21) Taft, R. W. *J. Am. Chem. Soc.* **1952**, *74* (12), 3120.
- (22) Harper, K. C.; Sigman, M. S. *Science* **2011**, *333* (6051), 1875.
- (23) Harper, K. C.; Bess, E. N.; Sigman, M. S. *Nat. Chem.* **2012**, *4* (5), 366.
- (24) Verloop, A.; Hoogenstraaten, W.; Tipker, J. In *Drug Design*; Ariëns, E. J., Ed.; Medicinal Chemistry: A Series of Monographs; Academic Press: Amsterdam, 1976; Vol. 11, Part G, pp 165–207.
- (25) Milo, A.; Bess, E. N.; Sigman, M. S. *Nature* **2014**, *507* (7491), 210.
- (26) Hunter, C. A.; Sanders, J. K. M. *J. Am. Chem. Soc.* **1990**, *112* (14), 5525.
- (27) Cozzi, F.; Cinquini, M.; Annuziata, R.; Siegel, J. S. *J. Am. Chem. Soc.* **1993**, *115* (12), 5330.
- (28) Bloom, J. W. G.; Wheeler, S. E. *Angew. Chem. Int. Ed.* **2011**, *50* (34), 7847.
- (29) Raju, R. K.; Bloom, J. W. G.; An, Y.; Wheeler, S. E. *ChemPhysChem* **2011**, *12* (17), 3116.
- (30) Martinez, C. R.; Iverson, B. L. *Chem. Sci.* **2012**, *3* (7), 2191.
- (31) Riley, K. E.; Hobza, P. *Acc. Chem. Res.* **2013**, *46* (4), 927.
- (32) Sherrill, C. D. *Acc. Chem. Res.* **2013**, *46* (4), 1020.
- (33) Hohenstein, E. G.; Sherrill, C. D. *J. Phys. Chem. A* **2009**, *113* (5), 878.
- (34) Wheeler, S. E. *Acc. Chem. Res.* **2013**, *46* (4), 1029.
- (35) Wheeler, S. E.; Houk, K. N. *J. Am. Chem. Soc.* **2008**, *130* (33), 10854.
- (36) Wheeler, S. E.; Houk, K. N. *Mol. Phys.* **2009**, *107* (8-12), 749.
- (37) Wheeler, S. E.; Houk, K. N. *J. Chem. Theory Comput.* **2009**, *5* (9), 2301.

- (38) Wheeler, S. E. *J. Am. Chem. Soc.* **2011**, *133* (26), 10262.
- (39) Wheeler, S. E. *CrystEngComm* **2012**, *14* (19), 6140.
- (40) Parrish, R. M.; Sherrill, C. D. *J. Am. Chem. Soc.* **2014**, *136* (50), 17386.
- (41) Wheeler, S. E.; Bloom, J. W. G. *J. Phys. Chem. A* **2014**, *118* (32), 6133.
- (42) O'Hagan, D. *Chem. Soc. Rev.* **2008**, *37* (2), 308.
- (43) Collins, K. D.; Gensch, T.; Glorius, F. *Nat. Chem.* **2014**, *6* (10), 859.
- (44) Reetz, M. T. *Angew. Chem. Int. Ed.* **2011**, *50* (1), 138.
- (45) Robbins, D. W.; Hartwig, J. F. *Science* **2011**, *333* (6048), 1423.
- (46) McNally, A.; Prier, C. K.; MacMillan, D. W. C. *Science* **2011**, *334* (6059), 1114.
- (47) Friedfeld, M. R.; Shevlin, M.; Hoyt, J. M.; Krska, S. W.; Tudge, M. T.; Chirik, P. J. *Science* **2013**, *342* (6162), 1076.
- (48) Metola, P.; Nichols, S. M.; Kahr, B.; Anslyn, E. V. *Chem. Sci.* **2014**, *5* (11), 4278.
- (49) Santanilla, A. B.; Regalado, E. L.; Pereira, T.; Shevlin, M.; Bateman, K.; Campeau, L.-C.; Schneeweis, J.; Berritt, S.; Shi, Z.-C.; Nantermet, P.; Liu, Y.; Helmy, R.; Welch, C. J.; Vachal, P.; Davies, I. W.; Cernak, T.; Dreher, S. D. *Science* **2015**, *347* (6217), 49.
- (50) Frisch, M. J.; Trucks, G. W.; Schlegel, H. B.; Scuseria, G. E.; Robb, M. A.; Cheeseman, J. R.; Scalmani, R.; Barone, G.; Mennucci, B.; Petersson, G. A.; others. *Inc Wallingford CT* **2009**.
- (51) Zhao, Y.; Truhlar, D. G. *Theor. Chem. Acc.* **2007**, *120* (1-3), 215.
- (52) Valero, R.; Gomes, J. R. B.; Truhlar, D. G.; Illas, F. *J. Chem. Phys.* **2008**, *129* (12), 124710.
- (53) Schäfer, A.; Horn, H.; Ahlrichs, R. *J. Chem. Phys.* **1992**, *97* (4), 2571.
- (54) Schäfer, A.; Huber, C.; Ahlrichs, R. *J. Chem. Phys.* **1994**, *100* (8), 5829.
- (55) Merrick, J. P.; Moran, D.; Radom, L. *J. Phys. Chem. A* **2007**, *111* (45), 11683.
- (56) Goodman, S. *Semin. Hematol.* **2008**, *45* (3), 135.
- (57) Goddard-Borger, E. D.; Stick, R. V. *Org. Lett.* **2011**, *13* (9), 2514.

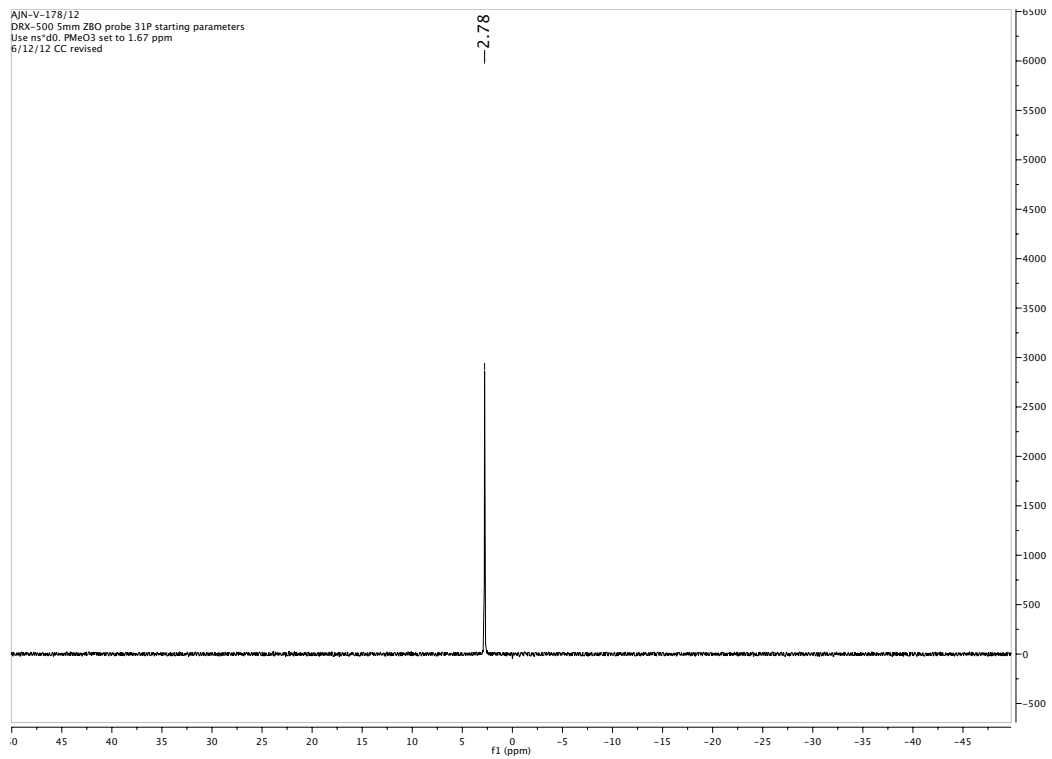
Appendix B. NMR Spectra for Compounds in Chapter 3

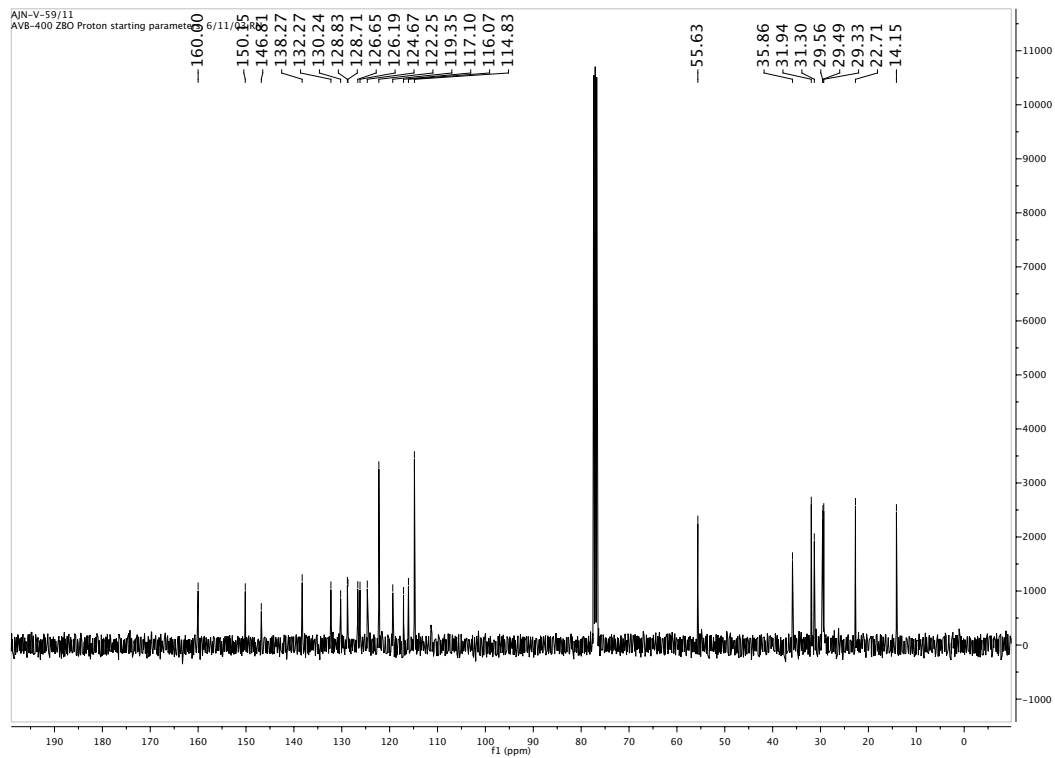
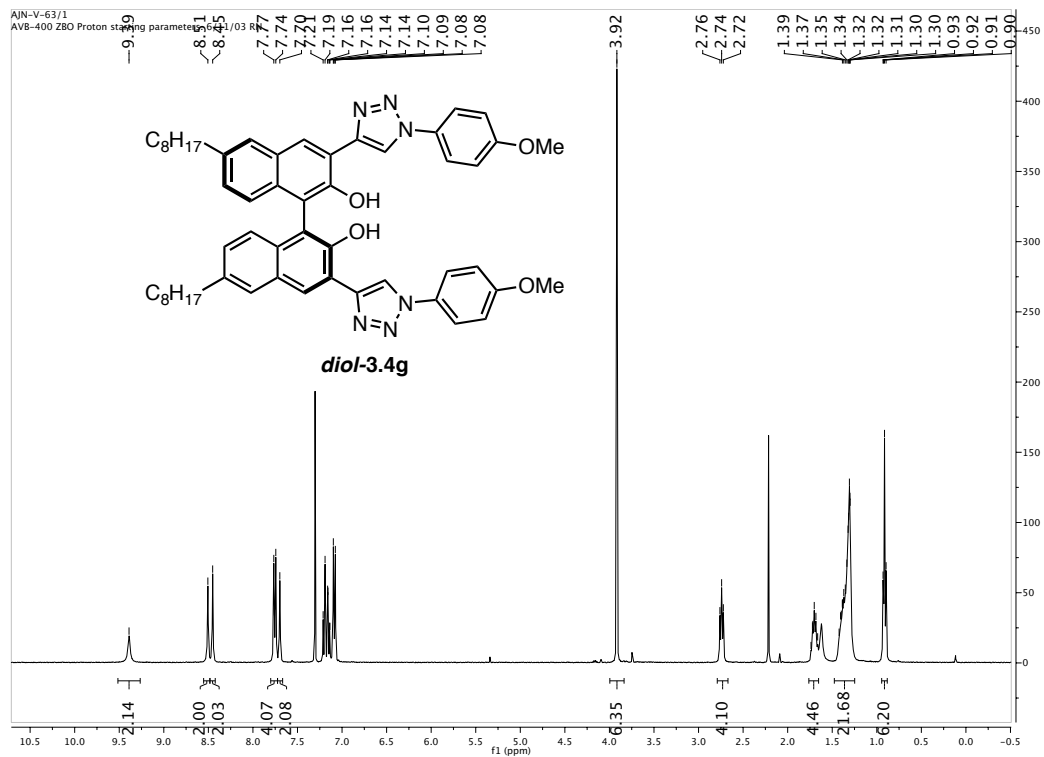


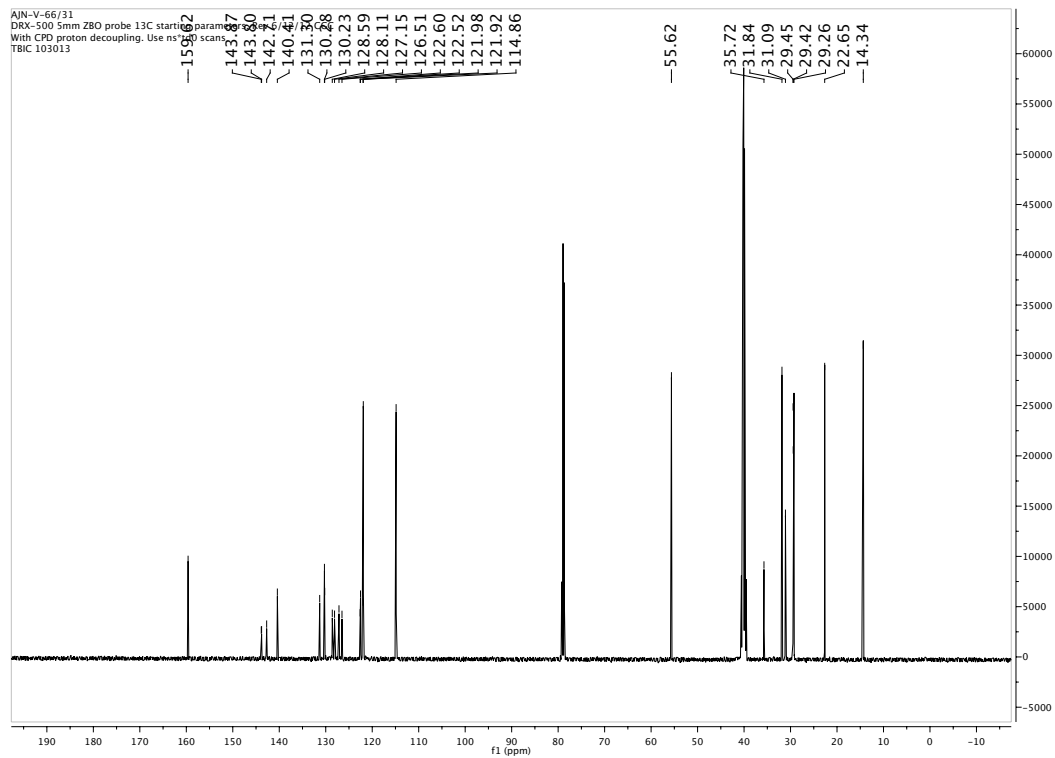
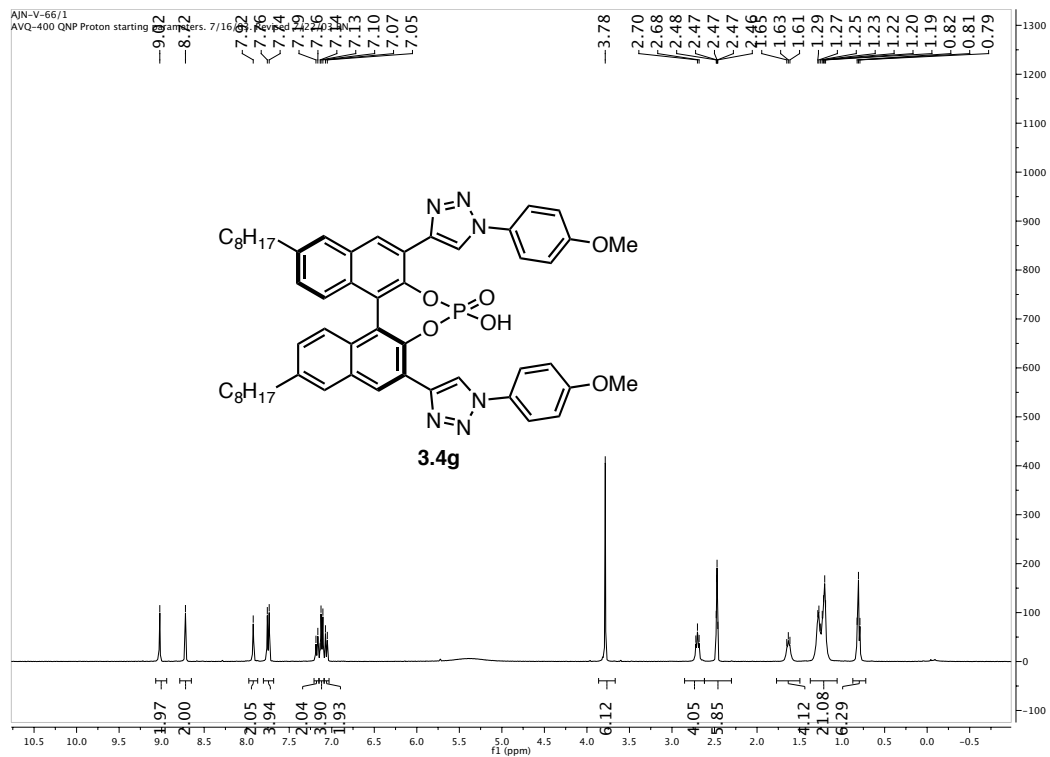


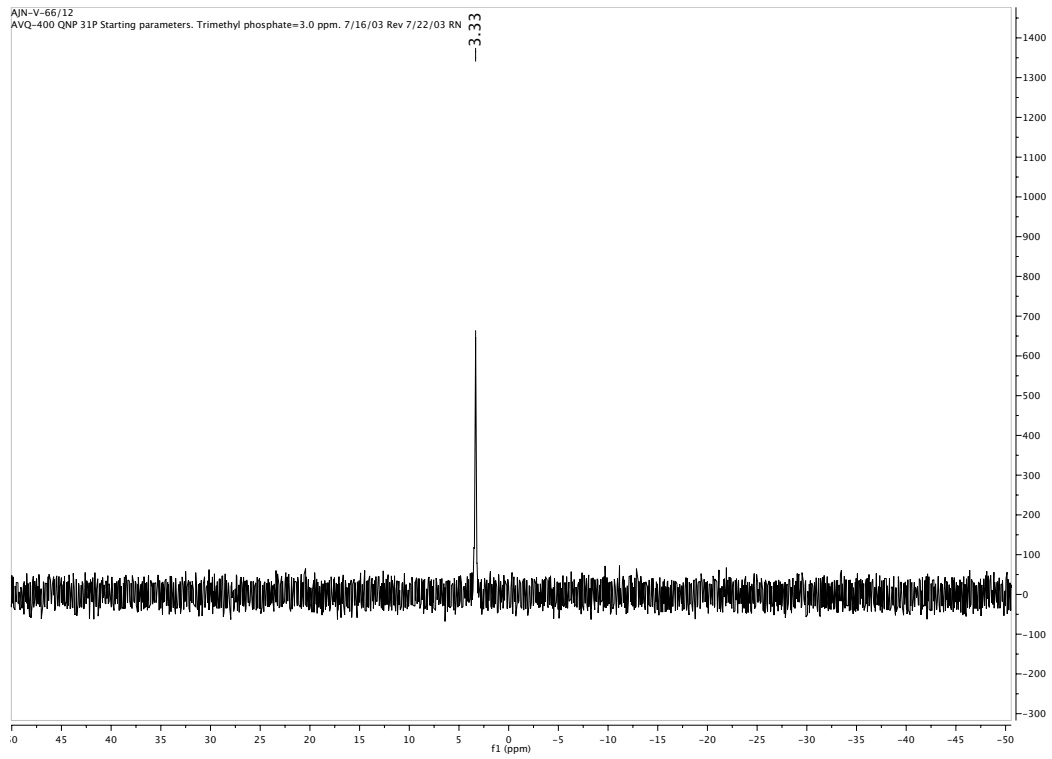


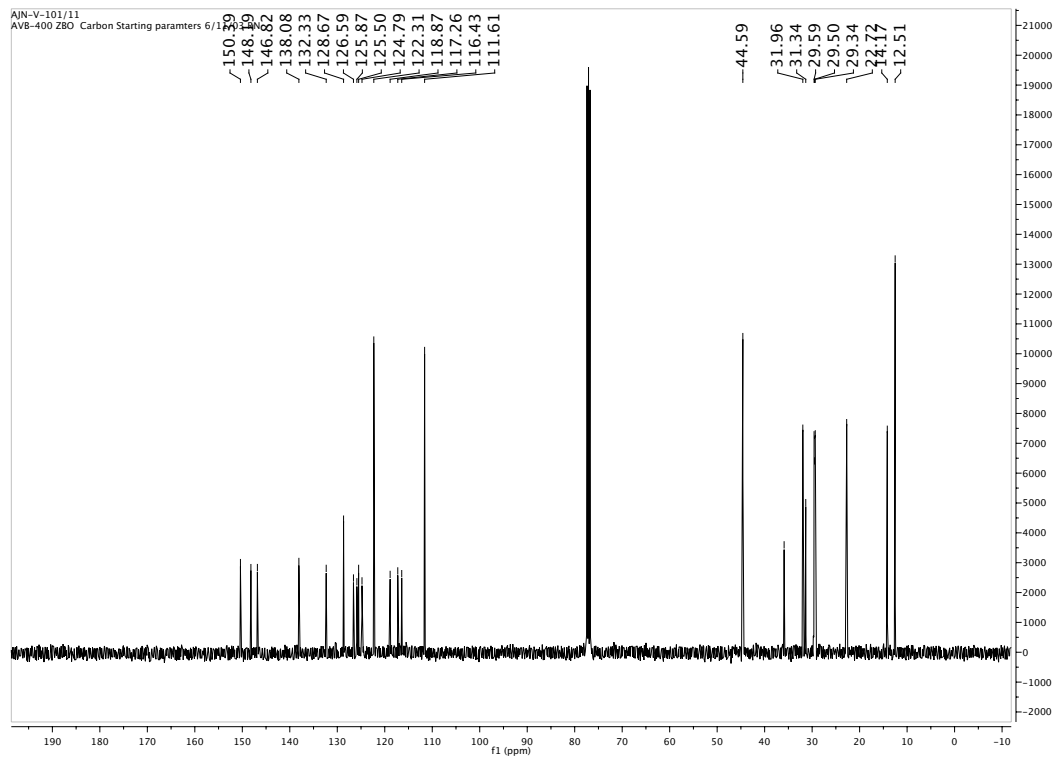
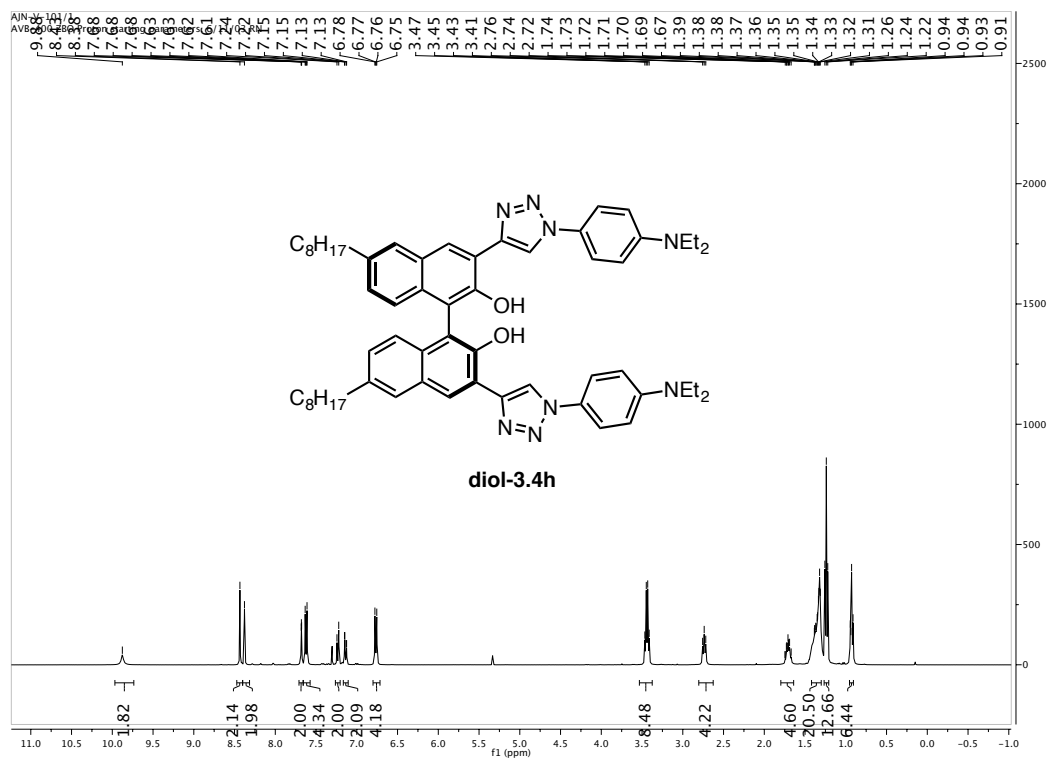
AJN-V-178/12
DRX-500 5mm Z80 probe 31P starting parameters
Use ns140, PMA03 set to 1.67 ppm
6/12/12 CC revised

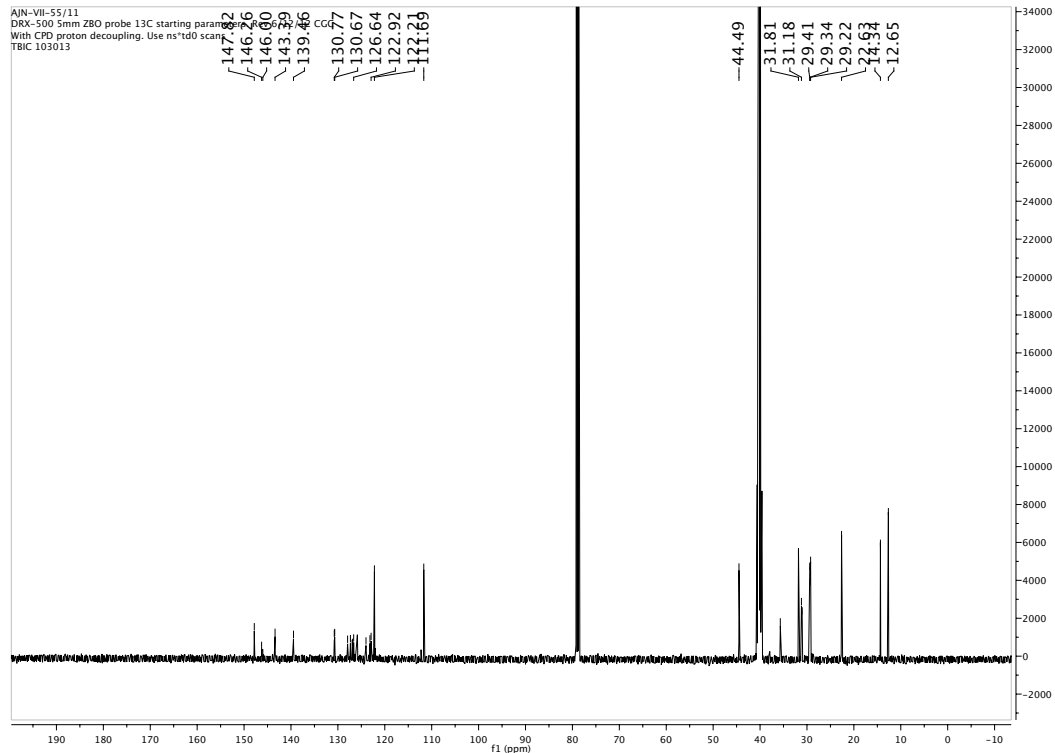
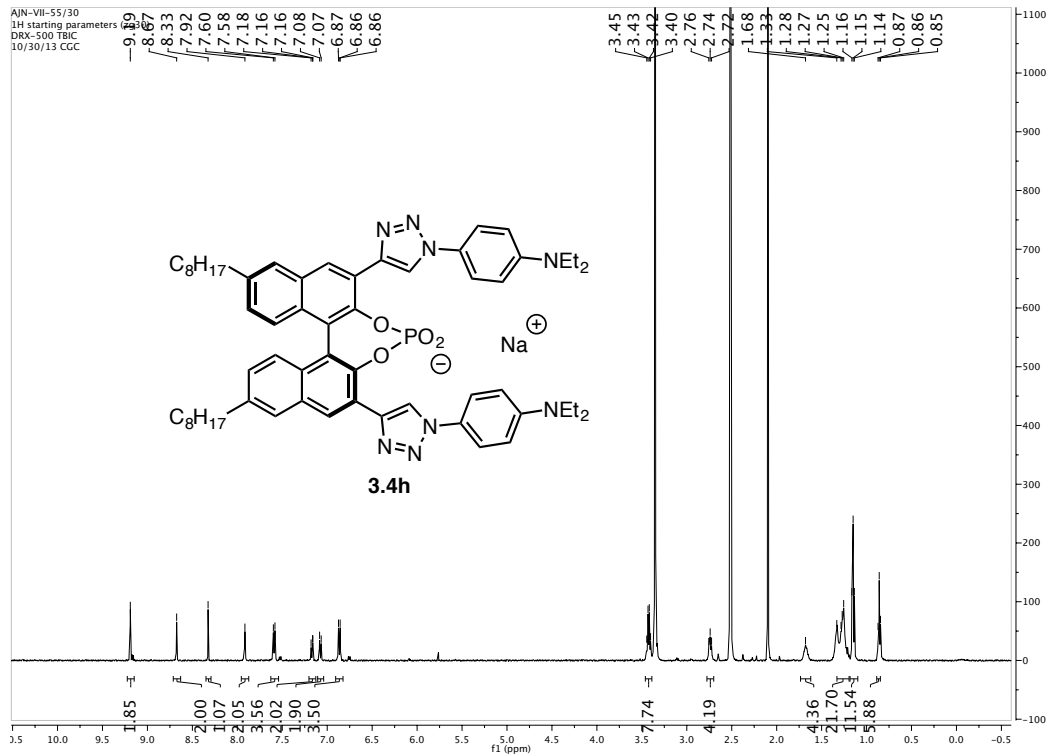


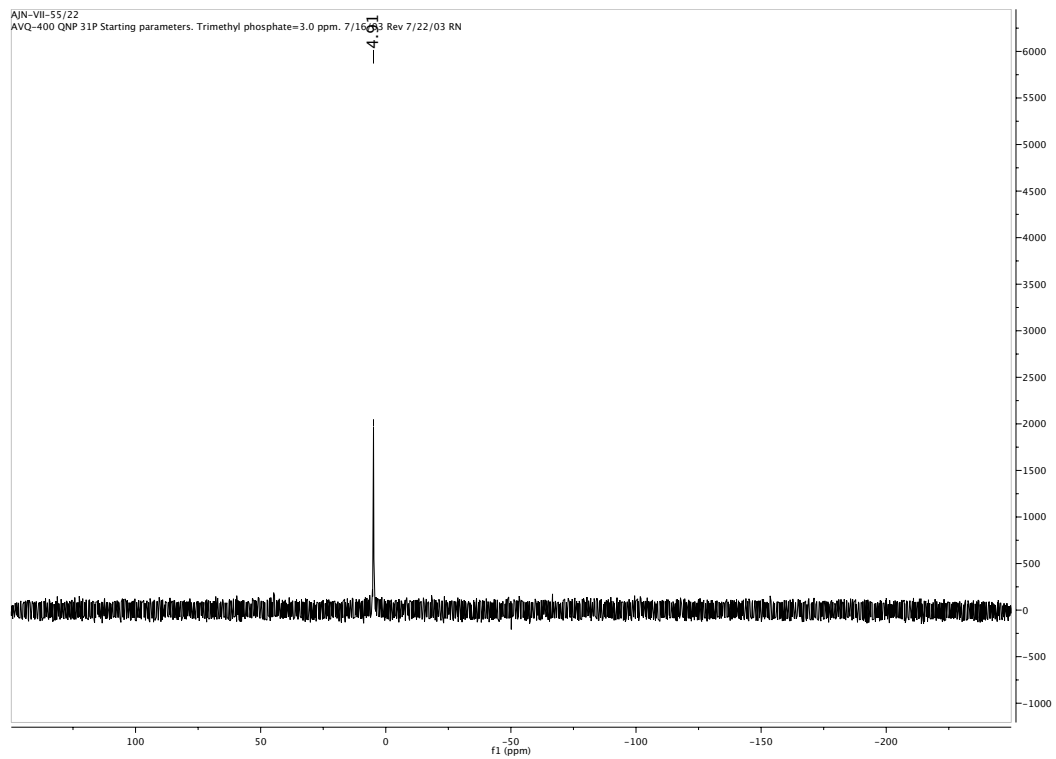


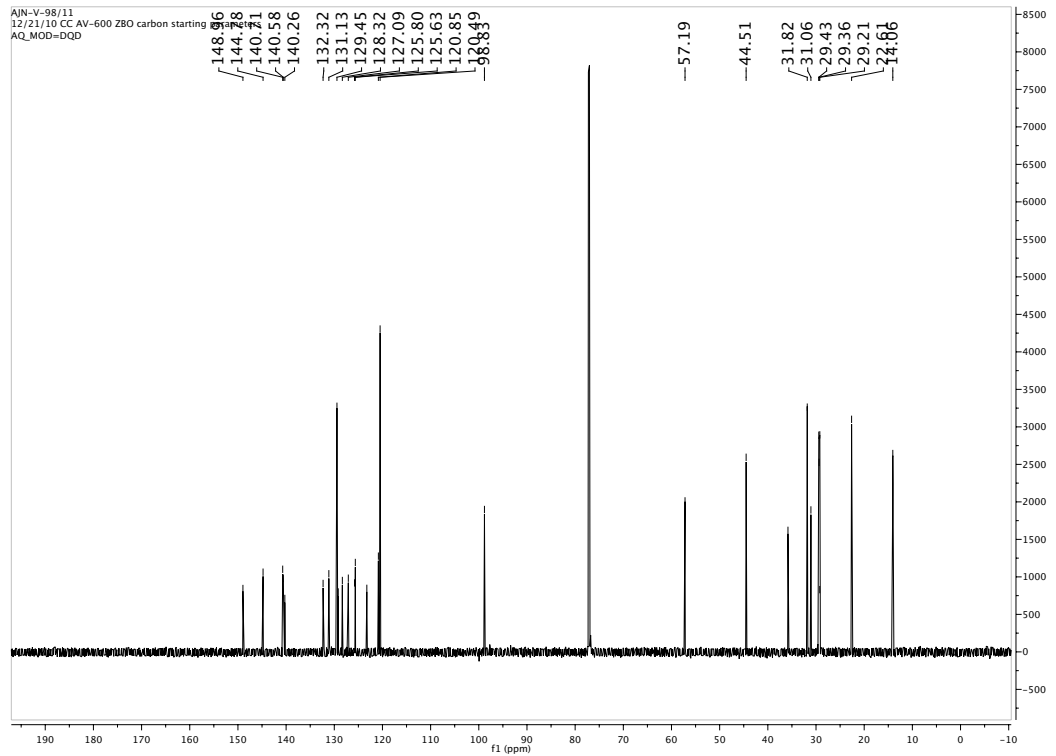
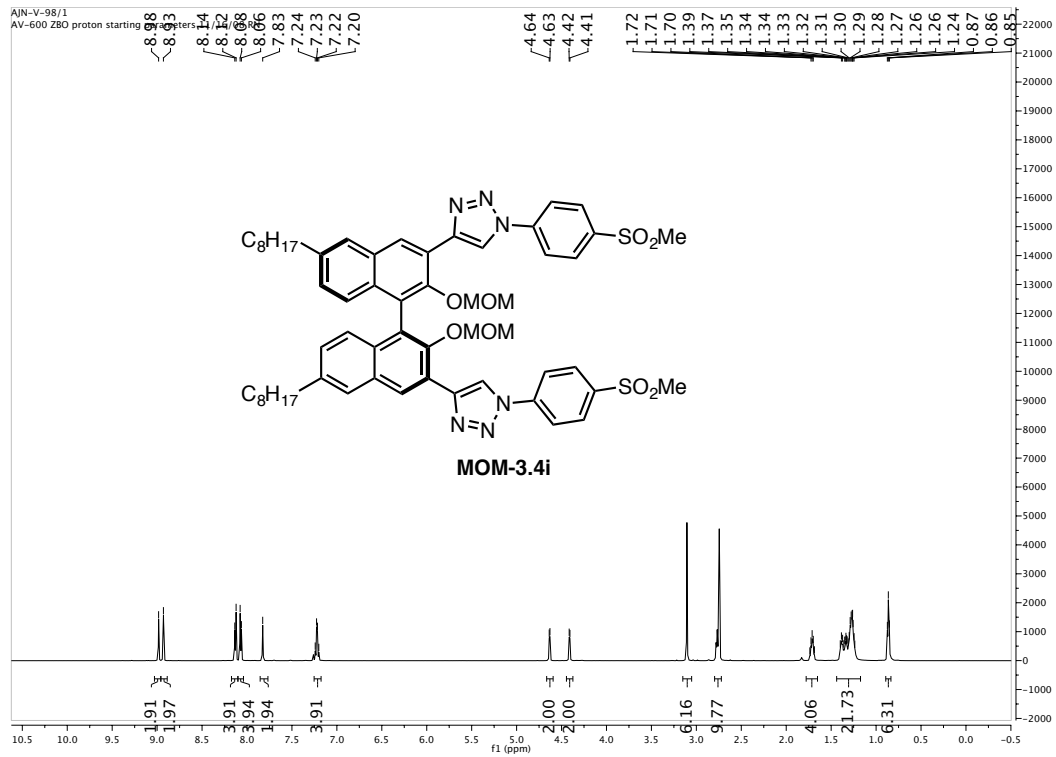


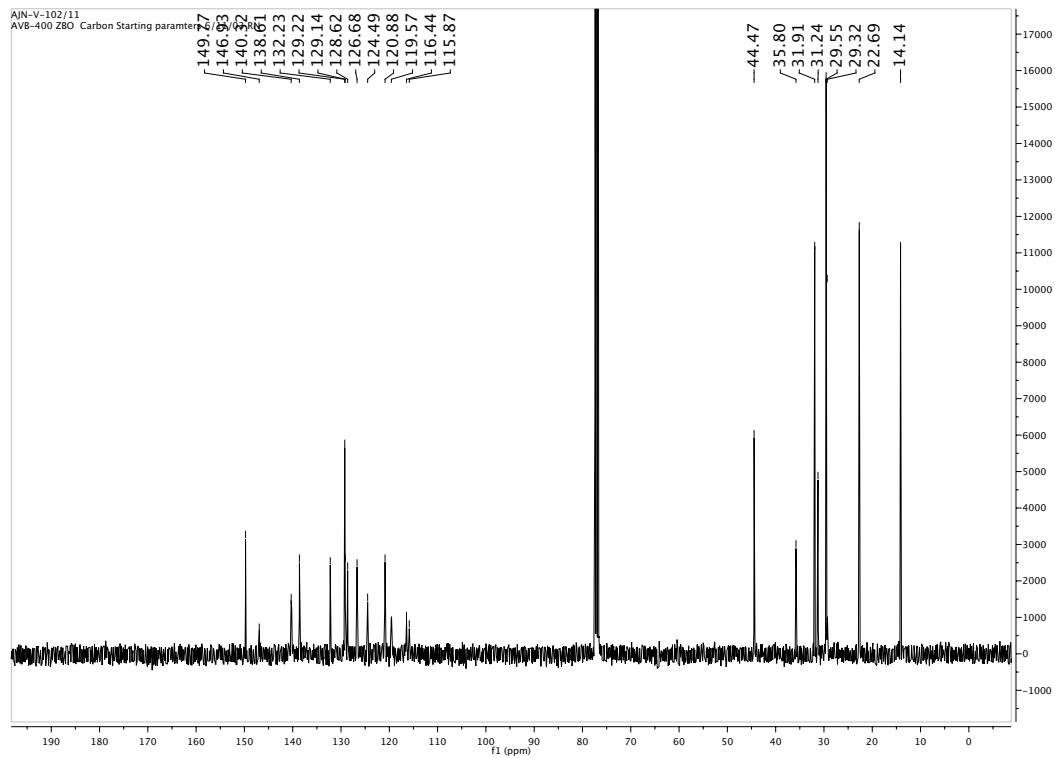
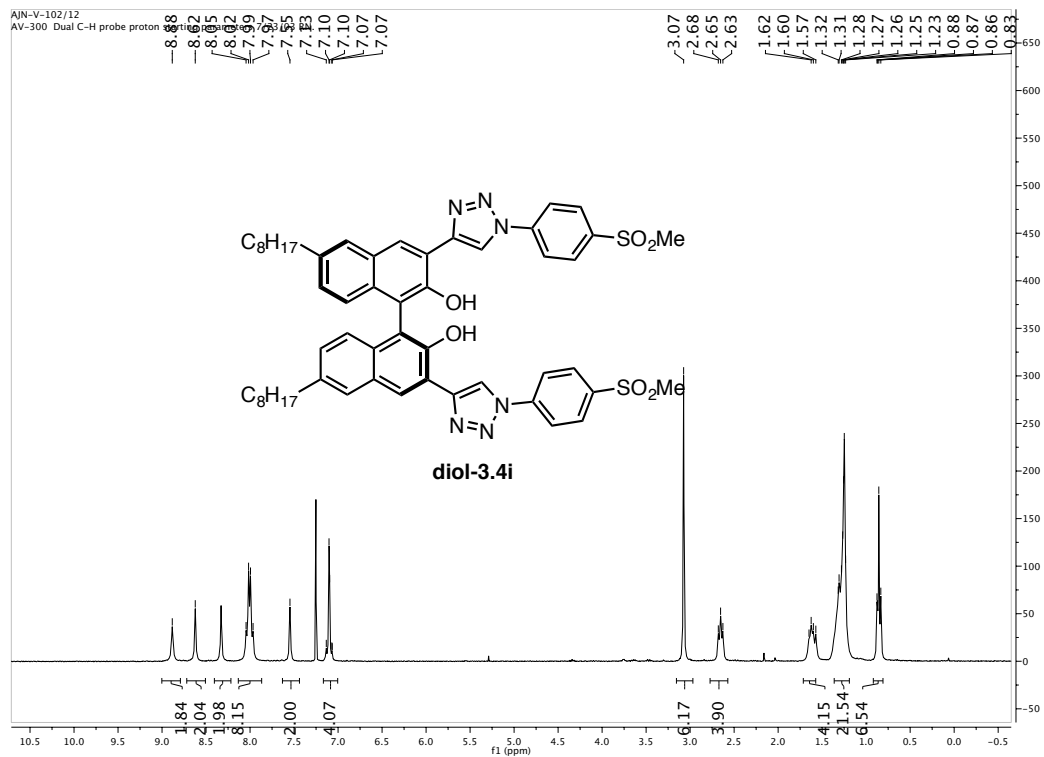




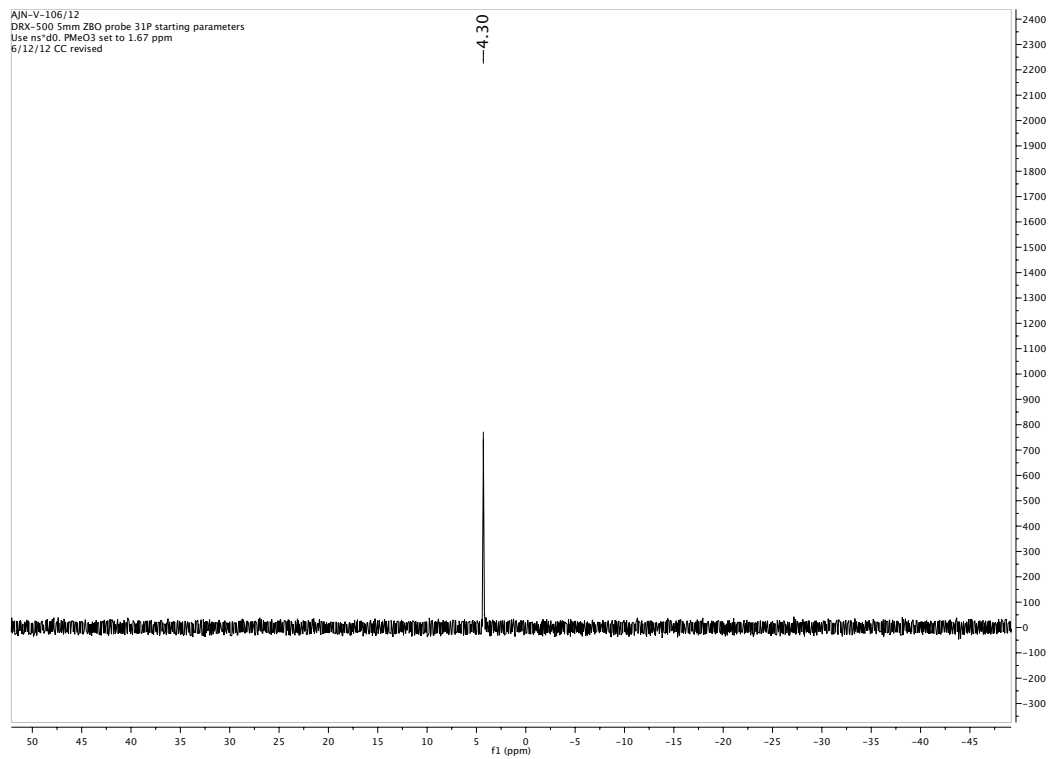


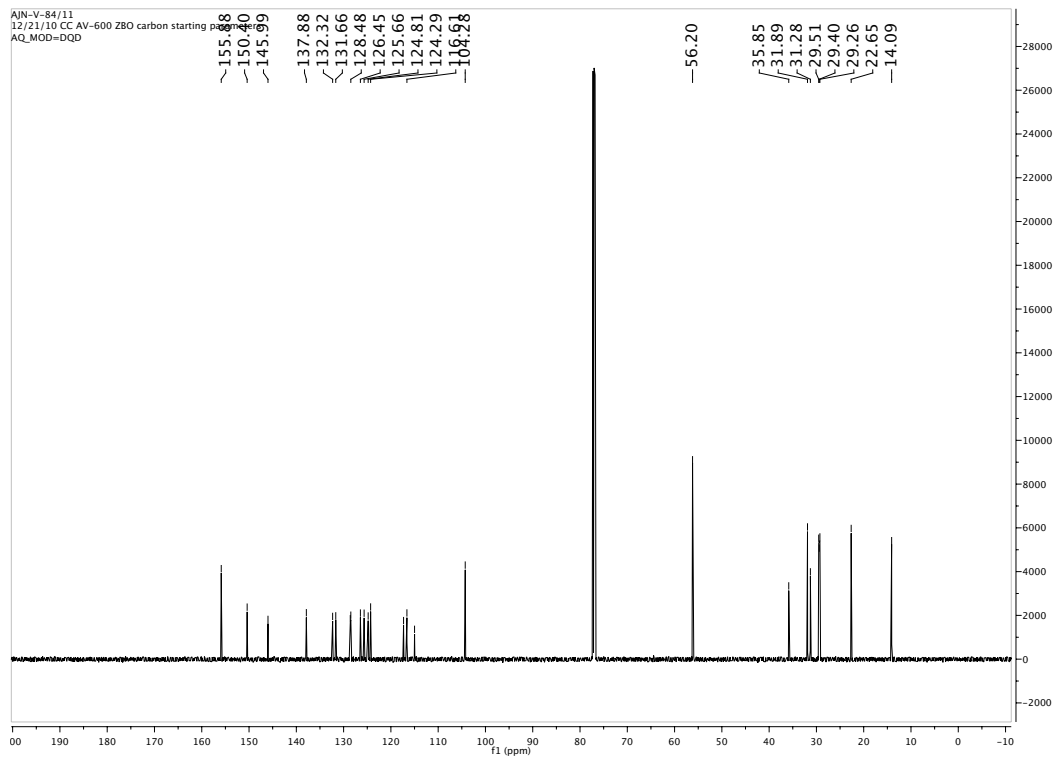
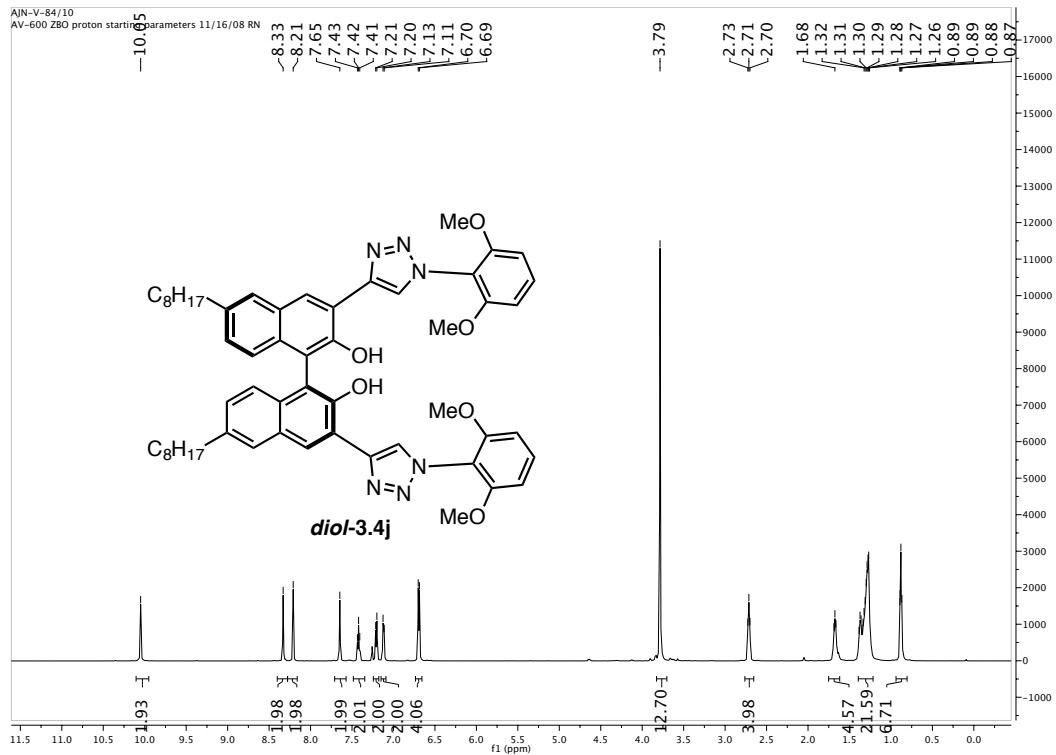


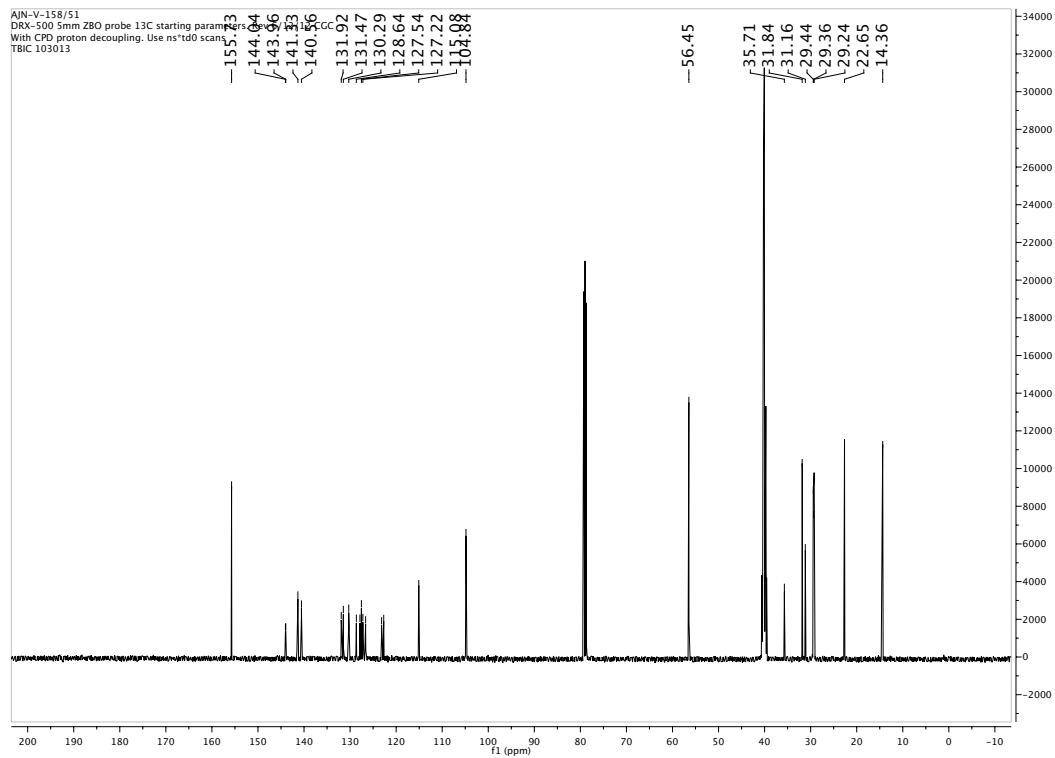
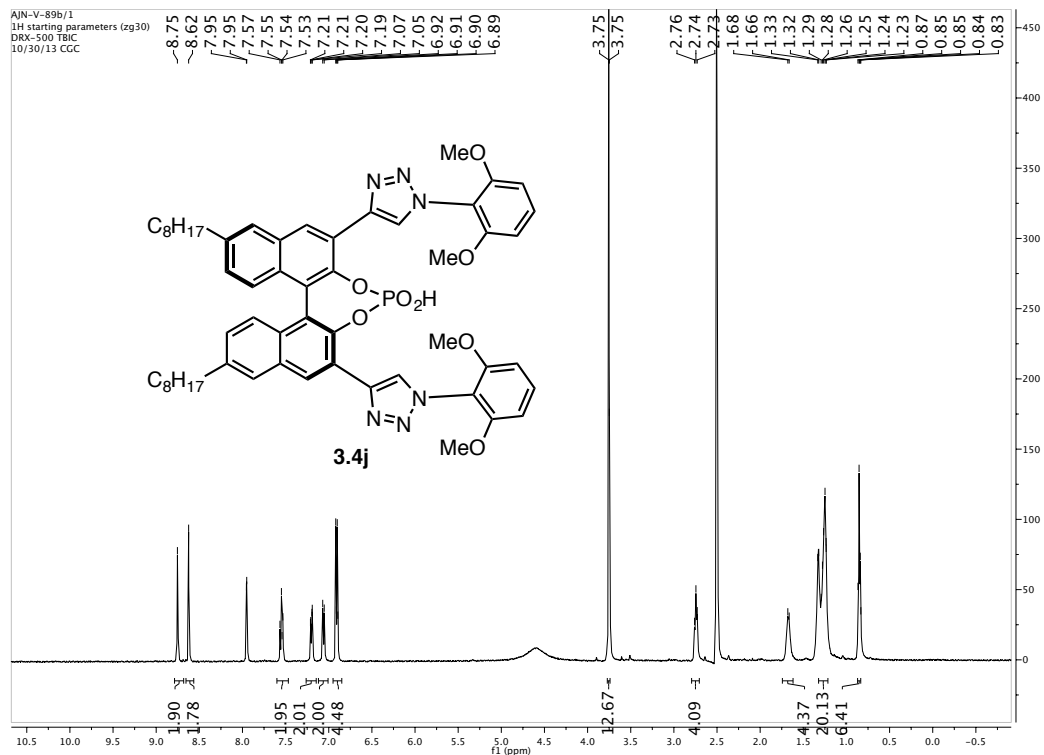




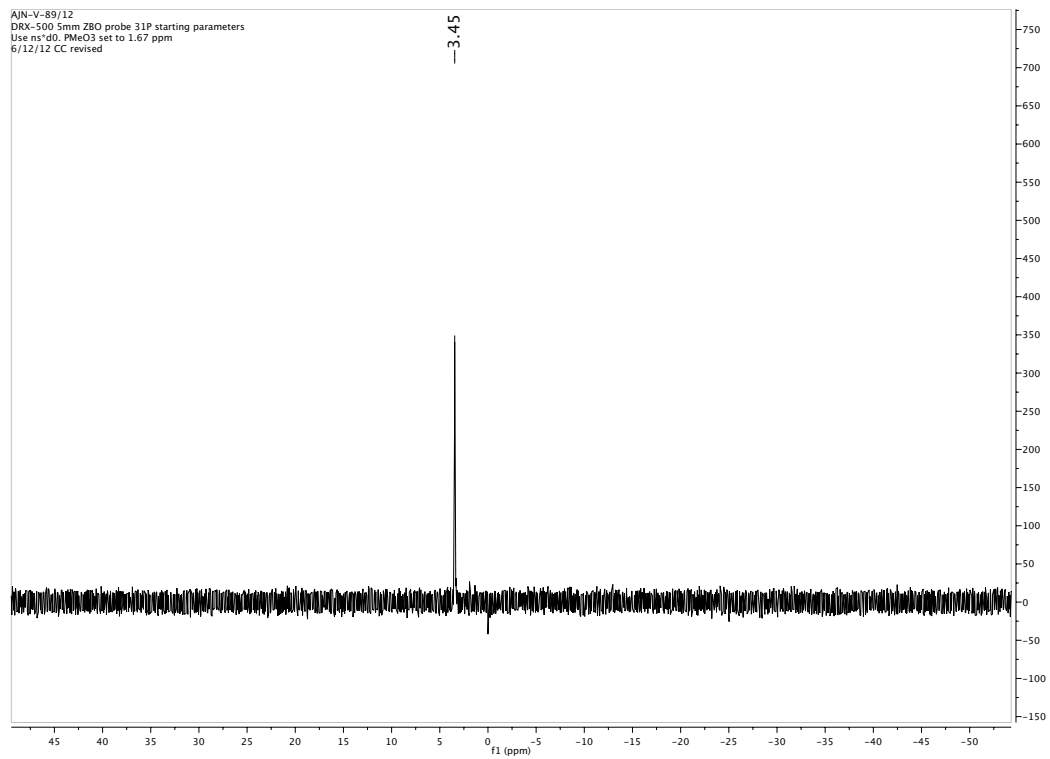
AJN-V-106/12
DRX-500 5mm Z80 probe 31P starting parameters
Use n140, PMeO3 set to 1.67 ppm
6/12/12 CC revised

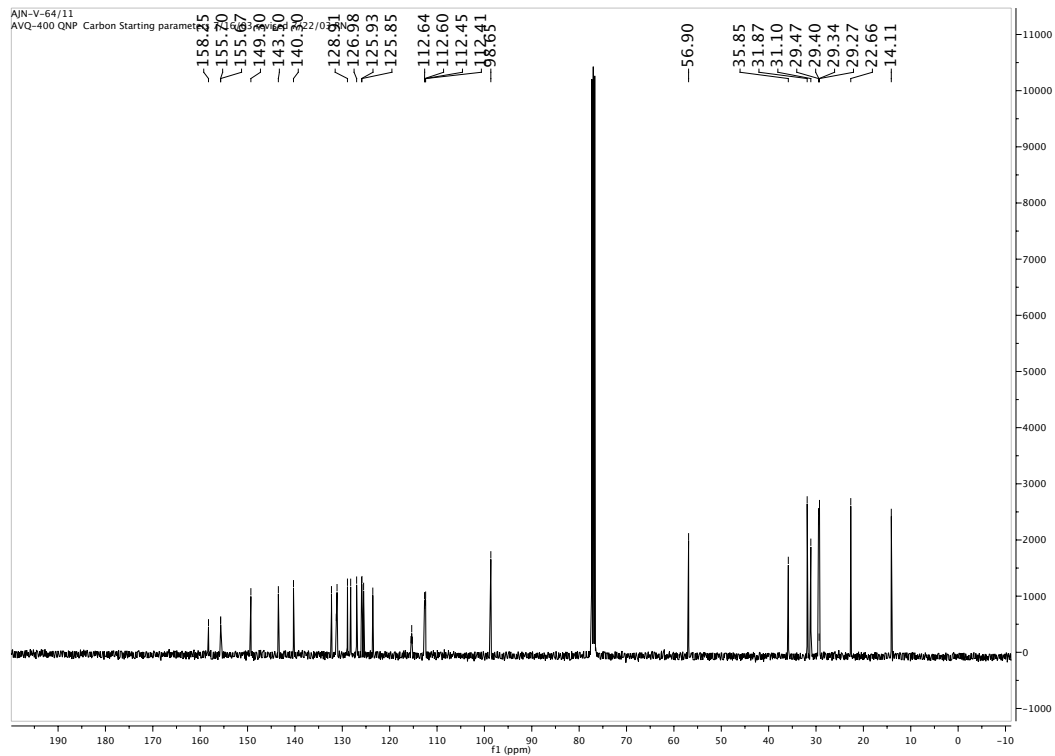
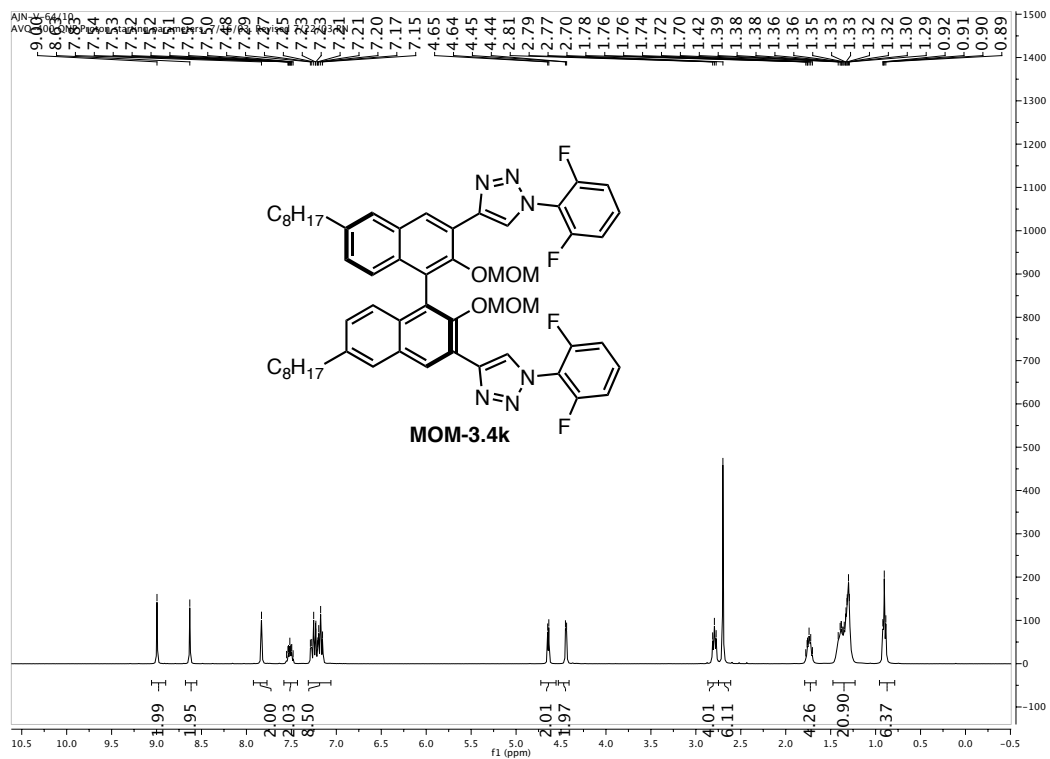


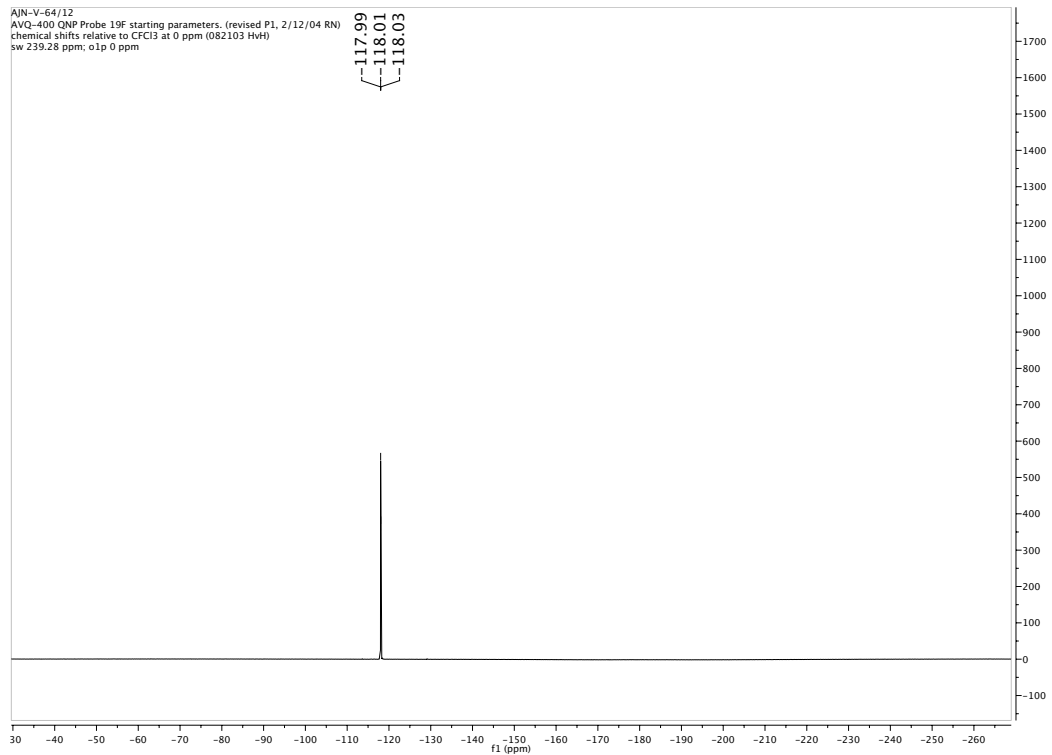


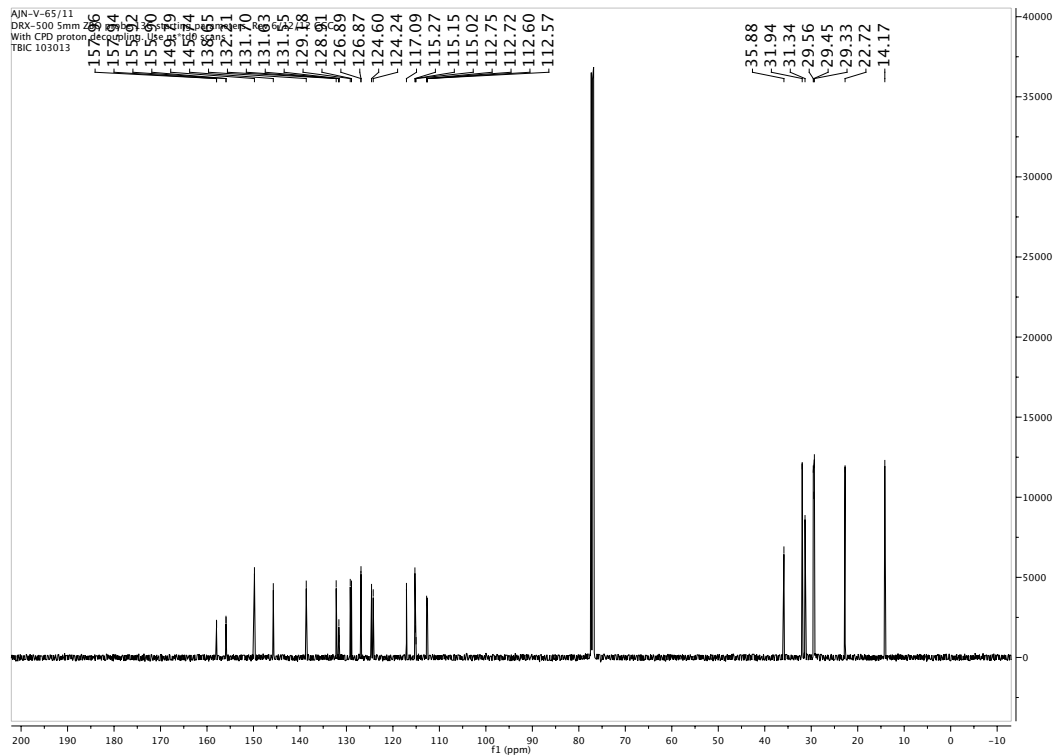
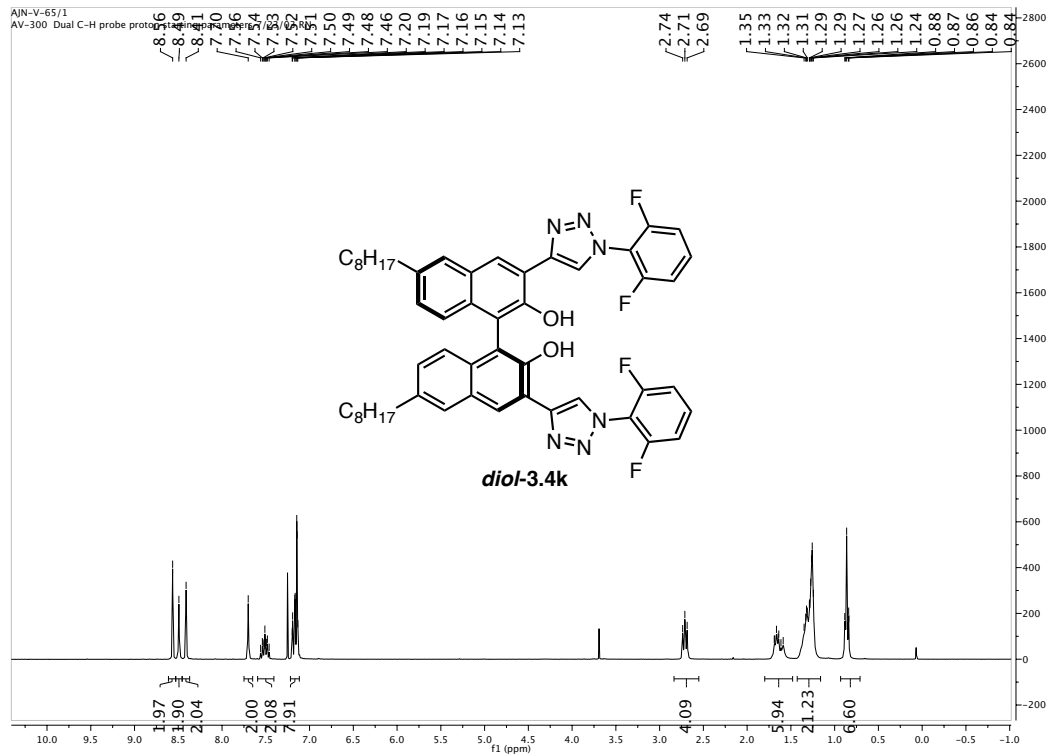


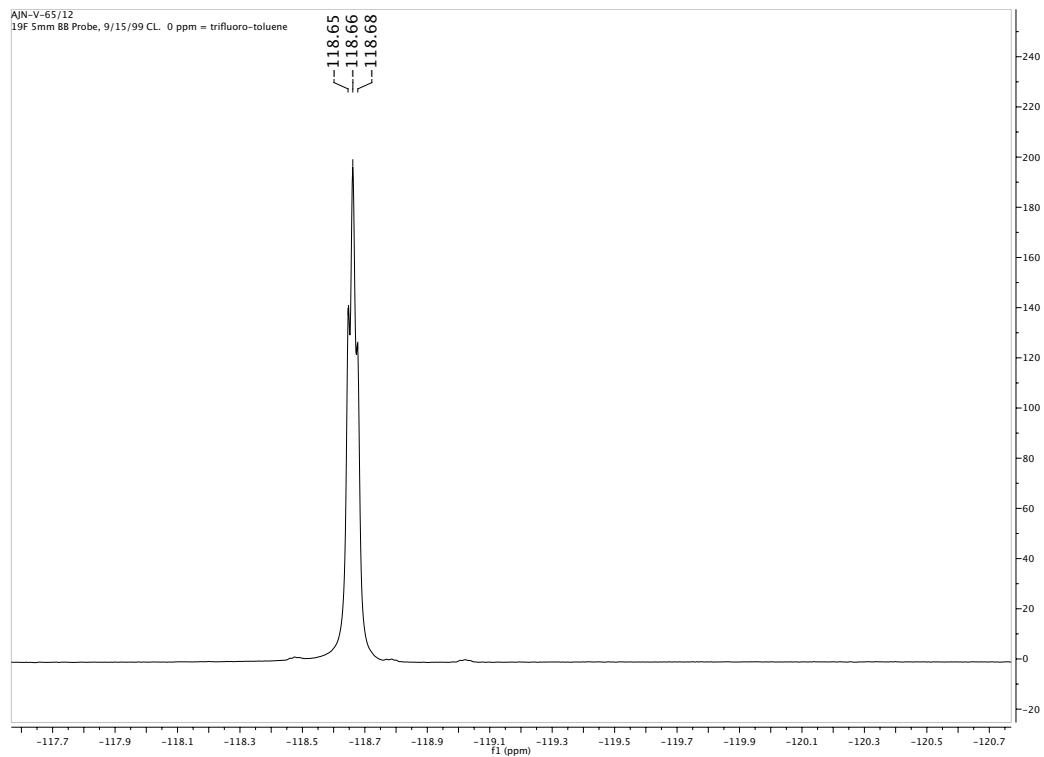
AJN-V-89/12
DRX-500 5mm ZBO probe 31P starting parameters
Use n140, PMeO3 set to 1.67 ppm
6/12/12 CC revised

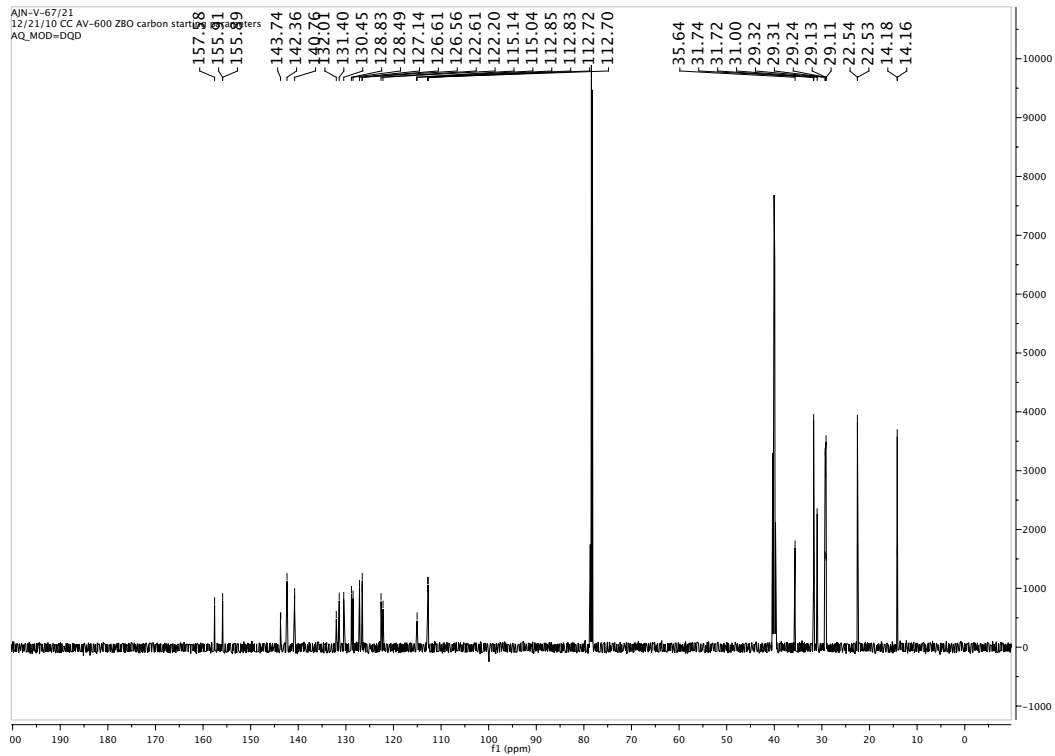
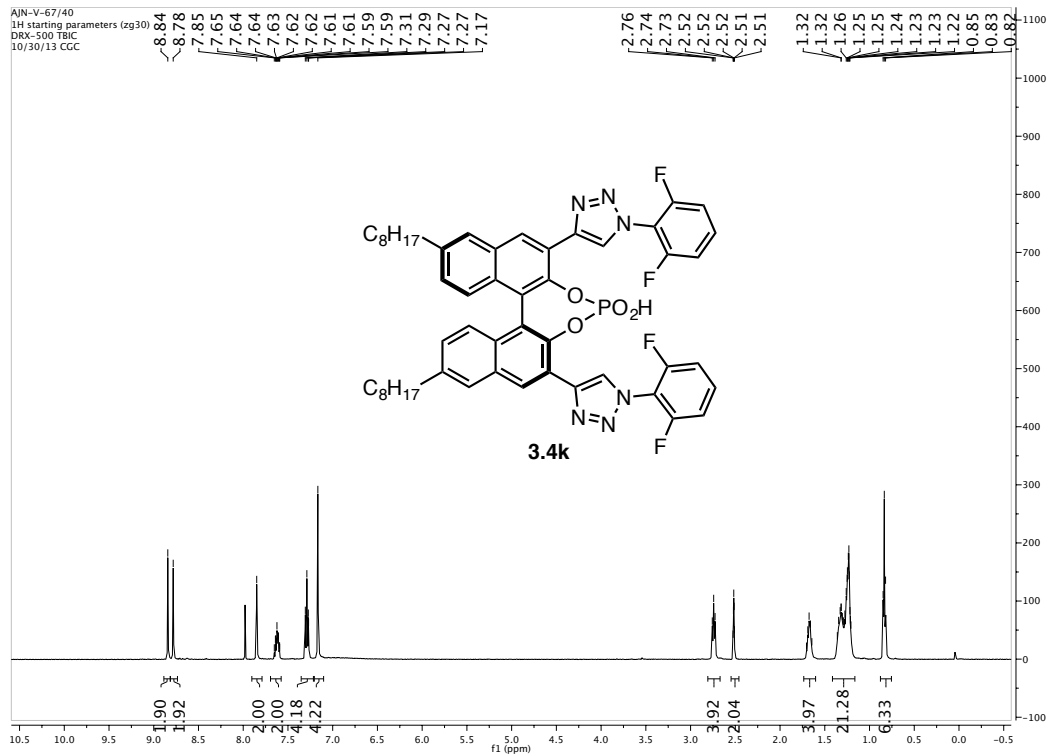


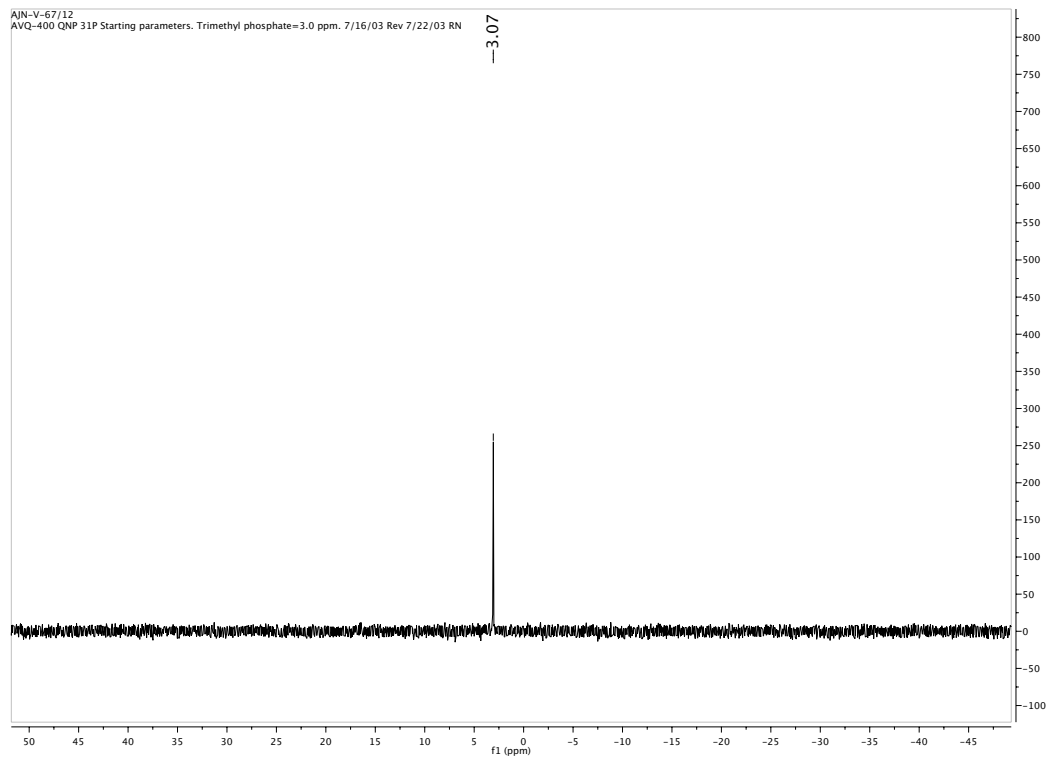
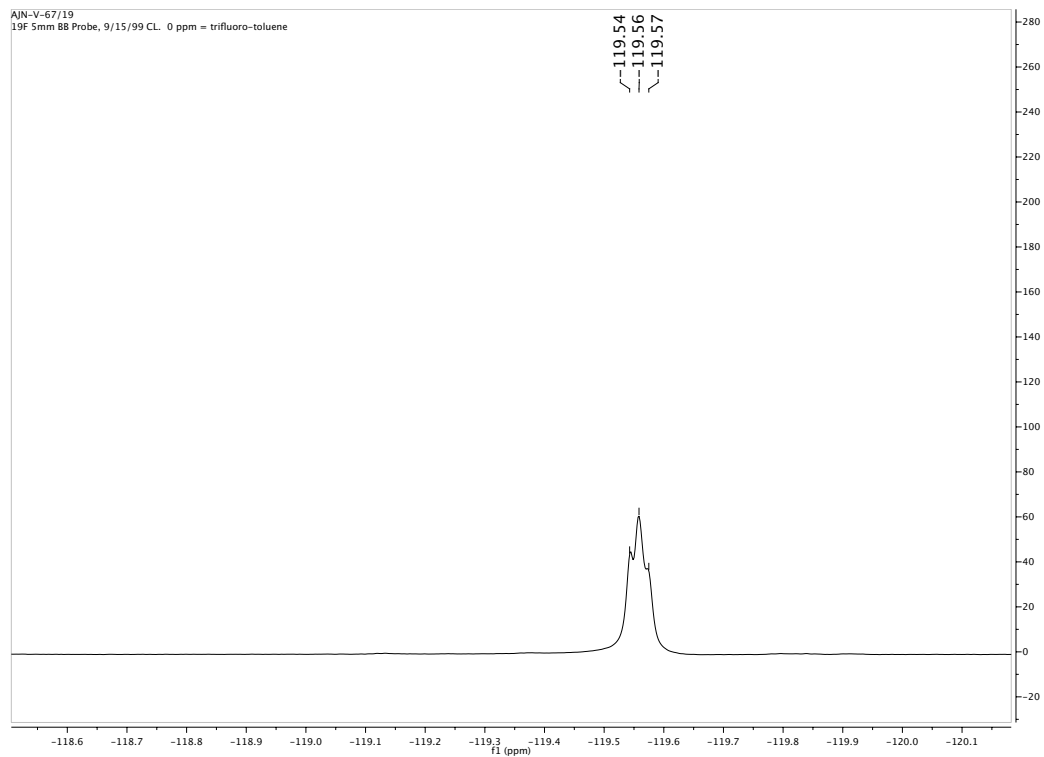


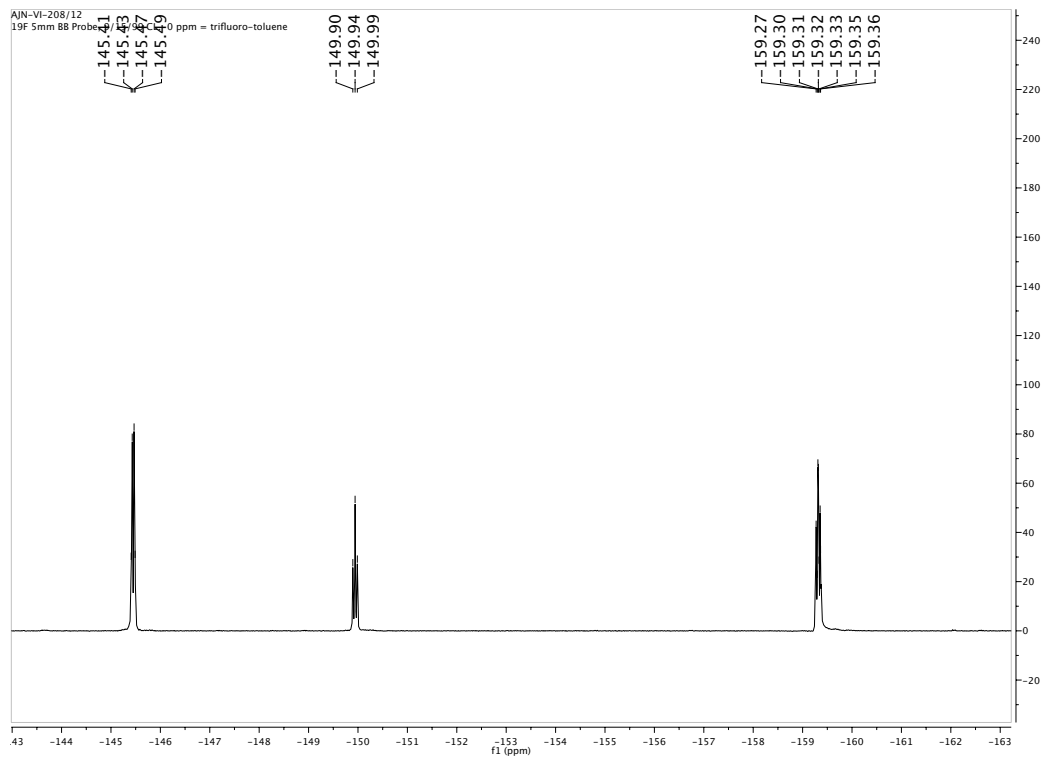


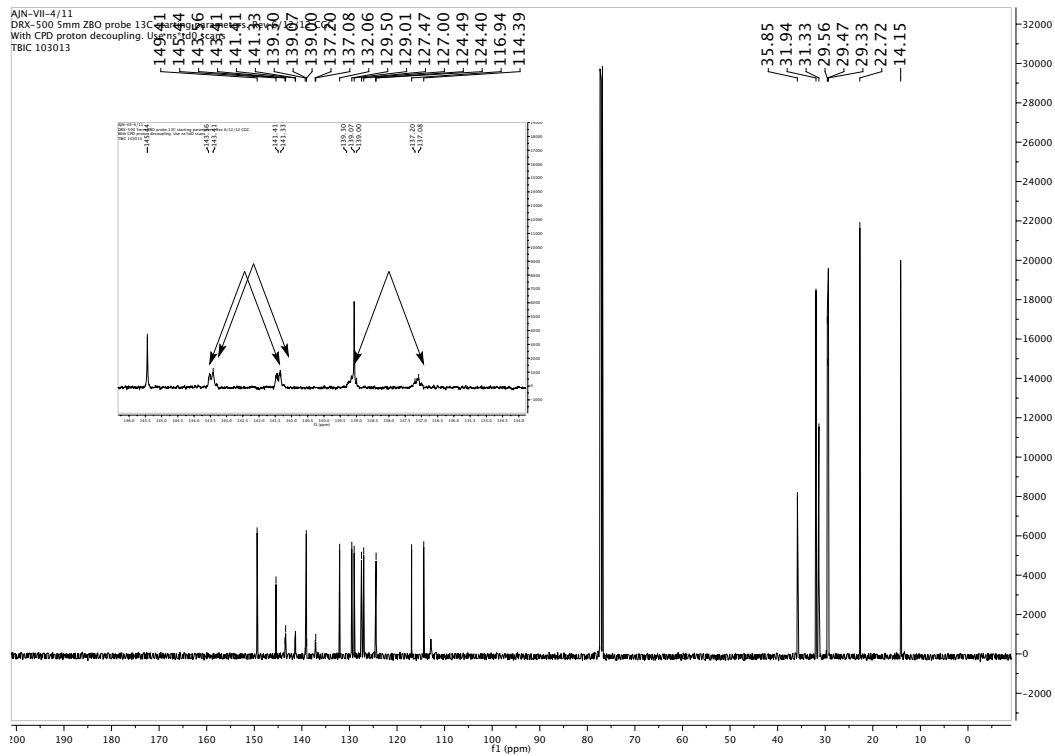
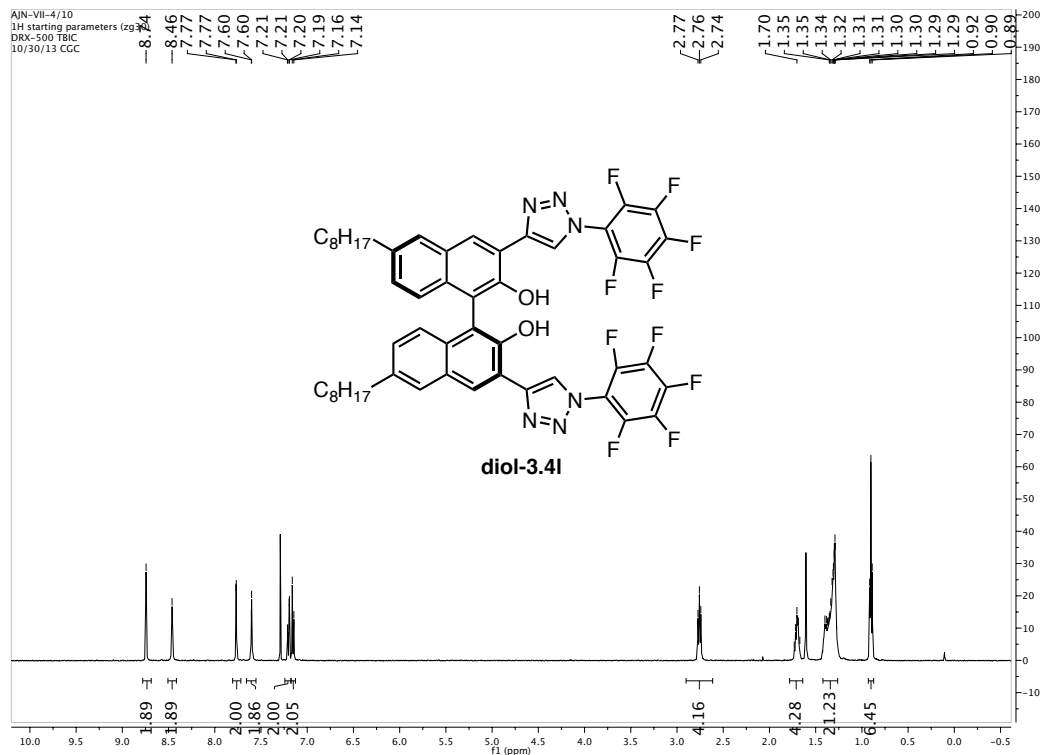


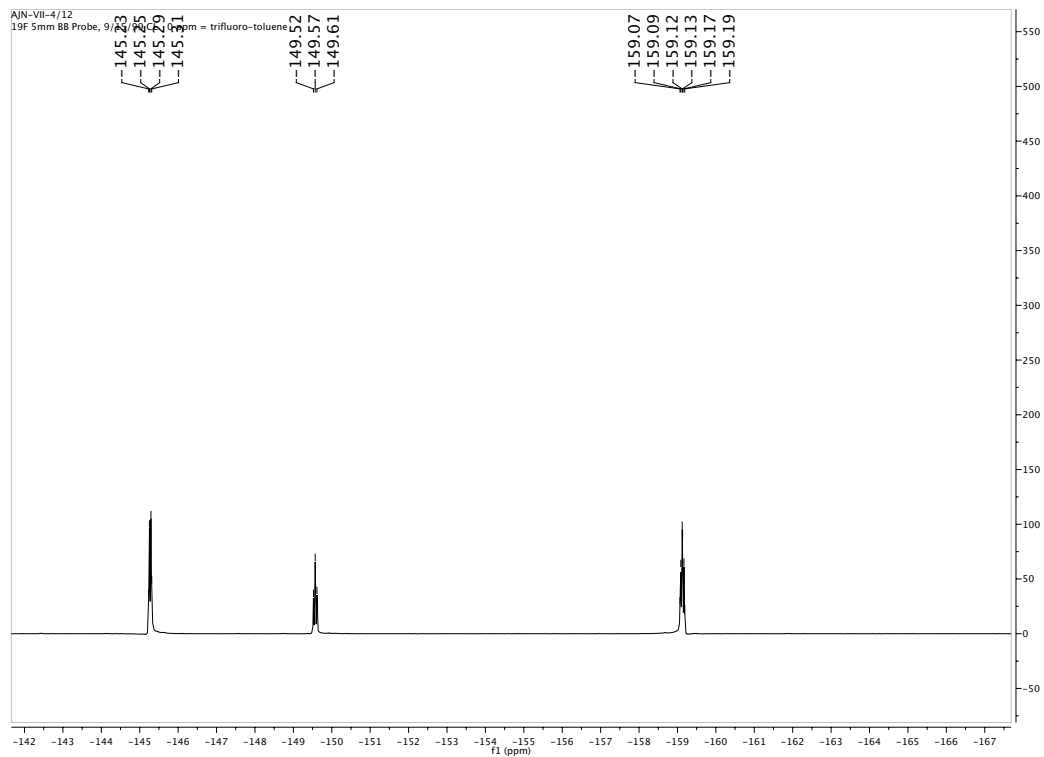


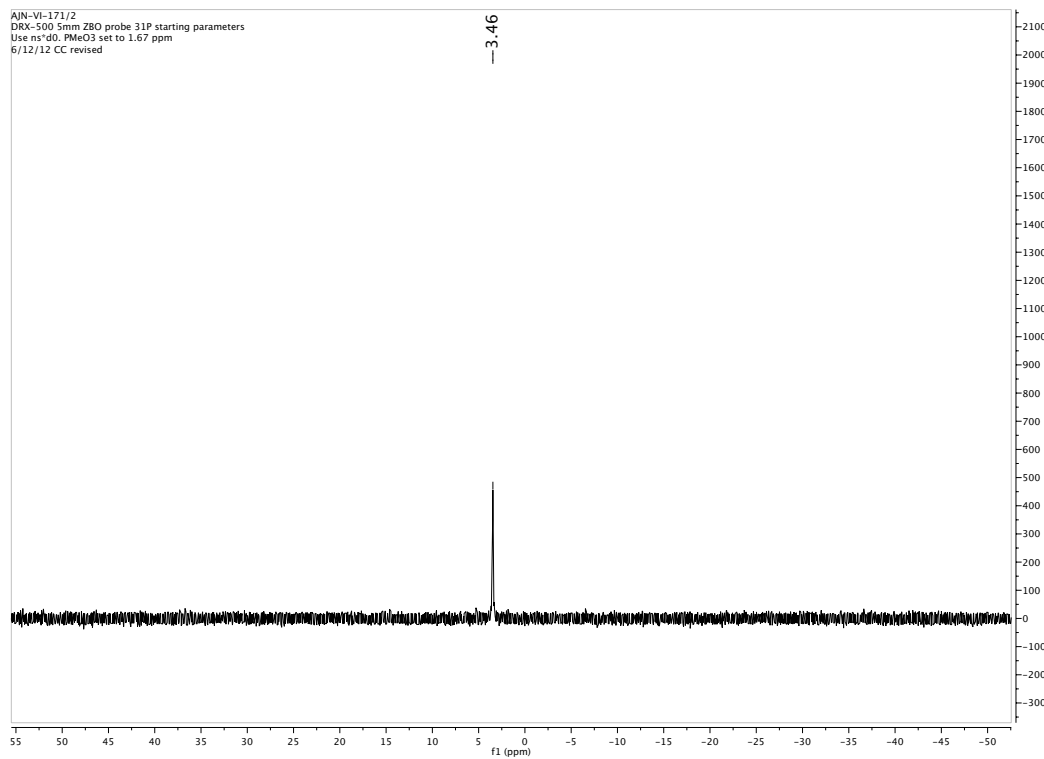
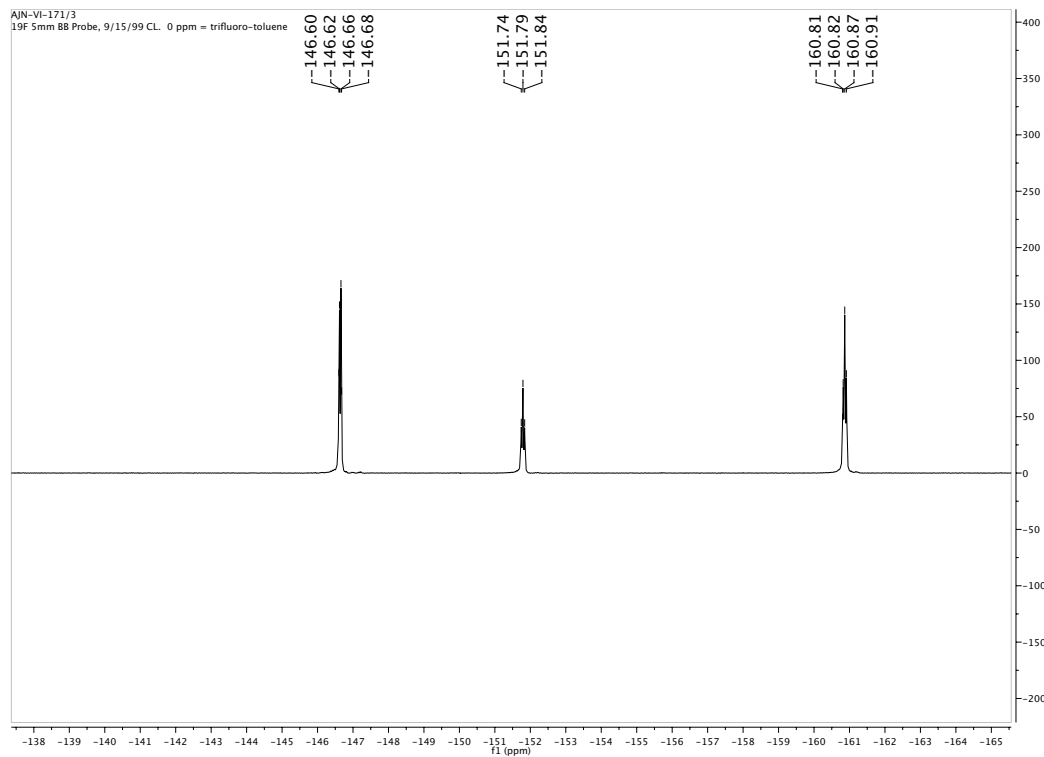


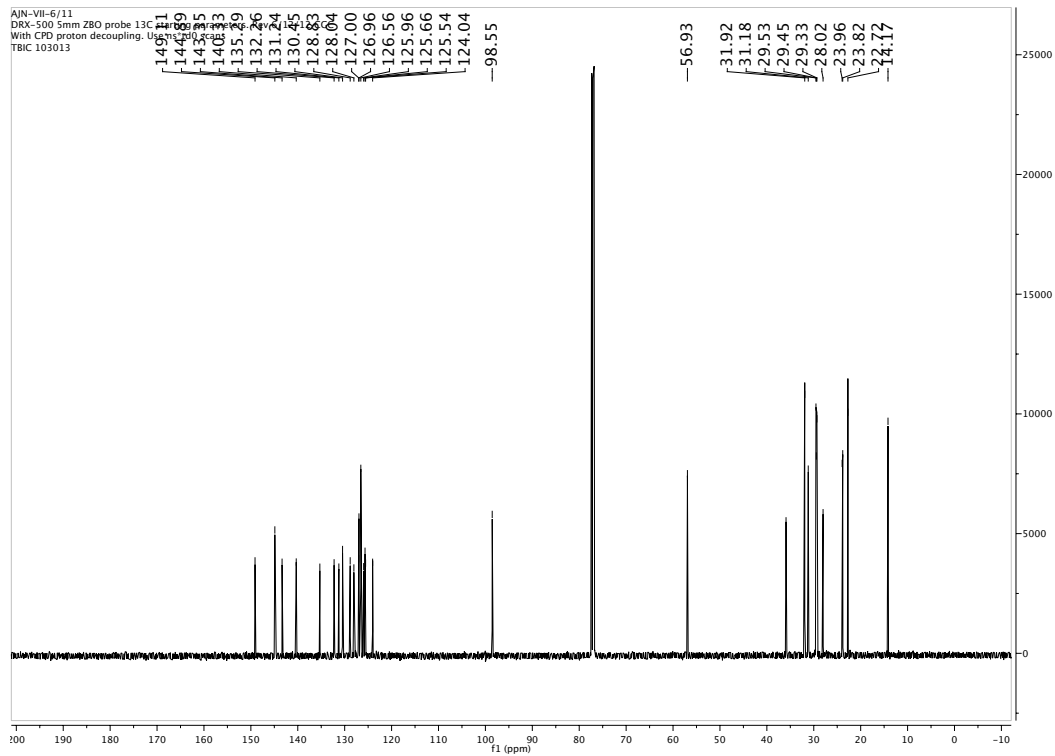
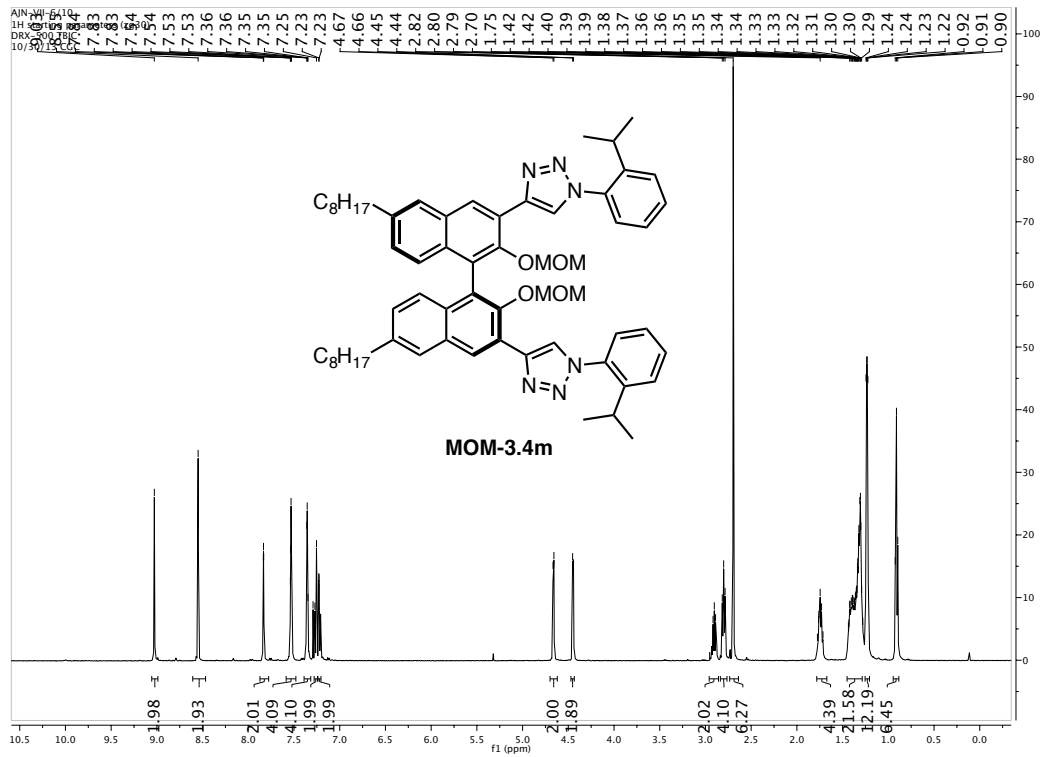


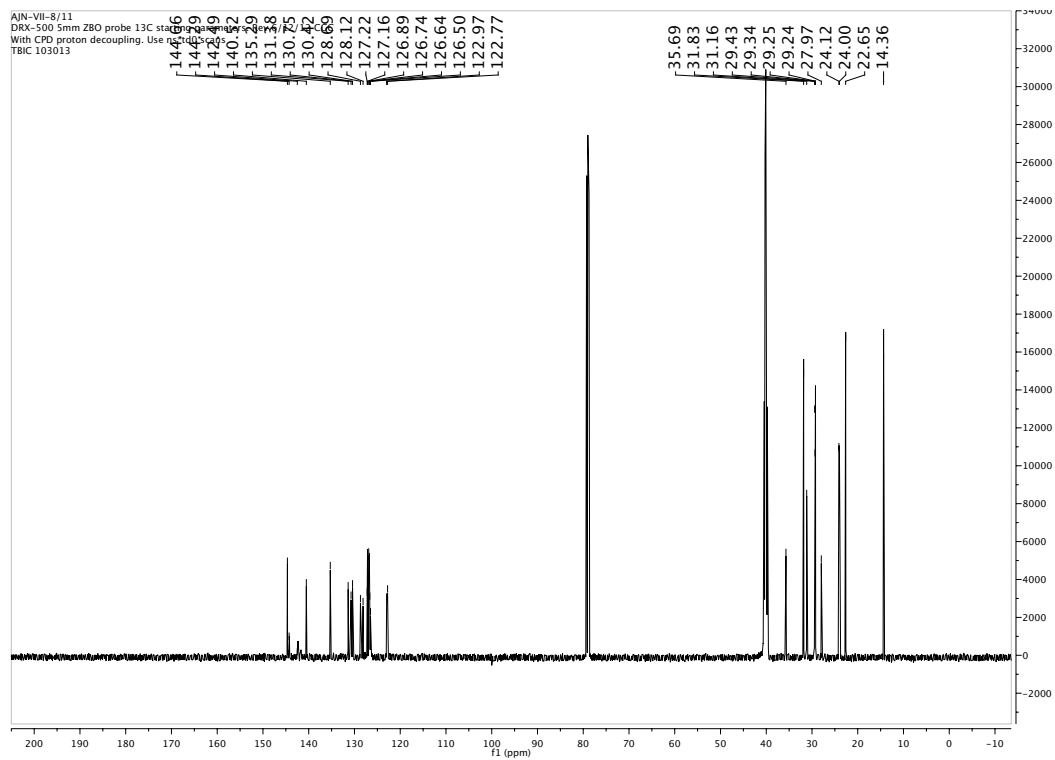
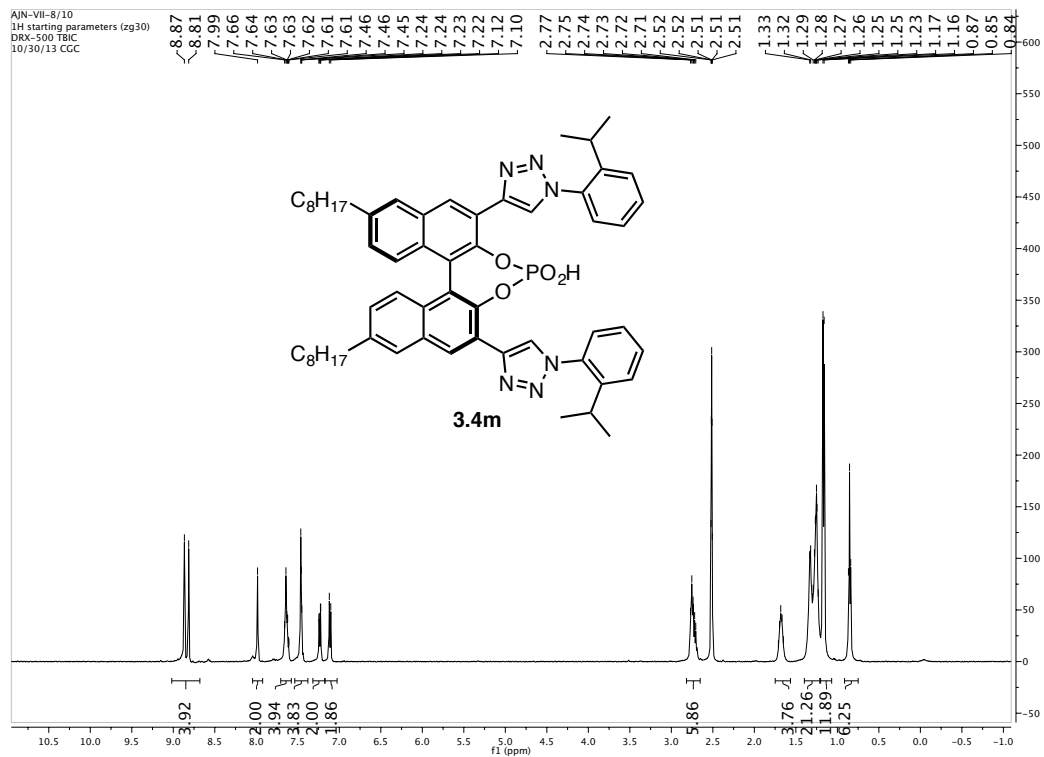




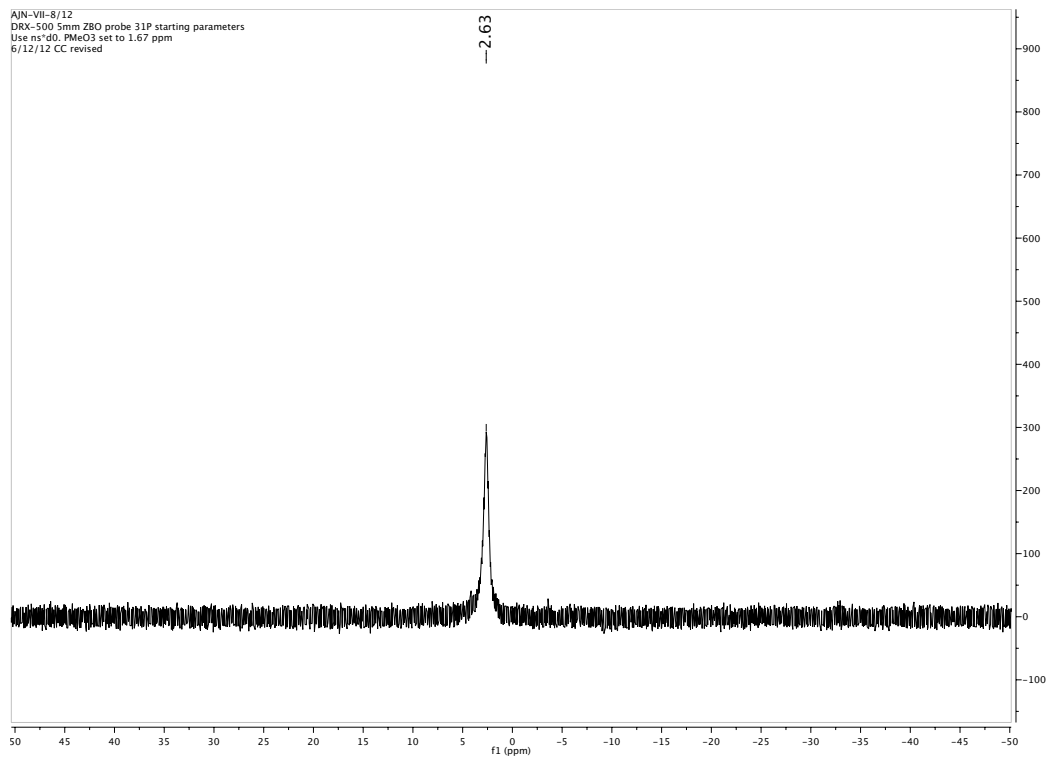


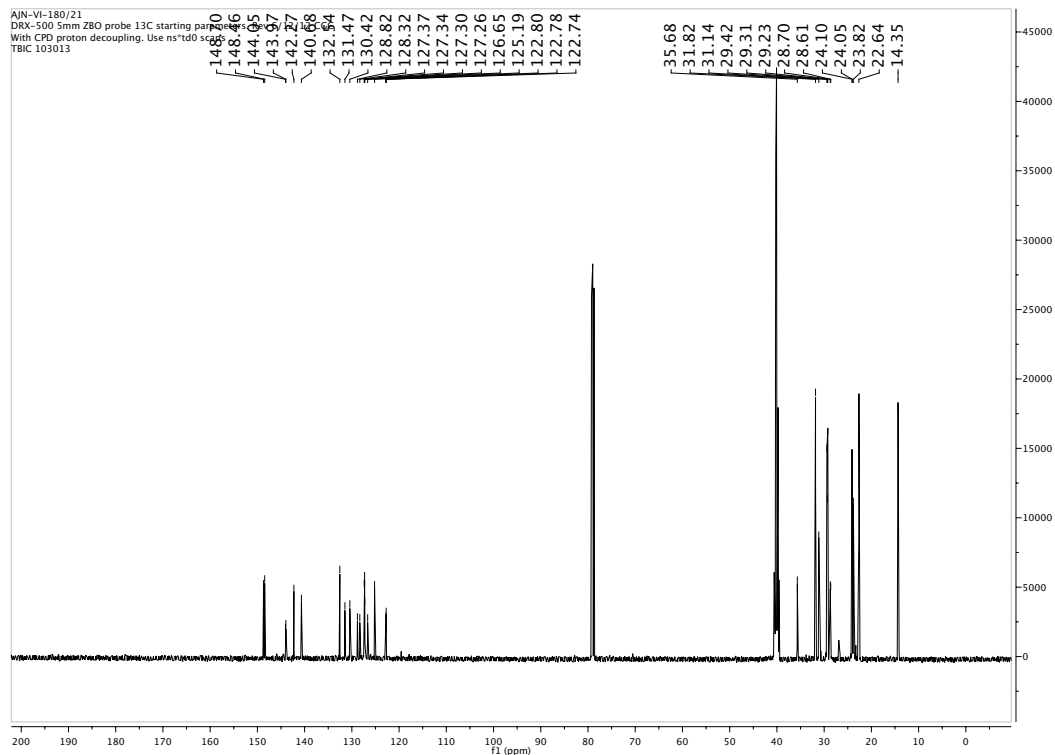
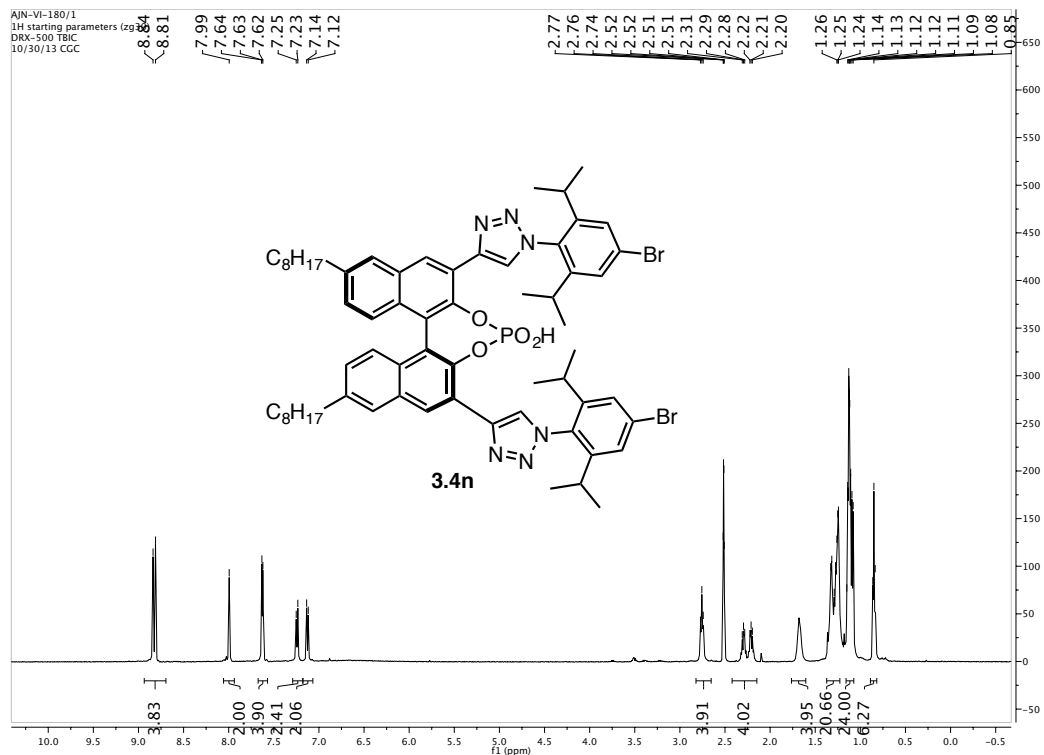




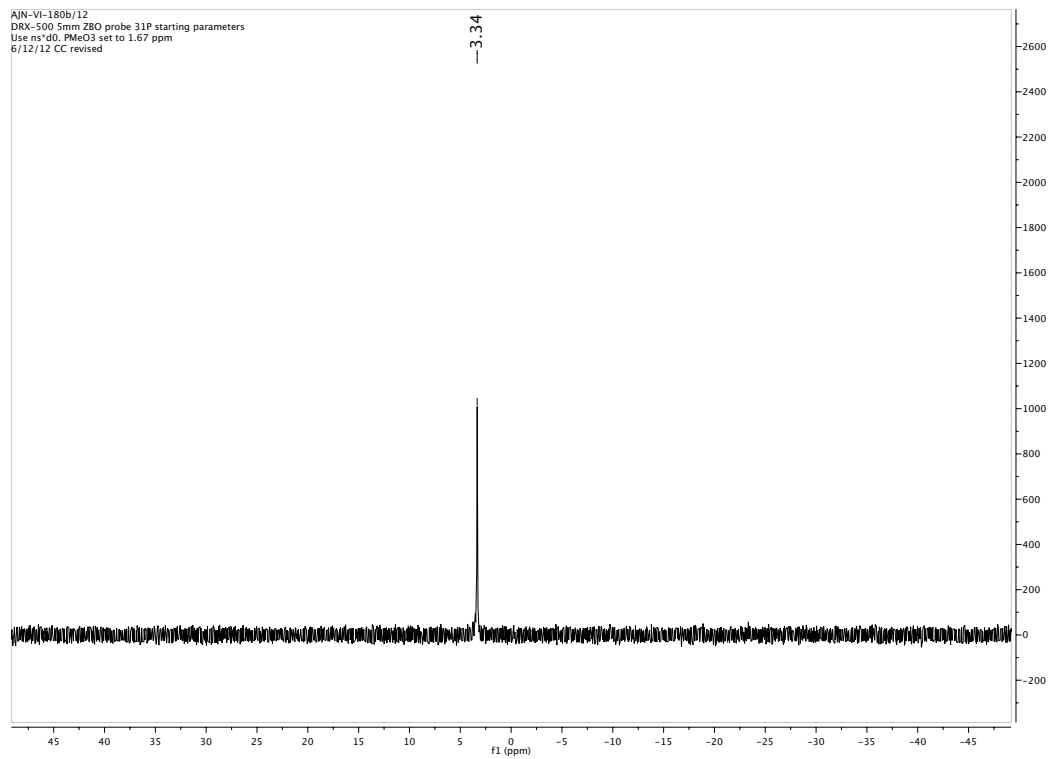


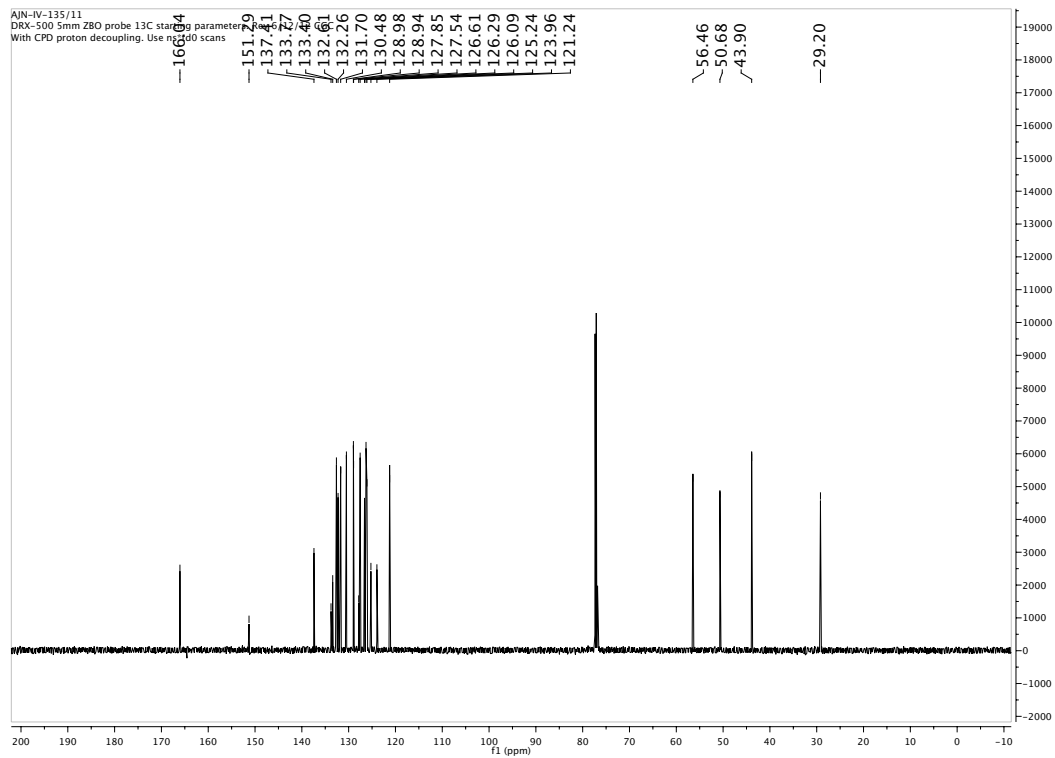
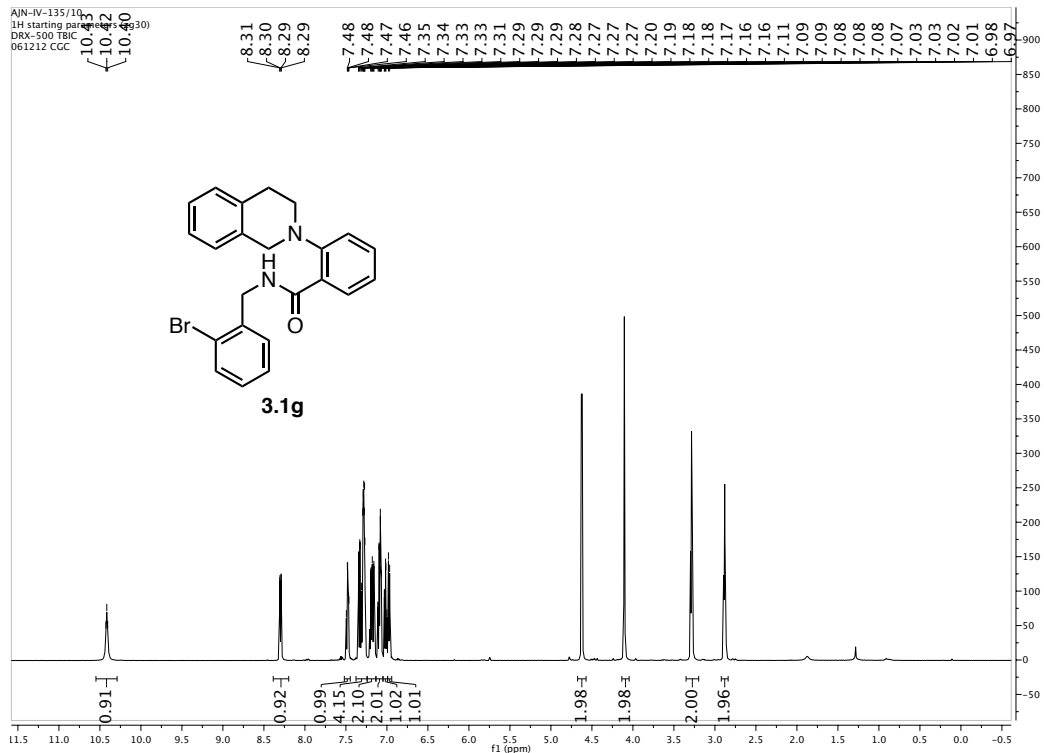
AJN-VII-8/12
DRX-500 5mm ZBO probe 31P starting parameters
Use n140, PMeO3 set to 1.67 ppm
6/12/12 CC revised

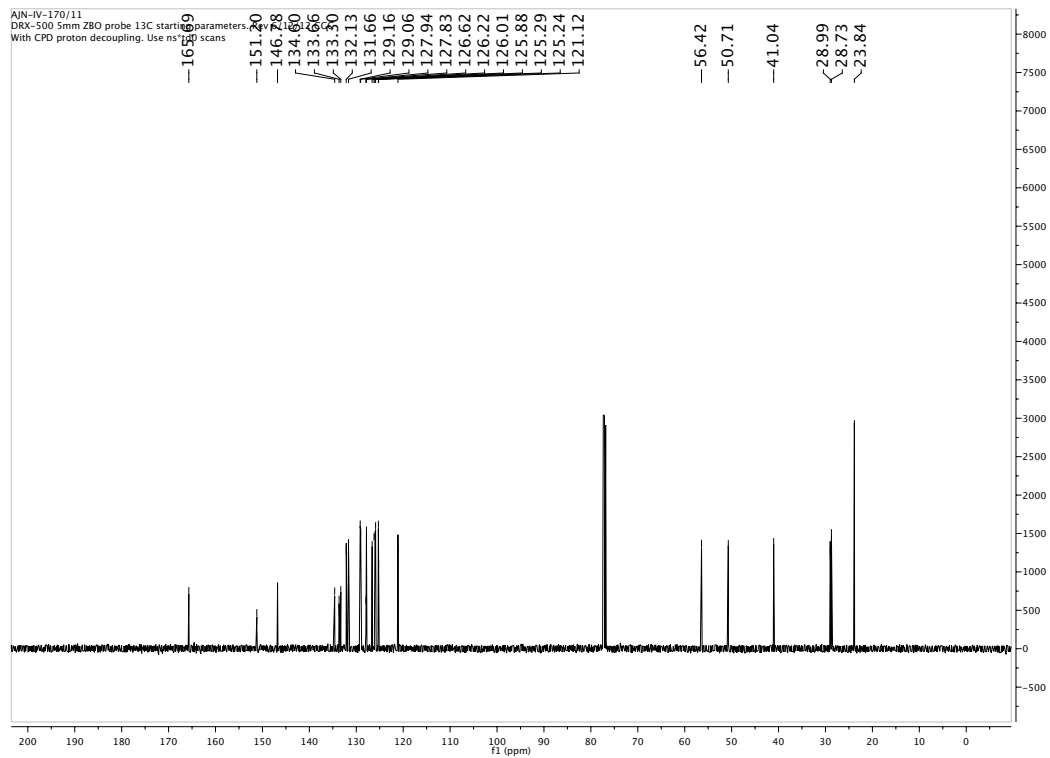
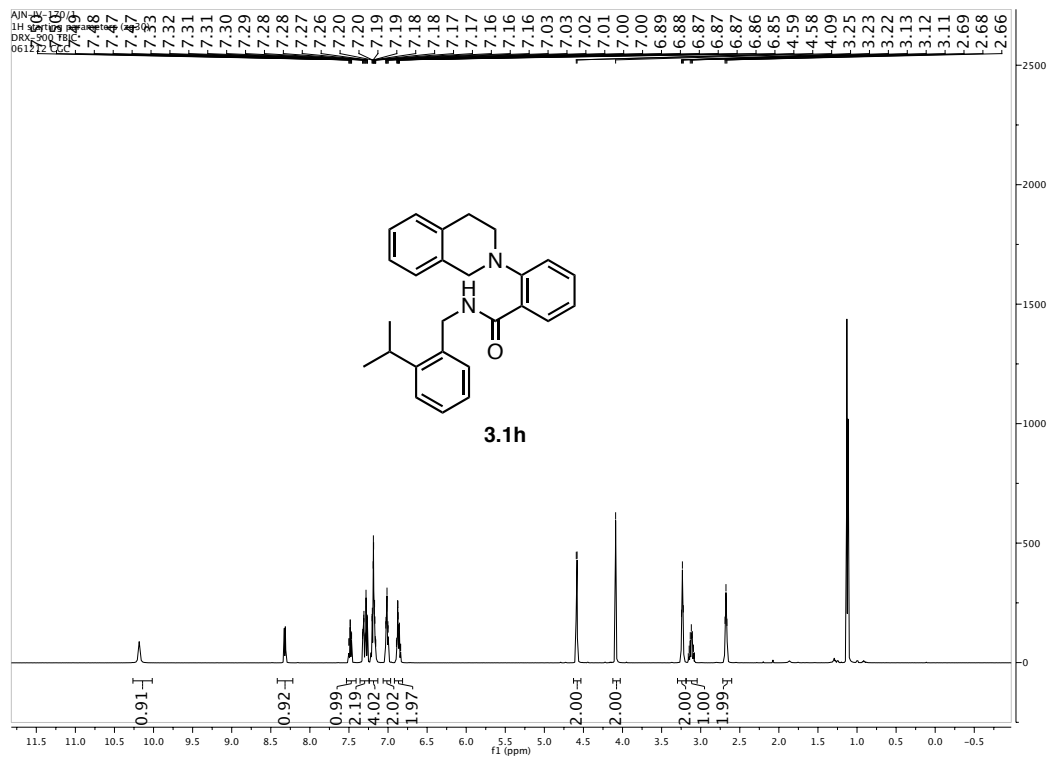


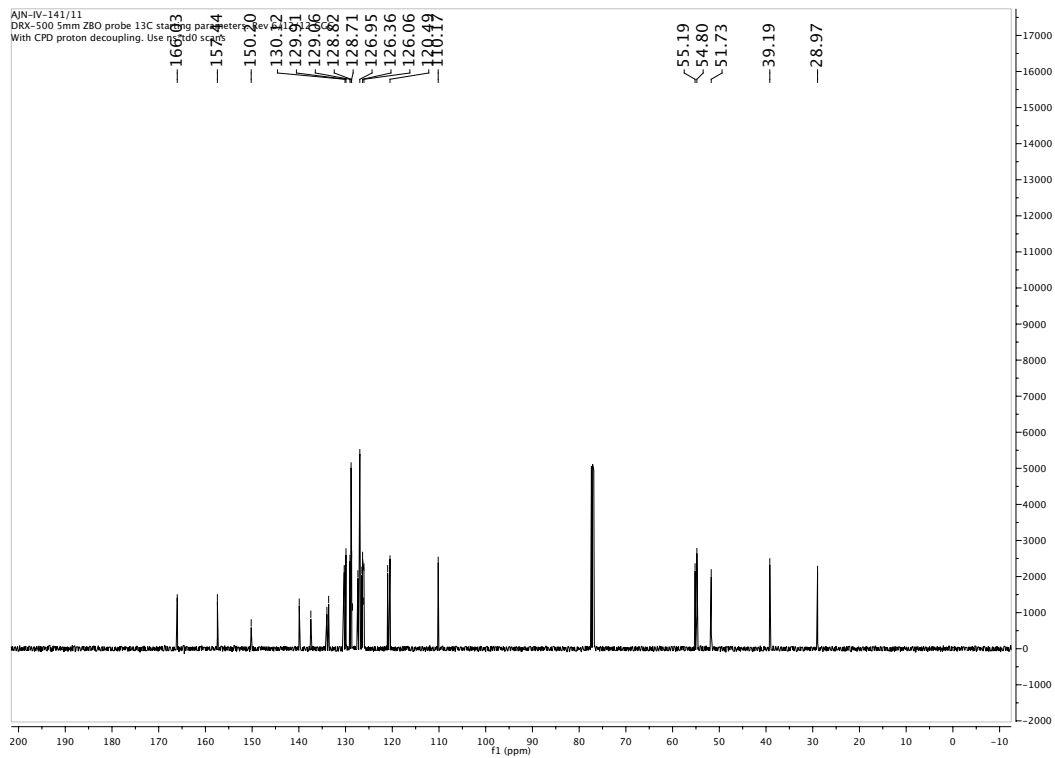
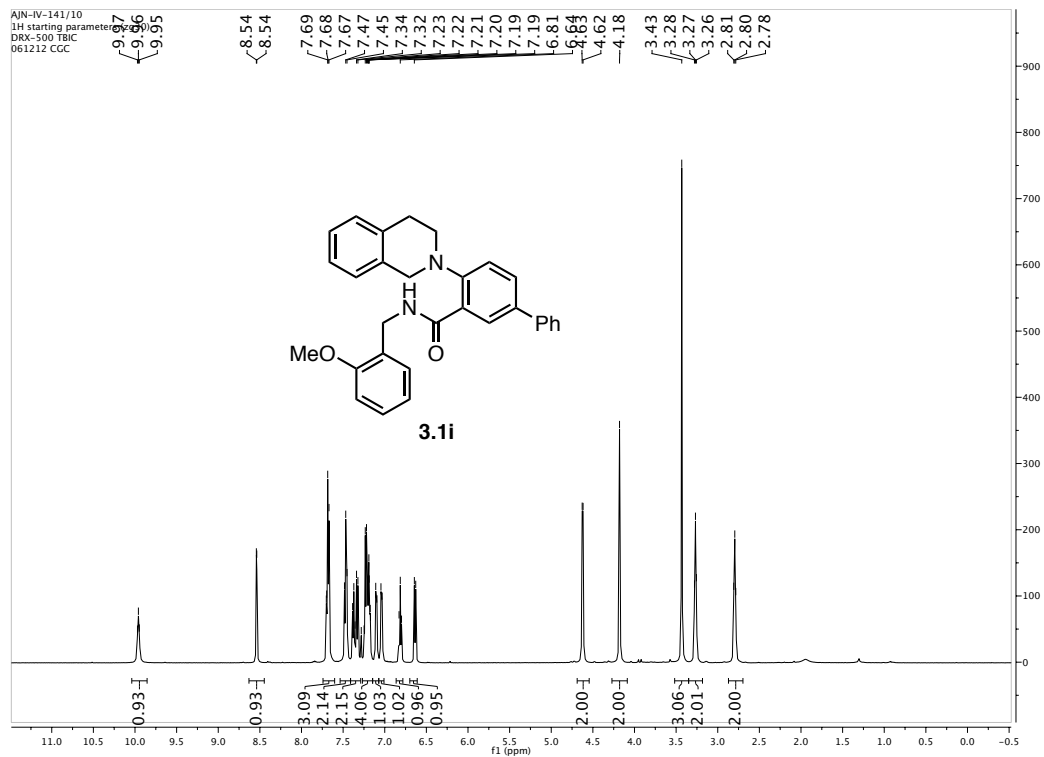


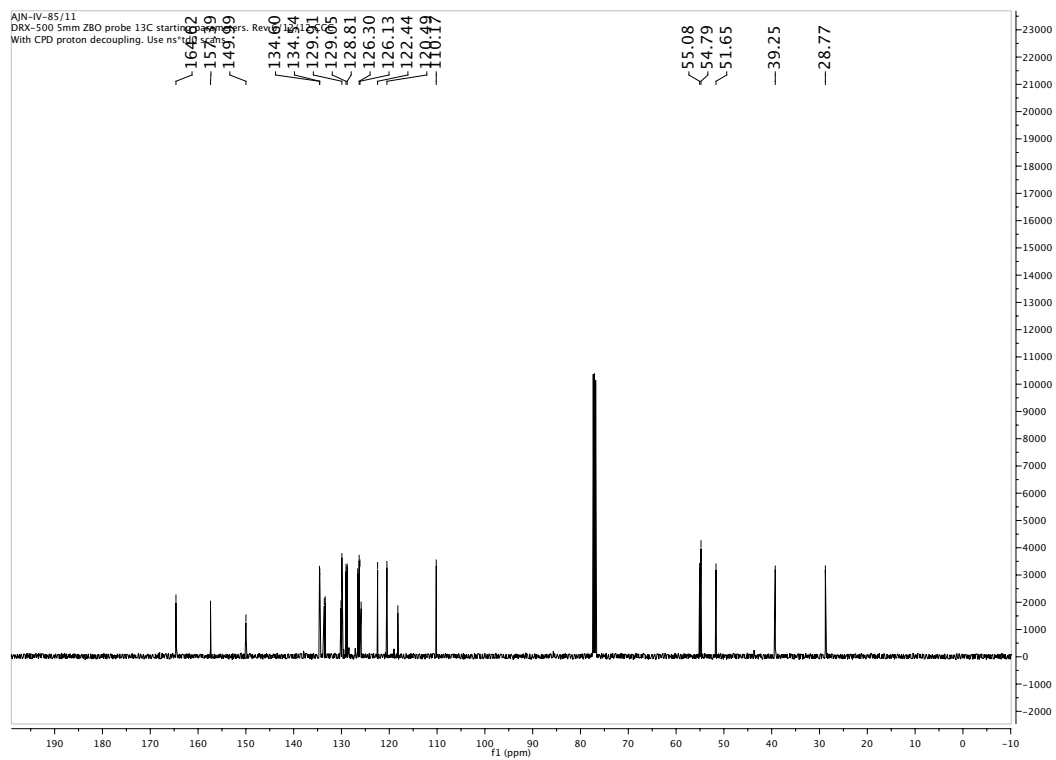
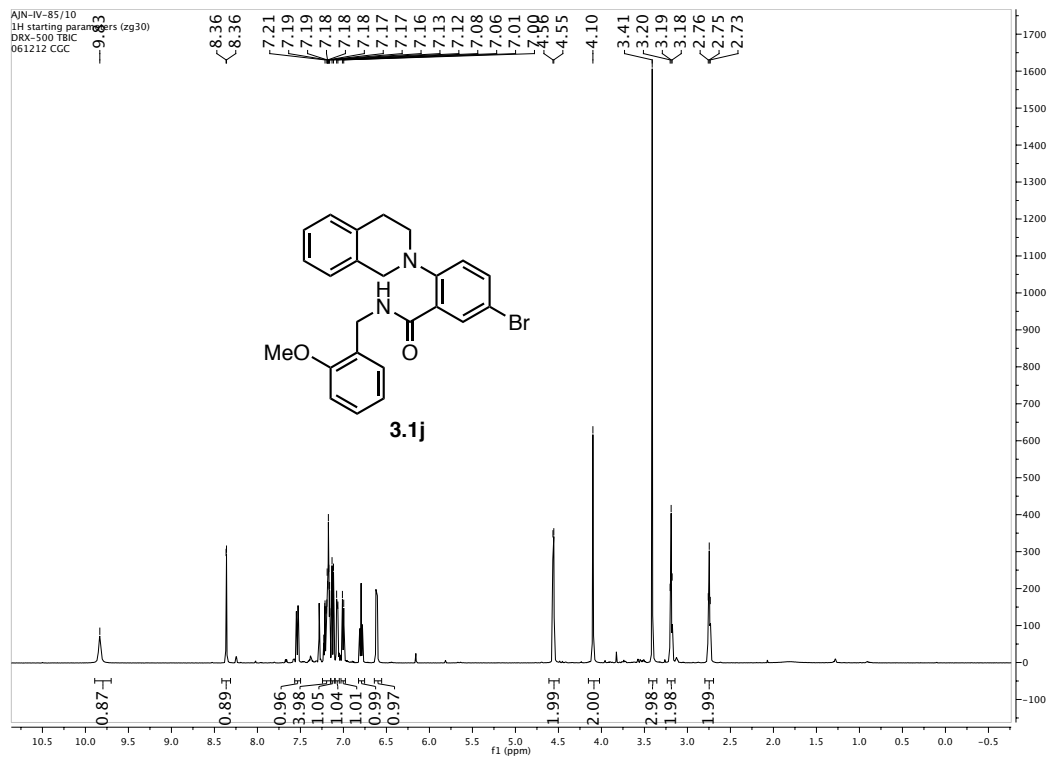
AJN-VI-180b/12
DRX-500 5mm Z80 probe 31P starting parameters
Use n140, PMeQ3 set to 1.67 ppm
6/12/12 CC revised

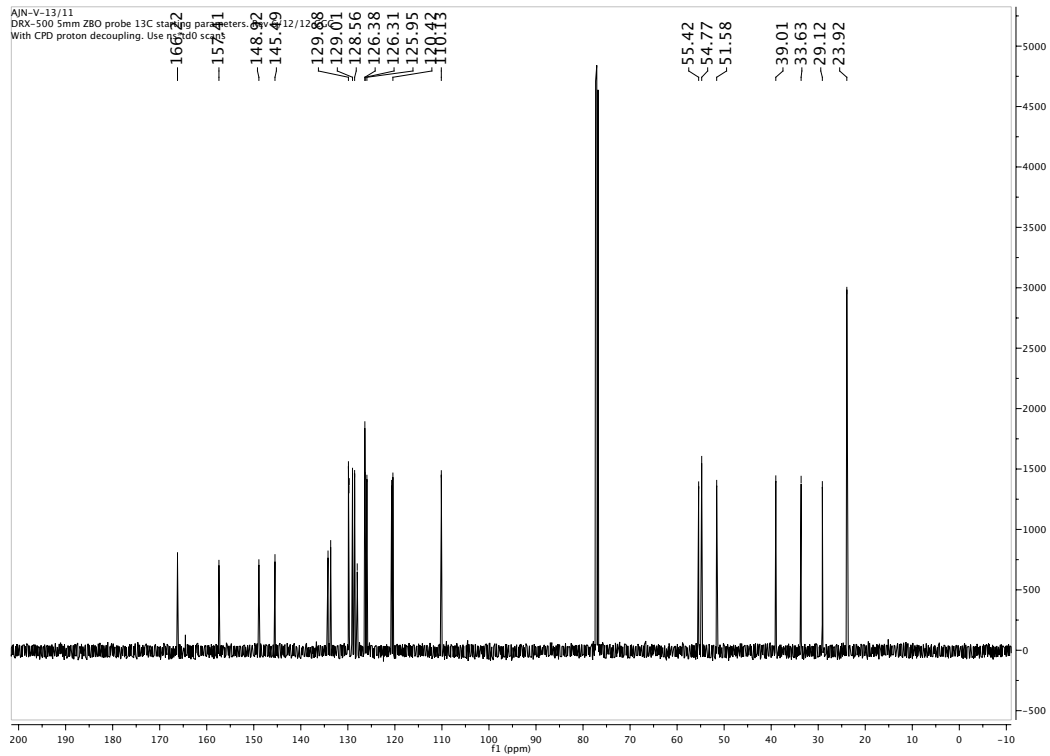
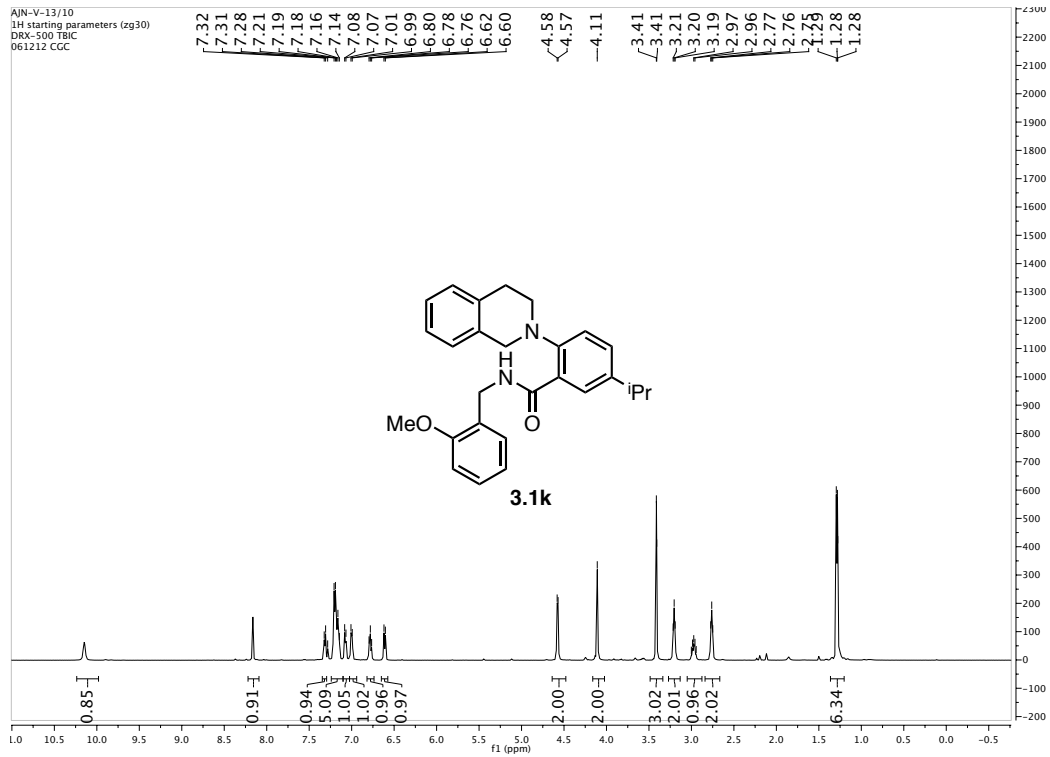


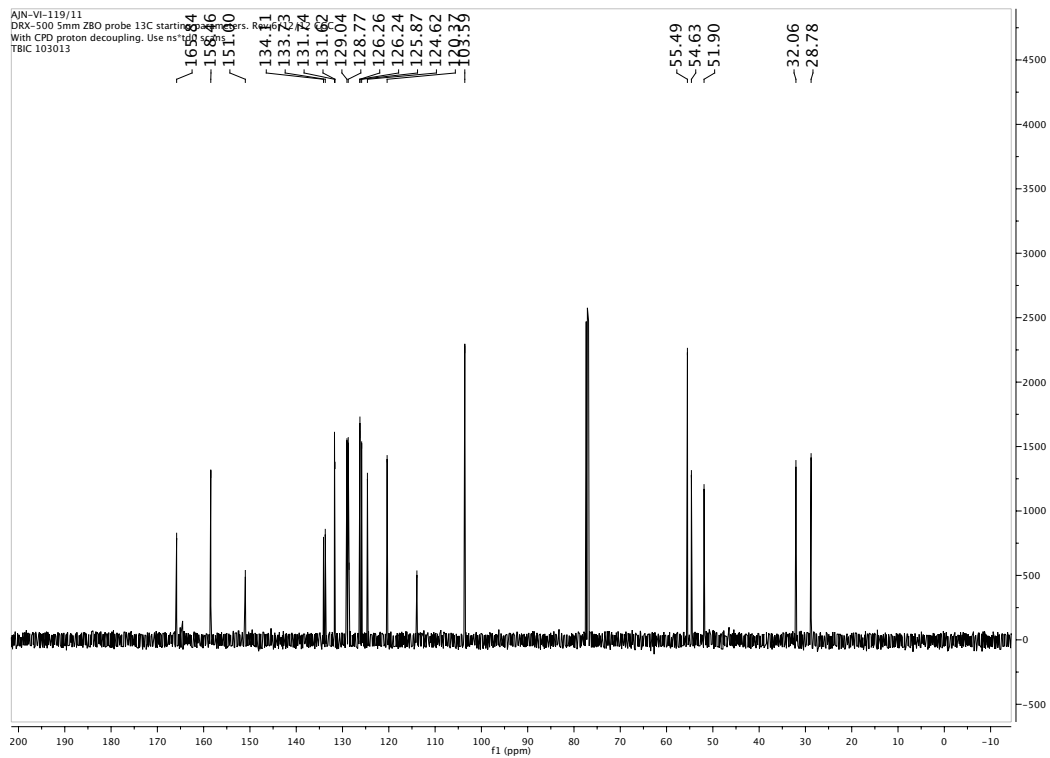
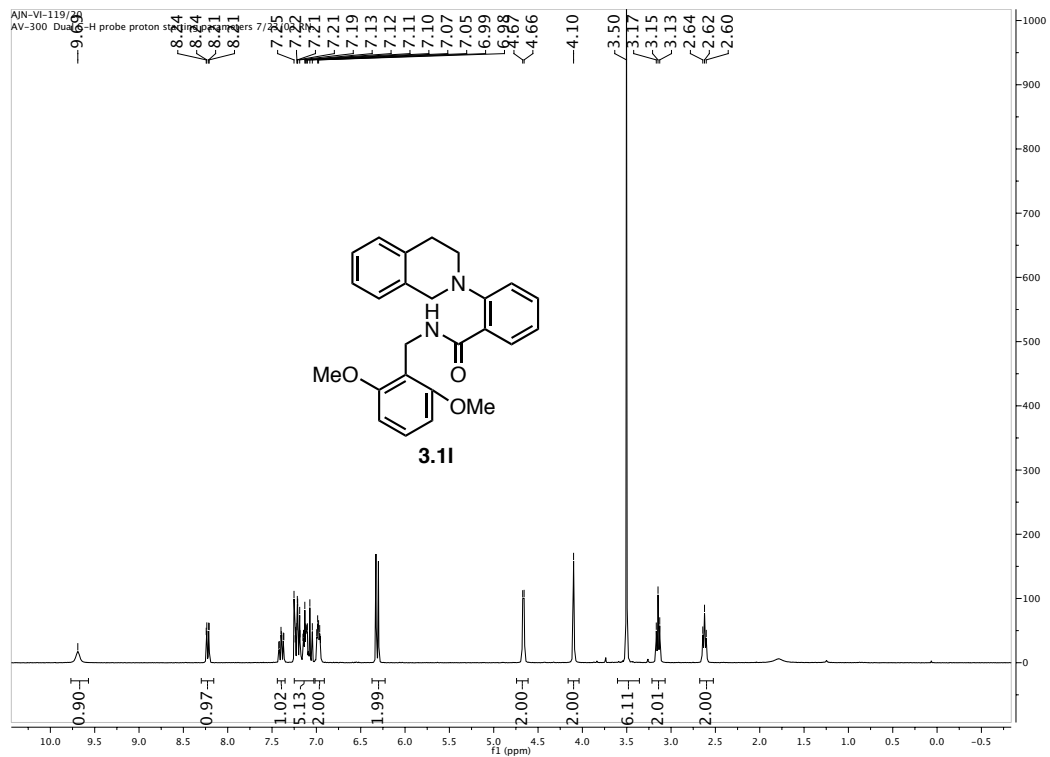


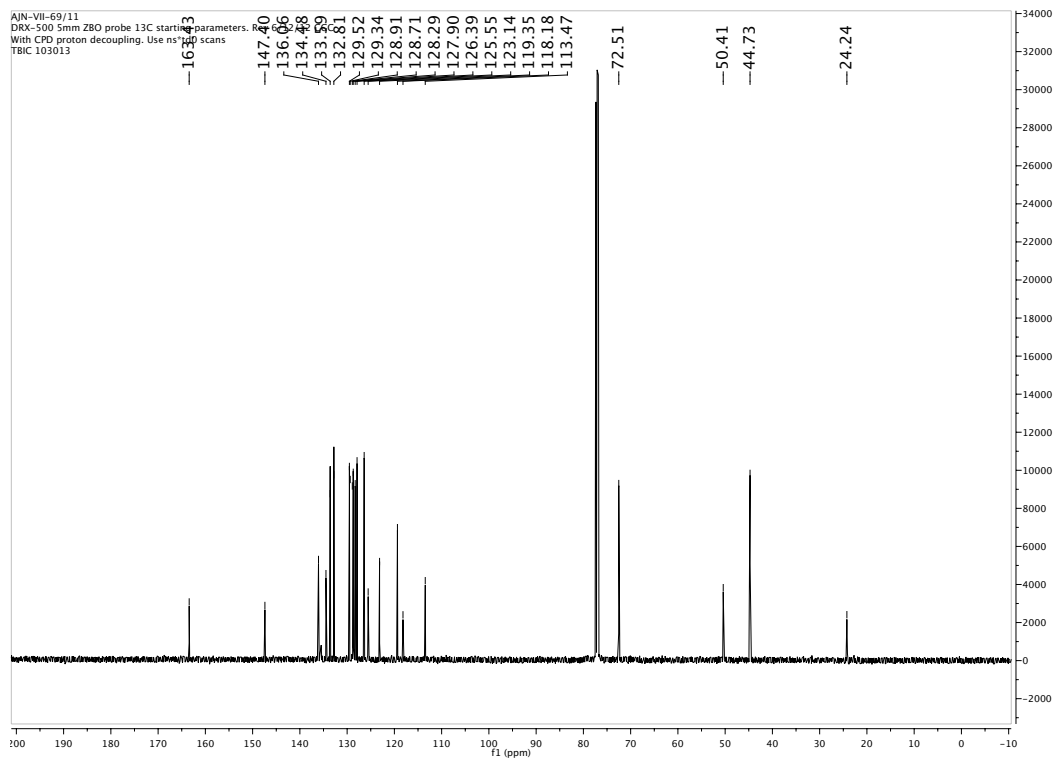
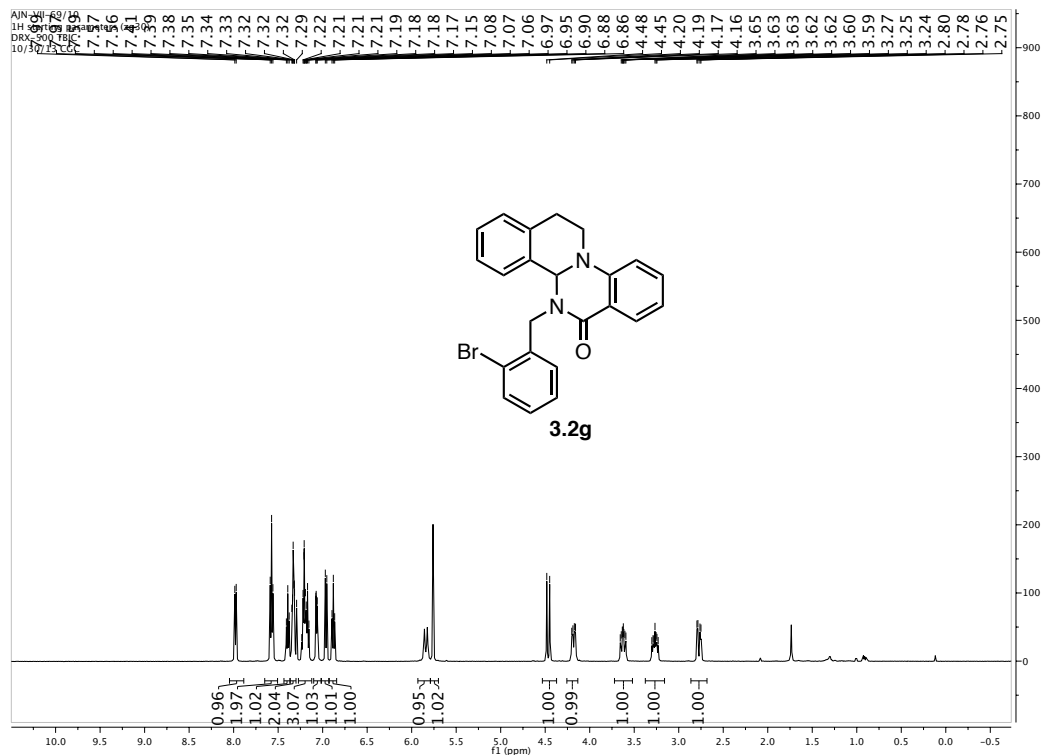


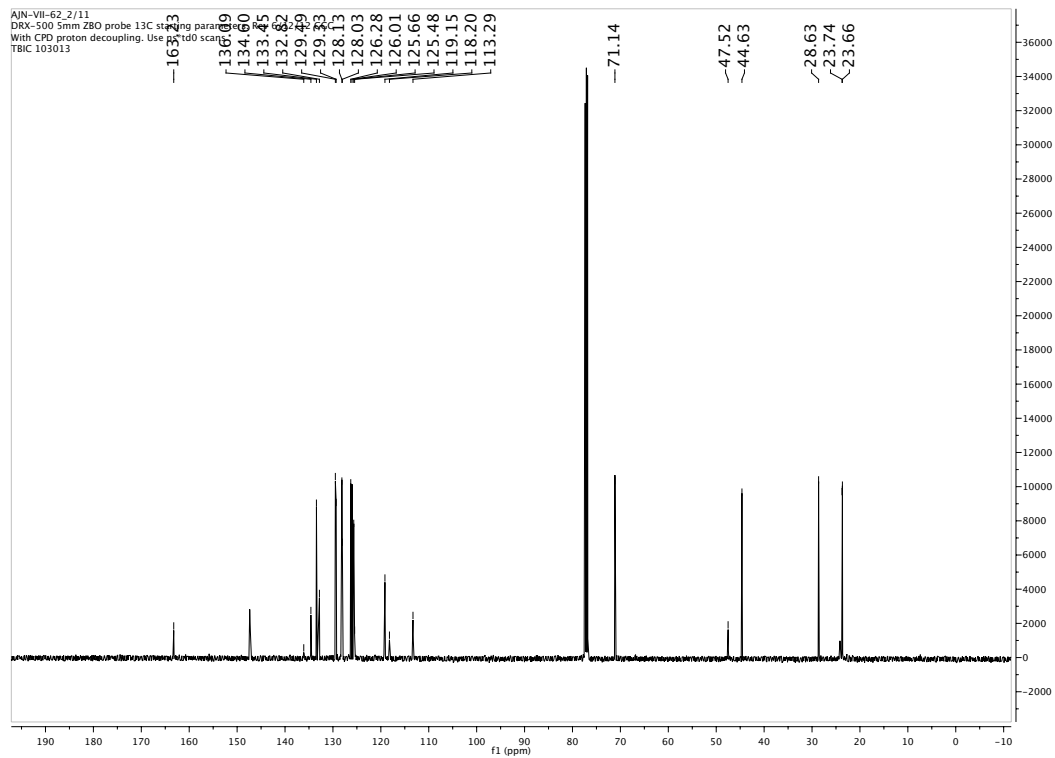
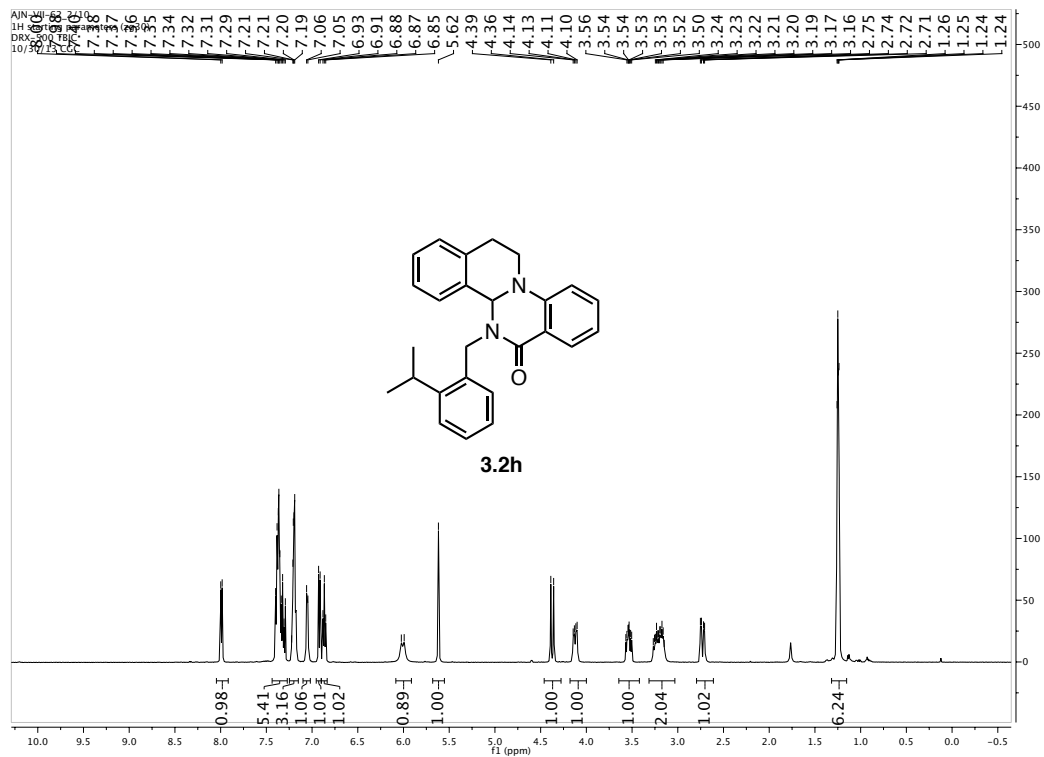


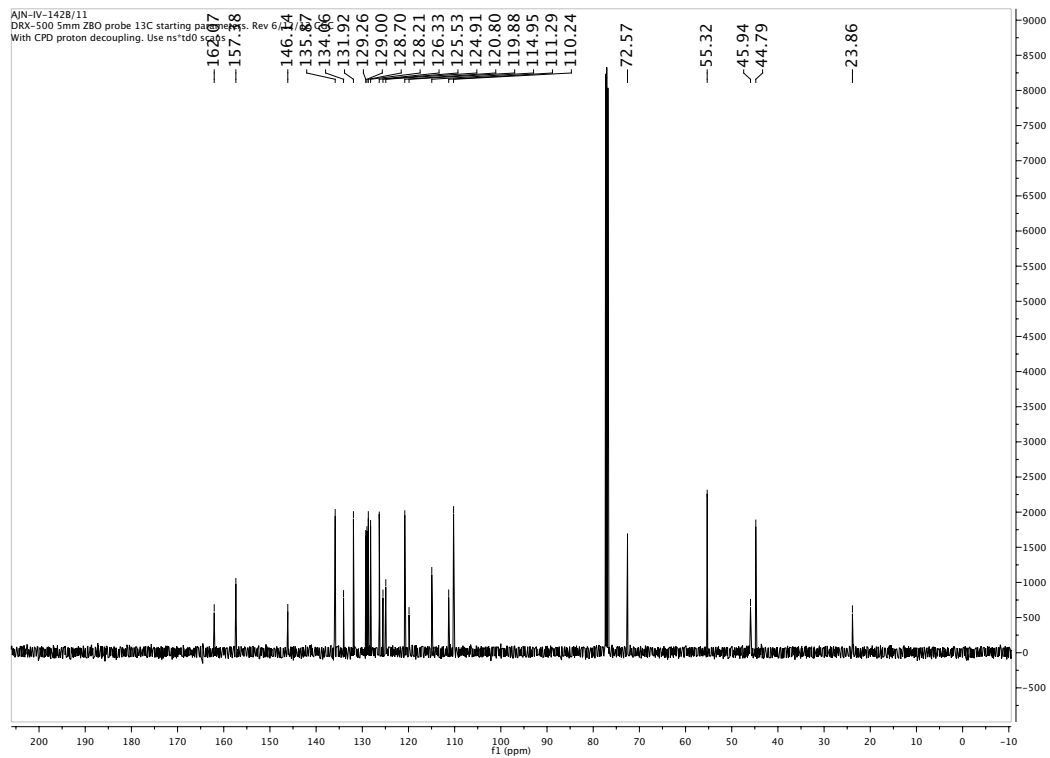
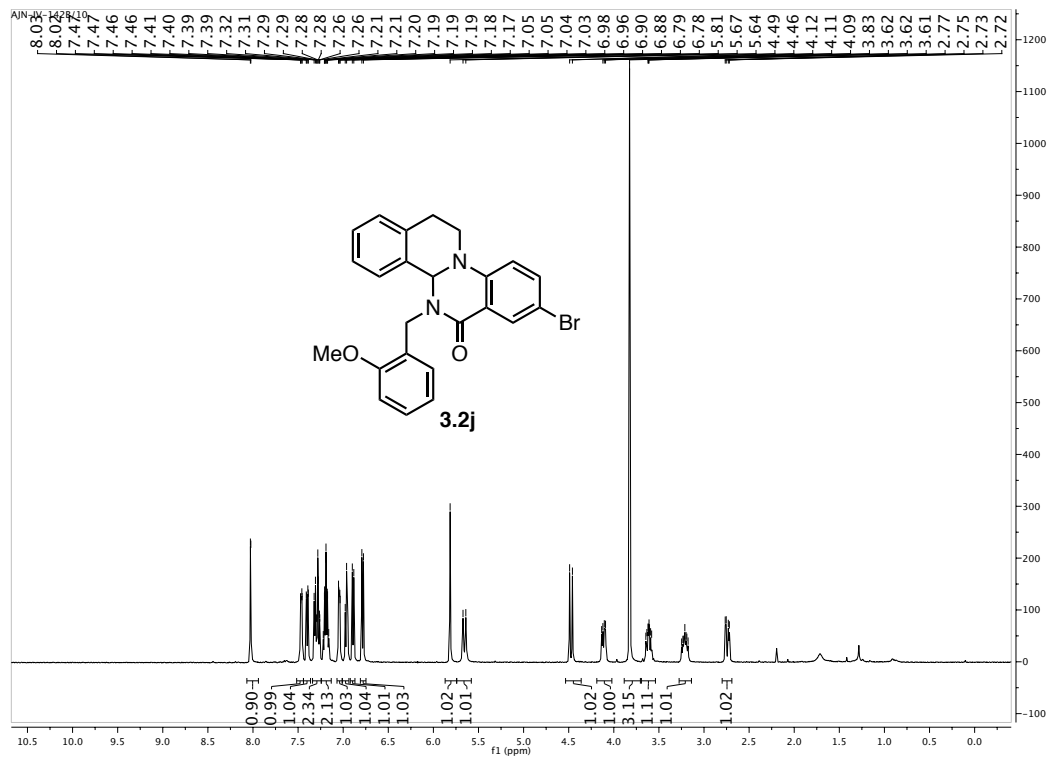


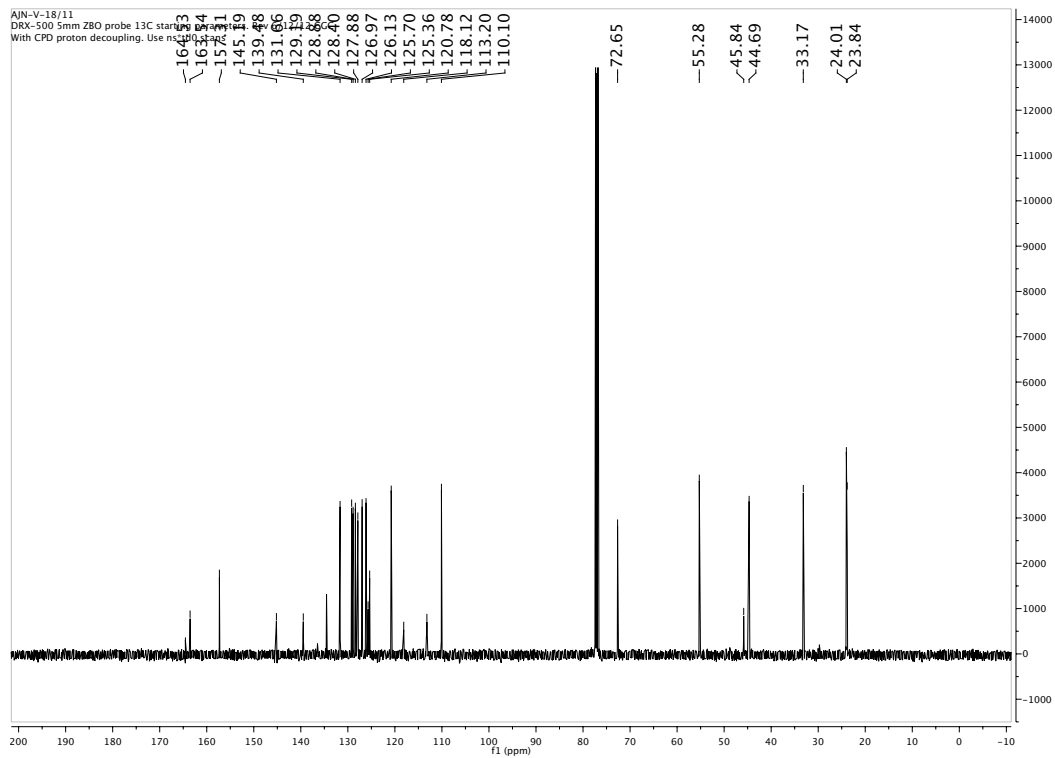
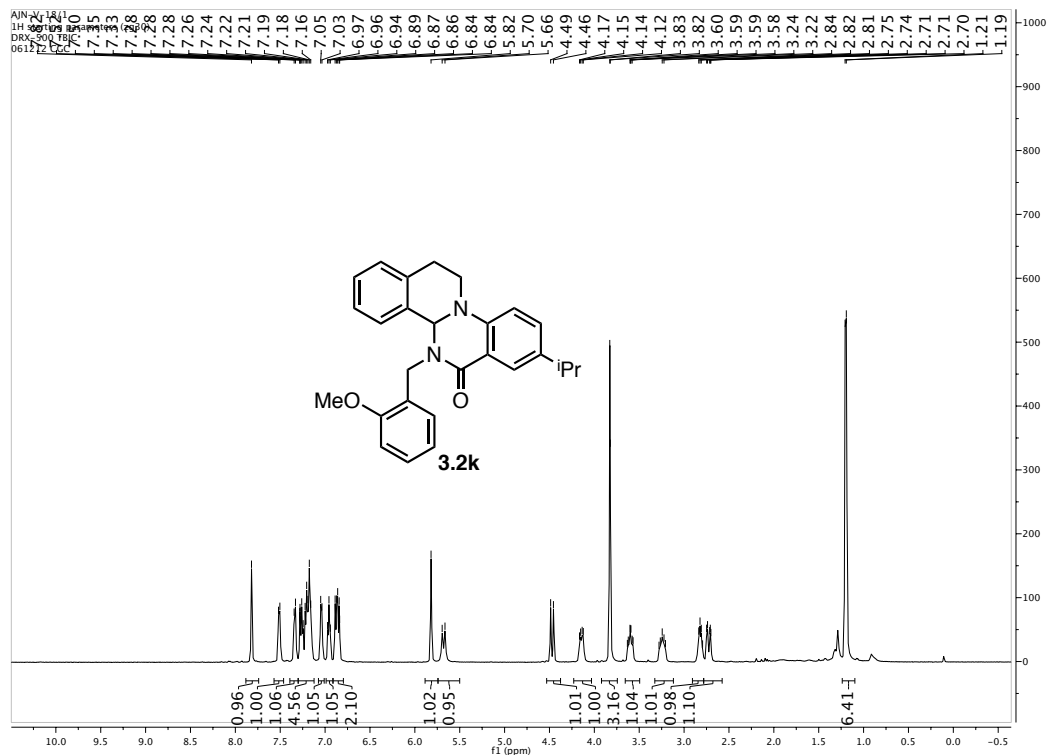


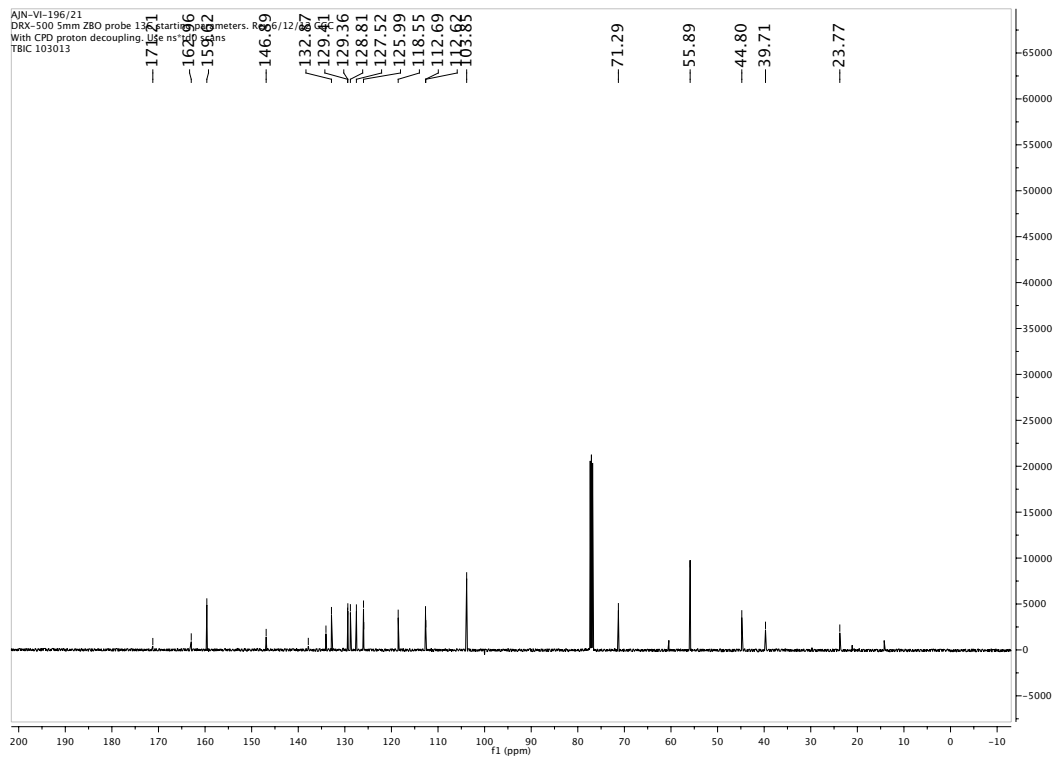
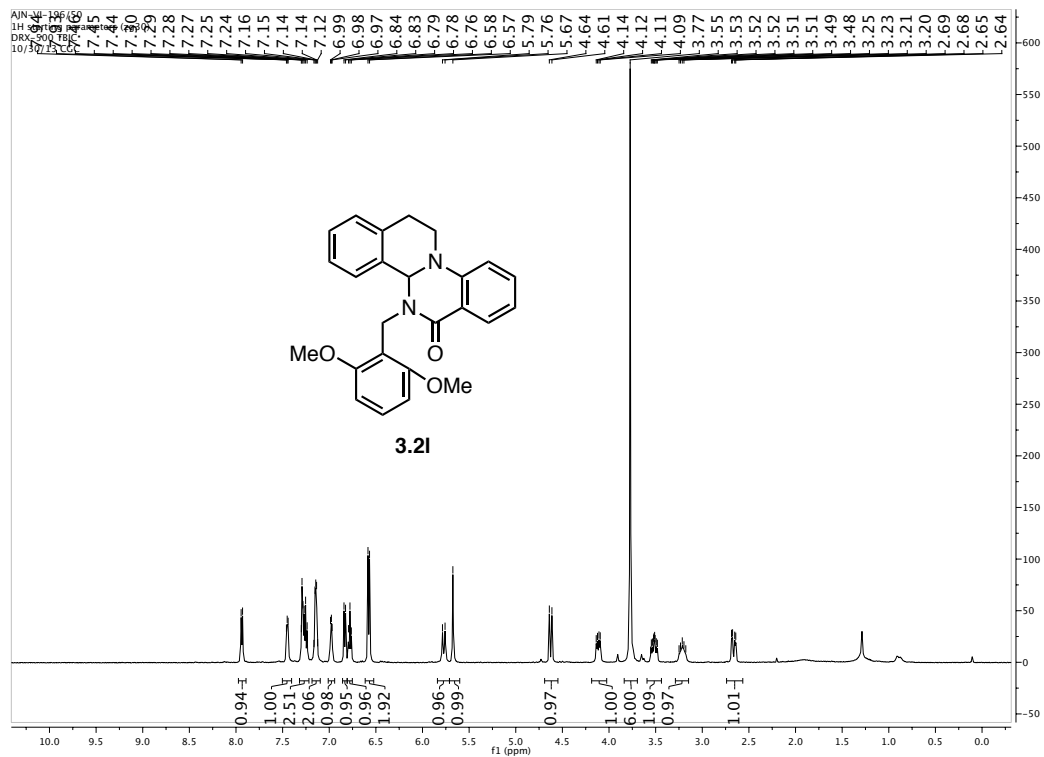












Chapter 4

Development of a Strategy for the Identification of Mechanistic Breaks using Judiciously Designed Enantioselectivity Datasets

Portions of this chapter were adapted with permission from (Neel, A. J.; Milo, A.; Sigman, M. S.; Toste, F. D. *J. Am. Chem. Soc.* **2016**, *138*, 3863. “Enantiodivergent Fluorination of Allylic Alcohols: Dataset Design Reveals Structural Interplay between Achiral Directing Group and Chiral Anion). Copyright (2016) American Chemical Society.

Introduction

Enantioselectivity values represent relative rate measurements that are sensitive to the structural features of the substrates and catalysts that interact to produce them. Therefore, well-designed enantioselectivity datasets are information rich and can provide key insights regarding specific molecular interactions. Chapter 3 described the development of a strategy to exploit this wealth of mechanistic information.¹ Briefly, this approach involves: 1) preparing a catalyst and substrate library of systematically perturbed structures, 2) identifying molecular descriptors that could serve to quantify these structural changes, 3) correlating these molecular descriptors with experimental selectivity outcomes of each catalyst and substrate combination in the dataset, 4) developing mechanistic hypotheses on the basis of the descriptors required for modeling, and 5) preparing tailored catalysts or substrates to probe these hypotheses. Using this approach, the key noncovalent interactions underlying asymmetric induction² were hypothesized, and consequently a series of catalysts that leveraged these putative interactions to improve selectivity over the entire dataset were prepared and validated.¹

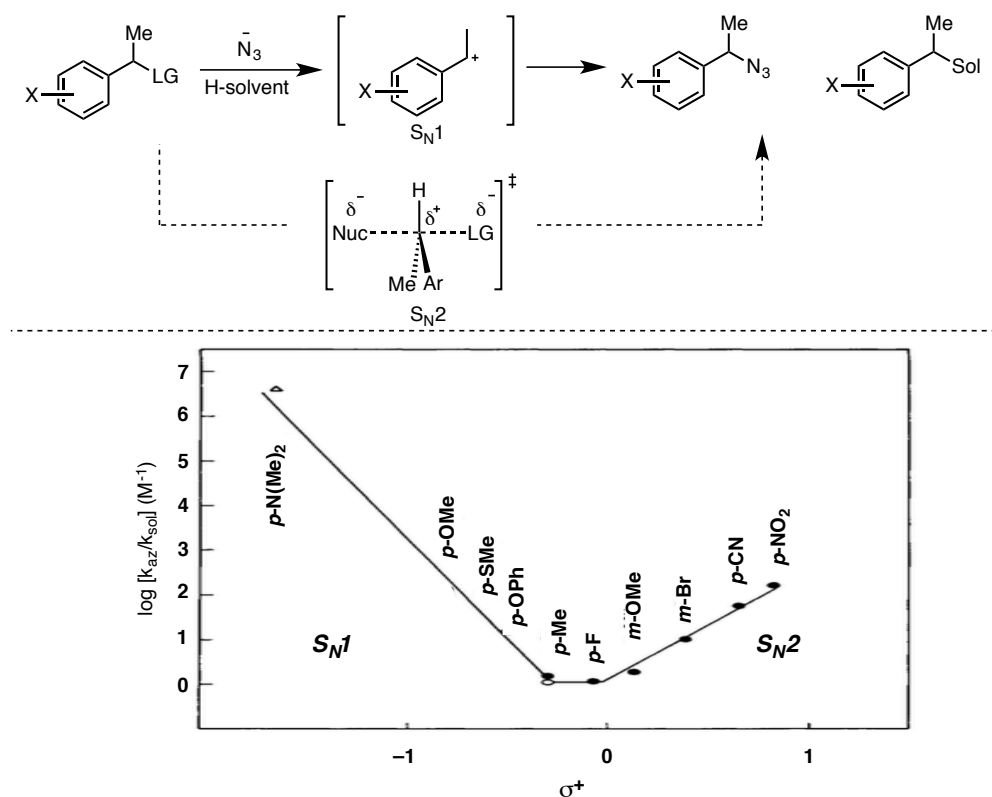


Figure 4.1. Example Hammett plot demonstrating how change in slope suggests change in mechanism (ref 17)

Although this strategy is general for the study of selective reactions, it is predicated on the assumption that any variation in selectivity stems from an analogous mechanism of asymmetric induction for each dataset member. If this assumption is not valid for certain examples in the dataset, they cannot be directly compared. Classically, such changes in mechanism have been revealed through changes in the slope of univariate correlations such as linear free energy relationships (LFERs, e.g. Hammett plots).³⁻²² A classic example from Jencks and coworkers illustrating the continuum between S_N1 and S_N2 mechanisms for nucleophilic substitution is

presented in Figure 4.1. Substituents that stabilize positive charge *via* resonance favor an S_N1 mechanism (Figure 4.1, left) whereas those that withdraw electron density (Figure 4.1, right) favor an S_N2 pathway. Because a single parameter is being used to describe reactivity (i.e. σ⁺), this mechanistic dichotomy is immediately apparent upon inspection.

However, in cases where multivariate correlations are applied, these changes become more challenging to identify, because the parameters employed could serve to account for this variance.⁶ We became interested in the question of how changes in mechanism could be identified in such scenarios, as this would allow for further generalization of our strategy that uses focused datasets to elucidate the structural origins of enantioselectivity. Herein, we demonstrate how dataset design and organization enable the rapid identification of mechanistic breaks that can be subsequently confirmed experimentally. This approach allows for valid comparisons to be made within a dataset, resulting in the identification of reasonable structural origins of enantioselectivity under different mechanistic regimes. As a demonstration of the insight gained, we have rationally designed a catalyst system capable of producing either enantiomer of a chiral fluorinated product in high enantioselectivity using the same enantiomer of chiral catalyst with a different achiral additive.^{23–26}

Background

The concept of chiral anion phase transfer (CAPT) catalysis (Figure 4.2) was introduced in Chapter 2.^{27–48} This strategy relies on employing an insoluble cationic electrophile in a nonpolar organic solvent, thus minimizing the unselective background reaction with a soluble substrate. The electrophile is solubilized through the action of a chiral, lipophilic, anionic phosphate salt,^{49–53} ensuring that it is in a chiral environment when it encounters the substrate in solution. This strategy has proven successful for several electrophiles, including diazonium salts,^{43,46,54} oxoammonium salts,^{36,38} and halogenating reagents (Selectfluor along with its bromo and iodo analogues). With respect to this latter reagent class, although a number of examples have been reported by our group^{30–35,37,42} and others,^{39–41,44,45,48,55} enantioselectivity has typically depended on the presence of a pre-installed directing group to facilitate the interaction between the substrate and phosphate catalyst in the enantiodetermining step.

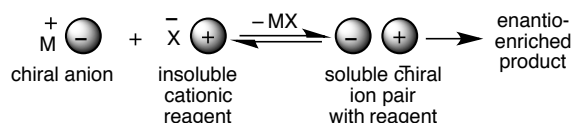


Figure 4.2. Conceptual diagram of chiral anion phase-transfer catalysis

To address this limitation, the Toste group recently demonstrated⁵⁶ that simple allylic alcohols could be fluorinated^{57–64} with ee values of up to 94 % using aryl boronic acids (BAs) as traceless, in situ directing groups (Figure 4.3).⁶⁵ The essential role of the aryl BA for high enantioselectivity was underlined by the formation of racemic product in its absence.

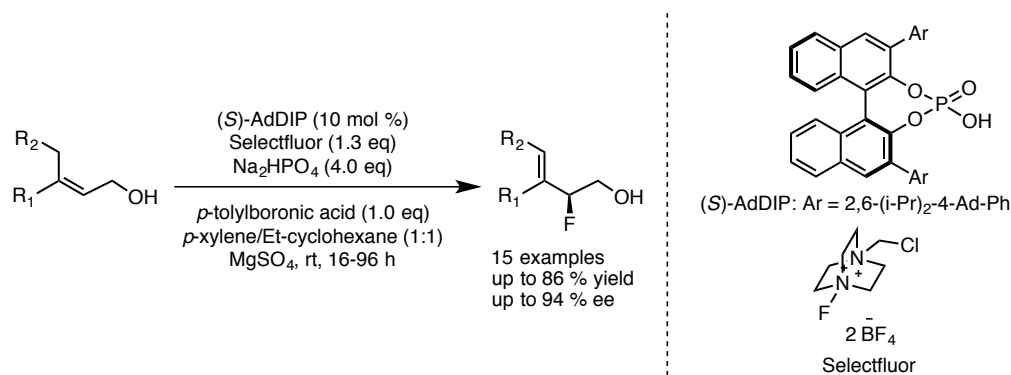


Figure 4.3. Phosphate-catalyzed aryl BA-directed asymmetric fluorination of allylic alcohols

However, it was observed that enantioselectivity was highly dependent on the structure of the aryl BA employed. For example, using (*S*)-TRIP as the catalyst, simply changing from 3,5-dimethylphenylboronic acid to *p*-tolylboronic acid resulted in an 81 % change in ee (1.3 kcal/mol, Figure 4.4). The notion that selectivity could be influenced to such an extent by an achiral additive is intriguing in terms of the structural underpinnings of this effect. We approached this problem within the framework of our hypothesis that enantioselectivity values can serve as sensitive mechanistic probes that report on specific interactions between reacting partners. Specifically, we anticipated that by designing a dataset in which the structural features of the aryl BA and phosphate catalyst were systematically perturbed, we could ascertain the manner in which they interact at the TS to control enantioselectivity in the fluorination of allylic alcohols

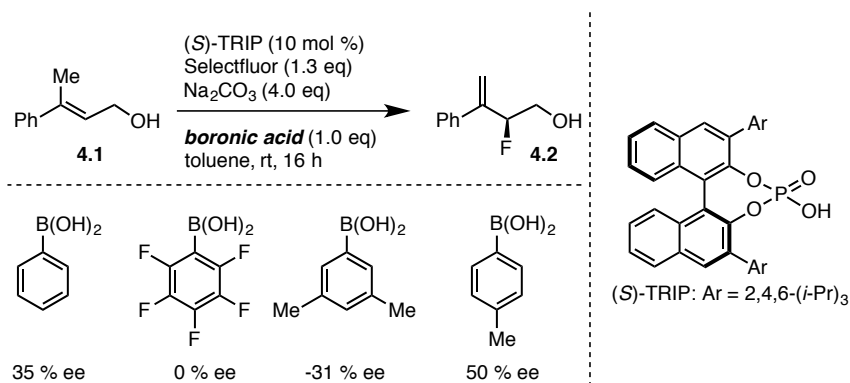


Figure 4.4. Preliminary results demonstrating effect of BA structure on enantioselectivity

Results and Discussion

Control Experiments

Figure 4.5 depicts our proposed mechanism for this transformation. Following anion metathesis between phosphate **4-A** and Selectfluor, chiral, soluble ion pair **4-B** encounters the condensation product (**4-E**) between allylic alcohol **4-C** and BA **4-D**. A concerted or stepwise fluorination-deprotonation sequence in the chiral environment of the phosphate (**4-G**) affords enantioenriched allylic fluoride **4-H** and phosphoric acid (PA) **4-I**, which can be regenerated to the anion by an inorganic base.

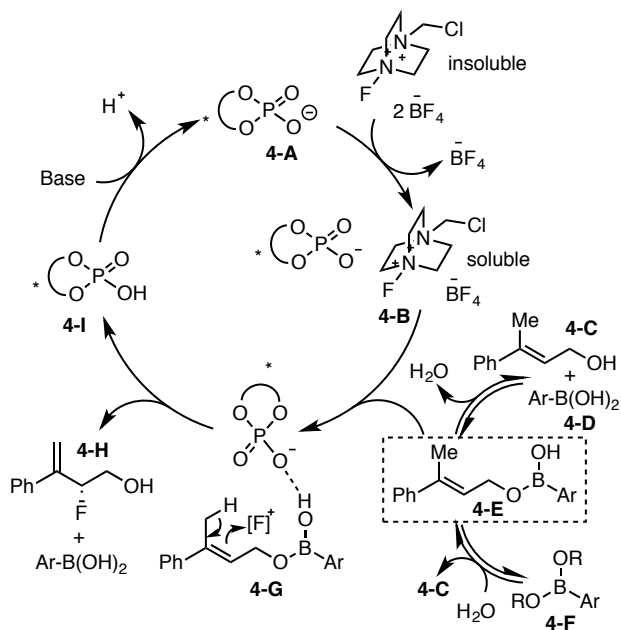
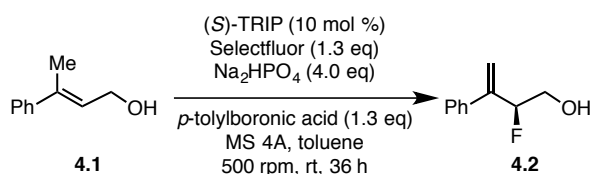


Figure 4.5. Proposed mechanism asymmetric fluorination

Prior to initiating our study of the relationship between PA/BA structures and enantioselectivity, we sought experimental evidence that BA monoester **4-E** was in fact the species undergoing enantioselective fluorination under catalytic conditions. Table 4.1 summarizes the relevant results using (*S*)-TRIP and *p*-tolylboronic acid as representative reaction components. In the absence of (*S*)-TRIP, the yield was greatly diminished (entry 2), supporting its role as a phase-transfer catalyst. Omission of *p*-tolylboronic acid from the reaction mixture somewhat restored the yield, but with a complete loss of enantioselectivity (entry 3). To better ascertain the relevance of this unselective pathway, a series of NMR titration experiments was performed to study the equilibrium depicted in Table 4.2.

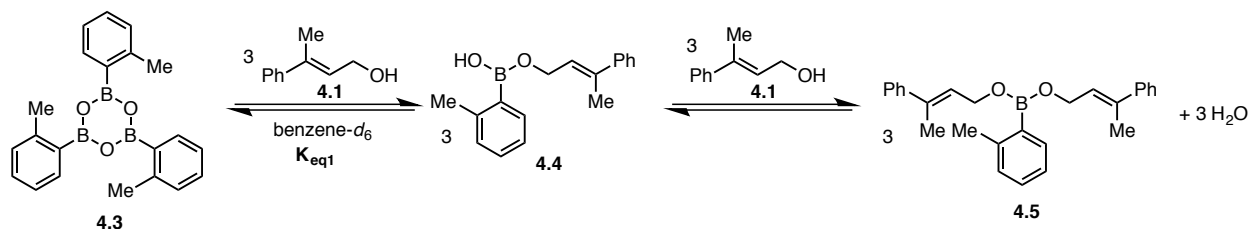
Table 4.1. Selected control experiments



entry	Omitted Reagent	yield (%)	ee(%)
1	none	52	66
2	(<i>S</i>)-TRIP	5	--
3	<i>p</i> -tolylboronic acid	39	5
4	MS 4A	62	66

Boroxine **4.3** was prepared by heating *o*-tolylboronic acid at 120 °C for 3h and its formation confirmed by ¹H NMR spectroscopy prior to use. A solution of boroxine **4.3** (0.35 mmol) in benzene-*d*₆ was treated with varying amounts of alcohol **4.1** and the resulting ¹H NMR spectra were recorded (see the Experimental Section for a sample spectrum).

Table 4.2. NMR Titration Experiments



entry	eq. 4.1 added	[4.1] added	[boroxine] _{eq} 4.3	[<i>mono-ester</i>] _{eq} 4.4	[<i>bis-ester</i>] _{eq} 4.4	[boron] _{total}	[alcohol] _{eq} 4.1	[alcohol] _{total} 4.1	K_{eq1}
1	0	0	0.0438	0	0	0.131	0	0	--
2	1	0.0438	0.0328	0.0144	0.0079	0.121	0.0013	0.0315	--
3	2	0.0875	0.0259	0.0276	0.0184	0.124	0.0171	0.0815	--
4	4	0.175	0.0114	0.0499	0.0381	0.122	0.0512	0.177	81.3
5	6	0.263	0.0031	0.0630	0.0499	0.122	0.0999	0.263	82.3
6	7	0.306	0.0018	0.0644	0.0499	0.120	0.121	0.284	86.6

Table 4.2 shows the data for several different concentrations of added **4.1** and Figure 4.6 depicts this data graphically. At all concentrations, an equilibrium is present between *mono-ester* **4.4** and *bis-ester* **4.5**. These data demonstrate that, under the employed reaction conditions (i.e. excess boronic acid relative to alcohol), essentially all of alcohol **4.1** is associated with a molecule of the boronic acid. Thus, although an unselective boronic acid-free pathway is possible (Table 4.1), its contribution to the observed enantioselectivity is likely minimal under the standard reaction conditions.

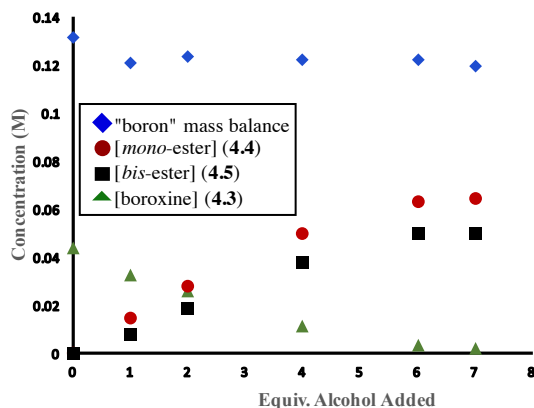


Figure 4.6. Boron speciation during titration of **4.3** with **4.1**

Finally, omission of molecular sieves resulted in an increased yield, while enantioselectivity remained unaffected (Table 4.1, entry 4).⁶⁶ The diminished yield in the presence of molecular sieves likely arises from the increased formation of BA *bis-ester* (**4-F**) under these dehydrating conditions, which serves as an unreactive reservoir of alcohol **4.1**. Collectively, these data sufficiently demonstrate that monoester **4-E** is likely the relevant species interacting with the

chiral phosphate in the enantiodetermining step of this reaction. The remainder of our study was devoted to uncovering the nature of this interaction within the relatively opaque region of the catalytic cycle from **4-E** to **4-G** to yield **4-H** (Figure 4.5).

Dataset Design

Prior to designing a dataset in which both BA and phosphate structures were systematically modified, we sought to establish the enantioselectivity range accessible by changing only the achiral aryl BA. It was reasoned that this approach would allow us to rapidly identify which BA structural features most affected enantioselectivity, enabling the effective design of a dataset of catalysts and BAs. To this end, 21 commercially available aryl BAs were selected with substituents that systematically spread the reaction space with respect to both their steric and electronic profiles at the 2-, 3-, 4-, 2,6-, and 3,5- positions of the aryl ring (Figure 4.7). (*S*)-TRIP was selected as the catalyst for these studies, given its ubiquity in the field of chiral PA/phosphate catalysis.^{67,68}

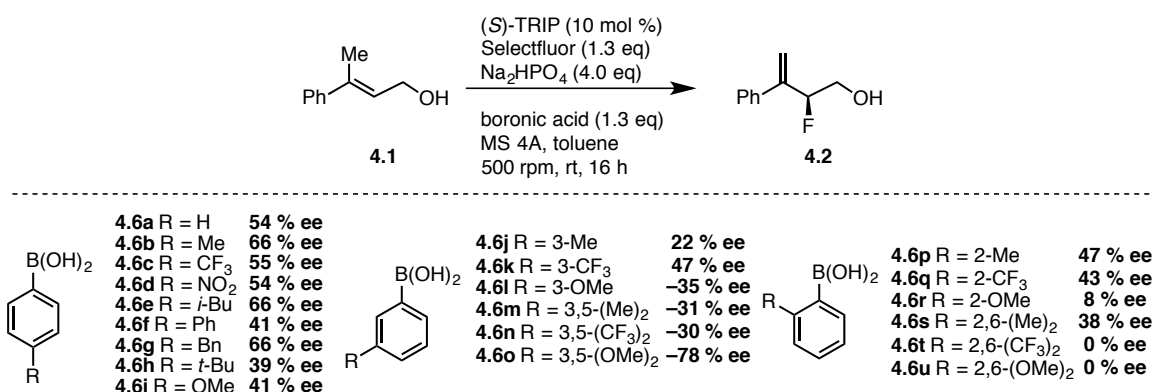


Figure 4.7. Effect of BA structure on enantioselectivity using (*S*)-TRIP

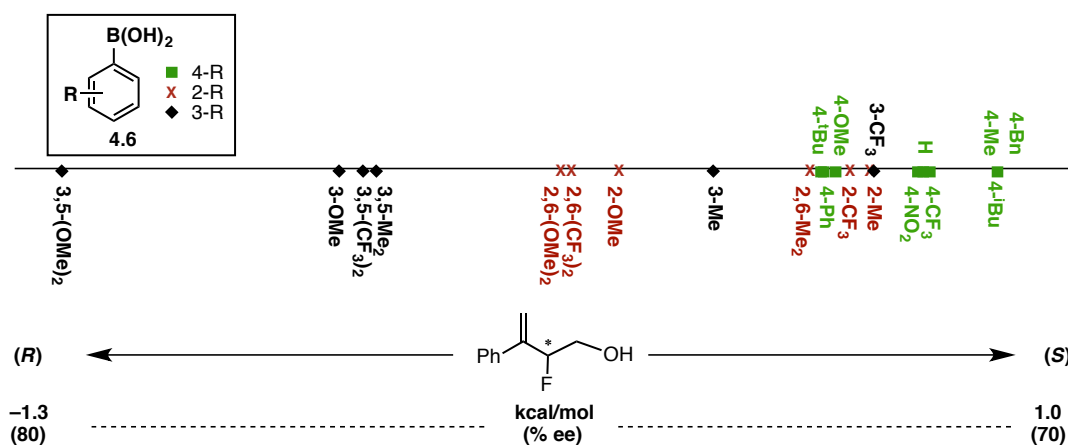


Figure 4.8. Visualization of enantioselectivity range accessible through alteration BA structure

Using conditions slightly modified from those previously reported, the enantioselectivity of **4.2** was measured using each of these BAs with (*S*)-TRIP, resulting in values ranging from 66% ee of the expected (*S*)-**4.2**, to 78% ee of the (*R*) enantiomer. Remarkably, this represents a 2.2 kcal/mol range based solely on the structure of the achiral BA (Figures 4.7 and 4.8). A notable

structural effect is apparent from these data as well: 4-substituted phenyl BA derivatives lead to the (*S*) enantiomer with the largest ee values, followed by their 2- and 3-substituted counterparts, with 3,5-substituted derivatives resulting in the highest enantioselectivities favoring the (*R*) enantiomer.

Having established this range, we turned to design a complete dataset in which both BA and phosphate structures were perturbed (Figure 4.9). To this end, eight BAs were selected that evenly covered the range of enantioselectivities representative of the different substitution patterns that were believed to influence selectivity (i.e. 2-, 4- and 3,5-substituted). Simultaneously, eight phosphate catalysts were prepared with variable substitution at the 3 and 3' positions of the binaphthyl backbone. Mesityl-substituted catalyst **4.7a** was selected as a less-encumbered version of TRIP (**4.7b**) to assess the potential role of sterics within the 2,4,6-substitution pattern, while 2,6-(*i*-Pr)₂-Ph (**4.7c**), 2-*i*-Pr-Ph (**4.7d**), and 4-*i*-Pr-Ph (**4.7e**) substituted catalysts were intended to serve as deconstructed derivatives of TRIP to assess any potential isolated effects of these positions. Finally, as the 3,5-disubstituted phenyl BAs **4.6m-4.6o** had been observed to afford inverted selectivity using TRIP as the catalyst (Figures 4.7 and 4.8), 3,5-disubstituted catalysts **4.7g** and **4.7h** were prepared to evaluate the possibility of shape complementarity between the BA and catalyst substituents.

Data Collection

With the appropriate libraries of phosphate catalysts and BAs in hand, the enantioselective outcome of each combination was measured with the goal of producing correlations between the experimental values and molecular parameters describing these structural variations.⁶⁹⁻⁷⁸ Figure 4.9 depicts the enantioselective outcome of each BA-phosphate combination. It was anticipated that the general trends observed using TRIP (Figures 4.7 and 4.8) would hold across the series of catalysts (e.g., 4-substituted BAs would display the highest propensity for one enantiomer, while 3,5-disubstituted BAs would favor the other). We were therefore surprised to observe that these trends were highly variable from one catalyst to the next, even as a result of seemingly minor structural changes. For example, the use of mesityl-substituted catalyst (**R**)-**4.7a** resulted in the formation of (**R**)-**4.2** as the major enantiomer across the entire BA series, in contrast to the use of structurally directly analogous (*R*)-TRIP (**4.7b**), which primarily formed (*S*)-**4.2** when used in combination with 3,5-disubstituted phenyl BA derivatives. Additionally, the use of catalyst (**R**)-**4.7e**, in which the *ortho* isopropyl groups of **4.7b** have been removed, afforded the enantiomeric product (*S*)-**4.2** across the entire dataset. Figure 4.10 provides a method to visualize this data simultaneously, where each line represents a BA and each x-axis tick mark represents a catalyst aryl group. This visualization scheme displays the same information contained in Figure 4.9, but in a manner that facilitates the identification of outliers and stark trend breaks. For example, upon moving from left to right, sharp breaks in the observed trends can be detected by distinct, significant changes to enantioselectivity and a reordering of the trend lines.

We have interpreted these sharp breaks in the trends as being indicative of a change in the mechanism of asymmetric induction for certain phosphate-BA combinations. For this reason, although our initial goal was the elucidation of the relevant selectivity-determining interactions across the entire dataset through a multivariate correlation, the required models would not necessarily account for these mechanistic breaks. However, we reasoned that a mechanistic understanding of the outliers would contextualize the remainder of the data, allowing meaningful conclusions to be drawn regarding the structural origins of selectivity. Because this dataset had

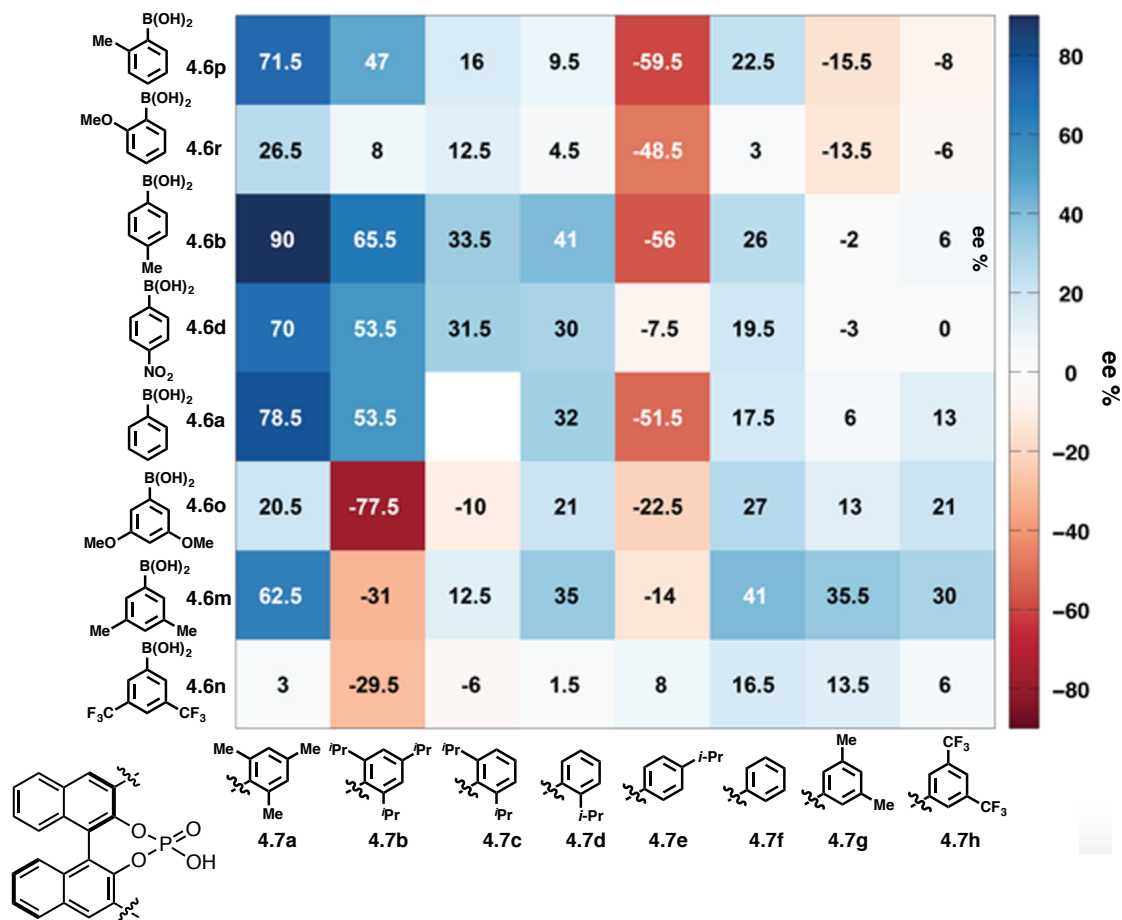


Figure 4.9. Enantioselectivity data obtained by variation of PA and BA substitution pattern. All reactions were conducted using 0.05 mmol **4.1**, 0.065 mmol **4.6**, 0.065 mmol Selectfluor, 0.200 mmol Na₂HPO₄, 0.005 mmol **4.7**, and 40 mg MS 4 Å in toluene (0.1 M)

been designed to cover a broad range of structure enantioselectivity relationships, Figures 4.9 and 4.10 could serve as a guide for experimentally interrogating regions of the dataset that seemed distinctive. Specifically, we were intrigued by the phenomenon that catalysts with the same backbone chirality could deliver either enantiomer of **4.2** in reasonably high ee. Based on the data in Figure 4.9, this divergence in enantioselectivity appears to manifest itself in two distinct respects: 1) by changing the catalyst substituent (compare (*R*)-**4.7e**, containing a 4-*i*-Pr-Ph substituent, and (*R*)-**4.7b**, containing a 2,4,6-*i*-Pr)₃-Ph substituent) and 2) by holding the catalyst constant while changing the achiral BA additive (compare **4.6b**, 4-Me-Ph BA, with **4.6o**, 3,5-(OMe)₂-Ph BA using (*R*)-**4.7b** as the catalyst). The ability of the described approach to provide a systematic guide for focused outlier identification steered our further studies toward selecting particular experiments that would reveal the mechanistic possibilities responsible for these observations.

Nonlinear Effect Studies

The aforementioned inversions of enantioselectivity are clearly indicative of a major change to the structure of the enantiodetermining TS(s). Given the doubly cationic nature of Selectfluor, we hypothesized that this change may be related to the number of phosphate molecules

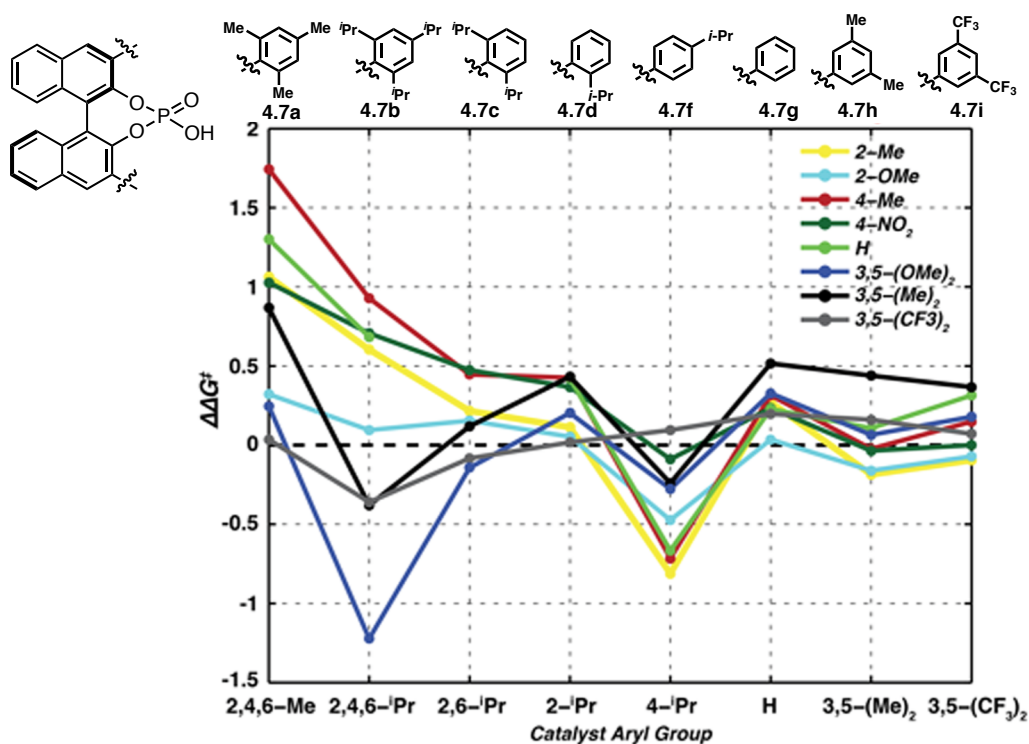


Figure 4.10. Graphical representation of BA structure-selectivity trends as a function of catalyst structure

associated with Selectfluor (i.e. 1 or 2) during C–F bond formation (**4-B**, Figure 4.5), as this speciation could conceivably be sensitive to the structure of the phosphate, BA or both. To test this possibility, we conducted a series of nonlinear effect (NLE) experiments^{79–102} using phosphate/BA combinations from different regions of the original dataset hypothesized to function by unique mechanisms (*vide supra*). As depicted in Figure 4.11, using *p*-tolyl BA **4.6b**, a linear relationship was observed between catalyst and product ee when using both (*S*)-**4.7a** and (*S*)-**4.7b** as catalysts, implicating only a single phosphate in the enantiodetermining TS in each of these scenarios. This result suggests that these two catalyst are directly comparable and that the improvement from 66% ee with **4.7b** to 91% ee with the structurally analogous **4.7a** is likely geometric in origin. However, a significant positive NLE was observed using (*S*)-**4.7e** as the catalyst with both **4.6b** and **4.6p** (Figure 4.11C and D), which is consistent with the involvement of multiple phosphate species in the enantiodetermining TS. The reduced steric profile proximal to the phosphate moiety in **4.7e** lends credence to the proposal that this catalyst is more likely to form a dimeric salt compared with the bulkier **4.7b**. Thus, we propose that the selectivity reversal observed using catalyst **4.7e** is a result of a fundamentally different mechanism of asymmetric induction when using this catalyst relative to the others in the dataset.

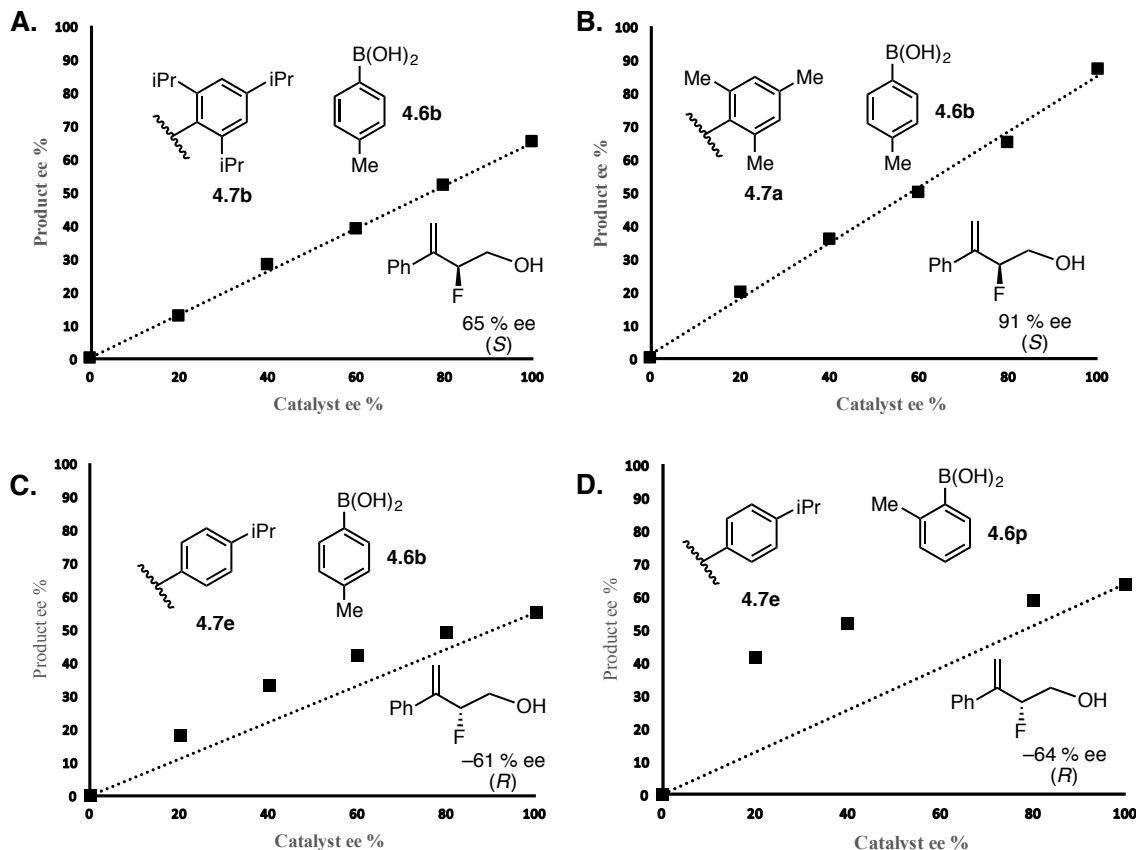
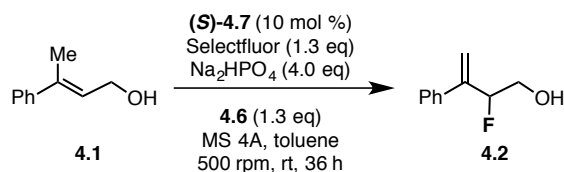


Figure 4.11. Relationship between product and catalyst enantiomeric excess for various PA-BA combinations.

Although the presence of a positive nonlinear effect using catalyst **4.7e** with both *p*-tolyl and *o*-tolylboronic acid is consistent with an active fluorinating species containing two chiral phosphates, it is also possible that a single phosphate is associated with Selectfluor during the enantiodetermining step, with the dimeric species serving as a reservoir for any racemic catalyst present under the reaction conditions. The heterogeneous nature of the reaction mixtures precludes a rigorous kinetic analysis to distinguish these possibilities. Monitoring of product formation vs. time for both enantiopure and scalemic (40 % ee) **4.7e** demonstrates a higher rate of product formation for the former (Figure 4.12), a result that is consistent with either scenario.

In attempts to distinguish between the presence of an active fluorinating species containing two phosphates versus an inactive reservoir in a qualitative manner, salts (**R**)-**4.8** and (**R**)-**4.9** were prepared by the method of Alexakis and coworkers⁵⁵ (Figure 4.13). Using these reagents, the fluorination reaction was performed under otherwise standard conditions with *p*-tolylboronic acid (**4.6b**). As shown in Figure 4.13, using reagent (**R**)-**4.8**, derived from catalyst **4.7b** (TRIP) for

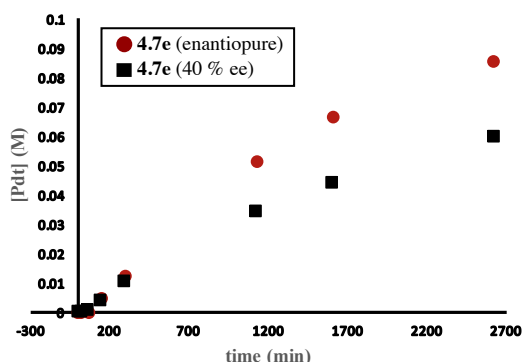


Figure 4.12. Effect of catalyst enantiopurity on rate of product formation

which there was no nonlinear effect, 0 % yield of **4.2** was observed after 20 h. In contrast, using (*R*)-**4.9** (derived from **4.7e**), for which a positive nonlinear effect was observed, **4.2** was obtained in 40 % yield (based on fluorinating reagent) and –62 % ee, the same enantioselectivity obtained under catalytic reaction conditions. Although this experiment does not rigorously exclude the possibility of an active fluorinating species containing a single phosphate that is in equilibrium with an off-cycle dimeric species such as **4.9**, we propose that this species is likely involved in the enantiodetermining TS when using catalyst **4.7e** given the complete inactivity of dimeric salt (*R*)-**4.8** (0% yield) compared to catalyst **4.7b** (82% yield).

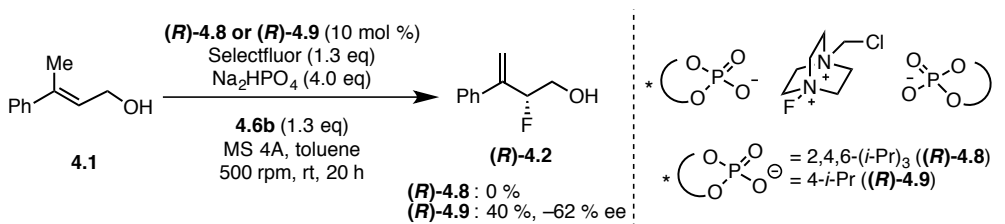


Figure 4.13. Effect of Selectfluor counteranion on reaction outcome

A primary objective of this study was to use the understanding of dataset outliers to contextualize the remainder of the data (*vide supra*). To this end, based on the hypothesis that catalysts lacking *ortho* substituents (such as **4.7e**) would associate with Selectfluor in duplicate, we anticipated similar aggregation behavior for unhindered phenyl substituted catalyst **4.7f**, despite the observation that it afforded **4.2** with “positive” 26 % ee (Figure 4.9). Figure 4.14 shows the results of the nonlinear effect experiment carried out using **4.7f**. The presence of an NLE (negative in this case) suggests aggregation behavior in analogy to that observed with 4-*i*-Pr substituted catalyst **4.7e**. This result is significant, as in the absence of the insight gained from the outliers, this “positive” data point would have been indistinguishable from the other “positive” values in the dataset that are the result of entirely different transition state structures.

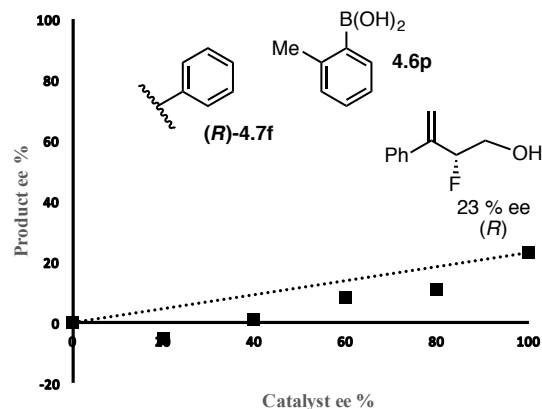


Figure 4.14. Relationship between product and catalyst enantiomeric excess for **4.7f** and **4.6p**

To explain the “negative” enantioselectivity using 4-*i*-Pr substituted catalyst **4.7e** relative the “positive” one observed with unsubstituted catalyst **4.7f**, we hypothesized that substituent shape dictated enantioselectivity within this mechanistic regime (i.e. two phosphates involved in enantioselection). Consistent with this hypothesis, catalysts bearing 4-Me-Ph, 4-*i*-Bu-Ph, and 4-*t*-Bu-Ph substituents at the 3 and 3' positions were evaluated with *o*-tolylboronic acid **4.6p**, affording the product in -11, -37, and -27 % ee respectively (**Figure 4.15**). We thus propose that catalysts **4.7f**, **4.7i**, **4.7e**, **4.7k**, and **4.7j** are all part of the same mechanistic regime (i.e. involving aggregation with Selectfluor), and that the ee range observed with boronic acid **4.6p** (-59.5 to 26, representing a 1.5 kcal/mol difference) is reflective of specific catalyst-boronic interactions that are sensitive to catalyst substitution pattern.

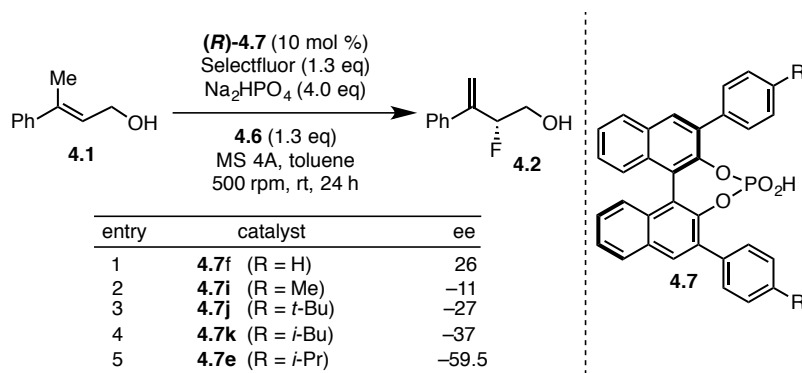


Figure 4.15. Effect of catalyst *para*-substituent identity on enantioselectivity

Finally, given the significantly inverted enantioselectivity observed using the combination of catalyst **4.7b** and 3,5-(OMe)₂-substituted BA **4.6o** (-78 % ee), the relationship between product and catalyst enantioselectivities was sought for this combination. Intriguingly, a linear relationship was observed (Figure 4.16), suggesting that a single phosphate molecule was involved in the enantiodetermining TS in this case and therefore, that the origin of selectivity inversion for this particular phosphate/BA combination is different than that of catalysts lacking *ortho* substituents (*vide infra*).

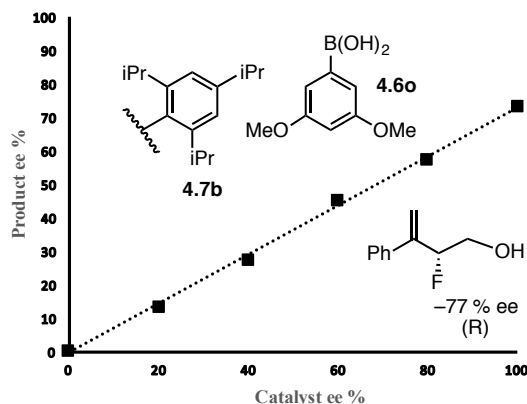


Figure 4.16. Relationship between product and catalyst enantiomeric excess for **4.7b** and **4.6o**.

Examination of 4-*i*-Pr substituted catalyst **4.7e**

As 4-*i*-Pr-Ph substituted catalyst **4.7e** likely operates via an alternative mechanism, the enantioselectivity data collected using it cannot be directly compared with those from the other catalysts in the dataset. However, we were interested in the source of the significant variation (8 to -61% ee) in the data obtained using this catalyst resulting from changes in BA structure. To obtain a more complete representation, several additional BAs were evaluated in combination with this catalyst. Figure 4.17 shows two Hammett plots correlating enantioselectivity to σ_{para} that include these results along with those from the original dataset. For a given substitution pattern (i.e. 3,5- or 4-), there is an excellent correlation between enantioselectivity (represented as $\Delta\Delta G^\ddagger$) and Hammett σ_{para} values, with electron-rich BAs generally affording higher enantioselectivities than electron-poor examples. The 3,5-substituted BAs cannot be correlated on the same plot as the 4-substituted BAs, yet independently, both plots reveal robust linear free energy relationships (LFERs) with electronic features of the BA substituent.¹⁰³

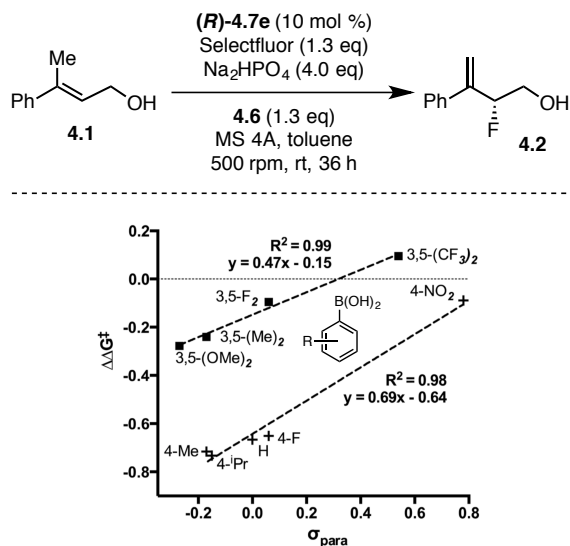


Figure 4.17. Correlation between enantiomeric excess of **4.2** ($\Delta\Delta G^\ddagger$) and σ_{para} for various BAs using catalyst **4.7e**

Martínez-Aguirre and Yatsimirsky recently reported that, in contrast to various other anions, H_2PO_4^- tends to form Lewis acid–Lewis base type tetrahedral adducts with aryl BAs.¹⁰⁴ Furthermore, Tokunaga and coworkers have demonstrated the increased electrophilicity of boron in electron poor aryl BAs by studying the thermodynamics of boroxine hydrolysis as a function of aryl substitution.¹⁰⁵ Based on this precedent, we propose that the sterically accessible phosphate moiety in **4.7e** is inhibited by the formation of a catalytically inactive covalent adduct with electron poor BAs under the reaction conditions. Therefore, the low enantioselectivities observed using electron poor BAs reflect an inability of the phosphate to serve as a phase transfer catalyst and thus to outcompete the unselective background reaction. This hypothesis was probed further by monitoring product formation in the presence and absence of catalyst.

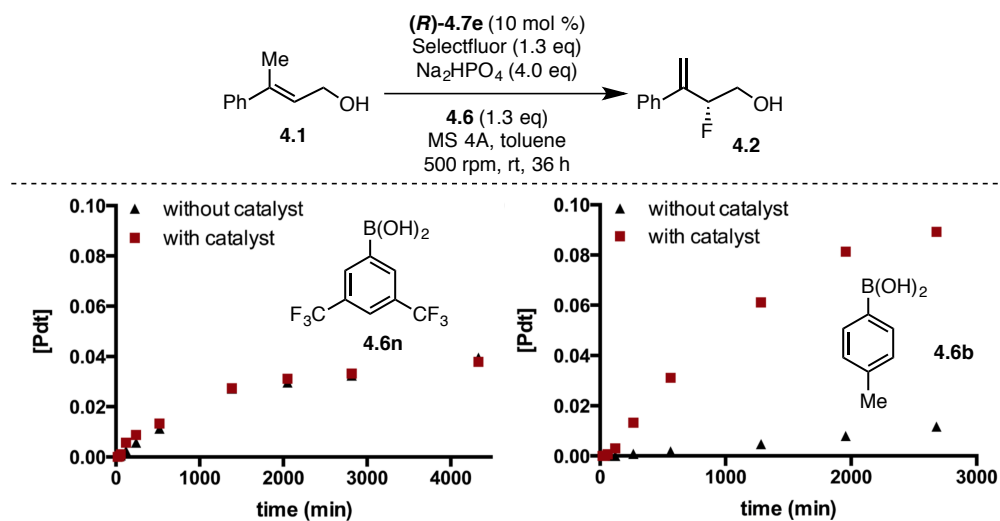


Figure 4.18. Reaction time course data for formation of **4.2** with varying BA structure

As shown in Figure 4.18, using 3,5-(CF_3)₂-substituted BA **4.6n**, fluorination occurred at nearly identical rates in the presence and absence of catalyst **4.7e**. However, using the more electron rich 4-Me substituted **4.6b**, a rate acceleration over the uncatalyzed background reaction was observed in the presence of catalyst (Figure 4.18, right). Thus, we propose that although the inverted sense of enantioselectivity using **4.7e** presumably results from the association of two chiral phosphates with Selectfluor, the variation in enantioselectivity observed for this catalyst over a set of BAs is predominantly electronic in origin, with electron poor BAs acting as catalyst poisons.

Isotopic Substitution Experiments

Having identified the likely cause for the inverted enantioselectivity displayed by **4.7e**, we sought a sufficient explanation for the anomalous enantioselectivity observed using **4.7b** and 3,5-(OMe)₂ substituted BA **4.6o** (−78% ee, Figure 4.9). The absence of an NLE (Figure 4.16), indicated that a single phosphate was presumably involved in this TS. This suggested that the inversion of selectivity relative to 4-substituted BAs was likely due to specific phosphate-BA interactions leading to a change in TS geometry. To gain better insight into this region of the

catalytic cycle, substrate **4.1-d₃** was prepared and subjected to the standard reaction conditions with three different phosphate/BA combinations. As demonstrated in Figure 4.19, the use of 4-Me substituted BA **4.6b** with both **4.7a** and **4.7b** afforded **4.2-d₂** with enantioselectivity nearly identical to that observed with its protonated analogue. However, the combination of **4.6o** and **4.7b** provided **4.2-d₂** in -90% ee, a 13% ee (0.6 kcal/mol) increase relative to **4.2**. These results suggest

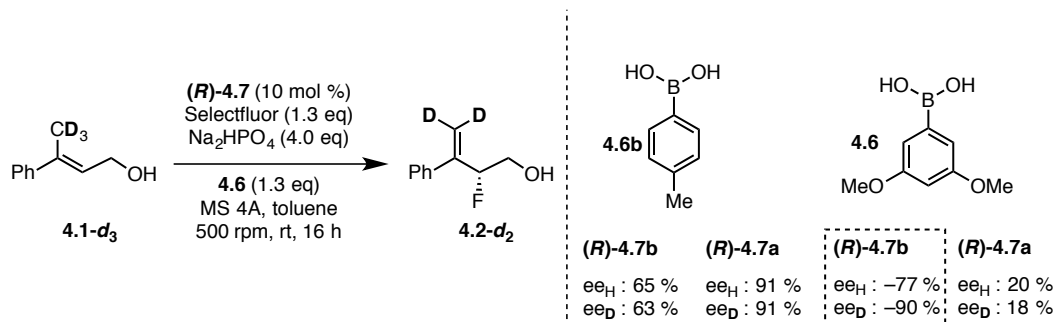


Figure 4.19. Comparison of enantiomeric excess of **4.2** and **4.2-d₂** for various BA-PA combinations.

that the cleavage of the C–H bond is involved in the enantiodetermining TS in the latter case, but not in the former. Figure 4.20 depicts a plausible mechanistic explanation for this situation, in which a continuum exists between two limiting scenarios: 1) irreversible, enantiodetermining fluorination followed by rapid deprotonation (pathway a) or 2) concerted enantiodetermining fluorination-deprotonation (pathway b). The enantioselectivity differences between the deuterated and protonated substrate along this mechanistic continuum depend on the substituents of the aryl BA, and are suggestive of a specific interaction between the BA and catalyst in the latter of the two limiting scenarios. The absence of an effect in the case of **4.6o** with **4.7a** demonstrates that phosphate structure also plays a role in this interaction. We thus focused our efforts on identifying the nature of the specific interaction(s) that were presumably responsible for the large inversion of enantioselectivity observed using **4.6o** with **4.7b**.

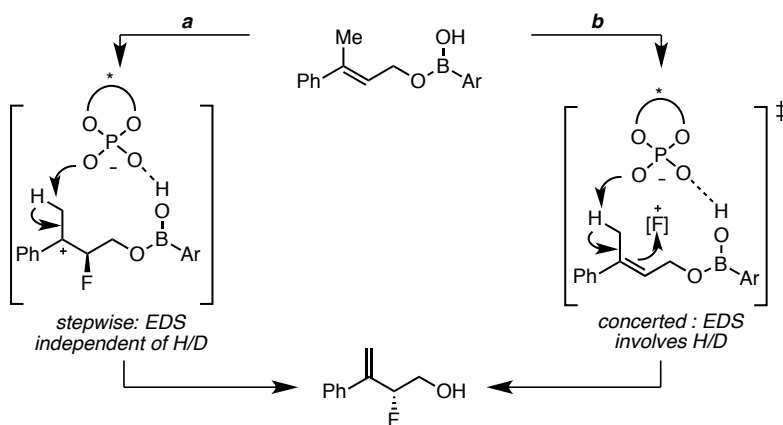


Figure 4.20. Plausible mechanistic rationale for variable dependence of enantioselectivity on isotopic substitution

Probing Direct Interaction

Inspection of our original dataset (Figure 4.9) revealed that 3,5-disubstituted BAs generally resulted in inverted enantioselectivities when used in combination with **4.7b**, but this effect appeared particularly pronounced with 3,5-(OMe)₂-substituted boronic acid derivative **4.6o**. In order to distinguish whether this marked effect using **4.6o** was simply a result of its steric profile or was due to a direct interaction with the methoxy substituent, hybrid 3-Me-5-OMe-substituted phenyl BA derivative **4.6w** was prepared and evaluated under the standard reaction conditions using each of the catalysts from the original dataset. The resulting enantioselectivities are presented in Figure 4.21A, alongside those obtained using 3,5-(OMe)₂ and 3,5-(Me)₂ substituted derivatives **4.6o** and **4.6m** respectively for comparison. With all catalysts other than **4.7b**, hybrid BA **4.6w** afforded the fluorinated product with enantioselectivity similar to that observed with 3,5-(Me)₂ substituted variant **4.6m**, suggesting that the BA steric profile is the dominant factor governing enantioselectivity in these cases. However, in combination with **4.7b**, **4.6w** behaved nearly identically to 3,5-(OMe)₂ substituted variant **4.6o**, suggesting the presence of a specific interaction between the BA methoxy group and the aryl substituent of **4.7b**.

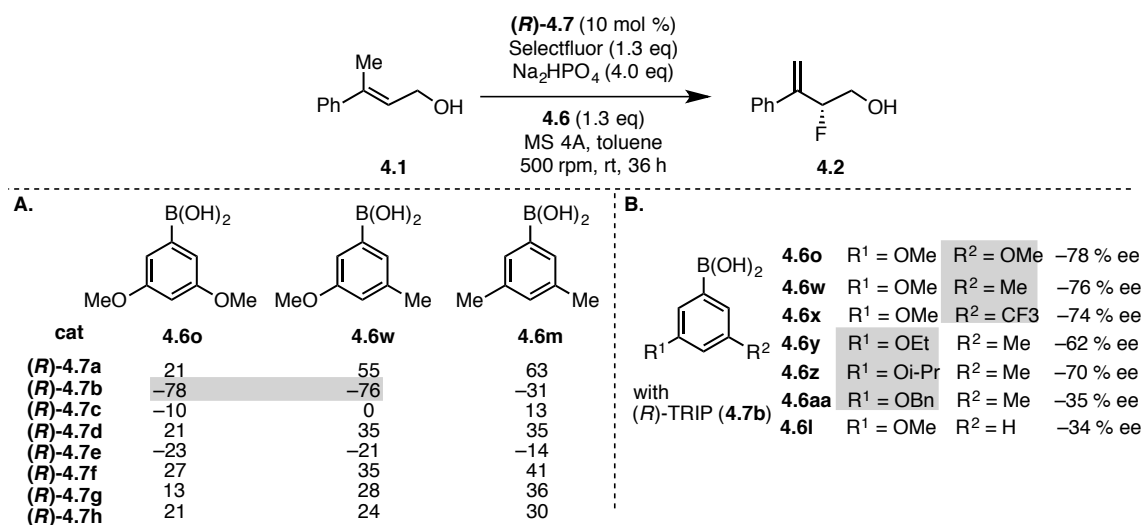


Figure 4.21. (A) Comparison of enantiomeric excess of **4.2** using hybrid BA **4.6w** vs. **4.6o** and **4.6m**. (B) Effect of variation of alkyl vs. alkoxy substituents for various 3,5-disubstituted hybrid BAs

This assertion is further supported by the results provided in Figure 4.21B. Employing a series of hybrid 3,5-disubstituted BAs, holding the alkoxy substituent constant (R₁ = OMe) while varying the second substituent (R₂ = OMe, Me, CF₃) displayed a minimal effect on enantioselectivity. However, for the inverse set of experiments in which the alkyl substituent was held constant (R₂ = Me), variation of the alkoxy group (R₁ = OEt, O*i*-Pr, OBn) had a significant impact on enantioselectivity, consistent with a structural perturbation at this position disrupting the interaction responsible for the observed inverted enantioselectivity. Notably, 3-OMe substituted BA **4.6l** also afforded inverted enantioselectivity but to a lesser degree (-34% ee), suggesting that while an interaction with the methoxy group is present, the overall steric profile of the 3,5-substituted derivatives does play a role. Finally, an intriguing dependence of the interaction in question on catalyst structure was observed. Particularly notable was the observation that

mesityl-substituted catalyst **4.7a**, which possesses the same substitution pattern as **4.7b**, did not furnish **4.2** with inverted selectivity when used in combination with BA **4.6o** (Figure 4.21A). However, an intermediate enantioselectivity value was obtained using hybrid BA **4.6w** compared with **4.6o** and **4.6m** (55% ee vs. 21 and 63% ee respectively), suggesting that the putative direct interaction may be present, but attenuated.

On the basis of the following observations, we propose that a lone pair- π interaction^{106–125} (Figure 4.22) is attenuating enantioselectivity: 1) our experiments isolated the interaction to an alkoxy group at a specific position of the aryl BA, 2) variation of this alkoxy group resulted in drastically altered selectivity, and 3) subtle changes to the catalyst aryl ring had a considerable impact on enantioselectivity. First discovered as a stabilizing element for the conformation of Z-DNA (Figure 4.22),¹¹⁶ the lone pair- π interaction entails an overlap between a heteroatom lone pair and the face of an aromatic ring, and has been demonstrated to be highly dependent on the geometries of both interacting partners.¹²⁰ Several studies have reported the ability of this interaction to alter the overall geometries of molecular complexes by acting in cooperation with other noncovalent interactions such as hydrogen bonding.^{113–115,117,121} Although lone pair- π interactions have been implicated as stereocontrolling elements in asymmetric catalysis computationally,^{124,125} our results serve as compelling experimental support to this end.

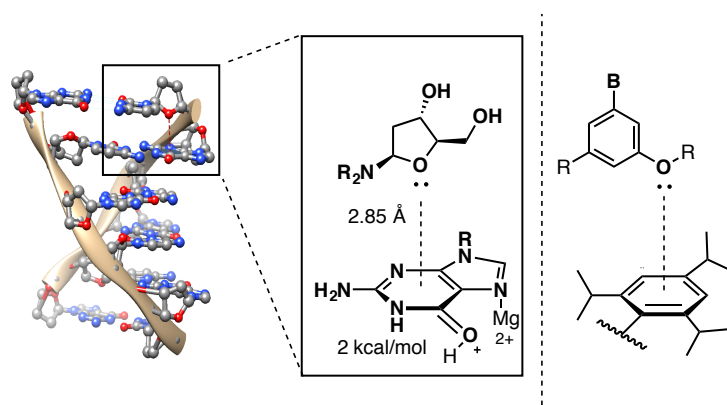


Figure 4.22. Qualitative depiction of the lone pair- π interaction as a stabilizing structural element of Z-DNA (left) and analogy to the present system (right).

We hypothesized that, if an interaction between a methoxy lone pair in **4.6o** and the catalyst aryl ring were important, then control of the orientation of this ring might provide a means to enhance it. Given the apparent trend moving from **4.7a** to **4.7b**, we reasoned that a catalyst with bulkier substituents at the 2,4,6- positions of its aryl rings may serve to reinforce the interaction in question due to better overlap, perhaps owing to a change in the torsional angle between the substituent and the binaphthyl backbone.

To this end, 2,4,6-(Cy)₃-Ph substituted catalyst (*R*)-TCYP (**4.7l**) was employed with **4.6o**, furnishing (*S*)-**4.2** in -92% ee (Figure 4.23). Using this same catalyst with the BA that gave the largest positive enantioselectivity in the initial screen with TRIP (**4.7b**) (4-*i*-Bu-substituted variant **4.6e**), resulted in the formation of (*R*)-**4.2** in 77% ee. Thus, simply by making a subtle structural change to an achiral additive, we are able to tune the enantioselectivity of fluorinated product **4.2** from 77% to -92% (a $\Delta\Delta G^\ddagger$ range of 3 kcal/mol) using the same chiral catalyst **4.7l**. We attribute

this remarkable inversion of enantioselectivity to a subtle, noncovalent interaction between the achiral additive and the chiral catalyst.

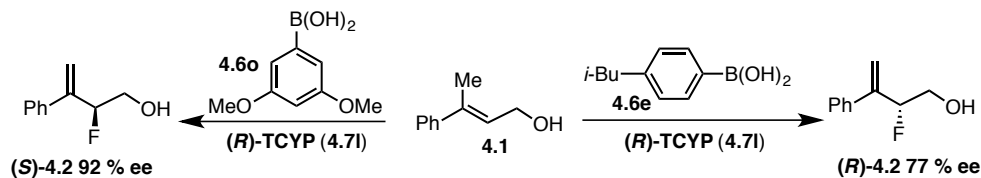


Figure 4.23. Inversion of enantiomeric excess of **4.2** using catalyst **4.71**

Trend Analysis

Having gained sufficient insight regarding several mechanistic regimes in the dataset, we sought to address our initial goal of producing multivariate correlations to describe the catalyst-substrate enantioselectivity imparting interactions (*vide supra*). Examination of Figure 4.9 revealed that the catalysts that were the most sensitive to changes in the BA structure were **4.7a** (2,4,6-(Me)₃-Ph, 3 to 90 % ee), **4.7b** (2,4,6-(*i*-Pr)₃-Ph, -78 to 66 % ee), and **4.7e** (4-(*i*-Pr)-Ph, -60 to 8 % ee). As previously discussed, catalyst **4.7e** likely operates in a mechanistically distinctive fashion and cannot be compared directly with the others. The remainder of the catalysts tested (**4.7c**, **4.7d**, **4.7f-h**) generally displayed ee values over a smaller range indicating less sensitivity to the structure of the BA and were therefore not considered for modeling purposes. Thus, **4.7a** and **4.7b** were selected for modeling, along with their 2,4,6-(Cy)₃-Ph substituted analogue **4.7i**. Figure 4.24 displays the enantioselectivity trend for each catalyst as a function of BA structure. The behavior of all three catalysts is clearly similar for 2- and 4- substituted BAs (Figure 4.24, left), indicating the same interactions are likely involved in determining selectivity in this mechanistic region. However, upon moving to the 3,5-substituted BAs (Figure 4.24, right) there is a noticeable break in the behavior of **4.7a** relative to **4.7b** and **4.7i** demonstrating that the latter two are behaving differently than **4.7a**. Thus, to aid the construction of correlations describing these trends, the dataset was initially divided according to the BA substitution pattern, separating the 2- and 4- from 3,5-substituted aryl BAs.

The first set, consisting of 2- and 4-substituted aryl BAs (Figure 4.25A, light blue), can be modeled using three descriptors that are sensitive to the structures of the reactive partners: the minimal and maximal width Sterimol¹²⁶ steric parameters (B_1 and B_5) describe the BA structure, and the torsion angle between the binaphthyl backbone and 3,3'-substituent describe the catalyst structure. As these are normalized models (see Experimental Section for details), the correlation coefficients denote the relative magnitude of each effect. Thus, we propose that in this region of the dataset, the location of the BA substituent and the accessible conformations of the catalyst aryl rings (represented by the catalyst torsion parameter) dictate the geometry of their interaction at the selectivity determining TS.

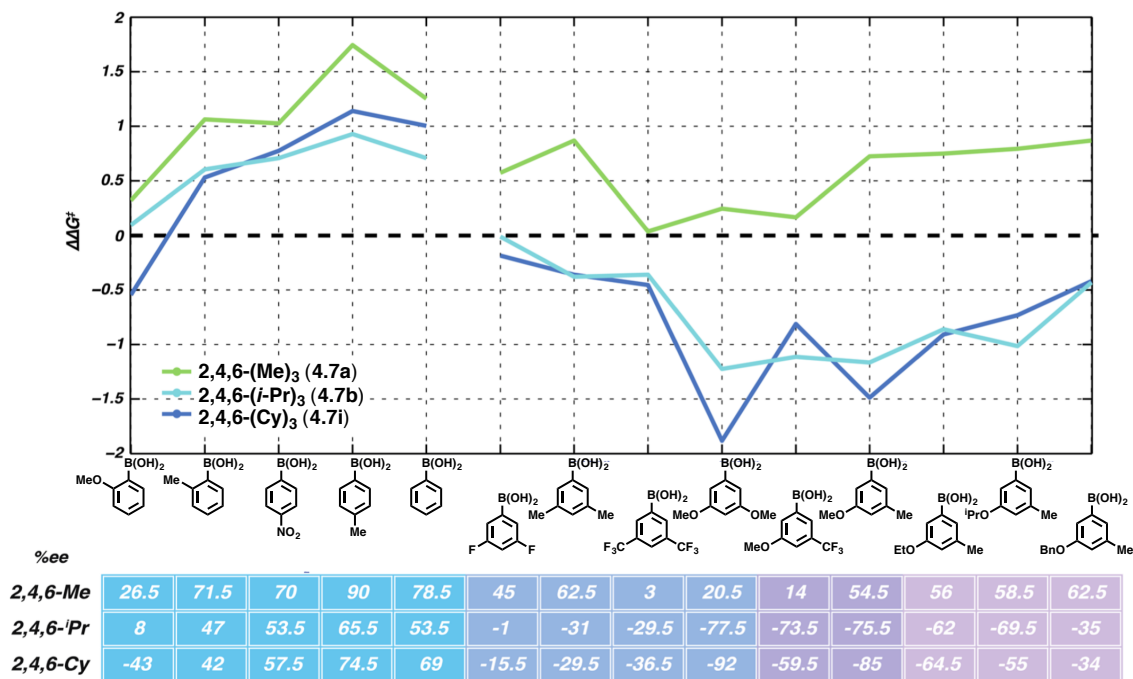


Figure 4.24. Graphical representation of catalyst structure-selectivity trends as a function of BA structure.

Although a statistically robust model was identified for the full set of 3,5-substituted BAs (Figure 4.25B, grey), in addition to catalyst torsion, several BA steric parameters are required to capture the possible TS geometries. Overall, this model seems complex and reveals little regarding the interactions at the origin of asymmetric induction. Thus, this set was further sub-divided according to substitution pattern: those with symmetric substitution or any methoxy substituent (Figure 4.25C, blue) and those with 3-alkoxy-5-methyl substitution (Figure 4.25D, purple). In line with probing a putative lone pair- π interaction, this sub-division keeps the alkoxy substituent constant in one set and the alkyl substituent constant in the other. Although these two models both contain the same molecular descriptors (BA length, L , and catalyst torsion angle), the correlation coefficients of each are slightly different, and the former contains an interaction cross-term (consisting of the infrared BA ring stretch (ν_3)¹²⁷ and catalyst torsion, Figure 4.25C). This cross-term may be necessary to differentiate members of this set containing a methoxy substituent from the other BAs, as the former are presumed to undergo a direct interaction with the catalyst. However, in the 3-alkoxy-5-methyl set (Figure 4.25D), all of the BAs are presumed to undergo the same type of interaction with the catalyst, and thus do not require this additional interaction term. It is particularly intriguing that catalyst torsion has the largest coefficient in both of these models (Figures 4.25C and 4.25D), as these BAs are proposed to undergo a direct interaction with the catalyst that is highly geometry dependent. Because torsion is a major feature differentiating catalyst **4.7a** (2,4,6-(Me)₃-Ph) from **4.7b** and **4.7i** (2,4,6-(*i*-Pr)₃-Ph and 2,4,6-(Cy)₃-Ph respectively), this is also consistent with the divergence in selectivity visibly noticeable in Figure 4.24. These results support the hypothesis that a direct, noncovalent interaction controls enantioselectivity in a manner that is greatly affected by the structures of both the BA and PA, and is proposed to be directing the sizable inversion in enantioselectivity.

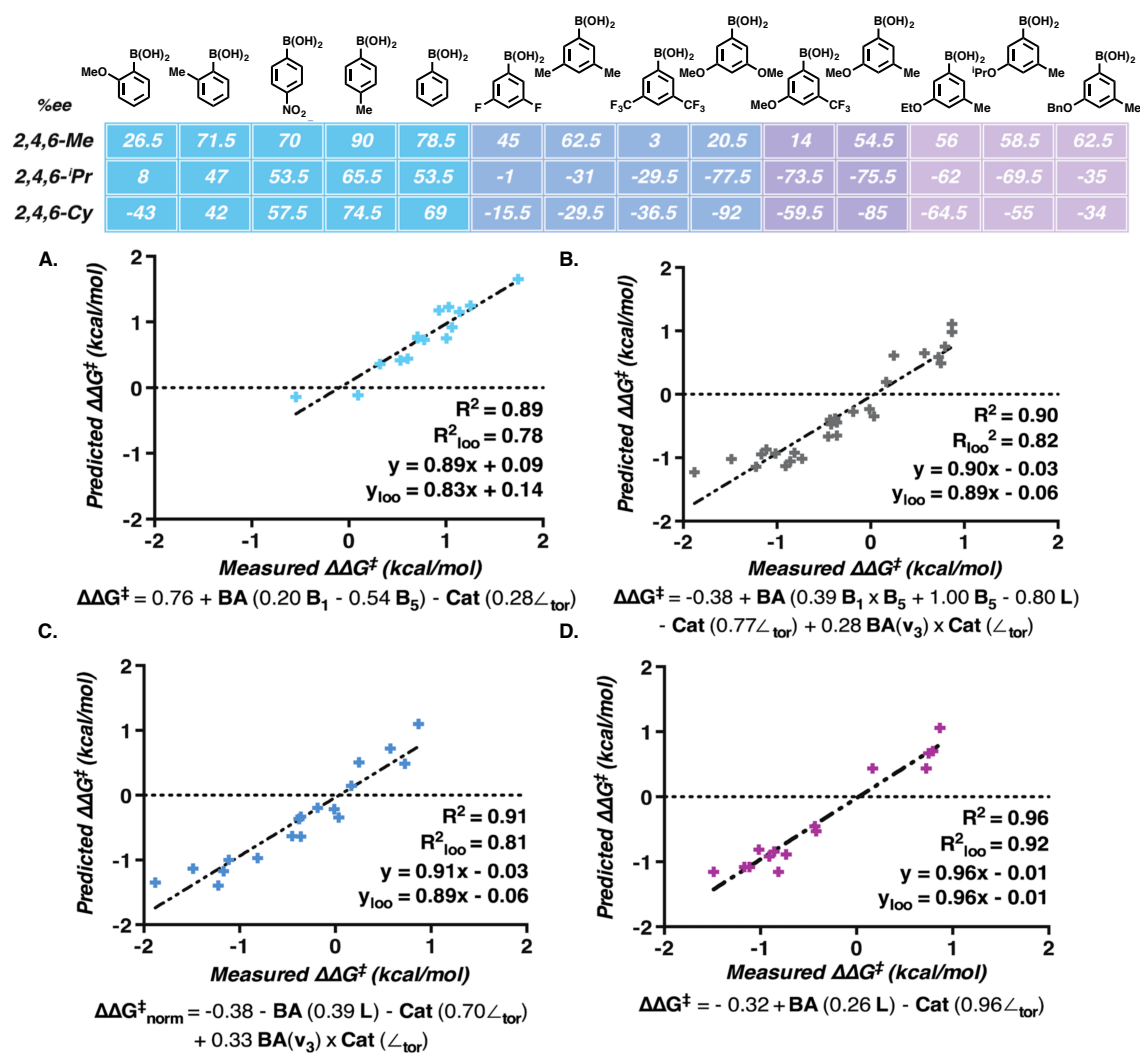


Figure 4.25. Mathematical correlations of normalized normalized catalyst and BA molecular descriptors to enantioselectivity ($\Delta\Delta G^\ddagger$) for 2- and 4-substituted aryl BAs (A), all 3,5-disubstituted aryl BAs (B), 3,5-disubstituted aryl BAs with symmetrical substitution or a methoxy substituent (C), and 3-alkoxy-5-methyl substituted aryl BAs (D).

Conclusion

Often in the field of asymmetric catalysis, there exists an infrequently acknowledged assumption that the trend observed for a particular catalyst with several substrates will hold when structurally analogous catalysts are tested. In fact, it is this line of reasoning that generally drives standard optimization studies. However, in many cases, this assumption does not prove valid. In these instances, the rational design of a dataset that takes the structural variation of multiple reaction components into account can greatly facilitate the identification of regions of structural space where trends break down. We contend that such regions signal potential changes in mechanism in a manner analogous to a break in slope in a classical linear free energy relationship. It is through an understanding of the mechanistic underpinnings of these phenomena that the remainder of the dataset can be contextualized. Furthermore, we contend that this approach facilitates the identification of specific dataset outliers that would be difficult to design *de novo*,

but which can be optimized once identified. Here, we have demonstrated these principles using a dataset of enantioselectivities from an asymmetric BA-directed phosphate-catalyzed fluorination of allylic alcohols. We initially set out to understand the structural underpinnings of enantioselectivity by producing statistical models to describe the entire dataset. However, the recognition that multiple mechanistic pathways may be operative called for a re-evaluation of our strategy. Guided by a highly organized dataset that was designed according to geometric, steric, and electronic criteria, we promptly recognized that not all of the values were directly comparable, presumably due to differences in the mechanisms of asymmetric induction. A series of mechanistic experiments was conducted that shed light on the structural origins of these effects, ultimately leading to a catalytic system capable of producing either enantiomer of a chiral fluorinated building block in high enantioselectivity. The insights gained in this study can be generalized to countless situations in which structural features of the catalysts and substrates may alter the mechanism through which selectivity is induced. It is our current goal to apply these approaches to new reaction development, facilitating both a foundational guide to catalyst design and a rapid identification of mechanistic outliers.

Experimental Section

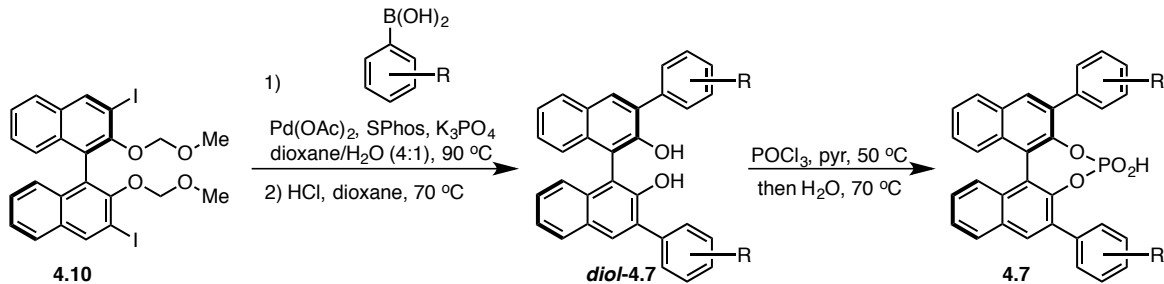
General Information

Unless otherwise noted, all reagents were purchased from commercial suppliers and used without further purification. Enantioselective fluorination reactions were run in 1 dram vials equipped with a screw cap and stirred using a magnetic Teflon stir bar, placed on the surface of a magnetic stir plate. Due to the heterogeneous nature of these reactions, it was important that fast and efficient stirring be maintained over the course of the reaction in order to obtain optimal results. Tetrahydrofuran, dichloromethane, diethyl ether, toluene, triethylamine and N,N-dimethylformamide were purified by passage through an activated alumina column under argon. Thin-layer chromatography (TLC) analysis of reaction mixtures was performed using Merck silica gel 60 F254 TLC plates, and visualized under UV or by staining with ceric ammonium molybdate or KMnO₄. Column chromatography was performed on Merck Silica Gel 60 Å, 230 X 400 mesh. Nuclear magnetic resonance (NMR) spectra were recorded using Bruker AV-600, AV-500, DRX-500, AVQ-400, AVB-400 and AV-300 spectrometers. ¹H and ¹³C chemical shifts are reported in ppm downfield of tetramethylsilane and referenced to residual solvent peak (CHCl₃; δH = 7.26 ppm and δC = 77.0 ppm, DMSO; δH = 2.50 and δC = 39.5 ppm). Multiplicities are reported using the following abbreviations: s = singlet, d = doublet, t = triplet, q = quartet, app t = apparent triplet, m = multiplet, br = broad resonance. Solvent abbreviations are reported as follows: EtOAc = ethyl acetate, hex = hexanes, DCM = dichloromethane, Et₂O = diethyl ether, MeOH = methanol, THF = tetrahydrofuran, DMF = N,N-dimethylformamide, Et₃N = triethylamine. Mass spectral data were obtained from the Micro-Mass/Analytical Facility operated by the College of Chemistry, University of California, Berkeley. Enantiomeric excesses were measured on a Shimadzu VP Series Chiral HPLC using Chiralpak IA, IB, or IC columns. The syntheses of catalysts **4.7a**,¹²⁸ **4.7b**,⁶⁷ **4.7c**,¹²⁹ **4.7f**,¹²⁸ **4.7g**,¹³⁰ **4.7h**,¹³¹ and **4.7l**,¹³² have been previously reported.

Synthesis of Catalysts

Catalysts **4.7d** and **4.7e** were prepared according to the reaction sequence depicted in Scheme 4.1.

Scheme 4.1. Synthesis of catalysts 4.7



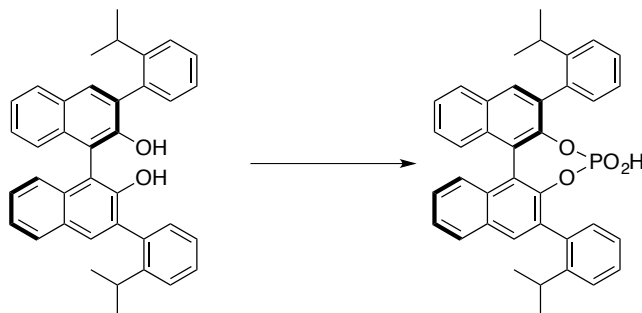
General Procedure A: Synthesis of diols *diol-4.7*:

To a magnetically-stirred solution of (*R*)-3,3'-diiodo-2,2'-bis(methoxymethoxy)-1,1'-binaphthalene¹³³ (**4.10**, 1.00 g, 1.6 mmol) in dioxane (16 mL) were added the appropriate aryl boronic acid (3.0 equiv, 4.8 mmol), palladium (II) acetate (0.05 equiv, 0.018 g, 0.08 mmol), SPhos (0.1 equiv, 0.066 g, 0.16 mmol) and tribasic potassium phosphate (4.0 equiv, 1.36 g, 6.4 mmol) which had been dissolved in H_2O (4 mL). After degassing this mixture under high vacuum (X 3), it has heated at 90 °C under and atmosphere of nitrogen with stirring. Upon complete consumption of **S1**, as judged by TLC analysis, the reaction mixture was allowed to cool to room temperature and filtered through Celite, the filter cake rinsed with EtOAc. After separating the organic layer, the aqueous layer was extracted with EtOAc (3 X 20 mL). The combined organic extracts were washed with brine (20 mL), dried (Na_2SO_4) and concentrated *in vacuo*. The crude residue was purified by column chromatography on silica gel using Hexs/EtOAc as eluent (20:1). The resulting purified material was dissolved in dioxane (0.05 M) and conc. HCl (1 mL) was added. This mixture was magnetically stirred at 70 °C for 2 h. After cooling to rt, the reaction mixture was concentrated *in vacuo*. The resulting residue was dissolved in DCM (25 mL) and washed with sat. aq. NaHCO_3 (40 mL), H_2O (25 mL) and brine (25 mL), dried (Na_2SO_4) and concentrated *in vacuo*. The crude residue was purified by column chromatography on silica gel using Hexs/EtOAc as eluent (20:1 to 10:1).

General Procedure B: Synthesis of Phosphoric Acids 4.7:

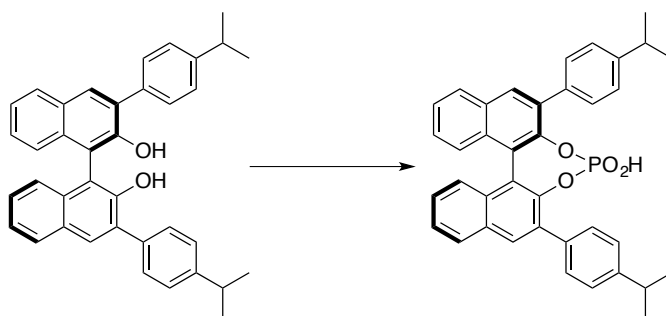
To a magnetically-stirred solution of diol *diol-4.7* (1.0 equiv) in pyridine (0.05 M) was added phosphorus (V) oxychloride (3.0 equiv) *via* syringe under an atmosphere of nitrogen and the resulting mixture was heated at 50 °C. After complete consumption of *diol-4.7*, as judged by TLC analysis (typically 1-6 h), H_2O (equal volume to pyridine) was added and the mixture heated at 70 °C. After 3h, the mixture was allowed to cool to room temperature and diluted with DCM (25 mL). The mixture was washed with 3 N HCl (3 X 25 mL) and concentrated *in vacuo*. The crude residue was purified by column chromatography using DCM/MeOH as eluent. The fractions that contained the desired product were concentrated to a volume of *ca.* 30 mL and washed with 3 N HCl.¹³⁴ The resulting organic layer was collected and concentrated to dryness *in vacuo*.

(R)-4-hydroxy-2,6-bis(2-isopropylphenyl)dinaphtho[2,1-d:1',2'-f][1,3,2]dioxaphosphepine 4-oxide (4.7d)



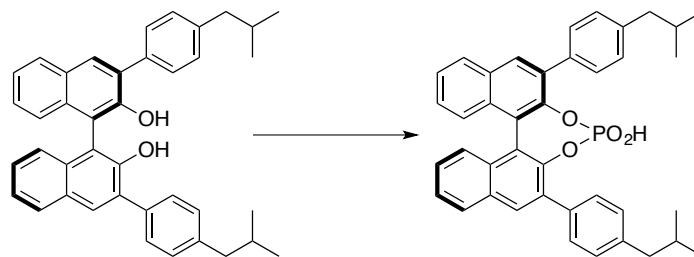
Subjection of *diol-4.7d*¹³⁵ (0.405 g, 0.776 mmol) to General Procedure B gave the title compound (0.346 g, 0.592 mmol, 76 % yield) as a white solid after purification by column chromatography on silica gel using DCM/MeOH as eluent (DCM to 10:1 DCM:MeOH). ¹H NMR (500 MHz, DMSO-*d*₆) δ 8.22-7.98 (m, 4H), 7.63-7.48 (m, 2.8H), 7.48-7.34 (m, 6.8H), 7.32-7.15 (m, 4.3H), 3.07-2.93 (m, 0.5H), 2.84-2.70 (m, 1.5H), 1.43-0.93 (m, 12H). This spectrum complicated due to presence of rotamers. A similar observation was noted by List and coworkers for a similar compound.⁹ ¹³C NMR (126 MHz, CDCl₃) δ 147.4, 147.0, 146.9, 145.0, 144.8, 134.9, 134.8, 134.7, 134.4, 133.4, 132.1, 132.0, 131.9, 131.7, 131.0, 130.9, 128.4, 128.3, 128.2, 127.2, 126.5, 126.4, 126.3, 126.0, 125.9, 125.3, 124.7, 124.6, 122.6, 121.8, 30.6, 30.0, 29.9, 26.1, 26.0, 25.4, 24.9, 23.6, 23.5, 23.4. These data include signals due to the presence of rotamers as well as unassigned C-P couplings. ³¹P NMR (243 MHz, CDCl₃) δ 4.5, 3.9, 3.4, 1.5. These data include signals due to the presence of rotamers.

®-4-hydroxy-2,6-bis(4-isopropylphenyl)dinaphtho[2,1-d:1',2'-f][1,3,2]dioxaphosphepine 4-oxide (4.7e)



Subjection of diol *diol-4.7e* (0.500 g, 0.956 mmol) to General Procedure B gave the title compound (0.463 g, 0.793 mmol, 83 % yield) as a white solid after purification by column chromatography on silica gel using DCM/MeOH as eluent (DCM to 20:1 DCM:MeOH). ¹H NMR (500 MHz, CDCl₃) δ 8.78 (brs, 1H), 8.02 (s, 2H), 7.95 (d, *J* = 8.1 Hz, 2H), 7.55 (app d, *J* = 7.7 Hz, 4H), 7.50 (app t, *J* = 7.3 Hz, 2H), 7.36 (d, *J* = 8.3 Hz, 2H), 7.31 (app t, *J* = 7.4 Hz, 2H), 7.17 (app d, *J* = 7.6 Hz, 4H), 2.73 (m, 2H), 1.05 (d, *J* = 6.5 Hz, 6H), 1.04 (d, *J* = 6.5 Hz, 6H). ¹³C NMR (126 MHz, CDCl₃) δ 148.2, 144.5 (d, *J* = 9.3 Hz), 134.1, 134.0, 131.8, 131.6, 131.3, 129.6, 128.3, 127.1, 126.4, 126.3, 125.9, 122.4, 33.7, 23.7, 23.6. ³¹P NMR (243 MHz, CDCl₃) δ 3.60. HRMS (ESI) found [M-H]⁻ 583.2028, C₃₈H₃₂O₄P requires 583.2044.

®-4-hydroxy-2,6-bis(4-isobutylphenyl)dinaphtho[2,1-*d*:1',2'-*f*][1,3,2]dioxaphosphepine 4-oxide (4.7k)

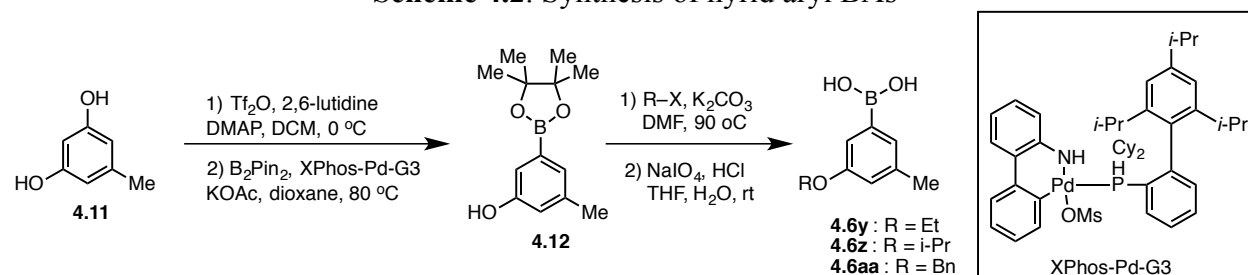


Subjection of **diol-4.7k** (0.542 g, 0.984 mmol) to General Procedure B gave the title compound (0.361 g, 0.589 mmol, 60 % yield) as a white solid after purification by column chromatography on silica gel using DCM/MeOH as eluent (DCM to 9:1 DCM:MeOH). ¹H NMR (500 MHz, CDCl₃) δ 8.04 (s, 2H), 7.98 (d, *J* = 8.0 Hz, 2H), 7.55 (app d, *J* = 7.4 Hz, 4H), 7.51 (app t, *J* = 7.5 Hz, 4H), 7.37 (d, 2H), 7.33 (d, *J* = 7.1 Hz, 2H), 7.10 (app d, *J* = 7.4 Hz, 4H), 2.34 (d, *J* = 6.8 Hz, 4H), 1.74 (hept, *J* = 6.6 Hz, 2H), 0.73 (d, *J* = 6.4 Hz, 12H). ¹³C NMR (126 MHz, CDCl₃) δ 144.6 (d, *J* = 9.1 Hz), 141.3, 134.0, 131.9, 131.6, 131.3, 129.5, 129.0, 128.4, 127.1, 126.4, 125.9, 122.5, 122.4, 45.1, 30.0, 22.4, 22.3. ³¹P NMR (202 MHz, CDCl₃) δ 3.64. HRMS (ESI) found [M-H]⁻ 611.2340, C₄₀H₃₆O₄P requires 611.2357.

Synthesis of Boronic Acids

Boronic acids **4.6y**, **4.6z**, and **4.6aa** were prepared according to the reaction sequence depicted in Scheme 4.2.

Scheme 4.2. Synthesis of hybrid aryl BAs



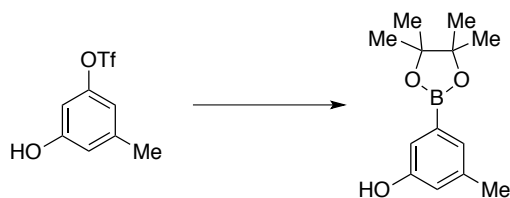
3-hydroxy-5-methylphenyl trifluoromethanesulfonate



To a magnetically-stirred solution of 5-methylbenzene-1,3-diol (5.50 g, 44.3 mmol) in DCM (50 mL) were added trifluoromethanesulfonic anhydride (7.45 mL, 44.3 mmol), 2,6-lutidine (5.65 mL, 48.9 mmol), and 4-dimethylaminopyridine (0.100 g, 0.820 mmol) at 0 °C. The reaction mixture was allowed to warm to rt and stirred for 3h. The reaction mixture was diluted with sat. aq. ammonium chloride (50 mL) and extracted with EtOAc (2 X 50 mL). The combined organic layers were washed with brine (50 mL), dried (Na₂SO₄) and concentrated *in vacuo*. The crude

residue was purified by column chromatography on silica gel using Hexs/EtOAc as eluent (6:1 to 4:1) to afford the title compound (5.18 g, 20.2 mmol, 46 % yield) as a viscous amber oil. $^1\text{H NMR}$ (500 MHz, CD_3CN) δ 7.53 (brs, 1H), 6.77 (s, 1H), 6.74 (s, 1H), 6.65 (s, 1H), 2.33 (s, 3H). The $^1\text{H NMR}$ data match those reported in the literature.¹⁰

3-methyl-5-(4,4,5,5-tetramethyl-1,3,2-dioxaborolan-2-yl)phenol (4.12)

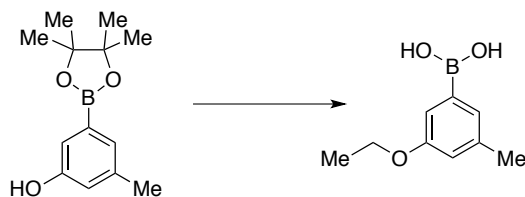


To a magnetically-stirred solution of 3-hydroxy-5-methylphenyl trifluoromethanesulfonate (2.56 g, 10.0 mmol) in toluene (25 mL) and dioxane (15 mL) was added bis(pinacolato)diboron (2.78 g, 11.0 mmol), potassium acetate (2.94 g, 30.0 mmol), and XPhos Pd G3 (0.169 g, 0.2 mmol). The mixture was heated at 95 °C with stirring under an atmosphere of nitrogen. After 16 h, the mixture was diluted with sat. aq. ammonium chloride and extracted with EtOAc (3 X 25 mL). The combined organic extracts were washed with brine (25 mL), dried (Na_2SO_4) and concentrated *in vacuo*. The crude residue was purified by column chromatography on silica gel using Hexs/EtOAc as eluent (12:1 to 10:1) to give the title compound (1.97 g, 8.4 mmol, 84 % yield) as a clear yellow oil. $^1\text{H NMR}$ (500 MHz, CDCl_3) δ 7.29 (s, 1H), 7.23 (s, 1H), 7.07 (s, 1H), 6.80 (s, 1H), 2.33 (s, 3H), 1.36 (s, 12H). The $^1\text{H NMR}$ data match those reported in the literature.¹³⁶

General Procedure C: Preparation of Boronic Acids 4.6y, 4.6z, and 4.6aa:

To a magnetically-stirred solution of phenol **4.12** (1.0 equiv) in DMF (0.2 M) were added alkyl halide (2.0 equiv) and potassium carbonate (3.0 equiv). The resulting mixture was heated at 90 °C with stirring. Upon complete consumption of **4.12**, as judged by TLC analysis, the reaction mixture was allowed to cool to room temperature and diluted with sat. aq. ammonium chloride (20 mL) and extracted with EtOAc (2 X 30 mL). The organic extracts were washed with H_2O (5 X 30 mL) and brine (30 mL), dried (Na_2SO_4) and concentrated *in vacuo*. The crude residue was purified by column chromatography on silica gel using Hexs/EtOAc as eluent (20:1). The resulting purified material was dissolved in THF/ H_2O (2:1, 0.2 M) and NaIO_4 (3.0 equiv) was added and the mixture was magnetically stirred. After 15 min, 1 M HCl (5 mL) was added and the reaction mixture was stirred at rt for 4h at which point it was extracted with EtOAc (3 X 15 mL). The combined organic extracts were washed with brine (20 mL), dried (Na_2SO_4) and concentrated *in vacuo*. The crude residue was triturated with hexanes and the resulting white solid collected *via* vacuum filtration.

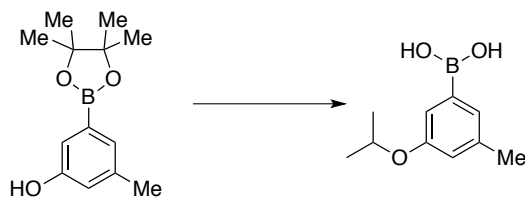
(3-ethoxy-5-methylphenyl)boronic acid (4.6y)



Subjection of phenol **4.12** (0.400 g, 1.71 mmol) and ethyl iodide (0.275 mL, 3.42 mmol) to General Procedure C gave the title compound (0.110 g, 0.611 mmol, 36 % yield over two steps) as a fluffy

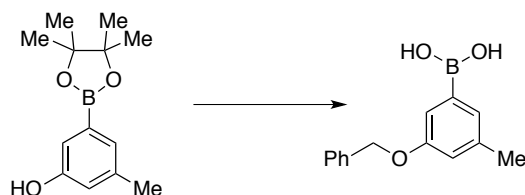
white solid. $^1\text{H NMR}$ (500 MHz, CDCl_3) δ 7.95 (s, 2H), 7.18 (s, 1H), 7.15 (s, 1H), 6.76 (s, 1H), 3.99 (app brs, 2H), 2.27 (s, 3H), 1.32 (app brs, 3H). $^{13}\text{C NMR}$ (126 MHz, CDCl_3) δ 158.4, 138.1, 135.8, 127.6, 117.4, 117.1, 63.1, 21.6, 15.3. **HRMS** (EI) found $[\text{M}-\text{H}]^-$ 179.0884, $\text{C}_9\text{H}_{12}\text{O}_3\text{B}$ requires 179.0885.

(3-isopropoxy-5-methylphenyl)boronic acid (4.6z)



Subjection of phenol **4.12** (0.400 g, 1.71 mmol) and isopropyl bromide (0.321 mL, 3.42 mmol) to General Procedure C gave the title compound (0.178 g, 0.918 mmol, 54 % yield over two steps) as a fluffy white solid. $^1\text{H NMR}$ (500 MHz, CDCl_3) δ 7.97 (s, 2H), 7.14 (s, 1H), 7.13 (s, 1H), 6.75 (s, 1H), 4.57 (hept, $J = 11.7, 5.7$ Hz, 1H), 2.26 (s, 3H), 1.25 (d, $J = 6.3$ Hz, 6H). $^{13}\text{C NMR}$ (126 MHz, CDCl_3) δ 157.4, 138.1, 127.6, 118.8, 118.4, 69.3, 22.5, 21.6. **HRMS** (EI) found $[\text{M}]^+$ 194.1114, $\text{C}_{10}\text{H}_{15}\text{BO}_3$ requires 194.1114.

(3-(benzyloxy)-5-methylphenyl)boronic acid (4.6aa)

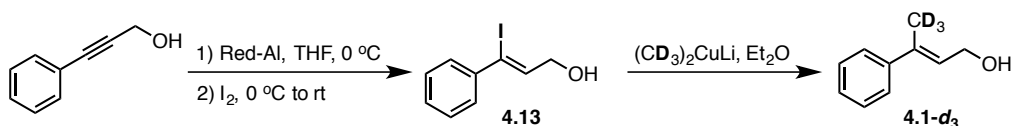


Subjection of phenol **4.12** (0.400 g, 1.71 mmol) and benzyl bromide (0.406 mL, 3.42 mmol) to General Procedure C gave the title compound (0.228 g, 0.942 mmol, 55 % yield over two steps) as a fluffy white solid. $^1\text{H NMR}$ (500 MHz, CDCl_3) δ 8.00 (s, 2H), 7.45 (d, $J = 7.3$ Hz, 2H), 7.40 (app t, $J = 7.4$ Hz, 2H), 7.33 (t, $J = 6.9$ Hz, 1H), 7.25 (s, 1H), 7.20 (s, 1H), 6.88 (s, 1H), 5.08 (s, 2H), 2.28 (s, 3H). $^{13}\text{C NMR}$ (126 MHz, CDCl_3) δ 158.3, 138.2, 137.9, 128.9, 128.2, 128.1, 128.0, 117.7, 117.5, 69.4, 21.6. **HRMS** (ESI) found $[\text{M}-\text{H}]^-$ 241.1040, $\text{C}_{14}\text{H}_{14}\text{BO}_3$ requires 241.1041.

Synthesis of Deuterated Substrate 4.1-d₃

The synthesis of substrate **4.1-d₃** was adapted from the previously-reported method,⁵⁶ and was accomplished according to the reaction sequence depicted in Scheme 4.3.

Scheme 4.3. Synthesis of deuterated substrate 4.1-d₃



(E)-3-phenylbut-2-en-1-ol-*d*₃ (4.1-*d*₃)



To a magnetically-stirred solution of iodomethane-*d*₃ (0.62 mL, 10.0 mmol) in Et₂O (20 mL) was added *tert*-butyllithium (1.7 M in pentane, 11.7 mL, 20.0 mmol) at -78 °C. After 30 min, the reaction mixture was warmed to 0 °C and copper (I) iodide (0.95 g, 5.0 mmol) was added. After 30 min at this temperature, the reaction mixture was again cooled to -78 °C and a solution of vinyl iodide **S5**¹³⁷ (0.52 g, 2.0 mmol) in Et₂O (20 mL) was added. The reaction mixture was allowed to warm to 0 °C and then rt. After complete consumption of the starting material, as judged by TLC analysis, sat. aq. ammonium chloride (50 mL) was added and the mixture was extracted with EtOAc (3 X 25 mL). The combined organic layers were washed with brine (25 mL), dried (Na₂SO₄) and concentrated *in vacuo*. The crude residue was purified by column chromatography on silica gel, using Hexs/EtOAc as eluent (6:1) to give the title compound (0.181 g, 1.20 mmol, 60 % yield) as a clear, colorless oil. *Note: As previously noted,⁵⁶ the purified product contained 15 mol % (89 wt. %) cinnamyl alcohol that was unable to be separated. This was taken into account when measuring material for the experiments reported herein.* ¹H NMR (500 MHz, CDCl₃) δ 7.44 (d, *J* = 7.4 Hz, 2H), 7.36 (t, *J* = 7.5 Hz, 2H), 7.30 (t, *J* = 5.9 Hz, 1H), 6.02 (t, *J* = 6.7 Hz, 1H), 4.40 (d, *J* = 6.6 Hz, 2H). ¹³C NMR (126 MHz, CDCl₃) δ 142.8, 137.8, 128.3, 127.3, 126.5, 125.8, 60.0, 15.3 (app t, *J* = 20.1 Hz). HRMS (EI) found [M]⁺ 151.1076, C₁₀H₉D₃O requires 151.1076.

General Procedure for Enantioselective Fluorination Reactions:

A stock solution of allylic alcohol **4.1** (0.1 M in toluene) was prepared immediately prior to use. A 1-dram vial was charged with the appropriate catalyst (0.005 mmol), boronic acid (0.065 mmol), Na₂HPO₄ (0.20 mmol), MS 4A (0.040 g) and an 8 mm Teflon magnetic stir bar. To this vial was added 0.5 mL of the substrate stock solution and the resulting mixture was placed directly onto the surface of a stirring plate and allowed to stir at 500 rpm. After 30 min, Selectfluor (0.023 g, 0.065 mmol) was added to the vial and the mixture was again placed directly on the surface of the stirring plate and allowed to stir at 500 rpm. After the designated time, the reaction mixture was filtered through a plug of silica gel using DCM (3 mL) as eluent. The filtrate was concentrated *in vacuo* and the residue taken up in 10 % IPA/hexs and the enantiomeric excess analyzed directly by HPLC using a chiral stationary phase (Chiralpak IB column, 99:01 hexanes:isopropanol, 1 mL/min); *t*_r = 26.2, 32.1 min). Spectral data for allylic fluoride **4.2** have been previously reported.⁵⁶

Note: Due to the heterogeneity of the reaction mixtures it was essential that fast and efficient stirring be maintained throughout the course of the reactions. This was achieved by placing the vials containing the reaction mixtures directly on the surface of the stir plate, maintaining a stir rate of 500 rpm.

Note: Each enantioselectivity value was obtained in duplicate to ensure reproducibility. In each case, it was confirmed that the enantioselectivity did not change as a function of conversion,

4.6g	4.6h	4.6i	4.6j	4.6k	4.6l
ee₁ ee₂	ee₁ ee₂	ee₁ ee₂	ee₁ ee₂	ee₁ ee₂	ee₁ ee₂
4.7a — —	4.7a — —	4.7a — —	4.7a — —	4.7a — —	4.7a — —
4.7b 65 67	4.7b 38 40	4.7b 41 41	4.7b 22 22	4.7b 46 47	4.7b -32 -35
4.7c — —	4.7c — —	4.7c — —	4.7c — —	4.7c — —	4.7c — —
4.7d — —	4.7d — —	4.7d — —	4.7d — —	4.7d — —	4.7d — —
4.7e — —	4.7e 0 -4	4.7e — —	4.7e — —	4.7e — —	4.7e — —
4.7f — —	4.7f — —	4.7f — —	4.7f — —	4.7f — —	4.7f — —
4.7g — —	4.7g — —	4.7g — —	4.7g — —	4.7g — —	4.7g — —
4.7h — —	4.7h — —	4.7h — —	4.7h — —	4.7h — —	4.7h — —
4.7i — —	4.7i — —	4.7i — —	4.7i — —	4.7i — —	4.7i — —

4.6m	4.6n	4.6o	4.6p	4.6q	4.6r
ee₁ ee₂	ee₁ ee₂	ee₁ ee₂	ee₁ ee₂	ee₁ ee₂	ee₁ ee₂
4.7a 62 63	4.7a 3 3	4.7a 20 21	4.7a 72 71	4.7a — —	4.7a 25 28
4.7b -31 -31	4.7b -28 -31	4.7b -77 -78	4.7b 47 47	4.7b 44 42	4.7b 9 7
4.7c 10 15	4.7c -7 -5	4.7c -12 -8	4.7c 18 14	4.7c — —	4.7c 13 12
4.7d 33 37	4.7d 2 1	4.7d 22 20	4.7d 11 8	4.7d — —	4.7d 7 2
4.7e -12 -16	4.7e 9 7	4.7e -23 -22	4.7e -61 -58	4.7e -12 -14	4.7e -49 -48
4.7f 40 42	4.7f 15 18	4.7f 23 31	4.7f 24 21	4.7f — —	4.7f 2 4
4.7g 37 34	4.7g 13 14	4.7g 12 14	4.7g -15 -16	4.7g — —	4.7g -12 -15
4.7h 29 31	4.7h 6 6	4.7h 21 21	4.7h -8 -8	4.7h — —	4.7h -6 -6
4.7i -30 -29	4.7i -37 -36	4.7i -91 -93	4.7i 44 40	4.7i — —	4.7i -44 -42

4.6s	4.6t	4.6u	4.6v	4.6w	4.6x
ee₁ ee₂	ee₁ ee₂	ee₁ ee₂	ee₁ ee₂	ee₁ ee₂	ee₁ ee₂
4.7a — —	4.7a — —	4.7a — —	4.7a 54 55	4.7a 13 15	4.7a 55 57
4.7b 40 35	4.7b 0 0	4.7b 0 0	4.7b -74 -77	4.7b -73 -74	4.7b -61 -63
4.7c — —	4.7c — —	4.7c — —	4.7c 0 —	4.7c — —	4.7c — —
4.7d — —	4.7d — —	4.7d — —	4.7d 36 34	4.7d — —	4.7d — —
4.7e — —	4.7e — —	4.7e — —	4.7e -21 -21	4.7e 11 10	4.7e — —
4.7f — —	4.7f — —	4.7f — —	4.7f 37 32	4.7f — —	4.7f — —
4.7g — —	4.7g — —	4.7g — —	4.7g 30 26	4.7g — —	4.7g — —
4.7h — —	4.7h — —	4.7h — —	4.7h 24 24	4.7h — —	4.7h — —
4.7i — —	4.7i — —	4.7i — —	4.7i -85 -85	4.7i -57 -62	4.7i -62 -67

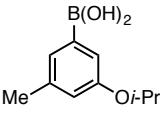
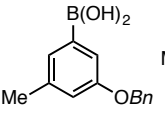
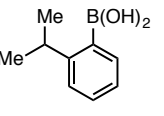
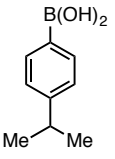
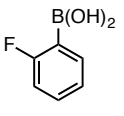
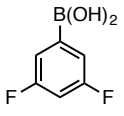
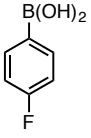
 4.6z			 4.6aa																	
ee₁	ee₂		ee₁	ee₂		ee₁	ee₂		ee₁	ee₂		ee₁	ee₂		ee₁	ee₂				
4.7a	57	60	4.7a	62	63	4.7a	—	—	4.7a	—	—	4.7a	46	44	4.7a	—	—			
4.7b	-68	-71	4.7b	-35	-35	4.7b	—	—	4.7b	—	—	4.7b	-2	0	4.7b	—	—			
4.7c	—	—	4.7c	—	—	4.7c	—	—	4.7c	—	—	4.7c	—	—	4.7c	—	—			
4.7d	—	—	4.7d	—	—	4.7d	—	—	4.7d	—	—	4.7d	—	—	4.7d	—	—			
4.7e	—	—	4.7e	—	—	4.7e	-13	-14	4.7e	-55	-55	4.7e	-8	-6	4.7e	-50	-48			
4.7f	—	—	4.7f	—	—	4.7f	—	—	4.7f	—	—	4.7f	—	—	4.7f	—	—			
4.7g	—	—	4.7g	—	—	4.7g	—	—	4.7g	—	—	4.7g	—	—	4.7g	—	—			
4.7h	—	—	4.7h	—	—	4.7h	—	—	4.7h	—	—	4.7h	—	—	4.7h	—	—			
4.7i	-55	-55	4.7i	-32	-36	4.7i	—	—	4.7i	—	—	4.7i	-16	-15	4.7i	—	—			

Figure 4.26. Complete set of enantioselectivity data for all BA-PA combinations

The raw data for the nonlinear effect (NLE) plots are presented in Figure 4.27.

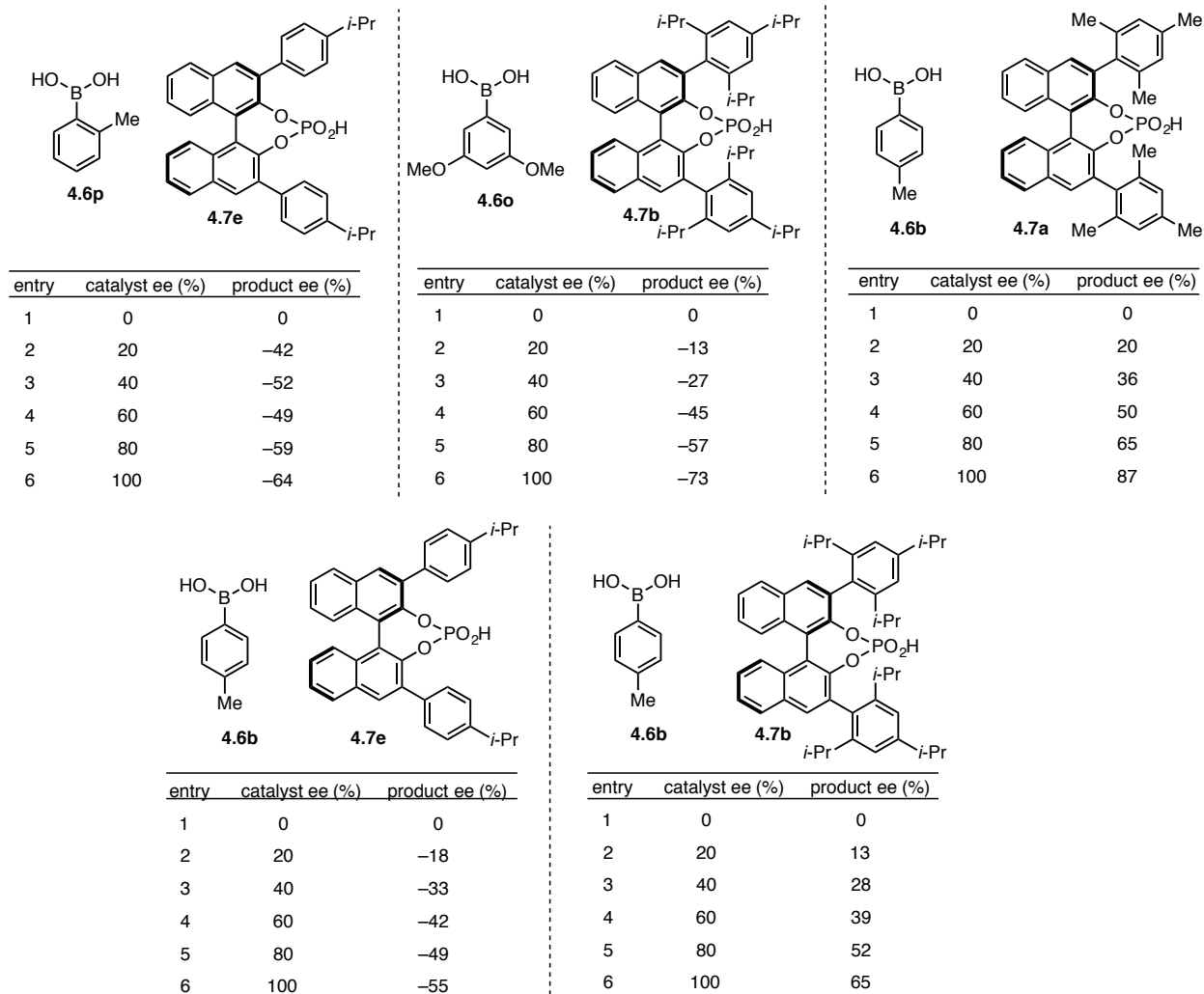
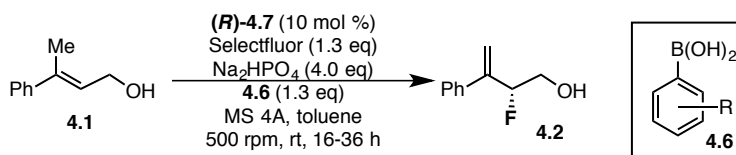


Figure 4.27. Enantioselectivity data used for creation of NLE plots

Hammett Plot

In addition to the data presented in Figure 4.9 of the main text, data was collected using catalyst **4.7e** in combination with several additional boronic acids. Table 4.3 presents all enantioselectivity data obtained with catalyst **4.7e**, organized from largest to smallest ee. Each enantioselectivity value was measured a minimum of two times. Qualitatively, electron rich boronic acids tend to result in larger enantioselectivities than their electron poor analogues, regardless of substitution pattern. For all 4- and 3- substituted boronic acids, the corresponding σ_{para} values used for the creation of the linear free energy relationship in Figure 4.17 are also presented.

Table 4.3. Complete enantioselectivity data using catalyst **4.7e**



entry	R	σ_{meta}	σ_{para}	ee ₁	ee ₂
1	2-Me	—	—	-61	-58
2	4- <i>i</i> -Pr	-0.04	-0.15	-55	-55
3	4-Me	-0.07	-0.17	-57	-55
4	H	0	0	-51	-52
5	4-F	0.34	0.06	-50	-48
6	2-OMe	—	—	-49	-48
7	2- <i>i</i> -Pr	—	—	-13	-14
8	3,5-(OMe) ₂	0.12	-0.27	-23	-22
9	3,5-(Me) ₂	-0.07	-0.17	-12	-16
10	2-CF ₃	—	—	-12	-14
11	3,5-(F) ₂	0.34	0.06	-8	-6
12	2-F	—	—	-8	-8
13	4-NO ₂	0.71	0.78	-8	-7
14	3,5-(CF ₃) ₂	0.43	0.54	9	7

Computations

Geometry optimizations and frequency calculations were carried out using Gaussian 09 software, Revision D.01.¹³⁹ The functional used for DFT calculation is M06-2X, which was previously benchmarked for thermodynamic and kinetic accuracy of main group elements, and for non-covalent interactions.^{140,141} A triple zeta potential basis-set (def2-TZVP)^{142,143} was chosen based on Zhao and Truhlar's evaluation of the M06-2x functional for organic molecules, indicating that a triple zeta quality is generally more quantitative.¹⁴⁰ As this study seeks correlations, we opted not to incorporate scaling factors for vibrational terms.¹⁴⁴ This simplification was justified by the assumption that a constant scaling factor would neither change the descriptive parameters identified, nor the relationship between them. Sterimol values were calculated for the geometry optimized structures using Molecular Modeling Pro[®].¹⁴⁵

Model development

In the current study, since aryl rings on both the catalyst and boronic acids were modified, a common parameter set was sought to simplify the computational procedure. Therefore, a combination of Sterimol¹²⁶ parameters and computationally-derived vibrational frequencies and intensities¹²⁷ were pursued from geometry optimized carboxylic acid structures, as these

measurements were thought to be descriptive of the structural features of the aryl rings at the catalyst 3, 3' positions, and those of the boronic acids. For this purpose, gas-phase ground-state energy minimization and vibrational frequency calculations were carried out. Additionally, for the boronic acids Hammett σ -meta and σ -para values were collected, and for the catalysts the torsion (dihedral) angles between the carboxylic acid carbonyl and aryl ring were measured. These carboxylic acid structures represent truncated moieties of the catalyst and boronic acid, while the acid moiety itself serves as a common additional electronic probe. Sterimol values were calculated over the full ring structure. Thus, L is the length of the ring from the carbon connected to the carboxylic acid, B_1 is the minimal width perpendicular to L (the thickness of the ring or its substituent), and B_5 is the maximal width perpendicular to L (the width of the ring or its substituents). Figure 4.28 depicts the ring stretches used for modeling. These represent 4 vibrational modes that appear in most cases between the C–O–H bending mode and the C=O stretching frequency. The full parameter set is attached in an excel spread sheet.

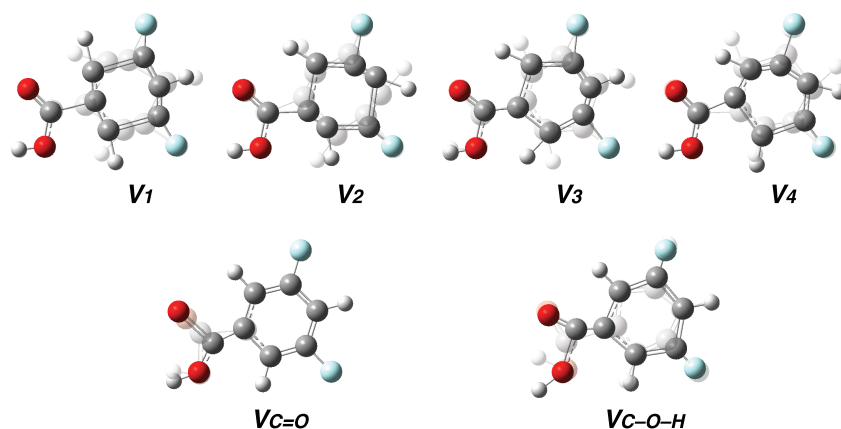
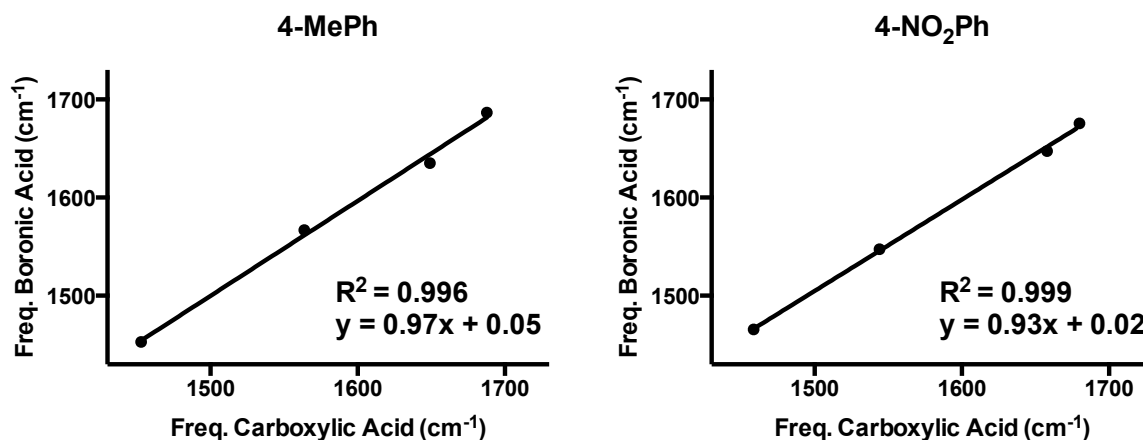


Figure 4.28. Carboxylic acid vibrational modes used for modeling enantioselectivity

In order to test the validity of this approach representative ring stretching modes of the carboxylic acids were compared to those of the BAs (Figure 4.29).



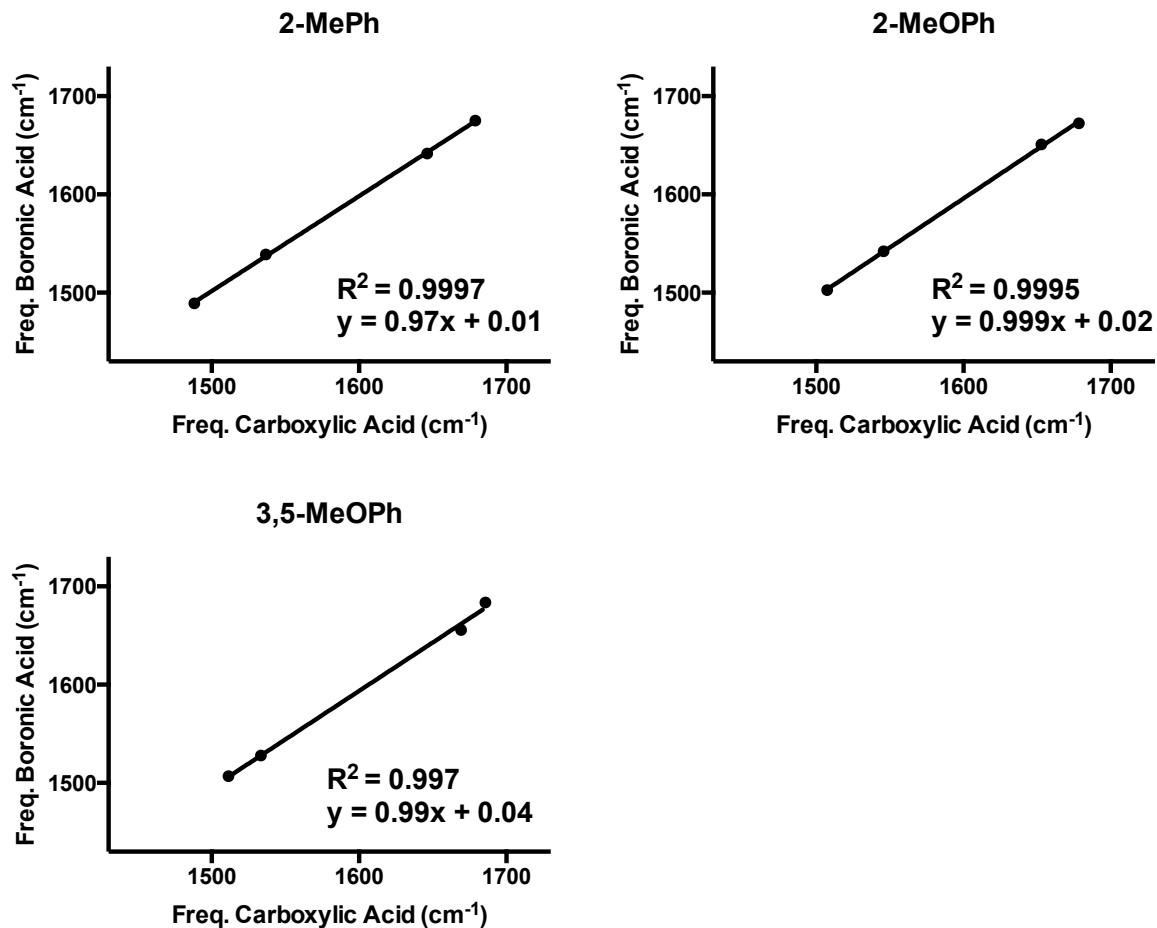


Figure 4.29. Correlation between carboxylic acid and boronic acid vibrational modes for various aryl substitution patterns.

Figure 4.30 depicts an example of changes to these parameters between different structures, the golden arrows are the overall dipole moments associated with specific vibration modes:

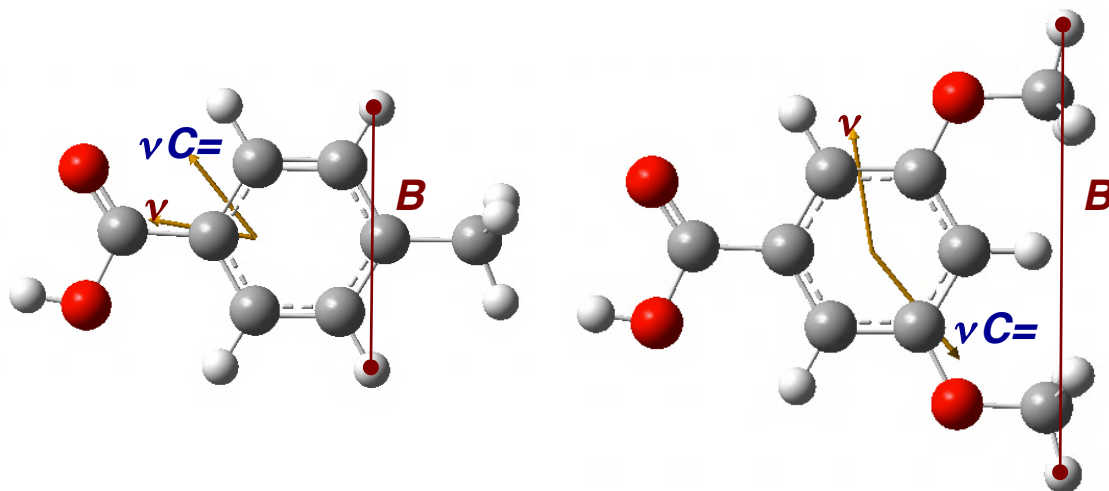


Figure 4.30. Examples of parameters used for modeling

Having defined the structural space to be sampled and the parameterization framework accordingly, enantioselectivities were measured for various substrate-catalyst combinations. Using these data, linear regression algorithms were implemented to relate relevant substrate and catalyst parameters to enantioselectivity, represented as $\Delta\Delta G^\ddagger$, which is the energy difference, in kcal/mol, between the diastereomeric transition states leading to opposite enantiomers. A number of different models were constructed by this process to explore different aspects of the system.

The boronic acid (Table 4.4) and catalyst (Table 4.5) parameters used for modeling the selectivity data are displayed below. Model development involved 4 stepwise regression algorithms that assess the significance of each parameter by applying statistical criteria. In order to realize this assessment, each set of parameter values was normalized by subtracting its respective mean and dividing by its standard deviation. The 4 stepwise regression algorithms are built in MATLAB[®] (version 7.14.0.739, R2012a)¹⁴⁶ statistical toolbox and add or remove normalized parameters from an initial model according to a p-value threshold.¹⁴⁷ Additional suggestions for models were inputted manually based on the results of the 4 preliminary algorithm results or based on our mechanistic hypotheses. A linear fit was performed to probe each manually suggested model's statistical probability, and each suggestion was examined as an initial model for stepwise regression to seek a more effective model.

Table 4.4. Full set of BA molecular descriptors used for modeling

BA	B1	B5	L	vCOH	iCOH
4-tBu	2.82	3.52	8.73	1396.62	153.10
4-F	1.85	3.23	7.50	1398.38	203.07
2-CF₃	1.99	4.97	6.35	1404.75	232.47
2-F	1.77	3.83	6.36	1389.31	125.14
4-ⁱPr	2.55	3.45	8.58	1397.38	174.36
2-ⁱPr	2.17	5.68	6.35	1382.69	80.73
H	1.77	3.19	6.36	1396.80	161.88
4-Me	1.88	3.23	7.39	1396.56	169.55
4-NO₂	1.77	3.23	7.81	1398.79	195.22
2-Me	1.86	4.51	6.34	1388.86	124.97
2-OMe	1.85	5.52	6.34	1410.16	124.26
3,5-(OMe)₂	2.08	4.83	7.21	1411.18	431.19
3,5-(Me)₂	1.95	4.58	6.32	1398.86	120.69
3,5-(CF₃)₂	2.50	4.99	7.00	1368.51	324.82
3,5-F₂	1.77	3.90	6.35	1423.08	288.96
3-MeO-5-Me	2.06	4.84	7.07	1404.51	214.63
3-MeO-5-CF₃	2.28	4.94	7.07	1431.64	446.18
3-EtO-5-Me	2.06	5.84	8.07	1406.26	104.53

3-BnO-5-Me	2.06	8.76	9.71	1404.67	274.26
3-iPrO-5-Me	2.27	6.00	8.20	1404.84	154.57

BA	v1	i1	v2	i2	v3	i3
4-tBu	1454.56	35.66	1562.69	3.96	1643.16	8.75
4-F	1462.27	24.69	1566.89	53.14	1669.57	7.22
2-CF₃	1499.59	4.23	1549.02	13.19	1657.99	9.08
2-F	1500.78	18.66	1547.07	73.28	1659.85	29.97
4-ⁱPr	1465.36	31.46	1562.32	3.10	1647.94	5.26
2-ⁱPr	1493.12	7.79	1539.58	20.83	1647.00	18.84
H	1497.60	19.07	1541.94	3.37	1660.88	4.19
4-Me	1452.93	16.21	1563.79	2.87	1649.00	5.66
4-NO₂	1458.56	52.46	1544.00	2.22	1657.98	116.47
2-Me	1505.43	21.78	1539.12	17.25	1647.76	19.25
2-OMe	1507.41	16.27	1545.74	113.20	1652.85	23.60
3,5-(OMe)₂	1511.43	1.65	1533.44	78.01	1669.20	270.53
3,5-(Me)₂	1516.29	27.41	1523.34	5.70	1675.56	5.13
3,5-(CF₃)₂	1511.70	5.87	1514.77	2.76	1692.75	26.70
3,5-F₂	1514.48	114.84	1525.63	29.41	1683.35	178.49
3-MeO-5-Me	1512.27	77.54	1524.92	45.20	1672.73	122.62
3-MeO-5-CF₃	1519.53	120.09	1526.45	65.99	1680.35	66.61
3-EtO-5-Me	1516.44	133.27	1520.19	12.11	1672.59	131.91
3-BnO-5-Me	1519.62	3.68	1525.12	80.54	1673.20	150.63
3-iPrO-5-Me	1517.90	121.38	1519.39	0.31	1670.31	135.93

BA	v4	i4	vC=O	iC=O	σ-meta	σ-para
4-tBu	1685.79	61.17	1848.89	426.09	-0.10	-0.20
4-F	1683.45	130.65	1852.00	395.02	0.34	0.06
2-CF₃	1682.02	6.37	1857.98	368.61	0.43	0.54
2-F	1687.50	55.54	1865.33	439.19	0.34	0.06
4-ⁱPr	1685.84	58.54	1848.78	418.76	-0.04	-0.15
2-ⁱPr	1676.55	10.68	1839.23	371.96	-0.04	-0.15
H	1679.11	15.36	1852.13	385.46	0.00	0.00

4-Me	1687.75	57.60	1848.99	413.29	-0.07	-0.17
4-NO₂	1679.99	8.57	1861.50	366.86	0.71	0.78
2-Me	1678.35	10.43	1840.76	374.94	-0.07	-0.17
2-OMe	1678.43	107.40	1826.12	439.85	0.12	-0.27
3,5-(OMe)₂	1685.72	44.27	1854.36	363.21	0.12	-0.27
3,5-(Me)₂	1679.70	32.13	1849.43	380.00	-0.07	-0.17
3,5-(CF₃)₂	1696.19	11.82	1864.49	364.46	0.43	0.54
3,5-F₂	1695.86	27.09	1860.31	354.15	0.34	0.06
3-MeO-5-Me	1682.39	9.54	1852.13	376.51		
3-MeO-5-CF₃	1691.77	11.31	1859.20	364.44		
3-EtO-5-Me	1681.66	9.83	1851.81	371.81		
3-BnO-5-Me	1682.54	8.69	1852.45	353.87		
3-iPrO-5-Me	1679.66	9.24	1851.71	370.49		

Table 4.5. Full set of catalyst molecular descriptors used for modeling

Cat	B1	B5	L	vCOH	iCOH
2,4,6-ⁱPr	3.31	5.76	8.61	1375.91	38.68
2,4,6-Me	2.03	4.53	7.36	1377.57	91.79
2-ⁱPr	2.17	5.68	6.35	1382.69	80.73
H	1.77	3.19	6.36	1396.80	161.88
2,6-ⁱPr	3.03	5.80	6.36	1365.44	56.24
4-ⁱPr	2.55	3.45	8.58	1397.38	174.36
3,5-(Me)₂	1.95	4.58	6.32	1398.86	120.69
3,5-(CF₃)₂	2.50	4.99	7.00	1368.51	324.82
2,4,6-Cy	3.34	7.57	10.71	1376.40	22.87

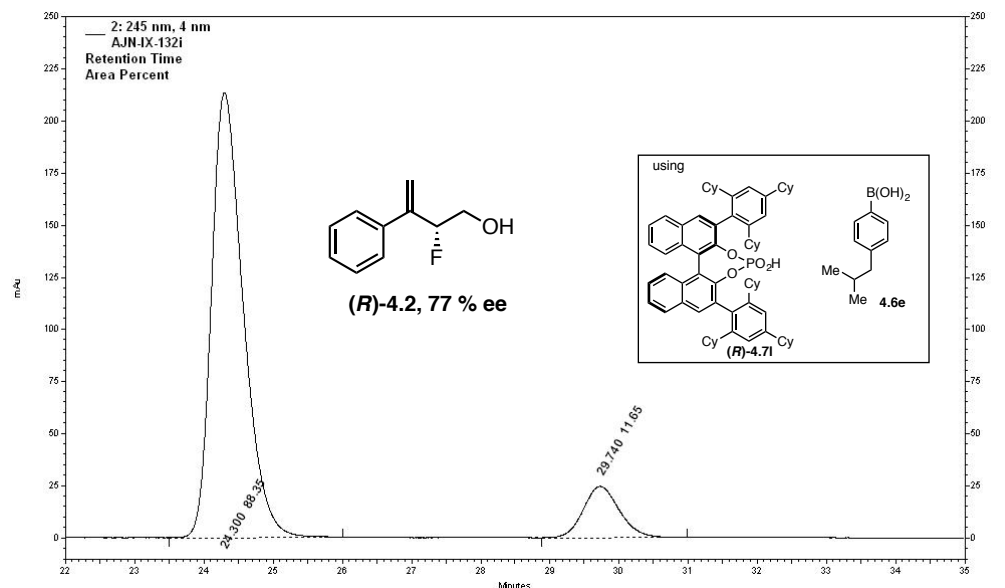
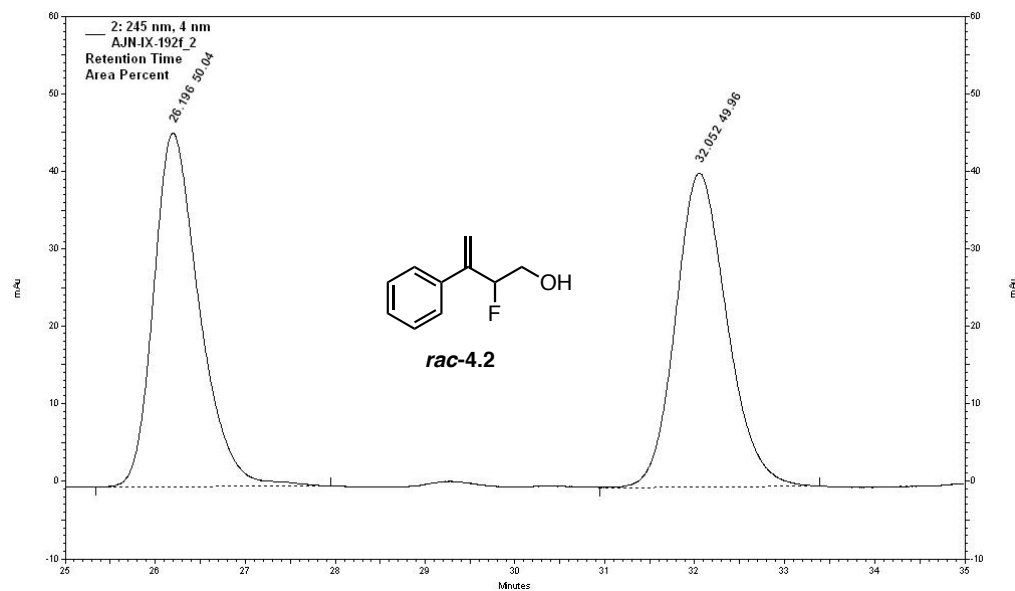
Cat	v1	i1	v2	i2	v3	i3
2,4,6-ⁱPr	1483.15	18.44	1529.17	6.20	1645.94	25.04
2,4,6-Me	1456.00	1.65	1532.60	1.90	1645.42	20.26
2-ⁱPr	1493.12	7.79	1539.58	20.83	1647.00	18.84
H	1497.60	19.07	1541.94	3.37	1660.88	4.19

2,6-ⁱPr	1520.18	3.63	1522.30	14.92	1659.18	15.51
4-ⁱPr	1465.36	31.46	1562.32	3.10	1647.94	5.26
3,5-(Me)₂	1516.29	27.41	1523.34	5.70	1675.56	5.13
3,5-(CF₃)₂	1511.70	5.87	1514.77	2.76	1692.75	26.70
2,4,6-Cy	1485.75	1.48	1525.15	5.18	1643.35	36.83

Cat	v4	i4	vC=O	iC=O	tor
2,4,6-ⁱPr	1677.87	46.13	1853.75	336.62	65.69
2,4,6-Me	1680.55	69.34	1842.66	386.83	39.67
2-ⁱPr	1676.55	10.68	1839.23	371.96	20.24
H	1679.11	15.36	1852.13	385.46	0.00
2,6-ⁱPr	1667.62	10.49	1855.04	273.49	89.26
4-ⁱPr	1685.84	58.54	1848.78	418.76	0.05
3,5-(Me)₂	1679.70	32.13	1849.43	380.00	0.05
3,5-(CF₃)₂	1696.19	11.82	1864.49	364.46	0.02
2,4,6-Cy	1675.74	64.56	1851.28	333.64	65.08

HPLC Traces

As part of this study, substrate **4.1**, was tested with 9 chiral phosphoric acid catalysts and 31 aryl boronic acids in various combinations, each in duplicate for a total of 234 independent measurements of enantioselectivity. Thus, only selected HPLC traces are provided, representing the enantioselectivity reversal (77 % (*R*) to 92 % (*S*)) reported in Figure 4.23 of the main text using catalyst (***R***)-**4.71** (TCYP) with boronic acids **4.6e** and **4.6o** respectively. The raw enantioselectivity data for each phosphoric acid/boronic acid combination are presented above..



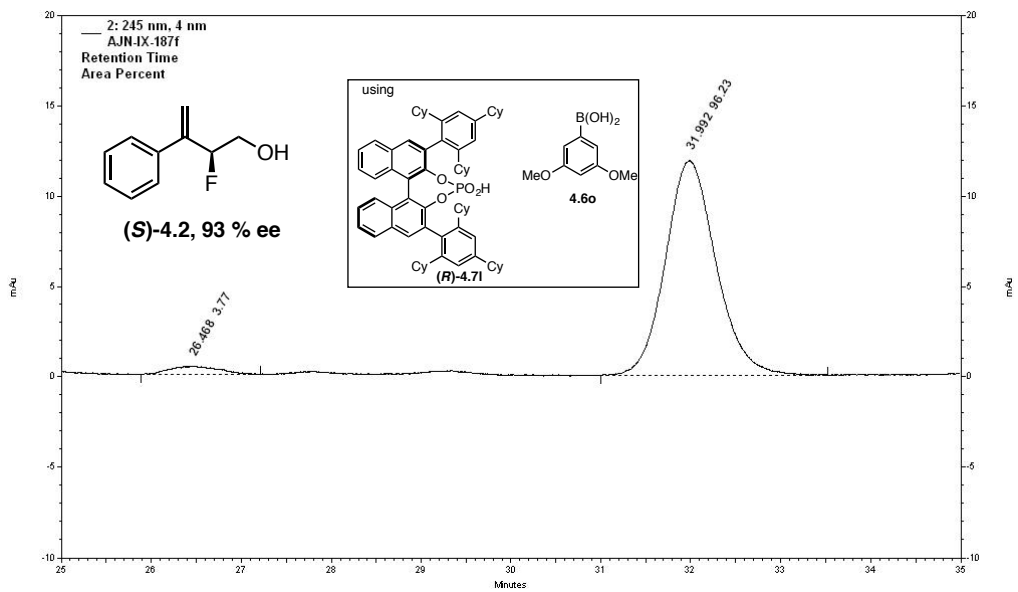


Figure 4.31 depicts a sample ^1H NMR spectrum for the equilibrium described in Table 4.2, corresponding to 4 equivalents of added **4.1** (0.140 mmol, 1.33 equiv with respect to “boron”).

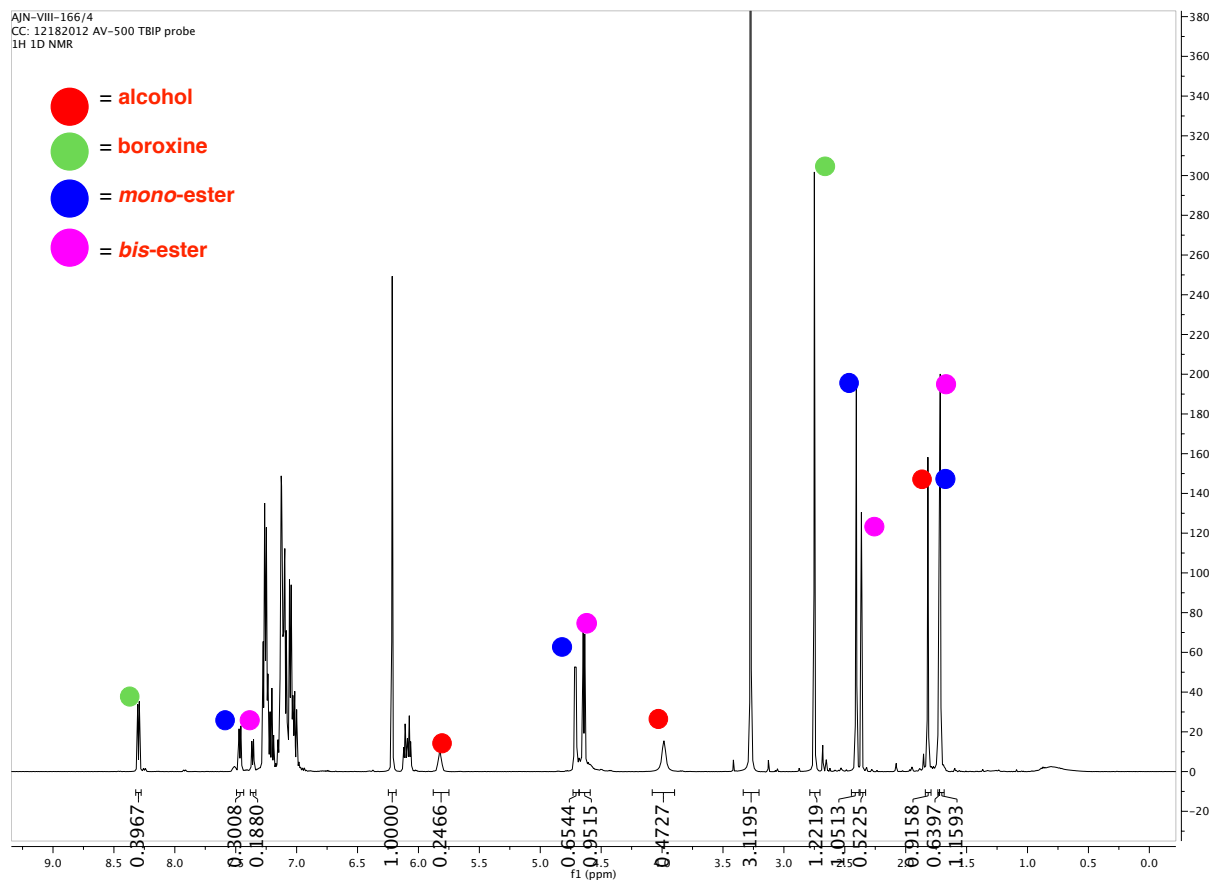


Figure 4.31. Sample ^1H NMR titration spectrum. Initial concentrations: 0.0438 M boroxine, 0.175 M alcohol in benzene- d_6 . Final concentrations: 0.0114 M boroxine, 0.0499 M mono-ester, 0.0381 M bis-ester, 0.0512 M alcohol.

References and Notes

- (1) Milo, A.; Neel, A. J.; Toste, F. D.; Sigman, M. S. *Science* **2015**, *347* (6223), 737.
- (2) Knowles, R. R.; Jacobsen, E. N. *Proc. Natl. Acad. Sci.* **2010**, *107* (48), 20678.
- (3) Jaffé, H. H. *Chem. Rev.* **1953**, *53* (2), 191.
- (4) Schreck, J. O. *J. Chem. Educ.* **1971**, *48* (2), 103.
- (5) Hoz, S.; Ben-Zion, M. *J. Chem. Soc. Chem. Commun.* **1980**, No. 10, 453.
- (6) Sjöström, M.; Wold, S.; Fredga, A.; Bonner, W. A.; Örn, U. *Acta Chem. Scand.* **1981**, *35b*, 537.
- (7) Jencks, W. P.; Brant, S. R.; Gandler, J. R.; Fendrich, G.; Nakamura, C. *J. Am. Chem. Soc.* **1982**, *104* (25), 7045.
- (8) Williams, A. In *New Comprehensive Biochemistry*; Page, M. I., Ed.; The Chemistry of Enzyme Action; Elsevier, 1984; Vol. 6, pp 127–201.
- (9) Greig, I. R. *Chem. Soc. Rev.* **2010**, *39* (6), 2272.
- (10) Swain, C. G.; Langsdorf, W. P. *J. Am. Chem. Soc.* **1951**, *73* (6), 2813.

- (11) Anderson, B. M.; Jencks, W. P. *J. Am. Chem. Soc.* **1960**, 82 (7), 1773.
- (12) Hart, H.; Sedor, E. A. *J. Am. Chem. Soc.* **1967**, 89 (10), 2342.
- (13) Ta-Shma, R.; Rappoport, Z. *J. Am. Chem. Soc.* **1977**, 99 (6), 1845.
- (14) Young, P. R.; Jencks, W. P. *J. Am. Chem. Soc.* **1979**, 101 (12), 3288.
- (15) Stein, A. R.; Tencer, M.; Moffatt, E. A.; Dawe, R.; Sweet, J. *J. Org. Chem.* **1980**, 45 (17), 3539.
- (16) Bergon, M.; Calmon, J.-P. *Tetrahedron Lett.* **1981**, 22 (10), 937.
- (17) Richard, J. P.; Jencks, W. P. *J. Am. Chem. Soc.* **1982**, 104 (17), 4689.
- (18) Meenakshisundaram, S.; Sockalingam, R. *Collect. Czechoslov. Chem. Commun.* **2001**, 66 (6), 897.
- (19) Um, I.-H.; Han, H.-J.; Ahn, J.-A.; Kang, S.; Buncl, E. *J. Org. Chem.* **2002**, 67 (24), 8475.
- (20) Ravi, R.; Sanjeev, R.; Jagannadham, V. *Int. J. Chem. Kinet.* **2013**, 45 (12), 803.
- (21) Jmaoui, I.; Boubaker, T.; Goumont, R. *Int. J. Chem. Kinet.* **2013**, 45 (3), 152.
- (22) Ciaccia, M.; Pilati, S.; Cacciapaglia, R.; Mandolini, L.; Di Stefano, S. *Org. Biomol. Chem.* **2014**, 12 (20), 3282.
- (23) Bartók, M. *Chem. Rev.* **2010**, 110 (3), 1663.
- (24) Lutz, F.; Igarashi, T.; Kawasaki, T.; Soai, K. *J. Am. Chem. Soc.* **2005**, 127 (35), 12206.
- (25) Lutz, F.; Igarashi, T.; Kinoshita, T.; Asahina, M.; Tsukiyama, K.; Kawasaki, T.; Soai, K. *J. Am. Chem. Soc.* **2008**, 130 (10), 2956.
- (26) Holland, M. C.; Metternich, J. B.; Daniliuc, C.; Schweizer, W. B.; Gilmour, R. *Chem. – Eur. J.* **2015**, 21 (28), 10031.
- (27) Phipps, R. J.; Hamilton, G. L.; Toste, F. D. *Nat. Chem.* **2012**, 4 (8), 603.
- (28) Mahlau, M.; List, B. *Angew. Chem. Int. Ed.* **2013**, 52 (2), 518.
- (29) Brak, K.; Jacobsen, E. N. *Angew. Chem. Int. Ed.* **2013**, 52 (2), 534.
- (30) Rauniyar, V.; Lackner, A. D.; Hamilton, G. L.; Toste, F. D. *Science* **2011**, 334 (6063), 1681.
- (31) Phipps, R. J.; Hiramatsu, K.; Toste, F. D. *J. Am. Chem. Soc.* **2012**, 134 (20), 8376.
- (32) Wang, Y.-M.; Wu, J.; Hoong, C.; Rauniyar, V.; Toste, F. D. *J. Am. Chem. Soc.* **2012**, 134 (31), 12928.
- (33) Honjo, T.; Phipps, R. J.; Rauniyar, V.; Toste, F. D. *Angew. Chem. Int. Ed.* **2012**, 51 (38), 9684.
- (34) Phipps, R. J.; Toste, F. D. *J. Am. Chem. Soc.* **2013**, 135 (4), 1268.
- (35) Shunatona, H. P.; Früh, N.; Wang, Y.-M.; Rauniyar, V.; Toste, F. D. *Angew. Chem. Int. Ed.* **2013**, 52 (30), 7724.
- (36) Neel, A. J.; Hehn, J. P.; Triplet, P. F.; Toste, F. D. *J. Am. Chem. Soc.* **2013**, 135 (38), 14044.
- (37) Wu, J.; Wang, Y.-M.; Drljevic, A.; Rauniyar, V.; Phipps, R. J.; Toste, F. D. *Proc. Natl. Acad. Sci.* **2013**, 110 (34), 13729.
- (38) Lackner, A. D.; Samant, A. V.; Toste, F. D. *J. Am. Chem. Soc.* **2013**, 135 (38), 14090.
- (39) Liu, H.; Jiang, G.; Pan, X.; Wan, X.; Lai, Y.; Ma, D.; Xie, W. *Org. Lett.* **2014**, 16 (7), 1908.
- (40) Romanov-Michailidis, F.; Guénée, L.; Alexakis, A. *Angew. Chem. Int. Ed.* **2013**, 52 (35), 9266.
- (41) Romanov-Michailidis, F.; Guénée, L.; Alexakis, A. *Org. Lett.* **2013**, 15 (22), 5890.
- (42) Yang, X.; Phipps, R. J.; Toste, F. D. *J. Am. Chem. Soc.* **2014**, 136 (14), 5225.
- (43) Nelson, H. M.; Reisberg, S. H.; Shunatona, H. P.; Patel, J. S.; Toste, F. D. *Angew. Chem. Int. Ed.* **2014**, 53 (22), 5600.

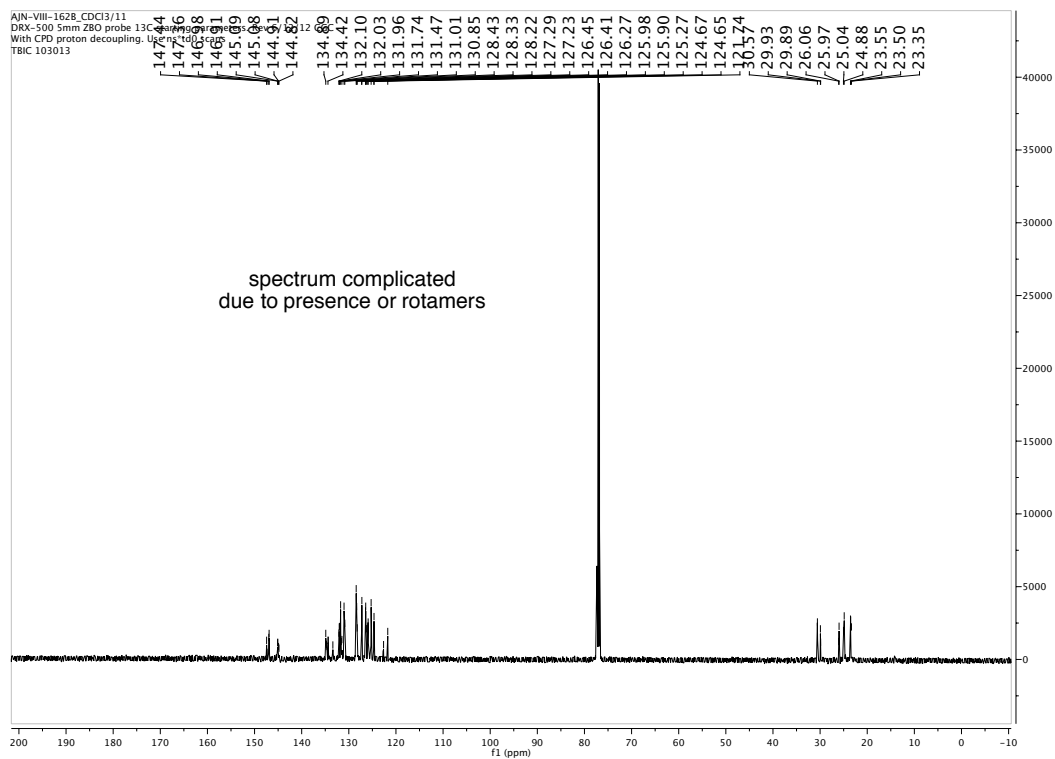
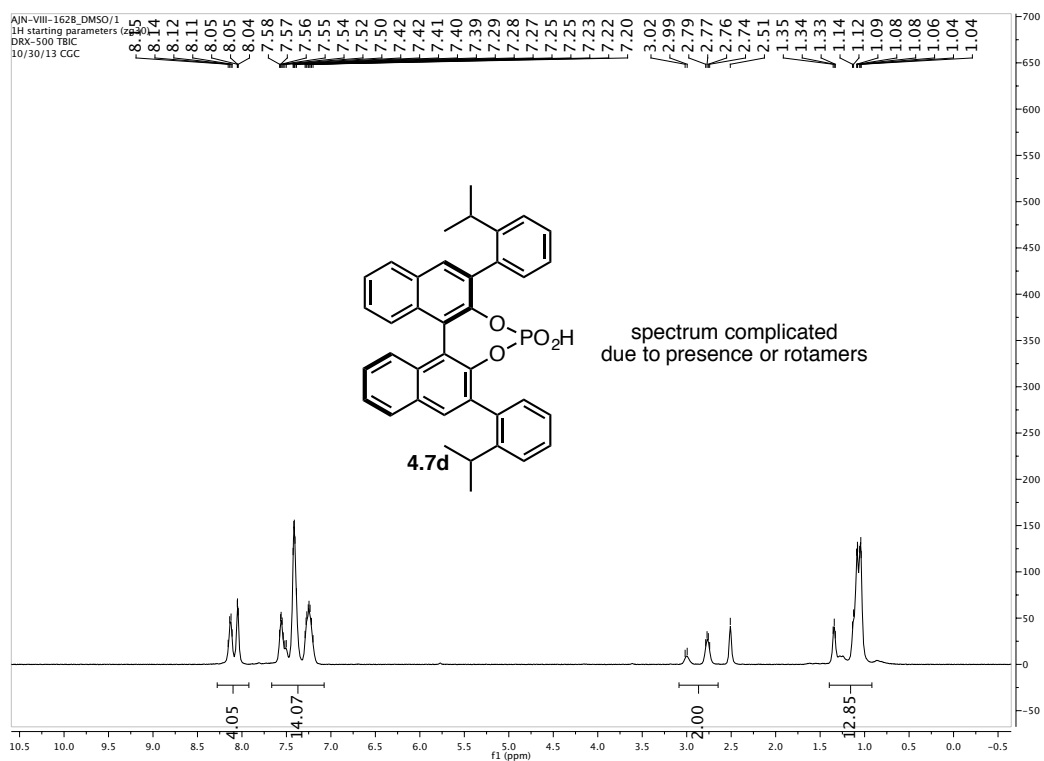
- (44) Romanov-Michailidis, F.; Pupier, M.; Guénée, L.; Alexakis, A. *Chem. Commun.* **2014**, 50 (88), 13461.
- (45) Romanov-Michailidis, F.; Pupier, M.; Besnard, C.; Bürgi, T.; Alexakis, A. *Org. Lett.* **2014**, 16 (19), 4988.
- (46) Nelson, H. M.; Williams, B. D.; Miró, J.; Toste, F. D. *J. Am. Chem. Soc.* **2015**, 137 (9), 3213.
- (47) Romanov-Michailidis, F.; Romanova-Michaelides, M.; Pupier, M.; Alexakis, A. *Chem. – Eur. J.* **2015**, 21 (14), 5561.
- (48) Egami, H.; Asada, J.; Sato, K.; Hashizume, D.; Kawato, Y.; Hamashima, Y. *J. Am. Chem. Soc.* **2015**, 137 (32), 10132.
- (49) Akiyama, T. *Chem Rev* **2007**, 107 (12), 5744.
- (50) Terada, M. *Synthesis* **2010**, 2010 (12), 1929.
- (51) Terada, M. *Curr. Org. Chem.* **2011**, 15 (13), 2227.
- (52) Mori, K.; Akiyama, T. In *Comprehensive Enantioselective Organocatalysis*; Dalko, P. I., Ed.; Wiley-VCH Verlag GmbH & Co. KGaA, 2013; pp 289–314.
- (53) Parmar, D.; Sugiono, E.; Raja, S.; Rueping, M. *Chem. Rev.* **2014**, 114 (18), 9047.
- (54) Nelson, H. M.; Patel, J. S.; Shunatona, H. P.; Toste, F. D. *Chem. Sci.* **2014**, 6 (1), 170.
- (55) Romanov-Michailidis, F.; Romanova-Michaelides, M.; Pupier, M.; Alexakis, A. *Chem. – Eur. J.* **2015**, 21 (14), 5561.
- (56) Zi, W.; Wang, Y.-M.; Toste, F. D. *J. Am. Chem. Soc.* **2014**, 136 (37), 12864.
- (57) Bobbio, C.; Gouverneur, V. *Org. Biomol. Chem.* **2006**, 4 (11), 2065.
- (58) Shibata, N.; Ishimaru, T.; Nakamura, S.; Toru, T. *J. Fluor. Chem.* **2007**, 128 (5), 469.
- (59) Ma, J.-A.; Cahard, D. *Chem. Rev.* **2008**, 108 (9), PR1.
- (60) Cahard, D.; Xu, X.; Couve-Bonnaire, S.; Pannecoucke, X. *Chem. Soc. Rev.* **2010**, 39 (2), 558.
- (61) Lectard, S.; Hamashima, Y.; Sodeoka, M. *Adv. Synth. Catal.* **2010**, 352 (16), 2708.
- (62) Valero, G.; Companyó, X.; Rios, R. *Chem. – Eur. J.* **2011**, 17 (7), 2018.
- (63) Ye, Z.; Zhao, G. *Chim. Int. J. Chem.* **2011**, 65 (12), 902.
- (64) Yang, X.; Wu, T.; Phipps, R. J.; Toste, F. D. *Chem. Rev.* **2015**, 115 (2), 826.
- (65) Li, D. R.; Murugan, A.; Falck, J. R. *J. Am. Chem. Soc.* **2008**, 130 (1), 46.
- (66) (a) Although reaction rates were qualitatively greater in the absence of activated molecular sieves, sieves were included in the standard reaction conditions as their presence generally resulted in more reproducible enantioselectivities. Additionally, toluene was used as the only solvent for operational simplicity. (b) For the entirety of this chapter, we have defined the result in Figure 4.8, as the standard enantioselectivity (i.e. the (*S*)-catalyst affords the (*S*)-product). On the basis of this convention, the predominant formation of the (*R*)-product was considered “negative” when using the (*S*)-catalyst. Similarly, if use of the (*R*)-catalyst resulted in the (*S*)-enantiomer as the major product, this result was considered “negative.” This convention was opted as it better alerts the reader to the fact that the enantioselectivity inversion is independent of the catalyst enantiomer used (as opposed to the (*R*) and (*S*) terminology).
- (67) Hoffmann, S.; Seayad, A. M.; List, B. *Angew. Chem. Int. Ed.* **2005**, 44 (45), 7424.
- (68) Tiago Menezes Correia, J. *Synlett* **2015**, 26 (03), 416.
- (69) Miller, J. J.; Sigman, M. S. *Angew. Chem. Int. Ed.* **2008**, 47 (4), 771.
- (70) Gustafson, J. L.; Sigman, M. S.; Miller, S. J. *Org. Lett.* **2010**, 12 (12), 2794.
- (71) Jensen, K. H.; Sigman, M. S. *J. Org. Chem.* **2010**, 75 (21), 7194.
- (72) Harper, K. C.; Sigman, M. S. *Proc. Natl. Acad. Sci.* **2011**.

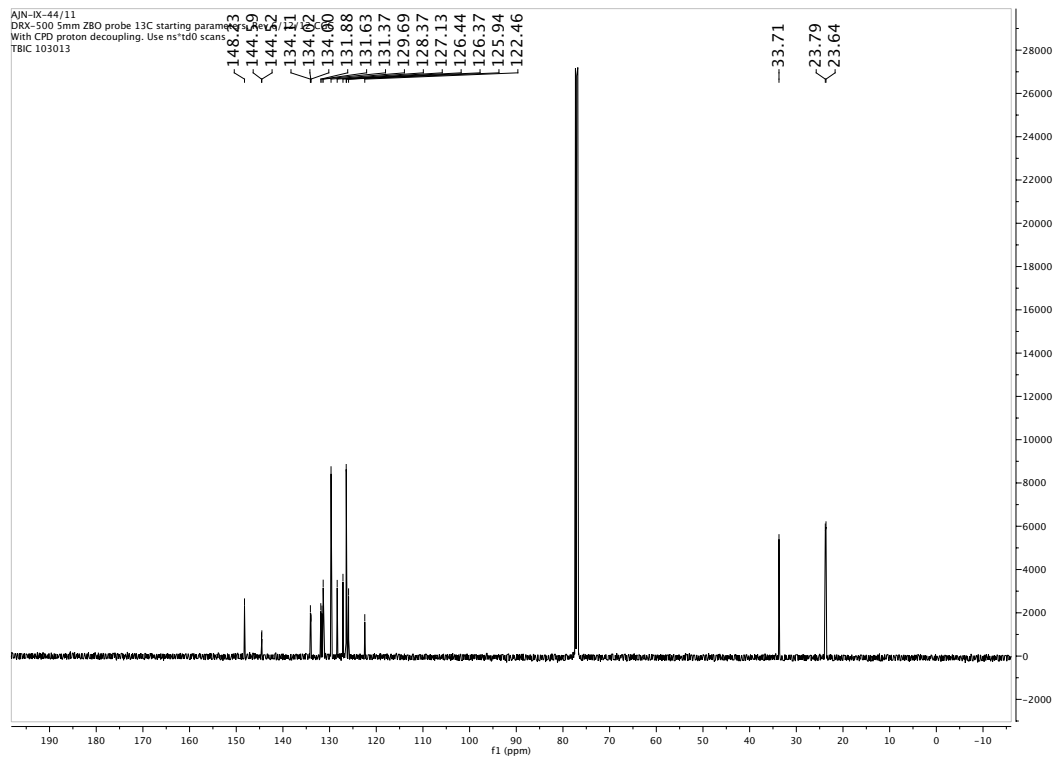
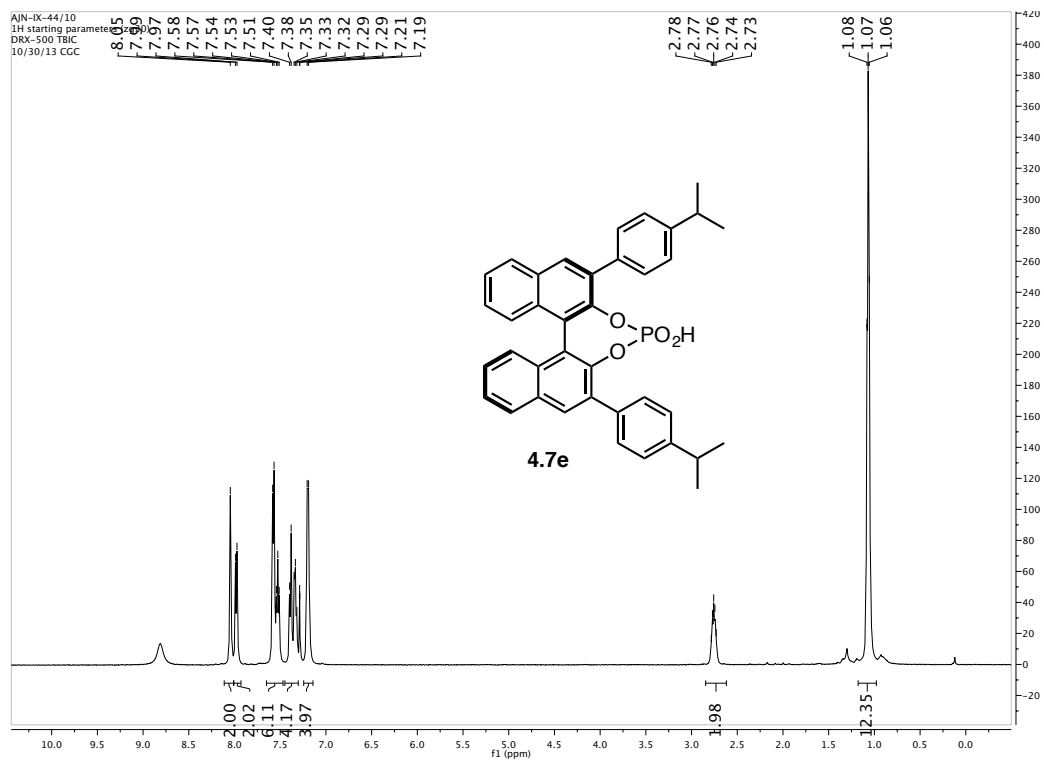
- (73) Harper, K. C.; Sigman, M. S. *Science* **2011**, 333 (6051), 1875.
- (74) Harper, K. C.; Bess, E. N.; Sigman, M. S. *Nat. Chem.* **2012**, 4 (5), 366.
- (75) Harper, K. C.; Sigman, M. S. *J. Org. Chem.* **2013**, 78 (7), 2813.
- (76) Harper, K. C.; Vilaridi, S. C.; Sigman, M. S. *J. Am. Chem. Soc.* **2013**, 135 (7), 2482.
- (77) McCammant, M. S.; Sigman, M. S. *Chem. Sci.* **2015**, 6 (2), 1355.
- (78) Zhang, C.; Santiago, C. B.; Kou, L.; Sigman, M. S. *J. Am. Chem. Soc.* **2015**, 137 (23), 7290.
- (79) Puchot, C.; Samuel, O.; Dunach, E.; Zhao, S.; Agami, C.; Kagan, H. B. *J. Am. Chem. Soc.* **1986**, 108 (9), 2353.
- (80) Guillaneux, D.; Zhao, S.-H.; Samuel, O.; Rainford, D.; Kagan, H. B. *J. Am. Chem. Soc.* **1994**, 116 (21), 9430.
- (81) Kagan, H. B.; Girard, C.; Guillaneux, D.; Rainford, D.; Samuel, O.; Zhang, S. Y.; Zhao, S. H.; Ciglic, M. I.; Haugg, M.; Trabesinger-Rüf, N.; Weinhold, E. G. *Acta Chem. Scand.* **1996**, 50, 345.
- (82) Heller, D.; Drexler, H.-J.; Fischer, C.; Buschmann, H.; Baumann, W.; Heller, B. *Angew. Chem. Int. Ed.* **2000**, 39 (3), 495.
- (83) Kagan, H. B. *Adv. Synth. Catal.* **2001**, 343 (3), 227.
- (84) Kagan, H. B. *Synlett* **2001**, 2001 (Special Issue), 0888.
- (85) Klusmann, M.; Mathew, S. P.; Iwamura, H.; Wells, D. H.; Armstrong, A.; Blackmond, D. G. *Angew. Chem.* **2006**, 118 (47), 8157.
- (86) Satyanarayana, T.; Abraham, S.; Kagan, H. B. *Angew. Chem. Int. Ed.* **2009**, 48 (3), 456.
- (87) Kitamura, M.; Suga, S.; Oka, H.; Noyori, R. *J. Am. Chem. Soc.* **1998**, 120 (38), 9800.
- (88) Chen, Y. K.; Costa, A. M.; Walsh, P. J. *J. Am. Chem. Soc.* **2001**, 123 (22), 5378.
- (89) Noyori, R.; Suga, S.; Oka, H.; Kitamura, M. *Chem. Rec.* **2001**, 1 (2), 85.
- (90) Buono, F.; Walsh, P. J.; Blackmond, D. G. *J. Am. Chem. Soc.* **2002**, 124 (46), 13652.
- (91) Oestreich, M.; Rendler, S. *Angew. Chem. Int. Ed.* **2005**, 44 (11), 1661.
- (92) Palomo, C.; Oiarbide, M.; Laso, A. *Angew. Chem. Int. Ed.* **2005**, 44 (25), 3881.
- (93) Portada, T.; Roje, M.; Hameršak, Z.; Žinić, M. *Tetrahedron Lett.* **2005**, 46 (35), 5957.
- (94) Dziedzic, P.; Zou, W.; Ibrahim, I.; Sundén, H.; Córdova, A. *Tetrahedron Lett.* **2006**, 47 (37), 6657.
- (95) Duan, W.-L.; Iwamura, H.; Shintani, R.; Hayashi, T. *J. Am. Chem. Soc.* **2007**, 129 (7), 2130.
- (96) Lou, S.; Moquist, P. N.; Schaus, S. E. *J. Am. Chem. Soc.* **2007**, 129 (49), 15398.
- (97) Gelalcha, F. G.; Anilkumar, G.; Tse, M. K.; Brückner, A.; Beller, M. *Chem. – Eur. J.* **2008**, 14 (25), 7687.
- (98) El-Hamdouni, N.; Companyó, X.; Rios, R.; Moyano, A. *Chem. – Eur. J.* **2010**, 16 (4), 1142.
- (99) Li, N.; Chen, X.-H.; Zhou, S.-M.; Luo, S.-W.; Song, J.; Ren, L.; Gong, L.-Z. *Angew. Chem. Int. Ed.* **2010**, 49 (36), 6378.
- (100) Chen, Z.; Wang, B.; Wang, Z.; Zhu, G.; Sun, J. *Angew. Chem. Int. Ed.* **2013**, 52 (7), 2027.
- (101) Wang, H.-Y.; Zhang, K.; Zheng, C.-W.; Chai, Z.; Cao, D.-D.; Zhang, J.-X.; Zhao, G. *Angew. Chem. Int. Ed.* **2015**, 54 (6), 1775.
- (102) Tanaka, K.; Iwashita, T.; Yoshida, E.; Ishikawa, T.; Otuka, S.; Urbanczyk-Lipkowska, Z.; Takahashi, H. *Chem Commun* **2015**, 51 (37), 7907.

- (103) It should also be noted that for both the BA subsets, σ_{para} values correlate with selectivity, indicating that asymmetric induction throughout either set was governed by a substantial resonance component (σ_{meta} values were not well-correlated).
- (104) Martínez-Aguirre, M. A.; Yatsimirsky, A. K. *J. Org. Chem.* **2015**, *80* (10), 4985.
- (105) Tokunaga, Y.; Ueno, H.; Shimomura, Y.; Seo, T. *HETEROCYCLES* **2002**, *57* (5), 787.
- (106) Egli, M.; Sarkhel, S. *Acc. Chem. Res.* **2007**, *40* (3), 197.
- (107) Singh, S. K.; Das, A. *Phys. Chem. Chem. Phys.* **2015**, *17* (15), 9596.
- (108) Gallivan, J. P.; Dougherty, D. A. *Org. Lett.* **1999**, *1* (1), 103.
- (109) Grimme, S. *J. Comput. Chem.* **2004**, *25* (12), 1463.
- (110) Amicangelo, J. C.; Gung, B. W.; Irwin, D. G.; Romano, N. C. *Phys. Chem. Chem. Phys.* **2008**, *10* (19), 2695.
- (111) Jain, A.; Ramanathan, V.; Sankararamakrishnan, R. *Protein Sci.* **2009**, *18* (3), 595.
- (112) Yang, T.; An, J.-J.; Wang, X.; Wu, D.-Y.; Chen, W.; Fossey, J. S. *Phys. Chem. Chem. Phys.* **2012**, *14* (30), 10747.
- (113) Singh, S. K.; Kumar, S.; Das, A. *Phys. Chem. Chem. Phys.* **2014**, *16* (19), 8819.
- (114) Mondal, S. I.; Dey, A.; Sen, S.; Patwari, G. N.; Ghosh, D. *Phys. Chem. Chem. Phys.* **2014**, *17* (1), 434.
- (115) Ao, M.-Z.; Tao, Z.; Liu, H.-X.; Wu, D.-Y.; Wang, X. *Comput. Theor. Chem.* **2015**, *1064*, 25.
- (116) Egli, M.; Gessner, R. V. *Proc. Natl. Acad. Sci.* **1995**, *92* (1), 180.
- (117) Korenaga, T.; Tanaka, H.; Ema, T.; Sakai, T. *J. Fluor. Chem.* **2003**, *122* (2), 201.
- (118) Gung, B. W.; Xue, X.; Reich, H. J. *J. Org. Chem.* **2005**, *70* (18), 7232.
- (119) Gung, B. W.; Zou, Y.; Xu, Z.; Amicangelo, J. C.; Irwin, D. G.; Ma, S.; Zhou, H.-C. *J. Org. Chem.* **2008**, *73* (2), 689.
- (120) Mooibroek, T. J.; Gamez, P.; Reedijk, J. *CrystEngComm* **2008**, *10* (11), 1501.
- (121) Korenaga, T.; Shoji, T.; Onoue, K.; Sakai, T. *Chem. Commun.* **2009**, No. 31, 4678.
- (122) Nijamudheen, A.; Jose, D.; Shine, A.; Datta, A. *J. Phys. Chem. Lett.* **2012**, *3* (11), 1493.
- (123) Pavlakos, I.; Arif, T.; Aliev, A. E.; Motherwell, W. B.; Tizzard, G. J.; Coles, S. J. *Angew. Chem. Int. Ed.* **2015**, *54* (28), 8169.
- (124) Duarte, V. C. M.; Faustino, H.; Alves, M. J.; Gil Fortes, A.; Micaelo, N. *Tetrahedron Asymmetry* **2013**, *24* (18), 1063.
- (125) Reddi, Y.; Sunoj, R. B. *ACS Catal.* **2015**, *5* (3), 1596.
- (126) Verloop, A.; Hoogenstraaten, W.; Tipker, J. In *Drug Design*; Ariëns, E. J., Ed.; Medicinal Chemistry: A Series of Monographs; Academic Press: Amsterdam, 1976; Vol. 11, Part G, pp 165–207.
- (127) Milo, A.; Bess, E. N.; Sigman, M. S. *Nature* **2014**, *507* (7491), 210.
- (128) Yamanaka, M.; Itoh, J.; Fuchibe, K.; Akiyama, T. *J. Am. Chem. Soc.* **2007**, *129* (21), 6756.
- (129) Mandai, H.; Murota, K.; Mitsudo, K.; Suga, S. *Org. Lett.* **2012**, *14* (13), 3486.
- (130) Hatano, M.; Ikeno, T.; Matsumura, T.; Torii, S.; Ishihara, K. *Adv. Synth. Catal.* **2008**, *350* (11-12), 1776.
- (131) Akiyama, T.; Morita, H.; Itoh, J.; Fuchibe, K. *Org. Lett.* **2005**, *7* (13), 2583.
- (132) Rauniyar, V.; Wang, Z. J.; Burks, H. E.; Toste, F. D. *J. Am. Chem. Soc.* **2011**, *133* (22), 8486.
- (133) Milburn, R. R.; Hussain, S. M. S.; Prien, O.; Ahmed, Z.; Snieckus, V. *Org. Lett.* **2007**, *9* (22), 4403.

- (134) Klusmann, M.; Ratjen, L.; Hoffmann, S.; Wakchaure, V.; Goddard, R.; List, B. *Synlett* **2010**, *2010* (14), 2189.
- (135) Kim, J. H.; Čorić, I.; Vellalath, S.; List, B. *Angew. Chem. Int. Ed.* **2013**, *52* (16), 4474.
- (136) Kobayashi, K.; Ishiwata, Y.; Takeuchi, K. Novel azo dye compound. US2006142553 (A1), June 29, 2006.
- (137) Wang, K. K.; Liu, C.; Gu, Y. G.; Burnett, F. N.; Sattsangi, P. D. *J. Org. Chem.* **1991**, *56* (5), 1914.
- (138) Murphy, J. M.; Tzschucke, C. C.; Hartwig, J. F. *Org. Lett.* **2007**, *9* (5), 757.
- (139) Frisch, M. J.; Trucks, G. W.; Schlegel, H. B.; Scuseria, G. E.; Robb, M. A.; Cheeseman, J. R.; Scalmani, R.; Barone, G.; Mennucci, B.; Petersson, G. A.; others. *Inc Wallingford CT* **2009**.
- (140) Zhao, Y.; Truhlar, D. G. *Theor. Chem. Acc.* **2007**, *120* (1-3), 215.
- (141) Valero, R.; Gomes, J. R. B.; Truhlar, D. G.; Illas, F. *J. Chem. Phys.* **2008**, *129* (12), 124710.
- (142) Weigend, F. *Phys. Chem. Chem. Phys.* **2006**, *8* (9), 1057.
- (143) Weigend, F.; Ahlrichs, R. *Phys. Chem. Chem. Phys.* **2005**, *7* (18), 3297.
- (144) Merrick, J. P.; Moran, D.; Radom, L. *J. Phys. Chem. A* **2007**, *111* (45), 11683.
- (145) Quinn, J. A. Molecular Modeling Pro, 6.36 (Norgwyn Montgomery Software, North Wales, PA).
- (146) MATLAB (The Math Works, Natick, MA).
- (147) Goodman, S. *Semin. Hematol.* **2008**, *45* (3), 135.

Appendix C. NMR Spectra for Compounds in Chapter 4





AJN-IX-44/31
AV-600 31P starting parameters 11/19/08
31P p1=12.Sus at 2dB. SW 400 ppm, O1P-50 ppm
With 1H decoupling

